AsCA2010

The 10th Conference of the Asian Crystallographic Association

Programme & Abstracts

October 31 (Sun) - November 3 (Wed), 2010
BEXCO, Busan, Korea
www.asca2010.org

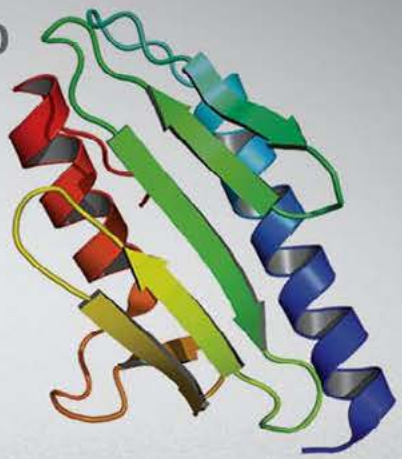

AsCA2010
Busan, Korea

Organized by Korean Crystallographic Association
Sponsored by Asian Crystallographic Association and International Union of Crystallography

Supported by

Greater Busan CVB

AsCA2010 Secretariat
LEE Convention Co., Ltd.
Tel. +82 51 711 0042 / Fax. +82 51 747 7030
E-mail. info@asca2010.org / www.asca2010.org

AsCA2010
Busan, Korea

Table of Contents

Welcome Message

Dear Colleagues:

The Asian Crystallographic Association is very pleased to invite delegates to attend the triennial scientific meeting to be held in Korea in 2010. The 10th Conference of the Association (AsCA'10) will be held in Busan, the second largest city of Korea, from October 31st to November 3rd 2010.

The meeting will bring together scientists, from the region and beyond, representing all aspects of the broad range of crystallographic research. It is my special pleasure to invite you to attend and participate in what promises to be a scientific and cultural delight.

J. Mitchell Guss,
President
Asian Crystallographic Association

Dear Colleagues:

We are very pleased to invite you to attend the AsCA'10 meeting, which will be held in Busan, Korea, from October 31st to November 3rd 2010. As is traditional at AsCA meetings, the program will be designed to cover diverse aspects of crystallography, ranging from structural chemistry to diffraction physics, from electrons to neutrons, from membrane proteins to drug design, from hot topics to cool results and, as they say, much much more.

We are delighted to chair the International Program Committee and the Local Organizing Committee. We extend a very warm welcome to you to join us in Busan, Korea, for what promises to be a terrific meeting.

Jennifer L Martin,
Chair
International Program
Committee

Se Won Suh,
Chair
Local Organizing
Committee

Committees

AsCA Executive Committee

President: Mitchell Guss (Australia)
Vice-President: Se Won Suh (Korea)
Secretary/Treasurer: Ken Haller (Thailand)

AsCA2010 International Program Committee

Chair: Jennifer Martin (Australia)
Members:

Stuart Batten (Australia)
Catherine Day (New Zealand)
Se-Young Jeong (Korea)
Zhi-Jie Liu (China)
Keiichiro Ogawa (Japan)
D M Salunke (India)
Mark Spackman (Australia)
J J Vittal (Singapore)
Wing-Tak Wong (Hong Kong)
Hanna Yuan (Taiwan)
Pinak Chakrabarti (India)
Hoong-Kun Fun (Malaysia)
Kyeong Kyu Kim (Korea)
Ashwini Nangia (India)
Zihe Rao (China)
Hiroshi Sawa (Japan)
Kenji Tsuda (Japan)
Andrew Wang (Taiwan)
Yuruko Yamagata (Japan)

AsCA2010 Local Organizing Committee

Chair: Se Won Suh (Seoul National University)
Members:

Yang Goo Cho (KRISS)
Soo Hyun Eom (GIST)
Taeghwan Hyeon (Seoul National Univ)
Eunice Kim (KIST)
Ki Bong Lee (Postech/PAL)
Tae Won Noh (Seoul National University)
Je-Geun Park (Seoul National University)
Ryong Ryu (KAIST)
Sung-Min Choi (KAIST)
Chang Sik Ha (Busan National University)
Cheol Jin Kim (Gyeongsang National Univ)
Hyung Joon Kim (Seoul National Univ)
Soon Won Lee (SungKyunKwan University)
Byung Ha Oh (KAIST)
Moonhor Ree (Postech/PAL)

AsCA2010 Local Working Committee

Chair: Kyeong Kyu Kim (SungKyunKwan University)
Members:

Nam-Chul Ha (Busan National Univ)
Se Bok Jang (Busan National Univ)
Hyun-Min Park (KRISS)
Byung Woo Han (Seoul National Univ)
Sangho Lee (SungKyunKwan Univ)
Kang Hyun Park (Busan National Univ)

IUCr Scientific Freedom Policy Statement

The International Union of Crystallography shall observe the basic policy of non-discrimination and affirms the right and freedom of scientists to associate in international scientific activity without regard to such factors as citizenship, religion, creed, political stance, ethnic origin, race, colour, language, age or gender, in accordance with the Statutes of the International Council for Science. At this Congress no barriers will exist which would prevent the participation of bona fida scientists.

Business Meeting

Monday, November 1
12:15-13:30 Meeting Room (Level 2)
IUCr Journal Commission Meeting [Lunches will be provided]

Tuesday, November 2
12:15-13:30 Meeting Room (Level 2)
AsCA Council Meeting [Lunches will be provided]

Tuesday, November 2
15:30-16:00 Meeting Room (Level 2)
18:00-18:30 Meeting Room (Level 2) – if necessary
Poster and AsCA Rising Stars Committee Meeting

Wednesday, November 3
12:15-13:30 Hall D
J-PARC Meeting

Satellite Meeting / Workshop

[1] Electron Crystallography in Physical and Biological Sciences

October 29-30, 2010, Korea Basic Science Institute, Daejeon, Korea.
Web site: http://hvem.kbsi.re.kr/eng/

[2] Workshop for ab initio Powder Structure Determination for Chemists and Materials Scientists & 3rd Powder Crystallography Tutorial Course

October 27-29, 2010, POSCO International Center, POSTECH, Pohang, Korea.
Web site: http://paleng.postech.ac.kr/workshop/

[3] Next Generation of Synchrotron Radiation Source Facilities and Their Applications in Ultra-fast and Ultra-small Sciences

November 4-5, 2010, POSCO International Center, POSTECH, Pohang, Korea.
Web site: http://paleng.postech.ac.kr/hrpd/

Evening Events and Luncheon Seminars

All the participants are invited to attend the Welcome Mixer on Sunday evening and the Conference Banquet on Tuesday evening. Limited number of lunch boxes will be provided during luncheon seminars.

Day 1:

Sunday, October 31 / 18:00-21:00 / Hall E (Level 3)
Bruker & Incoatec Welcome Mixer, Opening Ceremony, and Special Lecture

Day 2:

Monday, November 1 / 12:15-13:30 / Hall C (Level 2)
Bruker & Incoatec Luncheon Seminar (by invitation)
[Please pick up a luncheon seminar ticket at the Bruker & Incoatec exhibition booth.]

Day 3:

Tuesday, November 2 / 12:15-13:30 / Hall C (Level 2)
Rigaku Luncheon Seminar

Tuesday, November 2 / 12:15-13:30 / Hall D (Level 2)
GE Healthcare Luncheon Seminar

Tuesday, November 2 / 18:30-21:00 / Hall E (Level 3)
Rigaku Conference Banquet and Award Ceremony

Day 4:

Wednesday, November 3 / 12:15-13:30 / Hall C (Level 2)
IUCr Luncheon Seminar

Conference Sponsors/Exhibitors

Platinum Level

Rigaku / Rigaku USA / Korea ITS

Gold Level

Bruker & Incoatec
International Union of Crystallography (IUCr)

Silver Level

PANalytical
DECTRIS Ltd.
Pohang Light Source (PLS)
Agilent (formerly Oxford Diffraction Ltd.)
Asian Crystallographic Association (AsCA)
Korean Tourism Organization
Busan Convention & Visitors Bureau

Bronze Level

GE Healthcare
TTP LabTech Ltd.
MDXK Inc.
International Center for Diffraction Data (ICDD)
Oxford Cryosystems Ltd.
Bio-Medical Science Co., Ltd.
Molecular Dimensions
Formulatrix
Cambridge Crystallographic Data Centre (CCDC)
Area Detector Systems Corporation (ADSC)
Protein Data Bank Japan (PDBj)
Marresearch GmbH
Douglas Instruments Ltd.
Rayonix
Hyosung R&DB Labs

Venue and Floor Map

Busan Exhibition & Convention Center (BEXCO),

Convention Hall, Busan, Korea

Around BEXCO

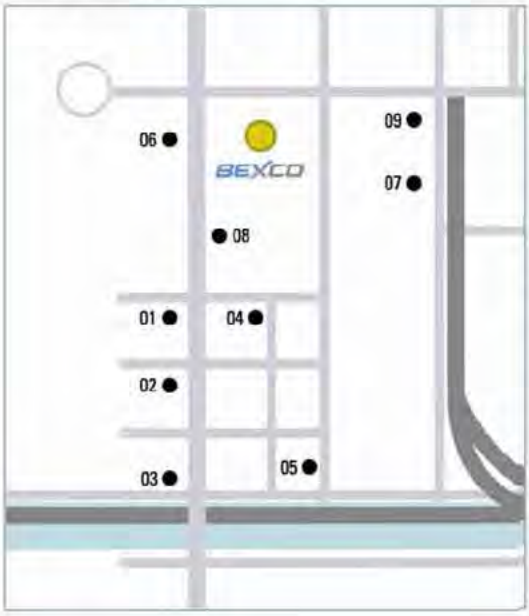

01. Lotte Department Store
(Movie Theater, Restaurant)

02. Shinsegae Department Store
(Movie Theater, Restaurant, Spa, Ice-rink)

03. APEC Park

04. Centum Hotel

05. Olympic Park

06. Home Plus
(Discount Store, Food Court, Fastfood, Drugstore)

07. Museum of Modern Art

08. Centun City Subway Station

09. Busan Museum of Modern Art Subway Station

BEXCO Map

❶ Exhibition Hall

❷ Convention Hall (AsCA2010 Venue)

❸ Glass Hall

❹ Open - Air Exhibition Space

❺ Office Block

❻ Parking Lot

❼ Museum of Modern Art

❽ Home Plus

❾ Centum City Subway Station

❿ Busan Museum of Modern Art Subway Station

BEXCO Convention Hall Floor Map

1st Floor

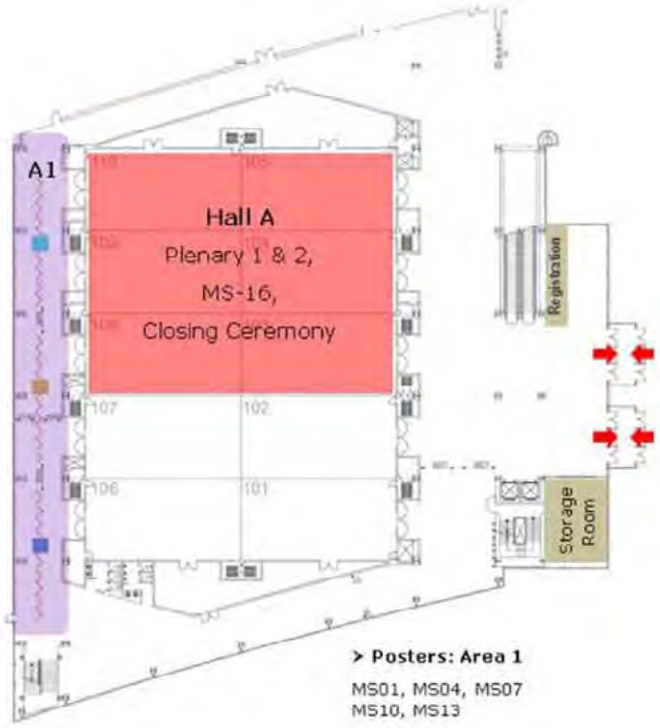

2nd Floor

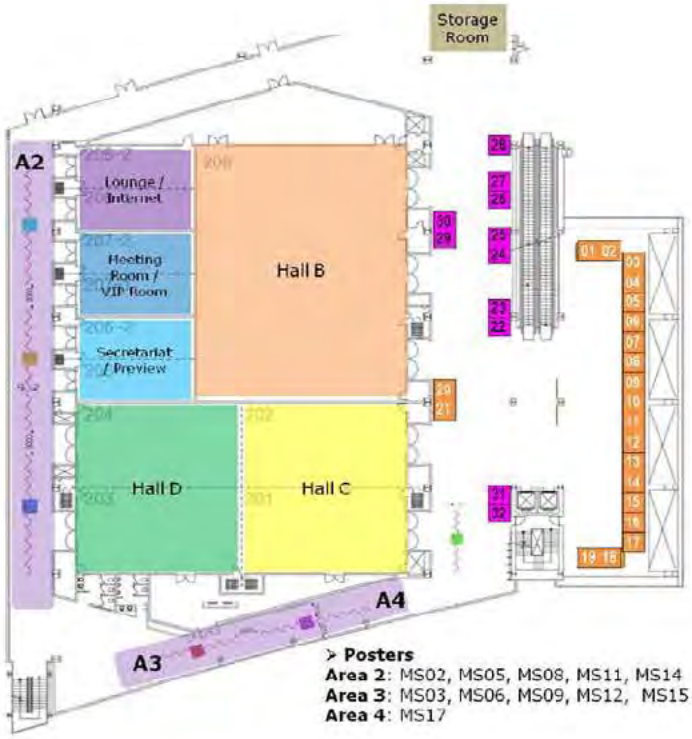

BEXCO Convention Hall Floor Map

2nd Floor Exhibition

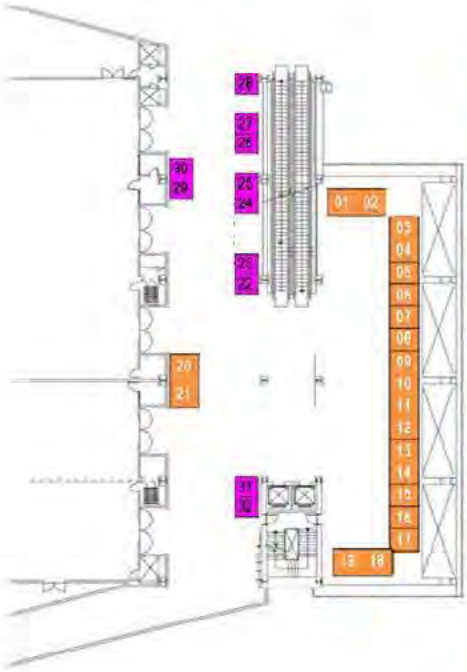

➢ **Exhibition Booth**
No. 1~21: Shell Scheme Booth (2mx2m)
No. 22~32: Table Only (1.6mx1.4m)

No	Company Name
1	Bruker AXS GmbH
2	
3	
4	
5	Pohang Accelerator Laboratory
6	TTP LabTech Ltd.
7	MDxK Inc.
8	ICDD
9	Rigaku Corporation
10	
11	
12	
13	DECTRIS Ltd.
14	
15	Oxford Cryosystems Ltd
16	Bio-Medical Science Co., Ltd.
17	Molecular Dimensions
18	Agilent Technologies
19	
20	PANalytical
21	
22	Formulatrix
23	Cambridge Crystallographic Data Centre
24	Area Detector Systems Corporation (ADSC)
25	
26	Protein Data Bank Japan
27	Marresearch GmbH
28	Douglas Instruments Ltd.
29	Rayonix
30	
31	IUCr
32	AsCA

3rd Floor

General Information

Name Tag

Name tags must be worn visibly during the conference and at the social activities.

Registration Desk

The Registration Desk is located on the first floor.

Opening Time:
Sunday, October 31, 13:30-18:00
Monday, November 1, 08:00-09:00
Tuesday, November 2, 08:00-09:00
Wednesday, November 3, 08:00-09:00

Exhibitions

The exhibition booths are located on the second floor.

Opening Time:
Monday, November 1, 09:00 - Wednesday, November 3, 17:30

Internet Access

Free wireless internet access is available for public use at BEXCO. However, it may be subject to slowdown and interruption in the case of too many users. The transmitted data may not be protected. We will also announce ID/password to provide additional wireless internet service free of charge to the participants of AsCA2010 in an internet room on the second floor (with a small number of PCs), conference lecture halls, and the exhibition area. This internet service may also be subject to slowdown and there may also be a problem in security.

Currency Exchange

The exchange rate of US Dollar to Korean Won fluctuates around KRW 1,150 / USD as of October, 2010.

Information for Authors and Presenters

Official Language

The official language of AsCA2010 will be English.

Oral Presentations

A set of notebook PC (Windows 7 with MS PowerPoint 2007) and LCD projectors are ready in each hall. All presenters are kindly requested to submit and check the presentation files (MS PowerPoint) at the preview room on the second floor at least 30 min before the session. Your talk time includes 5 min discussion/question.

Poster Presentations

All posters will be displayed for three days of the conference. The size of a poster will be 90 cm wide by 120 cm high. Mounting materials will be provided. Presenting authors are kindly requested to be present at the poster during one of the two poster sessions according to the last digit of their poster identification number. Please find the ID of your poster in the program/abstract book. The ID will also be attached to your poster wall.

For posters with last digit odd numbers:

Poster Session 1 on Monday, November 1, 13:30-15:30 (1st & 2nd Floor)

For posters with last digit even numbers:

Poster Session 2 on Tuesday, November 2, 13:30-15:30 (1st & 2nd Floor)

* Poster Installation: Prior to the Opening Ceremony on Oct. 31 (Sun), 18:00
* Poster Removal: Prior to the AsCA Rising Stars Symposium on Nov. 3 (Wed), 13:30

AsCA2010

The 10th Conference of the Asian Crystallographic Association

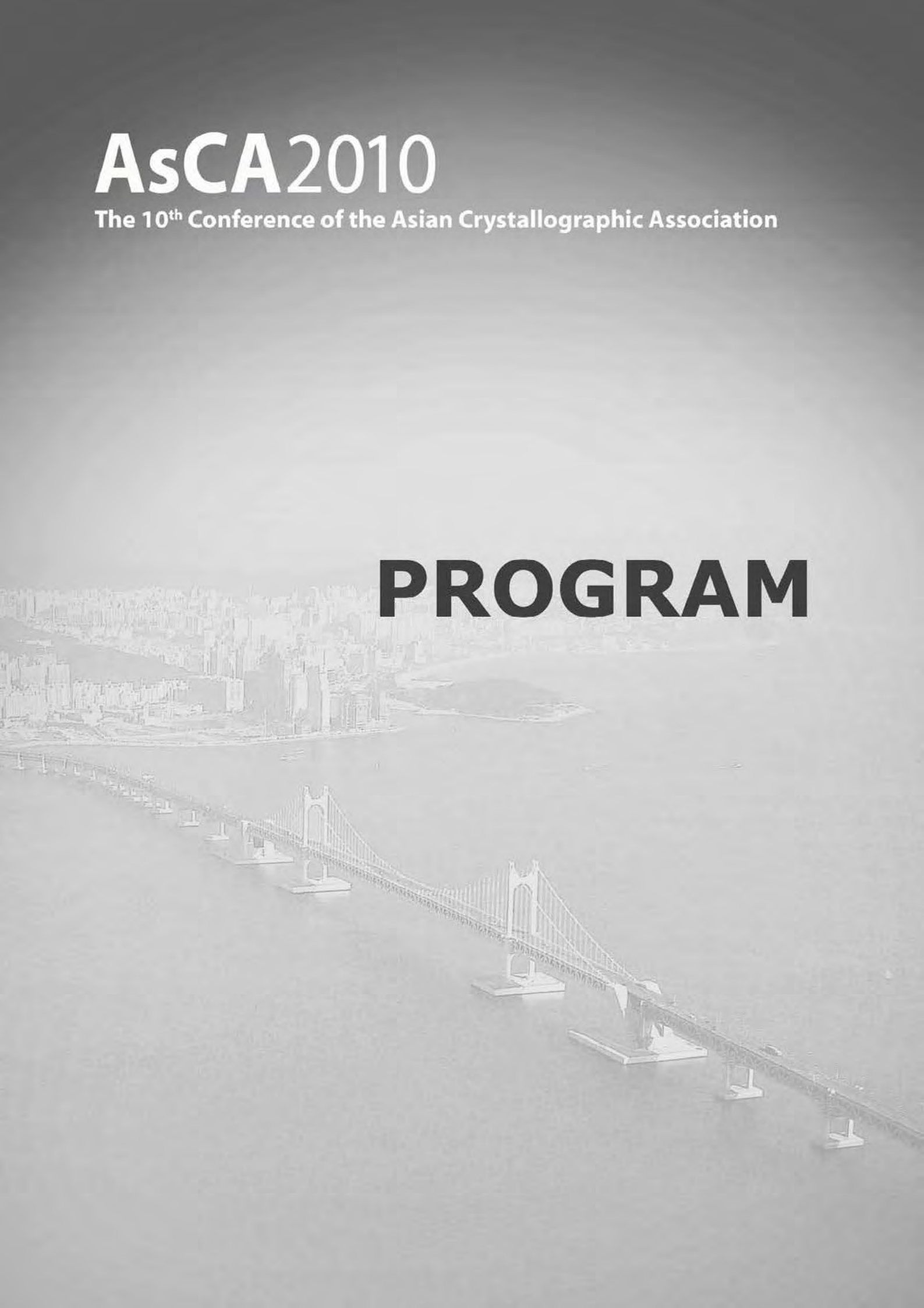

PROGRAM

Program Timetable

	Oct 31 (Sunday)	Nov 1 (Monday)	Nov 2 (Tuesday)	Nov 3 (Wednesday)
08:00		Registration (1st Floor)	Registration (1st Floor)	Registration (1st Floor)
09:00		***Plenary 1*** PL-1 (Hall A) 09:00-10:00	***Keynote 1, 2*** KN-1 (Hall C) KN-2 (Hall B) 09:00-10:00	***Keynote 3, 4*** KN-3 (Hall C) KN-4 (Hall B) 09:00-10:00
10:00	-	Break	Break	Break
10:15		***Oral session 1*** MS-1 (Hall B) MS-2 (Hall C) MS-3 (Hall D) 10:15-12:15	***Oral session 3*** MS-7 (Hall B) MS-8 (Hall C) MS-9 (Hall D) 10:15-12:15	***Oral session 5*** MS-13 (Hall B) MS-14 (Hall C) MS-15 (Hall D) 10:15-12:15
12:15		Lunch 12:15-13:30	Lunch 12:15-13:30	Lunch 12:15-13:30
13:30		***Poster Session 1*** Odd numbers (1st & 2nd Floor) 13:30-15:30	***Poster Session 2*** Even numbers (1st & 2nd Floor) 13:30-15:30	**AsCA rising stars symposium** MS-16 (Hall A) 13:30-15:30
15:30	Registration (1st Floor) 13:30-18:00	Break	Break	Break
16:00		***Oral session 2*** MS-4 (Hall B) MS-5 (Hall C) MS-6 (Hall D) 16:00-18:00	***Oral session 4*** MS-10 (Hall B) MS-11 (Hall C) MS-12 (Hall D) 16:00-18:00	***Plenary 2*** PL-2 (Hall A) 16:00-17:00
17:00				***Closing*** (Hall A) 17:00-17:30
17:30				-
18:00	***Opening, Welcome Mixer & AsCA Special Lecture*** SL-1 (Hall E) 18:00-21:00	-	-	
18:30			***Award Ceremony & Conference Banquet*** (Hall E) 18:30-21:00	
19:20		***Oral session 2e*** MS-10e (Hall B) 19:20-21:00		

Hall A (1st floor)
Hall B, C, D (2nd floor)
Hall E (3rd floor)

Session Topics

Area 1. Structural Biology

MS01: Membrane proteins
MS04: Macromolecular complexes including nucleic acids
MS07: Enzymes and enzyme inhibitors
MS10 and MS10e: Drug discovery/disease related proteins
MS13: Structural proteomics and bioinformatics

Area 2. Chemical Crystallography and Materials Science

MS02: Metal organic frameworks
MS05: Chemical crystallography - structure and properties
MS08: Dynamic aspects of molecular and solid state crystals
MS11: Magnetic structures/molecular magnets
MS14: Nanomaterials, surface, and interface

Area 3. Specialized Techniques

MS03: Synchrotron and neutron sources, instrumentation and applications
MS06: Small angle X-ray and neutron scattering
MS09: Combining methods/new tools in structural biology
MS12: Crystal growth and engineering
MS15: Powder diffraction

Area 4. Others

MS-16: AsCA rising stars symposium
MS-17: Other areas

Detailed Program

Day 1: October 31 (Sunday)

13:30-18:00 **Registration (Level 1)**

18:00-21:00 **Bruker & Incoatec Welcome Mixer, Opening Ceremony, and Special Opening Lecture**

Hall E / Special Opening Lecture

Chair: Se Won Suh

SL-1 **The Crystal Dragon: AsCA and crystallography in the Asia-Pacific region**
Gautam Desiraju (India)

Day 2: November 1 (Monday)

08:00-09:00 **Registration (Level 1)**

09:00-10:00 **Plenary Lecture-1 (PL-1)**

Hall A
Chair: Edward N. Baker
PL-1 **Demography and evolution of protein structural folds**
Sung-Hou Kim (USA)

10:00-10:15 **Break**

10:15-12:15 **Oral Sessions (MS01, 02, 03)**

Hall B / MS01 Membrane proteins
Chairs: Tomitake Tsukihara and Nieng Yan

10:15-10:45 MS01-O1 Daniela Stock (Australia)
Structure of the torque ring of the flagellar motor and the molecular basis for rotational switching

10:45-11:15 MS01-O2 Che Ma (Taiwan)
Structure of membrane proteins in drug discovery

11:15-11:45 MS01-O3 Megan Maher (Australia)
The molecular mechanism of the ferrous iron transporter, FeoB

11:45-12:15 MS01-O4 Wladek Minor (USA)
HKL-3000 - Toward the future of structural biology

Hall C / MS02 Metal Organic Frameworks
Chairs: Masaki Kawano and Wing-tak Wong

10:15-10:45 MS02-O1 Jaheon Kim (Korea)
Design and synthesis of highly porous Metal-Organic Frameworks

10:45-11:15 MS02-O2 Shuhai Furukawa (Japan)
Crystal interface functionalization of porous coordination polymers

11:15-11:45 MS02-O3 Ming-Liang Tong (China)
Metal-mediated in-situ ligand synthesis and application in const ruction of functional Metal-Organic Frameworks

11:45-12:00 MS02-O4 Masoumeh Tabatabaee (Iran)
Synthesis and crystal structure of a new cadmium metal–organic coordination polymer

12:00-12:15 MS02-O5 Apinpus Rujiwatra (Thailand)
Rapid crystal growth of two metal-organic frameworks constructed by linking of 1-D coordination polymers by hydrogen bonding

Hall D / MS03 Synchrotron and neutron sources, instrumentation and application
Chairs: S. C. Mande and Ian Gentle

10:15-10:45 MS03-O1 Masaki Yamamoto (Japan)
The SPring-8 high-brilliant beamlines for macromolecular crystallography

10:45-11:15 MS03-O2 Garry McIntyre (France)
Laue diffraction from spin-polarised protons: a new tool for neu tron protein crystallography?

11:15-11:45 MS03-O3 Toru Ishigaki (Japan)
The current status of versatile neutron diffractometer iMATERIA at J-PARC (II)

11:45-12:15 MS03-O4 Jey Jau Lee (Taiwan)
X-ray powder diffraction station at NSRRC for soft materials under non-ambient conditions

12:15-13:30 Lunch

Hall C ***Bruker & Incoatec Luncheon Seminar***
[Please pick up a ticket for lunch box at the Bruker & Incoatec exhibition booth.]

Meeting rm. ***IUCr Journal Commission Meeting***

13:30-15:30 Poster Session 1 (Last digit: Odd numbers)

15:30-16:00 Break

16:00-18:00 Oral Sessions (MS04, 05, 06)

Hall B / MS04 Macromolecular complexes including nucleic acids
Chairs: David Hsiao and Daniela Stock

16:00-16:30 MS04-O1 Hanna Yuan (Taiwan)
Structural basis of RNase T in stable RNA 3'-end maturation

16:30-17:00 MS04-O2 Osamu Nureki (Japan)
Structural analysis of bacterial Sec translocon machinery

17:00-17:30 MS04-O3 Kenji Inaba (Japan)
Structural basis of an ERAD pathway mediated by the ER-resident protein disulfide reductase ERdj5

17:30-18:00 MS04-O4 Takeshi Murata (Japan)
Structural studies of V_1-ATPase from Enterococcus hirae

Hall C / MS05 Chemical crystallography - structure and properties
Chairs: Wai-Yeung Wong and Kimoon Kim

16:00-16:30 MS05-O1 Song Gao (China)
Recent studies on single-ion magnets

16:30-17:00 MS05-O2 Masaki Kawano (Korea)
Kinetic syntheses of coordination networks and ab initio powder structure analysis

17:00-17:30 MS05-O3 Ian Williams (Hong Kong)
Metal imidazolate polymers: Synthesis, structure and properties of silica analogues
17:30-17:45 MS05-O4 Jason Cole (UK)
Crystal structure analysis in drug development
17:45-18:00 MS05-O5 Myoung Soo Lah (Korea)
Size- and shape-selective Metal-Organic Frameworks based on pillared Kagomé layers

Hall D / MS06 X-ray and neutron scattering
Chairs: Moonhor Ree and David Cookson
16:00-16:30 MS06-O1 Hyun Hoon Song (Korea)
Intermediate phase in oriented poly (pentamethylene 2,6-naphthalate)
16:30-17:00 MS06-O2 Michael James (Australia)
When explosives are welcome at your nuclear reactor ...
Molecular sensing using fluorescent dendrimer films and neutron reflectometry
17:00-17:30 MS06-O3 Atsushi Takahara (Japan)
Chain conformation of zwitter ionic polymers in solution and immobilized brush at solid/liquid interfaces
17:30-17:45 MS06-O4 Matthew Wilce (Australia)
Innate immunity and RNA sensing by the retinoic acid inducible gene I receptor
17:45-18:00 MS06-O5 Ross O. Piltz (Australia)
Structures determined by single crystal neutron diffraction with KOALA – what is possible now, what improvements are planned and when another experiment may be the answer!

18:00-19:20 Break for dinner

19:20-21:00 Oral Session (MS10e)

Hall B / MS10e Drug discovery and disease related proteins
Chairs: Sam-Yong Park and J. Shaun Lott
19:20-19:45 MS10e-O1 Yuh-Ju Sun (Taiwan)
The crystal structure of LipL32, a virulence factor from pathogenic Leptospira
19:45-20:10 MS10e-O2 Colin Groom (UK)
When does a disease-related protein become a viable target?
20:10-20:35 MS10e-O3 Cai-Hong Yun (USA)
Structure and mechanism-based discovery of mutant-selective inhibitors of the drug-resistant EGFR T790M mutant kinase
20:35-21:00 MS10e-O4 J. Shaun Lott (New Zealand)
The crystal structure of the N-terminal domain of human COMMD9 reveals an unexpected domain-swapped trimer

Day 3: November 2 (Tuesday)

08:00-09:00 **Registration (Level 1)**

09:00-10:00 **Keynote Lectures (KN-1, 2)**

Hall C
Chair: Alice Vrielink
KN-1 **Structure and assembly of Sesbania mosaic virus**
M. R. N. Murthy (India)

Hall B
Chair: Yoshio Matsui
KN-2 **Design and synthesis of porous metal-organic frameworks for gas storage and separation**
Myunghyun Paik Suh (Korea)

10:00-10:15 **Break**

10:15-12:15 **Oral Sessions (MS07, 08, 09)**

Hall B / MS07 Enzymes and enzyme inhibitors
Chairs: Isao Tanaka and K. Sivaraman

10:15-10:45 MS07-O1 Alice Vrielink (Australia)
Probing the structure of cholesterol oxidase by atomic resolution crystallography: Towards the design of novel antibiotics with high specificity and potency

10:45-11:15 MS07-O2 Masakazu Sugishima (Japan)
Structural insights into ferredoxin dependent bilin reductases

11:15-11:45 MS07-O3 Nobutaka Numoto (Japan)
Crystal structure and rotation mechanism of V_1-ATPase

11:45-12:00 MS07-O4 Chun-Jung Chen (Taiwan)
Crystal structures of Aspergillus japonicus fructosyltransferase in complex with donor/acceptor substrates reveal complete subsites for catalysis

12:00-12:15 MS07-O5 Dong Wu (China)
Structural basis for the inhibition of human MTHFS by N10-substituted folate analogues

Hall C / MS08 Dynamic aspects of molecular and solid state crystals
Chairs: Jun Harada and Hans-Beat Buergi

10:15-10:45 MS08-O1 Cameron Kepert (Australia)
Guest- and thermally-induced deformations of coordination framework materials

10:45-11:15 MS08-O2 Thammarat Aree (Thailand)
Thermodynamics properties of molecular crystals derived from multi-temperature diffraction data

11:15-11:45 MS08-O3 Hidehiro Uekusa (Japan)
Structural rearrangement of organic crystals in polymorphic transition investigated by ab initio structure determination from powder diffraction data

11:45-12:00 MS08-O4 Jagadese J. Vittal (Singapore/Korea)
Photoreactivity and structural rearrangements in the solid state
12:00-12:15 MS08-O5 Panče Naumov (Japan)
"Jumping crystals": Structural aspects of the thermosalient phenomenon

Hall D / MS09 Combining methods/new tools in structural biology
Chairs: Min Yao and R. Sankaranarayanan
10:15-10:45 MS09-O1 Nathan Cowieson (Australia)
Combining SAXS and CD to study flexibility and dynamics in multi-domain proteins
10:45-11:15 MS09-O2 Junichi Takagi (Japan)
Combination of correlative light-electron microscopy and X-ray crystallography reveals a unique trans-synaptic adhesion architecture
11:15-11:45 MS09-O3 Shekhar Mande (India)
Analysis of protein dynamics by crystallographic refinement and normal mode analysis
11:45-12:00 MS09-O4 Edward N. Baker (New Zealand)
Use of racemic protein crystallography to solve the structure of Rv1738, an essential protein from Mycobacterium tuberculosis
12:00-12:15 MS09-O5 Chae Un Kim (USA)
High pressure cryocooling at MacCHESS

12:15-13:30 Lunch

[A limited number of lunch boxes will be provided at the luncheon seminar lecture halls.]

Hall C ***Rigaku Luncheon Seminar***

Hall D ***GE Healthcare Luncheon Seminar***
Brian M. Baker (USA)
Modulation of T cell receptor binding affinity by targeted fluorine substitutions: Structural, thermodynamic, and kinetic effects

Meeting rm. ***AsCA Council Meeting***

13:30-15:30 Poster Session–2 (Last digit: Even numbers)

15:30-16:00 Break

16:00-18:00 Oral Sessions (MS10, 11, 12)

Hall B / MS10 Drug discovery and disease related proteins
Chairs: Sam-Yong Park and J. Shaun Lott
16:00-16:30 MS10-O1 Eiji Obayashi (Japan)
The structural study on influenza RNA polymerase for designing new anti-viral drug
16:30-17:00 MS10-O2 Hao Wu (USA)
Death domain interactions in apoptosis and immunity

17:00-17:30 MS10-O3 Catherine Day (New Zealand)
Regulating the ubiquitin E3 ligase activity of C-terminal RING domains
17:30-17:45 MS10-O4 Yang Wu (China)
Structures of EV71 RNA-dependent RNA polymerase in complex with substrate and inhibitor provide a drug target against the hand-foot-and-mouth disease pandemic in China
17:45-18:00 MS10-O5 Bostjan Kobe (Australia)
Structural basis of innate immunity in plants against fungal pathogens

Hall C / MS11 Magnetic structures and molecular magnets
Chairs: Je-Geun Park and Song Gao
16:00-16:30 MS11-O1 Yukio Noda (Japan)
Spin distribution of pi-electron in organic conductor studied by neutron magnetic structure analysis
16:30-17:00 MS11-O2 Seongsu Lee (Korea/USA)
The studies of multiferroric X-tal bismuth ferrite
17:00-17:30 MS11-O3 Jing-Lin Zuo (China)
Molecular magnetic semiconductors based on organic ligands with delocalized sulfur-rich core
17:30-17:45 MS11-O4 Deok-Yong Cho (Korea)
Anomalous L3/L2 X-ray absorption branching ratios in 5d transition metal oxides
17:45-18:00 MS11-O5 Jan Wikaira (New Zealand)
An investigation of magnetic exchange through double halide bridges

Hall D / MS12 Crystal growth and engineering
Chairs: A. Ramanan and Kumar Biradha
16:00-16:30 MS12-O1 Srinivasan Natarajan (India)
Polymorphism, solvotomorphism and related aspects in framework inorganic compounds
16:30-17:00 MS12-O2 Claude LeComte (France)
High resolution crystallography to understand the bonding between a transition metal and an alkyne
17:00-17:30 MS12-O3 Myoung Soo Lah (Korea)
Microporous Metal-Organic Frameworks based on Metal-Organic Supramolecules
17:30-17:45 MS12-O4 A. David Rae (Australia)
A compound with 6 chiral centers that uses the same unit cell and space group to grow either a racemate or an enantiomer
17:45-18:00 MS12-O5 Katsuhiro Tsukimura (Japan)
Kinetic theory of crystallization of nanoparticles

18:30-21:00 Award Ceremony and Rigaku Conference Banquet

Hall E / Award Ceremony and Rigaku Conference Banquet

Day 4: November 3 (Wednesday)

09:00-10:00 **Keynote Lectures (KN-3, 4)**

Hall C
Chair: Hanna Yuan
KN-3 **Structure and function of enzymes relevant in drug discovery**
Andrew H. Wang (Taiwan)

Hall B
Chair: Richard Tilley
KN-4 **New functional materials via crystal- and nano-engineering**
Wenbin Lin (USA)

10:00-10:15 **Break**

10:15-12:15 **Oral Sessions (MS13, 14, 15)**

Hall B / MS13 Structural proteomics and bioinformatics
Chairs: Zhi-Jie Liu and Seong Eon Ryu
10:15-10:45 MS13-O1 Satoshi Watanabe (Japan)
Crystal structures of the Hyp proteins for [NiFe] hydrogenase maturation
10:45-11:15 MS13-O2 Bill Duax (USA)
Combining sequence and structural analysis to obtain a perfect alignment essential to rational drug design
11:15-11:45 MS13-O3 Kwang Yeon Hwang (Korea)
Structural insights into the conformational change upon activation of tyrosine site-specific recombinase
11:45-12:00 MS13-O4 Muralidharan Muthu (New Zealand) - AsCA Rising Star
Crystal structures of the N-terminal dystrophin and utrophin spectrin repeats show a three helix bundle fold
12:00-12:15 MS13-O5 Maxim Titushin (China)
Structural basis of energy transfer in the bioluminescent system of jellyfish Clytia: the GFP-photoprotein complex

Hall C / MS14 Nanomaterials, surface and interface
Chairs: Joanne Etheridge and Taeghwan Hyeon
10:15-10:45 MS14-O1 Yoshio Matsui (Japan)
Nano magnetic structure analysis by cryo Lorentz TEM – visualization of the "Skirmion" crystal
10:45-11:15 MS14-O2 Richard Tilley (New Zealand)
Watching nanocrystals grow: In-situ synchrotron experiments
11:15-11:45 MS14-O3 Sunghoon Kwon (Korea)
Artificial structural colored microstructures via magnetically tunable photonic crystal
11:45-12:00 MS14-O4 Andrew Stewart (Germany)
Automated electron diffractometry: solving structures of nano crystals

12:00-12:15 MS14-O5 Daisuke Morikawa (Japan) - AsCA Rising Star
Structure analysis of charge-orbital ordered phases in A-site ordered perovskites $SmBaMn_2O_6$ and $NdBaMn_2O_6$ using CBED

Hall D / MS15 Powder diffraction
Chairs: Jungeun Kim and Kia Wallwork
10:15-10:45 MS15-O1 Makoto Sakata (Japan)
The challenge of highly reliable ab initio powder structure analysis by the novel concept of genetic algorithm
10:45-11:15 MS15-O2 Nathan Webster (Australia)
Industrial applications of in situ powder diffraction
11:15-11:45 MS15-O3 Bridget Ingham (New Zealand)
In situ studies using synchrotron powder diffraction
12:00-12:15 MS15-O4 Yongmoon Lee (Korea)
Structural study of monovalent cation-exchanged natrolites during dehydration
12:00-12:15 MS15-O5 Takashi Ida (Japan)
Particle statistics in high-resolution synchrotron powder X-ray diffractometry

12:15-13:30 Lunch

Hall C ***IUCr Luncheon Seminar***
Howard Einspahr (USA)
How to publish crystallographic results
[A limited number of lunch boxes will be provided at the luncheon seminar lecture hall.]

Hall D ***J-PARC Business Meeting***

13:30-15:30 Oral Session (MS16)

Hall A / MS16 AsCA Rising Stars Microsymposium
Chairs: Eunice Kim and Cameron Kepert
Speakers: Six speakers will be announced at the Tuesday Banquet.

15:30-16:00 Break

16:00-17:00 Plenary Lecture-2 (PL-2)

Hall A
Chair: Jennifer Martin
PL-2 Chirality in crystals
Reiko Kuroda (Japan)

17:00-17:30 Closing

Hall A / Closing ceremony

Poster Presentations

Area 1. Structural Biology

MS01: Membrane proteins

MS01-P01 **The structure of mouse anoctamin1 (mANO1) domains TM2↔TM3 (DTM1↔TM2) and TM5↔TM6 (DTM5↔TM6)**
Sang Ho Park, Ho Kyung Jung, and Byung Woo Han

MS01-P02 **Purification of LDL receptor-related protein and nano-gold labeling for structure analysis**
Kyung Eun Lee, Oh Yeun Kwon, and Hyesung Jeon

MS01-P03 **Interaction of PDZ adapter proteins NHERF and E3KARP in vitro**
Se Bok Jang, Eun Young Hwang, and Mi Suk Jeong

MS04: Macromolecular complexes including nucleic acids

MS04-P01 **In vitro reconstitution of the interactions in the PIDDosome**
Hyun Ho Park, Tae-ho Jang, Hao Wu, and Chao Zheng

MS04-P02 **High-resolution crystal structure of chicken cytokine interleukin-1β reveals differences in receptor binding compared to human interleukin-1β**
Chao-Sheng Cheng, Wen-Shiang Lu, I-Fan Tu, Ping-Chiang Lyu, Long-Huw Lee, and Hsien-Sheng Yin

MS04-P03 **Molecular interplay between the replicative hexameric helicase DnaC with ssDNA and its loader DnaI from Geobacillus kaustophilus**
Chwan-Deng Hsiao, Yu-Hua Lo, and Kuang-Lei Tsai

MS04-P04 **DNA/RNA binding properties of PCBP-1 KH domains**
Daouda AK Traore, Yano M Yoga, Matthew CJ Wilce, and Jackie A Wilce

MS04-P05 **Paraspeckle proteins: a novel arrangement of RNA-binding domains**
Mihwa Lee, Daniel Passon, Archa H. Fox, and Charles S. Bond

MS04-P06 **Structural study of RLR family innate immune proteins**
Hyunjin Moon and Jungwoo Choe

MS04-P07 **Translation elongation factor-P (EF-P) from Pseudomonas aeruginosa, a mimic of tRNA?**
Sarah choi and Jungwoo Choe

MS04-P08 **Nuclear translocation machinery of pre-microRNA**
Soo Jae Lee, Chimari Okada, Eiki Yamashita, Satoshi Shibata, Jun Katahira, Atsushi Nakagawa, Yoshihiro Yoneda, and Tomitake Tsukihara

MS04-P09 **Structural analysis of exosome from Thermoplasma acidophilum**
Hyun Sook Kim, Hye-Jeong Cho, Cho Gye Yoon, Ho Sam Ki, Moon Jung Song, and Kwang Yeon Hwang

MS04-P10 **An insight into the pairing geometry of DNA duplexes containing O6-carboxymethylguanine, a damaged base analogue relevant to gastrointestinal cancer**
Fang Zhang, Kaoru Suzuki, Md. Mominul Hoque, Masaru Tsunoda, Christopher L. Millington, David M. Williams, and Akio Takénaka

MS04-P11 **Crystal structures of E2-25K, E2-25K/Ub and E2-25K/UBB+1**
Jung-Gyu Lee, Gil Bu Kang, Sunggeon Ko, Sung Min Song, Yong-Keun Jung, Yung Joon Yoo, Weontae Lee, and Soo Hyun Eom

MS04-P12 **The role of the p-electron systems in regulation of reduction potentials of tetraheme cytochrome c_3**
Hideo Akutsu, Yuki Takayama, Midori Taketa-Sato, Hirofumi Komori, Kumiko Morita, Sujin Kang, and Yoshiki Higuchi

MS04-P13 **Two different modes of UvrD helicase by 2B domain movement**
Hyun Koo Yeo and Jae Young Lee

MS04-P14 **Functional implication of Ufd1-Npl4 complex in the FAF1 recognition mechanism by AAA-ATPase p97/VCP**
Joon Kyu Park and Eunice EunKyeong Kim

MS04-P15 **The structure of rat liver vault at 3.5 Å resolution**
Koji Kato, Hideaki Tanaka, Eiki Yamashita, Tomoyuki Sumizawa, Yong Zhouc, Min Yao, Kenji Iwasaki, Masato Yoshimura, and Tomitake Tsukihara

MS04-P16 **Biophysical investigation of RBP-ARE interactions: Application of SPR, NMR, and SAXS**
Henry Kim, Yano Yoga, Nathan Cowieson, Martin Scanlon, Steven Headey, Myriam Gorospe, Bryan Williams, Matthew Wilce, and Jackie Wilce

MS04-P17 **Identification and analysis of dominant negative mutants of RAIDD and PIDD**
Hyun Ho Park, Tae-ho Jang, Ju Young Bae, and Ok Kyeung Park

MS04-P18 **Human MTERF3 crystal structure of left-handed superhelical tandem repeat**
Dong-Uk Kim, Sang-Gil Cho, Kuk-Lea Kim, and Hyun-Soo Cho

MS04-P19 **Structure analysis of ligand-independent activation of Fushi tarazu factor-1 ligand binding domain from Drosophila melaganoster**
Ji-Ho Yoo, Sunggeon Ko, Hyeyon Kim, Kwang-Min Choe, Weon Tae Lee, and Hyun-Soo Cho

MS04-P20 **Structure of the entire ectodomain of gp130: Insights into the molecular assembly of cytokine receptor complexes**
Yibin Xu, Nadia J. Kershaw, Cindy S. Luo, Priscilla Soo, Michael J. Pocock, Peter E. Czabotar, Douglas J. Hilton, Nicos A. Nicola, Jian-Guo Zhang, and Thomas P. J. Garrett

MS07: Enzymes and enzyme inhibitors

MS07-P01 **Crystal structure of human transglutaminase 2 in complex with adenosine triphosphate**
Byeong-Gu Han, Jea-Won Cho, and Byung Il Lee

MS07-P02 **Structure and function of the Fibrobacter succinogenes 1,3-1,4-β-D-glucanase mutants F40I and W203F in complex with inhibitors**
Li-Chu Tsai, Hsiao-Chuan Huang, Ching-Hua Hsiao, Wei-Ru Li, and Li-Ming Yin

MS07-P03 **Investigating the structure and function of the redox folding factors αDsbA2 and αDsbB**
Walden, PM, Heras, B, Iturbe-Ormaetxe, I, and Martin, JL

MS07-P04 **Time-resolved X-ray crystal structure analysis of enzymatic reaction of copper amine oxidase from Arthrobacter globiformis**
Misumi Kataoka, Hiroko Oya, Ayuko Tominaga, Masayuki Otsu, Toshihide Okajima, Katsuyuki Tanizawa, and Hiroshi Yamaguchi

MS07-P05 **Metabolic adaptation for short-chain fatty acids degradation: crystal structure of 2-methylcitrate synthase from Salmonella typhimurium**
Sagar Chittori, H. S. Savithri, and M. R. N. Murthy

MS07-P06 **Crystal structures of Helicobacter pylori shikimate kinase reveal three conserved arginines involved in the induced movement**
Wen-Chi Cheng, Hung-Jung Wang, and Wen-Ching Wang

MS07-P07 **Involvement of scaffolding residues in efficient inhibition: Lesssons from chimeric proteins**
Sudip Majumder, Susmita Khamrui, Jhimli Dasgupta, J. K. Dattagupta, and Udayaditya Sen

MS07-P08 **Structural insights into catalysis of bC-S lyase from Streptococcus anginosus**
Yuichiro Kezuka, Yasuo Yoshida, and Takamasa Nonaka

MS07-P09 **SbcD, the subunit of SbcCD DNA strand break repair protein from Deinococcus radiodurans**
Mi Ra Han and Byung Woo Han

MS07-P10 **Structure of protochlorophyllide reductase: a greening mechanism of plants in the dark**
Norifumi Muraki, Jiro Nomata, Yuichi Fujita, and Genji Kurisu

MS07-P11 **Structural basis for the enantioselectivity of Est-Y29 toward S-ketoprofen**
Tri Duc Ngo, Seung Bum Kim, Sang Bum Joo, Sang Young Yoon, T. Doo Hun Kim, and Kyeong Kyu Kim

MS07-P12 **Crystal structure of M18 family dodecameric tetrahedral (TET) shape aminopeptidase from Pseudomonas aeruginosa**
Duy Nguyen Duc, Sampath Natarajan, Kap Sun Kim, Kyung Hee Yun, Hyejin Park, and Kyeong Kyu Kim

MS07-P13 **RNA binding mechanism of ThiI deduced from structural and binding analyses of a minimal RNA ligand**
Yoshikazu Tanaka, Shiori Yamagata, Yu Kitago, Yoko Yamada, Sarin Chimnaronk, Min Yao, and Isao Tanaka

MS07-P14 **Basis for the lack of stereospecificity in coenzyme B_{12}-dependent ethanolamine ammonia-lyase**
Naoki Shibata, Tetsuo Toraya, and Yoshiki Higuchi

MS07-P15 **Structural analysis and functional study of the human small MutS-related protein**
Euiyoung Jeong, Weejeong Jun, Seonghwan Lee, Sung-jin Choi, and Changill Ban

MS07-P16 **Structure and mechanism of XometC, a cystathionine γ-lyase from Xanthomonas oryzae pv. oryzae (Xoo): Insights for the substrate specificity and lyase mechanism of XometC**
Ho Phuong Thuy Ngo, Jin-Kwang Kim, Yeh-Jin Ahn, Jeong-Gu Kim, Byoung-Moo Lee, Hee-Wan Kang, and Lin-Woo Kang

MS07-P17 **Structure-based catalytic optimization of a type III Rubisco from a hyperthermophile**
Yuichi Nishitani, Shosuke Yoshida, Masahiro Fujihashi, Kazuya Kitagawa, Takashi Doi, Haruyuki Atomi, Tadayuki Imanaka, and Kunio Miki

MS07-P18 **Structural and functional analysis of the LMO2642 cyclic nucleotide phosphodiesterase from Listeria monocytogenes**
Yeon-Gil Kim1, Jae-Hee Jeong, Nam-Chul Ha, and Kyung-Jin Kim

MS07-P19 **Comparison of DNA translocators based on their structures**
Suk-Youl Park, Nguyen To Uyen, Ji-Woo Choi, Hyun-Ju Lee, Kosuke Nishi, and Jeong-Sun Kim

MS07-P20 **Structure and mechanism of the Nudix hydrolase Orf153 (YmfB) from E. coli**
Myoung-ki Hong, Jin-kwang Kim, Yeh-jin Ahn, and Lin-woo Kang

MS07-P21 **Crystal structure analysis of ATPase domain from Mycobacterium tuberculosis DosS protein**
Ha Yeon Cho and Beom Sik Kang

MS07-P22 **Crystal structure of LapB from Pseudomonas sp. strain KL28**
Jang-Hee Cho, Du-Kyo Jung, Kyoung Lee, and Sangkee Rhee

MS07-P23 **The crystal structure of D-ribose-5-phosphate isomerase B from Clostridium thermocellum with the unique high kinetic properties**
Jin Kwang Kim, Junho Jung, Soo Jin Yeom, Yeh Jin Ahn, Deok Kun Oh, and Lin Woo Kang

MS07-P24 **Structural feature of the extreme thermophile maltogenic amylase from Staphylothermus marinus**
Tae-Yang Jung, Dan Li, Jong-Tae Park, Se-Mi Yoon, KwanHwa Park, and Eui-Jeon Woo

MS07-P25 **Crystallization and preliminary X-ray analysis of a novel thermostable amylase from Pyrococcus furiosus (PFTA) in glycoside hydrolase 13 family**
Hyung-nam Song, Tae-yang Jung, Sae-mi Yoon, Sung-jae Yang, Kwan-hwa Park, and Eui-jeon Woo

MS07-P26 **Structural basis for the recognition of N-end rule substrates by the UBR box of ubiquitin ligases**
Woo Suk Choi, Byung-Cheon Jeong, Myeong-Ryeol Lee, Michael J. Eck, and Hyun Kyu Song

MS07-P27 **Structure basis of genetic encoded photosensitizer KillerRed**
Naoki Sakai, Yu Kitago, Kiwamu Takemoto, Tomoki Matsuda, Tokiyoshi Ayabe, and Takeharu Nagai

MS07-P28 **Crystal structures of ribosome-inactivating protein from barley seeds (Hordeum vulgare L.)**
Byung-Gil Lee, Min Kyung Kim, Se Won Suh, and Hyun Kyu Song

MS07-P29 **Crystal structure of human Evectin-2 PH domain and its complex with O-phospho-L-serine**
Seiji Okazaki, Yasunori Uchida, Ryuichi Kato, Takao Inoue, Yusuke, Yamada, Tomohiko Taguchi, Hiroyuki Arai, and Soichi Wakatsuki

MS07-P30 **Crystal structure analysis of the oxygenase component (GraA) of a resorcinol hydroxylase**
Yasuo Hata, Tomomi Fujii, Kazutaka Kobayshi, Masahiro Yoshida, and Tadao Oikawa

MS07-P31 **Structural basis of abscisic acid signaling**
Masaru Tanokura, Takuya Miyakawa, Ken-ichi Miyazono, Keiko Kubota, and Yoriko Sawano

MS07-P32 **X-ray structural analysis of N-terminal domain of KaiC for understanding of restrained ATPase activity**
Se-Young Son, Takao Kondo, and Shuji Akiyama

MS07-P33 **Unexpected substrate recognition and hydrolysis mechanisms of human NUDT5**
Takao Arimori, Haruhiko Tamaoki, Teruya Nakamura, Hiroyuki Kamiya, Shinji Ikemizu, Yasumitsu Takagi, Toru Ishibashi, Hideyoshi Harashima, Mutsuo Sekiguchi, and Yuriko Yamagata

MS07-P34 **Crystal structure of human ppGpp hydrolase**
Hye-Yeon Kim, Dawei Sun, and Young Ho Jeon

MS07-P35 **Crystal structures of extra cellular dermal glycoprotein from carrot and xyloglucan specific endo-β-1,4-glucanase from Aspergillus aculeatus**
Takuya Yoshizawa, Hiroshi Hashimoto, Toshiyuki Shimizu, Hisashi Hirano, and Mamoru Sato

MS07-P36 **Crystallization and preliminary X-ray analysis of a family 51 glycoside hydrolase, the α-L-arabinofuranosidase from Thermotoga maritima MSB8**
Arti Baban Dumbrepatil, Tae-Yang Jung, Jung Mi Park, Tae Jib Kim, and Eui-Jeon Woo

MS07-P37 **Structural and biological investigation of ppGpp hydrolase in Metazoa**
Dawei Sun, Gina Lee, Jun Hee Lee, Hye-Yeon Kim, Hyun-Woo Rhee, Seung-Yeol Park, Kyung-Jin Kim, Yongsung Kim, Bo Yeon Kim, Jong-In Hong, Chankyu Park, Hyon E. Choy, Jung-Hoe Kim, Young Ho Jeon, and Jongkyeong Chung

MS07-P38 **Structural insight into bacterial flavin containing monooxygenase**
Hyo Je Cho and Beom Sik Kang

MS07-P39 **Asymmetric dimeric structure of ferredoxin-NAD(P)$^+$ oxidoreductase from Chlorobaculum tepidum: Implications for binding ferredoxin and NADP$^+$**
Norifumi Muraki, Daisuke Seo, Takeshi Sakurai, and Genji Kurisu

MS07-P40 **Crystal structure and functional study of ureidoglycolate dehydrogenase from Escherichia coli**
Myung-Il Kim, Jeehyun Lee, and Sangkee Rhee

MS07-P41 **Structural and functional studies of an ureidoglycine-hydrolyzing enzyme from Arabidopsis thaliana**
Inchul Shin, Woo-Suk Jung, and Sangkee Rhee

MS07-P42 **Crystal structures of human peroxiredoxin VI in multiple oxidation states**
Kyung Hee Kim, Weon Tae Lee, and Eunice EunKyeong Kim

MS07-P43 **Crystal structures of malonyl-CoA-acyl carrier protein transacylase (MCAT) from Staphylococcus aureus and Streptococcus pneumoniae**
Seung Kon Hong, Kook Han Kim, Joon Kyu Park, and Eunice EunKyeong Kim

MS07-P44 **Characterization and crystallization of perakine reductase, an enzyme involved in monoterpenoid indole alkaloid biosynthesis**
Lianli Sun, Yixin Chen, Meitian Wang, Santosh Panjikar, and Joachim Stöckigt

MS07-P45 **Structural analysis of raucaffricine glucosidase, a central enzyme in the alkaloid biosynthetic network of the Indian plant Rauvolfia**
Liqun Xia, Martin Ruppert, Meitian Wang, Santosh Panjikar, and Joachim Stöckigt

MS07-P46 **Drug protein interaction studies of an antiviral agent garcinol targeting HIV-1 protease by in silico approach**
Prashantha Karunakar, Girija CR, Shalini S, Noor Shahina Begum, and Akheel Ahmed Syed

MS07-P47 **Structural and functional analyses of W272A and N277A mutant forms of prostacyclin synthase**
Yi-Ching Li, Shu-I Tsai, Lee-Ho Wang, and Nei-Li Chan

MS07-P48 **Structural and functional assay of AtTLP18.3 revealed its novel phosphatase activity involved in repair cycle of photosystem**
Hsin-Yi Wu, Mao-Sen Liu, Tsan-Piao Lin, and Yi-Sheng Cheng

MS07-P49 **Structural characterization of a serpin from the large beetle Tenebrio molitor and its regulation by heparin**
Sun Hee Park, Rui Jiang, Shunfu Piao, Bing Zhang, Eun-Hye Kim, Hyun-Mi Kwon, Xiao Ling Jin, Bok Luel Lee, and Nam-Chul Ha

MS07-P50 **The crystal structure of hexameric Lon protease: dynamics of the AAA+ module controls access to a sequestered proteolytic chamber**
Sun-Shin Cha, Young Jun An, Chang-Sook Jeong, and Sung Gyun Kang

MS07-P51 **X-ray structure of a 3-isopropylmalate isomerase large subunit from Methanococcus jannaschii**
Eun-Hye Lee and Kwang-Yeon Hwang

MS07-P52 **Crystal structure of enonyl-acyl carrier protein reductase (FabI) in complex with NADH and triclosan from Pseudomonas aeruginosa**
Jeong Hye Lee, Ae Kyung Park, Jin Ho Moon, and Young Min Chi

MS10: Drug discovery/disease related proteins

MS10-P01 **Crystal structure of human transglutaminase 2 in complex with adenosine triphosphate**
Byeong-Gu Han and Byung Il Lee

MS10-P02 **The c-AMP receptor-like protein CLP is a novel c-di-GMP receptor linking cell-cell signaling to virulence gene expression in Xanthomonas campestris**
Shan-Ho Chou, Ko-Hsin Chin, Yen-Chung Lee, and Andrew H.-J. Wang

MS10-P03 **Modulating immune function through chemokine binding – Orf virus presents a new twist on an old motif**
Kurt L. Krause, Rafael Counago, Stephen Fleming, and Andy Mercer

MS10-P04 **Structural and functional studies on thiolase from Mycobacterium smegmatis and Mycobacterium tuberculosis**
Neelanjana Janardan and M. R. N. Murthy

MS10-P05 **Crystal structure of the sensor domain of naphthalene chemoreceptor NahY from Pseudomonas putida**
Truc Kim and Kyeong Kyu Kim

MS10-P06 **Crystal structures and binding studies of atovaquone and its derivatives with cytochrome bc_1: Molecular basis for drug design**
Susanta K. Nayak, S. B. Mallik, S. P. Kanaujia, K. Sekar, and T. N. Guru Row

MS10-P07 **Structural basis of human p70 ribosomal S6 kinase-1 regulation by activation loop phosphorylation**
Sunami T, Byrne N, Diehl RE, Funabashi K, Hall DL, Ikuta M, Patel SB, Shipman JM, Smith RF, Takahashi I, Zugay-Murphy J, Iwasawa Y, Lumb KJ, Munshi SK, and Sharma S

MS10-P08 **Structural studies of TIRAP, an adaptor protein of Toll-like receptor signaling pathway**
Yoora Kang and Jungwoo Choe

MS10-P09 **Structural insights into the dual nucleotide exchange and GDI displacement activity of SidM/DrrA**
Kwang-Hoon Lee, Hye-Young Suh, and Byung-Ha Oh

MS10-P10 **Structural study of GTP-sensing pleiotropic transcriptional repressor CodY from Starphylococcus aureus**
Ah Reum Han, Kyung-Hee Rhee, Gye Yoon Cho, Hosam Ki, and Kwang Yeon Hwang

MS10-P11 **Structure-function analysis of human L-prostaglandin D synthase bound with fat**
Yangyan Zhou, Neil Shaw, Yang Li, Yu Zhao, Rongguang Zhang, and Zhi-Jie Liu

MS10-P12 **Recombinant fusion protein design for biophysical analysis of integrin subunit dimerization and function**
Andrea Francesca M. Salvador, Gabriel N. Valbuena, Lydia Teresa Isabel Salud-Bautista, and Neil Andrew D. Bascos

MS10-P13 **Structural study and antibacterial drug design against bacterial blight disease caused by Xanthomonas oryzae pv. Oryzae**
Sampath Natarajan, Thanh Thi Ngoc Doan, Phuong-Thuy Ho Ngo, Jae-Wook Jung, and Lin-Woo Kang

MS10-P14 **Crystal structure of D-alanine-D-alanine ligase a from Xanthomonas oryzae pathovar oryzae and its inhibitors from structure-based virtual screening**
Thi-Ngoc-Thanh Doan, Jin-Kwang Kim, Sam Natarajan, Yeh-Jin Ahn, and Lin-Woo Kang

MS10-P15 **Structure based design and synthesis of NAmPRTase inhibitors as anticancer agent**
Hyung-Seop Youn, Jung-Gyu Lee, Jun Yop An, Kyoung Ryoung Park, Woo Lai San, Youngjin Lee, Won Ju Jeong, Hyun You, Isak Im, Man-Ho Bae, Yong-Chul Kim, and Soo Hyun Eom

MS10-P16 **The structural and pharmacological studies of a dimeric acetylcholine binding protein**
Ching-I Anderson Wang, Vu Bach, and Richard Lewis

MS10-P17 **Cloning, expression, crystallization and preliminary X-ray crystallographic analysis of HrcN – an inner membrane ATPase from Xanthomonas oryzae pv. oryzae**
Viet Tan Pham, Yeh-Jin Ahn, and Lin-woo Kang

MS10-P18 **Molecular basis for recognition of paired immunoglobulin like type2 receptor (PILR) alpha to glycoprotein B (gB) of herpes simplex virus-1 (HSV-1)**
Osw Toyoyuki, Yamaguchi Munechika, Jing Wang, Kimiko Kuroki, Shigekazu Tabata, Nobuo Maita, Seiko Nakamura, Mizuho Kajikawa, Takeshi Satoh, Hisashi Arase, and Katsumi Maenaka

MS10-P19 **AraC transcription regulator in Bacillus cereus**
Mi Seul Park and Byung Woo Han

MS10-P20 **Crystal structures of murine norovirus RNA-dependent RNA polymerase and its complex with 5-fluorouracil and ribavirin**
Intekhab Alam, Ji-Hye Lee, and Kyung Hyun Kim

MS10-P21 **Molecular characterization of human influenza virus hemagglutinin**
Ki Joon Cho, Ji-Hye Lee, Seokha Kang, Yi Ho Park, Jun Young Lee, Taslima Gani Khan, Joo-Yeon Lee, Hee-Bok Oh, Chun Kang, and Kyung Hyun Kim

MS10-P22 **Comparison of the structures of horse spleen and Helicobacter pylori ferritins for iron uptake**
Yi-ho Park, Ki Joon Cho, and Kyung Hyun Kim

MS10-P23 **Structural study of aprotinin complexed with a pentapeptide, a conserved sequence responsible for Aβ aggregation**
Taslima Gani Khan, Ji-Hye Lee, and Kyung Hyun Kim

MS10-P24 **Structural basis of the interaction between FAF1 and p97/VCP**
Wonchull Kang, Ho Yeon Lee, Men Thi Ngoc Nguyen, Le Thi My Le, and Jin Kuk Yang

MS10-P25 **Crystal structure of thermostable direct hemolysin from Vibrio parahaemolyticus**
Hiroshi Hashimoto, Kumiko Nakahira, Tsutomu Yamane, Takashi Fukui, Kiyohisa Ohnishi, Toshiyuki Shimizu, Takeshi Honda, Mamoru Sato, Mitsunori Ikeguchi, and Itaru Yanagihara

MS10-P26 **Crystal structure of hypothetical protein HP0062 from Helicobacter pylori**
Ae-Ran Kwon

MS10-P27 **Structural analysis of Toll-like receptor 2-activating lipoprotein from Vibrio vulnificus**
Sangheon Yu, Na Yeon Lee, Soon-Jung Park, and Sangkee Rhee

MS10-P28 **Structure of EvpC: A type six secretion system protein from Edwardsiella tarda**
J. Sivaraman, Chacko Jobichen, Lissa Joseph, and Yu-Keung Mok

MS10-P29 **In silico search for putative GmhA binding compounds**
Mi-Sun Kim, Areum Lim, Sarinna Tumapa, Sharon Peacock, and Dong Hae Shin

MS10-P30 **2,3-difluoro-sialic acids as inactivators of influenza neuraminidases**
Victor Streltsov, Susan Barrett, Pat Pilling, Stefan B. Hader, Patricia Marcé, Andrew G. Watts, and Jennifer McKimm-Breschkin

MS10-P31 **Crystal structure of GmhA from Burkholderia pseudomallei, the causative agent of melioidosis**
Mi-Sun Kim, Areum Lim, Sarinna Tumapa, Sharon Peacock, and Dong Hae Shin

MS10-P32 **ABIN-1 senses linear ubiquitin chains: structural and biophysical insights**
Simin Rahighi, Fumiyo Ikeda, Masato Kawasaki, Ryuichi Kato, Ivan Dikic, and Soichi Wakatsuki

MS10-P33 **HIV-1 protease complexed to natural oligopeptide substrates**
Amit Das, S. C. Bihani, V. Prashar, J.-L. Ferrer, and M. V. Hosur

MS13: Structural proteomics and bioinformatics

MS13-P01 **Crystal structure of PPC protein from Pyrococcus furiosus**
Ji Young Yoon, Do Jin Kim, Kyoung Hoon Kim, Sang Jae Lee, Hyoun Sook Kim, Jun Young Jang, and Se Won Suh

MS13-P02 **Structural evidence for a dehydrated intermediate in green fluorescent protein chromophore biosynthesis**
Sergei Pletnev, Nadya V. Pletneva, Konstantin A. Lukyanov, Nadya G. Gurskaya, Ekaterina A. Goryacheva, Vladimir I. Martynov, Alexander Wlodawer, Zbigniew Dauter, and Vladimir Z. Pletnev

MS13-P03 **Crystal structure of Tpa1 from Saccharomyces cerevisiae, a component of the messenger ribonucleoprotein complex**
Hye-Jin Yoon, Ji Yong Kang, Hyung Ho Lee, and Se Won Suh

MS13-P04 **Crystal structure of phosphopantetheine adenylyltransferase from Enterococcus faecalis in the ligand-unbound state and in complex with ATP and pantetheine**
Hye-Jin Yoon, Ji Yong Kang, Hyung Ho Lee, and Se Won Suh

MS13-P05 **Crystal structures of LacD from Stapylococcus aureus and LacD.1 from Streptococcus pyogenes: Insights into substrate specificity and virulence gene regulation**
Sang Jae Lee , Hyoun Sook Kim, Do Jin Kim, Hye-Jin Yoon, Kyoung Hoon Kim, Ji Young Yoon, and Se Won Suh

MS13-P06 **Crystal structure of Hsm3p, an assembly chaperone of the 19S regulatory particle of the proteasome**
Sangwoo Kim, Tsunehiro Mizushima, Yasushi Saeki, Keiji Tanaka, and Koichi Kato

MS13-P07 **A structural genomics approach to the structure determination of macrophage proteins**
Kai-En Chen, Gautier Robin, Justine M. Hill, Matthew J. Sweet, Stuart Kellie, Bostjan Kobe, and Jennifer L. Martin

MS13-P08 **Crystal structure of the dimerization domain of human filamin A**
Bong-Jin Lee

MS13-P09 **Structural basis for the functional insight of HP0420-homologue from Helicobacter felis**
Shunfu Piao, Xiao Ling Jin, Bo-Young Yun, and Nam-Chul Ha

MS13-P10 **The hexameric structure of AcrA suggests the assembly of a bacterial multidrug efflux pump AcrAB-TolC**
Yongbin Xu1, Saemee Song, Shunfu Piao, Hong-Man Kim, Se-Hoon Sim, Xiao Ling Jin, Hyesung Jeon, Kangseok Lee, and Nam-Chul Ha

MS13-P11 **Crystal structure of the MukB hinge domain and its functional implications**
Bonsu Ku and Byung-Ha Oh

MS13-P12 **Crystal structure and functional characteristics of LmDPK, a novel DNA protection kinase, in Listeria monocytogenes**
Thao Thi Phuong Duong, Sung Wook Kang, Truc Dinh Trung Kim, Boi Hoa San, and Kyeong Kyu Kim

MS13-P13 **Structure mechanism of antigen recognition of the neural cell adhesion molecule L1 protein antibody**
Chunhua Wei, Eung Suk Lee, Jeong Yi Jeon, Seung Jun Kim, Young Ho Jeon, Hyo Jeong Hong, and Seong Eon Ryu

MS13-P14 **Crystal structure of Helicobacter pylori MinE, a cell division topological specificity factor**
Jun Yop An, Hyung-Seop Youn, Jung-Gyu Lee, Kyoung-Ryoung Park, Lai San Woo, Youngjin Lee, Won Ju Jeong, Gil Bu Kang, Hye-Eun Song, Mun-Kyoung Kim, Jang-Soo Chun, Hyesung Jeon, and Soo Hyun Eom

MS13-P15 **Ligand-binding-site prediction program POCASA**
MinYao, Jian Yu, Yong Zhou, and Isao Tanaka

MS13-P16 **Structures of enoyl-ACP reductase from Bacillus cereus**
Su Jin Kim, Byung Hak Ha, Kook-Han Kim, Seung Kon Hong, Key-Jung hin, Se Won Suh, and and Eunice EunKyeong Kim

MS13-P17 **PDBj Mine: Design and implementation of relational database interface for Protein Data Bank Japan**
Akira R. Kinjo, Reiko Yamashita, Haruki Nakamura

MS13-P18 **Crystallization and structural analysis of human Mitogen-Activated Protein Kinase Phosphatase (MAKP) proteins**
Song Yi Kim, A Young kyung, and Dae Gwin Jeong

MS13-P19 **Crystallization of human MST2 SARAH domain**
Jinsue Song, Saehae Choi, Il Young Park, and Soo Jae Lee

MS13-P20 **Structural basis for the specialization of Nur, a nickel-specific Fur homologue, in metal sensing and DNA recognition**
Young Jun An, Chang-Sook Jeong, Jung-Ho Shin, Jung-Hye Roe, and Sun-Shin Cha

Area 2. Chemical Crystallography and Materials Science

MS02: Metal organic frameworks

MS02-P01 **Metal-organic interpenetrated frameworks based on dipyridyl ligands bearing amide groups**
Pei-Chi, Cheng, Jian-Jr Cheng, Ya-Ting Chang, and Jhy-Der Chen

MS02-P02 **Calcium Metal-Organic Frameworks: Synthesis, structural transformations, and sorption properties**
Po-Ching Liang, Hsin-Kuan Liu, Chun-Ting Yeh, Chia-Her Lin, and Vítězslav Zim

MS02-P03 **Synthesis, structure and optical properties of new 4,4'-bipyridine - intercalated lanthanide sulfates layered framework**
Bunlawee Yotnoi, Apinus Rujiwatra, and Srinivasan Natarajan

MS02-P04 **X-ray structure of a nickel complex containing 2-aminopyrimidine and thiocyanate mixed ligands with a three-dimensional network structure**
Masoumeh Tabatabaee and Saina Saheli

MS02-P05 **Structural diversity of four Nd(III)-NDC MOFs based on different secondary building units (SUBs) showing interesting gas adsorption properties (NDC2 = 2,6-naphthalenedicarboxylate)**
Chih-Chieh Wang, Ching-Chun Yang, Chang-Tsung Yeh, and Gene-Hsiang Lee

MS02-P06 **Syntheses, structures and photoluminescence properties of hexanuclear gold(I)-silver(I) mixed metal complexes**
Hiroko Fujioka, Yoshiki Ozawa, and Koshiro Toriumi

MS02-P07 **Functional cyclobutane derivatives for metal organic frameworks**
Goutam Kumar Kole, Geok Kheng Tan, Lip Lin Koh, and Jagadese J. Vittal

MS02-P08 **Stepwise synthesis of charged and neutral 2-D networks via 1-D silver(I) coordination polymer based on bis(4-pyridylmethyl)sulfide**
Ki-Min Park, Joobeom Seo, Suk-Hee Moon, Jagadese J. Vittal, and Shim Sung Lee

MS02-P09 **Networking of O_2S_2-macrocycle with silver perchlorate into 1-D and 2-D coordination polymers: Kinetic and thermodynamic products**
So Young Lee, Jong Hwa Jung, Ki-Min Park, Jagadese J. Vittal, and Shim Sung Lee

MS02-P10 **Synthesis of 4d–4f heterometallic coordination framework by postsynthetic modification**
Young Ok Jang and Soon W. Lee

MS02-P11 **Reactivity of RhCp* complexes containing labile ligands toward potential linking ligands containing terminal thiophene or furan rings: preparation and structures of [Cp*Rh(L1)Cl_2], [Cp*Rh(h2-NO_3)(L1)](OTf), and {[Rh(L2)]·(OTf)}∞ [L1 = 1,2-bis((thiophen-2-yl)methylene)hydrazine); L2 = 1,2-bis((furan-2-yl)methylene)hydrazine]**
Kyung-Eun Lee and Soon W. Lee

MS02-P12 **Tailored thermal expansion in Metal-Organic Frameworks**
Yue Wu and Cameron J. Kepert

MS02-P13 **Cancelled**

MS02-P14 **Structurally responsive flexible PCPs to sorption of guests and ligand substitutions**
Joobeom Seo, Ryotaro Matsuda, Charlotte Bonneau, and Susumu Kitagawa

MS02-P15 **Solvothermal synthesis and structures of templated and hybrid solids in the imidazole manganese vanadate system**
Kittipong Chainok, Herman H-Y. Sung, and Ian D. Williams

MS05: Chemical crystallography - structure and properties

MS05-P01 **Supramolecular assemblies of 1,2,4,5-cyclohexanetetracarboxylic acid with various aza-donor compounds**
Manish Raut and V. R. Pedireddi

MS05-P02 **Unusual C--H...n interactions in the structure of 3,4,5-trimethoxy-N-p-tolylbenzamide**
Jim Simpson and Aamer Saeed

MS05-P03 **Using water as a design element in crystal engineering: Host-guest compounds of hydrated 3,5-dihydroxybenzoic acid**
Sunil Varughese and Gautam R. Desiraju

MS05-P04 **Investigation of the crystal structure of mixed $(Rb_{1-x}Tl_x)H_2PO_4$ by neutron diffraction**
In-Hwan Oh, Kwang-Sei Lee, Martin Meven, and Gernot Heger

MS05-P05 **Crystal and molecular structure of tris(tert-butyl-3-butanoato)gallium**
S. Brahma, S.A. Shivashankar, T. Narasimhamurthya, and Vasu

MS05-P06 **Molecular structure of fluorescent copper(II) complexes with anticancer activity**
Vedavati G. Puranik, Satish Bhat, Anupa Kumbhar, Huissain Heptullah, and Ayesha Khan

MS05-P07 **The relevance of unconventional hydrogen bonding in the polymerization and assembly of polydiacetylene DCHD**
Bagautdin Bagautdinov, Kunihisa Sugimoto, Sono Sasaki, Fumiko Yoshida, Che-Hsiu Shih, Jungeun Kim, Hiroshi Tanaka, Kohji Tashiro, and Masaki Takata

MS05-P08 **Crystal engineering of hydroxybenzoic acids: Influence of solvent in the synthon diversity and crystal packing**
SeethaLekshmi Sunil and T. N. Guru Row

MS05-P09 **Crystal structure of 7, 8-dimethyl-4-bromomethylcoumarin**
Ramakrishna Gowda, K.V. Arjuna Gowda, Mahantesha Basanagouda, and Manohar V. Kulkarni

MS05-P10 **The unusual phase behaviour of $Sr_2TiSi_2O_8$ and structurally related compounds**
Patryck Allen and Siegbert Schmid

MS05-P11 **Supramolecularly aggregated coordination solids containing 4-CNpy ligand**
Sanchay Jyoti Bora and Birinchi Kumar Das

MS05-P12 **Reinvestigation of structure-composition relationship in Na_xWO_3**
Tapas debnath, Claus H. Rüscher, and Altaf Hussain

MS05-P13 **Ordering in intercalated Co atoms and electron density distributions of layered compounds Co_xTiS_2**
Ken-ichi Ohshima and Takuro Kawasaki

MS05-P14 **Synthesis, structure and ionic conductivity in scheelite type $Li_{0.5}Ce_{0.5-x}Ln_xMoO_4$ (x = 0 and 0.25, Ln = Pr, Sm): A fast lithium-ion conductor**
Dipankar Saha, Giridhar Madras, Aninda J. Bhattacharyya and T. N. Guru Row

MS05-P15 **Polymorphism in benzyl alcohol: An in situ cryocrystallographic study**
Ranganathan Sathishkumar, Susanta K. Nayak, and T. N. Guru Row

MS05-P16 **Crystal structure and semi-empirical quantum chemical calculation of 3-dibromoacetyl-2H-1-benzopyran-2-one**
S. Shalini, C. R. Girija, T. V. Venkatesha, and M. M. Jotani

MS05-P17 **Influence of interstitial defects on the concentration of cation vacancies**
Anatoly M. Sazonov, Viktor V. Onufrienok, and Anatoly V. Chzhan

MS05-P18 **From coordinates to chemistry: 'decifering a cif'**
Colin R. Groom, Jason C. Cole, and Aurora J. Cruz-Cabeza

MS05-P19 **Photochromic property control using acid-base type co-crystal formation of salicylideneaniline derivatives**
Kohei Johmoto, Sekine Akiko, and Hidehiro Uekusa

MS05-P20 **Detail comparison on temperature dependence of XANES spectra for $PbTiO_3$, $ATiO_3$ and A_2TiO_4 compounds (A=Mg, Ca, Sr, Fe)**
Tomotaka Nakatani, Tatsuya Hiratoko, Maki Okube, Takashi Takeda, Keiichiro Murai, and Akira Yoshiasa

MS05-P21 **Temperature dependence of XANES spectra for $BaTiO_3$, $SrTiO_3$ and TiO_2 with structural phase transitions**
Tatsuya Hiratoko, Tomotaka Nakatani, Maki Okube, Akihiko Nakatsuka, Kei-ichiro Murai, and Akira Yoshiasa

MS05-P22 **Local structure analysis of tektites by Fe K-edge XAFS spectroscopy**
Takahiro Furuta, Ling Wang, Maki Okube, Takashi Takeda, Hiroki Okudera, and Akira Yoshiasa

MS05-P23 **H/D effect in a room temperature ionic liquid: N, N-diethyl-N-methyl-N-(2-methoxyethyl) ammonium tetrafluoroborate**
Hiroshi Abe, Yusuke Imai, Takahiro Takekiyo, and Yukihiro Yoshimura

MS05-P24 **A combined experimental and theoretical charge density study of di-chromium complex with a Cr-Cr quintuple bond**
Lai-Chin Wu, Chia-Wei Hsu, Yu-Chun Chuang, Gene-Hsiang Lee, Yi-Chou Tsai, and Yu Wang

MS05-P25 **In situ observation of crystal structure of $BaTiO_3$-based ceramics under high electric field**
Hisanori Ohkubo, Chikako Moriyoshi, Fumiko Yoshida, Yoshihiro Kuroiwa, Noriyuki Inoue, and Takafumi Okamoto

MS05-P26 **Nanoporous structures as a brand-new type of color conversion phosphor for solid-state lighting-LEDs**
Pei-Ci Jhang and Sue-Lein Wang

MS05-P27 **Preparation and characterization of a metformium salt of monoprotonated decavanadate**
Aungkana Chatkon and Kenneth J. Haller

MS05-P28 **Structural phase transition without accompanied spin transition of complex t-{$Fe(abpt)_2[N(CN)_2]_2$}**
Chou-Fu Sheu, Yu-Chun Chuang, Yi-Hung Liu, Hwo-Shuenn Sheu, Yu Wang

MS05-P29 **Electronic structures and luminescence properties of double activated $YTaO_4:Eu^{3+},Tb^{3+}$ and $YNbO_4:Eu^{3+},Tb^{3+}$ phosphors**
M. Nazarov, Do Young Noh, A. Zhbanov, and Yong-Gu Lee

MS05-P30 **Reversible phase transition in a new polymeric zinc metavanadate, $[Zn(Im)_4][V_2O_6]$**
Samroeng Krachodnok, Kenneth J. Haller, and Ian D. Williams

MS05-P31 **Study of intermolecular interactions in two imidazo[2,1-b] [1,3,4] thiadiazoles**
M. K. Kokila, G. N. Anil Kumar, Subhas S. Karki, R. Vinaya Kumar, and M. V. Kulkarni

MS05-P32 **Stereospecific metal bonding to cytosine in the tipodal tris(2-aminoethyl)amine (tren)-ligand system: Crystal structure of $[\{Cu(tren)\}_2(cytosinato)]\cdot(ClO_4)_3\cdot 0.5H_2O$**
M. S. Rahman and K. Aoki

MS05-P33 **Structures and bonding modes of tetra-bonded hypervalent oxygen compounds**
Etsuko Tomiyama, Kengo Yoshida, Masanobu Uchiyama, Yohsuke Yamamoto, and Daisuke Hashizume

MS05-P34 **Synthesis, structures, photophysical characterization and OLED applications of some multifunctional cyclometalated iridium metallophosphors containing 9-phenylcarbazoles**
Wai-Yeung Wong, Ching-Shan Lam, and Cheuk-Lam Ho

MS05-P35 **Concerted disorder through the hydrate region of tricyclic acyclovir: $C_{11}H_{13}N_5O_3\cdot 2H_2O$**
Montha Meepripruek and Kenneth J. Haller

MS05-P36 **Stability of clopidogrel bisulfate (PLAVIX), an antiplatelet drug, under elevated conditions**
Nongnuj Muangsin, Chuttree Phurut, and Thapong Teerawatananon

MS05-P37 **Successive volume expansion observed in a small-pore zeolite**
Yongjae Lee, Yongmoon Lee, and Dong-Hoon Seoung

MS05-P38 **Structural comparison of tetrapodal and bipodal host inclusion compounds with amine base**
Fumiaki Sano, Akiko Sekine, and Hidehiro Uekusa

MS05-P39 **Structural evolution of stoichiometric praseodymium silicate oxyapatite, $Pr_8Sr_2Si_4O_{26}$**
Terutoshi Sakakura, Minami Kamoshita, Jun Wang, and Nobuo Ishizawa

MS05-P40 **Crystal structure and magnetic behaviors of novel lanthanide(III) carboxylate compounds**
Hsiu-Mei Lin, Jen-Yun Wu, Pei-An Hsiung, Chi-Rung Lee, and I-Jui Hsu

MS05-P41 **Structural and electronic properties of tetrahedral fullerenes and diamond-like fullerene crystals**
Alexander Zhbanov, Yong-Gu Lee, Ching-Tarng Liang, and Yia-Chung Chang

MS05-P42 **Crystal structures of bipyridine–copper(II) complexes as anticancer agents**
A. Kaewthong, M. Sukwattanasinitt, and N. Muangsin

MS05-P43 **Visualisation and characterization of voids in molecular crystals**
Mark A. Spackman, Michael J. Turner, Joshua J. McKinnon, and Dylan JayAtilaka

MS05-P44 **The position determination of H/D in the protonated and deuterated $LaFeAsO_{1-y}H_x$**
Junrong Zhang, Chul-Ho Lee, Shuki Torii, Masao Yonemura, Toru Ishigaki, Teguh Panca Putra, Ping Miao, Takashi Muroya, Ryoko Tomiyasu1, and Takashi Kamiyama

MS05-P45 **High-temperature single-crystal X-ray diffraction study on the decarbonation of $FeCO_3$**
J. Wang, T. Sakakura, N. Ishizawa, and H. Eba

MS05-P46 **Model complexes of the active center in nitrite reductase**
Yasushi Kai, Kazue Ohmi, Haruka Teranishi, Tsuyoshi Inoue, Sinnichiro Suzuki, Akiko Minami, and Kazuya Yamaguchi

MS05-P47 **New pentanary thiophosphates, $A_x(Ta_{1-y}Ti_y)PS_5$ (A=K, Rb, Cs): A systematic approach toward new mixed-metallic phases**
Kyoung-hee Kim, Jae-min Yu, and Hoseop Yun

MS05-P48 **Gradual intermetallic bond formation controlled by alkali metals in quinternary metal thiophosphates, $A_y(Ta_xM_{1-x})PS_6$ (A=K, Rb; M=Ti, Zr)**
Sojeong Park, Eunsil Lee, and Hoseop Yun

MS05-P49 **Effect of 3d transition metal substitution on crystal structure in LaOMAs (M = Mn, Fe, Ni, Zn) by high-energy synchrotron radiation powder diffraction**
Shozo Hiramoto, Satoshi Yasuda, Chikako Moriyoshi, Fumiko Yoshida, Yoshihiro Kuroiwa, and Koichi Takase

MS05-P50 **Triplet biradical states of dibromo and dichloro mononuclear polypyridine iridium(III) complexes**
Naokazu Yoshikawa, Shinichi Yamabe, Nobuko Kanehisa, Tsuyoshi Inoue, Hiroshi Takashima, and Keiichi Tsukahara

MS05-P51 **Phase transitions of tetra-alkylammonium salts of deca-vanadates containing 1,4-dioxane molecules**
Tatsuhiro Kojima and Tomoji Ozeki

MS05-P52 **Two silver(I) complex structure in a single crystallization: flexible metallacyclodimer vs helical channel network**
Chi Won Kim, Eun Ji Kim, and Ok-Sang Jung

MS05-P53 **Fine competition and control among argentophilic, electrostatic, and π···π interactions in a molecular chair**
Jungmin Ahn and Ok-Sang Jung

MS05-P54 **Microwave-assisted preparation of an europium complex: $[Eu(NO_3)2(H_2O)_3(L)_2]\cdot(NO_3)(H_2O)$ {L = 2-(4-pyridylium)ethanesulfonate, (4-pyH)–CH_2CH_2–SO_3^-}**
Zhen Nu Zheng and Soon W. Lee

MS05-P55 **A terbium dimer bridged by (imidazol)benzoic acid: $[Tb(NO_3)_3(OMe)(ibaH)]_2$[iba = 4-(1H-imidazol-1-yl)benzoic acid]**
Yeong-Min Jung and Soon W. Lee

MS05-P56 **Crystal and molecular structure of 5-bromo-1H-indole-2,3-dione**
S. Shylaja, K.B.R. Varma, T. Narasimhamurthy, and Vasu

MS05-P57 **Progress in using short wavelength radiation for chemical crystallography**
T. Samtleben, J. Graf, B. Hasse, J. Wiesmann, C. Michaelsen, F. Fabbiani, T. Schulz, D. Stalke, and H. Ott

MS05-P58 **Molecular structure of 2-amino-N(2-fluorophenyl)-4, 5, 6, 7-tetrahydro-1-benzothiophene-3-carboxamide**
M. K. Kokila, K. Chandra Kumar, J. Saravanan, and M. V. Kulkarni

MS05-P59 **Synthesis, structures and characterization of organotin complexes derived from 3,5-di-tert-butyl-4-hydroxybenzyl alcohol**
S. M. Lee, H. Mohd. Ali, and K. M. Lo

MS05-P60 **Structure-property relationships in phosphous-based nanoporous metal oxides**
Sue-Lein Wang

MS05-P61 **Crystal morphological study on the solubility limits of synthetic Al-substituted goethite**
Fei Wu, Peter Smith, Bill Richmond, Franca Jones, and Kate Wright

MS05-P62 **Influence of cation vacancies on the phase composition of iron sulphides 29 years after synthesis**
Viktor V. Onufrienok and Anatoly M. Sazonov

MS05-P63 **The crystal structure of a new dioxo-molybdenium(VI) complex of a tridentate Schiff base ligand**
Iran Sheikhshoaie, Niaz Monadi, and Helen Stoeckli-Evans

MS05-P64 **Synthesis, crystal structure, and fluorescence property of chalcone derivatives**
Thawanrat Kobkeatthawin, Suchada Chantrapromma, and Hoong-Kun Fun

MS05-P65 **Partial resolution of racemic Cu(I) complex via crystallization**
Michael Y. Chiang and Jing-Yun Wu

MS05-P66 **Disordering of the $[NbOF_5]^{2-}$ anions in centrosymmetric structures of $(C_2H_6NO_2)_2[NbOF_5]$, $(C_3H_8NO_2)_2[NbOF_5]\cdot 2H_2O$, $[Sn_2F_2][NbOF_5]$, $K_4[Sb_2F_8][NbOF_5]$ and $Mn[NbOF_5]\cdot 4H_2O$**
Andrey V. Gerasimenko, Ivan A. Tkachenko, Ruven L. Davidovich, Tamara F. Antokhina, and Evgeny B. Merkulov

MS05-P67 **Crystal structure and microwave dielectric properties of indialite**
H. Ohsato, A-Y. Kim, T. Sakakura, N. Ishizawa, C-I. Cheon, and J-S. Kim

MS05-P68 **Novel anticancer agents: synthesis, crystal structures, cytotoxic activities, DNA-binding studies and topoisomerase II inhibitory of the sulfonyl containing 6-deoxyclitoriacetal derivatives**
Thapong Teerawatananond, Nattaya Ngamrojnavanich, Narongsak Chaichit, and N. Muangsin

MS05-P69 **Pressure-induced hydration and cation migration in a potassium-exchanged natrolite**
Dong-Hoon Seoung, Yongmoon Lee, and Yongjae Lee

MS05-P70 **Raman spectral and X-ray diffraction of CO2 absorption into natrolite under high-pressure**
Dan Liu, Zhenxian Liu, and Yongjae Lee

MS05-P71 **Structures of herbal compounds: 5-hydroxy substituted flavones**
Krishnaiah M, Ravi Kumar R, and Jagadeesh Kumar N

MS05-P72 **Crystal chemical screening of the ICSD for discovery of materials with high Li^+ mobility**
Matthew Sale and Maxim Avdeev

MS05-P73 **Capture of hydroxyl group (OH) cationic vacancies in structures of the Pyrrhotite**
Alexander G. Nikiforov, Viktor V. Onufrienok, and Anatoly V. Chzhan

MS05-P74 **Automation in single crystal X-ray diffraction (SC-XRD)**
Bernd Hinrichsen, Martin Adam, and Joerg Kaercher

MS05-P75 **Making the most of a SuperNova diffractometer equipped with both Mo and Cu micro-focus sources, an Atlas detector and AutoChem**
Zoltán Gál, Alexandra Griffin, and Oliver Presly

MS05-P76 **Photoinduced rearrangement of N-chlorinated acetanilides and benzanilides to chloroaromatic amides in the solid state: Inverted relative stability of Π_N and Σ_N amidyl radicals**
Panče Naumov, Yildiray Topcu, Mirjana Eckert-Maksić, Fabijan Pavošević, Manoj Kochunnoonny, and Zoran Glasovac

MS05-P77 **Topochemical limits for solid-state photoreactivity by fine tuning of the π---π interactions**
Shi-Yao Yang, Panče Naumov, and Shunichi Fukuzumi

MS05-P78 **Different complexation behavior of a proton transfer compound obtained from 2,9-dimethyl-1,10-phenanthroline and 4-hydroxy-pyridine-2,6-dicarboxylic acid with Cr(III), Co(III), Ni(II) and Cu(II)**
Janet Soleimannejad and Hossein Aghabozorg

MS08: Dynamic aspects of molecular and solid state crystals

MS08-P01 **Comparison with three H-, Si- and C-based giant materials on the various planetary materials**
Yasunori Miura

MS08-P02 **Local structure of Co-based additives in $LiBH_4$ + $LiNH_2$ system**
Takashi Asano, Daiju Matsumura, Yuka Okajima, Hai-Wen Li, Shin-ich Orimo, Hikaru Terauchi, Isao Takahashi, and Yasuo Nishihata

MS08-P03 **Molecular dynamics simulations of structure and dynamics of organic molecular crystals**
Alexandra Nemkevich, Hans-Beat Bürgi, Mark A. Spackman, and Ben Corry

MS08-P04 **Crystal structure of new cobaloxime complex with photochromic azobenzene derivatives as axial base ligand**
Hiroki Yamagiwa, Akiko Sekine, and Hidehiro Uekusa

MS08-P05 **Controllable photochromism in hybrid type cobaloxime complex**
Akiko Sekine, Sayaka Ina, Hiroki Yamagiwa, Kohei Johmoto, and Hidehiro Uekusa

MS08-P06 **Dehydration induced color switching of isophthalic acid crystal**
Aya Sakon, Akiko Sekine, and Hidehiro Uekusa

MS08-P07 **Hydration and dehydration transformation of sodium naproxen Pseudopolymorphs**
Takashi Miyamoto, Akiko Sekine, and Hidehiro Uekusa

MS08-P08 **Single crystal structure analyses of photo-excited states of photoluminescent hexanuclear d^{10} metal complexes**
Yoshiki Ozawa, Toru Ishida, Kimihiro Kimura, and Koshiro Toriumi

MS08-P09 **Selective pseudo-polymorphic transformation pathways of organic crystalline materials established using powder X-ray diffraction analysis**
Kotaro Fujii, Yasunari Ashida, Hidehiro Uekusa, Fang Guo, and Kenneth D.M. Harris

MS08-P10 **New insights into molecular mechanisms of photoinduced and thermally induced effects in crystals**
Panče Naumov

MS08-P11 **The origin of solid-state thermochromism of polycyclic overcrowded enes: A hundred-year old mystery resolved**
Panče Naumov, Nobuo Ishizawa, Jun Wang, Ljupčo Pejov, and Sang Cheol Lee

MS08-P12 **New type of dual solid-state thermochromism: Modulation of intramolecular charge transfer by intermolecular π–π interactions, kinetic trapping of aci-nitro group and reversible molecular locking**
Panče Naumov, Sang Cheol Lee, Nobuo Ishizawa, Young Gyu Jeong, Ihn Hee Chung, and Shunichi Fukuzumi

MS11: Magnetic structures/molecular magnets

MS11-P01 **Room temperature ferromagnetism in pure CdSe and CdSe:Ni nanorods**
Sanjeev Kumar, Sunil Kumar, and N. K. Verma

MS11-P02 **Doping effects of multiferroic $BiFeO_3$ ceramics**
Jun-Ki Hong, Jin-Ho Joo, Je-Geun Park, and Seongsu Lee

MS11-P03 **Magnetic and dielectric properties of multi-ferroic $YMn^{4+}(Mn_{1-x}T_x)^{3+}O_5$ (T = Ga and Fe)**
Hiroyuki Kimura, Kenta Yamazaki, Yuma Sakamoto, Mamoru Fukunaga, Yukio Noda, Nobuyuki Abe, Takahisa Arima, and Haruhiro Hiraka

MS11-P04 **Role of interlayer electrostatic interaction in superconductivity of $LaFeAsO_{1-x}F_x$**
J. Kim, T. Sawada, K. Sugimoto, K. Kato, M. Ishikado, S. Shamoto, A. Fujiwara, and M. Takata

MS11-P05 **X-ray magnetic circular dichroism study of $La_{1-x}Ba_xCoO_3$ at Co K absorption edge**
Hiroaki Morii, Takuya Yasue, Maki Okube, Takeshi Ohno, Takayasu Hanashima, and Satoshi Sasaki

MS11-P06 **Propeller-like thermal vibration of molecules in ferroelectric molecular crystal CCl_3CONH_2**
Chikako Moriyoshi and Yoshihiro Kuroiwa

MS11-P07 **The structural characterization and magnetic interactions in doped rare-earth manganites**
Wiqar Hussain Shah

MS14: Nanomaterials, surface, and interface

MS14-P01 **Cancelled**

MS14-P02 **Cancelled**

MS14-P03 **Mapping the strain field of chemically treated surface of semiconductor crystals using X-ray Bragg-surface diffraction**
Y. W. Tsai, C. H. Chu, S,-C. Weng, Y.-Z. Zeng, H.-Y. Chen, Y.-H. Yan, O. N. Zarubina, G. M. Mokrousov, and S.-L. Chang

MS14-P04 **Protein cages provide a platform of cell-permeable and biocompatible imaging probe in living cells**
Seung-Hye Choi, Kuiwon Choi, Ick Chan Kwon, Kwang Yeon Hwang, and Hyung Jun Ahn

MS14-P05 **Long-range-order and short-range-order structures of Co-doped Y_2O_3 nanocrystals**
Y. L. Soo, T. S. Wu, C. S. Wang, S. L. Chang, T. S. Chan, C. A. Hsieh, and J. F. Lee

MS14-P06 **Nano-particle formation by Pd complex deposited on polystyrene thin films**
Koyasu Naoki, Ohshima Yuji, Koiso Naohiro, Terauchi Hikaru, Hashimoto Takeji, and Takahashi Isao

MS14-P07 **Interfacial structure of polystyrene/polyhydroxybutyrate two-layer film revealed by X-ray diffraction**
K. Nozaki, K. Ishimoto, J. Takemoto, C. Yang, X. Sun, K. Shimizu, H. Terauchi, and I. Takahashi

MS14-P08 **Surface structure and morphology of PEG/PEO blends thin film: composition and temperature dependence study**
Yoshiki Kurokawa, Hideaki Takahashi, Hikaru Terauchi, Isao Takahashi, and Katsumi Shimizu

MS14-P09 **Glass transition and thermal expansion of ultrathin polystyrene films - An X-ray reflectivity study at various heating/cooling rates**
Chunming Yang, Shunsui Matsuura, Kiyoaki Inoue, Kohei Ishimoto, Naoki Koyasu, Hikaru Terauchi, and Isao Takahashi

MS14-P10 **Structure analysis of hydroxyapatite nano-crystals by electron powder diffraction**
Kyung Song, Jin-Gyu Kim, and Youn-Joong Kim

MS14-P11 **Symmetry determination of Ag_2Te nanowire using electron diffraction**
Jin-Gyu Kim, Sang-Gil Lee, Kyung Song, Juneho In, Bongsoo Kim, and Youn-Joong Kim

MS14-P12 **Development for X-ray crystal structure analysis of a surface-shallow layer and its application to the epitaxial crystals of halogen-bridged platinum(II,IV) complexes**
Hiroaki Yamanaka, Daisuke Yamashita, Aki Takazaki, Minoru Mitsumi, Yoshiki Ozawa, Koshiro Toriumi, and Osami Sakata

MS14-P13 **One-pot synthesis and application of magnetite containing mesoporous carbon via organic-organic self-assembly**
Sang-Wook Chu, Sung Soo Park, Jeong Hun Shin, and Chang-Sik Ha

MS14-P14 **Adsorption behavior of amino acids on periodic mesoporous organosilicas (PMOs)**
Jeong Hun Shin, Sung Soo Park, Sang-Wook Chu, and Chang-Sik Ha

MS14-P15 **First-principles calculation of dielectric function for graphite, graphene, and carbon nanotubes**
Alexander Zhbanov and Yong-Gu Lee

MS14-P16 **Moved to MS15-P13**

MS14-P17 **Synthesis of biocompatible and mechanically compatible Ti based solid material for implant prototyping**
A. A. Shaikha, S. Dudziakc, O. Meierc, and T. M. Gesingb

MS14-P18 **Analysis of electron diffraction patterns from bone minerals**
Chang-Yeon Kim, Tae-Hoon Jeon, Eun-Kyung Kim, Hyosun Lim, Seung-Won Nam, Kyung Song, Sang-Gil Lee, Woomi Yang, Jun-Ho Jeong, Jong-Man Jeong, Jin-Gyu Kim, Hwanuk Kim, and Youn-Joong Kim

MS14-P19 **Synthesis and characterization of Sb_2S_3 & Sb_2Se_3 nanorods via complex decomposition by hydrothermal method**
Abdolali Alemi and Younes Hanifehpour Firouzsalari

MS14-P20 **Preparation & characterization of Ho^{3+} doped Sb_2Te_3 nanoplates by hydrothermal method and investigation of optical properties**
Abdolali Alemi and Younes Hanifehpour Firouzsalari

MS14-P21 **Collecting complete 3D electron diffraction data using the automatic rotation method**
Sven Hovmöller, Peter Oleynikov, Daliang Zhang, and Xiaodong Zou

Area 3. Specialized Techniques

MS03: Synchrotron and neutron sources, instrumentation and applications

MS03-P01 **Site preference and electron-density distribution of Fe ions in magnetite by X-ray resonant and non-resonant scattering**
Takuya Yasue, Yuhei Kaneko, Maki Okube, and Satoshi Sasaki

MS03-P02 **Accurate determination of local structural properties by X-ray absorption fine structure**
Sang-Wook Han

MS03-P03 **Structure of transmembrane pore reconstructed by anomalous X-ray diffraction**
Ming-Tao Lee, Shiuan-Shiaou Wu, Wei-Yu Lin, and Yi-Ting Sun

MS03-P04 **MAX200x and max80 high-pressure / high-temperature experiments from Helmholtz Centre Potsdam, GFZ German Research Centre for Geosciences at DESY, German Electron synchrotron**
Christian Lathe, Hans Joachim Mueller, and Joern Lauterjung

MS03-P05 **Environmental structural analysis of hydrolytic condensed oxides with complex structure**
Reiko Murao and Kazumasa Sugiyama

MS03-P06 **Development of a micro-strip detector for high-energy XRD**
Taguchi Takeyoshi, Matsushita Kazuyuki, Maciej Kachel, Robert Szczygiel, and Pawel Grybos

MS03-P07 **Structural study of $Zr_{50}Cu_{40}Al_{10}$ and $Zr_{50}Ni_{40}Al_{10}$ amorphous alloys by anomalous X-ray scattering coupled with reverse Monte-Carlo simulation**
T. Kawamata, Y. Yokoyama, and K. Sugiyama

MS03-P08 **High brilliance laboratory sources for small X-ray beams**
T. Samtleben, C. Michaelsen, B. Hasse, J. Wiesmann, U. Heidorn, S. Kroth, and F. Hertlein

MS03-P09 **Synchrotron radiation beamline for macromolecular assemblies at SPring-8 operated by the Institute for Protein Research (BL44XU)**
Eiki yamashita, Masato Yoshimura, Mamoru Suzuki, Kazuya Hasegawa, Yukito Furukawa, Toru Ohata, Takashi Kumasaka, Go Ueno, Masaki Yamamoto, Shinya Yoshikawa, Tomitake Tsukihara, and Atsushi Nakagawa

MS03-P10 **Data processing software for a new TOF single crystal neutron diffractometer "iBIX" at J-PARC**
Takashi Ohhara, Katsuhiro Kusaka, Takaaki Hosoya, Kazuo Kurihara, Taro Yamada, Katsuaki Tomoyori, Takeshi Yokoyama, Yuki Onishi, Ichiro Tanaka, Nobuo Niimura, Toshiya Otomo, Jiro Suzuki, and Takeshi Nakatani

MS03-P11 **Development of a new beamline dedicated to low energy SAD experiments at the Photon Factory**
Naohiro Matsugaki, Yusuke Yamada, Leonard M.G. Chavas, Masahiko Hiraki, Masato Kawasaki, Ryuichi Kato, Noriyuki Igarashi, Atsushi Koyama, Shigeru Yamamoto, Kimichika Tsuchiya, Tatsuro Shioya, Tomohiro Aoto, Hideki Maezawa, Seiji Asaoka, Hiroshi Miyauchi, Toshihiro Tahara, Yasunori Tanimoto, and Soichi Wakatsuki

MS03-P12 **SENJU: A new time-of-flight single crystal neutron diffractometer at J-PARC**
Takuro Kawasaki, Kenichi Oikawa, Itaru Tamura, Takashi Ohhara, Koji Kaneko, Hiroyuki Kimura, Ryoji Kiyanagi, Miwako Takahashi, Tamiko Kiyotani, Masatoshi Arai, Yukio Noda, and Ken-ichi Ohshima

MS03-P13 **The Australian Synchrotron: research opportunities now and into the future**
Kia S. Wallwork, Chris Glover, Nigel Kirby, Tom Caradoc-Davies, and Ian Gentle

MS03-P14 **Introduction of 6B beamline at Pohang Accelerator Laboratory in Korea for the small molecule X-ray crystallography**
Dohyun Moon

MS03-P15 **A simulation report of a single crystal diffractometer using an image plate for nano-bio research**
Sang Jin Cho, Tae Sung Yoon, Chang Hee Lee, Shin Ae Kim, Ji Yong So, and Kyong-Pyo Kim

MS03-P16 **The first neutron structure analysis of biological macromolecule with IBARAKI Biological Crystal Diffractometer -iBIX- in J-PARC**
Katsuhiro Kusaka, Taro Yamada, Takaaki Hosoya, Takashi Ohhara2, Kazuo Kurihara, Ichiro Tanaka, and Nobuo Niimura

MS03-P17 **Highest brilliance X-ray sources for home lab instrumentation – From solid target anode to liquid metal jet micro-focus**
Martin Adam, Arnt Kern, Christoph Ollinger, Carsten Michaelson, Till Samtleben

MS03-P18 **New X-ray imaging cameras give insight into X-ray source characteristics**
Licai Jiang, Hugh Garvey, Nick Grupido, Bodo Ehlers, Bonglea Kim, Ladislav Pina, and Martin Horvath

MS06: Small angle X-ray and neutron scattering

MS06-P01 **Morphological structures of a polymethacrylate diblock copolymer bearing POSS moieties probed by grazing incidence X-ray scattering**
Byungcheol Ahn, Sangwoo Jin, Tomoyasu Hirai, Yecheol Rho, Sungmin Jung, Kwang-Woo Kim, Samdae Park, Jin Chul Kim, Wonsang Kwon, Junman Choi, Dong Min Kim, Jungwoon Jung, Kyungtae Kim, Mihee Kim, Yong-Gi Ko, Masa-aki Kakimoto, Padma Gopalan, Teruaki Hayakawa, and Moonhor Ree

MS06-P02 **Nanoporous conducting polymer thin films generated from ionic interaction block copolymers templates**
Yecheol Rho, Ayumi Takahashi, Tomoya Higashihara, Byungcheol Ahn, Samdae Park, Jin Chul Kim, Dong Min Kim, Jungwoon Jung, Wonsang Kwon, Kyungtae Kim, Mihee Kim, Yong-Gi Ko, Sungmin Jung, Junman Choi, Moonhor Ree, and Mitsuru Ueda

MS06-P03 **Effect of C_{60} fullerene on the duplex structure of i-motif DNA with complementary DNA in solution**
Byungcheol Ahn, Mihee Kim, Kyeong Sik Jin, Su Ryon Shin, Yecheol Rho, Kyungtae Kim, Sungmin Jung, Seon Jeong Kim, and Moonhor Ree

MS06-P04 **Molecular organization of laterally tethered rod-coil molecules**
Dong-Je Hong and Myongsoo Lee

MS06-P05 **Microstructure of PLA-PEG block copolymer aqueous solutions as studied by small angle X-ray scattering**
Hye-Jin Jeon, Yeon Hung Oh, Hak Seung Jeong, Woon Bo Shim, and Hyun Hoon Song

MS06-P06 **Surface-induced columnar structures of discotic liquid crystals in thin films**
Hyo-Sik Kim, Sung-Min Choi, Brian D. Pate, and Po Gyu Park

MS06-P07 **Fabrication of highly ordered SWNT superstructures in a polymeric system**
Changwoo Doe, Hyung-Sik Jang, Tae-Hwan Kim, Steven R. Kline, and Sung-Min Choi

MS06-P08 **Highly ordered self-assembly of negatively charged nanorods and cationic liposomes**
Tae-Hwan Kim, Shin-Hyun Kang, Changwoo Doe, Jihyun Yu, Jun-Bo Sim, Jehan Kim, Steven R. Kline, and Sung-Min Choi

MS06-P09 **Synchrotron grazing incidence wide-angle X-ray scattering analysis on molecular aggregation structure of full- or semi-aromatic polyimide films**
Byungcheol Ahn, Junji Wakita, Sangwoo Jin, Tae Joo Shin, Yecheol Rho, Samdae Park, Jin Chul Kim, Wonsang Kwon, Dong Min Kim, Jungwoon Jung, Kyungtae Kim, Mihee Kim, Yong-Gi Ko, Sungmin Jung, Junman Choi, Moonhor Ree, and Shinji Ando

MS06-P10 **Self-assembled brush polymers with glycine derivatives and its biocompatibility**

Yecheol Rho, Jungwoon Jung, Gahee Kim, Samdae Park, Hyunchul Kim, Jin Chul Kim, Dong Min Kim, Byungcheol Ahn, Wonsang Kwon, Kyungtae Kim, Mihee Kim, Yong-Gi Go, Sungmin Jung, Junman Choi, Sejin Son, Won Jong Kim, and Moonhor Ree

MS06-P11 **Structures characterization of star polystyrenes with varying numbers of arms through synchrotron X-ray scattering**

Yecheol Rho, Sangwoo Jin, Tomoya Higashihara, Samdae Park, Jin Chul Kim, Dong Min Kim, Jungwoon Jung, Byungcheol Ahn, Sungmin Jung, Wonsang Kwon, Kyungtae Kim, Mihee Kim, Yong-Gi Ko, Junman Choi, Moonhor Ree, and Akira Hirao

MS09: Combining methods/new tools in structural biology

MS09-P01 **A fast and fully automated solution for lipidic cubic screening (LCP) using Mosquito LCP**
Joby Jenkins, Patricia Edwards, Rob Lewis, and Joanne Franklin

MS09-P02 **macroSNAP: A computer program for comparing and clustering protein structures**
Christopher Gilmore, Gordon Barr, Wei Dong, Adrian Lapthorn, and Stuart MacKay

MS09-P03 **Automated crystal centering by use of UV LED**
Leonard M.G. Chavas, Yamada Yusuke, Masahiko Hiraki, Noriyuki Igarashi, Naohiro Matsugaki, and Soichi Wakatsuki

MS09-P04 **Improved technologies for high-resolution X-ray crystallography**
H. Tanaka, M. Sato, K. Inaka, N. Furubayashi, S. Takahashi, B. Yan, A. Higashiura, M. Suzuki, S.-Y. Park, Y. Higuchi, Y. Yoshimura, and A. Nakagawa

MS09-P05 **High-quality protein crystal growth experiment (JAXA PCG) onboard the Japanese experiment module 'Kibo' in the International Space Station**
M. Sato, H. Tanaka, K. Inaka, N. Furubayashi, S. Sano, S. Takahashi, B. Yan, E. Hirota, T. Ichikawa, S. Shinozaki, M. Shirakawa, and Y. Yoshimura

MS09-P06 **Analyses of X-ray damage on the oxidized form of high-potential iron-sulfur protein at ultra-high resolution**
Yu Hirano, Hiraku Ohno, Hideyuki Jonotsuka, Kazuki Takeda, and Kunio Miki

MS09-P07 **Towards efficient crystallization screening using high performance UV fluorescence imaging**
Jian Xu and Michael Willis

MS09-P08 **The high-pressure cryocooling for supramolecular crystals: In the case of Rice Dwarf Virus**
Akifumi Higashiura, Masaru Sato, Koji Inaka, Masaki Shirakawa, Yoshinori Yoshimura, and Atsushi Nakagawa

MS09-P09 **Fluorescence-based screening for soluble human proteins by POET in baculovirus-infected insect cells for structural studies**
Song-ying Ouyang, Neil shaw, and Zhi-Jie Liu

MS09-P10 **Hematin-hematin self-association in hemozoin by X-ray powder diffraction and X-ray absorption spectroscopy**
Victor Streltsov, Ruben Dilanian, Nectarios Klonis, Eric Hanssen, Harry Quiney, and Leann Tilley

MS09-P11 **Automating microseeding protein crystallography set-ups using Mosquito®**
Joby Jenkins, Rob Lewis, and David Smith

MS09-P12 **Getting the most out of your synchrotron**
Joseph D. Ferrara, Colin Acheson, Keith Crane, Angela Criswell, Pierre Le Magueres, and Bret Simpson

MS09-P13 **High-end solution for in-house protein crystallography**
Martin Adam, Marianna Biadene, Matt Benning, and Vernon Smith

MS12: Crystal growth and engineering

MS12-P01 Crystallization of catalytic domain of human MAP kinase phosphatase 5 for neutron diffraction experiments
Simranjeet Singh Sekhon, Elena Magay, and Tae-Sung Yoon

MS12-P02 Growing lysozyme crystals for neutron diffraction beamlines
Elena Magay and Tae-Sung Yoon

MS12-P03 Controlling the coordination numbers of lanthanoid atoms by the use of multidentate polyoxometalate ligands
Tomoji Ozeki, Yusuke Kato, and Takahiro Shimono

MS12-P04 The fascinating world of tautomers and their crystal structures
Aurora J. Cruz-Cabeza, Jason C. Cole, and Colin R. Groom

MS12-P05 Crystal engineering of rare-earth (Sm, Gd) molybdates based on organic linkers
Dinesh Kumar and A. Ramanan

MS12-P06 Protein crystallization with synthetic zeolite molecular sieves as hetero-epitaxic nucleants
Michihiro Sugahara, Yuko Kageyama-Morikawa, and Naoki Kunishima

MS12-P07 Crystal packing analysis of nonmolecular solids – A retrosynthetic approach
Monika Singh, Dinesh Kumar, and Arunachalam Ramanan

MS12-P08 Desktop Alchemist™: A high precision fine screen maker to automate crystallization optimization
Jian Xu and Michael Willis

MS12-P09 Growth and study of optical properties of polycrystalline and single crystals of CdI2
Alka Garg and Anita

MS12-P10 In situ diffraction: a powerful tool for studying undisturbed crystals in crystallization droplets
Tadeusz Skarzynski

MS12-P11 Gel crystallization of calcium-lead hydroxyapatite, MHAP (M = Ca^{2+} and/or Pb^{2+})
Oratai Saisa-ard and Kenneth J. Haller

MS15: Powder diffraction

MS15-P01 **Ab initio structure analysis of solid-state photodimerized methoxyazachalcone from powder diffraction data**
Hisashi Konaka, Yoko Tokugaw, and Shinji Yamada

MS15-P02 **Effect of pH on zinc oxide crystallographic structure**
Sanjeev Gautam, I. J. Lee, and Keun Hwa Chae

MS15-P03 **Structures differ from sodium and potassium urate crystals**
Hwo-Shuenn Sheu, Wei-Ju Shi, and Wei-Tsung Chuang

MS15-P04 **Diffraction vector approach and new detector for two-dimensional X-ray diffraction**
Bob B. He

MS15-P05 **Comparison of crystallite shape ellipsoid in various polymers**
H. Somashekarappa, R. Gopalakrishne Urs, V. Annadurai, S. S. Mahesh, and R. Somashekar

MS15-P06 **Using crystallographic knowledge to ease powder structure solution using DASH**
Jason C. Cole, Colin R. Groom, and Aurora J. Cruz-Cabeza

MS15-P07 **The importance of Mn(III) in phase transition of some Mn perovskites**
T. Y. Tan and B. J. Kennedy

MS15-P08 **Crystal structural change by guest sorption/release processes of the macrocyclic boronic ester investigated by laboratory powder X-ray diffraction analysis**
Kotaro Fujii, Hidehiro Uekusa, Yuji Kikuchi, Hiroki Takahagi, Kosuke Ono, and Nobuharu Iwasawa

MS15-P09 **Status report on super high resolution powder diffractometer at J-PARC**
Shuki Torii, Masao Yonemura, Teguh Panca Putra, Junrong Zhang, Miao Ping, Takashi Muroya, Ryoko Tomiyasu, Takahiro Morishima, Setsuo Sato, Hidenori Sagehashi, Toru Ishigaki, Yukio Noda, and Takashi Kamiyama

MS15-P10 **Research and developments at the Australian synchrotron powder diffraction beamline**
Kia S. Wallwork, Qinfen Gu, and Justin A. Kimpton

MS15-P11 **In situ powder X-ray diffraction for gas adsorption on ordered mesoporous materials**
Keiichi Miyasaka, Norihiro Muroyama, Kyoungmin Jung, Yoshiki Kubota, and Osamu Terasaki

MS15-P12 **X-ray diffraction analysis of carbon extracted from a fruit like fullerene**
B. Mallick, Sonam Narayan, Suraj Patra, Ashmaa Parvin, K. B. Sahu, B. Mishra, and S. Sahu

MS15-P13 **Moved to MS15-P13Development of defect perovskites for use as cathode materials in lithium ion batteries**
William R. Brant and Siegbert Schmid

Area 4. Others

MS-17: Other areas

MS17-P01 **Stacking faults in $Ca_4B_2B'O_9$-type layered brownmillerites**
H. Krüger, T. R. Welberry, J. D. FitzGerald, R. L. Withers, and S. Stöber

MS17-P02 **Enhancement of the ν4 band in heme at NIR laser enhancement attributed to supramolecular interactions**
Ratchadaporn Puntharod, Bayden R. Wood, and Kenneth J. Haller

MS17-P03 **Recombinant fusion protein design for biophysical analysis of integrin subunit dimerization and function**
Andrea Francesca M. Salvador, Gabriel N. Valbuena, Lydia Teresa Isabel Salud-Bautista, and Neil Andrew D. Bascos

MS17-P04 **Development of computer software for General Area Detector Diffraction System (GADDS)**
Hosung Kim and Hohyuk Kim

MS17-P05 **Mineralogy and geochemistry of volcanic rocks of Poledokhtar, Myaneh (NW Iran)**
Amin Kamali, Mohssen Moayed, Hadi Pirooj, and Mohamade Mehri

MS17-P06 **Evolution and development of CrysAlis^{Pro}**
Zoltan Gal, Alexandra Griffin, and Oliver Presly

MS17-P07 **Structure of Hibiscus latent Singapore virus by fiber diffraction: insights into evolution of a distinct Tobamovirus**
Kunchithapadam Swaminathan, Sunil Kumar Tewary, Toshiro Oda, Amy Kendall, Wen Bian, Gerald Stubbs, and Sek-Man Wong

AsCA2010

The 10th Conference of the Asian Crystallographic Association

ABSTRACTS

Special Lecture, Plenary Lectures, and Keynote Lectures

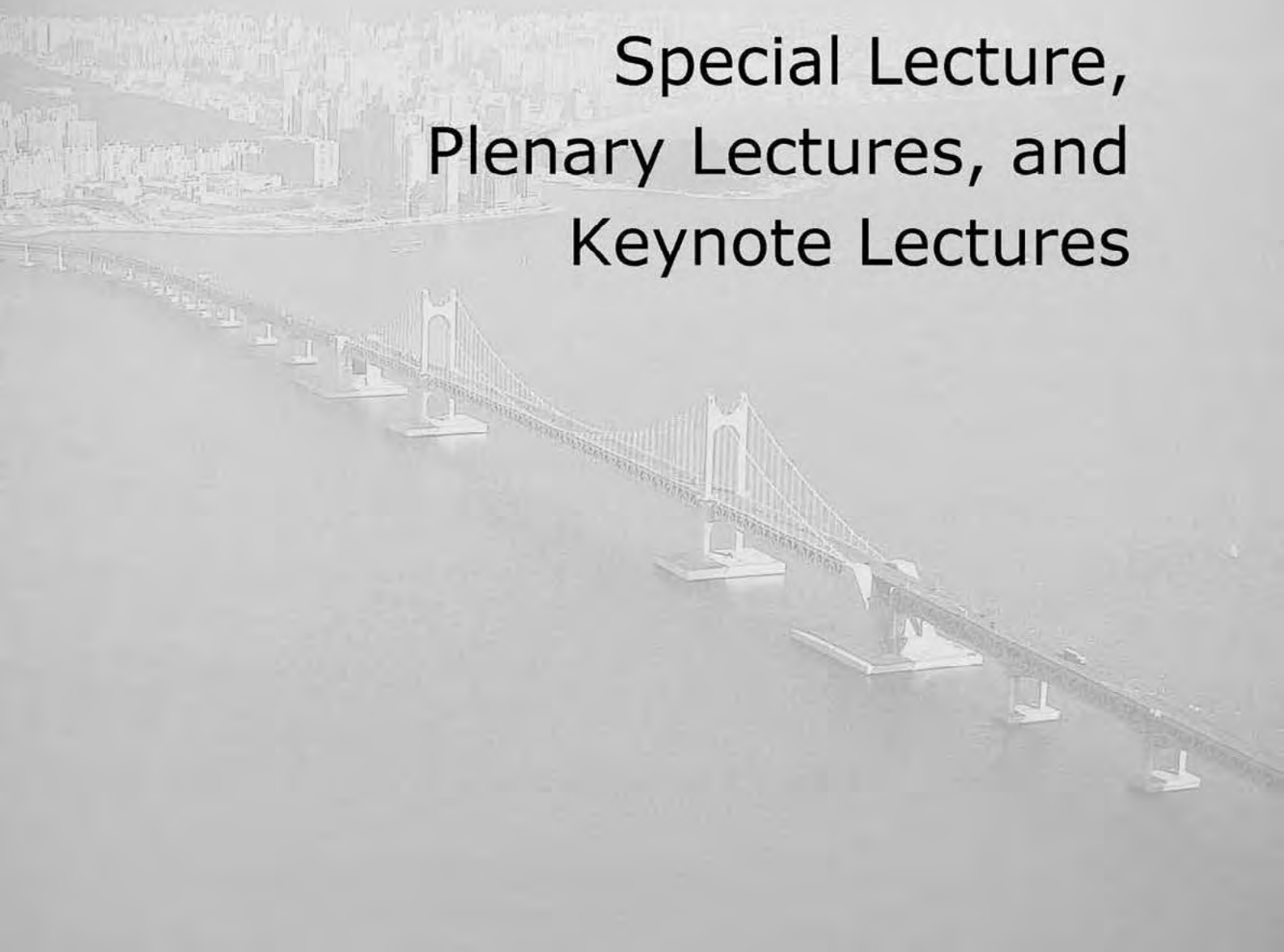

SL-1

The Crystal Dragon: AsCA and crystallography in the Asia-Pacific region

Gautam Desiraju

Indian Institute of Science, India

PL-1

Demography and eolution of protein structural folds

Sung-Hou Kim

Department of Chemistry, University of California, Berkeley CA, USA and WCU Program, Yonsei University, Seoul, Korea

Despite astronomically large numbers of theoretically possible protein sequences only a miniscule fraction of them are selected by evolution to exist in living organisms, and an even smaller number of 3-D architectural motifs (folds) are assumed by the proteins. Thus protein fold space is much less populated than protein sequence space, which is already very sparsely populated. Demographic distribution of the protein folds of all known 3-D structures of proteins has been "mapped" and represented in two ways: (1) as a 3-D map of the protein fold space, an approximation of a multidimensional map, and (2) as a "tree map," that reveals the relationship among the protein folds and possible evolutionary relationship in some cases. The 3-D demographic map of the fold space reveals four large regions populated by the folds of different secondary structure classes. The map also suggests an evolutionary history of the four fold classes. In the tree map, each fold class is subdivided into many folds, each fold representing protein structures of the same fold motif. Furthermore, the branching order of the tree map suggests a possible evolutionary relationship among the folds.

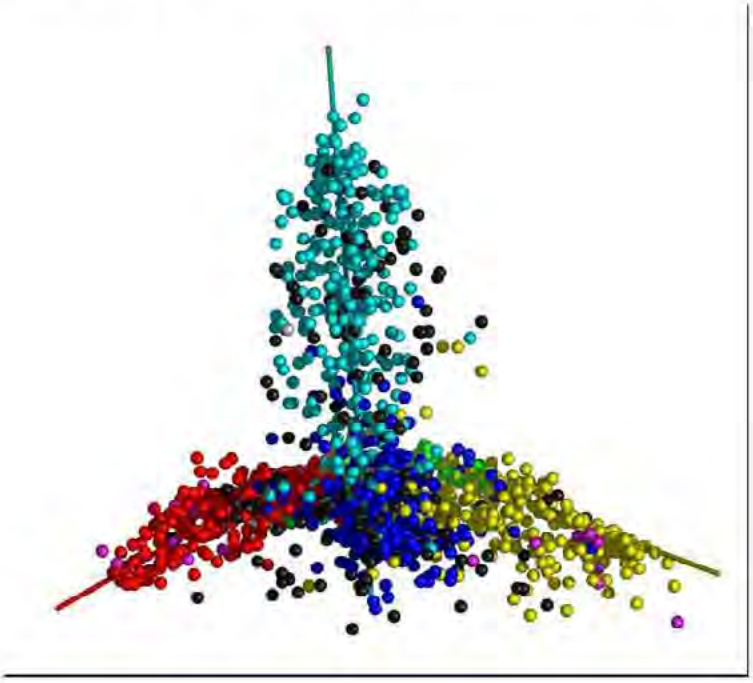

PL-2

Chirality in cystals

Reiko Kuroda

Department of Life Sciences, Graduate School of Arts and Sciences, The University of Tokyo, Komaba, Meguro-ku, Tokyo 153-8902, Japan
E-mail: ckuroda@mail.ecc.u-tokyo.ac.jp

Chirality is a fundamental aspect and is expressed throughout nature, whether microscopic or macroscopic, and whether animate or inanimate. We have been studying chirality at the molecular basis in both the biological and non-biological domains. In the non-biological world, which is the topic of this lecture, we have been investigating solid state chemistry, particularly that of crystals. Chiral discrimination, recognition, transfer and generation are realized strongly in the solid state and often only in that phase due to strong and fixed molecular interactions. The crystalline state has another advantage that we can make a direct use of structural information obtained by X-ray diffractometry. Thus, solid-state chiral chemistry provides rich science. Several of our latest results on solid-state chiral chemistry will be presented. For example, chiral or achiral molecules assemble to form chiral supramolecular crystals, which provide field for optical resolution or chirality transfer, the phenomena which cannot be achieved in solution. Thus, we could achieve extremely facile optical resolution of secondary alkyl alcohols [1], formation of crystals with unique stereochemistry by co-grinding of two or more kinds of crystals with or without annealing [2], and regio- and enantio-selective solid-state photoreactions.

CD spectra in the solid state often suffer from substantial artifact signals arising from the macroscopic anisotropy of samples which is intrinsic to the solid state such as linear birefringence (LB) and linear dichroism (LD), and their coupling with the non-ideal characteristics of the polarization-modulation instruments. Hence, they cannot, in general, be measured on commercially available instruments. Thus, we have developed UCS-1 (J-800KCM, UCS = Universal Chiroptical Spectrophotometer) which enables artifact-free solid-state CD, LD, LB and circular birefringence (CB) measurements [3], as well as UCS-2 (J-800KCMF) [4] and its upgraded version, UCS-3 [5], which can measure DR (diffuse reflectance) CD for in-situ measurements as well as transmittance CD of soft materials by holding samples on a horizontal sample stage. Using these, we could study aggregation process of peptides/proteins relevant to neurodegenerative diseases such as Alzheimer's [6] or Parkinson's diseases, chirality of inorganic and organic crystals consisting of achiral components etc. Further, we are currently developing an entirely new multichannel-CD (MC-CD) spectrophotometer that permits high-speed CD measurement without artifact contamination.

References

[1] Y. Imai, M. Takeshita, T. Sato and R. Kuroda, Chem. Comm., (2005), 3289-3291; Y. Imai, M. Takeshita, T. Sato and R. Kuroda, Chem. Comm., (2006), 1070-1072.
[2] R. Kuroda, Y. Imai and N. Tajima, Chem. Comm., (2002), 2848-2849; E. Y. Cheung, S. J. Kitchin, K. D.M. Harris, Y. Imai, N. Tajima., and R. Kuroda, J. Am. Chem. Soc., 125, 14658-14659 (2003); R. Kuroda,T. Sato, and S.Y. Imai, CrystEngComm, 10, (2008),1881-1890; Yoshida, S. Nishikiori and R. Kuroda, Chem. Eur. J., 14, (2008) 10570-10578; R. Kuroda, J. Yoshida, A. Nakamura and S. Nishikiori J, CrystEngComm, 11, (2009), 427-432.
[3] R. Kuroda, T. Harada and Y. Shindo, Review of Sci. Instruments, 72, (2001), 3802.
[4] T. Harada, H. Hayakawa, and R. Kuroda, ibid., 79, (2008), 073103.
[5] T. Harada, Y. Miyoshi and R. Kuroda, ibid., 80, (2009), 046101.
[6] T. Harada and R. Kuroda, Biopolymers, submitted.

KN-1

Structure and assembly of Sesbania mosaic virus

M.R.N. Murthy[1] and H.S. Savithri[2]

[1]*Molecular Biophysics Unit,* [2]*Dept of Biochemistry, Indian Institute of Science, Bangalore 560012, India*
E-mail: mrn@mbu.iisc.ernet.in

Sesbania mosaic virus (SeMV) is a ss-RNA (4149 nt) plant sobemovirus. SeMV capsids of diameter ~30 nm consist of 180 copies of a single species of protein (MW 29 kD) organized with icosahedral T=3 (Caspar and Klug, 1962) symmetry. The structure of the native virus has been determined (Bhuvaneswari et. al., 1995). In order to probe the mechanism of assembly of SeMV, a large number of deletion and substitution mutants of the coat protein (CP) were constructed. When expressed in *E. coli,* most of these CP mutants assembled into virus like particles (VLPs).

Structures of VLPs obtained with recombinant SeMV CP (rCP) as well as the rCP deletion mutant δN22 were similar to those of native particles. δN36 and δN65 formed mostly smaller (T=1, 60 subunits) particles. Particles of intermediate size were also observed with δN36. Calcium ions contribute to inter subunit interactions in the native virus particles and VLPs. Assembly of T=1 and T=3 particles was not affected by the substitution of D146 and D149 that coordinate calcium ions by asparagines. However, the stability of the resulting capsids was drastically reduced (Satheshkumar et. al., 2004).

A characteristic β-annulus structure present at the icosahedral 3-fold axes of the T=3 particles was believed to be essential for assembly. The structure of VLPs of rCP in which the residues forming the β-annulus were deleted was nearly identical to those of the native VLPs except for the absence of the β-annulus suggesting that the β-annulus is a consequence of assembly of CP into T=3 particles (Pappachan et. al, 2008). Mutation of a tryptophan close to the icosahedral five fold axis to glutamate or lysine disrupted assembly leading to the formation of soluble CP dimers (Pappachan et. al, 2009). The three dimensional structure of these dimers resembled the quasi-dimer structure of the native virus. Replacement of positively charged residues in the amino terminal segment of CP resulted in the formation of empty shells implicating the role of the N-terminal arginine rich motif in genomic RNA encapsidation.

Based on these observations, a plausible mechanism of SeMV assembly has been proposed (Savithri and Murthy, 2010). Evolution of the assembly pathway is being further probed by site mutations that might lead to domain swapping as observed in the structure of the homologous rice yellow mottle virus.

Reference

[1] Caspar, D.L.D. and Klug, A. (1962) Cold Spring Harbor Symp. Quant. Biol., 27, 1-24
[2] Bhuvaneshwari, M., Subramanya, K.Gopinath, K., Nayudu, Savithri, H.S. and Murthy, M.R.N. (1995), Structure, 3, 1021-1030.
[3] Pappachan, A., Subashchandrabose, C., Satheshkumar, P.S., Savithri, H.S. and Murthy, M.R.N. (2008), Virology, 375, 190-196
[4] Pappachan, A. Chinnatambi Subashchandrabose, Satheshkumar, P.S., Savithri, H.S. and Murthy, M.R.N. (2009), Virology, 392, 215-221.
[5] Satheshkumar, P.S., Lokesh, G.L, Sangita, V, Saravanan, V, Vijay, C.S, Murthy M.R.N., Savithri, H.S.(2004), J. Mol. Biol., 342, 1001-1014
[6] Savithri H. S. and Murthy M.R.N. (2010) Current Science, 98, 346-352

KN-2

Design and synthesis of porous metal-organic frameworks for gas storage and separation

Myunghyun Paik Suh and Hye Jeong Park

Department of Chemistry, Seoul National University, Seoul 151-747, Korea
E-mail: mpsuh@snu.ac.kr

Porous metal-organic frameworks (MOFs) have attracted great attention as new functional materials due to their high internal surface areas, tunable pore dimensions, and tailorable surface functionalities. In particular, hydrogen storage at the ambient temperature, carbon dioxide capture from the industrial flue gas, and O_2 separation from air have become highly important issues in the current scientific society, and MOFs are one of the best candidate materials for such applications.

We have prepared various MOFs from solvothermal reactions as well as room temperature self-assemblies. Depending on the design strategies, the MOFs show high H_2 storage capacities, O_2/N_2 separation capabilities, and highly selective CO_2 capture abilities. We could increase the hydrogen storage capacity by creating greater surface area, generating accessible metal sites, and embedding Pd nanoparticles in the channels.[1] We have offered highly selective CO_2 capture abilities in the MOFs by making them flexible so that their gates can open and close depending on the CO_2 pressure while not responding to other gases. [2] We have also modulate the gas sorption properties of a MOF by the post-synthetic insertion and removal of bridging linkers.[3] The MOFs for O_2/N_2 separation have been prepared by the modular pore size control.[4] Some MOFs show the single-crystal to single-crystal transformations in response to the external stimuli such as various activation methods, temperature change, and reversible incorporation of the bridging ligand, which will be also presented in the lecture.[1,3]

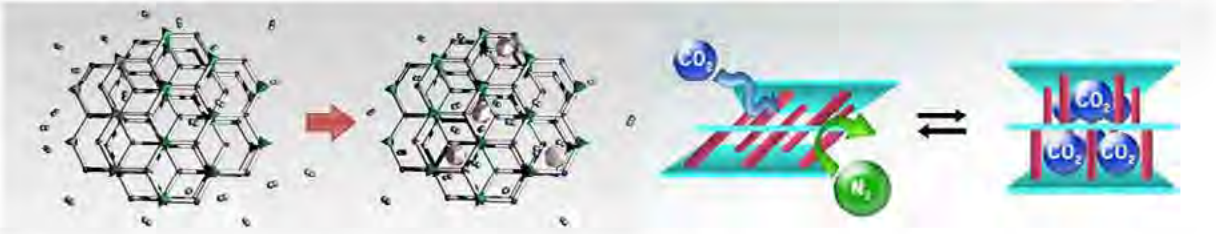

References

[1] (a) Cheon Y. E.; Suh M. P. *Angew. Chem. Int. Edit.* **2009**, *48*, 2899-2903. (b) Lee Y. G.; Moon H. R.; Cheon Y. E.; Suh M. P. *Angew. Chem. Int. Ed.* **2008**, *47*, 7741-7745. (c) Park H. J.; Suh M. P. *Chem. Eur. J.* **2008**, *14*, 8812-8821. (d) Park H. J.; Lim D. W.; Yang W. S.; Suh M. P. submitted.

[2] Choi H. S.; Suh M. P. *Angew. Chem. Int. Ed.* **2009**, *48*, 6865-6869.

[3] Park H. J.; Cheon Y. E.; Suh M. P. *Chem. Eur. J.* **2010**, in press.

[4] (a) Cheon Y. E.; Suh M. P. *Chem. Eur. J.* **2008**, 14, 3961-3967. (b) Cheon Y. E.; Suh M. P. *Chem. Commun.* **2009**, 17, 2296-2298. (c) Cheon Y E.; Park J. E.; Suh M. P. *Chem. Commun.* **2009**, 5436-5438.

KN-3

Structure and function of enzymes relevant in drug discovery

Andrew H.-J. Wang

Institute of Biological Chemistry, Academia Sinica, Taipei 115, Taiwan

Protein synchrotron crystallography is a powerful tool for drug discovery. Many important drug targets can be analyzed with relevant ligands (substrates, inhibitors) bound at the active site. In the lecture, I will discuss the following several enzymes and protein regulators that useful for antibiotics development.

Prenyltransferases are involved in many biological pathways; thus they are useful for developing new drugs for various diseases. We have studied several *trans*-type prenyltransferases, such as geranylgeranyl pyrophosphate synthase (GGPPS) complexed with several bisphosphonate inhibitors. In addition, dehydrosqualene synthase (CrtM) from *Staphylococcus aureus*, uses the head-to-head condensation of two molecules of farnesyl diphosphate (FPP) to produce the presqualene diphosphate C_{30} molecule, the precursor for of staphyloxanthin, the golden carotenoid pigment which promotes bacterial resistance to reactive oxygen species and host neutrophil-based killing. CrtM, therefore, has been tested as the target to treat infections by methicillin-resistant *S. aureus* (MRSA). We found squalene synthase inhibitors for cholesterol-lowering activity in humans bind to CrtM and block the biosynthesis of staphyloxanthin *in vitro*, resulting in colorless bacteria with increased susceptibility to killing by human blood and to innate immune clearance in a mouse infection model.

Another study related to MRSA is on TcaR and IcaR, a weak and a strong negative regulator of transcription of the *ica* locus, respectively, and their presence prevents the poly-N-acetylglucosamine production and biofilm formation in *S. aureus* and *S. epidermidis*. We solved the 3D structure of TcaR in its apo form and in complex with salicylate as well as several aminoglycoside and beta-lactam antibiotics. A comparison of the native and complex TcaR structures indicates that the mechanism of regulation involves a large conformational change in the DNA-binding lobe. The antimicrobial compounds we tested were shown not only to inhibit TcaR-DNA interaction but also to further induce biofilm formation in *S. epidermidis* in our in vivo assay. The results support a general mechanism for antibiotics in regulating TcaR-DNA interaction and thereby help understand the effect of antibiotic exposure on bacterial antibiotic resistance through biofilm formation.

KN-4

New functional materials via crystal- and nano-engineering

Wenbin Lin

Department of Chemistry, CB#3290, University of North Carolina at Chapel Hill, Chapel Hill, NC 27599, USA
E-mail: wlin@unc.edu

The chemistry of hybrid solids constructed from organic linkers and metal nodes has received much recent attention. The Lin group has explored the rational design of functional solids based on metal-organic frameworks (MOFs) over the past few years, with particular focuses on applying MOFs in nonlinear optics,[1] hydrogen storage,[2] biomedical imaging,[3] and drug delivery.[4] In this talk, I would like to discuss our recent success in the design and synthesis of chiral porous MOFs based on two complementary strategies.[5] In the first approach, the primary functional groups are linked by metal-connecting units to form extended networks whereas the orthogonal secondary chiral groups can then be used to generate asymmetric catalytic sites by postsynthetic modifications. Chiral Lewis acid catalysts with identical active sites and secondary environments are generated from the isoreticular mesoporous CMOFs via postsynthetic functionalization with $Ti(O^iPr)_4$, and are highly active for enantioselective diethylzinc and alkynylzinc additions to aromatic aldehydes to afford chiral secondary alcohols. The enantioselectivities of these reactions are highly dependent on the channel sizes of the isoreticular CMOFs, owing to different diffusion rates for the organic substrates.[5] In the second approach, the primary functional groups are used to generate robust transition metal precatalysts which are then linked by the metal nodes to form porous extended networks via the secondary functional groups. These chiral porous solids have been used for highly enantioselective reduction of unsaturated substrates such as ketones and ketoesters as well as oxidation reactions of alkenes.

I would also like to discuss our recent efforts in downsizing the MOFs to the nano-regime and to explore the applications of nanoscale metal-organic frameworks (NMOFs) in biomedical imaging and drug delivery. Imaging modalities such as magnetic resonance imaging (MRI), X-ray computed tomography (CT), and optical imaging (OI) require efficient contrast enhancement agents that can be selectively and specifically delivered to the diseased cells in vivo. We have synthesized a range of NMOFs that are highly luminescent with tunable emission wavelength and exhibit extraordinarily large relaxivities for magnetic resonance imaging. Preliminary results of in vitro and in vivo optical, MR, and CT imaging and anti-cancer drug delivery with cancer cells and tumor xenograft mouse models will be presented.

References

[1] Evans, O.R.; Lin, W. Acc. Chem. Res. 2002, 35, 511-522.
[2] Kesanli, B.; Cui, Y.; Smith, M.; Bittner, E.; Bockrath, B.; Lin, W. Angew. Chem. Int. Ed. 2005, 44, 72-75.
[3] Lin, W.; Rieter, W.L.; Taylor, K.M.L. Angew. Chem. Int. Ed. 2009, 48, 650-658.
[4] Huxford, R.C.; Della Rocca, J.; Lin, W. Curr. Opinion Chem. Biol. 2010, 14, 262-268.
[5] Ma, L.; Abney, C.; Lin, W. Chem Soc. Rev. 2009, 38, 1248-1256.
[6] Ma, L.; Falkowski, J.M.; Abney, C.; Lin, W. Nature Chem. in press.

AsCA2010

The 10th Conference of the Asian Crystallographic Association

ABSTRACTS

November 1, (Monday)

Morning Oral Sessions (MS01, 02, 03)
Afternoon Oral Sessions (MS04, 05, 06)

MS01-O1

Structure of the torque ring of the flagellar motor and the molecular basis for rotational switching

Daniela Stock[1], Lawrence K. Lee[1], Michael A. Ginsburg[1], Claudia Crovace[2] and Mhairi Donohoe[1]

[1]*Structural and Computational Biology Division, Victor Chang Cardiac Research Institute, 405 Liverpool St, Darlinghurst NSW 2010, Australia*
[2]*MRC Laboratory of Molecular Biology, Hills Road, Cambridge CB2 2QH, UK*
E-mail: d.stock@victorchang.edu.au

The bacterial flagellar motor is one of the most efficient rotary motors known to man. It rotates at hundreds of revolutions per second, yet can reverse its direction in less than one millisecond [1,2]. Both of these attributes facilitate the rapid movement of bacteria towards favourable environments. The motor uses the potential energy from an electrochemical gradient of anions [3,4] across the cytoplasmic membrane to generate torque. A rapid switch from counterclockwise to clockwise rotation determines whether a bacterium runs smoothly forward or tumbles to change its trajectory [5,6]. A protein called FliG forms a ring in the rotor of the flagellar motor that is involved in the generation of torque [7,8] through an interaction with the anion channel forming stator subunit MotA [9]. FliG has been suggested to adopt distinct conformations that induce switching but these structural changes and the molecular mechanism of switching are unknown. Here we report the molecular structure of the full-length FliG protein from Aquifex aeolicus [10], identify conformational changes that are involved in rotational switching and uncover the structural basis for the formation of the FliG torque ring. This allows us to propose a model of the complete ring and switching mechanism in which conformational changes in FliG reverse the electrostatic charges involved in torque generation.

References

[1] Berg, H. C., and Anderson, R. A., "Bacteria swim by rotating their flagellar filaments", Nature 245, (1973), pp 380–382.
[2] Magariyama, Y. et al., "Very fast flagellar rotation", Nature 371, (1994), p 752.
[3] Manson, M. D., Tedesco, P., Berg, H. C., Harold, F. M., and Van der Drift, C., "A protonmotive force drives bacterial flagella", Proc. Natl Acad. Sci. USA 74, (1977), pp 3060–3064.
[4] Hirota, N., and Imae, Y., "Na+-driven flagellar motors of an alkalophilic Bacillus strain YN-1", J. Biol. Chem. 258, (1983), pp 10577–10581.
[5] Berg, H. C., and Brown, D. A., "Chemotaxis in Escherichia coli analysed by three-dimensional tracking", Nature 239, (1972), pp 500–504.
[6] Turner, L., Ryu, W. S., and Berg, H. C., "Real-time imaging of fluorescent flagellar filaments", J. Bacteriol. 182, (2000), pp 2793–2801.
[7] Irikura, V. M., Kihara, M., Yamaguchi, S., Sockett, H., and Macnab, R. M., "Salmonella typhimurium fliG and fliN mutations causing defects in assembly, rotation, and switching of the flagellar motor", J. Bacteriol. 175, (1993), pp 802–810.
[8] Lloyd, S. A., and Blair, D. F., "Charged residues of the rotor protein FliG essential for torque generation in the flagellar motor of Escherichia coli", J. Mol. Biol. 266, (1997), pp 733–744.
[9] Zhou, J., Lloyd, S. A., and Blair, D. F., "Electrostatic interactions between rotor and stator in the bacterial flagellar motor", Proc. Natl Acad. Sci. USA 95, (1998), pp 6436–644.
[10] Lee, K. L., Ginsburg, M. A., Crovace, C., Donohoe, M., and Stock, D., "The structure of the torque ring of the flagellar motor and the molecular basis for rotational switching." Nature, accepted June 21, 2010.

MS01-O2

Structure of membrane proteins in drug discovery

Che Ma

Genomics Research Center, Academia Sinica, Taipei 115, Taiwan
E-mail: cma@gate.sinica.edu.tw

Membrane proteins are important drug targets and they represent 20-30% of all open-reading frames encoded in genomes. The approach using structural studies in combination with chemical biology methods will be presented, including two topics in infectious diseases. First, in order to overcome the problems of drug-resistant bacterial infection, a new enzyme target for antibiotic development, the membrane-bound bifunctional transglycosylase, has been chosen for structural and functional analysis. We have recently determined the X-ray crystal structure of this membrane-bound enzyme in complex with its inhibitor moenomycin, and studied its mechanism of peptidoglycan synthesis. In addition, a high-throughput screening method for finding new antibiotics has been developed using the purified full-length membrane protein. Structure-based drug design with our crystal structure is ongoing. Second, we have studied the effect of glycosylation on influenza virus major membrane glycoprotein hemagglutinin (HA) with regards to its role in receptor binding and immune response, and developed a new strategy for molecular vaccine design.

References

[1] Sung M.-T., Lai Y.-T., Huang C.-Y., Chou L.-Y., Shih H.-W., Cheng W.-C., Wong C.-H. and Ma C., "Crystal structure of the membrane-bound bifunctional transglycosylase PBP1b from Escherichia coli", Proc. Natl. Acad. Sci. U. S. A. 106, (2009), pp 8824-8829.

[2] Wang C.-C., Chen J.-R., Tseng Y.-C., Hsu C.-H., Hung Y.-F., Chen S.-W., Chen C.-M., Khoo K.-H., Cheng T.-J., Cheng Y.-S. E., Jan J.-T., Wu C.-Y., Ma C. and Wong C.-H., "Glycans on influenza hemagglutinin affect receptor binding and immune response", Proc. Natl. Acad. Sci. U. S. A. 106, (2009), pp 18137-18142.

MS01-O3

The molecular mechanism of the ferrous iron transporter, FeoB

Megan J. Maher[1], Miriam-Rose Ash[2], Amy Guilfoyle[1], Ronald J. Clarke[3], J. Mitchell Guss[2] and Mika Jormakka[1].

[1]*Centenary Institute, Locked Bag No 6, Newtown, NSW 2042, Australia*
[2]*School of Molecular Bioscience, University of Sydney, Sydney, NSW 2006, Australia*
[3]*School of Chemistry, University of Sydney, Sydney NSW, 2006, Australia*
E-mail: m.maher@centenary.org.au

Iron is an essential element for all living organisms, where it constitutes the active cofactor of many proteins and enzymes. Conversely, free forms of the metal are toxic even at very low concentrations. For bacteria, which grow in acidic, anaerobic environments, ferrous iron is the preferred form for iron uptake due to its solubility. The major route for bacterial ferrous iron uptake is through the integral membrane protein FeoB. In fact, FeoB has been found to be a major virulence factor in bacteria such as *Helicobacter pylori* (causative agent of gastric ulceration) and *Campylobacter jejuni* (gastroenteritis) and so is a potential target for the design of antibacterial lead compounds [1,2].

FeoB is unique amongst metal transport proteins, in that it contains a cytoplasmic G protein directly tethered to a polytopic membrane domain. GTP binding to the G protein domain (NFeoB) initiates the transport of Fe^{2+} across the membrane, which is halted by the hydrolysis of GTP to GDP. Previous studies have shown that NFeoB has slow GTPase activity (*E. coli* $k_{cat} = 0.0015\ s^{-1}$, equivalent to the hydrolysis of one GTP molecule in 11 minutes) [3,4]. This slow intrinsic hydrolysis rate is somewhat puzzling, being too slow to support an active Fe^{2+} transport mechanism. It is also too slow for FeoB to function as a G protein coupled channel.

Here, we will present our recent structural and functional work on FeoB, including results on the activation of the soluble domain of FeoB by potassium ions and the role of structural motifs such as the Switch I and G5 loops in the GTPase activity of FeoB [5,6].

References

[1] Velayudhan J., Hughes N. J., McColm A. A., Bagshaw J., Clayton C. L., Andrews S. C. and Kelly D. J. (2000) Mol. Microbiol., 37, 274-86.
[2] Naikare H., Palyada K., Panciera R., Marlow D. and Stintzi A. (2006) Infect. Immun., 74, 5433-44.
[3] Marlovits T. C., Haase W., Herrmann C., Aller S. G. and Unger V. M. (2002) Proc. Nat. Acad. Sci., 99, 16243-48.
[4] Eng E. T., Jalilian A. R., Spasov K. A. and Unger V. M. (2008) J. Mol. Biol., 375, 1086-97.
[5] Guilfoyle A., Maher M. J., Rapp M., Clarke R., Harrop S. and Jormakka M. (2009) EMBO J., 28, 2677-85.
[6] Ash M. R., Guilfoyle A., Clarke R. J., Guss J. M., Maher M. J. and Jormakka M. (2010) J. Biol. Chem., 285, 14594.

MS01-O4

HKL-3000 - Toward the future of structural biology

Wladek Minor[1], Marcin Cymborowski[1], Maksymilian Chruszcz[1], Zbyszek Otwinowski[2], and Dominika Borek[2]

[1]*Department of Molecular Physiology and Biological Physics, University of Virginia, Charlottesville, VA 22908, USA*
[2]*Department of Biochemistry, University of Texas, Southwestern Medical Center at Dallas, 5323 Harry Hines Boulevard, Dallas, TX 75390, USA*
E-mail: wladek@iwonka.med.virginia.edu

HKL-3000 integrates data collection, data reduction, phasing, and model building to significantly accelerate the process of structure determination, and on average, minimize the number of data sets and crystals required for structure solution. Upon execution, the package merges several modules and software applications into the structure determination pipeline. There are modules for experimental control of some beamlines and laboratory instruments, data reduction, phasing by SAD/MAD or molecular replacement, fast model building, and initial refinement. The system is being developed and tested in the high-throughput environments of the Midwest Center for Structural Genomics (MCSG), the Center for Structural Genomics of Infectious Diseases (CSGID), the New York Structural Genomics Consortium (NYSGRC) and the Enzyme Function Initiative (EFI). The robustness of HKL-3000 has improved considerably over time and currently over 1400 structures deposited in the PDB have been determined with it.

Continuous advancement of the decision-making procedures within HKL-3000 has made it the system of choice for SG projects. Transforming raw images into a solved structure (with 70% of the model built) in 10-15 minutes is no longer a surprise, but a routine operation for crystals that diffract to 2.5 Å or better. Our experience with the determination of hundreds of structures by experimental phasing methods helped us to establish rules for the best approaches when the available data fall into three categories: unsolvable with current data, borderline and straightforward. Current work concentrates on improving the approach to borderline cases of structure determination rather than optimizing intermediate calculations for straightforward cases, thus shifting borderline cases into the "easy" category and unsolvable into borderline.

An important implication is that simple experimental protocols are sufficient in most cases and may even be optimal for the most challenging ones. Feedback from fast preliminary structure solution has proven to be one of the critical components of success.

References

[1] Minor W, Cymborowski M, Otwinowski Z, Chruszcz M (2006) Acta Crystallographica Section D: Biological Crystallography 62: 859-66.
[2] Kirillova O, Chruszcz M, Shumilin IA, Skarina T, Gorodichtchenskaia E, Cymborowski M, Savchenko A, Edwards A, Minor W (2007) Acta Crystallographica Section D: Biological Crystallography 63: 348-54.
[3] Otwinowski Z, Borek D, Majewski W, Minor W (2003) Acta Crystallographica. Section A: Foundations of Crystallography 59: 228-34.
[4] Zheng H, Chruszcz M, Lasota P, Lebioda L, Minor W (2008) Journal of Inorganic Biochemistry 102(9): 1765-76.
[5] Chruszcz M, Wlodawer A, Minor W (2008) Biophysical Journal 95(1): 1-9.
[6] Wlodawer A, Minor W, Dauter Z, Jaskolski M (2008) Febs Journal 275: 1-21.
[7] Otwinowski Z, Minor W (1997) Methods in Enzymology 275: 307-326.

MS02-O1

Design and synthesis of highly porous Metal-Organic Frameworks

Jaheon Kim

Department of Chemistry, Soongsil University, Seoul 156-743, Korea
E-mail: jaheon@ssu.ac.kr

Porous metal-organic frameworks (MOFs) are crystalline materials, and therefore have regular pores and framework structures. As the framework surfaces of MOFs are almost exposed to pores, they have usually much larger surface areas than zeolites. MOFs can have exceptionally large Langmuir surface areas exceeding 5000 m^2/g. This is one of the most important properties of MOFs, which has led to many applications concerned with gas storage, separations, and catalysis. The simplest way to accomplish large surface areas is to use expanded organic linkers. However, this approach often yields fragile frameworks under reduced pressure, or self-interpenetration of frameworks with reduced porosity. In this talk, the synthesis of very porous MOFs will be presented with examples of MOFs prepared by design. Although the design has not worked perfectly, it was finally possible to obtain MOF-201 that has the largest surface area among porous solids until now.

MS02-O2

Crystal interface functionalization of porous coordination polymers

Shuhei Furukawa[1],[2]

[1]*Institute for Integrated Cell-Material Sciences, Kyoto University, Yoshida, Sakyo-ku, Kyoto 606-8501, Japan*
[2]*ERATO Kitagawa Integrated Pores Project, Japan Science and Technology Agency (JST), Kyoto Research Park Bldg #3, Shimogyo-ku, Kyoto 600-8815, Japan*
E-mail: shuhei.furukawa@kip.jst.go.jp

Porous coordination polymers (PCPs), assembled by metal ions and organic bridging ligands, are an intriguing class of crystalline porous materials, as it is possible to design their framework topologies and pore sizes and the functionality of the pore surfaces. On the other hand, functionalization of PCP other surfaces (crystal surfaces) is a great challenge, but it is a promising methodology not only for modification of the porous properties but also for the addition of a new function to the PCP without changing the characteristic features of the PCP crystal itself, resulting in the fabrication of multifunctional PCPs.

The relatively weak interactions of coordination bonds that dominate the construction of PCPs are also useful to modify the surfaces of PCPs or hybridize PCPs with other materials. This is because that the crystal surfaces once in solution will be extremely sensitive to the coordination equilibrium, whereby the organic ligand and solvent molecules compete to terminate the surfaces by coordination bonds. When appropriate postsynthetic reaction media have been found, that is, the crystals do not degrade and the reactivity of the crystal surfaces is preserved, the use of the coordination equilibrium then allows specific and selective functionalization of the surfaces by desirable organic molecules or bridging ligands.

One way to decorate the crystal surfaces of a PCP is to hybridize the core PCP crystal with a different shell crystal by epitaxial growth at the single-crystal level, thus creating core-shell PCP heteroepitaxial crystals [1,2]. Such a lattice match promises pore connections at the interface between crystals. We demonstrated the synthesis of hybridized PCP single crystals by taking the advantage of coordination equilibrium at the crystal interfaces and determined the structural relationship between the shell and the core by using surface X-ray diffraction analysis. Whereas the epitaxial growth of the shell crystal requires the careful choice of bridging ligands to laterally match the lattice distances at the interfaces, the ultimate thinning of the shell layer on the core PCP crystal, and thus the formation of a monolayer gives the free-usage of functional organic molecules [3]. Thanks to the coordination equilibrium at the crystal interface, we succeeded in the fabrication of functional organic monolayers on the crystal surface and the characterization by microscopic techniques.

References

[1] Furukawa S., Hirai K., Nakagawa K., Takashima Y., Matsuda R., Tsuruoka T., Kondo M., Haruki R., Tanaka D., Sakamoto H., Shimomura S., Sakata O. and Kitagawa S., "Heterogeneously hybridized porous coordination polymer crystals: Fabrication of heterometallic core-shell single crystals with an in-plane rotational epitaxial relationship", Angew. Chem. Int. Ed., 48, (2009), 1766-1770.

[2] Furukawa S., Hirai K., Takashima Y., Nakagawa K., Kondo M., Tsuruoka T., Sakata O. and Kitagawa S., "A block PCP crystal: anisotropic hybridization of porous coordination polymers by face-selective epitaxial growth", Chem. Commun., (2009), 5097-5099.

[3] Kondo M., Furukawa S., Hirai K. and Kitagawa S., "Coordinatively immobilized monolayers on porous coordination polymer crystals", Angew. Chem. Int. Ed., 49, (2010), in press.

MS02-O3

Metal-mediated in-situ ligand synthesis and application in construction of functional Metal-Organic Frameworks

Ming-Liang Tong

Key Laboratory of Bioinorganic and Synthetic Chemistry of Ministry of Education, School of Chemistry and Chemical Engineering, Sun Yat-Sen University, Guangzhou 510275, China
E-mail: tongml@mail.sysu.edu.cn

Hydro(solvo)thermal in-situ ligand reactions have been proved to be a newly created bridge between coordination chemistry and synthetic organic chemistry.[1] The interest in solvothermal metal/ligand reactions has been concerned with the discovery of new ligand reactions and their application in the crystal engineering of functional metal-coordination frameworks (MOFs) together with many interesting phenomena. In this lecture we will outline our recent progress in metal-mediated in-situ ligand synthesis and application in construction of functional MOFs. We have developed some in situ ligand syntheses including transition metal-mediated ligand oxidative coupling, hydrolysis, substitution and alkylation, in-situ cleavage of S-S and S-C(sp^2) bonds and re-arrangement reactions as well as stepwise oxidation of 2,3,5- and 2,4,6-trimethylpyridine to pyridinecarboxylates towards construction of novel metal-organic framework materials.[2,3]

References

[1] Chen, X.-M.; Tong, M.-L. Acc. Chem. Res., 2007, 40, 162.

[2] Hu, S.; Chen, J.-C.; Tong, M.-L.; Wang, B.; Yan, Y.-X.; Batten, S. R. Angew. Chem. Int. Ed. 2005, 44, 5471. Hao, H.-Q.; Lin, Z.-J.; Hu, S.; Liu, W.-T.; Zheng, Y.-Z.; Tong, M.-L. CrystCommEng 2010, 12, 2225. Hu, S.; Meng, Z.-S.; Tong, M.-L. Cryst. Growth Des. 2010, 10, 1742. Hu, S.; Zhang, Z.-M.; Meng, Z.-S.; Lin, Z.; Tong, M.-L. CrystEngComm, 2010, 12, in press.

[3] Wang, J.; Zheng, S.-L.; Hu, S.; Zhang, Y.-H.; Tong, M.-L. Inorg. Chem. 2007, 46, 795. Li, C.-J.; Lin, Z.; Yun, L.; Xie, Y.-L.; Leng, J.-D.; Ou, Y.-C.; Tong, M.-L. CrystEngComm 2010, 12, 425. Wang, J.; Lin, Z.-J.; Ou, Y.-C.; Shen Y.; Herchel, R.; Tong, M.-L. Chem. Eur. J. 2008, 14, 7218. Wang, J.; Zhang, Y.-H.; Tong, M.-L. Chem. Commun. 2006, 3166. Zheng, Y.-Z.; Zhang, Y.-B.; Tong, M.-L.; Xue, W.; Chen, X.-M. Dalton Trans. 2009, 1396. Wang, J.; Zhang, Y.-H.; Li, H.-X.; Lin, Z.-J.; Tong, M.-L. Cryst. Growth Des. 2007, 7, 2352. Wang, J.; Ou, Y.-C.; Shen Y.; Yun, L.; Leng, J.-D.; Lin, Z.-J.; Tong, M.-L. Cryst. Growth Des. 2009, 9, 2442. Liu, W.-T.; Ou, Y.-C.; Xie, Y.-L.; Lin, Z.; Tong, M.-L. Eur. J. Inorg. Chem. 2009, 4213. Zheng, L.-L.; Li, H.-X.; Leng, J.-D.; Wang, J.; Tong, M.-L. Eur. J. Inorg. Chem. 2008, 213. Zhang, Y.-H.; Wang, J.; Zheng, L.-L.; Hu, S.; Lin, Z.; Tong, M.-L. Chinese Sci. Bull. 2009, 54, 4277. Miao, Y.-L.; Liu, J.-L.; Lin, Z.; Ou, Y.-C.; Leng, J.-D.; Tong, M.-L. Dalton Trans. 2010, 39, 4893. Bao, X.; Liu, J.-L.; Leng, J.-D.; Lin, Z.; Tong, M.-L.; Nihei, M.; Oshio, H. Chem. Eur. J., 2010, 16, 7973.

MS02-O4

Synthesis and crystal structure of a new cadmium metal-organic coordination polymer

Masoumeh Tabatabaee,[1*] Elham Zare[1], Mitra Ghassemzadeh[2], Bernhard Neumüller[3]

[1]*Department of Chemistry, Islamic Azad University Yazd Branch, Yazd, Iran*
[2]*Chemistry & Chemical Engineering Research Center of Iran, Tehran, Iran*
[3]*Fachbereich Chemie, Universität Marburg, Marburg, Germany*
E-mail: tabatabaee45m@yahoo.com

An especially active research area in recent years has involved the preparation of metal–organic coordination polymers due to their tunable properties and functions. These compounds have been applied in many fields, such as molecular recognition, adsorption and separation processes, catalysis, ion exchange and molecular magnet [1]. The design and synthesis of novel coordination architectures controlled by varying the reaction conditions (including temperature, metal-to-ligand ratio, pH value, solvents, and counter anions) are of great interest in coordination chemistry [2]. In continuation of our recent works on selecting suitable multidentate organic ligands or mixed ligands under appropriate conditions to prepare novel metal–organic hybrids[3], in this communication we wish to report our results on the synthesis and characterization of the first two-dimensional Cd^{II} coordination polymer with bridging 2- aminopyrimidine and cyanide ligands. Reaction of $Cd(CH_3COO)_2$, 2-aminopyrimidine and potassium cyanide (molar ratio 1: 1:1) in C_2H_5OH/H_2O led to formation of $\{[Cd_4(C_4H_5N_3)_4(OAc)_4(CN)_4(OH_2)_2]\ .2H_2O\}$. Compound has been IR spectroscopy and X-ray diffraction studies. As shown if Fig. 1 every Cd^{II} stom is six coordinated, Cd1 ion is coordinated with two heterocyclic nitrogen atoms of two bridged 2- aminopyrimidine ligands, two nitrogen atoms from bridged CN^- ions, one oxygen atom from OAC ion and on O atom from coordinated water molecules.Cd2 is coordinated with two heterocyclic nitrogen atoms of two bridged 2- aminopyrimidine ligands, two carbon atoms from bridged CN^- ions and two oxygen of bidentate carboxylate ion.

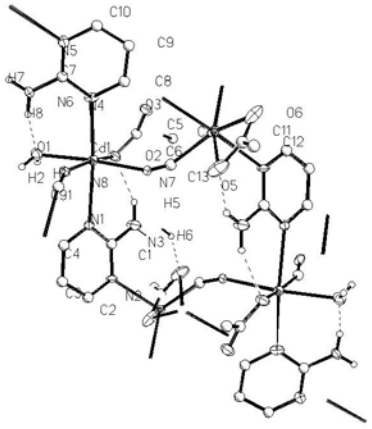

Fig. 1 Molecular structure of Cd complex

References

[1] [1] X. Lin C. Yun-Xia Z. Ji-Min, Chinese J. Struct. Chem. 2006, 25, 1250,
[2] 2 Y. Wen, J. Cheng Y. Feng, J. Zhang, Z. Li, Y. Yao, Inorg. Chim.a Acta , 2005, 358 2005, 3347.
[3] 3Tabatabaee, M., Sharif, M. A., Vakili F. & Saheli S. J. Rare. Earth., 2009, 27, 356.

MS02-O5

Rapid crystal growth of two metal-organic frameworks constructed by linking of 1-D coordination polymers by hydrogen bonding

Apinpus Rujiwatra[1], Bunlawee Yotnoi[1] and Timothy J. Prior[2]

[1]*Department of Chemistry, Faculty of Science, Chiang Mai University, Chiang Mai 50200, Thailand*
[2]*Department of Chemistry, University of Hull, Kingston Upon Hull, HU6 7RX, UK*
E-mail: apinpus@gmail.com

Two extended solids displaying both one-dimensional coordination polymer and two-dimensional hydrogen-bonded structural features has been prepared under microwave-assisted hydrothermal conditions. $[Co(H_2O)_4(4,4'\text{-bipyridine})](4,4'\text{-bipyridine}H_2).2(SO_4).2H_2O$ (**1**) crystallises in the centrosymmetric space group $P2_1/n$ with unit cell parameters a = 9.4120(18) Å, b = 13.0143(13) Å, c = 22.155(3) Å, β = 97.943(13) ° and unit cell volume 2687.8(7) Å^3. One dimensional coordination polymer chains of composition Co(4,4'-bipyridine)$(H_2O)_4$ are linked into a three dimensional framework by hydrogen bonding through uncoordinated sulfate and water. Within this framework is located a twice protonated 4,4'-bipyridine molecule ($C_{10}N_2H_{10}^{2+}$) which forms two short N-H···O hydrogen bonds and eight further non-classical C-H···O interactions. The close approach of guest and framework and the large number of interactions between them suggest the cation is important in templating this phase.

Co(4,4'-bipyridine)$(SO_4)(H_2O)_5$ (**2**) crystallises in the centric space group $P2_1/c$ with a = 7.4347(5) Å, b = 40.573(4) Å, c = 11.4833(8)Å, β = 117.405(5) ° and unit cell volume 3075.2(4) Å^3 and is considerably denser than **1**. It contains one dimensional chains of cobalt-bipyridine which are sinusoidal in nature. Two sets of these chains run parallel to the crystallographic $[212]$ and $[\bar{2}1\bar{2}]$ directions. Two dimensional hydrogen-bonded sheets parallel to the *xz* plane link these; further hydrogen bonds to uncoordinated water help to form a three dimensional honeycomb network with the centroids of the six-membered rings aligned parallel to the *a*-axis.

References

[1] Luachan S., Pakawatchai C and Rujiwatra A., Hydrothermal crystal growth, structures and thermal properties of Co(II)-4,4'-bipyridine-based coordination polymeric materials, J. Inorg. Organomet. Polym. Mater., vol. 17, (2001), pp 561-568.

[2] Steiner T and Desiraju G.R., Distinction between the weak hydrogen bond and the van der Waals interaction, Chem. Commun., vol. 8, (1998), pp 891-892.

MS03-O1

The SPring-8 high-brilliant beamlines for macromolecular crystallography

Masaki Yamamoto[1], Kunio Hirata[1], Yoshiaki Kawano[1], Kouichi Hashimoto[1], Hironori Murakami[1], Takaaki Hikima[1], Go Ueno[1], Masatomo Makino[2], Kazuya Hasegawa[2], Nobutaka Shimizu[1,2] and Takashi Kumasaka[1,2]

[1]*RIKEN SPring-8 Center, 1-1-1 Kouto, Sayo, Hyogo 679-5148, Japan*
[2]*JASRI/SPring-8, 1-1-1 Kouto, Sayo, Hyogo 679-5198, Japan*
E-mail: yamamoto@riken.jp

For the third generation synchrotron radiation, macromolecular crystallography is one of the major subjects in the past decade. At SPring-8, eight beamlines in total are dedicated for macromolecular crystallography. Each beamline is improving to meet broad requests from beamline users and to develop new applications for enhancing each characteristic property. We have been developing the beamlines with the view of two objectives. One is the high-quality data collection from small crystals and weakly-diffracting crystals, and the other is the high throughput data collection.

As the brightest beamline, BL41XU[1] equipping an in-vacuum undulator and a K/B mirror is dedicated to obtain high-quality data even from small crystals and weakly-diffracting crystals. To adapt to small crystals, the minimum beam size at sample position is achieved to 10×10 μm^2 using a pin-hole collimator. Its photon flux and flux density at 1 Å are 2.8×10^{11} photons/sec and 2.5×10^9 photons/sec/μm^2, respectively. This small beam coupled with irradiation point scanning method available with our data collection software BSS[2] is quite useful to take diffraction dataset from small crystals with suppressing the radiation damage by the brilliant beam.
A new undulator beamline dedicated for protein micro-crystallography, named RIKEN Targeted Proteins Beamline (BL32XU), has been constructed and has started the user operation from May 2010. In order to realize the protein micro-crystallography, we have developed the beamline optics and data collection system to acquire high S/N data even from weak diffractions and have designed the beamline to provide the focused beam size of 1 μm^2. An in-vacuum undulator and a K/B mirror fabricated with Elastic Emission Machinery technique[3] are equipped as the light source and the micro-focusing optics, respectively. The beamline has achieved the minimum beam size at sample position of 0.9×0.9 μm^2 with 7.6×10^{10} photons/sec/μm^2. The beam size can be changed up to the maximum size of 19 x 7 μm^2 according to the size of sample crystals or experimental condition.

At end station, R&D for indispensable components to achieve protein micro-crystallography with micro-beam, such as high-precision diffractometer, laser tweezers system for micro-crystal handling and so on, are progressing. Support of real-time damage monitoring system for radiation sensitive micro-crystals is also being planned. We will present here the present status and the future prospects of the high-quality data collection at SPring-8. BL32XU project was supported by Targeted Proteins Research Program from the Ministry of Education, Science and Culture (MEXT) of Japan.

References

[1] Kawamoto, M., et al., "SPring-8 Structural Biology Beamlines", AIP Conf. Proc. 879, 1920-1923 (2007).
[2] Ueno, G. et al., "Beamline Scheduling Software: administration software for automatic operation of the RIKEN structural genomics beamlines at SPring-8", J. Synchrotron Rad. 12, 380-384 (2005).
[3] Mimura H. et.al, "Hard x-ray diffraction-limited nanofocusing with Kirkpatrick–Baez mirrors" Jpn. J. Appl. Phys. 44, L539-L542 (2005).

Laue diffraction from spin-polarised protons: a new tool for neutron protein crystallography?

Garry J. McIntyre[1,*], Maths Karlsson[2], Florian Piegsa[1], Ben van den Brandt[3], Patrick Hautle[3], Ton Konter[3], Oliver Zimmer[1], Edward M. Forgan[4] and Colin J. Carlile[2]

[1]*Institut Laue-Langevin, BP 156, F-38042 Grenoble Cedex 9, France*
[2]*The European Spallation Source, Lund University, P.O. 117, S-22100 Lund, Sweden*
[3]*Paul Scherrer Institute, CH-5232 Villigen PSI, Switzerland*
[4]*School of Physics and Astronomy, University of Birmingham, Birmingham B15 2TT, UK*
E-mail: mcintyre@ill.fr

Neutron diffraction on samples with large hydrogen content, e.g. on large organic and protein samples, generally suffers from a strong featureless background due to strong incoherent scattering from the protons. This is particularly evident in the two-dimensional projection of Laue diffraction, a technique which is otherwise undergoing a renaissance thanks to the development of large-solid-angle image-plate detectors, notably on LADI [1] and VIVALDI [2] at the ILL, and most recently on KOALA [3] at the OPAL reactor at ANSTO. Despite the strong incoherent background, the larger coherent neutron scattering length of hydrogen relative to other elements compared with the situation in X-ray diffraction more readily yields answers to specific questions on, e.g. protonation states, hydrogen positions, and dynamic disorder of hydrogen. Deuteration can be used to reduce the incoherent background, but sample growth may be difficult or even impossible, and there may be an isotopic difference between the deuterated and non-deuterated structures. An intriguing alternative is parallel polarisation of the incident neutron beam and the nuclear spins of the hydrogen atoms [4].

We have performed a proof-of-principle polarised-neutron Laue diffraction experiment on a spin-polarised single crystal of Nd-doped lanthanum magnesium nitrate hydrate, $La_2Mg_3(NO_3)_{12}.24H_2O$. The experiment was carried out on the FUNSPIN beam line [5] at the continuous spallation neutron source SINQ (PSI) with the proton spins aligned by dynamic nuclear polarisation. It demonstrates that not only is the incoherent background indeed reduced but also that the intensity of the Laue reflections can be enhanced or diminished significantly to give a form of contrast variation. In the longer term, we foresee that the technique can be employed to improve substantially the poor signal-to-noise ratio in neutron Laue diffraction experiments on biological crystals.

Reference

[1] Blakeley M.P. "Neutron macromolecular crystallography", *Crystallography Reviews*, Vol. 15, No. 3, (2009), pp 157-218.
[2] McIntyre G.J., Lemée-Cailleau M.-H. and Wilkinson C. "High-speed neutron Laue diffraction comes of age", *Physica B* Vol. 385-386 (2006), pp 1055-1058.
[3] Sharma N., Soehnel T., McIntyre G.J., Piltz R.O. and Ling C.D. "Structure of $BiRe_2O_6$ re-investigated using single-crystal neutron Laue diffraction", *Journal of Physics: Conference Series*, In press.
[4] Hayter J.B., Jenkin G.T. and White J.W. "Polarized-neutron diffraction from spin-polarised protons: A tool in structure determination?" *Phys. Rev. Lett.* Vol. 33, No. 12, (1974) 696-699.
[5] Zejma J., Ban G., Beck M., Bialek A., Bodek K., Frei G., Hilbes C., Kühne G., Gorel P., Kirch K., Kistryn S., Kozela A., Kuzniak M., Lindroth A., Naviliat-Cuncic O., Pulut J., Severijns N., Stephan E. "FUNSPIN polarized cold-neutron beam at PSI", *Nucl. Instr. and Meth. A* Vol. 539 (2005) 622-639.

* Present address: *Bragg Institute, Australian Nuclear and Science Technology Organisation, Locked Bag 2001, Kirrawwee DC NSW 2232, Australia*

The current status of versatile neutron diffractometer iMATERIA at J-PARC (II)

Toru Ishigaki[1], Akinori Hoshikawa[1], Masao Yonemura[2], Kenji Iwase[1], D. S. Adipranoto[1], Hidetoshi Oguro[1], Takashi Kamiyama[2], Ryoko Tomiyasu-Oishi[2], Kazuhiro Mori[3], Ryoji Kiyanagi[4], Yukio Morii[5], Makoto Hayashi[5]

[1]*Frontier Research Center for Applied Nuclear Sciences, Ibaraki University, Tokai, Naka, Ibaraki, 319-1106, Japan*
[2]*Neutron Science Laboratory, KEK, Tsukuba, Ibaraki, Japan*
[3]*KUR, Kyoto University, Kumatori, Osaka, Japan*
[4]*IMRAM, Tohoku University, Sendai, Miyagi, Japan*
[5]*Ibaraki prefecture, Mito, Ibaraki, Japan*
E-mail: toru.ishigaki@j-parc.jp

Ibaraki prefecture, the local government of the area where J-PARC sites in Japan, has decided to build a versatile neutron diffractometer (IBARAKI Materials Design Diffractometer, iMATERIA [1]) to promote industrial applications for neutron beam in J-PARC. iMATERIA is planned to be a high throughput diffractometer so that materials engineers and scientists can use this diffractometer like the chemical analytical instruments in their materials development process. It covers the d in range $0.18 < d\ (Å) < 5$ with $\Delta d/d = 0.16$ % at high resolution bank, and $5 < d\ (Å) < 800$ with the resolution changing gradually at three detector banks of 90 degree, low angle and small angle. So, this diffractometer covers very wide d-range ($0.18 < d\ (Å) < 800$). It takes several minutes to obtain a "Rietveld-quality" data for the X-ray laboratory sized sample measured at 1MW. Currently, the beam power is limited for tuning the accelerator (~100kW), so that the measuring time is about 30min to one hours for standard oxide samples. To promote industrial applications, a utilization system of this diffractometer is required. Since several tens to thousands experiments will be carried out in one year, we have prepared an automatically sample exchange system and large numbers of sample holders. The analysis software is also very important for powder diffraction data, so that we prepare a software package consisting of combination of several powder-diffraction software, include Rietveld analysis software (Z-Rietveld [2]), structural databases and visualization. The construction of iMATERIA was completed and user program was already started since June 2009 for high resolution bank. The recent data of iMATERIA include low angle bank and small angle bank will be reported.

Reference

[1] T. Ishigaki et. al., "BARAKI materials design diffractometer (iMATERIA)-Versatile neutron diffractometer at J-PARC", Nucl. Instr. Meth. Phys. Res. A, 600, 189-191 (2009).
[2] R. Oishi, et. al., "Rietveld analysis software for J-PARC", Nuclear Instruments and Methods A600, 94–96 (2009).

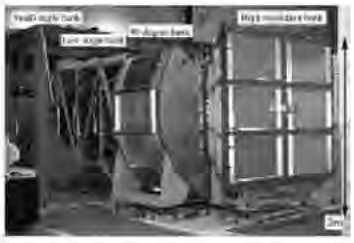

Fig.1 IBARAKI Materials Design Diffractometer, iMATERIA without detector for each bank and instrument shieldings. High-resolution bank, special environment bank (90 degree bank), low angle bank, can be seen from right to left, and small angle detector bank, which are not shown in picture, are situated in the low angle vacuum chamber (left hand of the picture).

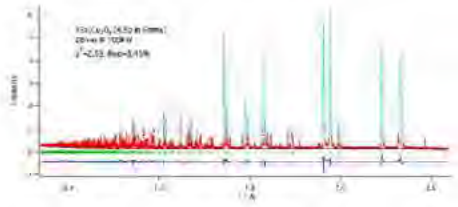

Fig. 2 Rietveld refinment pattern of $YBa_2Cu_3O_y$ by high resolution bank of iMATERIA using Z-Rietveld. The measurement time was 26 min for 4.5g samples at 100 kW.

MS03-O4

X-ray powder diffraction station at NSRRC for soft materials under non-ambient conditions

Jey Jau Lee[1], Ching Yuan Cheng[1]

[1] *National Synchrotron Radiation Research Center, Taiwan*
E-mail: jjlee@nsrrc.org.tw

We present a modified powder diffraction experimental station suitable for soft materials under non-ambient condition, which equipped at wiggler beamline BL17A1 of the National Synchrotron Radiation Research Center (NSRRC) of Taiwan. This beamline is fixed energy at 9.3 KeV, which can provide low Q information down to $0.024A^{-1}$ and moderate penetrate for general soft materials and other chemical species, such as polymer and liquid crystal samples. The normal operation temperature is 900 K to 100 K, 1300 K is also possible.
The non-ambient sample environment contain permanent magnets magnetic field (up to 1.8 Tesla at low temperature), electric field (maximum applied voltage: 10000 Volts) with program controllable sequence. Varied temperature diffraction and GIXS chamber with gas-line supplied atmosphere are also designed for in-situ diffraction signals measurements. In addition, a modified diamond anvil cell for low energy is also ready for soft materials under moderate high pressure (100bar-3GPa). The technical details and applied cases studies will be presented in the poster.

MS04-O1

Structural basis of RNase T in stable RNA 3'-end maturation

Hanna S. Yuan[1], Yu-Yuan Hsiao[1, 2] and Woei-Chyn Chu[3]

[1]*Institute of Molecular Biology, Academia Sinica, Taipei, Taiwan, ROC*
[2]*Institute of Bioinformatics and Structural Biology, National Tsing Hua University, Hsin-Chu, Taiwan, ROC*
[3]*Institutes of Biomedical Engineering, National Yang-Ming University, Taipei, Taiwan, ROC*
E-mail: hanna@sinica.edu.tw

Precursor RNA must undergo several processing steps to generate functional RNA molecules, which are crucial for many cellular processes. Despite its importance, the mechanisms of the end-processing steps by exonucleases on stable RNA, such as ribosomal and transfer RNA, are mostly unclear. Using RNase T as a model system, here we dissect the structural basis of its substrate specificity and derive the general principles of the final 3'-end trimming process made by RNase T in stable RNA maturation. Our crystal structural analyses on four RNase T-DNA complexes show that the two subunits of RNase T dimer work together in binding a double-stranded structure, producing a minimum product of a duplex with a 2-nt or 1-nt 3' overhang, depending on the last base pair composition in the duplex. A "C-filter" in RNase T screens out the nucleic acids with a 3'-terminal cytosine for the 3'-to-5' cleavage by inducing a disruptive conformational change at the active site. Our results reveal the general principles for the final trimming step made by RNase T in the maturation of stable RNA and provide a working mechanism for the DEDD family exonucleases, dysfunction of some these enzymes linking directly to human diseases.

MS04-O2

Structural analysis of bacterial Sec translocon machinery

Tomoya Tsukazaki[1], Hiroyuki Mori[2], Koreaki Ito[2] and Osamu Nureki[1]

[1]*Department of Biophysics and Biochemistry, Graduate School of Science, The University of Tokyo, Japan*
[2]*Institute for Virus Research, Kyoto University, Japan*

The Sec translocon functions as a protein-conducting channel to promote secretory protein export and membrane protein integration in all living cells. Here, we present the 3.2-Å crystal structure of the SecYE translocon from a SecA ATPase (bacterial translocation motor)-containing organism, *Thermus thermophilus*. The SecYE structure exhibits a 'pre-open' state, creating a hydrophobic crack open to the cytoplasm. Structural based functional analyses suggest that the pre-open state might represent a SecYE conformational transition that is induced by SecA association. Moreover, our results suggested that both the channel and the motor components of the Sec machinery undergo cooperative conformational changes on formation of the functional complex. Second, we have just solved the 3.3-Å crystal structure of SecDF, a translocon-associated membrane protein required for completion of the protein translocation and integration by SecYE, from the same organism and its periplasmic soluble domain structures at high resolution. We identified that SecDF is a novel proton channel and that the protein export acceleration by SecDF is driven by proton motive force across the membrane. The structure-based working model of the SecDF will be discussed.

MS04-O3

Structural basis of an ERAD pathway mediated by the ER-resident protein disulfide reductase ERdj5

Kenji Inaba

Division of Protein Chemistry, Post-Genome Science Center, Medical Institute of Bioregulation, Kyushu University, 3-1-1 Maidashi, Higashi-ku, Fukuoka 812-8582, Japan

The biological kingdoms have evolved elaborate systems that maintain protein homeostasis inside the cell. ER-associated degradation (ERAD) is an ER quality control process that eliminates terminally misfolded proteins. ERdj5, an ER-resident disulfide reductase, promotes ERAD by cleaving incorrect disulfide bonds of misfolded proteins, which are recruited by EDEM1, and transferring them to BiP. In this study, we solved the crystal structure of full-length ERdj5 at 2.4Å resolution. The structure revealed that ERdj5 was composed of the N-terminal J-domain and six tandem thioredoxin domains, which can be divided into N- and C-terminal clusters. The systematic *in vivo* and *in vitro* analyses indicated that the two thioredoxin domains that constitute the C-terminal cluster form the highly reducing platform that interacts with EDEM1 and reduces EDEM1-recruited substrates. The reduced substrates are subsequently captured by ATP-bound form of BiP, which in turn transfers the substrates to a retrotranslocation channel upon ATP hydrolysis. We here present the detailed structural and mechanistic basis of the ERdj5-mediated ERAD pathway.

MS04-O4

Structural studies of V_1-ATPase from *Enterococcus hirae*

Takeshi Murata[1,2,3], Shinya Saijo[4], Satoshi Arai[1], Yoshiko Ishizuka[2], Takaho Terada[2], Mikako Shirouzu[2], Ichiro Yamato[4], Shigeyuki Yokoyama[2] and So Iwata[2,3]

[1]*Department of Chemistry, Chiba University, 1-33 Yayoi-cho, Inage, Chiba 263-8522, Japan*
[2]*RIKEN SSBC, 1-7-22 Suehiro-cho, Tsurumi, Yokohama 230-0045, Japan*
[3]*Faculty of Medicine, Kyoto University, Yoshidakonoe-cho, Sakyo-ku, Kyoto 606-8501, Japan*
[4]*TB, Tokyo University of Science, 2641 Yamazaki, Noda-shi, Chiba 278-8510, Japan*
E-mail: t.murata@faculty.chiba-u.jp

Vacuolar ATPases (V-ATPases) function as ATP-dependent proton pumps in the membranes of acidic organelles and in plasma membranes of eukaryotic cells. This acidification is involved in concentration of neurotransmitters, processing of secretory proteins, endocytosis and other important cellular processes. V-ATPase contains a globular catalytic domain, V_1; 450 kDa, which hydrolyses ATP, attached by central and peripheral stalks to an integral membrane domain, V_o; 230 kDa, which pumps ions across the membrane. ATP hydrolysis generates rotation of the central stalk and an attached membrane rotor ring of hydrophobic subunits. Ions are pumped through a pathway at the interface between the rotating ring and a static membrane component, which is linked to the outside of the V_1 domain by the peripheral stalk. Precise mechanism of ATP hydrolysis of V_1-ATPase is not still clear, although crystal structure of V_1-ATPase from *Thermus thermophilius* have been solved at low resolution (4.5 Å), recently.

A V-ATPase in the non-respiring bacterium *Enterococcus hirae* acts as a primary sodium extrusion system. Its subunit composition is simpler than that of its eukaryotic counterparts, and its nine subunits (NtpA, B, C, D, E, F, G, I, K) are encoded in an operon. Here, we examined the in vitro reconstitution properties of NtpA, NtpB and NtpDG heterodimer which purified by using *E. coli* expression system in vitro. We have succeeded to solve the crystal structures of A_3B_3 heterohexamer and the DG complex at 2.8 Å and 1.9 Å, respectively. In my talk, I would like to present our recent studies of the V_1-ATPase, and discuss about reaction mechanism of the V_1-ATPase.

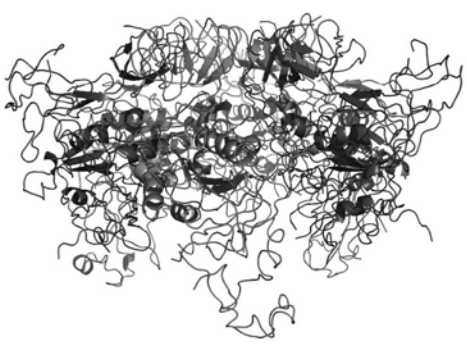

Crystal structures of A3B3 complex and NtpDG complex

MS05-O1

Recent studies on single-ion magnets

Song GAO

Beijing National Laboratory for Molecular Sciences, State Key Laboratory of Rare Earth Materials Chemistry and Applications, College of Chemistry and Molecular Engineering, Peking University, Beijing 100871, China
E-mail: gaosong@pku.edu.cn

Single-molecule magnets (SMMs) and single-chain magnets (SCMs) have been received great attention for their unique properties, such as very slow relaxation and quantum tunneling of magnetization, which offer the opportunity of potential application in information storage and quantum computation at molecular level. In the last decade, we obtained some homo-spin and/or hetero-spin SCMs and SMMs [1-2], and now we are going to explore the smallest molecular entity with isolated spin center showing SMM or SMM-like behavior, single-ion magnets, based on the previous work [3]. Some recent preliminary results on Dy(III) and Mn(III) based mononuclear molecules and their SMM behaviors will be presented [4].

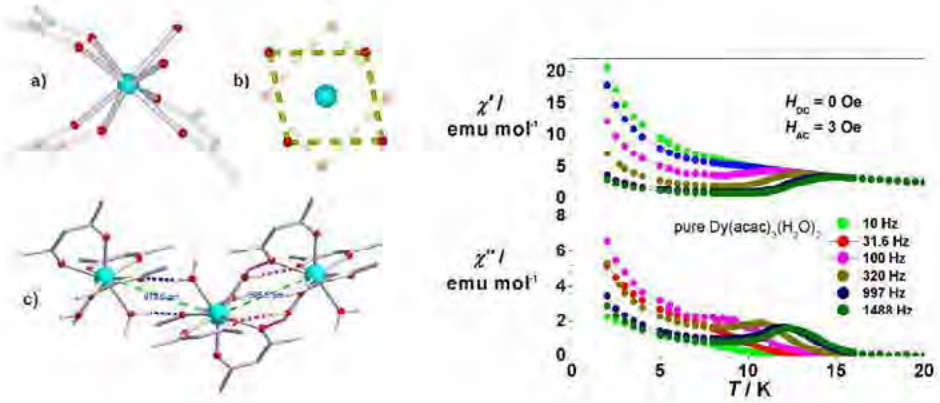

References

[1] Y.-Z. Zhang, W. Wernsdorfer, F. Pan, Z. M. Wang, S. Gao, *Chem. Commun.* 2006, 3302; (b) Z.-L. Lu, M. Yuan, F. Pan, S. Gao, D.-Q. Zhang, D.-B. Zhu, *Inorg. Chem.* 2006, 45, 3538; (c) M.-Y. Li, A. M. Ako, Y.-H. Lan, W. Wernsdorfer, G. Buth, C. E. Anson, A. K. Powell, Z.-M. Wang, S. Gao, *Dalton Trans.* 2010, 39, 3375.

[2] T.-F. Liu, D. Fu, S. Gao, Y.-Z. Zhang, H.-L.Sun, G. Su, Y.-J. Liu, *J. Am. Chem. Soc.* 2003, 125, 13976; (b) H.-B. Xu, B.-W. Wang, F. Pan, Z.-M. Wang, S. Gao, *Angew. Chem. Int. Ed.* 2007, 46, 7388; (c) H.-L. Sun, Z.-M. Wang, S. Gao, *Chem. Eur. J.* 2009, 15, 1757; (d) J.-F. Guo, X.-T. Wang, B.-W. Wang, G.-C. Xu, S. Gao, L. Szeto, W.-T. Wong, W.-Y. Wong, T.-C. Lau, *Chem. Eur. J. 2010, 16, 3524*; (e) H.-L. Sun, Z.-M. Wang, S. Gao, *Coord. Chem. Rev.* 2010, 254, 1081.

[3] B.-Q. Ma, S. Gao, G. Su, G.-X. Xu, *Angew. Chem. Int. Ed.* 2001, 40, 434; (b) Q.-D. Liu, J.-R. Li, S. Gao, B.-Q. Ma, Q.-Z. Zhou, Y. K. Bei, H. Liu, *Chem. Commun.* 2000, 1685; (c) S. Gao, G. Su, T. Yi, B.-Q. Ma, *Phys. Rev.* B 2001, 63, 054431; (d) Y.-Z. Zhang, G.-P. Duan, O. Sato, S. Gao, *J. Mater. Chem.* 2006, 16, 2625.

[4] S.-D. Jiang, B.-Wu Wang, G. Su, Z.-M. Wang, S. Gao, *Angew. Chem. Int. Ed.* 2010, accepted.

We acknowledge the support of NSFC, the National Basic Research Program of China.

MS05-O2

Kinetic syntheses of coordination networks and ab initio powder structure analysis

Masaki Kawano

Division of Advanced Materials Science, Pohang University of Science and Technology (POSTECH), Pohang 790-784, Korea
E-mail: mkawano@postech.ac.kr

The chemistry of porous coordination networks has undergone explosive growth in the last decade, mainly because its advantage over zeolite and related materials that detailed structure analysis can be done by the most reliable structure determination method, single crystal X-ray diffraction.[1-3] This powerful method is, however, limited to single crystals of network complexes prepared by slow crystallization methods, typically in small scale at room temperature in excess solvent. As a result, the crystals often include large quantities of solvent and do not have comparable thermal stability to zeolites. Stable structures often appear via thermal phase transitions and the new structures analyzed by powder X-ray analysis, but detailed structural information is usually difficult to obtain. Recently we reported selective synthesis of a porous coordination network via crystalline-amorphous-crystalline phase transitions and the ab initio powder structure analysis [4,5]. In this talk, we report a unique approach to the preparation of a porous coordination network by a kinetic effect and the ab initio powder structure analysis. After the solid-state phase transition of the kinetic networks, the resultant porous structures are remarkably robust and thermally stable. Solid-liquid interface syntheses of coordination networks will be reported as well.

References

[1] M. Kawano, T. Kawamichi, T. Haneda, T. Kojima, and M. Fujita, *J. Am. Chem. Soc.* **2007**, *129*, 15418-15419.
[2] T. Haneda, M. Kawano, T. Kawamichi and M. Fujita, *J. Am. Chem. Soc.* **2008**, *130*, 1578 -1579.
[3] T. Kawamichi, T. Haneda, M. Kawano and M. Fujita, *Nature*, **2009**, *461*, 633-635.
[4] M. Kawano, T. Haneda, D. Hashizume, F. Izumi, M. Fujita, *Angew. Chem. Int. Ed.* **2008**, *47*, 1269-1271.
[5] K. Ohara, J. Martí-Rujas, T. Haneda, M. Kawano, D.Hashizume, F. Izumi, M. Fujita, *J. Am. Chem. Soc.* **2009**, *131*, 3860-3861.

MS05-O3

Metal imidazolate polymers: Synthesis, structure and properties of silica analogues

Ian D. Williams, Herman H-Y. Sung, Fanny L-Y. Shek and Fion T-Y. Yeong

Department of Chemistry, Hong Kong University of Science and Technology, Hong Kong
E-mail: chwill@ust.hk

Metal imidazolates [MIm_2] have received much recent attention as a promising class of metal coordination polymer especially microporous phases for separation technology. Notably they have exceptional framework stability of 300-400°C. They are also of interest as topological analogues of Silica SiO_2 since they possess tetrahedral metal centers typically Zn, Co or Cd^{2+} rather than Si^{4+} and with bent linear bridges of Im^- anion ligands rather than bridging oxide O^{2-}. Much work has focused on the preparation of zeolitic analogues (ZIFs), however appropriate synthetic conditions can also result in more condensed 3D networks including quartz analogues. The effect of varying solvothermal conditions and imidazole substituent groups on framework topology will be discussed. The compounds may be made phase pure with high degree of crystallinity and single crystal structure determinations of many phases have been carried out. The structural aspects of these polymers, both local and topological, will be reviewed. Although local metal geometries are indeed tetrahedral and M---M distances fall in a narrow range, this geometry does not extend to next nearest neighbor M---M---M distances which fall into three sets due to syn and anti conformations. One interesting issue is that asymmetric imidazoles are found to be more problematic in forming crystalline phases; presumably since a high level of ordering is required for the nucleating cores, these tend to require higher temperature and time for crystallization to occur. Finally solid-state phase transitions of metal imidazolates are possible and examples are given of displacive and reconstructive types.

New Metal Imidazolide Polymers: Silica Analogues

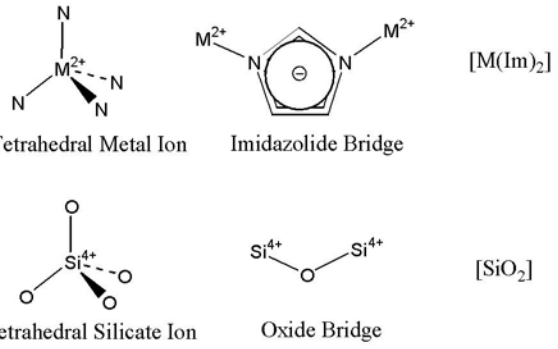

MS05-O4

Crystal structure analysis in drug development

Jason C. Cole, Aurora J. Cruz-Cabeza and Colin R. Groom

CCDC, 12 Union Road, Cambridge, CB2 1EZ, United Kingdom
E-mail: cole@ccdc.cam.ac.uk

Scientists in drug *discovery* benefit from a plethora of computational tools to assist with drug design. Many of these rely on knowledge extracted from small molecule crystal structures, including those to address molecular geometry and molecular interactions.
The adoption of such tools in drug *development* is less common, despite the dominance of crystalline materials as dosage form. The poor penetration of such tools is even more surprising when one considers the regulatory context in which drug development work is done, the high risk of drug candidate attrition and the financial commitments made by organisations when choosing to develop a specific compound.

This presentation will illustrate the role of computational methods in early drug development and describe the tools available to provide answers to key questions such as, 'Do I have the most stable polymorph?', 'Can I stop polymorph screening?', 'How can I describe the structural relationship between these crystal forms?', 'What might I be able to cocrystallise my molecule with?' , 'Can I replace my coformer and retain the same crystal form?' , 'How might I be able to generate a more soluble molecule?'

MS05-O5

Size- and shape-selective Metal-Organic Frameworks based on pillared Kagomé layers

Myoung Soo Lah*[1], Xinfang Liu[2], Minhak Oh[1]

[1]*Interdisciplinary School of Green Energy, Ulsan National Institute of Science & Technology, Ulsan, 689-798, Korea*
[2]*Department of Chemistry and Applied Chemistry, Hanyang University, Ansan, Kyunggi-do 426-791, Korea*
E-mail: mslah@unist.ac.kr

Hydrothermally stable two isostructural microporous metal-organic frameworks were prepared by employing a new ligand, 3-(3,5-dicarboxylphenylethynyl)pyridine, which has a 3,5-benzenedicarboxylate (bdc) unit for the construction of Kagomé layers and a 3-pyridine group as an internal pillaring residue between the layers. The combination of bent dicarboxylates and Cu (or Zn) square paddle-wheel secondary building units led to 2D Kagomé layers and these layers were further pillared by the internal pyridyl residues of the ligands to form a 3D microporous framework having two different types of cage-like pores, type A and type B pores, interconnected. While the type A pore with large enough window size allows most small gas molecules such as N_2, Ar, CO_2, and CH_4, the type B pore with small oval-shaped window distinguishes the absorbates, N_2 and Ar, based on the shape of the absorbates not based on their kinetic diameters. Even though the kinetic diameter of N_2 is larger than that of Ar, N_2 is preferred to the type B pore than the Ar because N_2 molecule better matches with the shape of the window than Ar. More interestingly, even though the static (or average) window size of the type B pore in Zn-MOF is similar to or even smaller than that in the isostructural Cu-MOF, the N_2 and Ar absorbates are more easily accessed to the type B pore of Zn-MOF than that of Cu-MOF. The maximum dynamic window size, the maximum allowed window size because of the thermal motion of the framework, may play more important role than the static size of the window for the discrimination of the absorbates. The larger average thermal factor of Zn-MOF than that of Cu-MOF might be responsible for such behavior. The details of the structure and the sorption behaviors will be discussed.

MS06-O1

Intermediate phase in oriented poly(pentamethylene 2,6-naphthalate)

Thi Cuc Do[1], Hye-Jin Jeon[1], Hyun Hoon Song[1], Kohji Tashiro[2]

[1]*Department of Advanced Materials, Hannam University, Daejeon, S. Korea*
[2]*Toyota Technological Institute, Nagoya, Japan*
E-mail: songhh@hnu.kr

The thermotropic liquid crystalline (LC) behavior of polymers with rigid mesogenic units interconnected through flexible spacers has been extensively over the past two decades. In the main-chain LC polymer flexible spacers are constrained by the mesogenic units to which they are linked, thus to have some orientational order. Among these polymers poly(alkylene 4,4'-bibenzoate)s whose mesophase existence and transition behavior have been intensively studied. These BB-*n* polyesters invariably form smectic mesophase when *n* varies from 3 to 9. Polyester based on 2,6-naphthalene dicarboxylic acid, poly(*m*-methylene 2,6-naphthalate) is another example of LC polymer that possibly show mesophase. In this family, as was noted in BB-n family, the macroscopic thermal and mechanical properties exhibit odd-even fluctuations as the number of methylene group in P*m*N increases. However, the existence of mesophase in these polymers is relatively rare and has been reported only in PEN and PBN. In this report, we present the mesophase structure in poly(pentamethylene 2,6-naphthalate) (PPN).

In order to examine the existence of mesophase and related structure in PPN, the sample was first quenched from the melt to obtain the complete amorphous structure and was then cold drawn at various strains. For the structural investigation we utilized the synchrotron X-ray scattering facility at Pohang Accelerator Laboratory (PAL) in S. Korea. From the WAXD pattern, the structure of un-drawn PPN is identified as the complete amorphous phase without any trace of the crystalline order. But, when the amorphous PPN is cold drawn, a structural order evolves in the polymer chains. Drawn samples (strain =1~3) exhibit two weak but sharp peaks at low angles in the meridian and two broad peaks in the equator. The sharp peak observed in the meridian implies a certain longitudinal order in the drawn PPN, similar to the fiber period in crystalline structure. On the other hand, the broad halo in the equator suggests the absence of long range order between the drawn PPN chains. These results suggest that the drawn PPN has certain low dimensional order, namely the mesophase, which resembles smectic LC order as has been observed in the oriented polymers having the flexible spacers between the rigid units. The smectic mesophase is a precursor of crystalline phase evolved. It is then quite reasonable to assume that the chain conformation within smectic layer resembles that of crystal structure. The crystal structure of PPN suggests that the neighboring mesogens in a chain are inclined toward each other The observation of splitting of broad equatorial reflection up and down the equator consolidates our assumption, especially the anti-clinically inclined mesogens, suggesting the smectic mesophase as the S_{CA} structure, where the mesogens are anti-clinically tilted with the molecular axes perpendicular to the layer surface.

MS06-O2

When explosives are welcome at your nuclear reactor... Molecular sensing using fluorescent dendrimer films and neutron reflectometry

Michael James[1,2], Hamish Cavaye[3] and Arthur Smith,[3] Paul Shaw,[3] Ian Gentle,[3] Paul Burn[3]

[1]*Bragg Institute, Australian Nuclear Science and Technology Organisation, Locked Bag 2001, Kirrawee DC, NSW 2232, Australia*
[2]*School of Chemistry, University of New South Wales, Kensington NSW 2052, Australia*
[3]*Centre for Organic Photonics and Electronics, University of Queensland, St Lucia QLD 4072, Australia*
E-mail: mja@ansto.gov.au

Events on Northwestern Flight 235 from Amsterdam to Detroit on Christmas Day 2009, saw airport security again become headline news. The proposed introduction of full body scanning at major international airports followed closely in its wake. The need for less invasive, yet highly sensitive screening for explosive materials is of supreme importance to security agencies around the globe. We have developed new classes of fluorescent dendrimer thin films as solid-state sensors to detect vapour molecules emitted by explosive materials using oxidative luminescence quenching. [1] We demonstrate that these films, can rapidly and reversibly detect explosive analogues for TNT such as para-nitrotoluene and 2,4-dinitrotoluene. Typically the photoluminescence is quenched by >90% in a few seconds, which is much faster than that reported for luminescent polymer films. Combined fluorescence spectroscopy and neutron reflectometry measurements were made using the *Platypus* time-of-flight neutron reflectometer at the OPAL reactor in Sydney for both pristine and analyte-saturated films, and gave important insights into the analyte adsorption process. It was found that during analyte adsorption the films swelled by ~4% in conjunction with the complete quenching of the photoluminescence. It was also clear that a single analyte molecule was able to quench the photoluminescence from more than one dendrimer molecule. On removal of the analyte the films returned to their original thickness and scattering length density, with the restoration of photoluminescence, indicating that the sensing process was fully reversible.

References

[1] Cavaye H., Smith A., James M., Nelson A., Burn P. L., Gentle I. R., Meredith P., "Solid-state dendrimer sensors: probing the diffusion of an explosive analogue using neutron reflectometry", *Langmuir*, Vol. 25, No. 21, (2009), pp 12800-12805.

MS06-O3

Chain conformation of zwitter ionic polymers in solution and immobilized brush at solid/liquid interfaces

Yuki Terayama[1], Moriya Kikuchi[2], Taiki Hoshino[2], Kohji Mitamura[2], Motoyasu Kobayashi2, Atsushi Takahara[1,2,3]

[1]*Graduate School of Engineering,* [3]*Institute for Materials Chemistry & Engineering, Kyushu University, Nishi-ku, Fukuoka 819-0395, Japan*
[2]*JST, ERATO Takahara Soft Interfaces Project, Nishi-ku, Fukuoka 819-0395, Japan*
E-mail: takahara@cstf.kyushu-u.ac.jp

Zwitter ionic polymers have positively and negatively charged groups on the polymer chain. Zwitter ionic polymers play an important role in various biological systems both in the solution and brush state. However, little is known on the chain conformation of Zwitter ionic polymers in the solution and brush state. The purpose of this study is to reveal the chain conformation of sulfobetaine and phosphobetaine polymers in the solution and immobilized brush state under various salt solutions.

Zwitter ionic polymers and their polymer brushes were prepared by surface-initiated atom transfer radical polymerization of 3-(*N*-2-methacryloyloxyethyl-*N*,*N*-dimethyl) ammonato propanesulfonate (MAPS) [1] and 2-methacryloyloxyethyl phosphorylcholine (MPC)[2]. Chain conformation in dilute solution and polymer brush on silica nanoparticles in aqueous solution with various ionic strengths were characterized by small angle X-ray scattering (SAXS) and static/dynamic light scattering (SLS/DLS). The molecular weight dependence of z-averaged mean-square radius of gyration and scattering factor of the poly(MAPS) were determined and analyzed in terms of the wormlike cylinder model taking into account the electrostatic interactions. The poly(MAPS) was insoluble in pure water, but soluble in NaCl aqueous solution above the Θ concentration, which was determined to be 74 mM at 25 °C by the light scattering when econd virial coefficient was vanished for high molecular weight. The radius of gyration for the poly(MAPS) increased with increasing ionic strength. Silica nanoparticle with 54 nm of radius was immobilized poly(MAPS) with 192,000 g/mol of molecular weight and M_w/M_n = 1.23 of polydispersity index. The relaxation spectrum obtained from DLS showed a unimodal distribution and sharp peak due to the homogeneous dispersion of poly(MPAS)-grafted SiO_2 in a solution without any aggregations, respectively. Hydrodynamic radius R_H of the poly(MAPS)-grafted SiO_2 was estimated to be 97 nm using the Einstein-Storks equation with diffusion constant D_o at the zero concentration. The thickness of polymer layer was found to be 43 nm, which is the 25% of the contour length of the fully-extended chain structure. Further precise molecular morphology of sulfobetaine polymer brush in a salt solution was analyzed by SAXS profiles using a core-shell model fitting. On the other hand, poly(MPC) was soluble both in pure water and NaCl aqueous solution. Concentration dependence of chain conformation was not observed below 1.0 M.

Polymer brushes on the Si-wafer substrate were characterized by contact angle measurement in air and water, adhesion force measurement, neutron reflectivity (NR) at aqueous solution interface, and AFM thickness measurement in aqueous solution. NR curves at poly(MAPS) brush/D_2O and poly(MPC) brush/D_2O interface *versus* scattering vector q ($4\pi \sin\theta/\lambda$) revealed that phosphobetaine polymer brush showed a completely different dependence of chain conformation on an ionic from that of sulfobetaine polymer brush.

References

[1] Y. Terayama, M. Kikuchi, M. Kobayashi, M. Hino, Atsushi Takahara, Influence of Salt Concentration on Swelling States of Poly(sulfobetaine) Brush at Aqueous Solution Interface, J. Phys. Conf. Ser. 184 ,012011(2009).

[2] M. Kobayashi, Y. Terayama, M. Kaido, A. Suzuki, K. Ishihara, A. Takahara, Friction Behavior of High-density Poly(2-methacryloyloxyethyl phosphorylcholine) Brush in Aqueous Media, Soft Matter, 3, 740-746(2007).

MS06-O4

Innate immunity and RNA sensing by the retinoic acid inducible gene I receptor

Matthew C. J. Wilce[1], Simone A. Beckham[1,2], Anna Roth[1], Die Wang[2], Anthony J. Sadler[2], Bryan R. G Williams[2] and Jackie A. Wilce[1].

[1]*Department of Biochemistry and Molecular Biology, Monash University, Clayton, Victoria, Australia*
[2] *Monash Institute of Medical Research, Monash University, Clayton, Victoria, Australia*

Organisms have evolved a range of mechanisms to sense viral infection and to block their replication and spread. Viral infection of human cells is primarily detected through sensing viral nucleic acids. The RIG-I-like helicases (RLH) sense viral RNA in the cytoplasm. Here we focus on the RLH, retinoic acid inducible gene I receptor, RIG-I. Selective recognition of viral RNA by RIG-I triggers the activation of NF-κB and interferon regulatory factors, leading to type I interferon production via the innate immune response. In the absence of its RNA ligands, RIG-I remains in an inactive state. RIG-I is a multidomain 103 kDa protein composed of two N-terminal caspase rectuirment domains (CARDs), a DEAD-box helicase domain and a C-terminal RNA recognition domain. It has been proposed that the CARD domains are not accessible until RIG-I forms a complex with dsRNA, but that upon this interaction the CARD domains are able to interact with IPS-1 to initiate downstream events. The molecular mechanism underlying this conformational change, however, has never been demonstrated.

We report the use of Small Angle X-ray Scattering (SAXS) to evaluate the conformational changes that occur to RIG-I upon binding to dsRNA. SAXS experiments were conducted for constructs representing full-length RIG-I and RIG-I without the card domains (deltaCARDs) both in and out of the presence of a 29-nt dsRNA target. The scattering data demonstrate that apo-RIG-I is more compact than the RIG-I/dsRNA complex: R_g and R_{max} change from 40 Å and 135 Å respectively to 45 Å and 170 Å upon binding RNA. Kratky plots also indicate that the apo-RIG-I is more ordered that the RIG-I/dsRNA complex. To evaluate the potential conformations of apo- and RNA bound RIG-I rigid body molecular dynamics[1] was applied to explore a large range of conformational space from which a genetic algorithm was used to select a minimal ensemble consistent with the scattering data. Furthermore, SAXS data acquired for deltaCARD RIG-I+/-RNA complex and RNA alone allowed the position of bound dsRNA to be ascertained from the contrast variation of the protein and RNA. Together this data has allowed us to propose a detailed molecular model of RIG-I and its conformation when bound to target dsRNA.

Reference

[1] Pelikan, M., Hura, G.L., and Hammel, M., Structure and flexibility within proteins as identified through small angle X-ray scattering, Gen. Physiol. Biophys. 28 (2009) 174-189

MS06-O5

Structures determined by single crystal neutron diffraction with KOALA - what is possible now, what improvements are planned and when another experiment may be the answer!

Alison J. Edwards and Ross O. Piltz

Bragg Institute, Australian Nuclear Science and Technology Organization, Lucas Heights, N.S.W., Australia
E-mail: Alison.Edwards@ansto.gov.au

The KOALA diffractometer is now in routine operation at the Bragg Institute. Our most recent call for proposals was oversubscribed and we anticipate a steady flow of publications to follow our early successes.

Software developments reported at the last AsCA conference have led to a steady flow of high quality neutron diffraction data for structures with modest sized unit cells (<2200 angstrom) where R- factors under 5% and C-C bond e.s.d.s of 0.001 - 0.002 angstrom are typically observed for refinements with all atoms anisotropic. Structures with larger unit cells are found to refine to a lower precision but nonetheless, in most instances structures are obtained which provide definitive answers for the questions posed – most particularly as regards that presence or absence of hydrogen whatever its oxidation state – protic, "atomic" or hydridic. We are now well placed to assess the applicability of the instrument to a particular problem and what if any modifications to hardware or software may be needed to improve the chances of a successful experiment.

In the immediate future we will be implementing flash freezing of crystals using a cold nitrogen gas stream which we hope will reduce one significant source of experimental failure which has plagued many experiments to date – cracking of crystals under the cooling regime inside bottom loading cryostats.

This paper will discuss both the successes to date together with our understanding of the present limitations of KOALA.

MS10e-O1

The crystal structure of LipL32, a virulence factor from pathogenic *Leptospira*

Yuh-Ju Sun[1], Jung-Yu Tung[1], Shao-Wen Chou[1], Chien-Chih Lin[1], Yi-Ching Ko[2], and Chih-Wei Yang[2]

[1]*Institute of Bioinformatics and Structural Biology, National Tsing Hua University, Hsinchu, Taiwan*
[2]*Kidney Institute and Graduate Institute of Clinical Medical Science, Chang Gung Memorial Hospital, Taiwan*
E-mail: yjsun@life.nthu.edu.tw

Tubulointerstitial nephritis is a cardinal renal manifestation of leptospirosis. LipL32, a virulence factor of pathogen *Leptospira*, is the major lipoprotein of outer membrane proteins. LipL32 recognizes extracellular matrix components and adheres to the host cell to evade an immune response. The crystal structure of Ca^{2+}-bound LipL32 was determined by multiwavelength anomalous dispersion at 2.3 Å LipL32 consists of a novel polyD sequence with a cluster of seven aspartate residues to form a continuous acidic surface patch for Ca^{2+} binding. A significant conformational change was induced when Ca^{2+} bound to LipL32. The calcium binding to LipL32 was determined by ITC. The binding of fibronectin to LipL32 was observed by Stains-all circular dichroism and ELISA experiments. The interaction between fibronectin F30 and LipL32 is associated with Ca^{2+} binding. Based on the Ca^{2+}-bound LipL32 crystal structure and the Stains-all circular dichroism results, a LipL32-F30 complex model was proposed. The fibronectin-binding site of LipL32 is near to the polyD region, and LipL32 interacts with F30 through significant electrostatic interactions. The Ca^{2+} binding to LipL32 might be important for extracellular matrix interaction with the host cell in *Leptospira*.

References

[1] Tung, J-Y, Yang, C.-W., Chou, S.-W., Lin, C.-C. and Sun, Y.-J. (2010) Calcium Binds to LipL32, a Lipoprotein from Pathogenic *Leptospira*, and Modulates Fibronectin Binding *J. Biol. Chem.* 285(5):3245-52.

MS10e-O2

When does a disease-related protein become a viable target?

Colin R. Groom, Jason C. Cole and Aurora J. Cruz-Cabeza

CCDC, 12 Union Road, Cambridge, CB2 1EZ, United Kingdom
E-mail: groom@ccdc.cam.ac.uk

Confirming a therapeutically beneficial link of a protein to a disease is a tremendous achievement. However, one must also confirm the potential of modulating the activity of protein for it to join only several hundred precedented drug targets. Whilst the success of therapeutic proteins, including antibodies, has opened up many new opportunities, traditional small molecule therapeutics continue to dominate.

The concepts of druggability and ligand efficiency are now well established, but should we really be deterred from tackling difficult targets? This presentation will focus on knowledge based computational methods for assessing the challenge a novel target might present; including exploratory docking experiments with small fragments and structure-based binding cavity comparisons.

MS10e-O3

Structure and mechanism-based discovery of mutant-selective inhibitors of the drug-resistant EGFR T790M mutant kinase

Cai-Hong Yun[1,2] and Michael Eck[1,2]

[1]*Department of Cancer Biology, Dana-Farber Cancer Institute, Boston, MA 02115, USA*
[2]*Department of Biological Chemistry and Molecular Pharmacology, Harvard Medical School, Boston, MA 02115, USA*
E-mail: yunch@red.dfci.harvard.edu

Mutations in the epidermal growth factor receptor (EGFR) kinase domain occur in approximately 16% of non-small-cell lung cancer (NSCLC). Lung cancers caused by most of these mutations are initially responsive to small molecule tyrosine kinase inhibitors (TKIs), but the efficacy of these agents is limited because of the emergence of drug resistance. In about 50% of the cases the resistance is conferred by a second mutation, T790M. Threonine 790 is the "gatekeeper" residue, an important determinant of inhibitor specificity in the ATP binding pocket. The T790M mutation has been thought to cause resistance by sterically blocking binding of TKIs such as gefitinib and erlotinib, but we show by a direct binding assay that T790M mutants retain low-nanomolar affinity for gefitinib, and by crystallographic analysis that the T790M mutant can adapt to accommodate tight binding of diverse inhibitors. Furthermore, we show that the T790M mutation increases the ATP affinity of the primary oncogenic L858R mutant by more than an order of magnitude. The increased ATP affinity is the primary mechanism by which the T790M mutation confers drug resistance[1-3].

Strategies targeting EGFR T790M with irreversible inhibitors have been shown in *in vitro* studies an option to overcome drug-resistance caused by the increased ATP affinity, but have had limited success in clinical trials and are associated with toxicity due to concurrent inhibition of wild-type EGFR. All current EGFR inhibitors possess a structurally related quinazoline-based core scaffold and were identified as ATP-competitive inhibitors of wild-type EGFR. Through three-dimensional structure directed drug design and screening an irreversible kinase inhibitor library we identify a covalent pyrimidine EGFR inhibitor scaffold specifically against EGFR T790M. These agents are 30- to 100-fold more potent against EGFR T790M, and up to 100-fold less potent against wildtype EGFR, than quinazoline-based EGFR inhibitors *in vitro*. They are also effective in murine models of lung cancer driven by EGFR T790M mutations. Co-crystallization studies reveal a structural basis for the increased potency and mutant selectivity of these agents. These mutant-selective irreversible EGFR kinase inhibitors may be clinically more effective and better tolerated than quinazoline-based inhibitors. Our findings demonstrate that three-dimensional structure directed drug design and functional pharmacological screens against clinically important mutant kinases represent a powerful strategy to identify new classes of mutant-selective kinase inhibitors[4].

References

[1] Yun C.H., Boggon T.J., Li Y., Woo M.S., Greulich H., Meyerson M. and Eck M.J., "Structures of lung cancer-derived EGFR mutants and inhibitor complexes: mechanism of activation and insights into differential inhibitor sensitivi", *Cancer Cell*, Vol. 11, No. 3, (2007), pp 217-227.

[2] Yun C.H., Mengwasser K.E., Toms A.V., Woo M.S., Greulich H., Wong K.K., Meyerson M. and Eck M.J., "The T790M mutation in EGFR kinase causes drug resistance by increasing the affinity for ATP", *Proc Natl Acad Sci U S A*, Vol. 105, No. 6, (2008), pp 2070-2075.

[3] Eck M.J. and Yun C.H., "Structural and mechanistic underpinnings of the differential drug sensitivity of EGFR mutations in non-small cell lung cancer", *Biochim Biophys Acta*, Vol. 1804, No. 3, (2010), pp 559-566.

[4] Zhou W.*, Ercan D.*, Chen L.*, Yun C.H.*, Li D., Capelletti M., Cortot A.B., Chirieac L., Iacob R.E., Padera R., Engen J.R., Wong K.K., Eck M.J., Gray N.S. and Jänne P.A., "Novel mutant-selective EG FR kinase inhibitors against EGFR T790M", *Nature*, Vol. 462, No. 7276, (2009), pp 1070-107 4. (*These authors contributed equally to this work.)

MS10e-O4

The crystal structure of the N-terminal domain of human COMMD9 reveals an unexpected domain-swapped trimer

Manuela Hospenthal[1], Treena Blythe[1], Fiona J. McDonald[2] and J. Shaun Lott[1]

[1]*School of Biological Sciences, University of Auckland, 3 Symonds Street, Auckland 1142, New Zealand*
[2]*Department of Physiology, University of Otago, Dunedin, New Zealand*
E-mail: s.lott@auckland.ac.nz

The COMMD (*Copper metabolism gene Murr1 (Mouse U2af1-rs1 region 1) Domain)* family is composed of ten proteins that share a conserved C-terminal 'COMM' domain but contain apparently unrelated N-terminal domains. Originally identified as critical for correct copper metabolism in dogs[1], it is now apparent that the COMMD proteins are vital components in the proteolytic regulation of several important cellular proteins[2]. They have been shown to regulate the degradation of the copper transporter ATP7B[3], the epithelial sodium channel ENaC[4], the serum- and glucocorticoid-regulated kinase SGK1[7], and the key transcription factors NF-κB[5] and HIF-1α[6]. In most cases, such as NF-κB, the regulation acts via ubiquitin-dependent degradation; in others, such as HIF-1α, the degradation is ubiquitin-independent, and in the case of SGK1, we have shown that COMMD1 protects the kinase from ubiquitin-dependent degradation[7]. Decreased expression of COMMD proteins is observed in many cancers, and has been shown to correlate with disease severity[8].

Despite many observational studies showing the *in vivo* association of COMMD proteins with their targets, the structures and the mechanism of action of the COMMD proteins remain largely unknown. The only structural information about the protein family is the NMR structure of the N-terminal domain of COMMD1. In order to address these issues, we have set out to determine the crystal structures of COMMD proteins, both alone and in complex with target proteins.

We here report the first crystal structure of a COMMD family member: the N-terminal domain of human COMMD9 (N-COMMD9) determined to 1.6 Å using SeMet-MAD. Despite a lack of sequence conservation, the core structure has the same overall fold as the equivalent domain in COMMD1: a distinctive helical bundle not observed in any other protein. The COMMD proteins are known to bind to each other *in vivo*, but their normal multimeric state is unclear. In one crystal form, N-COMMD9 forms a head-to-head dimer, but most unexpectedly, in a second crystal form the protein forms an intimately associated domain-swapped trimer. The implications of this structural plasticity to the possible mechanistic roles of the COMMD proteins will be discussed.

References

[1] van de Sluis, B., *et al.*, *Human Molecular Genetics*, 11: 165-173 (2002).
[2] van de Sluis, B., *et al.*, *Cell Cycle*, 6: 2091-8 (2007).
[3] de Bie, P., *et al.*, *Gastroenterology*, 133: 1316-26 (2007).
[4] Biasio, W., et al., Journal of Biological Chemistry, 279: 5429-5434 (2004).
[5] Ganesh, L., *et al.*, *Nature*, 426: 853-857 (2003).
[6] van de Sluis, B., *et al.*, *PLoS ONE*, 4: e7332 (2009).
[7] Ke, Y., *PhD Thesis, Department of Physiology*, University of Otago (2008).
[8] van de Sluis, B., et al., The Journal of Clinical Investigation, 120: 2119-30 (2010).

AsCA2010

The 10th Conference of the Asian Crystallographic Association

ABSTRACTS

November 2, (Tuesday)

Morning Oral Sessions (MS07, 08, 09)
Afternoon Oral Sessions (MS10, 11, 12)

MS07-O1

Probing the structure of cholesterol oxidase by atomic resolution crystallography: Towards the design of novel antibiotics with high specificity and potency

Alice Vrielink

School of Biomedical, Biomolecular and Chemical Sciences, University of Western Australia, 35 Stirling Highway, Crawley 6009, Australia
E-mail: alice.vrielink@uwa.edu.au

Cholesterol oxidase is a bifunctional flavoenzyme that catalyzes the oxidation and isomerization of Δ5-6-ene-3β-ketosteroids. The enzyme is an important virulent factor in patients suffering from tuberculosis and coccobacillus infections and thus constitutes a potential new target for antibacterial drug design. Such work would benefit from a detailed understanding of the structural events that occur along the catalytic pathway of the enzyme. Sub-Ångstrom resolution structures of the enzyme from *Streptomyces* sp. using crystals grown at different pH reveal changes to the structure as a function of electrostatic changes. These electrostatic changes can be correlated with spectral features and kinetic data. Further structural studies of a double mutant of the enzyme in the presence of a bound ligand identify a proposed Michaelis complex. A distortion of the isoalloxazine moiety of the cofactor suggests that tuning of the FAD redox potential is caused by Michaelis complex formation during catalysis. Finally, structural and kinetic analyses of the enzyme support the hypothesis that a gated hydrophobic channel provides O_2 access for the oxidative half reaction of the enzyme. These structural studies have expanded our understanding of the interplay between the enzyme, cofactor and substrates.

MS07-O2

Structural insights into ferredoxin dependent bilin reductases

Masakazu Sugishima

Department of Medical Biochemistry, Kurume University School of Medicine, Kurume 830-0011, Japan
E-mail: sugishima_masakazu@med.kurume-u.ac.jp

Phycobilisome, which is a light-harvesting system for photosynthesis in most of cyanobacteria and red algae, contains various type of phycobilins for efficient light-harvesting. A variety of phycobilins are produced by the site-specific reductions of heme catabolites, biliverdin (BV), catalyzed by ferredoxin dependent bilin reductases (FDBRs). Further, a phytochrome chromophore, phytochromobilin, is also biosynthesized in plants as well as the biosynthesis of phycobilins in red algae and cyanobacteria. Thus FDBRs are essential for the photosynthesis in cyanobacteria and red algae and the light-sensing in plants. Indeed, FDBR-deficient mutants in plants (*hy2* in *Arabidopsis* and *aurea* in tomato) show phytochrome-deficient phenotypes.

FDBRs catalyze the site-specific reductions of BV and other bilins using reducing equivalents from ferredoxin to produce phycobilins and phytochromobilin. No metals and cofactors are involved in the reductions, therefore a radical specie is formed by one-electron reduction during the catalysis. FDBRs regulate the reactivity of a radical specie and site-specifically reduce the substrate by site-specifically donating protons. To obtain the structural basis of FDBRs, we determined the crystal structure of the BV-bound PcyA [1], which is one of FDBRs and catalyzes the sequential reductions of the vinyl group of D-ring and the A-ring of BV to produce phycocyanobilin. Further we determined the structure of the reaction intermediate (18EtBV) bound PcyA [2]. PcyA folds into an α/β/α sandwich, in which BV and 18EtBV are bound between the central β-sheet and C-terminal α-helices. All of the polar groups of BV and 18EtBV form hydrogen bonds with PcyA, thus the substrate-binding of PcyA seems very tight. Although some aromatic residues of PcyA exist nearby BV/18EtBV, π-π stacking interactions are not used for BV/18EtBV binding to prevent the radical transition from one-electron reduced BV/18EtBV to PcyA. Moreover, unusual OH/π hydrogen bond is found between the carboxy group of Glu76 and the vinyl group of BV, the first reduction site by PcyA. This unusual hydrogen bond appears essential for the first reduction of BV by PcyA. Charge distribution on the molecular surface suggests that ferredoxin is bound on the surface close to the entrance of the BV-binding pocket, indicating ferredoxin directly transfers one-electron to BV. The carboxy group of Asp105 hydrogen bonds with the pyrrol nitrogen atoms of BV and the lactim/lactam oxygen atom of the D-ring. The imidazole group of His88 forms hydrogen bonds with the lactim/lactam oxygen atoms of BV. Asp105 and His88 are essential for the D- and A-rings reductions. Mechanistic implications for PcyA reaction will be discussed.

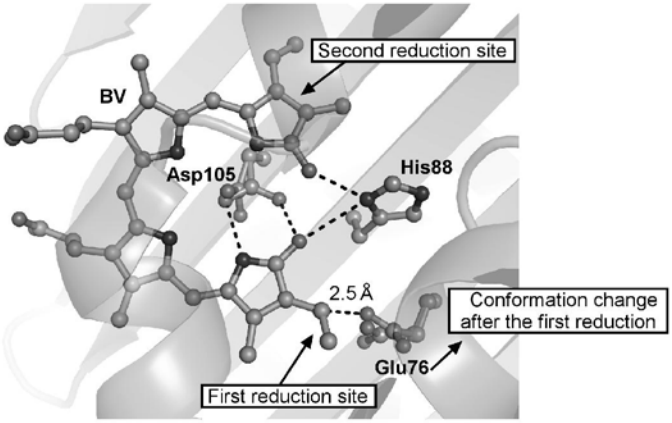

References

[1] Hagiwara Y., Sugishima M., Takahashi Y. and Fukuyama K., "Crystal structure of phycocyanobilin:ferredoxin oxidoreductase in complex with biliverdin IXα, a key enzyme in the biosynthesis of phycocyanobilin." Proc. Natl. Acad. Sci. USA, Vol. 103, No. 1, (2006), pp 27-32.

[2] Hagiwara Y., Sugishima M., Khawn H., Kinoshita H., Inomata K., Shang L., Lagarias J.C., Takahashi Y. and Fukuyama K., "Structural insights into vinyl reduction regiospecificity of phycocyanobilin:ferredoxin oxidoreductase (PcyA)." J. Biol. Chem., Vol. 285, No. 2, (2010), pp 1000-1007.

MS07-O3

Crystal structure and rotation mechanism of V_1-ATPase

Nobutaka Numoto[1,*], Yu Hasegawa[1], Kazuki Takeda[1] and Kunio Miki[1,2]

[1]*Department of Chemistry, Graduate School of Sciences, Kyoto University, Sakyo-ku, Kyoto, Japan*
[2]*RIKEN Spring-8 Center, Harima Institute, Sayo, Hyogo, Japan*
[*]*Present address: Research Reactor Institute, Kyoto University, Kumatori, Osaka, Japan*
E-mail: numoto@kuchem.kyoto-u.ac.jp

V-ATPases and F-ATPases belong to the rotary ATPase/synthase superfamily. V-ATPases occur in the membranes of acidic organelles in eukaryotic cells, maintaining acidic pH by pumping protons, and are also found in the plasma membranes of archaea and some eubacteria. These prokaryotic V-ATPases are primarily responsible for ATP synthesis, which is the reverse of the ATP-driven proton pumping reaction. V-ATPases consist of water-soluble components (V_1-ATPases), catalyze ATP hydrolysis and synthesis, and contain membrane-embedded components (V_o) involved in proton and ion pumping. It has been shown that isolated V_1-ATPases and F_1-ATPases show ATPase activities and rotate during ATP hydrolysis. However, detailed analyses of rotation kinetics have revealed some differences between V_1- and F_1-ATPase in the generated torque and rotation steps. Many crystallographic studies have been reported for F_1-ATPases, but no structure of the whole V_1 complex is available. Therefore, the detailed rotation mechanism of V_1-ATPase, and the reason for the difference in the rotation kinetics between V_1- and F_1-ATPases still remain open questions.

Recently, we have determined crystal structure of whole V_1-ATPase from thermophilic eubacterium, *Thermus thermophils* in nucleotide-free and nucleotide-bound forms at 4.8 and 4.5 Å resolutions, respectively. The structures were determined by using a combination of molecular replacement and multiple isomorphous replacement with anomalous scattering methods. The subunit composition for V_1-ATPase is A_3B_3DF. The central stalk composed of the D and F subunits protrudes from the cylindrical A_3B_3 hexamer, similarly to that of F_1-ATPase. A comparison of the structure of V_1- with F_1-ATPases reveals some differences in the conformation or structural motif between each subunit. In particular, the D subunit, which is main component of the central stalk in V_1-ATPase, shows apparently more straight conformation than the γ subunit of F_1-ATPase. This difference can influence on the generating and transmitting torque during the rotation. Moreover, little conformational differences are observed among the three catalytic A subunits of V_1-ATPase. In contrast, quaternary changes around nucleotide binding sites located at the interfaces of the A and B subunits are quite similar to both the enzymes. Therefore, the common structural property between V_1- and F_1-ATPases is only in the subunit interfaces around the active sites, strongly suggesting that the rotation of V_1-ATPase is primarily driven by the quaternary changes around the interface of nucleotide binding sites.

References

[1] Numoto N., Hasegawa Y., Takeda K. and Miki K., "Inter-subunit interaction and quaternary rearrangement defined by the central stalk of prokaryotic V1-ATPase", EMBO Rep., Vol. 10, No. 11, (2009), pp 1228-1234.

MS07-O4

Crystal structures of Aspergillus japonicas fructosyltransferase in complex with donor/acceptor substrates reveal complete subsites for catalysis

Phimonphan Chuankhayan[1], Chih-Yu Hsieh[2], Yen-Chieh Huang[1], Yi-You Hsieh[2], Hong-Hsiang Guan[1,4], Yin-Cheng Hsieh[1,4], Yueh-CHu Tien[1,4], Cheng-De Chen[1,3], Chien-Min Chiang[2] and Chun-Jung Chen[1,3,5]

[1]*Life Science Group, Scientific Research Division, National Synchrotron Radiation Research Center, Hsinchu 30076, Taiwan*
[2]*Department of Biotechnology, Chia Nan University of Pharmacy & Science, Tainan 71710, Taiwan*
[3]*Department of Physics, National Tsing Hua University, Hsinchu 30043, Taiwan*
[4]*Institute of Bioinformatics and Structural Biology, National Tsing Hua University, Hsinchu 30043, Taiwan*
[5]*Institute of Biotechnology, National Cheng Kung University, 1 University Road, Tainan City 701, Taiwan*
E-mail: cjchen@nsrrc.org.tw

Fructosyltransferases catalyze the transfer of a fructose unit from one sucrose/fructan to another, and are engaged in the production of fructooligosaccharide/fructan. The enzymes belong to the glycoside hydrolase family 32 (GH32) with a retaining catalytic mechanism. Here we describe the crystal structures of recombinant fructosyltransferase (*Aj*FT) from *Aspergillus japonicus* CB05 and its mutant D191A complexes with various donor/acceptor substrates, including sucrose, 1-kestose, nystose and raffinose. This is the first structure of fructosyltransferase of the GH32 with a high transfructosylation activity. The structure of *Aj*FT comprises two domains with an N-terminal catalytic domain containing a five-blade β-propeller fold linked to a C-terminal β-sandwich domain. Structures of various mutant *Aj*FT-substrate complexes reveal complete four substrate-binding subsites (-1 to +3) in the catalytic pocket with shapes and characters distinct from those of clan GH-J enzymes. Residues Asp60, Asp191 and Glu292 that are proposed for nucleophile, transition-state stabilizer and general acid/base catalyst, respectively, govern the binding of the terminal fructose at the -1 subsite and the catalytic reaction. Mutants D60A, D191A and E292A completely lost their activities. Residues Ile143, Arg190, Glu292, Glu318 and His332 combine the hydrophobic Phe118 and Tyr369 to define the +1 subsite for its preference of fructosyl and glucosyl moieties. Ile143, Gln327 define the +2 subsite for raffinose, whereas Tyr404 and Glu405 define the +2 and +3 subsites for inulin-type substrates with higher structural flexibilities. Structural geometries of 1-kestose, nystose and raffinose are different from previous data. All results shed light on the catalytic mechanism and substrate recognition of *Aj*FT and other clan GH-J fructosyltransferases.

References

[1] Chuankhayan, P., Hsieh, C.-Y., Huang, Y.-C., Hsieh, Y.-Y., Guan, H.-H., Hsieh, Y.-C., Tien, Y.-C., Chen, C.-D., Chiang, C.-M. and Chen, C.-J., "Crystal structures of *Aspergillus Japonicus* fructosyltrance complex with donor/acceptor substrates reveal complete subsites for catalysis The title of the journal paper", *J. Biol. Chem.* Vol. 285, (2010), Epub on May 13, 2010, doi:10.1074/jbc.M110.113027

MS07-O5

Structural basis for the inhibition of human MTHFS by N10-substituted folate analogues

Dong Wu[1], Yang Li[1], Gaojie Song[1], Chongyun Cheng[1], Rongguang Zhang[1], Neil Shaw[1], and Zhi-Jie Liu[1]

[1]*National Laboratory of Biomacromolecules, Institute of Biophysics, Chinese Academy of Sciences, Beijing 100101, China*
E-mail: wudong@moon.ibp.ac.cn

5,10-Methenyltetrahydrofolate synthetase (MTHFS) regulates the flow of carbon through the one-carbon metabolic network, which supplies essential components for the growth and proliferation of cells. Inhibition of MTHFS in human MCF-7 breast cancer cells has been shown to arrest the growth of cells. Absence of the three-dimensional structure of human MTHFS (hMTHFS) has hampered the rational design and optimization of drug candidates. Here, we report the structures of native hMTHFS, a binary complex of hMTHFS with ADP, hMTHFS bound with the N5-iminium phosphate reaction intermediate, and an enzyme-product complex of hMTHFS. The N5-iminium phosphate captured for the first time in our crystal structure unravels a unique strategy used by hMTHFS for recognition of the substrate and provides structural basis for the regulation of enzyme activity. Binding of N10-substituted folate analogues places Y152 in the middle of the channel connecting ATP binding site with the substrate binding pocket, precluding the positioning of ;-phosphate for a nucleophilic attack. Using the structures of hMTHFS as a guide, we have probed the role of residues surrounding the active site in catalysis by mutagenesis. The ensemble of hMTHFS structures and the mutagenesis data yield a coherent picture of the MTHFS active site, determinants of substrate specificity, and new insights into the mechanism of inhibition of hMTHFS.

References

[1] Chen, S., Yakunin, A.F., Proudfoot, M., Kim, R., and Kim, S.H., "Structural and functional characterization of a 5,10-methenyltetrahydrofolate synthetase from Mycoplasma pneumoniae (GI: 13508087)", *Proteins* , Vol. 2, No. 61, (2005), pp 433-443.

[2] Field, M.S., Szebenyi, D.M., Perry, C.A., and Stover, P.J., "Inhibition of 5,10-methenyltetrahydrofolate synthetase", *Arch Biochem Biophys* , Vol. 2, No. 458, (2007), pp194-201.

[3] Fox, J.T., and Stover, P.J. , "Folate-mediated one-carbon metabolism", *Vitam Horm* , No. 79, (2008), pp1-44.

[4] Wu, D., Li, Y., Song, GJ., Cheng,CY., Zhang R G., Joachimiak, A., Shaw, N., and Liu, Z. J., "Structural basis for the inhibition of human MTHFS by N10-substituted folate analogues", *Cancer Research* , Vol. 18, No. 69, (2009), pp7294-7301.

MS08-O1

Guest- and thermally-induced deformations of coordination framework materials

Cameron J. Kepert

School of Chemistry, University of Sydney, Camperdown NSW 2006, Australia
E-mail: c.kepert@chem.usyd.edu.au

The comparatively low energies associated with the deformation of coordination frameworks, a feature that emerges from the comparative flexibility of their molecular building units and from their commonly highly underconstrained and open topologies, means that these materials display a very rich array of dynamic lattices properties. Two very interesting consequences of the pronounced flexibility of these materials will be discussed:
1) Guest-induced framework flexibility; through novel *in-situ* single crystal and powder X-ray diffraction measurements we have followed the response of porous framework hosts to the desorption and sorption of a range of guest molecules and observed a range of novel lattice behaviours.[1-4]
2) Anomalous thermal expansion behaviour; we have recently found that the thermal excitation of transverse molecular vibrations within open coordination framework lattices leads to unprecedented negative thermal expansion (NTE) behaviours – an effect that can be moderated through control of the host-guest chemistry to yield near-perfect zero thermal expansion (ZTE).[5-10]

References

[1] Halder G.J. and Kepert C.J., "In situ single-crystal X-ray diffraction studies of desorption and sorption in a flexible nanoporous molecular framework material", *J. Am. Chem. Soc.*, Vol. 127, (2005), pp 7891-7900.
[2] Chapman K.W., Chupas P.J. and Kepert C.J., "Selective recovery of dynamic guest structure, in a nanoporous Prussian blue through in situ X-ray diffraction: A differential pair distribution function analysis", *J. Am. Chem. Soc.*, Vol. 127, (2005), pp 11232-11233.
[3] Neville S.M., Halder G.J., Chapman K.W., Duriska M.B., Southon P.D., Cashion J.D., Létard J.-F., Moubaraki B., Murray K.S. and Kepert C.J., "Single-crystal to single-crystal structural transformation and photomagnetic properties of a porous iron(II) spin-crossover framework", *J. Am. Chem. Soc.*, Vol. 130, (2008), pp 2869-2876.
[4] Southon P.D., Liu L., Fellows E.A., Price D.J., Halder G.J., Chapman K.W., Moubaraki B., Murray K.S., Létard J.F. and Kepert C.J., "Dynamic Interplay between Spin-Crossover and Host-Guest Function in a Nanoporous Metal-Organic Framework Material", *J. Am. Chem. Soc.*, Vol. 131, (2009), pp 10998-11009.
[5] Goodwin A.L. and Kepert C.J., "Negative thermal expansion and low-frequency modes in cyanide-bridged framework materials", *Phys. Rev. B: Condens. Matter*, Vol. 71, (2005), pp.
[6] Chapman K.W., Chupas P.J. and Kepert C.J., "Direct Observation of a Transverse Vibrational Mechanism for Negative Thermal Expansion in $Zn(CN)_2$: An Atomic Pair Distribution Function Analysis", *J. Am. Chem. Soc.*, Vol. 127, (2005), pp 15630-15636.
[7] Phillips A.E., Goodwin A.L., Halder G.J., Southon P.D. and Kepert C.J., "Nanoporosity and Exceptional Negative Thermal Expansion in Single-Network Cadmium Cyanide", *Angew. Chem., Int. Ed.*, Vol. 47, (2008), pp 1396-1399.
[8] Wu Y., Kobayashi A., Halder G.J., Peterson V.K., Chapman K.W., Lock N., Southon P.D. and Kepert C.J., "Negative Thermal Expansion in the Metal-Organic Framework Material Cu_3(1,3,5-benzenetricarboxylate)$_2$", *Angew. Chem., Int. Ed.*, Vol. 47, (2008), pp 8929-8932.
[9] Peterson V.K., Kearley G.J., Wu Y., Ramirez-Cuesta A.J., Kemner E. and Kepert C.J., "Local Vibrational Mechanism for Negative Thermal Expansion: A Combined Neutron Scattering and First-Principles Study", *Angew. Chem., Int. Ed.*, Vol. 49, (2010), pp 585-588.
[10] Phillips A.E., Halder G.J., Chapman K.W., Goodwin A.L. and Kepert C.J., "Zero Thermal Expansion in a Flexible, Stable Framework: Tetramethylammonium Copper(I) Zinc(II) Cyanide", *J. Am. Chem. Soc.*, Vol. 132, (2010), pp 10-11.

MS08-O2

Thermodynamics properties of molecular crystals derived from multitemperature diffraction data

Thammarat Aree[1] and Hans-Beat Bürgi[2]

[1]*Department of Chemistry, Faculty of Science, Chulalongkorn University, Bangkok 10330, Thailand*
[2]*Department of Chemistry and Biochemistry, University of Berne, CH-3012 Berne, Switzerland*
E-mail: thammarat.aree@gmail.com

Single-crystal X-ray analysis routinely provide accurate atomic coordinates and displacement parameters (ADPs). Atomic coordinates are generally interpreted in terms of molecular geometrical parameters (e.g., bond lengths, bond angles, torsion angles) and intra- and intermolecular interactions (e.g., hydrogen bonds, van der Waals interactions). By contrast, the ADPs of a single temperature study are merely depicted as ORTEP plots. Here we apply normal mode analysis of variable-temperature ADPs to determine thermodynamic properties of the molecular crystals of naphthalene, anthracene and hexamethylenetetramine. More recent results on the glycine polymorphs will also be presented. The thermodynamic parameters (heat capacity, enthalpy, entropy) obtained agree well with those from calorimetry.

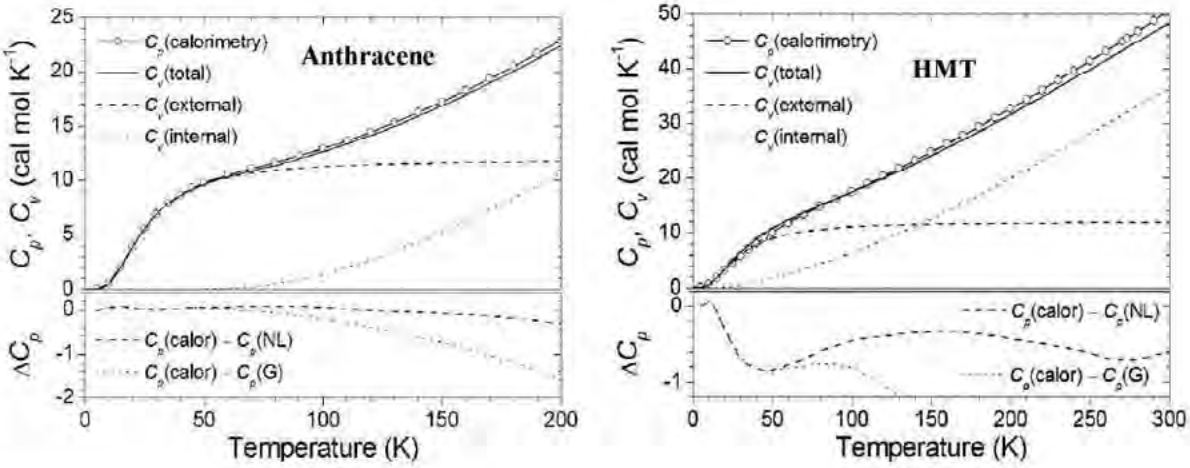

References

[1] Bürgi H.-B. and Capelli S. C. "Dynamics of molecules in crystals from multi-temperature anisotropic displacement parameters. I. Theory", Acta Crystallogr. Vol. A56, No. 5, (2000), pp 403–412.

[2] Aree T. and Bürgi H.-B., "Specific Heat of Molecular Crystals from Atomic Mean Square Displacements with the Einstein, Debye, and Nernst–Lindemann Models", J. Phys. Chem. B, Vol. 110, No. 51, (2006), pp 26129–26134.

MS08-O3

Structural rearrangement of organic crystals in polymorphic transition investigated by *ab initio* structure determination from powder diffraction data

Hidehiro Uekusa

Department of Chemistry and Materials Science, Tokyo Institute of Technology, Tokyo 152-8551, Japan
E-mail: uekusa@cms.titech.ac.jp

Many organic crystals show (pseudo-) polymorphism including hydrate or solvate crystals. Also among polymorphs, unexpected polymorphic transition including hydration / dehydration transition often occurs depending on its storage environment or by a mechanical treatment. Since their physicochemical properties such as color, stability, and solubility largely differ depending on the crystal structures, the structural investigation of phase transition is important especially to utilize the pharmaceutical polymorphic crystals. However, after the phase transition, single crystal integrity tends to degrade and powdery crystals are formed. In such case, *ab initio* Structure Determination from Powder X-ray Diffraction data (SDPD) is efficient technique. This technique is also important for the structure analysis of powdery co-crystals made by solid-state grinding, and of minor polymorphic phase. In this study, the rearrangement of crystal structures caused by pseudo-polymorphic transition are investigated by SDPD technique [1-6].

Tunnel water hydration/dehydration of Cephalexin hydrates: Pharmaceutical hydrates are well used as API (Active Pharmaceutical Ingredients) and often show hydration / dehydration transition. Cephalexin (cephem antibiotic) has five hydrated forms and their reversible transformations are induced by the change of relative humidity. Three psudopolymorphs (anhydrate, monohydrate, and dihydrate) were successfully analyzed by SDPD technique to show water tunnel structures between building blocks formed by three independent cephalexin molecules. In the hydration process, the blocks slide each other to increase the tunnel volume from 0 to 280 $Å^3$ (see figure), which is accompanied by elongation of the *a*-axis length by 17%. This reversible tunnel volume change associated with hydration/dehydration process indicates that water molecules go in and out through the tunnel with retention of crystallinity.

Two step dehydration process of Lisinopril dihydrate: Lisinopril is used as an anti-hypertension drug in the dihydrate form. A DSC-PXRD measurement indicated that water molecules were released at 373K and 383K to form monohydrate and anhydrate form, respectively. Both crystal structures were successfully analyzed from high resolution PXRD. The dehydration mechanism is illustrated as the two step water molecule releasing from two different channel structures in order. During the process, terminal phenylethyl group turns to close the empty channel and to stabilize the structure.

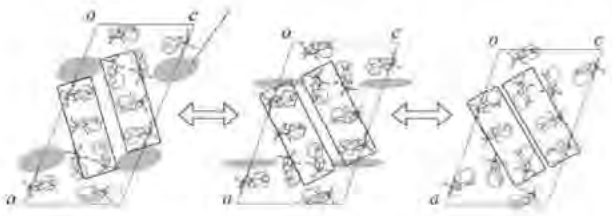

Structural rearrangement of Cephalexin
(di-, mono-, and an-hydrate)

References

[1] Angew. Chem. Int. Ed., 45, 6013 (2006).
[2] Int. J. Pharm., 369, 12 (2009).
[3] Cryst. Growth Des., 9, 1201 (2009).
[4] J. Phys. Chem. C., 114, 580 (2010).
[5] Chem. Comm., 46, 4264 (2010).
[6] Cryst. Growth Des., 10, 2116 (2010).

MS08-O4

Photoreactivity and structural rearrangements in the solid state

Jagadese J. Vittal,[1,2]

[1]*Department of Chemistry, National University of Singapore, Singapore 117543*
[2]*Department of Chemistry, Gyeongsang National University, Jinju, S. Korea 660-701*
E-mail: chmjjv@nus.edu.sg

For the past few decades the photochemical [2+2] cycloaddition reactions in the solid state have been extensively studied. It may be possible to align the C=C bonds favorable for the photoreactions, but this does not guarantee the reaction to take place in the crystals. For example, a number of compounds containing C=C bonds do not undergo photodimerization in the solid state despite satisfying Schmidt's criteria, whereas there are a number of cases where photocyclization is not expected, surprisingly found to be reactive. Crystal structure analyses of these systems exhibiting unexpected photoreactivity unraveled several pieces of new information about the mobility of the molecules.

Of the organic molecules studied so far, *trans* 1,2-bis(4-pyridyl)ethene (bpe) containing two pyridyl nitrogen atoms has been extensively investigated in our laboratory. For instance, a ladder coordination polymer where infinite pairs of C=C bonds in bpe are aligned has been found to undergo single-crystal to single-crystal structural transformation under UV light. Whereas a Ag(I) 1D coordination polymer reorganized to a ladder structure upon desolvation and further undergoes [2+2] cycloaddition under UV irradiation quantitatively. Similar observation has been noted in another 1D coordination polymer also. On the other hand, during the grinding process the infinitely packed *trans*-3-(4-pyridyl) acrylic acid salt in head-to-head fashion with one third of C=C bonds in crisscross fashion in the single crystals takes up a water molecule and rearranges to form isolated pairs congenial for [2+2] cycloaddition quantitatively. Similarly, cycloaddition reaction in a triple-stranded ladder coordination polymer has been found to take place in two steps via cooperative molecular movements of the partially dimerized products formed initially. We will highlight the role of solvents in the structural rearrangements to assist the alignment of C=C bonds for [2+2] cycloaddition reactions in the talk.

References

[1] Vittal, J.J., *Coord. Chem. Rev*. 251 (2007) 1781-1795.
[2] Nagarathinam, N.; Peedikakkal, A.M.P.; Vittal, J.J. *Chem. Comm*. (2008) 5277-5288.
[3] Nagarathinam, M.; Vittal, J.J. *Angew. Chem. Int. Ed*., 45 (2006) 4337-4341.
[4] Peedikakkal, A.M.P.; Vittal, J.J. *Chem. – A Eur. J*. 14 (2008) 5329-5334.
[5] Nagarathinam, M.; Vittal, J.J. *Chem. Commun*., (2008) 438-440.
[6] Kole, G.K.; Tan, G.K.; Vittal, J.J. *Org. Lett*, 12 (2010) 128-131
[7] Kole, G.K.; Koh, L.L.; Lee, S.Y.; Lee, S.S.; Vittal, J.J. *Chem. Comm.* 46 (2010) 3660-3662

"Jumping crystals": Structural aspects of the thermosalient phenomenon

Željko Skoko[1], Sharona Zamir[2], Panče Naumov[1] and Joel Bernstein[2]

[1]*Department of Material and Life Science, Graduate School of Engineering, Osaka University, 2–1 Yamada-oka, Suita 565–0871, Osaka, Japan*
[2]*Department of Chemistry, Ben-Gurion University of the Negev, Beer Sheva 84105, Israel*
E-mail: npance@wakate.frc.eng.osaka-u.ac.jp

An increasing amount of experimental evidence on mechanically, thermally or photochemically induced mechanical deformations of organic or metal-organic materials, where the supramolecular structure is based on non-covalent interactions, sharply contradicts the common perception of these entities as soft, rigid and fragile state of matter.[1-3] In this report the *thermosalient ("jumping crystal") effect*[4,5] – a mechanical property that can be an important physical foundation of organic-based actuators – has been investigated in detail for oxitropium bromide (OXTB), a potent anticholinergic active pharmaceutical ingredient. Although being of extreme importance for understanding issues of fundamental or practical interest, this phenomenon is usually only accidentally observed, rarely reported, and its origin and detailed structural basis have remained enigmatic.

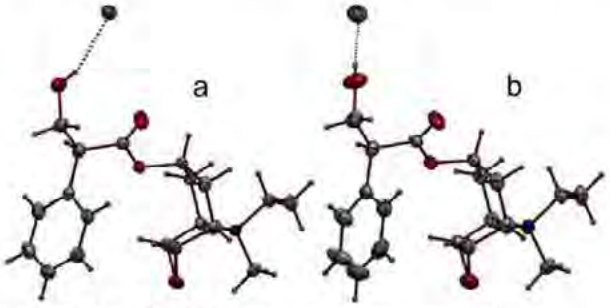

Figure 1. ORTEP-style representation of the molecular structures (30% probability level) of phase A (a) and phase B (b) of OXTB.

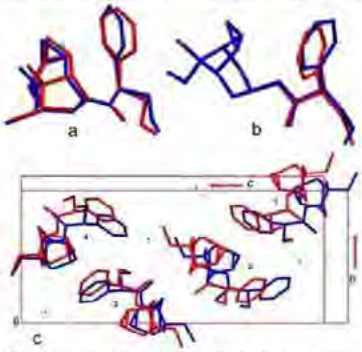

Figure 2. Overlapped molecular (a,b) and crystal (c) structures of the low-temperature (blue) and high-temperature phase (red).

Upon heating, unattached single crystals of OXTB exhibit forceful jumps of up to several centimeters as result of structure switching over a thermal two-phase hysteresis. Application of a combination of structural, microscopic, spectroscopic and thermoanalytical techniques has clarified the origin and mechanism of the significant thermosalient effect. Direct observation of the effect in a single crystal and the structure determination of both phases revealed that the jumping is a macroscopic manifestation of a highly anisotropic change in the cell volume. At the molecular level, the cation acts as a molecular shuttle composed of two rigid parts (epoxy-aza-tricyclic-nonyl portion and phenyl ring) that are bridged by a flexible ester linkage. The structure of the rigid, inert aza-tricyclic portion remains practically unaffected by the temperature, suggesting a mechanism in which the accumulated strain is transferred over the bridge to the phenyl ring, which rotates to trigger the transition.

References

[1] Reddy, C. M., Gundakaram, R. C., Basavoju, S., Kirchner, M. T., Padmanabhan, K. A. and Desiraju, G R., *Chem. Commun.* **2005**, 3945–3947.
[2] Reddy, C. M., Kirchner, M. T., Gundakaram, R. C., Padmanabhan, K. A. and Desiraju, G R., *Chem.–Eur. J.* **2006**, *12*, 2222–2234.
[3] Reddy, C. M., Basavoju, S. and Desiraju, G R. *Chem. Commun.* **2005**, 2439–2441.
[4] Etter, M. C. and Siedle, A. R., *J. Am. Chem. Soc.* **1983**, *105*, 641–643.
[5] Ding, J., Herbst, R., Praefcke, K., Kohne, B. and Saenger, W., *Acta Crystallogr.* **1991**, *B47*, 739–742.

MS09-O1

Combining SAXS and CD to study flexibility and dynamics in multi-domain proteins

Cowieson NP[1], Hijnen M[2,3], Pendini N[2], Wilce J[2], Wilce M[2] and Mak J[3]

[1]*Australian Synchrotron, 800 Blackburn Road, Clayton, VIC 3168, Australia*
[2]*Monash University, Clayton, VIC 3800, Australia*
[3]*Burnet Institute, 85 Commercial Rd, Melbourne, VIC 3004, Australia*
E-mail: nathan.cowieson@synchrotron.org.au

Protein crystallography is an excellent tool for measuring protein structure to high-resolution while being less well suited to measuring flexibility and dynamics. Small-angle x-ray scattering (SAXS) and circular dichroism (CD) are solution-based methods that can be used alongside crystallography to study conformational change, dynamics and flexibility in the tertiary and secondary structure of proteins respectively. SAXS and CD analysis of retroviral Gag proteins, eukaryotic biotin protein ligases and murine cortactin will be used to illustrate the application of these methods to the study of multi-domain, flexible proteins.

The HIV Gag poly-protein is the main structural component of the viral capsid and is sufficient to form virus-like particles in vitro. We have used a combination of small angle x-ray scattering, circular dichroism and other biophysical methods to analyse the orientation of the four domains of Gag in solution and to track how their relative orientation changes during the proteolytic processing that is part of this proteins normal life cycle.

MS09-O2

Combination of correlative light-electron microscopy and X-ray crystallography revealed a unique trans-synaptic adhesion architecture

Junichi Takagi[1], Hiroki Tanaka[1], Naoyuki Miyazaki[1], Terukazu Nogi[1] and Kenji Iwasaki[1]

[1]*Institute for Protein Research, Osaka University, Osaka 565-0871, Japan*
E-mail: takagi@protein.osaka-u.ac.jp

Synapse formation at the neuronal membrane junctions is a dynamic process involving orchestrated assembly/disassembly of multiple classes of membrane proteins and cytosolic proteins. It is becoming clear that cell adhesion molecules play more than structural and "scaffolding" roles in this process. Neurexin (NX) and neuroligin (NL) are membrane spanning adhesion molecules expressed on neurons, and the *trans* association of presynaptic NX and postsynaptic NL across the synaptic cleft is required for the functional maturation of synapses. Recently several groups have reported crystal structures of complex between ectodomain fragments of NX and NL, revealing a unique 2:2 stoichiometry [1-3]. We have also obtained crystals of the NX/NL complex in a unique condition. The crystal formation was induced by addition of physiological concentration of Ca^{2+}, and did not require addition of any precipitants. In the crystal, the 2:2 complex formed two-dimensional array that is compatible with the membrane topology of the asymmetric synaptic cleft. We hypothesize that this NX/NL "2D array meshwork" corresponds to the ordered molecular complexes that span the synaptic cleft previously visualized by cryo-EM. In order to confirm this hypothesis, we turned to a combinatory technique using light microscopy (LM) and electron microscopy (EM). First, we expressed NX-DsRed and NL-GFP on HEK cell surface and analyzed the colocalization of the two molecules at the heterophilic cell-cell junction using fluorescent live LM. The cells were then processed in a high pressure freezing followed by freeze substitution and resin embedding to preserve the fine structure of the specimen. The resultant EM image of the cell-cell junction clearly showed a presence of sheet-like density in the middle of the narrow extracellular space between the cell membranes. This density was present exclusively at the heterophilic contacts between NX- and NL-expressing cells, strongly suggesting the formation of 2D array by the NX-NL trans-cellular adhesion complex. This higher-order membrane platform may send bidirectional signal across the synaptic membrane, leading to the recruitment of specific post- and pre-synaptic cytoplasmic components. Our hybrid approach represents a successful application of Correlative Light-Electron Microscopy (CLEM) technique in the visualization of higher-order molecular complex *in situ*, as a complimentary way to verify the biological relevance of a crystal structure.

References

[1] Fabrichny IP, Leone P, Sulzenbacher G, Comoletti D, Miller MT, Taylor P, Bourne Y, and Marchot P., " Structural analysis of the synaptic protein neuroligin and its beta-neurexin complex: determinants for folding and cell adhesion ", Neuron, *56,* (2007), pp 979-991.

[2] Araç D, Boucard AA, Ozkan E, Strop P, Newell E, Südhof TC, Brunger AT., " Structures of neuroligin-1 and the neuroligin-1/neurexin-1 beta complex reveal specific protein-protein and protein-Ca2+ interactions", Neuron, *56,* (2007), pp 992-1003.

[3] Chen X, Liu H, Shim AH, Focia PJ, and He X., " Structural basis for synaptic adhesion mediated by neuroligin-neurexin interactions", *Nat Struct Mol Biol.* 15 (2008), pp 50-56.

MS09-O3

Analysis of protein dynamics by crystallographic refinement and normal mode analysis

Pramod Kumar[1] and Shekhar C. Mande[1]

Centre for DNA Fingerprinting and Diagnostics, 5-4-399/B, Nampally, Hyderabad 500 001, India
E-mail: shekhar@cdfd.org.in

Crystallographic analysis of biological macromolecules yields deep insights in their biological function. One aspect of this analysis that has received less attention pertains to the dynamics of macromolecules. As is well known, dynamics plays an important role in attempting to address biological problems such as explaining enzyme catalysis, allostery and cooperativity. Especially, addressing problems such as large conformational changes in enzymes which occur during catalysis are less amenable by routine crystallographic analysis. We have attempted to address this problem by combining TLS refinement in standard crystallographic refinement, and by supplementing the refinement by normal mode analysis. We show that correlation between the two has the capability to address such complex dynamics problems. Two such examples will be presented- thioredoxin reductase[1], where the enzyme undergoes large conformational changes; and cAMP receptor protein[2], which acts allosterically.

References

[1] Akif M., Suhre K., Verma C. and Mande S. C. Conformational flexibility of Mycobacterium tuberculosis thioredoxin redictase: crystal structure and normal mode analysis. *Acta crystal*logr. vol. D61, (2005), 1603- 1611.

[2] Kumar P., Joshi D., Akif M., Akhter Y., Hasnain S. E. and Mande S. C. Mapping conformational transitions in cyclic AMP receptor protein: crystal structure and normal mode analysis. *Biophys J.*, vol 98, 305- 314.

Use of racemic protein crystallography to solve the structure of Rv1738, an essential protein from *Mycobacterium tuberculosis*

Edward N. Baker[1], Richard D. Bunker[1], Jessica J. Chaston[1], Kalyaneswar Mandal[2], Brad Pentelute[2], Geoffrey B. Jameson[3], J. Shaun Lott[1], and Stephen B. H. Kent[2]

[1]*Maurice Wilkins Centre for Molecular Biodiscovery and School of Biological Sciences, University of Auckland, Private Bag 92019, Auckland, New Zealand*
[2]*Department of Biochemistry and Molecular Biology, Department of Chemistry and Institute for Biophysical Dynamics, University of Chicago, Chicago, IL 60637, USA*
[3]*Institute of Fundamental Sciences, Massey University, Private Bag 11222, Palmerston North, New Zealand*
E-mail: ted.baker@auckland.ac.nz

Naturally-occurring proteins are chiral molecules, being built solely from L-amino acids. As such, they can only be crystallized in acentric space-groups, which do not contain mirror symmetry or inversion centres. This limits the number of potential packing arrangements. A possible strategy to improve the chances of crystallization is to crystallize a racemic mixture comprising the D- and L-forms of a protein [1,2]. The D-form must be synthesized chemically from D-amino acids, which can readily be achieved by modern methods of native chemical ligation [3]. This strategy means that all 230 possible crystal space-groups become accessible instead of only the 65 acentric space-groups. Crystallization in a centrosymmetric space-group also means that structure determination is greatly simplified since the phases are limited to 0° or 180°.

Microarray experiments show that *Rv1738* is highly up-regulated in *Mycobacterium tuberculosis* (*Mtb*) under conditions of hypoxia or nitric oxide challenge. *Mtb* must adapt to hypoxia as it undergoes the transition from active infection to persistence, and Rv1738 is therefore predicted to have an important role in this transition. Transposon mutagenesis also identifies Rv1738 as essential for growth, but the function of Rv1738 is unknown. All attempts to crystallize recombinant Rv1738, using varied constructs, chemical modification and mutagenesis, failed. In contrast, a racemic mixture of D- and L-forms crystallized easily from multiple conditions and the structure was solved in the centrosymmetic space group C2/c at 1.7 Å resolution. The 94-residue protein forms an intimate dimer by crystallographic twofold symmetry with one molecule in the crystal asymmetric unit. Both D- and L-dimers are found in the crystal, related by a crystallographic glide plane.

As a further demonstration of the advantages afforded by racemic protein crystallography, a novel fragment-based *ab initio* procedure was developed and successfully used to quickly determine the correct Rv1738 model starting by the positioning of short, idealized poly-Ala α-helices.

References

[1] Pentelute B., Gates Z., Tereshko V., Dashnau J., Vanderkooi J., Kossiakov A. and Kent S., "X-ray structure of snow flea antifreeze protein determined by racemic crystallization of synthetic protein enantiomers", *J. Amer. Chem. Soc*., Vol. 130, (2008), pp 9695-9701.
[2] Matthews B., "Racemic crystallography – easy crystals and easy structures: what's not to like?", *Protein Sci*., Vol. 18, (2009), pp 1135-1138.
[3] Pentelute B., Gates Z., Dashnau J., Vanderkooi J. and Kent S., "Mirror image forms of snow flea antifreeze protein prepared by total chemical synthesis have identical antifreeze activities", *J. Amer. Chem. Soc*., Vol. 130, (2008), pp 9702-9707.

MS09-O5

High pressure cryocooling at MacCHESS

Chae Un Kim[1], Irina A. Kriksunov[1], William A. Miller[1], Mike Cook[1], Doletha M. E. Szebenyi[1] and Sol M. Gruner[2,3]

[1]*Macromolecular diffraction at CHESS (MacCHESS), Cornell University, Ithaca, NY 14853, USA*
[2]*Cornell High Energy Synchrotron Source (CHESS), Cornell University, Ithaca, NY 14853, USA*
[3]*Physics Department, Cornell University, Ithaca, NY 14853, USA*
E-mail: ck243@cornell.edu

A novel high-pressure cryocooling technique for macromolecular crystallography has been developed and explored at the Macromolecular Diffraction Facility at the Cornell High Energy Synchrotron Source (MacCHESS) [1]. The method involves cooling macromolecular crystals to cryogenic temperatures (~ 100 K) in high-pressure (up to 200 MPa) helium gas. Applications include successful cryocooling with little or no penetrating cryoprotectant, and native sulfur SAD phasing. Samples in capillaries can also be pressure cryocooled [2]. The method has been extended to other gases, e.g. Kr or Xe (followed by He) for single-wavelength anomalous dispersion (SAD) phasing [2,3], and CO2 (alone at lower pressure) to visualize an enzymatic intermediate state in carbonic anhydrase [4]. Surprising results include visualization of ligands which could not be seen using other methods [5], and unusual phase behavior of water in protein crystals [6, 7]. The method also can be used to study pressure effects on protein structures [8,9]. A mechanism involving high-density amorphous (HDA) ice is used to explain why the method works [1,6,7].

The high pressure cryocooling method is available to researchers with suitable crystals. More details can be found in the following link.

http://www.macchess.cornell.edu/MacCHESS/about_macchess.html#Pressure

References

[1] Kim C.U., Kapfer R. and Gruner S.M., "High pressure cooling of protein crystals without cryoprotectants", *Acta Cryst.* D**61**, (2005), 881-890.
[2] Kim C.U., Hao Q. and Gruner S.M., "High pressure cryocooling for capillary sample cryoprotection and diffraction phasing at long wavelengths", *Acta Cryst.* D**63**, (2007), 653-659.
[3] Kim C.U., Hao Q. and Gruner S.M., "Solution of protein crystallographic structures by high pressure cryocooling and noble gas phasing", *Acta Cryst.* D**62**, (2006), 687-694.
[4] Domsic J.F., Avvaru B.S., Kim C.U., Gruner S.M., Agbandje-McKenna M., Silverman D.N. and McKenna R., "Entrapment of carbon dioxide in the active site of carbonic anhydrase II", *J. Biol. Chem.* **283**, (2008), 30766-30771.
[5] Albright R.A, Ibar J.-L.V., Kim C.U., Gruner S.M. and Morais-Cabral J.H., "The RCK domain of the KtrAB K+ transporter: multiple conformations of an octameric ring", *Cell* **126**, (2006), 1147-1159.
[6] Kim C.U., Chen Y.-F, Tate M.W. and Gruner S.M., "Pressure induced high-density amorphous ice in protein crystals", *J. Appl. Cryst.* **41**, (2008), 1-7.
[7] Kim C.U., Barstow B., Tate M.W. and Gruner S.M. "Evidence for liquid water during the high-densi ty to low-density amorphous ice transition", *Proc. Natl. Acad. Sci.*, **106**, (2009), 4596-4600.
[8] Barstow B., Ando N., Kim C.U. and Gruner S.M., "Alteration of citrine structure by hydrostatic pressure explains the accompanying spectral shift", *Proc. Natl. Acad. Sci.*, **105**, (2008), 13362-13366 .
[9] Barstow B., Ando N., Kim C.U. and Gruner S.M., "Coupling of pressure-induced structural shifts to spectral changes in a yellow fluorescent protein", *Biophys. J.* **97**, (2009), 1719-1727.

MS10-O1

The structural study on influenza RNA polymerase for designing new anti-viral drug

Eiji Obayashi

Protein Design Laboratory, Yokohama City University, Yokohama 230-0045, Japan
E-mail: eijioba@tsurumi.yokohama-cu.ac.jp

The recent outbreak of a new, swine-related H1N1 influenza virus in Mexico has affected the entire world economy, even though it is not as pathogenic as imagined at first. Standard medication, such as NA inhibitors Tamiflu and Relenza, have proved effective against this virul strain, but present vaccines are not. This current pandemic shows that there is still danger of the emergence of new type influenza viruses. New viral strains against which humans have no immunity are spread rapidly from person to person. Furthermore, the swine-related H1N1 influenza virus is a hybrid of human, swine and highly pathogenic avian strains. This means that it is only a matter of time before a new highly pathogenic and Tamiflu-resistant influenza virus emerges, and we have to prepare for it.

The viral RNA-polymerase is not yet a target of any approved pharmaceutical, but has recently become a focus for the development of new anti-influenza drugs since it is highly conserved in avian and human influenza. It carries out a number of essential processes in the viral life cycle, many of which remain poorly understood. The three subunits, PB1, PB2 and PA play different roles within the polymerase, and are all essential for viral replication, but despite considerable functional analysis relatively little is known about their structure. PA and PB2 both bind PB1, but not each other. Here, we have solved crystal structures of the two subunit interaction surfaces, PA-PB1 and PB2-PB1. We have found highly conserved residues which are essential for these interactions, and demonstrated that the interruption of these interfaces dramatically reduces viral replication. These interfaces have considerable potential as a drug target sites, which are entirely independent of surface antigen type.

References

[1] Obayashi E., Yoshida H., Kawai F., Shibayama N., Kawaguchi A., Nagata K., Tame, J.R.H. and Park S.-Y. "The structural basis for an essential subunit interaction in influenza virus RNA polymerase" *Nature*, Vol.454 (2008), pp1127-1131

[2] Sugiyama K., Obayashi E., Kawaguchi A., Suzuki Y., Tame, J.R.H., Nagata, K. and Park S.-Y. "Structural insight into the essential PB1-PB2 subunit contact of the influenza virus RNA polymerase" *EMBO J.,* Vol.28 (2009), pp1803-1811

MS10-O2

Death domain interactions in apoptosis and immunity

Hao Wu, Su-Chang Lin, Hyun Ho Park, Jin Kuk Yang, Liwei Wang and Venkataraman Kabaleeswaran

Department of Biochemistry, Weill Cornell Medical College, 1300 York Avenue, New York, NY 10021, USA
E-mail: haowu@med.cornell.edu

Proteins of the death domain (DD) superfamily share a common fold with six anti-parallel α-helices. They mediate assembly of oligomeric signaling complexes for the activation of caspases and kinases [1]. Structures of three oligomeric DD complexes will be presented, the 6: 4: 4 MyD88: IRAK4: IRAK2 complex in Toll-like receptor signaling [2], the 5: 7 PIDD: RAIDD complex in caspase-2 activation [3] and the 5: 5 Fas: FADD complex in death receptor signaling. These structures collectively reveal common mechanisms of DD interactions including helical symmetry, versatility and high cooperativitiy.

References

[1] Park H. H., Lo Y.-C., Lin S.-C., Wang L., Yang J. K., and Wu H. (2007). "The Death Domain Superfamily in Intracellular Signaling of Apoptosis and Inflammation", *Ann. Rev. Immunol.* 25: 561-86.

[2] Lin S.-C., Lo, Y.-C. and Wu H. (2010). "Helical assembly in the MyD88:IRAK4:IRAK2 complex in TLR/IL-1R signaling", *Nature,* 465: 885-90.

[3] Park H. H., Logette E., Raunser S., Cuenin S., Walz T., Tschopp J. & Wu H. (2007). "Death domain assembly mechanism revealed by crystal structure of the oligomeric PIDDosome core complex", *Cell* 128: 533–546.

MS10-O3

Regulating the ubiquitin E3 ligase activity of C-terminal RING domains

Catherine L. Day, Chu Wai Liew, Peter D. Mace, Katrin Linke

Department of Biochemistry, University of Otago, Dunedin 9054, New Zealand
Email: catherine.day@otago.ac.nz

RING domains are found at the C-terminus of a number of proteins including MDM2, which has a key role in regulating p53 activity, the inhibitor of apoptosis (IAP) proteins, which block cell death in response to diverse stimuli and RNF4, which regulates the abundance of SUMOylated proteins in cells. The RING domains from RNF4, IAPs and MDMs can promote ubiquitylation of themselves and of substrate proteins that are recruited by N-terminal protein interaction domains. This allows them to regulate their own abundance and that of substrate proteins. The RING domains in RNF4, IAP and MDM proteins are critical to their function as they are required for dimerisation and for E3-ligase activity.

Our analysis of proteins that have a C-terminal RING domain suggests that they form comparable dimers and that RING dimerization has an essential role in regulating ubiquitin transfer. We show that E2 binding does not correlate with activity, but RING dimerization is required to promote release of ubiquitin from an E2~ubiquitin conjugate and correlates with activity. This suggests that RING dimerization directly alters the stability of the E2~ubiquitin thioester bond so that the rate of discharge is significantly increased upon dimerization. Recent advances in our understanding of the structure and function of C-terminal RING domains will be discussed, with a particular focus on the regulatory role of RING dimerization.

MS10-O4

Structures of EV71 RNA-dependent RNA polymerase in complex with substrate and inhibitor provide a drug target against the hand-foot-and-mouth disease pandemic in China

Yang Wu[1, $], Zhiyong Lou[2, $], Yi Miao[2], Yue Yu[2], Hui Dong[2], Wei Peng[1], Mark Bartlam[3], Xuemei Li[1] and Zihe Rao[1,2,3,*]

1 National Laboratory of Macromolecules, Institute of Biophysics, Chinese Academy of Science, Beijing, 100101, China
2 Structural Biology Laboratory, Tsinghua University, Beijing, 100084, China
3 College of Life Sciences and Tianjin State Laboratory of Protein Science, Nankai University, Tianjin 300071, China
$ These authors contribute equally to this work
E-mail: wuy@xtal.tsinghua.edu.cn

Enterovirus 71 (EV71), one of the major causative agents for hand-foot-and-mouth disease (HFMD), has caused more than 100 deaths among Chinese children since March 2008. The EV71 genome encodes an RNA-dependent RNA polymerase (RdRp), denoted 3Dpol, which is central for viral genome replication and is a key target for the discovery of specific antiviral therapeutics. Here we report the crystal structures of EV71 RdRp ($3D^{pol}$) and in complex with substrate guanosine-5'-triphosphate and analog 5-bromouridine-5'-triphosphate best to 2.4 Å resolution. The structure of EV71 RdRp ($3D^{pol}$) adopts the usual "closed-right-hand" conformation of an RdRp consisting of fingers, palm, and thumb domains. It has a rearrangement of the thumb domain compared with the crystal structure of poliovirus RdRp, suggesting a possible concerted movement of both the thumb and finger tips during translocation of the RNA template-primer in successive rounds of polymerization. The EV71 RdRp ($3D^{pol}$) /GTP complex shows the vital amino acid residues in incoming NTP binding. The model of the complex with the template:primer derived by superimposition with foot-and-mouth disease virus (FMDV) 3D/RNA complex reveals the majority of EV71 RdRp ($3D^{pol}$) amino acid residues that are likely to be implicated in binding to RNA. A ribonucleotide analogue, 5-bromouridine-5'-triphosphate, in the crystal structure of EV71 RdRp ($3D^{pol}$) /Br-UTP, guides inhibitor design targeting the EV71 RdRp ($3D^{pol}$). These results together provide a molecular basis for EV71 RNA replication and reveal a potential target for anti-EV71 drug discovery.

References

[1] Yang, Y., Wang, H., Gong, E., Du, J., Zhao, X., McNutt, M. A., Wang, S., Zhong, Y., Gao, Z., & Zheng, J. (2009) *Hum Pathol*.
[2] McMinn, P. C. (2002) *FEMS microbiology reviews* 26, 91-107.
[3] King, A. M. Q., Brown, F., Christian, P., Hovi, T., Hyypia, T. et al. (2000) *Seventh Report of the International Committee for the Taxonomy of Viruses* (Van Regen-mortel, M.H.V., Fauquet, C.M., Bishop, D.H.L., Calisher, C.H. et al., Eds.), pp. 657-673.
[4] Racaniello, V. R. (2001) *In Fields Virology*, D.M. Knipe and P.M. Howley, eds. (Philadelphia: Lippincott Williams & Wilkins), pp. 685–722.
[5] Hansen, J. L., Long, A. M., & Schultz, S. C. (1997) *Structure* 5, 1109-1122.
[6] Thompson, A. A. & Peersen, O. B. (2004) *The EMBO journal* 23, 3462-3471.
[7] Thompson, A. A., Albertini, R. A., & Peersen, O. B. (2007) *Journal of molecular biology* 366, 1459-1474.
[8] Love, R. A., Maegley, K. A., Yu, X., Ferre, R. A., Lingardo, L. K., Diehl, W., Parge, H. E., Dragovich, P. S., & Fuhrman, S. A. (2004) *Structure* 12, 1533-1544.
[9] Campagnola, G., Weygandt, M., Scoggin, K., & Peersen, O. (2008) *Journal of virology* 82, 9458-9464.
[10] Ferrer-Orta, C., Arias, A., Perez-Luque, R., Escarmis, C., Domingo, E., & Verdaguer, N. (2004) *The Journal of biological chemistry* 279, 47212-47221.

MS10-O5

Structural basis of innate immunity in plants against fungal pathogens

Thomas Ve[1], Simon Williams[1,2], Eugene Valkov[1], Anna Stamp[1], Pradeep Sornaraj[2], Emma de Courcy-Ireland[2], Jeffrey G Ellis[3], Peter N Dodds[3], Peter A Anderson[2] and Bostjan Kobe[1]

[1]*School of Chemistry and Molecular Biosciences, Institute for Molecular Bioscience, and Centre for Infectious Disease Research, University of Queensland, Brisbane 4072, Australia*
[2]*School of Biological Sciences, Flinders University, G.P.O. Box 2100, Adelaide 5001, Australia*
[3]*CSIRO Plant Industry, Canberra, Australia*
E-mail: b.kobe@uq.edu.au

Plant diseases have a significant effect on economically important crops. Plant immunity is triggered through the recognition of a pathogen effector protein by a plant resistance (R) protein, leading to the activation of plant defenses and a localized cell death response. The effectors usually have roles in virulence and are structurally diverse, while R proteins generally fall into a few conserved families. The effector-R recognition event is poorly understood at molecular and structural levels. We have used the fungal pathogen flax rust interaction with flax as a model system to characterize this process. The flax R proteins consist of a core nucleotide-binding domain, an N-terminal Toll-interleukin 1-receptor (TIR) domain, and a C-terminal leucine-rich repeat (LRR) domain. Previously, we have shown the direct interaction of the effector proteins AvrL567 and AvrM with R proteins L6 and M, respectively [1,2]. We also determined the crystal structure of AvrL567 [3,4]. Here, we report the first crystal structure of a TIR domain from a plant R protein (L6) at 2.3 Å resolution. The structure reveals important differences from the structures of mammalian TIR domains, and highlights three separate functionally important protein surfaces, involved in oligomerization, interaction with a downstream signaling partner, and regulatory intramolecular interactions, respectively. We also determined the crystal structure of flax rust effector protein AvrM, which has no significant sequence similarity with proteins of known structure. The 2.7 Å resolution structure reveals a novel L-shaped helical fold, with two chains forming a dimer with an unusual non-globular shape. Our results bring us a step closer to understanding the molecular basis for the disease resistance process and the ability to engineer novel resistance specificities.

References

[1] Dodds PN, Lawrence GJ, Catanzariti A-M, Teh T, Wang C-I, Ayliffe MA, Kobe B and Ellis JG, "Direct protein interaction underlies gene-for-gene specificity and co-evolution of the flax L5/L6/L7 resistance genes and flax rust AvrL567 avirulence genes", *Proc Natl Acad Sci USA,* 103, 23, (2006), 8888-8893.

[2] Catanzariti A-M, Dodds PN, Ve T, Kobe B, Ellis JG and Staskawicz BJ (2010) "The AvrM effector from flax rust has a structured C-terminal domain and interacts directly with the M resistance protein", *Mol Plant Microbe Interact* 23, 1, (2010), 49-57.

[3] Wang C-IA, Guncar G, Forwood JK, Teh T, Catanzariti A-M, Lawrence GJ, Loughlin FE, Mackay JP, Schirra HJ, Anderson PA, Ellis JG, Dodds PN and Kobe B, "Crystal structures of flax rust avirulence proteins AvrL567-A and -D reveal details of the structural basis for flax disease resistance specificity", *Plant Cell* 19, 9 (2007) 2898-2912.

[4] Guncar G, Wang C-I, Forwood JK, Teh T, Catanzariti A-M, Ellis JG, Dodds PN and Kobe B, "The use of Co2+ for crystallization and structure determination, using a conventional monochromatic X-ray source, of flax rust avirulence protein", *Acta Crystallograph Sect F: Struct Biol Cryst Commun,* 63, 3, (2007), 209-213

MS11-O1

Spin distribution of pi-electron in organic conductor studied by neutron magnetic structure analysis

Yukio Noda

Institute of Multidisciplinary Research for Advanced Materials, Tohoku University 2-1-1 Katahira, Aoba-ku, Sendai 980-8577, Japan
E-mail: ynoda@tagen.tohoku.ac.jp

Magnetism of organic material is still rare to be studied compared to the ordinal d-element metal and oxide compounds. There are two categories of magnetic order in organic compounds; one is d-element moment, which is embedded in an organic molecule, and the other is pi-electron moment, which plays an important role for the bonding in organic system. Obviously, the latter case is interesting to discuss the characteristics of organic compounds.

For the study of magnetic ordering pattern in a crystal unite cell, neutron magnetic scattering is powerful tool. If the magnetic order is antiferromagnetic, macroscopic magnetic quantity is hard to observe. However, neutron scattering clearly shows the new magnetic Bragg peak, which corresponds to the magnetic order parameters. Based on the conventional magnetic structure analysis, we can determine the magnetic moment of the particular atoms. Further, we can extend the analysis to get magnetic moment distribution using so-called Fourier synthesis and maximum entropy method. Usually, the magnetic moment is assumed to be spherical, as is usual case of the x-ray atomic form factor corresponding to the electron cloud distribution. However, if we carefully measure the diffraction intensity and analyze them with much precise form factor, we can get the information of electron orbit distribution [1].

In my talk, I will demonstrate the ability of the single crystal neutron diffraction experiment to show the magnetic moment distribution, which correspond to 3d-electron orbital. One example is MnF_2 ($3d^5$) [2], and the other is Nd_2CuO_4 ($3d^1$:dx^2-y^2) [3]. As an example of organic compound case, I will show the recent experiment of beta'-ET_2ICl_2 [4]. Here, ET is the abbreviation of the molecule BEDT-TTF (bisethylenedithio tetrathiafulvalene). It contains only light atoms (H, C, O and S), and transforms to a magnetic ordered phase at 22K[5]. Our single crystal neutron experiments clearly shows the antiferromagnetic Bragg reflections below 22K. Not only that, the intensity is extraordinary steeply decreased as a function of Q. Fourier synthesis analysis shows the wide distribution of pi-electron extending to the all over region of the unit cell. There is a slight overlapping to one direction to the next unit cell, which will produce the semiconductor type hopping of electrons.

References

[1] Akimitsu J., Ito Y., "Magnetic form-factor of Cu^{2+} in K_2CuF_4", J. Phys. Soc. Jpn **40**(1976) pp 1621-1629.
[2] Noda Y., Kimura H., Komiyama S., Kiyanagi R., Kojima A., Yamada I., Morii Y., Minakawa N. and Takesue N., "Development of a new neutron 4-circle diffractometer and application to the crystal and magnetic structure of MnF_2", Applied Physics A**74** Suppl. (2002) pp 121-123.
[3] Kimura H., Kadoshita K., Noda Y. and Yamada K., "Imaging of Spin Density Distribution by Magnetic Structure Analysis in Nd_2CuO_4", Physica B **385-386** (2006) pp133-136.
[4] Matsunaga A., "Master thesis of Tohoku University (*in Japanese*)", (2005).
[5] Yoneyama N., Miyazaki A., Enoki T. and Saito G., "Magnetic properties of $(BEDT\text{-}TTF)_2X$ with localized spins", Synthetic Metals **86** (1997) pp 2029-2030.

MS11-O2

The studies of multiferroric X-tal bismuth ferrite

Seoungsu Lee[1,3,*], Taekjib Choi[3], W. Ratcliff II[2], R. Erwin[2], S-W. Cheong[3], and V. Kiryukhin[3]

[1]*Neutron Science Division, Korea Atomic Energy Research Institute, Daejeon 305-600, Korea*
[2]*NIST Center for Neutron Research, NIST, Gaithersburg, Maryland 20899, USA*
[3]*Rutgers Center for Emergent Materials and Department of Physics and Astronomy, Rutgers University, Piscataway, New Jersey 08854, USA*
E-mail: seongsulee@kaeri.re.kr

Ferroelectricity and magnetism coexist in multiferroics. These materials have attracted significant attention recently because of an intriguing possibility of control of their magnetic properties with an electric field and vice versa, leading to the discovery of new physical phenomena. Among these materials, $BiFeO_3$ (BFO) is debatably the most extensively studied multiferroic due to its large polarization at room temperature. Multiferroics provide opportunities for devices with unique functionalities utilizing the coupling between different order parameters. Controlling magnetism with an external electric field is one of the most important of these opportunities. This changed with the important discovery of room-temperature magnetoelectric ME coupling in thin films of BFO, in which spins are strongly coupled to ferroelastic domains. Main studies of BFO have studied mainly thin-film form because suitable single crystals were unavailable. Unfortunately, BFO thin films exhibit poor crystallinity and are influenced by substrate strain. Now, our studies of single crystals are required to uncover intrinsic properties of this unique material. This is direct relevance for thin films whose properties are strongly affected by extrinsic strain. In addition, demonstration of electric field induced changes in the magnetic structure by direct methods neutron scattering until now was lacking for BFO.

Here, we will report on several studies of single crystal BFO. One is the studies about the transform of magnetic domain of BFO as function of an external electric field [1]. Another one is the single domain physics of x-tal BFO studied by polarized neutron-scattering and piezoresponse force microscopy [2]. Finally, the unique property of the single crystal BFO [3] and the effort for the realization of multiferroic materials with ferromagnetic property at room temperature will be shown in our presentation [3].

References

[1] Seongsu Lee, W. Ratcliff II, S-W. Cheong, and V. Kiryukhin, APPLIED PHYSICS LETTERS 92, 192906 (2008)
[2] Seongsu Lee,Taekjib Choi,W. Ratcliff II, R. Erwin, S-W. Cheong, and V. Viryukhin, PHYSICAL REVIEW B 78, 100101(R)(2008)
[3] T. Choi, S. Lee, Y. J. Choi, V. Kiryukhin, and S-W. Cheong, Science 324, 63 (2009)

MS11-O3

Molecular magnetic semiconductors based on organic ligands with delocalized sulfur-rich core

Jing-Lin Zuo, Xiao-Zeng You

State Key Laboratory of Coordination Chemistry, School of Chemistry and Chemical Engineering, Nanjing University, Nanjing 210093, China
Email: zuojl@nju.edu.cn

Owing to unique π electron-donating-properties, tetrathiafulvalene and its derivatives (TTFs) have been extensively studied for decades to achieve molecular conductors and superconductors.[1] The investigation of magnetic conductor and magnetic semiconductor based on TTFs has been receiving much attention,[2] due to its potential application in spintronics.[2-3]

Using different chemical synthetic methods, for example, hybridizing two individual magnetic and conducting part, or direct coordination of paramagnetic metal ions to organic ligands with TTF derivatives, many metal complexes possessing both the conducting π-electrons and magnetic d-electrons (π-d system) have been synthesized. Some d-d and π-π interactions are observed in these systems and it leads to the coexistence of magnetic and conducting properties. Recently, we have prepared some versatile ligands of with delocalized sulfur-rich cores, for example, polypyridine or carboxylate ligands containing TTF units.[3-5] They are useful bridges for heteronuclear complexes. Some deprotected ligands offer feasibility to be modified by introducing selected functional groups at peripheral sites. It is anticipated that, multi-functional properties, such as magnetic semi-conductive, and cooperative behaviors could be achieved through modification. Furthermore, with the use of some molecular magnetic semiconductors, the spin injection and transportation into the TTF molecules have been studied.

References

[1] a) Kobayashi H., Cui H. B. and Kobayashi A., *Chem. Rev.* 104 (2004) 5265; b) Tanaka M., Okano Y., Kobayashi H., Suzuki W. and Kobayashi A., *Science*, 291 (2001) 285.
[2] a) Coronado E., Galán-Mascarós J. R., Gómez-García C. J. and Laukhin V., *Nature*, 408 (2000) 447; b) Kosaka Y., Yamamoto H. M., Nakao A., Tamura M. and Kato R., *J. Am. Chem. Soc.*, 129 (2007) 3054.
[3] a) Chen Y., Li C. H., Wang C. F., Zuo J. L. and You X. Z., *Science in China, Series B*, 52 (2009) 1596; b) Peng Y. H., Meng Y. F., Hu L., Li Q. X., Li Y. Z., Zuo J. L. and You X. Z. *Inorg. Chem.*, 49 (2010) 1905.
[4] Wen H. R., Li C. H., Song Y., Zuo J. L., Zhang B. and You X. Z., *Inorg. Chem.*, 46 (2007) 6837.
[5] a) Liu W., Wang R., Zhou X. H., Zuo J. L. and You X. Z., *Organometallics*, 27 (2008) 126; b) Liu W., Chen Y., Wang R., Zhou X. H., Zuo J. L. and You X. Z., *Organometallics*, 27 (2008) 2990.

Anomalous L3/L2 X-ray absorption branching ratios in 5d transition metal oxides

Deok-Yong Cho, Junghwan Park and Je-Geun Park

Department of Physics and Astronomy, Seoul National University, Seoul 151-747, Korea
E-mail: zax@snu.ac.kr

The L_3 and L_2 edge white-line intensities in the X-ray absorption spectra were examined for a variety of 5d transition metal binary oxides. The white-line intensities at both edges decreased with increasing 5d electron number due to decreasing number of the final states in the 2p - 5d transition. The intensity ratio between the two white lines, or the L_3/L_2 branching ratio, showed a large deviation from the statistical value of 1/2 in contrast to the case of the 3d transition metal oxides. This branching ratio increased systematically with increasing 5d electron number. The anomalous behavior can be interpreted as a signature of strong spin-orbit coupling in the 5d shells because the spin-orbit coupling promotes the J quantum states so as to make extremely biased J occupations in the photoabsorption process. The similar works have already been preformed for the 5d elements and metallic alloys [1]. However, the recent interests in novel 5d oxides reinstated the general attention on the spin-orbit coupling in the 5d transition metal oxides [2,3].

References

[1] Qi B., Perez I., Ansari P. H., Lu F. and Croft M., "L_2 and L_3 measurements of transition-metal 5d orbital occupancy, spin-orbit effects, and chemical bonding", *Phys. Rev. B,* Vol 36, No. 5, (1987), pp 2972-2975.

[2] Kim B. J., Ohsumi H., Komesu T., Sakai S., Morita T., Takagi H. and Arima T., "Phase-Sensitive Observation of a Spin-Orbital Mott State in Sr_2IrO_4", *Science*, Vol. 323, (2009), pp 1329-1332.

[3] Shitade A., Katsura H., Kuneš J., Qi X.-L., Zhang S.-C. and Nagaosa N., "Quantum Spin Hall Effect in a Transition Metal Oxide Na_2IrO_3", *Phys. Rev. Lett.*, Vol. 102, No. 25, (2009), p 256403.

MS11-O5

An investigation of magnetic exchange through double halide bridges

Jan Wikaira 1, Mark M. Turnbull2, Christopher P. Landee2 and Chris Saunders1

1Department of Chemistry, University of Canterbury, PB 4800, Christchurch, 8410, New Zealand
2Carlson School of Chemistry and Biochemistry, Clark University, 950 Main St, Worcester, MA 01610, USA
E-mail: jan.wikaira@canterbury.ac.nz

After extensive investigation, a variety of pathways for magnetic exchange in cuprate salts has been elucidated. One of these, which involves magnetic exchange via non-bonding contacts between halide ions attached to a variety of metals, is of particular interest in this study. This pathway, M-X ••••X-M, is described as a double halide bridge. As the factors controlling the sign and strength of the magnetic exchange through double halide bridges are not currently well understood, a considerable library of compounds is needed to facilitate this investigation. A series of Cu(II) compounds containing the CuX42+ anion are being synthesised and their crystal structures and magnetic behaviour determined to the end that the appropriate magnetostructural correlations may be added to those already reported in the literature. A proposed system for the interaction topology is fully explained in reference 3.

The packing of the CuX42+ anions in A2CuX4 complexes (AH = protonated organic base), and as a result the distances and angles in these double-halide bridges, are significantly affected by the packing of the molecules in the crystals. Changes in the crystal packing can be effected by changing the cationic portion (AH) of the molecule. Turnbull et.al., have undertaken a systematic series of investigations of the compounds (5-S-2-aminopyridinium)2CuX4 (X=Cl, Br) and S=F, Cl, Br, I and Me. In this family, the crystal packing is affected by the size of the S-substituent, and in part dominated by the hydrogen-bond dominating properties of the 2-aminopyridinium N-H groups. More recent results in this series and in the new series 6-S-3-aminopyridinium will be discussed.

References

[1] (a) R.H. White, Quantum Theory of Magnetism, 2nd ed., Springer-Verlag, Berlin. 1983;
(b) R.L. Carlin, Magnetochemistry, Springer-Verlag, Berlin. 1986;
(c) O.Kahn, Moleculare Magnetism, VCH Publishers, New York, 1993.
(d) L.J. Longh (ED.), Magnetic Properties of Layered Transition Metal Compounds, Kluwer Academic Publishers, Dordrecht, 1990.
[2] W.E. Marsh, E.J. Valence, D.J. Hodgson, Inorg. Chim. Acta 51, (1981), 49.
[3] M.M. Turnbull, C. P. Landee, B.M. Wells, Coord. Chem. Rev., **249**, 2567 (2005).
[4] (a) F.M. Woodward, A.S. Albrecht, C.M. Wynn, C.P. Landee, M.M. Turnbull, Phys. Rev. B 65(2002) 144412.
(b) C.P. Landee, M.M. Turnbull, C. Galeriu, J. Giantsidis, F.M. Woodward, Phys. Rev. B: Rapid Commun. 63 (2001) 100402R.
(c) F.M. Woodward, C.P. Landee, J. Giantsidis, M.M. Turnbull, C. Richardson, Inorg. Chim. Acta 324 (2001) 324.
(d) T.J. Coffey, C.P. Landee, W.T. Robinson, M.M. Turnbull, M. Winn, F.M. Woodward, Inorg. Chim. Acta 303 (2001) 54.
[5] Jan L. Wikaira,* Lixin Li, Ray Butcher, Christopher M. Fitchett, Geoffrey B. Jameson, Christopher P. Landee, Shane G. Telfer and Mark M. Turnbull.* J.Coord. Chem (2010), *I.P.*

MS12-O1

Polymorphism, solvotomorphism and related aspects in framework inorganic compounds

Srinivasan Natarajan

Framework Solids Laboratory, Solid State and Structural Chemistry Unit, Indian Institute of Science, Bangalore 560 012, India
E-mail: snatarajan@sscu.iisc.ernet.in

Polymorphism, one of the earliest known structural modifications, defined as the existence of at least two different structural forms for a particular molecular formula. The occurrences of polymorphism are quite prevalent in the area of organic chemistry and also in inorganic chemistry. The subtle differences in the structural arrangements and interactions within the crystal structures of some of the pharmaceutical drugs are believed to have profound effect in their therapeutic use. In spite of the common occurrences, there are not many polymorphic structures that are known in amine templated inorganic compounds. The formation of closely related structures (polymorphs) in zeolites have been known and observed in electron microscopy investigations. Recently, the first example of polymorphic structures has been reported in open-framework amine templated inorganic arsenate and phosphite structures from our group.[1-4] In addition, we have also observed closely related structural forms in amine templated inorganic borates.[1] The present talk would highlight these interesting findings.

References

[1] Stabilization of Graphite and Diamond Nets in a Family of Aluminoborates, A.K. Paul and S. Natarajan, *Crystal Growth & Design*, **2010**, *10*, 765 – 774.
[2] Synthesis, Structure and Transformation Studies in a Family of Inorganic-Organic Hybrid Fram ework Structures Based on Indium, P. Ramaswamy, N. N Hegde, R. Prabhu, V.M.Vidya, A. Datta and S. Natarajan, *Inorg. Chem.*, **2009**, *48*, 11697 – 11711.
[3] Synthesis, Structure and Polymorphism Studies in Amine-Templated Open-Framework Zinc Pho sphites, S. Mandal and S. Natarajan, *Inorg. Chem.*, **2008**, *47*, 5304 – 5313.
[4] Amine-Templated Open-Framework Zinc Arsenates of Varying Dimensionalities: Synthesis, Stru cture, Polymorphism and Transformation Reactions, V.K. Rao, S. Chakrabarti and S. Natarajan, *Inorg. Chem.*, **2007**, *46*, 10781 – 10790.

High resolution crystallography to understanding the bonding between a transition metal and an alkyne

C. Lecomte,[a] N. Claiser,[a] S. Pillet,[a] H. Nuss,[a] M. Etienne[b] and N. Lugan[b]

[a] *Laboratoire de Cristallographie Résonance Magnétique et Modélisations, UMR CNRS 7036, Institut Jean Barriol, Nancy-Université, BP 239 54506 Vandoeuvre-lès-Nancy, France*
[b] *Laboratoire de Chimie de Coordination du CNRS, UPR8241, 205 Route de Narbonne 31077, Toulouse, France*
E-mail: claude.lecomte@crm2.uhp-nancy.fr

Since many years, the study of the experimental electron density and its latest developments has proven to be a powerful tool to a better understanding of the metal-ligand interactions. We have applied this method, based on high resolution X-ray diffraction data, to investigate a series of metal-alkyne complexes.
The studied compounds are a manganese complex, MnCp(PhC≡CPh)(CO)2, for which the alkyne is considered as a 2e donor, and a niobium compound, Nb(C14H23N2O)(H3CC≡CCH3)Cl2 in which the alkyne should act as a 4e donor. Both complexes were studied at 100 K (structures on figure 1).

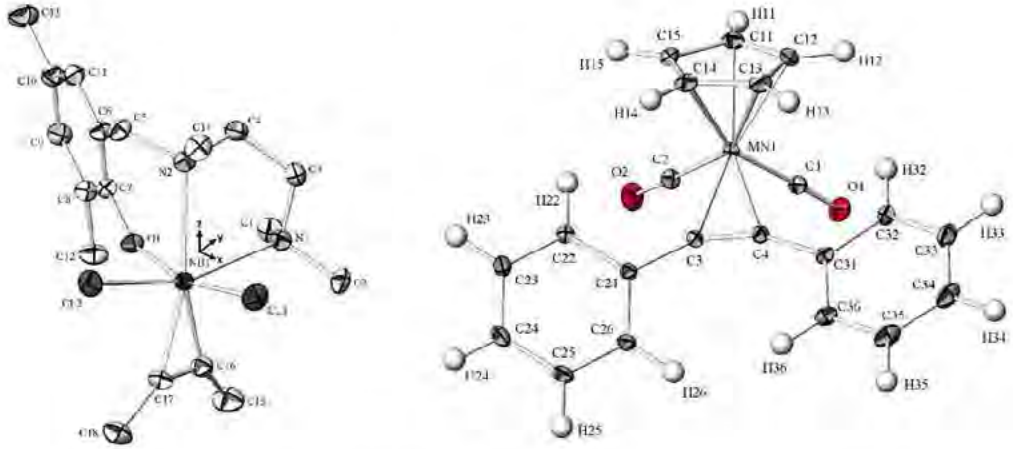

Figure 1: ORTEP plots of the two crystal structures at 100K (75% probability level)

Our aim is to define precisely the bonding situation of each metal in order to identify and characterize the electronic specificities of a 2e versus a 4e donor complex.

We shall discuss various electron density and topological descriptors which may be appropriate for that respect.

MS12-O3

Microporous Metal-Organic Frameworks Based on Metal-Organic Supramolecules

Myoung Soo Lah and Minhak Oh

Interdisciplinary School of Green Energy, Ulsan National Institute of Science & Technology, Ulsan, 689-798, Korea
E-mail: mslah@unist.ac.kr

Microporous metal–organic frameworks (MOFs) based on porous metal–organic supramolecules have been prepared using carefully designed ligands [1]. The ligands with multiple bdc units connected with various covalent linking groups were used for the construction of MOFs covalently interconnected with cuboctahedral metal–organic polyhedra (MOPs) generated by edge-directed corner-linkage strategy. Two isostructural MOFs based on MOPs have been prepared using a rigid C_3 symmetric hexacarboxylic ligand, 1,3,5-tris(3,5-dicarboxylphenylethynyl)benzene, in which three 3,5-benzenedicarboxylate (bdc) units were connected via the 1,3,5-ethynylbenzene group [2]. In these MOFs, the bdc unit is involved in the formation of an edge-directed corner-linked MOP by use of a Cu(II) paddle-wheel secondary building unit, and the MOPs are interconnected via quadruple covalent linkages to a cubic close packing arrangement. The Zn-polyhdron-based MOF (Zn-PMOF-2) did not show any significant gas sorption behavior, whereas the Cu analogue (Cu-PMOF-2) with exposed metal sites is theramlly and hygrically stable. Cu-PMOF-2 has a large surface area, large H_2 adsorption enthalpy, and very large excess H_2 storage capacity. Another type of two-fold interpenetrating Cu-polyhdron-based MOF (Cu-PMOF-3) with exposed metal sites was prepared using a rigid and bent C_2 symmetric ligand containing two bdc units [3]. In spite of the interpenetration, the PMOF still has a large solvent cavity inherited from the MOC building unit, the corresponding large surface area and high uptake capacities for various gas molecules. A powder X-ray diffraction pattern and sustained N_2 sorption behavior of Cu-PMOF-3 soaked in water, under even reflux conditions, strongly support its high hydrothermal stability.

References

[1] Prakash M. J. and Lah M. S., "Metal-organic macrocycles, metal-organic polyhedra, and metal-organic frameworks", *Chem. Commun.* (2009), 3326.

[2] Hong S., Oh M., Park M., Yoon J., Chang J.-S. and Lah M. S., "Large H_2 Storage Capacity of a New Polyhedron-based Metal-Organic Framework with High Thermal and Hygroscopic Stability", *Chem. Commun.* (2009), 5397.

[3] X. Liu, M. Park, S. Hong, M. Oh, J. Yoon, J.-S. Chang, M. S. Lah, "A twofold interpenetrating porous metal–organic framework with high hydrothermal stability: structure and gas sorption behavior", *Inorg. Chem. 48,* (2009), 11507.

MS12-O4

A compound with 6 chiral centers that uses the same unit cell and space group to grow either a racemate or an enantiomer

A. David Rae[1], Mukesh K. Sharma[1], Anthony C. Willis[1] and Martin G Banwell[1]

[1]*Research School of Chemistry, Australian National University, Canberra, ACT 0200, Australia*
E-mail: rae@rsc.anu.edu.au

The diol (5R,6S)-1-iodo-4,5,6-trimethylcyclohexa-1,3-diene5,6-diol was used as a precursor in the manufacture of a penta-annulated bicyclo[2.2.2]octane compound, C18H26O3 that contains six chiral centers. The diol was not pure and contained 20% of its mirror image. Much of the crystalline material in the bulk sample of the C18H26O3 was unsuitable but a limited number of usable small thin plates were observed. It gave a ratio for mirror related molecules of 0.595(1) : 0,405. In view of this curious result, a second smaller crystal was examined and gave essentially the same result. ie a ratio for mirror related molecules of 0.602(1) : 0.398.

The structure was solved and refined as an average structure in space group P21212 (a 13.6886(3), b 27.1933(7), c 8.7038(2) Å, T 200 K) with two molecules on general positions in the asymmetric unit. Molecule 1 was ordered but molecule 2 was 0.810(2) : 0.190 disordered. The major component has the opposite chirality to molecule 1 whereas the minor component has the same chirality as molecule 1. R(F) = 0.051 for 2611 independent reflections out of 4187 where both Iobs and Icalc were > 3 (Iobs). There appears to be very little diffuse scattering so it is reasonable to assume we have reasonably large domains of two ordered structures approximated by the average structure.

Refinement used the program RAELS2008 as it allowed the use of a single set of refinable local orthonormal coordinates to describe all three molecules as a constraint. It also allowed the anisotropic atom displacement parameters of the disordered molecule to be sensibly constrained using an equality of single atom parameters described relative to the axial systems used to locate the disordered molecule in the crystal from the local coordinates. An additional TLX model (a single re-orientable re-locatable libration axis, 11 variables) was applied to all atoms in the 1:4 disordered molecule. The refinement used 334 parameters to refine 63 non-hydrogen atom positions and their atom displacement parameters. Hydrogen atoms were reinserted in sensible positions each refinement cycle and given anisotropic atom displacement parameters determined by the parameters used to describe the atoms to which they were attached.

MS12-O5

Kinetic theory of crystallization of nanoparticles

Katsuhiro Tsukimura[1], Masaya Suzuki[1], Yohey Suzuki[1], Takashi Murakami[2]

[1]*Geological Survey of Japan, National Institute of Advanced Industrial Science and Technology, Tsukuba, Ibaraki 305-8567, Japan*
[2]*Department of Earth & Planetary Sciences, the University of Tokyo, Bunkyo, Tokyo 113-0033, Japan*
E-mail: tsukimura-katsuhiro@aist.go.jp

We here describe a kinetic theory of the crystallization of nanoparticles, where nanoparticles are dissolving and crystals are forming in solution. The theory assumes that a crystal nucleates only on a nanoparticle, the crystal stops growing at a certain size, and the concentration of metal ion in solution is close to the solubility of the nanoparticles. On the basis of these assumptions, we have derived integral equations for $R(t)$ (crystal ratio as a function of time). We have solved the integral equations with a successive approximation method. When time t is less than t_{inflec} (=r_{max}/G, r_{max}= maximum radius of crystal, G = growth rate of crystal), $R(t)$ is close to fourth power of time; when t is larger than t_{inflec}, $R(t)$ is close to an exponential-type function. The kinetic theory has been applied successfully to the transformation of ferrihydrite nanoparticles to goethite or hematite crystals, and the crystallization of TiO_2 (Fig. 1). The theory shows that the nucleation rate of crystal essentially determines the crystallization rate, and that induction period is observed when the growth of crystal is slow.

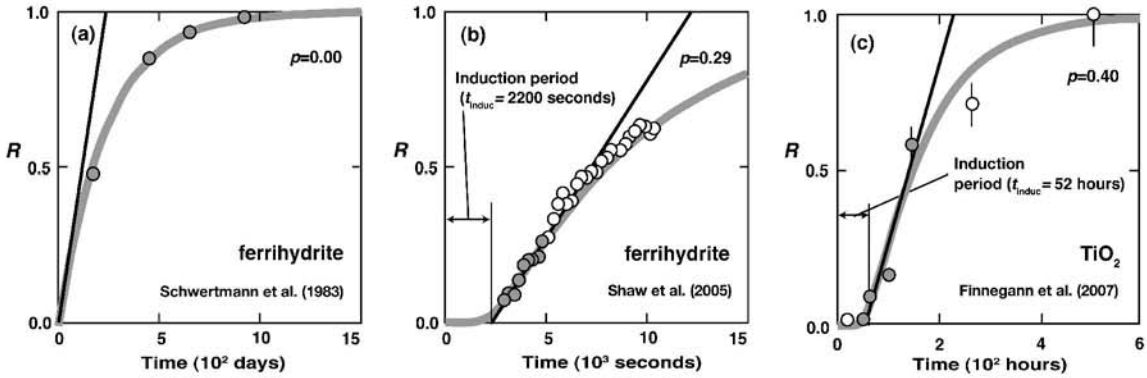

Fig. 1. Relation between observed and calculated values of R [1]; (a) the transformation of ferrihydrite at pH 6 and 297 K by Schwertmann et al. [2], (b) the transformation of ferrihydrite at pH 10.7 and 361 K by Shaw et al. [3], and (c) the crystallization of TiO_2 at pH 1 and 473 K [4]. Circles denote experimental data points and solid curves calculated values based on the present theory. Data points in grey symbols were used for the determination of parameters p and t_{inflec} (=4/3 t_{induc}) . We assume that errors in (c) and (d) are ±10% of

References

[1] Tsukimura, K., Suzuki, M., Suzuki, Y., Murakami, T., "Kinetic theory of crystallization of nanoparticles", *Crystal Growth & Design,* Vol. 10,(2010).
[2] Schwertmann U., Murad E., "Effect of pH on the formation of goethite and hematite from ferrihydrite", *Clays & Clay Mineral*, Vol 31, (1983), pp. 277-284.
[3] Shaw S., Pepper S. E., Bryan N. D., Livens F. R. "The kinetics and mechanisms of goethite and hematite crystallization under alkaline conditions, and in the presence of phosphate", *Am. Mineral.*, Vol. 90, (2005), pp. 1852-1860.
[4] Finnegan M. P., Zhang H., Banfield J. F., "Phase stability and transformation in titania nanoparticles in aqueous solutions dominated by surface energy", *J. Phys. Chem. C*, Vol. 111, (2007), pp 1962-1968.

AsCA2010

The 10th Conference of the Asian Crystallographic Association

ABSTRACTS

November 3, (Wednesday)

Morning Oral Sessions (MS13, 14, 15)

MS13-O1

Crystal structures of the Hyp proteins for [NiFe] hydrogenase maturation

Satoshi Watanabe[1], Takayuki Arai[1], Rie Matsumi[2], Haruyuki Atomi[2], Tadayuki Imanaka[3] and Kunio Miki[1]

[1]*Department of Chemistry, Graduate School of Science, Kyoto University, Sakyo-ku, Kyoto 606-8502, Japan*
[2]*Department of Synthetic Chemistry and Biological Chemistry, Graduate School of Engineering, Kyoto University, Katsura, Nishikyo-ku, Kyoto 615-8510, Japan*
[3]*Department of Biotechnology, College of Life Sciences, Ritsumeikan University, Kusatsu 525-8577, Japan*
E-mail: watanabe@kuchem.kyoto-u.ac.jp

[NiFe] hydrogenases catalyze the reversible oxidation of molecular hydrogen. The active site is composed of a Ni atom and a Fe atom. Furthermore the two CN and one CO are attached to the Fe atom. The biosynthesis/maturation of [NiFe] hydrogenases is a stepwise process that requires six hydrogenase maturation proteins (HypABCDEF)[1]. To elucidate each step of the maturation at an atomic resolution, we have determined crystal structures of HypA, HypC, HypD and HypE from *Thermococcus kodakaraensis* KOD1[1,2].

HypA and HypB are involved in the insertion of the Ni atom into the large subunit of the hydrogenase. The monomer structure of HypA consists of Ni- and Zn-binding domains[1]. Local conformations of the conserved Ni-binding motif affect the relative arrangement of the two metal binding domains, suggesting a communication between the Ni- and Zn-binding sites. The HypA dimer is unexpectedly formed by domain swapping through archaea specific linker helices. In addition, the hexameric structure of HypA is observed in the crystal packing. These findings suggest the functional diversity of HypA proteins.

HypCDEF are involved in the synthesis and insertion of the $Fe(CN)_2CO$ ligand. The crystal structures of HypC, HypD and HypE reveal structural features of each protein and functional roles of conserved motifs of these proteins[2]. It is remarkable that HypD has a redox cascade similar to the ferredoxin:thioredoxin reductase system, in which two redox thiols are regulated by an 4Fe-4S cluster. In order to obtain further insight into the maturation process, we have determined the structure of the HypC-HypD complex at 2.55Å resolution. In the HypCD complex, the β-barrel domain of HypC is tightly bound to the central cleft of HypD, which is highly conserved region of HypD. On the other hand, the C-terminal α-helix of HypC shows large conformational changes and does not interact with any part of HypD. The N-terminal residues of HypC are located near the conserved motifs of HypD. These observations support a hypothetical cyanation mechanism by thiol redox signaling in the HypCDE complex.

References

[1] Watanabe, S., Arai, T., Matsumi, R., Atomi, H., Imanaka, T. & Miki, K. "Crystal structure of HypA, a nickel-binding metallochaperone for [NiFe] hydrogenase maturation", *J Mol Biol,* Vol. 394, (2009), pp 448-59.

[2] Watanabe, S., Matsumi, R., Arai, T., Atomi, H., Imanaka, T. & Miki, K. "Crystal structures of [NiFe] hydrogenase maturation proteins HypC, HypD, and HypE: insights into cyanation reaction by thiol redox signaling", *Mol Cell,* Vol. 27, (2007), pp 29-40.

MS13-O2

Combining sequence and structural analysis to obtain a perfect alignment essential to rational drug design

W.L. Duax, R. Huether, D. Dziak

Hauptman-Woodward Medical Research, Institute, 700 Ellicott St., Buffalo, NY. 14203 U.S.A.
E-mail: duax@hwi.buffalo.edu

The sequences of families of proteins found in all bacterial species can be accurately and perfectly aligned by locating Glycine (G), Alanine (A), Arginine (R) and Proline (P) residues [GARP] that are 100% conserved in fixed positions in all members of the family and by locating precisely the sites of amino acid insertions or deletions in the sequence alignment. All fundamental folds found in essential proteins that are present in all bacteria contain one or more Glycine residues that cannot be replaced by any other amino acid and most contain one or more prolines, alanines or arginines that are not replaced by any other amino acid. Proof of principal is provided for 1800 genes for ribosomal protein L1 from all bacterial genomes. The accuracy of the alignment is demonstrated by our ability to separate Gram positive and Gram negative bacteria and co-isolate L1 proteins in cyanobacteria and chloroplasts on the basis of only two sequence positions each. Application of the [GARP] based perfect alignment to the short chain oxido reductase (SCOR) family of 20,000 enzymes allows sequence analysis of the three loops that define substrate binding. Combinations of 5 to 9 residues in the three loops unequivocally identify specific substrates. Proof of principal is demonstrated for 1600 β-keto (acyl carrier protein) reductase enzymes present in all bacteria and 500 acetyl CoA reductase enzymes primary present in proteobacteria.

MS13-O3

Structural insights into the conformational change upon activation of tyrosine site-specific recombinase

Ki-Hyun Nam, Gye Yoon Cho, Hyun-suk Kim, Hosam Ki, Kwang Yeon Hwang

Division of Biotechnology, School of Life Sciences and Biotechnology, Korea University, Anam-Dong, Seongbuk-Gu, Seoul 136-713, Korea
E-mail: chahong@korea.ac.kr

In microorganism, tyrosine site-specific recombination plays a pivotal role in reshuffle their genetic information as a chromosome separation. In the bacteria system, FtsK promotes a complete Xer recombination reaction by switching the state of activity of the XerCD recombinase. Whereas integrase family in archaea is commonly shared the sequence of recombinase/integrase without activation of FtsK protein. Here we reported the sequential and structural analysis of site-specific integrase/recombinase from archaeon *Thermoplasma acidophilum*. This crystallographic data has the novel conformation between core-binding and catalytic domain, and it given insight into the large conformational change between two domains. As well as, we propose the conformational change for the cleavage mode of nucleophile tyrosine by interaction between the C-terminal helix and partner molecules. This structure studies will contribute the understanding the archaea recombination system, and providing the framework for commonly architectural mechanisms in the integrase family.

References

[1] Arciszewska, L.K., Grainge, I., and Sherratt, D.J. "Action of site-specific recombinases XerC and XerD on tethered Holliday junctions." *EMBO J.* Vol.16, (1997). pp. 3731-3743.
[2] Blakely, G. W., Davidson, A. O., and Sherratt, D. J. "Binding and cleavage of nicked substrates by site-specific recombinases XerC and XerD." *J. Mol. Biol.* Vol.265, (1997). pp. 30-39.
[3] Le Bourgeois, P., Bugarel, M., Campo, N., Daveran-Mingot, M.L., Labonté, J., Lanfranchi, D., Lautier, T., Pagès, C., Ritzenthaler, P. "The unconventional Xer recombination machinery of Streptococci/Lactococci." *PLoS Genet.* Vol. 3, (2007). e117.

MS13-O4

Crystal structures of the N-terminal dystrophin and utrophin spectrin repeats show a three helix bundle fold

Muralidharan Muthu and Andrew J Sutherland-Smith

Center for Structural Biology, Institute of Molecular Biosciences, Massey University, Palmerston North, New Zealand
E-mail: M.A.Muthu@massey.ac.nz

Duchenne and Becker muscular dystrophies (DMD & BMD) are muscle-wasting disorders caused by mutations in the X-linked dystrophin gene. Utrophin is a widely expressed protein with high sequence similarity to dystrophin that has been shown to functionally compensate for dystrophin in cultured muscle cells and in the muscular dystrophy *(mdx)* mice model. Replacement of utrophin for dystrophin in DMD and BMD patients is a potential therapeutic strategy [1].

Dystrophin and utrophin are large cytoskeletal proteins, belonging to the spectrin superfamily, that link intracellular F-actin and the extracellular matrix via a membrane-associated protein complex. Utrophin and dystrophin are characterized by N-terminal actin binding domains and C-terminal variable domains separated by 22 or 24 spectrin-like repeats respectively. Certain utrophin and dystrophin spectrin repeats can bind F-actin, and was hypothesized to act as a shock absorbers or molecular springs. The aim of this research is a structural and biochemical comparison of utrophin and dystrophin N-terminal spectrin repeats. Studies have shown that spectrin repeats of utrophin are required for a higher affinity interaction of the actin binding domain with F-actin. It is unclear whether the N-terminal repeats have an intrinsic affinity for F-actin and in the current study we are determining the actin-binding properties of these spectrin repeats. The crystal structure of the N-terminal repeats from utrophin and dystrophin have been determined and exhibit the characteristic triple-helix structure folded into a left-handed coiled-coil [2].

References

[1] Tinsley JM, Deconinck N, Fisher R, Kahn D, Phelps S, Gillis JM and Davies KE. Expression of full-length utrophin prevents muscular dystrophy in *mdx* mice. *Nat. Med.* **4** (1998), 1441-14 44.

[2] Parry DA, Dixon TW and Cohen C. Analysis of the three-α-helix motif in the spectrin superf amily of proteins. *Biophys. J.* **61** (1992) 858–867

MS13-O5

Structural basis of energy transfer in the bioluminescent system of jellyfish *Clytia*: the GFP-photoprotein complex

Maxim Titushin*[1,2], Yingang Feng*[1], Galina Stepanyuk[2,3] and Zhi-Jie Liu[1]

[1]*National Laboratory of Biomacromolecules, Institute of Biophysics, Chinese Academy of Sciences, Datun Road 15, Beijing 100101, China*
[2]*Laboratory of Photobiology, Institute of Biophysics Russian Academy of Sciences, Siberian Branch, Akademgorodok 50/50, Krasnoyarsk 660036, Russia*
[3]*Department of Biochemistry and Molecular Biology, University of Georgia, Athens, GA 30602, USA*
**These authors contributed equally to this work*
E-mail: maxim_titushin@moon.ibp.ac.cn

Förster resonance energy transfer within a protein-protein complex has previously been invoked to explain emission spectral modulation observed in several bioluminescence systems [1]. Here we present a spatial structure of a complex of the Ca^{2+}-regulated photoprotein clytin with its Green-fluorescent Protein (*cg*GFP) from the jellyfish *Clytia gregaria*, and show that it accounts for the bioluminescence properties of this system *in vitro*. We adopted an indirect approach of combining X-ray crystallography determined structures of the separate proteins, NMR spectroscopy, computational docking and mutagenesis. Heteronuclear NMR spectroscopy using variously ^{15}N,^{13}C,^{2}H-enriched proteins enabled assignment of backbone resonances of more than 94% of the residues of both proteins. In a mixture of the two proteins at millimolar concentrations, complexation was inferred from perturbations of certain ^{1}H-^{15}N HSQC-resonances, which could be mapped to those residues involved at the interaction site. A docking computation using HADDOCK [2] was employed constrained by the sites of interaction, to deduce an overall spatial structure of the complex (Fig. 1). Contacts within the clytin-*cg*GFP complex and electrostatic complementarity of interaction surfaces argued for a weak protein-protein complex. Mutation of clytin residues located at the interaction site, reduced the degree of protein-protein association concomitant with a loss of effectiveness of *cg*GFP in color-shifting the bioluminescence. It is suggested that this clytin-*cg*GFP structure corresponds to the transient complex previously postulated to account for the energy transfer effect of GFP in the bioluminescence of aequorin or Renilla luciferase.

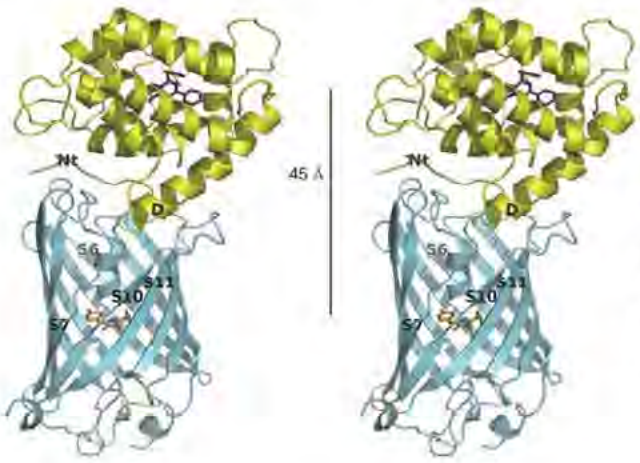

Fig. 1. Stereoview representation of the spatial structure of the clytin-*cg*GFP complex derived from X-ray structures of clytin and *cg*GFP, NMR-mapping of the interaction surfaces and computational docking in HADDOCK. The 45 Å is the distance between the two chromophores. α-helix D and the N-terminus of clytin (top molecule) carry the positive charge and occupy, with good shape complementarity, the negatively charged gutter on the top of the *cg*GFP barrel (bottom molecule) formed by the S3-S4, the distal part of the S6-S7, and the S10-S11, loops.

References

[1] Morin J G, Hastings J W (1971) Energy transfer in a bioluminescence system. *J Cell Physiol* 88:313-318.
[2] Dominguez C, Boelens R, Bonvin A M (2003) HADDOCK: a protein-protein docking approach based on biochemical or biophysical information. *J Am Chem Soc* 125:1731-1737.

MS14-O1

Nano magnetic structure analysis by cryo Lorentz TEM - Visualization of the "Skirmion" crystal

Xiuzhen Yu[1,2], Yoshinori Tokura[2,3] and Yoshio Matsui[1]

[1]*National Institute for Materials Science, 1-1 Namiki, 305-0044, Japan*
[2]*Multi-Ferroics Projekt, ERATO-JST, Tokyo 113-8656, Japan*
[3]*Department of Applied Physics, University of Tokyo, Tokyo 113-8656, Japan*
E-mail: MATSUI.Yoshio@nims.go.jp

We have so-far studied plenty of singular magnetic nanostructures in various materials. Among them is the unusual, topologically stable "skyrmion" spin texture, in which the spins point in all the directions wrapping a sphere. The skyrmion configuration in a magnetic solid is anticipated to produce unconventional spin–electronic phenomena such as the topological Hall effect. The crystallization of skyrmions as driven by thermal fluctuations has recently been confirmed in a narrow region of the temperature/magnetic field (T–B) phase diagram, by neutron scattering studies of helical magnets MnSi[1)] and $Fe_{1-x}Co_xSi$[2)]. Here, on the other hand, we report "real-space imaging" of a two-dimensional skyrmion lattice in a thin film of $Fe_{0.5}Co_{0.5}Si$ by Lorentz transmission electron microscopy[3)]. This compound has a typical helical spin order at low-temperature without the magnetic field[4)]. With a magnetic field of 50–70mT applied normal to the film, however, we observe skyrmions in the form of a hexagonal arrangement of swirling spin textures, with a lattice spacing of 90 nm. The related T–B phase diagram is found to be in good agreement with Monte Carlo simulations. In such two-dimensional case, the skyrmion crystal seems very stable and appears over a wide range of the phase diagram, including near zero temperature. Such a controlled nanometre-scale spin topology in a thin film may be useful in observing unconventional magneto-transport effects.

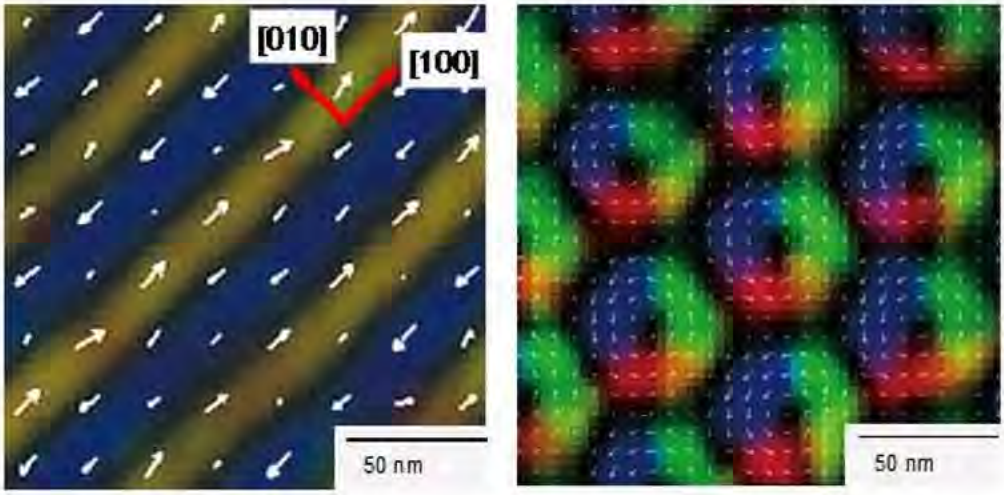

Fig. 1 Helical spin texture of $Fe_{0.5}Co_{0.5}Si$ without magnetic field (left), and the "Skirmion" lattice observed under 50mT of magnetic field at 25K[3)]. The data was processed by Transport of Intensity Equation (TIE) analysis of the Lorentz TEM images.

References

[1] Muhlbauer, S. et al. "Skyrmion lattice in a chiral magnet". Science 323, 915–919 (2009)
[2] Munzer, W. et al. "Skyrmion lattice in the doped semiconductor $Fe_{1-x}Co_xSi$". Phys. Rev. B 81, 04 1203(R) (2010).
[3] Yu X.Z. et al., "Real-space observation of a two-dimensional skyrmion crystal". Nature 465, 9 01-904 (2010)
[4] Uchida, M., et. al.. "Real-space observation of helical spin order". Science 311, 359–361 (2006).

MS14-O2

Watching nanocrystals grow: in-situ synchrotron experiments

Richard D Tilley

School of Chemical and Physical Sciences, Victoria University of Wellington and MacDiarmid Institute, Wellington, New Zealand
E-mail: richard.tilley@vuw.ac.nz

Liquid phase synthesis is a powerful method for the formation of uniform sized nanoparticles and nanoparticles with a faceted morphology. General strategies for the formation of nanoparticles and quantum dots through chemical synthesis will be outlined. The results presented will include the formation of noble metal. In-situ synchrotron studies along with HRTEM observations have been used to illucidate growth mechanisms of how the nanoparticles form and will also be presented. [1-2]

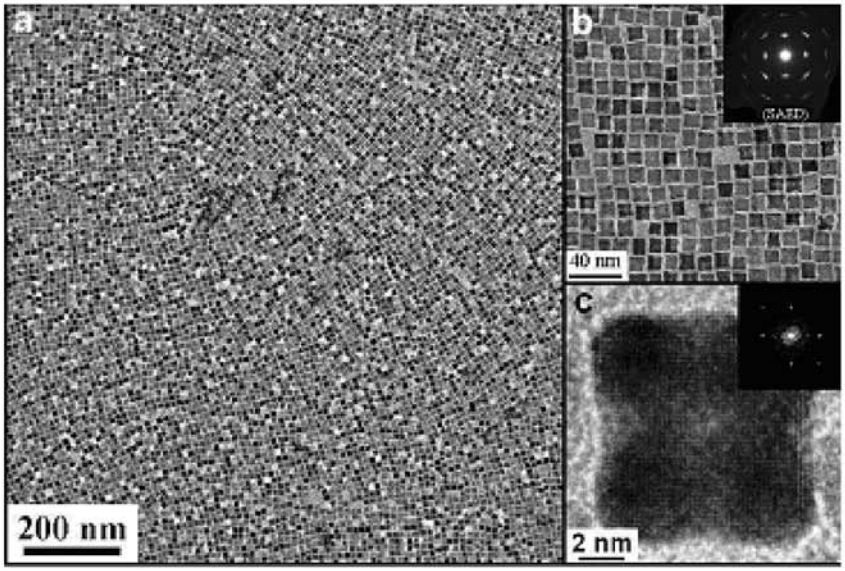

Figure 1. Monodispersed platinum nanocubes. a, low-resolution TEM image of self-assembled highly monodispersed nanocubes. b, mid-resolution TEM image. c, high resolution TEM image of platinum nanocube. Inset is a FFT of the image of the particle.

References

[1] S. Cheong, J. Watt, B. Ingham, M. F. Toney and R. D. Tilley 'In Situ and Ex Situ Studies of Platinum Nanocrystals: Growth and Evolution in Solution' *Journal of the American Chemical Society*, 131, (2009) 14590–14595.

[2] Watt J., Cheong S., Toney M. F., Ingham B., Cookson J., Bishop P. T., Tilley R. D. 'Ultra-fast Growth of Highly Branched Palladium Nanostructures for Catalysis' *ACS Nano*, 4, (2010) 396–402.

MS14-O3

Artificial structural colored microstructures via magnetically tunable photonic crystal

Howon Lee and Sunghoon kwon

School of Electrical Engineering and Computer Science, Seoul National University, San 56-1, Shillim 9-dong, Gwanak-ku, Seoul 151-744, South Korea
E-mail: skwon@snu.ac.kr

Many creatures in nature, such as butterflies and peacocks display unique brilliant colors, known as "structural colors", which result from the light interaction with periodic nanostructures on their surface. Unlike chemical dyes, structural color originating from the physical structures shows iridescent, metallic, and free from photobleaching. Mimicking such nanostructures found in nature, however, requires state-of-the-art nanofabrication techniques that are expensive and not scalable. Especially, productions of multicolors and high resolution patterning of such structures were hard to achieve. Here in this talk, we first introduce our recent demonstration of high resolution patterning of multiple structural colors that is based on successive tuning and fixing of color using a single material along with a special instrumentation[1]. Then we introduce our recent application of the patterning method to create vivid, free-floating structural coloured particles with multi-axis rotational control [2]. Our colour-barcoded magnetic microparticles offer a coding capacity easily into the billions with distinct magnetic handling capabilities including active positioning for code readouts and active stirring for improved reaction kinetics in microscale environments. A DNA hybridization assay is done using the colour-barcoded magnetic microparticles to demonstrate multiplexing capabilities.

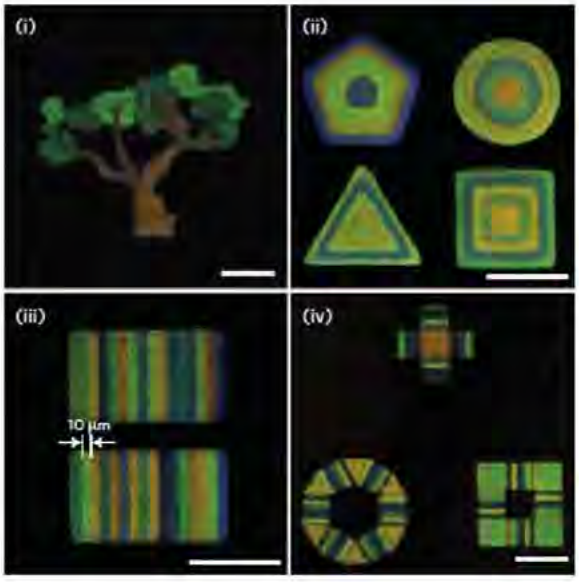

Figure 1. Generation of high-resolution multiple structural colour patterns using M-Ink[1]
(ii, iii, scale bars100mm; i, iv, scale bars 250mm)

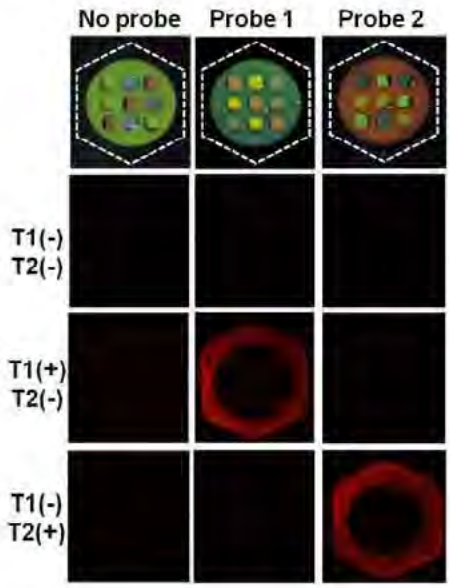

Figure 2. Multiplexed DNA detection assay using colour-barcoded magnetic microparticles[2]

References

[1] Hyoki Kim, Jianping Ge, Junhoi Kim, Sung Eun Choi, Hosuk Lee, Howon Lee, Wook Park, Yadong Yin and Sunghoon Kwon, "Structural color printing using a magnetically tunable and lithographically fixble photonic crystal", Nature Photonics, 3, 534-540, 2009

[2] Howon Lee, Junhoi Kim, Hyoki Kim, Jiyun Kim and Sunghoon Kwon, "Colour-barcoded magnetic microparticles for multiplexed bioassays", Nature Materials, 2010 (in press)

MS14-O4

Automated electron diffractometry: solving structures of nano crystals

Tatiana Gorelik, Enrico Mugnaioli, Andrew Stewart, Iryna Andrusenko, Ute Kolb

Institute of Physical Chemistry, Johannes-Gutenberg University, Jackb-Welderweg11, 55099 Mainz, Germany
E-mail: gorelik@uni-mainz.de

Many compounds of different material classes do not crystallize as large enough crystals for single crystal X-ray structure analysis. Powder diffraction data is often difficult to index due to reflection overlap, several crystalline phases present in the sample, preferred orientation effects etc. Crystal-size driven peak broadening of X-ray diffraction data can be a severe difficulty for data indexing and subsequent structure solution. Although X-ray powder diffraction data clearly states that the material is crystalline to a certain extent, the structure of the crystallites can often not be determined. On the other hand exactly the structure of the nano phase can be of particular importance, since it may differ from that realized in larger crystals [1].

Electron diffraction, due to its high scattering efficiency and small probe size, was long used to characterize the structure of nano materials [2]. It is for the first time, however, a set of automated routines was developed for structure solution of nano materials [3, 4]. The electron diffraction data is acquired similarly as it is done on a four-circle single crystal X-ray diffractometer. A selected nano crystal is tilted in fine steps and diffraction data is collected sequentially. Data processing routines accounting for specialties of electron diffraction are elaborated. The processing package delivers the information about the unit cell parameters unambiguously. This information can either be used to index an X-ray powder diagram, or, more important, knowing the orientation matrix a 3D (*h k l Int*) data set of electron diffraction intensities can be extracted. This data set can then be used for a structure solution by direct methods implemented, for instance, in SIR software [5].

Structure solution from automatically collected electron diffraction data is demonstrated for various kinds of materials including minerals (pure and polyphasic systems), zeolites, metal organic polymers, organic molecular crystals, and pharmaceutical compounds.

References

[1] Bernstein, J., "*Polymorphism in Molecular Crystals*", Oxford University Press, (2002).
[2] Vainstein, B.K., "*Structural Analysis by Electron Diffraction*", Oxford Pergamon, (1964).
[3] Kolb, U., Gorelik, T., Kübel, C., Otten, M., Hubert, D., "Towards automated diffraction tomography: Part I—Data acquisition", *Ultramicroscopy*, 107, (2007), pp 507-513.
[4] Kolb, U., Gorelik, T., Otten, M., "Towards automated diffraction tomography: Part II—Cell param eter determination", *Ultramicroscopy*, 108, (2008), pp 763-772.
[5] Burla, M. C., Caliandro, R., Camalli, M., Carrozzini, B., Cascarano, G. L., De Caro, L., Giacovazzo, C., Polidori, G., Siliqi, D. and Spagna, R., "IL MILIONE: a suite of computer programs for crystal structure solution of proteins", *J. Appl. Crystallogr.*, 40, (2007), pp. 609-613.

MS14-O5

Structure analysis of charge-orbital ordered phases in *A*-site ordered perovskites $SmBaMn_2O_6$ and $NdBaMn_2O_6$ using CBED

Daisuke Morikawa[1], Kenji Tsuda[1], Shigeki Yamada[2] and Takahisa Arima[1]

[1]*Institute of Multidisciplinary Research for Advanced Materials, Tohoku University, 2-1-1 Katahira, Aoba -ku, Sendai, 9808577, Japan*
[2]*International Graduate School of Arts and Science, Yokohama City University, 22-2 Seto, Kanazawa-ku, Yokohama, 236-0027, Japan*
E-mail: morikawa@mail.tagen.tohoku.ac.jp

A structure analysis method using convergent-beam electron diffraction (CBED), which was developed by Tsuda and co-workers [1,2], enables us to directly determine the electrostatic potential and crystal structure from a nanometer-scale specimen area. *A*-site ordered perovskites have the alternate stack of SmO (or NdO) and BaO sheets along *c*-axis with intervening MnO_2 sheets [3]. *A*-site ordered perovskites show high crystallinity than *A*-site disordered perovskites. Thus, these perovskites are suitable for the defect-free analysis. In this study, we aim to reveal the relations between microscopic crystal structure and macroscopic physical properties. CBED patterns were obtained at 300K for $SmBaMn_2O_6$ and at 300K and 90K for $NdBaMn_2O_6$ using an energy-filter transmission electron microscope JEM-2010FEF with an accelerating voltage of 100kV. Atom positions, atomic displacement parameters and low-order structure factors were refined by nonlinear least square fitting between the CBED patterns and dynamical diffraction calculations using original analysis software MBFIT [1].

Figure (a) shows CBED pattern of $SmBaMn_2O_6$ taken with the [001] incidence at 300K and (b) shows that of $NdBaMn_2O_6$ at 90K. Both CBED patterns exhibit *2mm* whole pattern symmetry, but the pattern of $SmBaMn_2O_6$ has a slightly larger deviation from the *4mm* symmetry of the high temperature phase than that of $NdBaMn_2O_6$. It is noted that there is difference in the intensities of higher-order laue zone reflections. From many CBED patterns taken with other incidences, it has been found that the unit cell of $NdBaMn_2O_6$ at 90K is identical with that of $SmBaMn_2O_6$. The space group of these materials determined by CBED and the result of refinement using MBFIT will be presented.

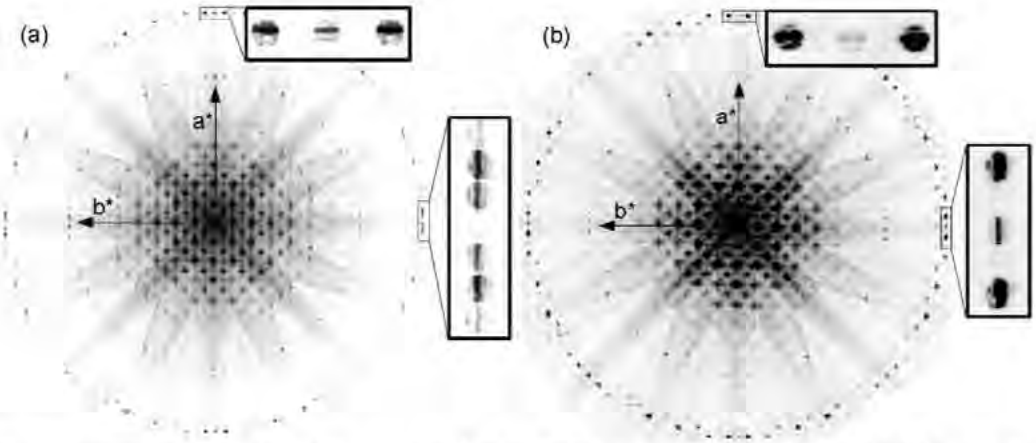

Fig. CBED patterns taken with [001] for (a) $SmBaMn_2O_6$ at 300K and (b) $NdBaMn_2O_6$ at 90K.

References

[1] K. Tsuda & M. Tanaka, *Acta Cryst.* A55, 939-954 (1999).
[2] K. Tsuda *et al.*, *Phys. Rev.* B81, 180102 (2010).
[3] D. Akahoshi *et al.*, *Phys. Rev.* B70, 064418 (2004).

MS15-O1

The challenge of highly reliable *ab initio* powder structure analysis by the novel concept of genetic algorithm

Makoto Sakata

Visiting Chief Scientist, Japan Synchrotron Radiation Research Institute, SPring-8, 1-1-1, Kouto, Sayo, Hyogo, 679-5198, Japan
E-mail: mttsakata@spring8.or.jp

Since the advent of synchrotron radiation, the capability of powder diffraction has been greatly extend.
The modern synchrotron powder diffraction can tackle many structural problems, which would not be possible to handle by conventional laboratory based powder diffraction system. It should be, however, emphasized that the improvement of experimental powder data by utilizing synchrotron radiation could not have been solely attained to the present capability of structural problems for powder crystalline materials. There is another important factor, *i. e.* new ideas of analytical methods. This is the main interest of this talk.

In this talk, two different analytical methods will be mentioned, which are necessary for highly reliable *ab-initio* powder structure analysis. One is the Maximum Entropy Method (MEM) [1], which seems now well established as a structural refinement method beyond Rietveld refinements. More specifically speaking as an analytical method for powder diffraction data, it should be assigned as MEM/Rietveld method [2]. The other is hybrid Genetic Algorithm (GA) for *ab initio* structure determination for materials with rather complicated structures such as pharmaceutical compounds [3]. The concept of the methods will be mentioned in the talk in detail. In addition the difficulties of the method will be also described in the talk.

The both of the analytical methods are completely different and independent. But one thing is common. Both of them are heavily depend on computer resources. It is, therefore, important what kind of computer system will be used to analyze synchrotron powder diffraction data. This seems a main reason why these methods did not developed in crystallography until late 20^{th} century. Reflecting this fact, more complicated structures are now becoming target materials by synchrotron powder diffraction, although there must be a limit where powder diffraction could not be no longer useful to solve structural problems. Considering computer systems are still very rapidly developing, the above mentioned methods are still high potential to answer many structural questions for relatively complicated structural materials such as pharmaceutical compounds, functional materials and so on.

References

[1] Sakata M. and Sato M., "The Accurate Structure Analysis by the Maximum Entropy Method", Acta Cryst. **A46** (1990), pp263-270
[2] James J., Takata M., Umeda B., Nishibori N., Sakata M., Ohno M., and Shinohara H., " Confirmation by X- Ray Diffraction of the Endohedral Nature of the Metallofullerene Y@C_{82}." Nature, **377,** (1995) pp46-49
[3] James Nishibori E., Ogura T., Aoyagi S. and Sakata M., "Ab initio structure determination of a pharmaceutical compound, predonisolone succinate, from synchrotron powder data by combin ation of agenetic algorithm and the maximum entropy method" J. Appl. Cryst. (2008) 41, pp2 92-301

MS15-O2

Industrial applications of *in situ* powder diffraction

Nathan A.S. Webster[1,2], Ian C. Madsen[1], Nicola V.Y. Scarlett[1], Matthew R. Rowles[1,3] and Helen E.A. Brand[1,2]

[1]*CSIRO Process Science and Engineering, Box 312, Clayton South, VIC 3169, Australia*
[2]*ANSTO, PMB 1, Menai, NSW 2234, Australia*
[3]*CSIRO Light Metals National Research Flagship, Box 312, Clayton South, Victoria 3169 Australia*
E-mail: nathan.webster@csiro.au

The implementation of powder diffraction methods to follow reactions in industrial processes has the benefit over other analysis techniques because it allows for simultaneous determination of phase structure and composition. When performing powder diffraction measurements in an industrial context, an *in situ* approach is favourable over an *ex situ* one since it allows for reactions to be followed in real time, avoiding artifacts that can occur when a sample is extracted from its environment for analysis. Analysis of the *in situ* data using the Rietveld method then allows for the extraction of information such as relative and absolute phase abundances, and lattice parameter and unit cell site occupancy variation. *In situ* diffraction studies in an industrial context often involve the design and implementation of novel reaction cells so that the reactions being investigated are meaningful in terms of the larger scale industrial process.

In this presentation, recent *in situ* powder diffraction research within our research group will be discussed. For example, *in situ* XRD investigations of scale formation in the Bayer process have focused on the characterisation of $Al(OH)_3$ scale deposition on mild steel substrates [1], and the determination of the kinetics and mechanisms of $Al(OH)_3$ precipitation from supersaturated sodium aluminate liquors seeded with iron oxides and oxyhydroxides [2]. The formation of scale in the Bayer process is a costly problem for the global alumina industry, and an increased understanding of scale nucleation and growth mechanisms is necessary for the development of strategies for scale prevention. Other examples include the application of energy dispersive XRD to the characterisation of inert anodes used in the production of titanium [3], and investigations of the thermal decomposition [4] and co-precipitation [5] of jarosite minerals.

References

[1] Webster N.A.S., Madsen, I.C., Loan M.J., Scarlett N.V.Y. and Wallwork K.S., "A flow cell for *in situ* synchrotron X-ray diffraction studies of scale formation under Bayer processing conditions", *Review of Scientific Instruments*, Vol. 80, (2009), 084102.

[2] Webster N.A.S., Madsen, I.C., Loan M.J., Knott R.B., Naim F., Wallwork K.S. and Kimpton, J.A., "An investigation of goethite-seeded $Al(OH)_3$ precipitation using in situ X-ray diffraction and Rietveld-based quantitative phase analysis", *Journal of Applied Crystallography*, Vol. 43, (2010), pp. 466-472.

[3] Scarlett N.V.Y., Madsen, I.C., Evans J.S.O, Coelho A.A., McGregor K., Rowles M., Lanyon M.R. and Urban A.J., "Energy dispersive studies of inert anodes", *Journal of Applied Crystallography*, Vol. 42, (2009), pp. 502-512.

[4] Madsen I.C., Grey I.E. and Mills S., "*In situ* Diffraction Studies: Thermal Decomposition of a Natural Plumbojarosite and the Development of Rietveld-based Data Analysis Techniques", *Materials Science Forum*, Vol. 651, (2010), pp. 37-64.

[5] Scarlett N.V.Y., Grey I.E. and Brand H.E.A., "Ordering of iron vacancies in monoclinic jarosites", *American Mineralogist*, in press.

MS15-O3

In situ studies using synchrotron powder diffraction

Bridget Ingham[1,2]

[1]*Industrial Research Limited, P. O. Box 31-310, Lower Hutt 5040, New Zealand*
[2]*The MacDiarmid Institute for Advanced Materials and Nanotechnology, Victoria University of Wellington, P. O. Box 600, Wellington 6140, New Zealand*
E-mail: b.ingham@irl.cri.nz

The development of high flux synchrotron X-ray sources allows diffraction measurements to be recorded from much smaller amounts of material, much faster, than laboratory sources. The high energy of synchrotron X-ray sources enables penetration through windows of a variety of materials. This allows chambers to be designed for *in situ* experiments under extreme environments (e.g. immersed in liquid, high temperatures, high pressures). Both of these aspects open up possibilities for studying physical transformations and chemical reactions *in situ* and in some cases, in real time.

In this presentation, the advantages and limitations of in situ synchrotron X-ray diffraction techniques will be discussed. The presentation will feature examples of real-time, in situ X-ray diffraction studies performed at synchrotron facilities, including nanoparticle formation in solution [1,2], carbon dioxide corrosion of steel [3], and thermally-induced coalescence of metallic nanoparticles. For each case, the design of the experimental method and apparatus will be described in detail, along with the major results.

Acknowledgements
Portions of this research were undertaken on the powder diffraction beam line at the Australian Synchrotron, Victoria, Australia, and at the Stanford Synchrotron Radiation Lightsource (SSRL), a national user facility operated by Stanford University on behalf of the U. S. Department of Energy, Office of Basic Energy Sciences.

References

[1] Watt J., Cheong S., Toney M. F., Ingham B., Cookson J., Bishop P. and Tilley R. D., "Ultra-fast growth of highly branched palladium nanostructures for catalysis", *ACS Nano* Vol. 4, No. 1, (2010), pp 396-402.
[2] Cheong S., Watt J., Ingham B., Toney M. F. and Tilley R. D., "In situ and ex situ studies of platinum nanocrystals: growth and evolution in solution", *J. Am. Chem. Soc.* Vol. 131, (2009), pp 14590-14595.
[3] Ingham B., Ko M., Kear G., Kappen P., Laycock N., Kimpton J. A. and Williams D. E., "In-situ synchrotron x-ray diffraction study of surface scale formation during CO_2 corrosion of carbon steel at temperatures up to 90°C", *Corrosion Science* (2010, in press. DOI: 10.1016/j.corsci.2010.05.025).

Structural study of monovalent cation-exchanged natrolites during dehydration

Yongmoon Lee, Taehwa Kim, Donghoon Seoung and Yongjae Lee*

Department of Earth System Sciences, Yonsei University, Seoul 120-749, Korea
E-mail: lym1229@yonsei.ac.kr

Gas separation and catalytic applications of zeolites require activation process to remove volatile species such as water from the molecular-sized pores and channels. In many cases, the framework geometry changes either isotropically or anisotropically with temperature, and nonframework cations can migrate to either open or block the entrance to the pores and channels upon dehydration or decomposition of volatile molecules. It is, therefore, important to understand the structural changes as a function of temperature in order to gain any control over zeolitic applications. Natrolite is one of the small-pore zeolites potentially suitable for separation or adsorption for small molecules such as CO2, CH4, N2, and H2. We have recently identified a method to prepare alkali metal substituted natrolites and characterized their hydrated ambient structures using synchrotron X-ray powder diffraction and Rietveld methods. From the original sodium-natrolite to potassium-, rubidium- and cesium-exchanged natrolites, there is drastic yet systematic increase in the channel opening via unit cell expansion of up to 18.5 %. We show here how these structures change upon the loss of water molecules and suggest their potential usages as adsorbents for small gas molecules.

References

[1] Baur, W.H., Kassner, D., Kim, C.-H., and Sieber, N.H. (1990) Flexibility and distortion of the framework of natrolite: crystal structures of ion-exchanged natrolites. European Journal of Mineralogy, 2, 761-769.
[2] Elli STUCKENSCHMIDT, Dethard KASSNER, Werner JOSWIG, Werner H. BAUR, (1992), Flexibility and distortion of the collapsible framework of NAT topology: the crystal structure of NH4-exchanged natrolite. Euroupean journal of mineralogist, 92.
[3] Breck, D. W. et al., U.S. Patent (1958), 711,565,
[4] Breck, D. W. et al., *Zeolite Molecular Sieves, Structure, Chemistry and Use*, New York (1974), Chapter 2.
[5] Yamazaki, A., Kamioka, K., Matsumoto, H., and Otsuka, R. (1987) Structure Refinement of K-exchanged Natrolite by Rietveld Method. Memoirs of the School of Science and Engineering, Waseda University, 118, 40-44.

MS15-O5

Particle statistics in high-resolution synchrotron powder X-ray diffractometry

Takashi Ida, Takuya Iwamoto, Taishi Goto and Hisashi Hibino

Ceramics Research Laboratory, Nagoya Institute of Technology, Asahigaoka 10-6-29, Tajimi, Gifu, 507-0071, Japan
E-mail: ida.takashi@nitech.ac.jp

Analysis of observed powder diffraction intensity data generally assumes a sufficiently large number of crystallites that satisfy the diffraction condition in a powder specimen. However, it is difficult to justify this assumption for powder samples with average crystallite size larger than several μm, where statistical variation of the effective number of crystallites (particle statistics) becomes more significant [1]. It is also known that continuous in-plane rotation of a flat powder specimen considerably reduces the effect of particle statistics, as has been theoretically explained by the wider tolerable orientation of the diffraction plane along the axial direction as compared with the equatorial direction of the goniometer [2]. Recently, we have shown that quantitative evaluation of particle statistics for stationary specimens is enabled by the statistical analysis of the measured diffraction intensities collected on step-wise rotation of flat specimens [3]. In this study, we have compared the particle statistics for rotating and stationary flat specimens by applying a Ω–scan method in a parallel-beam geometry using a synchrotron powder diffractometer on the BL-4B2 at the Photon Factory in Tsukuba.

First, the ratios of the effective number of diffracting crystallites N_{eff} to the multiplicity of reflections m were evaluated for 19 reflection peaks of a standard Si powder sample (NIST SRM640c) by a spinner-scan method [3] in a symmetric reflection mode. It has been found that the dependence on the diffraction angle is well modeled by $N_{\mathrm{eff}} / m \sim 1.04(2)\ \mathrm{cosec}\ \theta$ throughout the observed range of diffraction angles. The effective tolerable angle along the equatorial direction, estimated at 0.0072° was quite narrower than the value about 0.03° for a typical laboratory diffractometer.

The systematic behaviors of the Ω-scan intensity profiles $I(\Omega)$ measured for 10 reflection peaks of the standard Si powder are modeled by the dependence of the effective irradiated volume upon the incident glancing angle Ω, which is given by

$$I(\Omega) = 2I(\theta)\ [\ \mathrm{cosec}\ \Omega + \mathrm{cosec}(2\theta - \Omega)\ ]^{-1}\ \mathrm{cosec}\ \theta,$$

for the fixed Bragg angles θ. The statistical deviation was evaluated by subtraction of the optimized model profile from the observed intensity at each measurement point. The effective number N_{eff} was evaluated by applying a normalization based on the effective irradiated volume. The ratios of N_{eff} to m have been estimated at $N_{\mathrm{eff}} / m \sim 1.02(4)\ \mathrm{cosec}\ \theta$ and $\sim 34(2)\ \mathrm{cosec}^2\ \theta$ from the Ω-scan measurements for the stationary and rotating specimens, respectively. It is suggested that the effect of particle statistics should not be neglected in high-resolution synchrotron powder diffractometry, even if continuous rotation of a flat specimen is applied.

References

[1] Alexander, L., Klug, H. P. and Kummer, E., "Statistical factors affecting the intensity of x-rays diffracted by crystalline powders", *J. Appl. Phys.*, Vol. 19, (1948), pp 742-753.
[2] De Wolff, P. M., "Particle statistics in x-ray diffractometry I. general theory", *Appl. Sci. Res. B*, Vol. 7, (1958), pp 102-112.
[3] Ida T., Goto, T. and Hibino, H. "Evaluation of particle statistics in powder diffractometry by a spinner-scan method", *J. Appl. Cryst.*, Vol. 42, (2009), pp 597-606.

AsCA2010

The 10th Conference of the Asian Crystallographic Association

ABSTRACTS

Poster Sessions

Area 1. Structural Biology
(MS01, 04, 07, 10, 13)

MS01-P01

The Structure of Mouse Anoctamin1(mANO1) Domains TM2↔TM3 ($D_{TM1↔TM2}$) and TM5↔TM6($D_{TM5↔TM6}$)

Sang Ho Park[1], Ho Kyung Jung[1], and Byung Woo Han[1]

[1]*Department of Pharmacy, College of Pharmacy, Seoul National University, Seoul 151-742, Korea*
E-mail: pksangho@snu.ac.kr

Calcium-activated chloride channels play an important role in a variety of physiological functions, including transepithelial ion absorption/reabsorption, neuronal excitation, smooth and skeletal muscle contraction and sensory transduction. Transmembrane protein 16A (TMEM16A), also called as anoctamin1(ANO1), is known to be a calcium-activated chloride channel and classified as a new class of ionic channels. ANO1 consists of eight transmembrane domains with intracellular and extracelluar regions. ANO1 is known to participate in tumorigenesis and may play some roles for tumor cell proliferation. Despite the importance of ANO1, the three-dimensional structure of ANO1 is still unknown. To elucidate the structure-function relationship of mANO1, we are purifying various truncated constructs of mANO1 including $D_{TM1↔TM2}$ and $D_{TM5↔TM6}$ which are assumed to play essential functions for the mechanism of channel proteins. Since ANO1 is activated by Ca^{2+} and voltage, crystal structures of mANO1 from our constructs will be able to explain the mode of calcium binding and the voltage-dependant action.

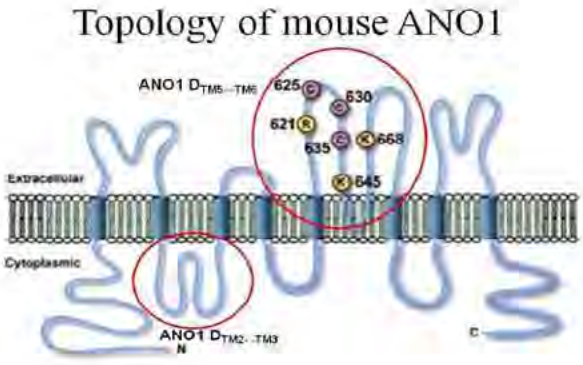

References

[1] Yang Y.D, Cho H, Koo J.Y, Tak M.H, Cho Y, Shim W.S et al "TMEM16A confers receptor-activated calcium-dependent chloride conductance", Nature, (2008)

[2] Luis J.V., "The TMEM16 Protein Family: A New Class of Chloride Channels?", Biophysical Journal Vol. 97 (2009)

MS01-P02

Purification of LDL receptor–related protein and nano-gold labeling for structure analysis

Kyung Eun Lee, Oh Yeun Kwon, Hyesung Jeon

Biomedical Research Center, Korea Institute of Science and Technology, Seoul, Korea
E-mail: hjeon@kist.re.kr

Low-density lipoprotein receptor–related protein (LRP) is a multifunctional endocytic receptor that interacts with more than 30 different ligands. It is hard to purify such a large protein of ~600 kDa by conventional purification methods, since the structural analysis using X-ray crystallography or NMR spectroscopy needs the high quality and large quantities of protein. Transmission electron microscopy (TEM) is one of the techniques that are used to analyze the large protein structures, because it can obtain the images of less purified protein from a very little amount. Furthermore, cryo-TEM is useful to observe the membrane proteins like LRP, as it shows the fully hydrated state of protein itself and also the integrated state into lipid bilayer. In this study, His-tagged LRP was transfected and expressed in mammalian cells, and purified using immobilized metal-affinity to the His-tag. Then it was labeled with Nano-gold on His-tags and reconstituted into the liposomes. The results confirmed by TEM showed the potential for LRP structure analysis through this semi-purification and Nano-gold labeling method.

References

[1] Herz J. and Strickland D.K., "LRP: A multifunctional scavenger and signaling receptor", *J. Clin. Invest.*, 108, (2001), pp 779-784.
[2] Rigaud J.L., Le'vy D. and Nejat D., "Reconstitution of Membrane Proteins into Liposomes", *Methods Enzymol.*, 372, (2003), pp. 65–86.
[3] Jeon H. and Shipley G.G., "Localization of the N-terminal domain of the low density lipoprotein receptor", *J. Biol. Chem.*, 275, 39, (2000), pp 30458–30464.
[4] L. Bumba, M. Tichy, M. Dobakova, J. Komenda, F. Vacha, "Localization of the PsbH subunit in photosystem II from the Synechocystis 6803 using the His-tagged Ni-NTA nanogold labeling", *J. Struct. Biol.*, 152, (2005), pp. 152:28-35

MS01-P03

Interaction of PDZ adapter proteins NHERF and E3KARP in vitro

Se Bok Jang, Eun Young Hwang, and Mi Suk Jeong

[1]*Department of Molecular Biology, College of Natural Sciences, Pusan National University, Jangjeon-dong, Geumjeong-gu, Busan 609-735, Korea*
E-mail: sbjang@pusan.ac.kr

NHERF (Na^+/H^+ exchanger regulatory factor) and E3KARP (NHE3 kinase A regulatory protein) play an important roles in the membrane targeting, trafficking, and sorting of several ion channels, transmembrane receptors, and signaling proteins in many tissues. These proteins contain two PDZ (PSD-95/Dlg-1/ZO-1) domains that mediate the assembly of transmembrane and cytosolic proteins into functional signal transduction complexes. The expression and purification of the full-length NHERF and E3KARP proteins were successfully performed in *E. coli*. The binding of both NHERF and E3KARP proteins was detected by surface plasmon resonance spectroscopy (BIAcore), fluorescence measurement, His pull-down experiment, and size-exclusion column (SEC) chromatography. NHERF indeed binds to E3KARP with an apparent K_D of 7 nM. After measuring the fluorescence emission spectra of purified NHERF and E3KARP, it was found that the tight interaction of these proteins is accompanied by significant conformational changes of one or both. These results indicate that NHERF and E3KARP complex provide ability to form intracellular signaling complexes through PDZ-PDZ interactions.

References

[1] Maudsley, S., Zamah, A. M., Rahman, N., Blitzer, J. T., Luttrell, L. M., Lefkowitz, R. J. and Hall, R. A. *Mol. Cell. Biol.* 20, 8352-8363 (2000).
[2] Morales, F. C., Takahashi, Y., Kreimann, E. L. and Georgescu, M.-M. *Proc. Natl. Acad. Sci. USA* 101, 17705-17710 (2004).
[3] Takahashi, Y., Morales, F. C., Kreimann, E. L. and Georgescu, M. M. *EMBO J.* 25, 910-920 (2006).

MS04-P01

In vitro Reconstitution of the Interactions in the PIDDosome

Hyun Ho Park[1], Tae-ho Jang[1], Hao Wu[2], and Chao Zheng[2]

[1]*School of Biotechnology and Graduate School of Biochemistry at Yeungnam University, Gyeongsan, South Korea*
[2]*Department of Biochemistry, Weill Medical College and Graduate School of Medical Sciences of Cornell University, New York, NY 10021*
E-mail: hyunhopark@yu.ac.kr

Caspase-2 is critical for genotoxic stress induced apoptosis and is activated by formation of the PIDDosome, an oligomeric caspase-2 activating complex. The PIDDosome comprises three protein components, PIDD, RAIDD and caspase-2. RAIDD contains both a death domain (DD) and a caspase recruitment domain (CARD). It acts as the bridge to recruit PIDD using the DD: DD interaction and to recruit caspase-2 via the CARD: CARD interaction. Here we report biochemical characterization and in vitro reconstitution of the core interactions in the PIDDosome. We show that RAIDD CARD and RAIDD DD interact with their binding partners, caspase-2 CARD and PIDD DD, respectively. However, full-length RAIDD fails to interact with either caspase-2 CARD or PIDD DD under a physiological buffer condition. We reveal that this lack of interaction of full-length RAIDD is not due to its tendency to aggregate under the physiological buffer condition, as decreasing full-length RAIDD aggregation using high salt or high pH is not able to promote complex formation. Instead, full-length RAIDD forms both binary and ternary complexes under a low salt condition. Successful in vitro reconstitution of the ternary complex provides a basis for further structural studies of the PIDDosome.

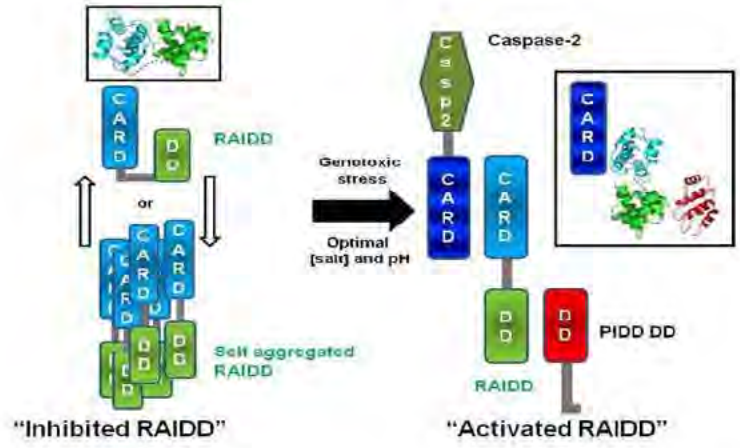

References

[1] Park HH., Lo YC., Lin SC., Wnag L., Yang JK. and Wu H., "The death domain superfamily in intracellular signaling of apoptosis and inflammation", *Annu Rev Immunol*, Vol. 25, (2007), pp 561-586.

[2] Park HH., Logette E., Raunser S., Cuenin S., Walz, T., Tschopp J. and Wu H., "Death domain assembly mechanism revealed by crystal structure of the oligomeric PIDDosome core complex", *Cell*, Vol. 128, (2007), pp 533-546.

[3] Tinel A. and Tschopp J., "The PIDDosome, a protein complex implicated in activation of caspase-2 in response to genotoxic stress", Science, Vol. 304, (2004), pp 843-846.

MS04-P02

High-Resolution Crystal Structure of Chicken Cytokine Interleukin-1β Reveals Differences in Receptor Binding Compared to Human Interleukin-1β

Chao-Sheng Cheng[1], Wen-Shiang Lu[1], I-Fan Tu[1], Ping-Chiang Lyu[1], Long-Huw Lee[2] and Hsien-Sheng Yin[1]

[1]*Institute of Bioinformatics and Structural Biology and College of Life Sciences, National Tsing Hua University, Hsinchu 300, Taiwan*
[2]*Department of Veterinary Medicine and College of Veterinary Medicine, National Chung Hsing University, Taichung, Taiwan*
E-mail: hsyin@life.nthu.edu.tw

Human interleukin-1β (IL-1β), an important cytokine in the immune system, has been studied extensively. Avian IL-1βs share 31-35% sequence identity and are less well understood. Here, we report the crystal structure of recombinant chicken IL-1β, to 1.58 Å. The protein structure is comprised of 14 β-strands and an α-helix, which form a barrel-shaped conformation. Modeling ligand docking of IL-1β to its receptor reveals some differences at the site of interaction compared to human IL-1β. MD simulations reveal significant changes in the dynamic range of motion on receptor binding. Loops 3 and 9 have the greatest atomic fluctuation before binding. After binding, the flexibility of these loops, which are in direct contact with the receptor, significantly decreases. This indicates ligand binding leads to not only favorable enthalpy but lower conformational entropy.

References

[1] Arend W. P., Palmer G. and Gabay C., IL-1, IL-18 and IL-33 Families of Cytokines, Immunol ogical Reviews. Vol. 223, (2008), pp 20-38.
[2] Wu Y. F., Liu H. J., Chiou S. H. and Lee L. H., Sequence and Phylogenetic Analysis of Inte rleukin (IL)-1Beta-encoding Genes of Five Avian Species and Structural and Functional Homol ogy Among these IL-1Beta Proteins, Veterinary Immunology and Immunopathology. Vol. 116, (2001), pp 37–46.

MS04-P03

Molecular interplay between the replicative hexameric Helicase DnaC with ssDNA and its Loader DnaI from *Geobacillus kaustophilus*

Chwan-Deng Hsiao, Yu-Hua Lo and Kuang-Lei Tsai

Institute of Molecular Biology, Academia Sinica, Taipei, 115, Taiwan
E-mail: hsiao@gate.sinica.edu.tw

DNA helicases are motor proteins that play essential roles in DNA replication, repair, and recombination. In the replicative hexameric helicase, the fundamental reaction is the unwinding of duplex DNA. In addition, the helicase loading factors are thought to transfer the hexameric ring-shaped helicases onto the replication fork during DNA replication. However, the mechanism of how helicase transfer onto DNA under the help of helicase loading factors help remains unclear. To date, intense biochemical, genetic, and structural approaches are being pursued to gain insight into both the mechanism and role of helicase and its loader in varied biological processes. However, in different organisms have a number of different mechanisms for DNA helicase loading. Therefore, the exact function of replicative helicase and the interaction with its loader in replication initiation are uncertain. In order to delineate the interaction and possible mechanism between helicase with ssDNA and its loader, we report here the structures and biochemical characterization of the DnaC replicative helicase in conjunction with the loader DnaI from *Geobacillus kaustophilus*.

References

[1] Lo, Y.-H., Tsai, K.-L., Sun, Y.-J., Chen, W.-T., Huang, C.-Y. and Hsiao, C.-D. The crystal structure of a replicative hexameric helicase DnaC and its complex with single-stranded DNA. *Nucleic Acids Res.* Vol. 37, (2009), pp 804-814.

[2] Tsai, K.-L., Lo, Y.-H., Sun, Y.-J. and Hsiao, C.-D. Molecular Interplay between the Replicative Helicase DnaC and its Loader Protein DnaI from *Geobacillus kaustophilus*. *J. Mol. Biol.* Vol. 393, (2009), pp 1056-1069.

MS04-P04

DNA/RNA binding properties of PCBP-1 KH domains

Daouda AK Traore, Yano M Yoga, Matthew CJ Wilce and Jackie A Wilce

Department of Biochemistry and Molecular Biology, School of Biomedical Sciences, Monash University, Australia
E-mail: daouda.traore@monash.edu

Poly-C binding proteins are ubiquitous oligonucleotide-binding proteins in eukaryotic cells that play fundamental role in regulation of gene expression via interaction with C-rich oligonucleotides. PCBP-1 (αCP-1 or hnRNP E1) is involved in the post-transcriptional regulation of mRNA by binding to the 3'-UTR and has been found to interact with a variety of mRNA such as Androgen Receptor, αGlobin, Tyrosine Hydroxylase and Lipoxygenase. PCBP binding to RNA can result in both silencing and enhancement of translation through a diverse set of mechanisms. PCBPs have also been found to be important for the replication of viral RNA which utilise them in both the translation and replication of the viral genome of picornaviruses. In addition to its RNA binding properties, PCBP-1 has been shown to bind ssDNA. Such interactions play a role in transcriptional regulation with PCBP identified as the ssDNA binding protein underlying proximal promoter activity of mouse μ-opioid receptor.

The aim of this work understand the molecular basis of DNA/RNA recognition by PCBP-1 using biophysical methods including Surface Plasmon Resonance and X-ray Crystallography.

MS04-P05

Paraspeckle proteins: a novel arrangement of RNA-binding domains

Mihwa Lee[1], Daniel Passon[1], Archa H. Fox[2] and Charles S. Bond[1]

[1]*School of Biomedical, Biomolecular and Chemical Sciences, University of Western Australia, Crawley WA 6009, Australia*
[2]*Western Australian Institute for Medical Research, Perth WA 6000, Australia*
E-mail: Mihwa.Lee@uwa.edu.au

Paraspeckles are sub-nuclear bodies found in the interchromatin space of mammalian cell nuclei [1]. Implicated in regulation of gene expressions by nuclear retention of RNA, paraspeckles are ribonucleoprotein bodies of which identified core components are a long non-protein coding RNA, NEAT1 and core paraspeckle proteins, PSPC1, PSF/SFPQ, and P54NRB/NONO. The three main core paraspeckle proteins are members of the *Drosophila melanogaster* behavior, human splicing (DBHS) family. The conserved regions of these proteins, comprised of two RNA recognition motifs (RRMs) and a C-terminal coiled-coil domain, share more than 50% sequence identity. Reported interactions between DBHS proteins suggest that they exist as either homo-or heterodimers *in vivo*. The three proteins appear to play a key role in the structural integrity of paraspeckles, because knockdown of these proteins results in a loss of parapeckles. Here we present the first structure of a paraspeckle-specific heterodimer, PSPC1/P54NRB. The structure of a 60kDa heterodimer of the conserved regions of PSPC1 and P54NRB reveals a novel arrangement of four RRM domains, an antiparallel right-handed coiled coil and a new protein:protein interaction motif. The structure provides a wealth of detail regarding possible RNA binding modes as well as insight into paraspeckle assembly.

References

[1] Bond C.S. and Fox A.H., "Paraspeckles: nuclear bodies built on long noncoding RNA", *Journal of Cell Biology*, Vol. 186, No. 5, (2009), pp 637-644.

MS04-P06

Structural Study of RLR family Innate immune proteins

Hyunjin Moon, Jungwoo Choe

University of Seoul, Siripdea-gil 13(jeonnong-dong 90), Dongdaemun-gu, Seoul 130-743 Korea
E-mail: hjmoon83@gmail.com

RLR family proteins (RIG-I–Like Family) play essential roles for the early recognition of various pathogens and activation of adaptive immunity. This family is a critical component of innate immune system that is responsible for the detection and elimination of invading viruses in cytoplasm and induction of the antiviral response. The RLR family consists of three members; RIG-I (Retinoic acid inducible gene-I), MDA5 (Melanoma Differentiation-Associated gene 5), and LGP2 (Laboratory of Genetics and Physiology 2). These proteins have a central DExD/H-box RNA helicase domain for viral RNA recognition. RIG-I and MDA5 also have two N-terminal CARDs (Caspase Activation and Recruitment Domains) for the initiation of downstream signaling to activate IRF-3 and NF-kB genes after interaction with an downstream adaptor protein, IPS-I(also Knowns as MAVS, VISA, and Cardif) that leads to the type I interferon production. Despite the domain similarity between the RLR families, they recognize different RNA molecules. MDA5 senses long dsRNA. On the other hand, RIG-I is response for the detection of short dsRNAs and 5'-triphosphate ssRNAs with base-paired structures, although it is still controversial. Since the role of RLR family proteins to recognize viral RNAs is very important in initiating innate immune responses, we are undergoing structural and biochemical studies of RLR family using X-ray crystallography. Especially, we focus on RIG-I : RNA complex structure. Thus, to determinate the structure, Seleno-Methionine incorporated RIG-I was expressed using E.coli and purified for crystallization. RIG-I : RNA binding was studied by EMSA method to investigate the RIG-I : RNA binding property in vitro. Crystals of RIG-I: RNA complex were obtained byvapor diffusion method. The crystal diffracted to 2.8 Å using synchrotron radiation. Attempts to determine the structure and obtain improved crystals is in progress. Structural studies of RIG-I : RNA complex will reveal how RIG-I can recognize viral RNA and discriminate it from self RNA and show the mechanism of RNA-induced conformational changes.

References

[1] Yoneyama M and Fujita, "RIG-I family RNA helicases : cytoplasmic sensor for antiviral innate immunity", Cytokine & Growth Factor Reviews, Vol.18, Issues 5-6, (2007), pp 545-551
[2] Schlee M, et al., "Approaching the RNA ligand for RIG-I?", Immunological Reviews, Vol. 227, Issue 1, (2009), pp 66-74
[3] Schmidt A, et al., "5'-triphosphate RNA requires base-paired structures to activate antiviral signaling via RIG-I", Proc Natl Acad Sci USA, Vol. 106, Issue 29, (2009), pp 12067–12072

MS04-P07

Translation Elongation Factor-P (EF-P) from Pseudomonas aeruginosa, a mimic of tRNA?

Sarah choi , Jungwoo Choe

University of Seoul, Siripdea-gil 13(jeonnong-dong 90), Dongdaemun-gu, Seoul 130-743 Korea
E-mail: chltkfk0728@naver.com

P. aeruginosa is prominent pathogenic bacteriumand it has intrinsic resistance to antibiotics and disinfectants. It can lead to various opportunistic human infections: bacteramia in burn victims, urinary-tract infections in catheterized patients and hospital-acquired pneumonia in patients on respirators. Translation factor P (EF-P) was found as a protein that stimulates the peptidyltransferase activity of 70S ribosome in Escherichia coli. E.coli EF-P is encoded by efp gene and the efp gene is essential for cell viability and is necessary for protein synthesis. The structure of EF-P is similar to transfer RNA in biophysical characteristics such as shape and charge distributions. The exact mechanism of EF-P as a translation factor is still unknown. EF-P from the P. aeruginosa was expressed as a solution protein in E.coli and crystallized. Data sets were collected to 2.2 Å from frozen crystals at 90K by using synchrotron radiation at SPring-8 beam lines (Hyogo, Japan). The data were processed with the program HKL2000, and the structure was determined from a SAD dataset using SOLVE/RESOLVE. The structural analysis of EF-P from P. acruginosa will be presented.

Reference

[1] C.K Stover 'Complete genome sequence of *Pseudomonas aeruginosa* PAO1, an opportunistic pathogen' NATURE / Vol 406 / 31AUGUST 2000
[2] Kyoko Hanawa-Suetsugu 'Crystal structure of elongation factor P from *Thermus thermophilus* HB8' PNAS / June 29, 2004 / Vol. 101 / no.26
[3] Aoki, H., Dekany, K., Adams, S. L. &Ganoza, M .C. 'The gene encoding the elongation factor P protein is essential for viability and is required for protein synthesis' *J. Biol. Chem.* / 1997

MS04-P08

Nuclear translocation machinery of pre-microRNA

Soo Jae Lee[1] Chimari Okada[2,6], Eiki Yamashita[2] Satoshi Shibata[3], Jun Katahira[3,4], Atsushi Nakagawa[2] Yoshihiro Yoneda[3,4], Tomitake Tsukihara[2,5]

[1]*College of Pharmacy, CBITRC, Chungbuk National University, Cheongju, Chungbuk 361-763, Korea*
[2]*Institute for Protein Research, Osaka University, Osaka 565-0871, Japan*
[3]*Department of Frontier Biosciences, Osaka University, Osaka 565-0871, Japan*
[4]*Department of Biochemistry, Graduate School of Medicine, Osaka University, Osaka 565-0871, Japan*
[5]*Department of Life Science, University of Hyogo, Hyogo 678-1297, Japan*
E-mail: sjlee@chungbuk.ac.kr

The translocation of proteins and RNAs between nucleus and cytoplasm plays important roles in the regulation of cytoplasmic and nuclear events. These exchanges occur at the nuclear pore complex (NPC) which spans the lipid bilayer of the nuclear envelope, and is mainly mediated by importin-β family transport factors family, importins and exportins. Interactions between cargoes and carriers are regulated by the nucleotide state of Ran, which cycles between GTP- and GDP-bound states in the nucleus and cytoplasm, respectively.

Nuclear export of pre-miRNAs by Exp-5 is an essential step in miRNA biogenesis. The crystal structure of the pre-miRNA nuclear export machinery formed by pre-miRNA complexed with Exp-5 and RanGTP shows that Exp-5:RanGTP recognizes the 2-nt 3' overhang structure and the double-stranded stem of pre-miRNA. Exp-5:RanGTP appears to shield the fragile pre-miRNA in a molecular cage-like complex that protects pre-miRNA from degradation by exonucleic RNase in the nucleus and safely delivers it from the nucleus to the cytoplasm. The tunnel-like structure of Exp-5 tightly grasps the 2-nt 3' overhang through specific hydrogen bonding and ionic interactions, while its cage-like structure loosely holds the double-stranded region of the pre-miRNA through a range of ionic interactions that are quite different from those previously reported in dsRNA recognition systems. Furthermore, RNA recognition by Exp-5:RanGTP does not depend on RNA sequence, which implies that Exp-5:RanGTP can recognize a variety of pre-miRNAs.

References

[1] Okada, C., Yamashita, E., Lee, S. J., Shibata, S., Katahira, J., Nakagawa, A., Yoneda, Y., and Tsukihara, T., "A high-resolution structure of the pre-microRNA nuclear export machinery" *Science*, Vol. 326, (2009), pp 1275-1279

MS04-P09

Structural analysis of exosome from *Thermoplasma acidophilum*

Hyun Sook Kim, Hye-Jeong Cho, Cho Gye Yoon, Ho Sam Ki, Moon Jung Song and Kwang Yeon Hwang*

Division of Biotechnology, College of Life Science, Korea University, Seoul 136-713, Korea
E-mail: chahong@korea.ac.kr

The exosome is a conserved protein complex containing 3'→5' exoribonuclease in archaea and eukaryotes. The complex has fundamental roles in RNA metabolic pathways such as the maturation, degradation and quality control of RNA molecules. To understand the crystal structure of the Thermoplasma acidophilum exosome, the Rrp41-Rrp42 complex was crystallized in space group $P2_13$ with two copies of Rrp41-Rrp42 in the asymmetric unit and the structure has determined at 2.4 Å resolution to an R_{factor} of 23 % and an R_{free} of 26 %. The overall structure is similar to the reported archaeal exosome with a hexameric ring containing arrangement of three Rrp41-Rrp42 heterodimers with the central channel. Both Rrp41 and Rrp42 contain RNase phosphorolytic (PH) domain with the β-α-β-α layers of secondary structure. Three RNA are predicted to recognize by the interface of the Rrp41 and Rrp42 on one side of the hexameric ring structure via charge-charge interactions between phosphate backbone and arginine side chains contributed by Rrp41 and Rrp42. Structural analysis of the complex structure is in progress.

References

[1] Büttner K., Wenig K. and Hopfner KP., "Structural framework for the mechanism of archaeal exosome in RNA processing", *Mol Cell*, Vol. 20, No. 3, (2005), pp 461-471.
[2] Lorentzen E. and Conti E., "Structural basis of 3' end RNA recognition and exoribonucleolytic cleavage by an exosome RNase PH core", *Mol Cell*, Vol. 20, No. 3, (2005), pp 473-481.
[3] Lorentzen E., Dziembowski A., Lindner D., Seraphin B. and Conti E., "RNA channelling by the archaeal exosome", *EMBO J*, Vol. 8, No. 5, (2007), pp 470-476.
[4] Lorentzen E., Walter P., Fribourg S., Evguenieva-Hackenberg E., Klug G. and Conti E., "The archaeal exosome core is a hexameric ring structure with three catalytic subunits", *Nat Struct Mol Biol*, Vol. 12, No. 7, (2005), pp 575-581.
[5] Navarro MV., Oliveira CC., Zanchin NI. and Guimarães BG., "Insight into the mechanism of progressive RNA degradation by the archaeal exosome", *J Biol Chem*, Vol. 283, No. 20, (2008), pp 14120-14131.

MS04-P10

An insight into the pairing geometry of DNA duplexes containing O^6-carboxymethylguanine, a damaged base analogue relevant to gastrointestinal cancer

Fang Zhang[1], Kaoru Suzuki[2], Md. Mominul Hoque[1], Masaru Tsunoda[3], Christopher L. Millington[4], David M. Williams[4] and Akio Takénaka[1, 3, 5,*]

[1]Graduate School of Science and Engineering, [2]Faculty of Science and Engineering, [3]Faculty of Pharmacy, Iwaki-Meisei University, Iwaki 970-8551, Japan, [4]Center for Chemical Biology, Krebs Institute, University of Sheffield, Sheffield S3 7HF, UK, and [5]Graduate School of Bioscience and Biotechnology, Tokyo Institute of Technology, Yokohama 226-8501, Japan
E-mail: zhangfanguknow@hotmail.com

Red meat stimulates endogenous intestinal *N*-nitrosation of glycine or glycine derivatives that can induce DNA mutations by reacting with DNA to form O^6-carboxymethylguanine (hereafter X) which is associated with increased risk of gastrointestinal cancer. In order to obtain an insight into the pairing geometry of DNA duplexes containing O^6-carboxymethylguanine and to further understand its biological implications, we synthesized two self-complementary DNA dodecamers with the sequences d(CGCGXATTCGCG) (X:T) and d(CGCXAATTCGCG) (X:C) and began attempts to obtain their structures by X-ray analyses.

Crystals of X:C were obtained under several conditions by the hanging drop vapor diffusion method at 277K in the presence of Hoechst 33258. X-ray diffraction data were collected at 100K with synchrotron radiation (λ=1.00Å) of the Photon factory. The initial structure has been solved by the molecular replacement method, and the atomic parameters were refined at 1.9 Å resolution with the programs, *Refmac 5* and *CNS*. During this process, the X residues of the two strands moved toward the major groove side from the canonical Watson-Crick type pairing position, and their electron density maps also supported this.

The DNA duplex adopts the B-form conformation, in which the two modified X residues form a pair with cytosine residues. However, it is noteworthy that the X residues form a reversed wobble base pair with cytosine with the O^6-alkyl group displaced into the major groove. In addition, this pairing is further stabilized by an additional hydrogen bond between the carboxyl oxygen and the paired cytidine amino group. The reversed wobble pair occurring can be reasonably explained from the chemical structure of X. A similar reversed wobbling has been observed in DNA duplex containing 5-formyl-2'-deoxyuridine derived from 2'-deoxythymidine damaged by oxygen radicals, which also induce gene mutations. In the oral session, we will explain the details of interaction geometry of the modified base X, and discuss its implications for inducing transition mutations during replication.

MS04-P11

Crystal structures of E2-25K, E2-25K/Ub and E2-25K/UBB^{+1}

Jung-Gyu Lee[1], Gil Bu Kang[1], Sunggeon Ko[2], Sung Min Song[3], Yong-Keun Jung[3], Yung Joon Yoo[1], Weontae Lee[2] and Soo Hyun Eom[1]

[1]*School of Life Science, Gwangju Institute of Science and Technology, Gwangju 500–712, Korea*
[2]*Department of Biochemistry, College of Life Science and Biotechnology, Yonsei University, Seoul 120-749, Korea*
[3]*School of Biological Science/Bio-Max Institute, Seoul National University, Seoul 151–742, Korea*
E-mail: meteo@gist.ac.kr

Aggregated proteins, neuritic plaques, neuropil threads and neurofibrillary tangles are molecular hallmarks of neurodegenerative disease. In particular, Aβ (amyloid-β peptide) and UBB^{+1} (a frameshift mutant of ubiquitin B) accumulate in Alzheimer's disease patients. E2-25K and polyglutamine-expanded huntingtin accumulate in patients with Huntington's disease. The ubiquitin (Ub)-proteasome system (UPS) has the function as proteolytic degradation of aberrant proteins via an Ub tagging mechanism. Within the UPS, Ub tagging of target molecules entails enzymatic reactions catalyzed by E1 (Ub-activating), E2 (Ub-conjugating), E3 (Ub-lagating) enzymes. The Ub tagged molecule is recognized by the 26S proteasome and degraded.

To study the molecular function in neurotoxicity by E2-25K, we determined the three-dimensional structures of UBB^{+1}, E2-25K and the E2-25K/Ub and E2-25K/UBB^{+1} complex. Structures revealed that the UBA domain of E2-25K is intricately associated with the E2 domain and that Ub or UBB^{+1} bound via the MGF motif and residues in α9 of the UBA domain. E2-25K mutations that disrupted Ub/UBB^{+1} binding markedly diminished synthesis of UBB^{+1}-anchored polyUb, inhibition of 26S proteasome activity, and neuronal cell death. We propose that interaction between the E2-25K UBA domain and UBB^{+1} is critical for the synthesis and accumulation of UBB^{+1}-anchored polyUb, which results in proteasomal inhibition and neuronal cell death.
This study was supported by a grant of the Korea Healthcare technology R&D Project, Ministry for Health, Welfare & Family Affairs, Republic of Korea (A092006).

References

[1] Lee V.M., Goedert M. amd Trojanowski J.Q., "Neurodegenerative tauopathies", *Annu. Rev. Neurosci.*, Vol. 24, (2001), pp 1121-1159.
[2] de Pril R., Fischer D.F., Roos R.A. and van Leeuwen F.W., "Ubiquitin-conjugating enzyme E2-25K increases aggregate formation and cell death in polyglutamine diseases", *Mol. Cell Neurosci.* 34, (2007), pp 10-19.
[3] van Leeuwen F.W., et al., "Frameshift mutants of beta amyloid precursor protein and ubiquitin-B in Alzheimer's and Down patients", *Science*, 279, (1998), pp 242-247.
[4] Hilbich C., Monning U., Grund C., Masters C.L. and Beyreuther K., "Amyloid-like properties of peptides flanking the epitope of amyloid precursor protein-specific monoclonal antibody 22C11", *J. Biol. Chem.*, 268, (1993), pp 26571-26577.
[5] van Leeuwen F.W., Hol E.M. and Fischer D.F., "Frameshift proteins in Alzheimer's disease and in other conformational disorders: time for the ubiquitin-proteasome system", *J. Alzheimers Dis.*, 9, (2006), pp 319-325.
[6] Fang S. and Weissman A.M., "A field guide to ubiquitylation", *Cell Mol. Life Sci.*, 61, (2004), pp 1546-1561.

MS04-P12

The role of the π-electron systems in regulation of reduction potentials of tetraheme cytochrome c_3

Hideo Akutsu[1,2], Yuki Takayama[1], Midori Taketa-Sato[3], Hirofumi Komori[3], Kumiko Morita[3], Sujin Kang[2] and Yoshiki Higuchi[3]

[1]*Institute for Protein Research, Osaka University, Suita 565-0871, Japan*
[2]*Department of Biophysics and Chemical Biology, College of Natural Sciences, Seoul National University, Seoul 151-747, Korea*
[3]*Graduate School of Life Science, University of Hyogo, Koto, Kamigori, Hyogo 678-1297, Japan*
E-mail: akutsu@protein.osaka-u.ac.jp

Cytochrome c_3 (cyt c_3) isolated from sulfate-reducing bacteria possesses four *c*-type hemes making a cyclic configuration in the single polypeptide whose molecular weight is typically ~14 kDa. Three-dimensional structures of ferrous and ferric cyts c_3 from various strains have been determined by x-ray crystallography and nuclear magnetic resonance (NMR) spectroscopy. One of its characteristic properties is extremely low reduction potentials, ranging from –90 mV to –380 mV [1]. We assessed the contributions of each amino acid residue to lowering the reduction potentials of *Desulfovibrio vulgaris* Miyazaki F (*Dv*MF) cyt c_3 by site-directed mutagenesis [1-4]. In these investigations, the overexpression system for cyt c_3 developed in our laboratory [2] has been shown powerful. The coordinated histidines were found to be essential [3,4]. There are 14 aromatic residues and four heme rings as π-electron systems in a 107-residue protein. In the mutational analysis of noncoordinated aromatic residues of cyt c_3 [2,3] only conserved residues, Phe20, Tyr43, Tyr65 and Tyr66, showed large contributions to the extremely low reduction potentials. Especially Phe20 is the most conserved residue among all type I cyts c_3 so far sequenced. We focused our attention on this residue to investigate the role of the π-electron systems using NMR and X-ray crystallography.

The effects of mutation at a noncoordinated aromatic residue on the coordination structure of heme irons and the microscopic reduction potentials were investigated on the basis of His C2H NMR signals and crystal structures for F20H, F20M, F20Y, Y65A and Y66L cytochromes c_3. Changes in the coordination structures were generally subtle in crystal structures in spite of significant changes in the reduction potentials and NMR spectra, suggesting that the dynamic structure and its physicochemical properties in solution are important in regulation of the redox reaction. The effect of the mutation on the reduction potential of each heme at each oxidation state reveals that the π-electron system composed of heme rings and aromatic amino acid rings play a key role in the regulation of reduction potentials.

References

[1] Akutsu, H. and Takayama, Y. "Functional roles of the heme architecture and its environment in tetraheme cytochrome *c*", *Acc. Chem. Res.* 40, (2007), 171-178.
[2] Ozawa, K., Takayama, Y., Yasukawa, F., Ohmura, T., Cusanovich, M.A., Tomimoto, Y., Ogata, H., Higuchi, Y., and Akutsu, H. "Role of the aromatic ring of Tyr43 in tetraheme cytochrome c_3 from *Desulfovibrio vulgaris* Miyazaki F", *Biophys. J.* 85, (2003), 3367-3374.
[3] Takayama, Y., Harada, E., Kobayashi, R., Ozawa, K., and Akutsu, H. "Roles of noncoordinated aromatic residues in redox regulation of cytochrome c_3 from *Desulfovibrio vulgaris* Miyazaki F", *Biochemistry* 43, (2004), 10859-10866.
[4] Takayama, Y., Werbeck, N.D., Komori, H., Morita, K., Ozawa, K., Higuchi, Y., and Akutsu, H. "Strategic roles of axial histidines in structure formation and redox regulation of tetraheme cytochrome c_3" *Biochemistry*, 47, (2008), 9405-9415.

MS04-P13

Two different modes of UvrD helicase by 2B domain movement

Hyun Koo Yeo[1] and Jae Young Lee[1]

[1]*Department of Life Science, Dongguk University, Seoul 100-715, Korea*
E-mail: yhk5442@dongguk.edu

Helicases use the energy derived from nucleoside triphosphate hydrolysis to unwind double helices in essentially every metabolic pathway involving nucleic acids. Earlier crystal structures have suggested that DNA helicases translocate along a single-stranded DNA in an inchworm fashion or unwind duplex DNA in a combined wrench-and-inchworm mechanism with the step size of 1 base pair. UvrD helicases contain domains 1B and 2B in addition to 1A and 2A. Domain 2B, which undergoes on ~150° rotation upon binding to a double- and single-stranded (ds-ss) DNA junction and transforms the helicase from an "open" to "closed" state, has been shown to be essential for duplex binding and unwinding. In order to probe the role of the 2B domain in dsDNA binding and helicase activity, several mutations were introduced in to UvrD. The biochemical studies of UvrD mutants reveal that UvrD helicases have two different modes depending on the 2B domain. In the wrench-and-inchworm mode, the closed conformation of 2B domain is essential for binding and unwinding the duplex region of DNA. All four key helicase-DNA contact points are engaged and the movements of ds-ss DNA are highly coordinated. But the presence of helicase activity that is independent of the 2B domain and dsDNA binding leads that there is a strand displacement mode as an alternative to the wrench-and-inchworm mode. In the strand displacement mode, the open conformation of 2B domain appears to work most efficiently. The strand displacement mode may be adopted in the absence of dsDNA or by UvrD mutants that are unable to bind dsDNA.

References

[1] Lee J.Y. and Yang W., "UvrD Helicase Unwinds DNA One Base Pair at aTime by a Two-Part Power Stroke", *Cell*, Vol. 127, No. 7, (2006), pp 1349-1360.

[2] Velankar, S.S., Soultanas, P., Dillingham, M.S., Subramanya, H.S., and Wigley, D.B. "Crystal structures of complexes of PcrA DNA helicase with a DNA substrate indicate an inchworm mechanism", *Cell*, Vol. 97, No. 1, (1999), pp 75–84.

MS04-P14

Functional implication of Ufd1-Npl4 complex in the FAF1 recognition mechanism by AAA-ATPase p97/VCP

Joon Kyu Park and Eunice EunKyeong Kim

Life Sciences Division, Korea Institute of Science and Technology, Seoul 136-791, Korea
E-mail: dansoons@kist.re.kr

The highly conserved p97 (also known as VCP and Cdc48 in yeast) is multifunctional AAA-family ATPase that is involved in a wide range of biological activities such as ERAD, membrane fusion, transcriptional activation, cell-cycle control and apoptosis. Mutations in human p97/VCP are reported to trigger the human multisystem disorder IBMPFD and elevated levels of p97/VCP have been reported to correlate with increased incidences of metastasis in various types of cancer. It is also co-localizes with protein depositions characteristic for various neurodegenerative disorders such as polyglutamine, Parkinson's and Alzherimer's diseases. It consists of three domains: the N-terminal domain and two ATPase domains called as D1 and D2. Although the precise regulatory mechanisms are not yet well understood, p97/VCP is believed to mediate these processes through the binding of various adaptor proteins. Two most well characterized adaptors are p47, and the Ufd1-Npl4 complex. P47 is known to direct p97/VCP to membrane fusion events and protein degradation other than ERAD while the Ufd1-Npl4 complex is known to direct p97/VCP to an essential role in ERAD. It has been shown that both p47 and Ufd1-Npl4 bind to the N-domain of p97/VCP through its UBX and UBD, respectively. A number of UBX containing proteins have been discovered in last few years and they are expected to be involved in substrate recruitment to p97/VCP and in the temporal and spatial regulation of its activity. Among them is FAF1, a highly conserved novel protein with multi-ubiquitin related domains. In this study we try to elucidate the interaction between FAF1 and various forms of p97/VCP and Ufd1-Npl4 complex using ITC, EM and X-ray crystallography and the results will be presented.

This work was supported by grants from the Functional Proteomics Center, the 21C Frontier Research & Development Program of the Korea Ministry of Science and Technology, and the Korea Institute of Science and Technology Institutional Program.

References

[1] Zhang X., Shaw A., Bates P.A., Newman R.H., Gowen B., Orlova E., Gorman M.A., Kondo H., Dokurno P., Lally J., Leonard G., Meyer H., van Heel M. and Freemont P.S., "Structure of the AAA ATPase p97", *Mol. Cell*, Vol. 6, No. 6, (2000), pp 1473-1484.

[2] Chu K., Niu X. and Williams L.T. "A Fas-associated protein factor, FAF1, potentiates Fas- m ediated apoptosis", *Proc. Natl. Acad. Sci. USA*., Vol. 92, No. 25, (1995), pp 11894-11898.

[3] Buchberger A. "From UBA to UBX: new words in the ubiquitin vocabulary", *Trends Cell. Biol*., Vol. 12, No. 5, (2002), pp 216-221.

MS04-P15

The structure of rat liver vault at 3.5 Å resolution

Koji Kato 1, Hideaki Tanaka2, Eiki Yamashita2, Tomoyuki Sumizawa3, Yong Zhouc4, Min Yao4, Kenji Iwasaki2, Masato Yoshimura5, and Tomitake Tsukihara1

1 Department of Life Science, University of Hyogo, 3-2-1 Koto, Kamighori, Akoh, Hyogo 678-1297, Japan
2 Institute for Protein Research, Osaka University, 3-2 Yamada-oka, Suita, Osaka 565-0871, Japan
3 Kagoshima women's junior college, 6-9 Kourai, Kagoshima, Kagoshima 890-8565, Japan
4 Faculty of Advanced Life Sciences, Graduate School of Life Sciences, Hokkaido University, Sapporo, Hokkaido 060-0810, Japan
5 National Synchrotron Radiation Research Center, 101 Hsin-Ann Road, Hsinchu Science Park, Hsinchu 30076, Taiwan
E-mail: k-kato@protein.osaka-u.ac.jp

Vault is a 10-MDa ribonucleoprotein particle with a barrel-like shape, two protruding caps, and an invaginated waist structure that is highly conserved in a wide variety of eukaryotes. The rat liver vault is composed of three proteins: the 99-kDa major vault protein (MVP), the 193-kDa vault poly(ADP-ribose)polymerase (VPARP), and the 290-kDa telomerase-associated protein TEP1. Additionally, the complex contains a small untranslated RNA consisting of 141 bases (vRNA). Although several functions have been proposed for vaults since their first discovery in 1986, including roles in multidrug resistance, cell signaling and innate immunity, their cellular function remains unclear. To elucidate the structure, structural organization and physiological function of this macromolecular complex, we determined the X-ray crystal structure of the rat liver vault at 3.5 Å resolution**[1,2]**. The X-ray structure reveals that the vault particle has a unique cage-like shape, consisting of 78 identical MVP chains with 39-fold dihedral symmetry. MVP monomer folded into 12 domains; nine structural repeat domains, a shoulder domain, a cap-helix domain and a cap-ring domain. I would like to explain the structure of rat liver vault in detail.

References

[1] Hideaki Tanaka, Koji Kato, Eiki Yamashita, Tomoyuki Sumizawa, Yong Zhou, Min Yao, Kenji Iwasaki, Masato Yoshimura, and Tomitake Tsukihara, "The structure of rat liver vault at 3.5 Å resolution", *Science* (**323**), 384-388, 2009

[2] Koji Kato, Hideaki Tanaka, Tomoyuki Sumizawa, Masato Yoshimura, Eiki Yamashita, Kenji Iwasaki, Tomitake Tsukihara, "A vault ribonucleoprotein particle exhibiting 39-fold dihedral symmetry.", *Acta Crystallogr D Biol Crystallogr*. (64), 525-531, 2008

MS04-P16

Biophysical investigation of RBP-ARE interactions: Application of SPR, NMR, and SAXS

Henry Kim[1], Yano Yoga[1], Nathan Cowieson[2], Martin Scanlon[3], Steven Headey[3], Myriam Gorospe[4], Bryan Williams[5], Matthew Wilce[1] and Jackie Wilce[1]

[1] *Biochemistry and Molecular Biology, Monash University, Clayton, Australia*
[2] *Australian Synchrotron, Clayton, Australia*
[3] *Monash Institute of Pharmaceutical Sciences, Parkville, Australia*
[4] *NIH, Baltimore USA*
[5] *Monash Institute of Medical Research, Clayton, Australia*
E-mail: hkimproject@gmail.com

The control of mRNA stability is a key factor in the regulation of gene expression. The competing events of translation and mRNA decay ultimately dictate the level of protein expressed and are readily affected in response to changes in cellular conditions. mRNA transcripts bearing AU-rich sequences in their 3'UTR, in particular, appear to be under the control of many factors that determine whether the transcript is destined for translation, degradation or held in a translationally repressed state. These factors include RNA-binding proteins such Hu proteins which are protective against degradation and TIA proteins which are involved in sequestering mRNA into stress granules under conditions of cellular stress. Exactly how these proteins recognise and interact with AU-rich sequences is only partially understood, including whether they actually compete for the same target mRNAs.

We have focused on two of these proteins, HuR and TIAR which are both triple RNA recognition motif (RRM) proteins that bind AU-rich RNA with nM affinity. We report our studies using SPR that reveal similar mRNA target sequence preferences, yet differences in their stringency of interaction. We also explore the importance of the separate RRMs, as well as the protein regions beyond the RRMs, for the mRNA interaction using NMR spectroscopy and differences in molecular shape of the protein/RNA complex using SAXS. Together these data bring us closer to an understanding of the dynamic interplay that takes place in the cell in the regulation of gene expression at the level of mRNA.

MS04-P17

Identification and analysis of dominant negative mutants of RAIDD and PIDD

Hyun Ho Park, Tae-ho Jang, Ju Young Bae, and Ok Kyeung Park

School of Biotechnology and Graduate School of Biochemistry at Yeungnam University, Gyeongsan, South Korea
E-mail: hyunhopark@yu.ac.kr

Caspases are cysteine proteases that are essential during the initiation and execution of apoptosis and inflammation. The formation of large oligomeric protein complexes is critical to the activation of caspases in apoptotic and inflammatory signaling pathways. These oligomeric protein complexes function as a platform to recruit caspases, which leads to caspase activation via a proximity-induced mechanism. One well-known oligomeric caspase-activating complex is the PIDDosome for caspase-2 activation, which is composed of 3 protein components, PIDD, RAIDD and Caspase-2. Despite the significant role that caspase-2 activated by PIDDosome plays important role during genotoxic stress-induced apoptosis, the oligomerization mechanism and the method by which the caspase activating process is mediated by the formation of PIDDosome is currently not well understood. Here, we show that the assembly mechanism of core of PIDDosome is time-dependent and salt concentration-dependent. In addition, we demonstrate that point mutations on RAIDD (R147E) and on PIDD (Y814A) exert a dominant negative effect on formation of the PIDDosome, and that this effect cannot be applied after the PIDDosome has been formed.

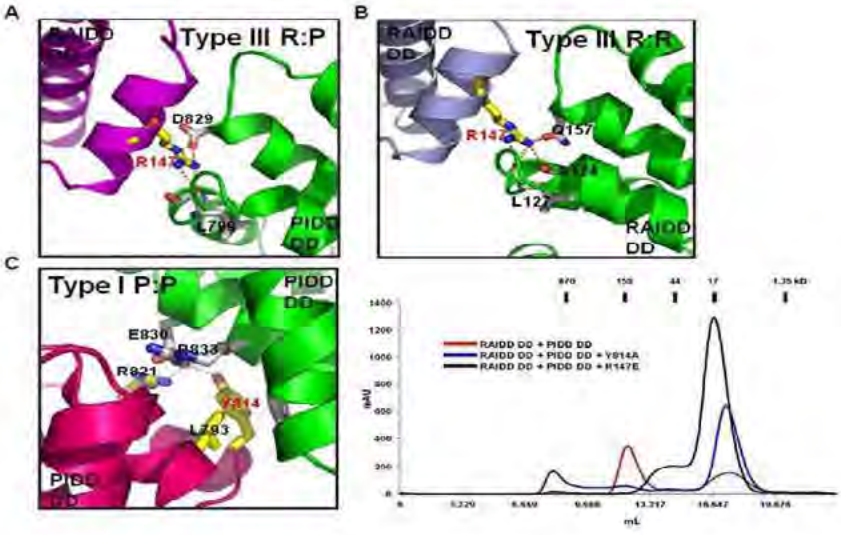

References

[1] Park HH., Lo YC., Lin SC., Wnag L., Yang JK. and Wu H., "The death domain superfamily in intracellular signaling of apoptosis and inflammation", *Annu Rev Immunol*, Vol. 25, (2007), pp 561-586.

[2] Park HH., Logette E., Raunser S., Cuenin S., Walz, T., Tschopp J. and Wu H., "Death domain assembly mechanism revealed by crystal structure of the oligomeric PIDDosome core complex", *Cell*, Vol. 128, (2007), pp 533-546.

[3] Tinel A. and Tschopp J., "The PIDDosome, a protein complex implicated in activation of caspase-2 in response to genotoxic stress", Science, Vol. 304, (2004), pp 843-846.

MS04-P18

Human MTERF3 crystal structure of left-handed superhelical tandem repeat

Dong-Uk Kim, Sang-Gil Cho, Kuk-Lea Kim, and Hyun-Soo Cho*

Department of Biology, College of Life Science and Biotechnology, Yonsei University, 134 Shinchon-dong, Seodaemun-gu, Seoul 120-749, Republic of Korea
E-mail: biokim@yonsei.ac.kr

The mitochondrial transcription termination factors (MTERFs) play an important role in the transcriptional regulation of mitochondrial genes. In mammals, the MTERF1-4 protein subfamilies one through four contain all the mTERF domains needed to interact with mitochondrial DNA (mtDNA). To understand the molecular function of these domains, we solved the crystal structure of MTERF3 at 2.8 Å and did performed homology modeling of the complex structure between an mTERF domain and mtDNA. It shows the left-handed superhelix resulting in a half-donut shape. Especially the positive charged concave in the central region of the structure suggests this region might be mtDNA binding interface, where accommodate and interact with mtDNA well according to the modeling structure. We compared MTERF3 to DNA-bound MTERF1 to explain the structural and functional characteristics of MTERF3.

References

[1] C.B. Park, J. Asin-Cayuela, Y. Camara, Y. Shi, M. Pellegrini, M. Gaspari, R. Wibom, K. Hultenby, H. Erdjument-Bromage, P. Tempst, M. Falkenberg, C.M. Gustafsson, N.G. Larsson, MTERF3 is a negative regulator of mammalian mtDNA transcription, Cell 130 (2007) 273-285.

[2] E. Yakubovskaya, E. Mejia, J. Byrnes, E. Hambardjieva, M. Garcia-Diaz, Helix unwinding and base flipping enable human MTERF1 to terminate mitochondrial transcription, Cell 141 (2010) 982-993.

[3] N. Jimenez-Menendez, P. Fernandez-Millan, A. Rubio-Cosials, C. Arnan, J. Montoya, H.T. Jacobs, P. Bernado, M. Coll, I. Uson, M. Sola, Human mitochondrial mTERF wraps around DNA through a left-handed superhelical tandem repeat, Nat Struct Mol Biol (2010).

MS04-P19

Structure analysis of ligand-independent activation of Fushi tarazu factor-1 ligand binding domain from *Drosophila melaganoster*

Ji-Ho Yoo[a], Sunggeon Ko[b], Hyeyon Kim[a], Kwang-Min Choe[a], WeonTae Lee[b] and Hyun-Soo Cho[a]

[a]*Department of Biology, College of Life Science and Biotechnology, Yonsei University, Seoul 120-749, Korea*
[b]*Department of Biochemistry, College of Life Science and Biotechnology, Yonsei University, Seoul 120-749, Korea*

Drosophila melanogaster Fushi tarazu factor 1 (Ftz-F1) is an orphan nuclear receptor of which ligand has not been identified until now. The Ftz-F1 regulate gene expression for development, reproduction and cholesterol homeostasis. Also, It is known that the Ftz-F1 interacts with segmentation gene '*Fushi tarazu*' (*Ftz*) for activation of the Ftz-F1. The Ftz-F1 is divided two parts, DNA-binding domain (DBD) and ligand-binding domain (LBD). It is known which ligand binding domain of Ftz-F1 is crucial part to regulate gene expression. Here we report the crystal structure analysis of the Ftz-F1 LBD bound to the peptide containing LXXLL co-activator motif of Ftz. The Ftz-F1 LBD structure consists of twelve α-helices and two β- strands which form a fourth-layer alpha-helical sandwich. Compared with structures of Liver receptor holmologue-1 and Steroidogenic factor-1 in the same subfamily of nuclear receptor, the Ftz-F1 LBD does not have an enough space for ligand-binding which explains in structural points why the ligand for Ftz-F1 regulation have not been found even though extensive efforts searching for it. Interestingly Ftz-F1 has the AF-2 in the active conformation without ligand binding. With mutagenesis assays, these suggest that Ftz-F1 is a constitutively active nuclear receptor which does not need ligand implying another regulation mechanism of the Ftz-F1.

Reference

[1] Carol J.E.Schwartz, Heidi M.Sampson, Daniela Hlousek, Anthony Percival-Smith, Yussa, Wei Han, Norbert Perrimon, Leslie Pick. The nuclear hormone receptor Ftz-F1 is a cofactor for *Drosophila* homeodomain protein Ftz. Nature, Vol 385 (1997) 552-555.

[2] Weiru Wang, Chao Zhang, Adhirai Marimuthu, Heike I. Krupka, Maryam Tabrizizad, Rafe Shelloe, Upasana Mehra, Kevin Eng, Hoa Nguyen, Calvin Settachatgul, Ben Powell, Michael V. Milburn, Brian L. West. The crystal structures of human steroidogenic factor-1 and liver receptor homologue-1. Proc Natl Acad Sci U S A Vol 102 (2005) 7505-7510.

[3] Elena P. Sablin, Irina N. Krylova, Robert J. Fletterick, Holly A. Ingraham. Structural basis for Ligand-Independent Activation of the Orphan receptor LRH-1. Mol Cell Vol 11 (2003) 1575-1585.

MS04-P20

Structure of the entire ectodomain of gp130: Insights into the molecular assembly of cytokine receptor complexes

Yibin Xu, Nadia J. Kershaw, Cindy S. Luo, Priscilla Soo, Michael J. Pocock, Peter E. Czabotar, Douglas J. Hilton, Nicos A. Nicola, Jian-Guo Zhang and Thomas P. J. Garrett

Walter + Eliza Hall Institute of Medical Research, 1G Royal Parade, Parkville, Victoria 3052, Australia
E-mail: tgarrett@wehi.edu.au

The cell surface receptor, gp130, is the required signaling subunit in the interleukin 6 (IL-6)-like cytokine family, which includes, IL-6, IL-11, leukemia inhibitory factor (LIF), oncostatin M (OSM) and ciliary neurotrophic factor (CNTF). This family of cytokines is involved in inflammatory and immune responses and also plays crucial roles in hematopoiesis, liver and neuronal regeneration, embryonic development, and fertility. Dysregulation of signaling contributes to diseases such as inflammatory bowel disease, osteoporosis, multiple sclerosis, multiple myeloma, and prostate cancer.

Although crystal structures have been determined for receptor:ligand complexes of this family, they lacked the C-terminal domains required for effective signal transduction. Here we present the crystal structure of the entire extracellular portion of human gp130 (D1-D6) at 3.6 Å resolution and D4-D6 at 1.9 Å resolution. This represents the first atomic resolution structure of the complete ectodomain for any "tall" cytokine receptor. The structures show that there is little structural change in gp130 upon ligand binding, other than a reorientation of the D1 domain. It also reveals that the interface between the D4 and D5 domains forms an acute bend in the gp130 structure. Key residues at this interface are highly conserved across the entire "tall" receptor family, suggesting that this acute bend may be a common feature of these receptors.

This structure, together with our structure of the LIF:LIF receptor complex allows us to construct models for the two types of receptor:ligand complexes which occur in this family, namely the hexameric $(gp130{:}IL\text{-}6R{:}IL\text{-}6)_2$ and the trimeric gp130:LIF:LIFR complexes. In each of these complexes the geometry of the membrane-proximal FnIII domains brings the transmembrane regions in close proximity, thus bringing together the cytoplasmic receptor-associated Janus kinases to trans-phosphorylate and activate each other.

MS07-P01

Crystal structure of human transglutaminase 2 in complex with adenosine triphosphate

Byeong-Gu Han[1], Jea-Won Cho[1] and Byung Il Lee[1]

[1]*Cancer Cell and Molecular Biology Branch, Division of Cancer Biology, Research Institute, National Cancer Center, Goyang, Gyeonggi 410-769, Korea*
E-mail: hanbyeonggu@gmail.com

Transglutaminase 2 (TG2) is a calcium-dependent multifunctional protein associated with various human diseases. We determined the crystal structure of human TG2 in complex with adenosine triphosphate (ATP). The ATP molecule binds to the previously identified guanosine diphosphate (GDP) binding pocket but has different hydrogen bonds and ion interaction with protein. The four residues Arg476, Arg478, Val479 and Tyr583, all of which are involved in both ATP and GDP binding by hydrogen bonds, might play important roles in the stabilization of TG2 by ATP or GDP. However, Ser482 and Arg580, which are involved in GDP binding, do not form hydrogen bond with ATP. Additionally, we newly discovered an intramolecular disulfide bond between Cys230 and Cys370, which formation might regulate the enzymatic activity of TG2.

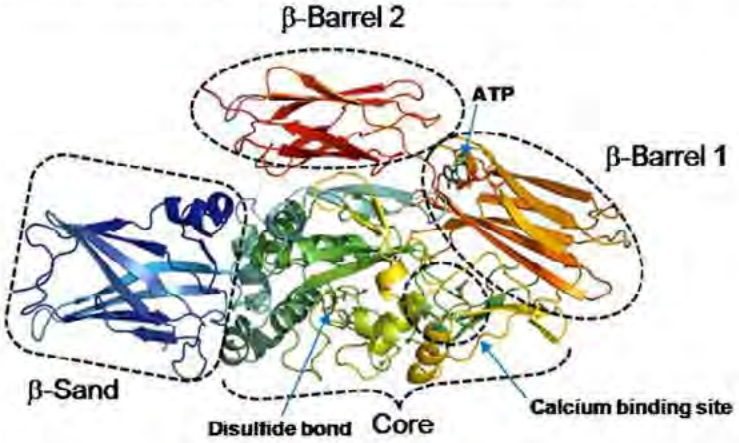

References

[1] Jeon J.H., Cho S.Y., Kim C.W., Shin D.M., Kweon J.C., Choi K.H., Park S.C. and Kim I.G., "GTP is required to stabilize and display transamidation activity of transglutaminase 2", Biochem Biophys Res Commun, Vol. 294, (2002), pp 818-822.

[2] Liu S., Cerione R.A. and Clardy J., "Structural basis for the guanine nucleotide-binding activity of tissue transglutaminase and its regulation of transamidation activity", Proc Natl Acad Sci, Vol. 99, (2002), pp 2743-2747.

[3] Pinkas D.M., Strop P., Brunger A.T. and Khosla C., "Transglutaminase 2 undergoes a large conformational change upon activation", PLoS Biol, Vol. 5, (2007), pp e3270.

[4] Han B.G., Cho J.W., Cho Y.D., Jeong K.C., Kim S.Y. and Byung Il Lee B.IL., "Crystal structure of human transglutaminase 2 in complex with adenosine triphosphate", Int J Biol Macromol, (2010).

MS07-P02

Structure and function of the Fibrobacter succinogenes 1,3-1,4-β-D-glucanase mutants F40I and W203F in complex with inhibitors

Li-Chu Tsai, Hsiao-Chuan Huang, Ching-Hua Hsiao, Wei-Ru Li and Li-Ming Yin

Department of Molecular Science and Engineering, Institute of Organic and Polymeric Materials, National Taipei University of Technology, Taipei 10608, Taiwan, R.O.C.
E-mail: lichu@ntut.edu.tw

Four aromatic residues, Phe40, Tyr42, Trp203 and Phe205 located in active site of the catalytic domain of *Fibrobacter succinogenes* 1,3-1,4-β-D-glucanase (TFsβ-glucanase) interact with sugar units of the product via hydrophobic stacking interactions. The role of aromatic residues at the carbohydrate-binding site was confirmed by mutational, structural, and functional analyses. Kinetic data reveal that substitution of aromatic residue with non-aromatic residue significantly affects enzyme activity. The mutant crystal structures of F40I and W203F were determined at 1.7 and 1.4 Å resolution, respectively. This study suggests that aromatic residues at the active site of enzyme play critical roles in protein-carbohydrate binding, stabilization and catalysis. Further analysis of the mutant structures revealed that two extra calcium ions and a Tris molecule have been identified in both mutants. It is interesting to note for the first time that two extra calcium ions and a Tris molecule have been identified in glycosyl hydrolase family 16. The Tris molecule, bound to catalytic residues Glu56 and Glu60, was found at the position normally taken by substrate binding to the -1 subsite. One calcium ion was found near the active site residue Asp202. Kinetics experiments show that Tris is a competitive inhibitor of the enzyme, while calcium ion is a non-competitive inhibitor.

MS07-P03

Investigating the structure and function of the redox folding factors αDsbA2 and αDsbB

Walden, P.M.[1], Heras, B.[1], Iturbe-Ormaetxe, I.[2], Martin, J.L[1].

1 Insitute for Molecular Bioscience, University of Queensland, St Lucia, QLD 4072, Australia
2 School of Biological Science, University of Queensland, St.Lucia, QLD 4072, Australia
E-mail: p.walden@uq.edu.au

To function correctly proteins need to be assembled and folded. For secreted proteins, a key step in the folding process is the introduction of disulfide bonds between cysteine residues, which gives stability in the harsh extracellular environment. This step is also known as oxidative protein folding. The process of oxidative protein folding requires thiol-disulfide exchange [1]. In prokaryotes, correct oxidative folding is influenced by disulfide bond forming proteins called Dsb-proteins. In *Escherichia coli*, the disulfide bond forming machinery has two pathways, oxidation and isomerization. In the oxidative pathway, disulfide bonds are introduced into proteins whereas in the isomerization pathway non-native disulfides are corrected by reshuffling [2].

While the Dsb pathway in *E. coli* K-12 is the best-characterized oxidative pathway, the Dsb pathway in other bacteria, like *Wolbachia pipientis*, is still unclear. *Wolbachia pipientis* is the most common Gram-negative α-proteobacterial endosymbiont worldwide since it is able to infect more than 65% of all insect species [3]. This bacterium has the unique ability to alter the reproduction of its host in several ways and so has become an interesting topic of current research [4]. *Wolbachia's wMel* genome encodes three Dsb proteins, with no apparent isomerization pathway [5], indicating a very different folding pathway from that of *E. coli*.

It is now interesting to investigate the *Wolbachia* Dsb pathway to obtain a comprehensive picture of how disulfide bond catalysis occurs in this organism and how disulfide-containing proteins are folded in *Wolbachia*. This research will improve our understanding of how the Dsb candidates interact with each other and how, in a bigger picture, this organism influences its hosts. Therefore, my research focuses on the characterization of two Dsb proteins in *Wolbachia*. I investigate the structure and function of the DsbA-like protein α-DsbA2 and the membrane protein α-DsbB. Biochemical analysis of their redox functions and determination of their structures by X-ray crystallography will provide a better understanding of their role in the *Wolbachia*-host relationship.

Reference

[1] Wedemeyer WJ, Welker E, Narayan M, Scheraga HA. Disulfide bonds and protein folding (vol 39, pg 4207, 2000). Biochemistry 2000;39(23):7032-7032.
[2] Heras B, Shouldice SR, Totsika M, Scanlon MJ, Schembri MA, Martin JL. DSB proteins and bacterial pathogenicity. Nature Reviews Microbiology 2009;7(3):215-225.
[3] Hilgenboecker K, Hammerstein P, Schlattmann P, Telschow A, Werren JH. How many species are infected with Wolbachia? - a statistical analysis of current data. Fems Microbiology Letters 2008;281(2):215-220.
[4] Travis J. Undesirable Sex Partners- Bacteria manipulate reproduction of insects and other species Science News Online 1996;11/16/96.
[5] Kurz M, Iturbe-Ormaetxe I, Jarrott R, Shouldice SR, Wouters MA, Frei P, Glockshuber R, O'Neill SL, Heras B, Martin JL. Structural and Functional Characterization of the Oxidoreductase alpha-DsbA1 from Wolbachia pipientis. Antioxidants & Redox Signaling 2009;11(7):1485-1500

MS07-P04

Time-resolved X-ray crystal structure analysis of enzymatic reaction of copper amine oxidase from *Arthrobacter globiformis*

Misumi Kataoka[1,2,4], Hiroko Oya[1], Ayuko Tominaga[1], Masayuki Otsu[1], Toshihide Okajima[3], Katsuyuki Tanizawa[3] and Hiroshi Yamaguchi[1,2]
[1]*School of Science and Technology, Kwansei Gakuin University, 2-1 Gakuen, Sanda, Hyogo 669-1337, Japan*
[2]*Physical Science Center for Biomolecular Systems Research, Kwansei Gakuin University, 2-1 Gakuen, Sanda, Hyogo 669-1337, Japan*
[3]*Institute of Scientific and Industrial Research, Osaka University, 8-1 Mihogaoka, Ibaraki, Osaka 567-0047, Japan*
[4]*Research Fellow of the Japan Society for the Promotion of Science (JSPS Research Fellow), 1-8 Chiyoda, Tokyo 102-8472, Japan*
E-mail: m-kataoka@kwansei.ac.jp

To reveal the chemical changes and geometry changes of active site residues and water molecules that cooperate with the reaction is important for appreciating the functional mechanism of proteins. And, in order to elucidate the catalytic reaction mechanisms of proteins, it is necessary to trace structural changes of reaction intermediates. And, geometry changes of active site residues that cooperate with the reaction are important for understanding the functional mechanism of proteins.

Amine oxidases catalyze the oxidative deamination of various primary amines to the corresponding aldehydes. In the active site, the enzyme has Cu and quinone cofactor, topaquinone (TPQ) which is converted from tyrosine residue by post-translational modification. A catalytic mechanism is proposed, which is composed of former reductive and latter oxidative half-reactions. In the former step, TPQ reacts with 2-phenylethylamine (PEA) substrate to give rise to topasemiquinone formed Schiff-base and produces phenylacetaldehyde. In the following step, TPQ is generated from topasemiquinone, releasing ammonia and peroxide aerobically. To elucidate this reaction mechanism of catalytic reaction, we are studying phenylethylamine oxidase from *Arthrobacter globiformis* (AGAO).

The solution of purified precursor apo-AGAO was dialyzed against buffer containing Cu^{2+} to convert to active holo-AGAO. The holo-AGAO solution was crystallized anaerobically. The crystals were soaked in the PEA solution and freeze-trapped in liquid nitrogen. Each step of crystals was confirmed by single-crystal microspectrometry before X-ray diffraction measurements. Diffraction data were collected at 100 K in the BL38B1, BL44B2 and BL44XU at SPring-8, Japan. Four structures of reaction intermediate were determined at atomic resolution. We revealed that TPQ and some residues in the substrate channel were flipped via catalytic reductive half-reaction of AGAO

References

[1] Kim M., Okajima T., Kishishita S., Yoshimura M., Kawamori A., Tanizawa K. and Yamaguchi H., "X-ray snapshots of quinone cofactor biogenesis in bacterial copper amine oxidase", *Nat. Struct. Biol.*, Vol. 9, No. 8, (2002), pp 591-596.
[2] Mure M., Mills A. S. and Klinman P. J., "Catalytic Mechanism of the Topa Quinone Containing Copper Amine Oxidases", *Biochemistry*, Vol. 41, No. 30, (2002), pp 9269-9278.
[3] Chiu Y. C., Okajima T., Murakawa T., Uchida M., Taki M., Hirota S., Kim M., Yamaguchi H., Kawano Y., Kamiya N., Kuroda S., Hayashi H., Yamamoto Y. and Tanizawa K., "Kinetic and structural studies on the catalytic role of the aspartic acid residue conserved in copper amine oxidase", *Biochemistry*, Vol. 45, No. 13, (2006), pp 4105-4120

MS07-P05

Metabolic adaptation for short-chain fatty acids degradation: crystal structure of 2-methylcitrate synthase from *Salmonella typhimurium*

Sagar Chittori[a], H. S. Savithri[b], and M. R. N. Murthy[a]
[a]*Molecular Biophysics Unit, Indian Institute of Science, Bangalore, Karnataka, 560012, India,*
[b]*Department of Biochemistry, Indian Institute of Science, Bangalore, Karnataka, 560012, India*
E-mail: sagar@mbu.iisc.ernet.in

Short chain fatty acids, like acetate and propionate, are byproducts of bacterial fermentation and are in turn shown to be inhibitors of bacterial growth. Metabolic pathways for the utilization of short-chain fatty acids as a source of carbon and energy are found in bacteria such as *Salmonella typhimurium* and *Escherichia coli*. These pathways could serve as a defense mechanism in these organisms against the negative effects of SCFAs. 2-methylcitric acid (2-MCA) cycle is one of the widely distributed and biochemically well studied pathways of propionate metabolism. 2-methylcitrate synthase (2-MCS), a polypeptide of 43 kDa, catalyzes the conversion of oxaloacetate and propionyl-CoA to 2-methylcitrate and CoA in the second step of 2-MCA cycle. Examination of *S. typhimurium* 2-MCS amino acid sequence showed the presence of a Prosite motif (PS00480) corresponding to the active site of citrate synthases (CSs), implying similarities in the catalytic function of 2-MCS and CSs. CSs are extremely well studied enzymes and catalyze the condensation of acetyl-CoA and oxaloacetate to citrate and CoA. In the present work, the gene coding for 2-MCS from *S. typhimurium* was cloned in pRSET-C vector, overexpressed in *E. coli* and purified to homogeneity using Ni-NTA affinity chromatography (Chittori *et al*., 2010). Kinetic analysis on *Salmonella typhimurium* 2-MCS (*St*PrpC) showed 26 times higher catalytic efficiency (K_{cat}/K_m) of the enzyme for propionyl-CoA over acetyl-CoA. This is in contrast to *E. coli* CS (*Ec*CS), which catalyzes the condensation reaction at significant rate only with acetyl-CoA. *St*PrpC was crystallized in the triclinic space group P1 using the under-oil-microbatch method (Chittori *et al*., 2010). Crystal structure of *St*PrpC, determined at 2.4 Å resolution, revealed that the polypeptide fold was similar to those of CSs. In the triclinic P1 cell, *St*PrpC molecules were organized as decamers composed of five identical dimer units with 52 point group symmetry. CSs are usually dimeric proteins but higher oligomeric states have been reported in Gram-negative bacteria like *E. coli*. The hexameric *Ec*CS is allosterically regulated by NADH and KCl. DLS experiments performed with different concentrations of *St*PrpC showed a direct correlation between protein concentration and hydrodynamic radius, with the largest observed species (132.2 Å) corresponding to the decameric form. Despite low sequence identity (29%), the core of the *St*PrpC polypeptide fold is similar to that of *Ec*CS. However, the conformation of the segment corresponding to residues 234-270 of *St*PrpC is different from that of the equivalent residues (263-298) of *Ec*CS. It has been proposed that this region of *Ec*CS is involved in allosteric regulation resulting from conformational changes upon binding of acetyl-CoA. Further structural comparisons suggested that the key residues of CSs involved in NADH binding are not conserved in *St*PrpC, indicating that the *Salmonella* 2-MCS is not regulated in a manner similar to *Ec*CS. The catalytic residues of CSs were found to be conserved in *St*PrpC (His235, His274 and Asp325) suggesting similarities in the catalytic mechanisms of citrate and 2-methylcitrate synthases. Structural comparison with the ligand free and bound states of CSs showed that *St*PrpC is in a nearly closed conformation despite the absence of bound ligands. The closed conformation of *St*PrpC permitted identification of ligand binding residues. It was found that Tyr197 and Leu324 of *St*PrpC are structurally equivalent to His and Val, respectively, of CSs. These substitutions might determine the specificities for acyl-CoAs of these enzymes.

References

[1] Chittori S., Simanshu D.K., Savithri H.S. and Murthy M.R., "Preliminary X-ray crystallographic analysis of 2-methylcitrate synthase from Salmonella typhimurium". *Acta Crystallogr Sect F Struct Biol Cryst Commun*. Apr 1;66, (2010), pp 467-70.

MS07-P06

Crystal structures of Helicobacter pylori shikimate kinase reveal three conserved arginines involved in the induced movement

Wen-Chi Cheng,[1] Hung-Jung Wang,[1] and Wen-Ching Wang[1]*

[1]*Institute of Molecular and Cellular Biology & Department of Life Sciences, National Tsing Hua University, Hsinchu, Taiwan*

The seven-enzyme shikimate pathway including shikimate kinase absent in mammals is an attractive target pathway for herbicides, antimicrobial and antiparasitic agent. Site-directed mutagenesis studies of shikimate kinase from *Helicobacter pylori* (HpSK) revealed critical conserved residues (S15, D33, F48, R57, R116, and R132) involved in catalysis. Crystal structure of the mutant R57A shows a significant shift of the shikimate binding domain owing to the interactions between E53 and R132 rather than those between E53 and R57 in the wild-type structure. We have also determined structures of HpSK·SO_4 and HpSK·shikimate-3-phosphate (S3P)·ADP. These structures show a characteristic three-layer alpha-beta-alpha architecture and a closed complex form owing to the lid closure. Analysis of various HpSK structures reveals that three strictly conserved arginines (R57, R116, and R132) make hydrogen binds with shikimate/S3P. Of these, R57 stays at a relatively identical site, R132 has a small shift, whereas R116 that is located in the lid loop shows a significant move. Our results together suggest that these arginines contribute to the movement of the lid region and the shikimate-binding domain upon shikinate/S3P binding, hence locking into a closed form.

MS07-P07

Involvement of scaffolding residues in efficient inhibition: lessons from chimeric proteins

Sudip Majumder[1], Susmita Khamrui[1], Jhimli Dasgupta[2], J.K.Dattagupta[1] ,Udayaditya Sen[1,3]

[1]*Crystallography and Molecular Biology Division, Saha Institute of Nuclear Physics, Kolkata 700064, India*
[2]*Department of Biotechnology, St. Xavier's College, Kolkata 700016, India*
[3]*Structural Genomics Section, Saha Institute of Nuclear Physics, Kolkata 700064, India*
E-mail : sudip.majumder@saha.ac.in

For serine protease inhibitors, scaffolding spacer residue Asn or Arg religates cleaved scissile peptide bond to offer efficient inhibition(1). However, several designed 'mini-proteins', containing the inhibitory loop and the spacer(s) with trimmed scaffold behave like substrates, indicating that scaffolding region beyond the spacer is also important in the inhibitory process. To understand the loop-scaffold compatibility we prepared three chimeric proteins ECI^{L}-WCI^{S}, ETI^{L}-WCI^{S}, STI^{L}-WCI^{S}, where the inhibitory loop of ECI, ETI, STI are placed on the scaffold of their homolog WCI. Results show that while ECI^{L}-WCI^{S} and STI^{L}-WCI^{S} behave like good inhibitors,ETI^{L}-WCI^{S} behaves like a substrate (2,3). That means a set of loop residues ('SRLRSAFI'), offering strong trypsin inhibition in ETI, acts as substrate when they seat on the scaffold of WCI. Crystal structure of ETI^{L}-WCI^{S} shows that the inhibitory loop is adopts a non-canonical conformation. We identified three novel scaffolding residues Trp88, Arg74 and Tyr113 in ETI that act as barrier to confine the inhibitory loop to canonical conformation. Absence of this barrier in the scaffold of WCI makes the inhibitory loop flexible in ETI^{L}-WCI^{S} leading to a loss of canonical conformation, explaining its substrate like behavior. Incorporation of this barrier back in ETI^{L}-WCI^{S} through mutations increases its inhibitory power, supporting our proposition. Structural studies of the double mutant A76R-L115Yon ETI^{L}-WCI^{S} shows that the conformation of the inhibitory loop is restored back. This can be reckoned as a case of 'conformational epistasis' where introduction of some 'lost contacts' introduces functionality at one site by readjusting the protein conformational backbone on another site. Our study provides structural evidence for the contribution of remote scaffolding residues in the inhibitory process of serine protease inhibitors. Additionally we rationalize why the loop-scaffold swapping is not permitted even among the members of highly homologous inhibitors, which might be important in the light of inhibitor designing.

References

[1] Dasgupta J., Khamrui S., Dattagupta J.K., Sen U., "Spacer Asn determines the fate of Kunitz (STI) inhibitors, as revealed by structural and biochemical studies on WCI mutants." , Biochemi stry. 2006 Jun 6;45(22):6783-92.

[2] Khamrui S, Dasgupta J, Dattagupta JK, Sen U., "Single mutation at P1 of a chymotrypsin inhibit or changes it to a trypsin inhibitor: X-ray structural (2.15 A) and biochemical basis", Biochim Bi ophys Acta. 2005 Aug 31;1752(1):65-72

[3] Khamrui S, Majumder S, Dasgupta J, Dattagupta JK, Sen U., "Identification of a novel set of sca ffolding residues that are instrumental for the inhibitory property of Kunitz (STI) inhibitors, Protei n Sci. 2010 Mar;19(3):593-602.

MS07-P08

Structural insights into catalysis of βC-S lyase from *Streptococcus anginosus*

Yuichiro Kezuka[1], Yasuo Yoshida[2,3], Takamasa Nonaka[1]

[1]*School of Pharmacy, Iwate Medical University, Yahaba, Iwate 028-3694, Japan*
[2]*School of Dentistry, Iwate Medical University, Morioka, Iwate 020-8505, Japan*
[3]*School of Dentistry, Aichi Gakuin University, Nagoya, Aichi 464-8650, Japan*
E-mail: ykezuka@iwate-med.ac.jp

Hydrogen sulfide (H_2S), a gas with the odor of rotten eggs, is a causative agent of oral malodor. The gas is generally produced from L-cysteine by some enzymes of oral bacteria. Reports have indicated that H_2S is (i) highly toxic to mammalian cells; (ii) associated with endotoxin-induced inflammation and apoptosis; and (iii) one of the predominant volatile sulfur compounds in periondontal pockets. These findings suggest that H_2S may contribute to the pathogenesis of gingivitis and periodontitis.

Streptococcus anginosus βC-S lyase, encoded by the lcd gene, is a homodimeric pyridoxal-5′-phosphate (PLP)-dependent enzyme that catalyzes the α,β-elimination of sulfur amino acids containing αC-N and βC-S linkages, such as L-cysteine and L-cystathionine, to generate sulfur-containing molecules, pyruvate, and ammonia. Interestingly, the capacity of βC-S lyases from the anginosus group, represented by *S. anginosus*, to produce H_2S from L-cysteine was found to be considerably higher than that from other oral streptococci. The high H_2S-production capacity of *S. anginosus* is caused by this enzymatic property of βC-S lyase. As initial steps toward elucidating the relationship between the structure and properties of *S. anginosus* βC-S lyase, we performed the X-ray crystallographic analysis of the βC-S lyase and its L-serine (substrate analogue) complexes.

The fold of βC-S lyase resembles that of other PLP-dependent enzymes of the aspartate aminotransferase family (type I). The ε-amino group of Lys234 located in the catalytic cleft between two domains forms a covalent linkage with the PLP cofactor in the absence of L-serine. The complex crystals were prepared by a combination of soaking and freeze trapping at various time intervals. We observed well-defined electron densities for two reaction intermediates covalently bound to the PLP cofactor. The intermediates were identified as an external Schiff base and an α-aminoacrylate intermediate, which are the key species of PLP-dependent-enzyme catalysis, by microspectroscopic measurement.

MS07-P09

SbcD, the subunit of SbcCD DNA strand break repair protein from *Deinococcus radiodurans*

Mi Ra Han[1] and Byung Woo Han[1]

[1]*Department of Pharmacy, College of Pharmacy, Seoul National University, Seoul 151-742, Korea*
E-mail: m2727273@snu.ac.kr

Deinococcus radiodurans is an extremophilic bacterium, one of the most radioresistant organisms known. To understand why bacteria such as *Deinococcus radiodurans* are extremely resistant to high doses of ionising and ultraviolet (UV) radiation and hydrogen peroxide, its DNA repair systems have been studied during recovery from high dose exposure UV. Recenlty, it was emphasized that the role of SbcCD is similar to that of DSB repair proteins, which have single-stranded endonuclease and 3'→5' double-stranded DNA exonuclease activities of DNA strand break repair system in higher organisms. Here, we report structural study on SbcD, subunit of the SbcCD complex, using protein X-ray crystallography. Further study, we expect to reveal the DNA repair mechanism of *Deinococcus radiodurans* and adapt it to other higher organisms or industrial purposes.

References

[1] J.R. Battista, "Against all odds, the survival strategies of Deinococcus radiodurans" *Ann. Rev. Microbiol.* 51 (1997) 203–224
[2] M. J. Daly and K. W. Minton "Resistance to radiation." *Science* 270, (1995) 1318.
[3] Vidya A. Kamble, Hari S. Misra "The SbcCD complex of Deinococcus radiodurans contributes to radioresistance and DNA strand break repair in vivo and exhibits Mre11–Rad50 type activity in vitro *DNA Repair* 9 (2010) 488–494
[4] E. Bentchikou, P. Servant, G. Coste, S. Sommer " Additive effects of SbcCD and polX deficiencies in the in vivo repair of DNA double-strand breaks in Deinococcus radiodurans" *J. Bacteriol.* 189 (2007) 4784–4790.

MS07-P10

Structure of protochlorophyllide reductase: a greening mechanism of plants in the dark

Norifumi Muraki[1], Jiro Nomata[2], Yuichi Fujita[2], Genji Kurisu[1, 3]

[1]*Institute for Protein Research, Osaka University, Osaka 565-0871, Japan*
[2]*Graduate School of Bioagricultural Sciences, Nagoya University, Aichi 464-8601, Japan*
[3]*Departmet of Macromolecular Science, Graduate School of Science, Osaka University, Toyonaka, Osaka 560-0043, Japan*
E-mail: nmuraki@protein.osaka-u.ac.jp

Chlorophyll (Chl) is a tetrapyrrole macrocycle containing Mg and phytol chain. The Chl biosynthetic pathway consists of the multi-enzymatic reactions. An asymmetric conjugated double bond system of Chl *a*, which is crucial for efficient light absorption, is formed in the penultimate step of biosynthesis, reducing protochlorophyllide (Pchlide) to form chlorophyllide *a*. Photosynthetic organisms adopt two different strategies for the reduction of Pchlide; one is the light-dependent Pchlide oxidoreductase, the other is the dark-operative (light-independent) Pchlide oxidoreductase (DPOR) that operates even in the dark. The greening ability of plant in the dark is attributed to the activity of DPOR. DPOR is characterized to be a nitrogenase-like enzyme requiring ATP hydrolysis and electron supply from Ferredoxin. As same as nitrogenase which catalyzes reduction of molecular nitrogen, DPOR consists of the electron transfer component, L-protein, and the catalytic component, NB-protein.
We show a crystal structure of the catalytic component, NB-protein, of the DPOR from *Rhodobacter capsulatus* at 2.3-angstrom resolution [1]. Overall structure with two copies of homologous BchN and BchB subunits is similar to that of nitrogenase MoFe-protein. Each catalytic BchN-BchB unit contains one Pchlide held without any axial ligations from amino acid residues and one [4Fe-4S] cluster (NB-cluster) at the subunit interface. A surprise of the structure is direct coordination of BchB-Asp36 to the cluster, instead of BchB-Cys95 anticipated to coordinate the cluster based on the sequence similarity. The orientation of bound Pchlide is mainly provided by hydrophobic interaction, keeping the reduction site of Pchlide away from the NB-cluster. The structure in the presence or absence of Pchlide has revealed the displacement of C-terminal helix of BchB when accommodating Pchlide. Intriguingly, NB-cluster and Pchlide are arranged spatially as almost identical to P-cluster and FeMo-cofactor in MoFe-protein of nitrogenase, illustrating a common architectire to reduce chemically stable multi-bonds such as porphyrin and dinitrogen.

In order to examine the contribution of some residues near the substrate-binding site, we created some variants. At the poster presentation, we will propose a novel catalytic reaction mechanism in DPOR based on the analysis of DPOR variants.

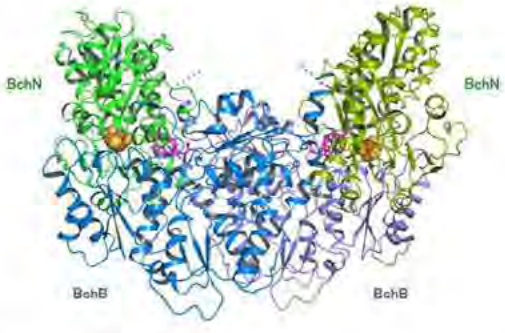

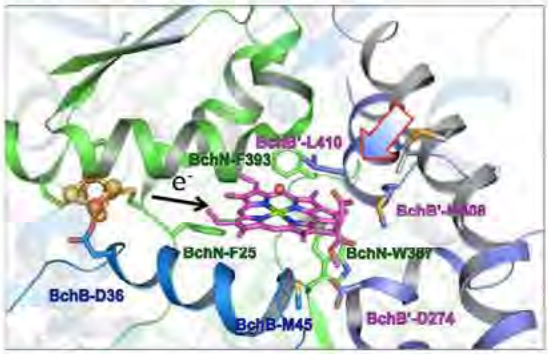

References

[1] Norifumi M., Nomata J., Ebata K., Mizoguchi T., Shiba T., Tamiaki H., Kurisu G and Fujita Y., "X-ray crystal structure of the light-independent protochlorophyllide reductase".
[2] Nature, Nature Publishing Group, Volume 465, (2010), pp 110-114.

MS07-P11

Structural basis for the enantioselectivity of Est-Y29 toward S-ketoprofen

TriDuc Ngo[1], SeungBum Kim[2], SangBum Joo[1], SangYoung Yoon[2], T. DooHun Kim[2], KyeongKyu Kim[1]

[1]*Department of Molecular Cell Biology, School of Medicine, Sungkyunkwan University, Suwon 440-746, Korea*
[2]*Department of Biological and Molecular Engineering, College of Engineering, Ajou University, Suwon 443-749, Korea*
E-mail: tringo@skku.edu

Thermostable esterase Est-Y29 isolated from metagenome shows high selectivity against S-ketoprofen, an important member of the non-steroidal anti inflammatory drugs (NSAIDs). To investigate the structural basis for the enantioselectivity of Est-Y29, we determined crystal structures of Est-Y29 and its complexes with various enantiomers of ketoprofen ethyl ester at 1.7 – 2.4 Å resolution range. Est-Y29 with racemic ketoprofen ethyl ester revealed that the S enantiomer binding to the active site is preferred due to the larger binding area than R enantiomer. Most importantly, water bound to the oxygen of S-ketoprofen formed hydrogen bonds with residues Y69 and S260 of Est-Y29, suggesting that high enantioselectivity observed in Est-Y29 is likely to be contributed by the substrate-bound water. Taken together, crystal structure analyses of Est-Y29 in complex with substrates provided the structure-based understanding of the enantioselectivity of Est-Y29 and proposed that solvent can take a critical role in enzyme selectivity.

Reference

[1] Kim, S., et al. "Purification, Crystallization and Preliminary Crystallographic Analysis of Est-Y29: A Novel Oligomeric Beta-Lactamase." Acta Crystallogr Sect F Struct Biol Cryst Commun 65.Pt 3 (2009): 310-2.
[2] Yoon, S., et al. "Identification and Characterization of a Novel (S)-Ketoprofen-Specific Esterase." Int J Biol Macromol 41.1 (2007): 1-7.
[3] Wagner, U. G., et al. "Estb from Burkholderia Gladioli: A Novel Esterase with a Beta-Lactamase Fold Reveals Steric Factors to Discriminate between Esterolytic and Beta-Lactam Cleaving Activity." Protein Sci 11.3 (2002): 467-78.

MS07-P12

Crystal structure of M18 family dodecameric tetrahedral (TET) shape aminopeptidase from *Pseudomonas aeruginosa*

Duy Nguyen Duc[1], Sampath Natarajan[2], Kap Sun Kim, Kyung Hee Yun, Hyejin Park, Kyeong Kyu Kim[1,2]

Department of Molecular Cell Biology, Samsung Biomedical Research Institute, Sungkyunkwan University, School of Medicineof Chemistry, Suwon 440-746, Korea
E-mail: duy84@skku.med.ac.kr

Peptidase family of M18 contains metalloaminopeptidases which utilize co-catalytic metal ions for catalysis. By solving the crystal structure of M18 aminopeptidase from *Pseudomonas aeruginosa* at 2.0 Å, we conclude that this structure shows high identity with dodecameric tetrahedral (TET) shape aminopeptidase from family M42. A single subunit of M18-TET structure is composed of two domains, a catalytically active domain which contains two Zn ions, and a PDZ like domain responsible for dimerization with other symmetry related subunit. Each dodecamer assembly of catalytically active molecule is constructed with six anti-parallel pairs forming a regular TET. Our results, combining with the multiple sequence alignment and DALI analysis with other metallopeptidases (LAD, AAP and Frvx) indicate that they share the catalytic mechanism, substrate entry and product release..

Reference

[1] Yifat Fundoiano Hershcovitz, Larisa Rabinovitch, Yael Langut, Vera Reiland, Gil Shoham, and Yuval Shoham.," Identification of the catalytic residues in the double-zinc aminopeptidase from Streptomyces griseus", *FEBS Letters*, Vol 571, No 1, (2004), 192–196.
[2] Ljudmila Borissenko, and Michael Groll. "Crystal Structure of TET Protease Reveals Complementary Protein Degradation Pathways in Prokaryotes". *J. Mol. Biol*. Vol 346, No.5, (2005), 1207–1219.
[3] Santina Russo, and Ulrich Baumann.," Crystal Structure of a Dodecameric Tetrahedral-shaped Aminopeptidase", *J. Biol. Chem*. Vol 279**,** No 49, (2004), 51275–51281,

MS07-P13

RNA binding mechanism of ThiI deduced from structural and binding analyses of a minimal RNA ligand

Yoshikazu Tanaka[1,2], Shiori Yamagata[3], Yu Kitago[2], Yoko Yamada[3], Sarin Chimnaronk[2,4], Min Yao[2,3], and Isao Tanaka[2,3]

[1] *Creative Research Institute "Sousei," Hokkaido University, Sapporo, 001-0021, Japan*
[2]*Faculty of Advanced Life Sciences, Hokkaido University, Sapporo, 060-0810, Japan*
[3]*Graduate School of Life Science , Hokkaido University, Sapporo, 060-0810, Japan*
[4]*Institute of Molecular Biology and Genetics, Mahidol University, Nakornpathom, 73170, Thailand*
E-mail: tanaka@cris.hokudai.ac.jp

ThiI catalyzes the thio-introduction reaction to tRNA, and a truncated tRNA consisting of 39 nucleotides, TPHE39A, is the minimal RNA substrate for modification by ThiI. To examine the molecular basis of the recognition of tRNA by ThiI, we solved the crystal structure of TPHE39A, which showed that base pairs in the T-stem were almost completely disrupted although those in the acceptor-stem were preserved. Gel shift assays and isothermal titration calorimetry experiments showed that ThiI can bind with not only tRNAPhe but also TPHE39A. Binding assays using truncated ThiI, i.e., N- and C-terminal domains of ThiI, showed that the N-domain can bind with both tRNAPhe and TPHE39A, whereas the C-domain cannot. These results indicated that the N-domain of ThiI recognizes the acceptor-stem region. Thermodynamic analysis indicated that the C-domain also affects RNA binding by its enthalpically favorable but entropically unfavorable contribution. In addition, circular dichroism spectra showed that the C-domain induced a conformation change in tRNAPhe. Based on these results, a possible RNA binding mechanism of ThiI in which the N-terminal domain recognizes the acceptor-stem region and the C-terminal region causes a conformational change of RNA is proposed.

References

[1] Tanaka Y., Yamagata S., Kitago Y., Yamada Y., Chimnaronk S., Yao M. and Tanaka I., Deduced RNA binding mechanism of ThiI based on structural and binding analyses of a minimal RNA ligand, *RNA*, Vol. 15, No. 8, (2009), pp 1498–1506.

MS07-P14

Basis for the lack of stereospecificity in coenzyme B_{12}-dependent ethanolamine ammonia-lyase

Naoki Shibata[1,2], Tetsuo Toraya[3] and Yoshiki Higuchi[1,2]
[1]Department of Life Science, Graduate School of Life Science, University of Hyogo, 3-2-1 Koto, Kamigori-cho, Ako-gun, Hyogo 678-1297, Japan
[2]RIKEN Harima Institute, SPring-8 Center, 1-1-1 Koto, Sayo-cho, Sayo-gun, Hyogo Japan 679-5148
[3]Department of Bioscience and Biotechnology, Graduate School of Natural Science and Technology, Okayama University, Tsushima-naka, Okayama 700-8530, Japan
E-mail: shibach@sci.u-hyogo.ac.jp

Ethanolamine ammonia-lyase (EAL) catalyses the formation of acetaldehyde and ammonia from a physiological substrate, 2-aminoethanol. The reaction is initiated by cleavage of the cobalt-carbon bond of coenzyme B_{12} (adenosylcobalamin) to form cob(II)alamin-5'-deoxyadenosyl radical pair. The 5'-deoxyadenosyl radical abstracts a hydrogen atom from the C1 carbon atom of the substrate to form a substrate radical, followed by migration of an amino group between substrate carbon atoms. This enzyme also reacts with a non-physiological slower substrate, 2-amino-1-propanol. Interestingly, both enantiomers of this compound can serve as substrate for this enzyme although their k_{cat} and K_m are significantly different; the (*S*)-enantiomer shows two times faster k_{cat} and eleven times smaller K_m then the (*R*)-enantiomer [1]. To elucidate this lack of stereospecificity of the enzyme, we determined the crystal structures of EAL complexed with each enantiomer of 2-amino-1-propanol.

Crystals of EAL complexed with (*S*)-2-amino-1-propanol and cyanocobalamin (EAL·S-AP·CN-Cbl) and (*R*)-2-amino-1-propanol and cyanocobalamin (EAL·R-AP·CN-Cbl) were obtained by soaking substate-free form crystals [2,3] in the crystallization solution containing each enantiomer of 2-amino-1-propanol. Diffraction data sets were collected at the SPring-8 beamlines BL44XU for EAL·S-AP·CN-Cbl and BL38B1 for EAL·R-AP·CN-Cbl.

The structures of EAL·S-AP·CN-Cbl and EAL·R-AP·CN-Cbl were determined at 2.25 and 2.10 Å, respectively. Electron density maps clearly showed that a substrate molecule was bound at the substrate-binding site of the enzyme and indicated the orientation and configuration of the molecule. Both enantiomers share the same position and the same binding mode as in the structure of the enzyme in the presence of racemic 2-amino-1-propanol [3] although their methyl group occupies a different position from each other. The same substrate-binding mode enables the enzyme to catalyze both enantiomers. Details of the steric courses of the reaction for each enantiomer based on the present structures will be discussed.

References

[1] Poyner R. R., Anderson M. A., Bandarian V., Cleland W. W., and Reed G. H. (2006) Probing nitrogen-sensitive steps in the free-radical-mediated deamination of amino alcohols by ethanolamine ammonia-lyase, *J. Am. Chem. Soc. 128*, 7120-7121.
[2] Shibata N, Tamagaki H, Ohtsuki S, Hieda N, Akita K, Komori H, Shomura Y, Terawaki S, Toraya T, Yasuoka N, and Higuchi Y. (2010) Expression, crystallization and preliminary X-ray crystallographic study of ethanolamine ammonia-lyase from *Escherichia coli*. *Acta Crystallogr. Sect. F*, 709-711
[3] Shibata N, Tamagaki H, Hieda N, Akita K, Komori H, Shomura Y, Terawaki S, Mori K, Yasuoka N, Higuchi Y, and Toraya T. (2010) Crystal structures of ethanolamine ammonia-lyase complexed with coenzyme B_{12} analogs and substrates. *J. Biol. Chem.*, in press.

MS07-P15

Structural analysis and functional study of the human small MutS-related protein

Euiyoung Jeong, Weejeong Jun, Seonghwan Lee, Sung-jin Choi, Changill Ban*

Department of Chemistry, Pohang University of Science and Technology, San 31, Hyoja-dong, Pohang, Gyeongbuk 790-784, Korea
E-mail: eyjeong@postech.ac.kr

The Small MutS-related domains (Smr domain), which are widely conserved from prokaryote to eukaryote, possess nicking endonuclease activity, incising the phosphate at the 3′ backbone position of DNA. In eukaryote proteins, human Bcl-3 binding protein (B3bp) has a C-terminal Smr domain that functions as a nicking endonuclease. In order to verify the importance of N-terminal region connecting the Smr domain, we investigated the N-terminal extended Smr domain (exHSMRD; residues 1618-1770) and the Smr domain (HSMRD; residues 1691-1770) of B3bp through the use of a functional assay, SAXS (small-angle X-ray scattering analysis) and X-ray crystallography. The exHSMRD showed a random DNA endonucleolytic activity unlike the nicking endonuclease activity of the HSMRD. The low-resolution structure of the exHSMRD has been acquired by SAXS, and the crystal structure of the HSMRD was solved at 1.9 Å resolution with a crystallographic R-factor of 18.7%. We showed that the exHSMRD structure has an N-terminal elongated form rather than a globular HSMRD structure. Based on comparisons with other Smr structures, we might predict the amino acids that bind to DNA/RNA nucleotides. We suggest that the structural and functional differences between the nicking endonuclease HSMRD and the DNaseI-like endonuclease exHSMRD are affected by connecting the N-terminal region with the Smr domain.

References

[1] Moreira D., Philippe H., "Smr: a bacterial and eukaryotic homologue of the C-terminal region of the MutS2 family", *Trends Biochem. Sci.*, 24, (1999), 298-300
[2] Fukui K., Kosaka H., Kuramitsu S., Masui R., "Nuclease activity of the MutS homologue MutS2 from *Thermus thermophilus* is confined to the Smr domain", *Nucleic Acids Res.*, 35, (2007), 850-860
[3] Malik HS., Henikoff S., "Dual recognition-incision enzymes might be involved in mismatch repair and meiosis", *Trends Biochem. Sci.*, 25, (2000), 414-418

MS07-P16

Structure and mechanism of XometC, a cystathionine γ-lyase from *Xanthomonas oryzae* pv. *oryzae* (Xoo): insights for the substrate specificity and lyase mechanism of XometC

Ho Phuong Thuy Ngo[1], Jin-Kwang Kim[1], Yeh-Jin Ahn[2], Jeong-Gu Kim[3], Byoung-Moo Lee[3], Hee-Wan Kang[4] and Lin-Woo Kang[1]

[1]*Department of Advanced Technology Fusion, Konkuk University, Hwayang-dong, Gwangjin-gu, Seoul 143-701 Korea*
[2]*Major in Life Science, College of Natural Sciences, Sangmyung University,7 Hongji-dong, Jongno-gu, Seoul 110-743, Korea*
[3]*Microbial Genetics Division, National Institute of Agricultural Biotechnology (NIAB), Rural Development Administration (RDA), Suwon 441-707, Korea*
[4]*Graduate School of Biotechnology and Information, Hankyong National University, Ansung 456-749, Korea*
E-mail: nhpthuy@gmail.com

XometC, a cystathionine γ lyase from rice pathogenic bacteria *Xanthomonas oryzae* pv. *oryzae* (Xoo), is a pyridoxal phosphate (PLP)-dependent enzyme that catalyzes the conversion of L-cystathionine to cysteine, which is essential for the metabolic interconversion of the sulfur-containing amino acids. *XometC* gene was selected from a genetic screen to search Xoo pathogenicity related genes. *XometC* gene was not essential for Xoo viability, but *XometC* knockout mutant lost the ability to cause bacterial blight in rice. Therefore, XometC is of interest as a potential antivirulence drug target against Xoo. Here, we characterize the enzymatic activity of XometC using HPLC and report its crystal structures in native form; in complex with aminocrotonate intermediate and propagylglycine (PPG). HPLC analysis of enzyme assay products showed that XometC can catalyze both of γ-elimination and β-elimination reactions toward L-cystathionine. Native structure of XometC was determined to 2.0Å resolution. The structure of XometC in complex with ligand reveals a change in conformation. In addition, XometC bound with the aminocrotonate intermediate from γ-elimination reaction can be trapped and the crystal structure was solved to 1.95Å resolution. Such intermediate of γ-elimination reaction hitherto was not reported. Besides, structure of XometC in complex with propagylglycine (PPG), a well-known inhibitor of cystathionine γ-lyase ezyme family, was determined to 2.2Å resolution. It showed a different binding mode compared to PPG-enzyme complexes previously, at which PLP cofactor was dissociated from the enzyme upon PPG bound to enzyme. These results can help to explain the lyase mechanism of XometC and provide a framework for further designing of specific inhibitor against XometC.

References

[1] Wang, J. C., So, B. H., Kim, J. H., Park, Y. J., Lee, B. M. and Kang, H. W., "Genome-WideIdentification of pathogenicity genes in Xanthomonas oryzae pathovar oryzae by Transposon Mutagenesis", Plant Pathology, Vol. 57, (2008), pp 1136-1145.

[2] Sun Q.X. and et al., "Structural Basis for the inhibition mechanism of human Cystathionine gamma lyase: an enzyme responsible for the production of H2S", The Journal of Biological Chemistry, Vol. 284, (2009), pp 3076-3085.

MS07-P17

Structure-based catalytic optimization of a type III Rubisco from a hyperthermophile

Yuichi Nishitani[1], Shosuke Yoshida[2], Masahiro Fujihashi[1], Kazuya Kitagawa[1], Takashi Doi[1], Haruyuki Atomi[2], Tadayuki Imanaka[2], and Kunio Miki[1]

[1]*Department of Chemistry, Graduate School of Science, Kyoto University, Sakyo-ku, Kyoto 606-8502, Japan.*
[2]*Department of Synthetic Chemistry and Biological Chemistry, Graduate School of Engineering, Kyoto University, Katsura, Nishikyo-ku, Kyoto 615-8510, Japan.*
E-mail: ynishi@kuchem.kyoto-u.ac.jp

The Calvin-Benson-Bassham cycle is responsible for carbon dioxide fixation in all plants, algae, and cyanobacteria. The enzyme that catalyzes the carbon dioxide-fixing reaction is ribulose-1,5-bisphosphate carboxylase/oxygenase (Rubisco). Rubisco from a hyperthermophilic archaeon Thermococcus kodakarensis (Tk-Rubisco) belongs to the type III group, and it shows high activity at high temperatures. We have previously determined the crystal structure in the apo-form of this enzyme [1]. We have also found that replacement of the entire α-helix 6 of Tk-Rubisco with the corresponding region of the spinach enzyme (SP6 mutant) results in an improvement of catalytic performance at mesophilic temperatures, both in vivo and in vitro, whereas the former and latter half replacements of the α-helix 6 (SP4 and SP5 mutants) do not yield such improvement [2]. We report here the crystal structures of the wild-type Tk-Rubisco and the mutants SP4 and SP6 in complex with its reaction-intermediate analogue, and discuss the relationships between their structures and enzymatic activities.

A comparison among these structures shows the movement and the increase of temperature factors of α-helix 6 induced by four essential factors. We thus supposed that an increase in the flexibility of the α-helix 6 and loop 6 regions was important to increase the catalytic activity of Tk-Rubisco at ambient temperatures. Based on this structural information, we constructed a new mutant, SP5-V330T, which was designed to have significantly greater flexibility in the above region, and it proved to exhibit the highest activity among all mutants examined to date. Thermostability of the SP5-V330T mutant was lower than that of wild-type Tk-Rubisco, providing further support on the relationship between flexibility and activity at ambient temperatures.

References

[1] Kitano, K., Maeda, N., Fukui, T., Atomi, H., Imanaka, T., and Miki, K., "Crystal structure of a novel-type archaeal rubisco with pentagonal symmetry", *Structure*, 9, (2001), pp 473-481.
[2] Yoshida, S., Atomi, H., and Imanaka, T., " Engineering of a type III rubisco from a hyperthermophilic archaeon in order to enhance catalytic performance in mesophilic host cells", *Appl. Environ. Microbiol.*, 73, (2007), pp 6254-6261.

MS07-P18

Structural and functional analysis of the LMO2642 cyclic nucleotide phosphodiesterase from *Listeria moncytogenes*

Yeon-Gil Kim[1*], Jae-Hee Jeong[1], Nam-Chul Ha[2], Kyung-Jin Kim[1*]

[1]*Pohang Accelerator Laboratory, Pohang University of Science and Technology, Pohang, Kyungbuk 790-784, Republic of Korea*
[2]*Department of Manufacturing Pharmacy, College of Pharmacy and Research Institute for Drug Development, Pusan National University, Busan 609-735, Republic of Korea*
[*]*Correspondence should be addressed to: Yeon-Gil Kim, Ph.D. San31, Hyoja-Dong, Nam-Gu, Pohang, Kyungbuk 790-784, Korea*
Email: ygkim76@postech.ac.kr

Listeria monocytogenes is a facultative intracellular pathogen invading humans and animals with the highest fatality rate among the food-borne pathogens. The *Listerial* pathogenic processes such as cell entry, escape from phagosomes and intracellular motility mostly depend on the actions of surface proteins. Therefore, revealing the functions of bacterial cell surface proteins is crucial to understand the bacterial pathogenesis and to develop defensive strategies. Here, we report the crystal structure of Lmo2642, a highly conserved surface protein containing a Ser/Thr phosphatase domain. The protein consists of two distinct domains: a catalytic domain that belongs to the metallophosphoesterase superfamily and an auxiliary α-helical bundle domain. We also reveals that Lmo2642 contains, for the phosphodiesterase activity, a dinuclear metal center in which Mn^{2+} and Fe^{3+} are preferentially positioned at the site1 and site2, respectively. Based on the structural analysis and enzymatic assays, we identified the biochemical activity of the protein as a cyclic nucleotide phosphodiesterase toward 2', 3'- and 3', 5'-cyclic nucleotides. Considering the localization of Lmo2642 exposed to host cytosol during *Listerial* infection and the 3', 5'-cAMP, an important signaling molecule, hydrolyzing activity of the protein, we speculate that the Lmo2642 protein has some potential roles for the host-pathogen interactions by subverting the cAMP concentration of host cells during its infection.

References

[1] Swaminathan, B., and Gerner-Smidt, P. , "The epidemiology of human listeriosis.", *Microbes Infect* **9**,(2007), pp 1236-1243
[2] Lecuit, M. , 'Human listeriosis and animal models", *Microbes Infect* **9**, (2007), pp 1216-1225
[3] Roberts, A. J., and Wiedmann, M., "Pathogen, host and environmental factors contributing to the pathogenesis of listeriosis. ' (2003) *Cell Mol Life Sci* 60, 904-918
[4] Cabanes, D., Dehoux, P., Dussurget, O., Frangeul, L., and Cossart, P. 'Surface proteins and the pathogenic potential of Listeria monocytogenes.", (2002) *Trends Microbiol* **10**, 238-245

MS07-P19

Comparison of DNA translocators based on their structures

Suk-Youl Park, Nguyen To Uyen, Ji-Woo Choi, Hyun-Ju Lee, Kosuke Nishi & Jeong-Sun Kim

Department of Chemistry, Chonnam National University, Gwangju, 500-757, Korea
E-mail: jsunkim@chonnam.ac.kr

Among four types of bacterial restriction enzymes that cleave a foreign DNA depending on its methylation status, type I enzymes composed of three subunits are interesting because of their unique DNA cleavage and translocation mechanisms performed by the restriction subunit (HsdR). The elucidated N-terminal fragment structure of a putative HsdR subunit from *Vibrio vulnificus* YJ016 reveals three globular domains. The nucleolytic core within an N-terminal nuclease domain (NTD) is composed of one basic and three acidic residues, which include a metal binding site. An ATP hydrolase (ATPase) site at the interface of two RecA-like domains (RDs) is located close to the probable DNA binding site for translocation, which is far from the NTD nucleolytic core. Comparison of relative domain arrangements with other functionally related ATP and/or DNA complex structures suggests a possible translocation and restriction mechanism of the HsdR subunit. Furthermore, careful analysis of its sequence and structure implies that a linker helix connecting two RDs and an extended region within the nuclease domain may play a central role in switching the DNA translocation into the restriction activity.

References

[1] Nguyen TU., Park SY., Choi JW., Lee HJ., Nishi K. Kim JS., "The fragment structure of a putative HsdR subunit of a type I restriction enzyme from *Vibrio vulnificus* YJ016: Implications for DNA restriction and translocation activity", *Nucleic Acids Research*, Vol. 37, No. 20, (2009), pp 6960-6969.

[2] Lapkouski M., Panjikar S., Janscak P., Smatanova I., Carey J., Ettrich R. and Csefalvay E., "Structure of the motor subunit of type I restriction-modification complex EcoR124I." *Nat. Struct. Mol. Biol.* Vol. 16, No. 1, (2009), 94-95.

MS07-P20

Structure and mechanism of the Nudix hydrolase Orf153 (YmfB) from *E. coli*

Myoung-ki Hong[1], Jin-kwang Kim[1], Yeh-jin Ahn[2] and Lin-woo Kang[1]

[1]*Department of Advanced Technology Fusion, Konkuk University, Seoul 143-701, Korea*
[1]*Major in Life science, college of Natural sciences, Sangmyung University, Seoul 110-743, Korea*
E-mail: myoungkihong@gmail.com

YmfB from *E. coli* is the Nudix hydrolase which can hydrolyze a broad spectrum of nucleoside phosphates. YmfB is also involved in the thiamine metabolism. Thiamin pyrophosphate is important in the primary metabolism and a cofactor of many enzymes. Although most Nudix hydrolases cleave (d)NTPs into (d)NMPs and pyrophosphates, YmfB atypically cleaves (d)NTPs into (d)NMPs and inorganic orthophosphates. To elucidate the unique hydrolysis mechanism of YmfB, YmfB structure was compared with structures of other Nudix hydrolases such as MutT, Ap4Aase, and DR1025. In comparison, YmfB had the larger negatively charged area in the substrate binding pocket, which was covered with glutamate and aspartate residues. We mutated the acidic residues by site-directed mutagenesis and studied the kinetic properties of all mutants. The mass spectrometric analysis of the hydrolysis reaction products was also carried out. Based on the results, the novel hydrolysis mechanism of YmfB was proposed, and the information could be used to understand the structure and function of the versatile Nudix hydrolase superfamily better.

References

[1] Xu, W., Dunn, C. A., O'Handley S, F., Smith, D. L. & Bessman, M. J., "Three new Nudix hydrolases from Escherichia coli", *J Biol Chem,* 281, (2006), 22794-8.
[2] Lawhorn, B. G., Gerdes, S. Y. & Begley, T. P., "A genetic screen for the identification of thiamin metabolic genes", *J Biol Chem,* 279, (2004), 43555-9.

MS07-P21

Crystal structure analysis of ATPase domain from *Mycobacterium tuberculosis* DosS protein

Ha Yeon Cho and Beom Sik Kang

School of Life Science and Biotechnology, Kyungpook National University, Daegu 702-701, Korea
E-mail: nisus85@knu.ac.kr

DosS is a sensor histidine kinase and essential for undergo the dormant state in the hypoxic condition. DosS is composed of a sensor domain in the N-terminal region and conserved kinase core in the C-terminal region. A conserved kinase core of DosS has HisKA domain and ATPase domain. Here, we report the crystal structure of DosS ATPase domain from *Mycobacterium tuberculosis* at 1.8 Å resolution by the single anomalous dispersion method. The ATPase domain crystal was obtained under the condition of 15 % (w/v) polyethylene glycol 1500, 0.2 M zinc acetate and 0.1 M citrate buffer pH 6.0. It belongs to the space group P41212 with unit cell parameters of a=53.19, b=53.19, c=184.61 Å. There are two molecules in the asymmetric unit. The ATPase domain shown α/β sandwich fold which composed of five-stranded β-sheet and three α-helices. DosS ATPase domain is similar to those of other PhoQ and CheA, but the ATP-lid loop of DosS is much shorter than others. It suggests that a conformational change will be required to bind ATP in DosS ATPase.

References

[1] Cho, H. Y., Cho,H. J., Kim, Y. M., Oh, J. I., and Kang, B. S., "Structural insight into the heme-based redox sensing by DosS from Mycobacterium tuberculosis", *J. Biol. Chem*, Vol. 284, No. 19, (2009), pp 13057-13067.

[2] Marina A., Mott C., Auyzenberg A., Hendrickson WA. and Waldburger CD., "Structural and mutational analysis of the PhoQ histidine kinase catalytic domain. Insight into the reaction mechanism" , *J. Biol. Chem*, Vol. 276, No. 44, (2001), pp 41182-41190.

[3] Bilwes AM., Quezada CM., Croal LR., Crane BR. and Simon MI., "Nucleotide binding by the histidine kinase CheA", *Nat Struct Biol,* Vol 8, No. 4, (2001), pp 353-360.

MS07-P22

Crystal structure of LapB from *Pseudomonas* sp. strain KL28

Jang-Hee Cho[1], Du-Kyo Jung[1], Kyoung Lee[2] and Sangkee Rhee[1]

[1]*Department of Agricultural Biotechnology, Seoul National University, Seoul 151-747, Korea*
[2]*Department of Microbiology, Changwon National University, Kyongnam 641-773, Korea*
E-mail: janghee2@snu.ac.kr

LapB is a non-heme Fe(II)-dependent 2,3-dioxygenase that catalyzes the second step of a *l*ong-chain *a*lkyl*p*henol (lap) degradation pathway in *Pseudomonas* sp. KL28, and belongs to the superfamily of type I extradiol dioxygenases. In this study, the crystal structures of substrate-free LapB and its complexes with a substrate or product were determined, along with a functional analysis of the active site residues. Structural features of the homotetramer are similar to those of other type I extradiol dioxygenases. In particular, the active site is located in the C-domain of each monomer, with a 2-His-1-carboxylate motif as the first coordination shell to Fe ion. A comparison of three different structures in the catalytic cycle indicated catalysis-related local conformational changes in the active site. Specifically, the active site loop containing His248 exhibits positional changes upon binding of the substrate and establishes a hydrogen-bonding network with Tyr257, which is near the hydroxyl group of the substrate. Kinetic analysis of the mutant enzymes H248A, H248N, and Y257F showed that these three mutant enzymes are inactive, suggesting that this hydrogen-bonding network plays a crucial role in catalysis by deprotonating the incoming substrate and leaving it in a monoanionic state. Additional functional analysis of His201, by using H201A and H201N mutants, near the dioxygen-binding site also supports its role as base and acid catalyst in the late stage of catalysis. We also noticed a disordered-to-ordered structural transition in the C-terminal region, resulting in the opening or closing of the active site. These results provide detailed insights into the structural and functional features of an extradiol dioxygenase that can accommodate a wide range of alkylcatechols.

References

[1] Cho JH., Jung DK., Lee K. and Rhee S., "Crystal structure and functional analysis of extradiol dioxygenase LapB from a long-chain alkylphenol degradation pathway in *Pseudomonas*", Journal of Biological Chemistry, Vol. 284, No. 49, (2009), pp 34321-34330.

MS07-P23

The crystal structure of D-ribose-5-phosphate isomerise B from Clostridium thermocellum with the unique high kinetic properties

Jin Kwang Kim[1], Junho Jung[1], Soo Jin Yeom[2], Yeh Jin Ahn[3], Deok Kun Oh[2] and Lin Woo Kang[2]

[1]*Department of Advanced Technology Fusion, Konkuk University, Hwayang dong, Gwangjin-gu, Seoul 143-701, Korea*
[2]*Department of Bioscience and Biotechnology, Hwayang dong, Gwangjin-gu, Seoul 143-701, Korea*
[3]*Major in Life Science, College of Natural Sciences, Sangmyung University, 7 Hongji-dong, Jongno-gu, Seoul 110-743, Korea*
E-mail: liebesky@gmail.com

Ribose-5-phosphate isomerase (Rpi) catalyzes the conversion between ribose-5-phosphate (R5P) and ribulose 5-phosphate, and plays important roles in the non-oxidative pathway of the pentose phosphate pathway and the calvin cycle of photosynthesis. Rpis also have many industrial uses to produce valuable rare sugars. Recently D-Ribose-5-phosphate isomerase B from Clostridium thermocellum (CtRpi) was studied due to its high kinetic properties with a narrow spectrum for substrate. The substrate preferences of CtRpi and Thermotoga maritime Rpi (TmRpi) are the same, however the kinetic properties of CtRpi on average 200 folds higher than those of TmRpi for substrates. We determined crystal structures of CtRpi by itself and in complex with substrates of R5P, D-allose, and D-ribose at 2.1 Å resolution or higher. The structure comparison between CtRpi and TmRpi showed overall structures were highly conserved even in the active site, however the substrate binding pocket (SBP) of CtRpi was 20% smaller than TmRpi SBP. Thus CtRpi recognized substrates more tightly. We switched the key different residues between CtRpi and TmRpi by site-directed mutagenesis, and studied the kinetic activities of mutants. The results showed several different structural motifs or residues rather than a single residue contribute the high kinetic activities of CtRpi in the concerted way. The information could be used to engineer better Rpi for the industrial purposes.

References

[1] Xu, Q., Schwarzenbacher, R., McMullan, D., von Delft, F., Brinen, L. S., Canaves, J. M., Dai, X., Deacon, A. M., Elsliger, M. A., Eshagi, S., Floyd, R., Godzik, A., Grittini, C., Grzechnik, S. K., Jaroszewski, L., Karlak, C., Klock, H. E., Koesema, E., Kovarik, J. S., Kreusch, A., Kuhn, P., Lesley, S. A., Levin, I., McPhillips, T. M., Miller, M. D., Morse, A., Moy, K., Ouyang, J., Page, R., Quijano, K., Robb, A., Spraggon, G., Stevens, R. C., van den Bedem, H., Velasquez, J., Vincent, J., Wang, X., West, B., Wolf, G., Hodgson, K. O., Wooley, J. & Wilson, I. A. (2004). Crystal structure of a ribose-5-phosphate isomerase RpiB (TM1080) from Thermotoga maritima at 1.90 A resolution. *Proteins* **56**, 171-5.

[2] Roos, A. K., Andersson, C. E., Bergfors, T., Jacobsson, M., Karlen, A., Unge, T., Jones, T. A. & Mowbray, S. L. (2004). Mycobacterium tuberculosis ribose-5-phosphate isomerase has a known fold, but a novel active site. *J Mol Biol* **335**, 799-809.

[3] Roos, A. K., Mariano, S., Kowalinski, E., Salmon, L. & Mowbray, S. L. (2008). D-ribose-5-phosphate isomerase B from Escherichia coli is also a functional D-allose-6-phosphate isomerase, while the Mycobacterium tuberculosis enzyme is not. *J Mol Biol* **382**, 667-79.

MS07-P24

Structural feature of the extreme thermophile maltogenic amylase from *Staphylothermus marinus*

Tae-Yang, Jung[1], Dan Li[2], Jong-Tae, Park[2], Se-Mi, Yoon[1], KwanHwa, Park[2,3] and Eui-Jeon, Woo[1]

[1]*Medical Proteomics Research Center, Korea Research Institute of Bioscience and Biotechnology, Daejeon 305-333, Korea*
[2]*Center for Agricultural Biomaterials and Department of Food Science and Biotechnology, Seoul National University, Seoul 151-921, Korea*
[3]*Department of Biology, University of Incheon, Incheon 402-749, Korea*
E-mail: sunny@kribb.re.kr

SMMA (*Staphylothermus marinus* maltogenic amylase) is an extreme thermophile maltogenic amylase from archaea, hydrolyzing cyclodextrin and linear maltooligosaccharide of a-(1-4) glycosyl linkages. This enzyme has an additional N-terminal extension (N'-domain) of ~110 amino acid that is conserved among archaeal hyperthermophile amylases but not found in other hydrozying enzymes of GH13 subfamily. To understand the functional role of the N'-domain, we determined the crystal structures of SMMA at the resolution of 2.28 Å. The structure revealed a unique architecture of the N'-domain, a domain topology similar to Carbohydrate Binding Module (CBM) 48 family. The strand-loop-strand region of the N'-domain that interacts to carbohydrate in CBM 48 family protrudes out and provides substrate binding surface at the active site. It is positioned adjacent to the active site forming one part of the substrate binding groove at the reducing end of substrate. Unlike other mesophilic bacterial maltogenic amylases, SMMA contains the complete components for the enzyme activity in a monomer subunit. This is the first observation of the involvement of CBM 48 in the maltogenic amylase activity mechanism suggesting that extreme thermophilic archaea utilize the carbohydrate interaction property to the binding of substrate at the active site. In addition, the extreme thermostability can be explained by many non-polar amino acid residues exposed at the surface of SMMA. The structures would provide a molecular basis for functional properties unique to extreme thermophile maltogenic amylases from archaea.

References

[1] Park KH, Kim TJ, Cheong TK, Kim JW, Oh BH, Svensson B., "Structure, specificity and function of cyclomaltodextrinase, a multispecific enzyme of the alpha-amylase family.", *Biochim Biophys Acta*, Vol. , No. 1478(2) (2000), pp 165-185.

[2] Li D, Park JT, Li X, Kim S, Lee S, Shim JH, Park SH, Cha J, Lee BH, Kim JW, Park KH., "Overexpression and characterization of an extremely thermostable maltogenic amylase, with an optimal temperature of 100 degrees C, from the hyperthermophilic archaeon Staphylothermus marinus.", N Biotechnol, (2010).

[3] Greaves RB, Warwicker J., "Mechanisms for stabilisation and the maintenance of solubility in proteins from thermophiles.", BMC Struct Biol, Vol 7, No.18, (2007)

[4] Boraston AB, Bolam DN, Gilbert HJ, Davies GJ., "Carbohydrate-binding modules: fine-tuning polysaccharide recognition.", Biochem J, Pt.3, No.382, (2004), pp 769-781.

MS07-P25

Crystallization and preliminary X-ray analysis of a novel thermostable amylase from *Pyrococcus furiosus* (PFTA) in glycoside hydrolase 13 family

Hyung-nam Song[1], Tae-yang Jung[1], Sae-mi Yoon[1], Sung-jae Yang[2], Kwan-hwa Park[2], and Eui-jeon Woo[1*]

[1]*Medical Proteomics Research Center, Korea Research Institute of Bioscience and Biotechnology, 111 Gwahangno, Yuseong-gu, Daejeon305-806, Republic of Korea*
[2]*Center for Agricultural Biomaterials and Department of Food and Animal Biotechnology, School of Agricultural Biotechnology, Seoul National University, Shillim-dong, Kwanak-gu, Seoul 151-921, Korea*
E-mail: hotdog77@kribb.re.kr

Pyrococcus furiosus thermostable amylase (PFTA) is a extremophile enzyme with a novel catalytic properties as both an a-amylase and a cyclodextrin hydrolyzing enzyme. PFTA exhibits a distinguishable substrate preference for cyclic maltodextrins over linear maltooligosaccharides. Its unique catalytic properties are useful for producing high-value-added maltooligosaccharides with defined lengths, such as maltohexaose (G6), maltoheptaose (G7), and maltooctaose (G8) from commercially available cyclodextrins. In this study, the first crystallization and preliminary X-ray analysis of PFTA, a family 13 glycoside hydrolase, is described. PFTA is a dimeric protein consisting of two identical subunits of 645 amino acids and with a calculated molecular weight of 76 KDa for each monomer subunit. Purified recombinant protein was crystallized by the sitting-drop method in space group P41 (unit-cell parameters a=150.065, b=150.065, c=67.856 Å). The crystals diffracted X-rays to a resolution of 2.34 Å. The three dimensional structure of this enzyme would provide the molecular basis for the unique substrate preferences for cyclic maltodextrins. The detailed information would be useful in developing and engineering thermostable CD degrading enzyme to produce functional maltooligosaccharides.

References

[1] ClaireVieille, Gregory J. Zeilus, "Hyperthermophilic Enzymes: Sources, Uses, and Molecular Mechanisms for Thermostability", *Microbiologyand molecular biology reviews,* Vol. 65, No. 1, (Mar. 2001), p. 1–43.
[2] Sung-Jae Yang, Byoung-Chul Min, Young-Wan Kim, Sang-Mok Jang, Byong-Hoon Lee, and
[3] Kwan-Hwa Park, "Changes in the Catalytic Properties of *Pyrococcus furiosus* Thermostable Amylase by Mutagenesis of the Substrate Binding Sites", *Applied and Environmental Microbiology*, Vol. 73, No. 17, (Sept. 2007), p. 5607-5612.
[4] Sung-Jae Yang, Hee-Seob Lee, Jung-Woo Kim, Myoung-Hee Lee, Joong-HyuckAuh,Byong-HoonLee, and Kwan-Hwa Parka, "Enzymatic preparation of maltohexaose, maltoheptaoseand maltooctaose by the preferentialcyclomaltooligosaccharide (cyclodextrin) ring-opening reactionof Pyrococcusfuriosusthermostable amylase", *Carbohydrate Research*, Vol. 341, (2006),p. 420–424.
[5] Sung-Jae Yang, Hee-Seob Lee,Cheon-Seok Park, Yong-Ro Kim, Tae-Wha Moon,and Kwan-Hwa Park, "Enzymatic Analysis of an Amylolytic Enzyme from the Hyper thermophilic Archaeon *Pyroccus furiosus* Reveals Its Novel Catalytic Properties as α-amylase and a Cyclodextrin-Hydrolyzing Enzyme", *Applied and Environmental Microbiology*, Vol. 70, No. 10, (Oct. 2004), p. 5988-5995.

MS07-P26

Structural basis for the recognition of N-end rule substrates by the UBR box of ubiquitin ligases

Woo Suk Choi[1], Byung-Cheon Jeong[1], Myeong-Ryeol Lee[1], Michael J. Eck[2,3], and Hyun Kyu Song[1]

[1]*School of Life Science and Biotechnology, Korea University, Anam-Dong, Seoungbuk-Gu, Seoul, 136-701, Korea*
[2]*Department of Biological Chemistry and Molecular Pharmacology, Harvard Medical School, Boston, Massachusetts 02115, USA*
[3]*Department of Cancer Biology, Dana-Farber Cancer Institute, 44 Binney Street, Boston, Massachusetts 02115, USA*
E-mail: ws821@naver.com

The N-end rule pathway is a regulated proteolytic system that targets proteins containing destabilizing N-terminal residues for ubiquitylation and proteosomal degradation. N-end rule mediated degradation underlies many cellular processes, from chromosome segregation to apoptosis. The N-terminal degradation signals (N-degrons) of type-1 substrates of this pathway contain an N-terminal arginine, lysine or histidine residue that is required for their recognition by the ~80-residue UBR-box domain of an E3 ubiquitin (Ub) ligase. Here we describe crystal structures of the UBR box of the *S. cerevisiae* E3 ligase Ubr1 alone and in complexes with N-degron peptides. The structures reveal a previously unknown protein fold that is stabilized by coordination of three zinc ions, two of which form a novel di-nuclear zinc center. The N-degron binds in a groove on the surface of the domain, forming a short β-strand. The basic N-terminal residue of the N-degron binds in a negatively charged cleft, and a conserved aspartate of UBR forms a critical salt-bridge with the α-amino group of the N-degron. Interestingly, the side-chains of N-terminal Arg, Lys or His are coordinated by distinct residues of the UBR binding site. These structures and our biochemical analyses also reveal a previously unknown modulation of binding specificity by the residue at position 2 of the N-degron.

References

[1] Varshavsky, "The N-end rule : functions, mysteries, uses", *Proc Natl Acad Sci USA*, Vol. 93, (1996), pp 12142-12149.
[2] Rao, H., Uhlmann, F., Nasmyth, K. & Varshavsky, A. Degradation of a cohesin subunit by the N-end rule pathway is essential for chromosome stability. *Nature,* Vol. 410, (2001), pp 955 – 959.
[3] Ditzel, M. *et al*. Degradation of DIAP1 by the N-end rule pathway is essential for regulating apoptosis. *Nat Cell Biol,* Vol. 5, (2003), pp 467 – 473.
[4] Varshavsky, A. The N-end rule and regulation of apoptosis. *Nat Cell Biol.* Vol. 5, (2003), pp 373 -376.

MS07-P27

Structure basis of genetic encoded photosensitizer KillerRed

Naoki Sakai[1], Yu Kitago[2], Kiwamu Takemoto[3], Tomoki Matsuda[3], Tokiyoshi Ayabe[1] and Takeharu Nagai[3]

[1]*Innate Immunity Laboratory, Faculty of Advanced Life Science, Hokkaido University, Sapporo 001-0021, Japan*
[2]*Laboratory of X-ray Structural Biology, Faculty of Advanced Life Science, Hokkaido University, Sapporo 063-0810, Japan*
[3]*Research Institute for Electronic Sciences, Hokkaido University, Sapporo 001-0020, Japan*
E-mail: nsakai@sci.hokudai.ac.jp

Most of biological phenomena are consisted of the complicated network of molecular interactions in cells. Therefore, to know the molecular role of proteins in vivo is a pivotal step for cellular biology, molecular biology etc. Several methods to elucidate the protein functions have been developed. Among them tools for loss of function of proteins derived meaningful data from biochemical and cellular biological experiments. Therefore some kinds of specific inhibitors such as RNA interference and neutralizing antibodies were developed and applied to inhibit the functions of proteins in vivo and in vitro. However, all of these methods could not regulate time and site specific inhibition. Chromophore-assisted light inactivation (CALI) is a promising technique to overcome this disadvantage [1]. In CALI chromophore molecules are used as photosensitizer, which produce highly reactive free radicals incuding reactive oxygen species (ROS) by irradiation of intense light. ROS have short lifetime, therefore the damage radius is limited to approximately 3-4 nm [2]. This indicates that inactivation of the protein(s) is limited in short timescales and very small regions, where the inactivation light is exposed. So far some fluorescent small molecules such as malachite green and fluorescein were used as photosensitizer for CALI applications. These photosensitizers should exogenously introduce into living specimen, which is the bottleneck of developing versatile application of CALI. KillerRed is the first genetically encoded photosensitizer, which has notable phototoxicity. KillerRed is developed by protein engineering from the hydrozoan chromoprotein anm2CP, a homolog of GFP [3]. Using KillerRed as photosensitizer of CALI, the difficulty of introducing any compound exogenously in cells is overcame. For the farther development of KillerRed, genetically encoded protein photosensitizer, we determine the crystal structure of KillerRed to understand the structural basis for the phototoxicity. The crystal structure of KillerRed was solved by S-SAD at 2.8Å resolution. The data sets were collected using the loopless data-collection method [4] with chromium Kα X-rays. The overall structure of KillerRed was 11-stranded β-barrel with an internal α-helix passing through inside of the barrel, which is characteristic of the fluorescent protein family. The chromophore formed by the autocatalytic cyclization and oxidation of three residues (Gln65-Tyr66-Gly67) located at the center of internal α-helix. The imidazolinone moiety of chromophore was exposed to the outside of the β-barrel through the characteristic water-filled channel. It is considered that oxygen molecules are converted to ROS with light induced energy transfer at chromophore, followed by ROS diffuse to outside of β-barrel through this channel.

References

[1] Wang, F.S. & Jay, D.G., Chromophore-assisted laser inactivation (CALI): probing protein function *in situ* with a high degree of spatial and temporal resolution. *Trends Cell Biol.* **6**, (1996) pp 442-445.
[2] Beck S., Sakurai T., Eustace B.K. , Baste G., Schier R., Rudert F. and Jay D. G., Fluorophore-ass isted light inactivation: a high-throughput tool for direct target validation of proteins. *Proteomics* **2**, (2002) pp 247-255.
[3] Bulina M. E., Chudakov D. M., Britanova O. V., Yanushevich Y. G., Staroverov D. B., Chepurny kh T. V., Merzlyak E. M., Shkrob M. A., Lukyanov S., Lukyanov K. A., A genetically encoded p hotosensitizer. *Nat. Biotechnol.* **24**, (2006) pp 95-99.
[4] Kitago, Y., Watanabe, N. and Tanaka, I., *Acta Cryst.* D**61**, (2005) pp 1013-1021.

MS07-P28

Crystal structures of ribosome-inactivating protein from barley seeds (*Hordeum vulgare L.*)

Byung-Gil Lee[1], Min Kyung Kim[1], Se Won Suh[2] and Hyun Kyu Song[1]

[1]*School of Life Sciences and Biotechnology, Korea University, Seoul, 136-701, Korea*
[2]*Department of Chemistry, College of Natural Sciences, Seoul National University, Seoul 151-747, Korea*
E-mail: pkthis@korea.ac.kr

The ribosome-inactivating protein (RIP) is widely distributed in plant kingdom, which inactivates ribosome of the pathogen by removing a specific adenine from the rRNA and plays a role in the plant defense. RIP from barley (*Hordeum vulgare L.*; bRIP) seeds was previously identified, isolated (Leah *et al.,* 1991) and crystallized (Song *et al.,* 1994), but no structural information is available so far because of phasing problem. The crystal from natural barley seeds is in complex with AMP and belongs to the monoclinic space group C2, with unit-cell parameters of a=88.36, b=62.59, c=53.18 Å and β=108.62° to 1.9 Å (Song *et al.,* 1994). The bRIP was over-expressed in *E. coli* using codon-optimized synthetic gene, and we obtained phase information using a selenomethionine derivatized crystal and determined the structures of bRIP at high resolution. The SER technique (Surface Entropy Reduction; Goldschmidt *et al.,* 2007) was used for crystallization of protein expressed from *E. coli*, and the crystal belongs to space group C2, with cell parameters of a=130.5, b=142.1, c=85.9 Å and β=127.0°, and diffracts to 1.75 Å. We also obtained the crystal in complex with adenine through soaking method, which diffracts to 1.85 Å. The structures of bRIP alone and in complex with adenine and AMP were currently refined to crystallographic R factor of 0.22~0.24 and free R factor of 0.25~0.28. The comparison between apo- and adenine-bound form shows catalytic mechanism of bRIP, an RNA N-glycosidase.

References

[1] Leah R., Tommerup H., Svendsen I. And Mundy J. "Biochemical and molecular characterization of three barley seed proteins with antifungal properties" *J. Biol. Chem.* Vol. 266, No. 3, (1991), pp 1564-1573.

[2] Song, H. K., Hwang, K. Y., Kim, K. K. & Suh, S. W. "Crystallization and preliminary X-ray crystallographic study of ribosome inactivating protein from barley seeds" *Acta Crystallogr. D.* Vol. 50, (1994), pp 910-912.

[3] Goldschmidt L., Cooper D., Derewenda Z. and Eisenberg D. "Toward rational protein crystallization: A Web server for the design of crystallizable protein variants" *Protein Sci.* Vol. 16, (2007) pp 1569-1576.

MS07-P29

Crystal structure of human Evectin-2 PH domain and its complex with O-phospho-L-serine

Seiji Okazaki[1], Yasunori Uchida[2], Ryuichi Kato[1], Takao Inoue[2], Yusuke, Yamada[1], Tomohiko Taguchi[3,4], Hiroyuki Arai[2] and Soichi Wakatsuki[1]

[1]*Structural Biology Research Center, Photon Factory, Institute of Materials Structure Science, High Energy Accelerator Research Organization (KEK), Tsukuba, Ibaraki 305-0801, Japan*
[2]*Department of Health Chemistry, Graduate School of Pharmaceutical Sciences, University of Tokyo, To kyo 113-0033, Japan*
[3]*Department of Biochemistry, Osaka University Graduate School of Medicine, Osaka 565-0871, Japan*
[4]*Institute for Molecular Bioscience, University of Queensland, Brisbane, Queensland 4072, Australia*
E-mail: okazakis@post.kek.jp

Evectin-2, a pleckstrin homology (PH)-domain–containing protein, is implicated to be a regulator of the retrograde transport from plasma membrane to Golgi. Furthermore, it is implicated that Evectin-2 PH domain plays an important role in the retrograde transport by binding to phosphatidylserine (PS) on Recycling Endsomes. To clarify the detailed binding mode between human Evectin-2 PH domain and PS, the crystal structures of the native and O-phospho-L-serine complex were determined at 1.75 and 1.00 Å resolutions, respectively. The overall structure follows the standard PH domain fold. O-phospho-L-serine binds to positively charged pocket near β1/β2 loop, and this binding mode confers the structural basis of the phosphor lipid binding specificity. Based on these structures, potential functional implications of human Evectin-2 PH domain are discussed.

MS07-P30

Crystal structure analysis of the oxygenase component (GraA) of a resorcinol hydroxylase

Yasuo Hata[1,2], Tomomi Fujii[1], Kazutaka Kobayshi[1], Masahiro Yoshida[3] and Tadao Oikawa[3]

[1]*Institute for Chemical Research, Kyoto University, Uji, Kyoto 611-0011, Japan*
[2]*Institute of Sustainability Science, Kyoto University, Uji, Kyoto 611-0011, Japan*
[3]*Department of Life Science and Biotechnology, Faculty of Chemistry, Materials and Bioengineering, Kansai University, Suita, Osaka 564-8680, Japan*
E-mail: hata@scl.kyoto-u.ac.jp

The resorcinol hydroxylase is involved in the first step of the resorcinol catabolic pathway and catalyzes hydroxylation of resorcinol to hydroxyquinol. The enzyme consists of two components: an oxygenase and a flavin reductase. It uses molecular oxygen and reduced flavin for hydroxylation and NAD(P)H for flavin reduction. The small component, flavin reductase, generates reduced flavin for the oxygenase component to oxygenate the substrate. Thus, the enzymatic reaction is separated into two steps. However, hydroxylation activity is exhibited in the cooperative presence of both the components. To understand the structural basis for the catalytic mechanism, we first performed the crystal structure analysis of the oxygenase component (GraA) from *Rhizobium* sp. strain MTP-10005. GraA is an oligomer and its subunit consists of 409 amino acid residues with the mass of 43,305.

The N-terminal His-tagged GraA was used for crystallization. Tetragonal-bipyramidal crystals with typical size of 0.17 x 0.30 x 0.025 mm^3 were obtained in about 6 days by a vapor diffusion method using PEG3350 as a precipitating agent. They belonged to the tetragonal space group $I4_122$ with unit cell dimensions of a=b=101.1 Å, c=319.4 Å and contained one GraA subunit in asymmetric unit. Diffraction data were collected up to 2.6 Å resolution under cryogenic conditions at beamline BL5A, PF, Tsukuba, Japan. The structure was determined by molecular replacement and refined at 2.6 Å resolution up to R=0.211 and R_{free}=0.253. The current structure of GraA subunit contains 374 of 409 residues (residue number 17–166, 171–269, 285–409) and 115 water molecules.

GraA is a tetramer of four identical subunits related to one another by three molecular two-fold axes which are identical to crystallographic two-fold axes. A given pair of two subunits in the molecule form a close dimer with C-terminal α-helical domains crossed together around a crystallographic two-fold axis. Then, two of the close dimers form a loose dimer around another crystallographic two-fold axis crossing perpendicular to the former two-fold axis. Finally, the GraA tetrameric molecule adopts the structure of a dimer of dimers with three molecular two-fold axes perpendicular to one another. The subunit consists of three domains. The N-terminal domain (residues Met1–Ala121) has an α-structure mainly of antiparallel α-helices, the central domain has a β-structure of two β-sheets stacked together, and the C-terminal domain (residues Phe218–Tyr409) has a four-helix-bundle structure of long antiparallel α-helices involved in tetramer formation.

MS07-P31

Structural basis of abscisic acid signaling

Masaru Tanokura [1], Takuya Miyakawa [1], Ken-ichi Miyazono [1], Keiko Kubota [1] and Yoriko Sawano [1]

[1] *Department of Applied Biological Chemistry, Graduate School of Agricultural and Life Sciences, University of Tokyo, Japan*
E-mail: amtanok@mail.ecc.u-tokyo.ac.jp

The phytohormone abscisic acid (ABA) mediates the adaptation of plants to environmental stresses such as drought and regulates developmental signals such as seed maturation. Studies on ABA signaling has rapidly been making progress since recent discovery of PYR/PYL/RCAR protein as ABA receptor [1,2]. Within plants, the receptor protein receives ABA to inhibit the phosphatase activity of type 2C protein phosphatase (PP2C) that is major negative regulator in ABA signaling. However, it remained unclear how the receptor percepts the ABA molecule and ABA binding leads to inhibition of PP2C. Elucidation of these critical questions is also required for development of stress-tolerant crops.

We determined the crystal structures of the ABA receptor PYL1 bound with ABA, and the complex formed by the further binding of ABA-bound PYL1 with the PP2C protein ABI1 (Fig.1) [3]. PYL1 exhibits a helix-grid fold with a large internal water-filled cavity. This receptor protein binds an ABA molecule in the cavity, thereby forming a hydrophobic pocket between two closed loops. The hydrophobic pocket of ABA-bound PYL1 provides the continuous binding interface of ABI1 and one of the closed loops covers the active site of ABI1 like a plug. Thus, ABA-bound PYL1 is capable to competitively inhibit the phosphatase activity of ABI1. Our results revealed the structural mechanism of ABA-dependent ABI1 inhibition that underlies the regulation of phosphorylation signaling in plant stress responses and seed developmental processes by ABA sensing of PYL1.

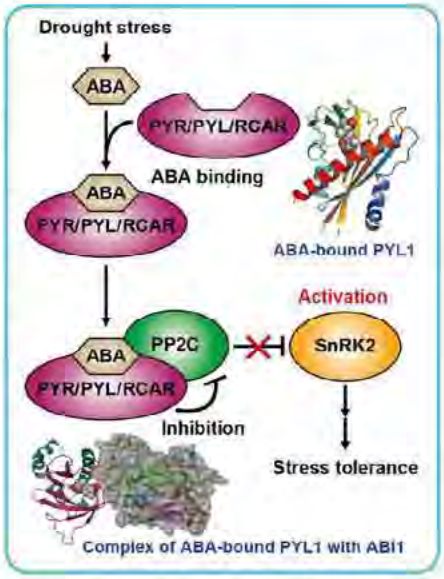

Fig. 1 Schematic diagram of the ABA signaling.

References

[1] Ma Y., Szostkiewicz I., Korte A., Moes D., Yang Y., Christmann A., Grill E., "*Regulators of PP2C phosphatase activity function as abscisic acid sensors*", *Science*, Vol. 324, No. 5930, (2009), pp 1064-1068.

[2] Park S.Y., Fung P., Nishimura N., Jensen D.R., Fujii H., Zhao Y., Lumba S., Santiago J., Rodrigues A., Chow T.F., Alfred S.E., Bonetta D., Finkelstein R., Provart N.J., Desveaux D., Rodriguez P.L., McCourt P., Zhu J.K., Schroeder J.I., Volkman B.F., Cutler S.R., "*Abscisic acid inhibits type 2C protein phosphatases via the PYR/PYL family of START proteins*", *Science*, Vol. 324, No. 5930, (2009), pp 1068-1071.

[3] Miyazono K., Miyakawa T., Sawano Y., Kubota K., Kang H.J., Asano A., Miyauchi Y., Takahashi M., Zhi Y., Fujita Y., Yoshida T., Kodaira K.S., Yamaguchi-Shinozaki K., Tanokura M., "*Structural basis of abscisic acid signalling*", *Nature*, Vol. 462, No. 7273, (2009), pp 609-614.

MS07-P32

X-ray structural analysis of N-terminal domain of KaiC for understanding of restrained ATPase activity

Se-Young Son[1,2], Takao Kondo[1,2] and Shuji Akiyama[1,2]

[1] *Division of Biological Science, Graduate School of Science, Nagoya University*
[2] *CREST, Japan Science and Technology Agency (JST)*
E-mail: sonseyoung@bio.nagoya-u.ac.jp

Cyanobacteria, known as the simplest organism that exhibits circadian rhythm, possesses an oscillator composed of three clock proteins termed KaiA, KaiB, and KaiC. [1] Incubation of these three proteins in vitro induces a KaiC phosphorylation cycle, whose frequency is positively correlated to the ATPase activity of KaiC. [2,3] The KaiC ATPase has two unusual characters. One is the extremely low activity as compared to those of AAA family (15 ATP/day/monomer). The other is that the apparent rate of ATP hydrolysis is insensitive to the change in ambient temperature. Although these features are relevant to a determinant of the oscillatory frequency, little is known about the details of ATPase cycle in KaiC. [3]

To understand a mechanism by which the ATPase activity is restrained, we focused on the structure of the N-terminal domain in KaiC (KaiCI) retaining the 70% of the activity of full-length KaiC. Here, we show the X-ray crystal structure of ATP-bound KaiCI at 2.8 Å. We found several signs of asymmetric structures in the KaiCI hexamer. By structural comparison between wild-type and modulated-ATPase mutants of KaiC-CI, we will discuss some information of several structural characteristics as well as consideration of extremely restrained activity of KaiC ATPase.

References

[1] Masahiro Ishiura, Shinsuke Kutsuna, Setsuyuki Aoki, Hideo Iwasaki, Carol R. Andersson, Akio Tanabe, Susan S. Golden, Carl H. Johnson and Takao Kondo "Expression of a Gene Cluster kaiABC as a Circadian Feedback Process in Cyanobacteria", Science, Vol. 281, (1998) pp 1519-1523
[2] Masato Nakajima, Keiko Imai, Hiroshi Ito, Taeko Nishiwaki, Yoriko Murayama, Hideo Iwasaki, Tokitaka Oyama and Takao Kondo, "Reconstitution of Circadian Oscillation of Cyanobacterial KaiC Phosphorylation in Vitro", Science, Vol. 308, (2005) pp 414-415
[3] Kazuki Terauchi, Yohko Kitayama, Taeko Nishiwaki, Kumiko Miwa, Yoriko Murayama, Tokitaka Oyama and Takao Kondo, "ATPase activity of KaiC determines the basic timing for circadian clock of cyanobacteria" PNAS, Vol.104, (2007) pp 16377-16381

MS07-P33

Unexpected substrate recognition and hydrolysis mechanisms of human NUDT5

Takao Arimori[1], Haruhiko Tamaoki[2], Teruya Nakamura[1], Hiroyuki Kamiya[3], Shinji Ikemizu[1], Yasumitsu Takagi[4], Toru Ishibashi[4], Hideyoshi Harashima[3], Mutsuo Sekiguchi[4], Yuriko Yamagata[1]

1Graduate School of Pharmaceutical Sciences, Kumamoto University, Kumamoto 862-0973, Japan
2Graduate School of Medical Sciences, Kumamoto University, Kumamoto 860-8556, Japan
3Faculty of Pharmaceutical Sciences, Hokkaido University, Sapporo 060-0812, Japan
4Fukuoka Dental College, Fukuoka 814-0193, Japan
E-mail: yamagata@gpo.kumamoto-u.ac.jp

Human NUDT5 (hNUDT5) hydrolyzes 8-oxo-dGDP into 8-oxo-dGMP and inorganic phosphate and prevents mutations caused by misincorporation of 8-oxoG into DNA. In addition, hNUDT5 displays extremely broad substrate specificity for various modified nucleoside diphosphates, including 8-oxo-dADP and ADP-ribose. However, the structural basis of the broad substrate specificity remains unknown. Here, we report the crystal structures of hNUDT5 complexed with 8-oxo-dGDP and 8-oxo-dADP. These structures reveal an unusually different substrate-binding mode: particularly, binding occurred in the opposite direction of the pyrophosphate group, compared with the previously reported hNUDT5-ADP-ribose complex structure [1]. As a result, the β-phosphorus of 8-oxo-dGDP and the α-phosphorus of ADP-ribose are superposed on the same position. If these crystal structures are not artificial, this result suggests that the nucleophilic substitution sites of the substrates involved in hydrolysis reactions differ despite the similarities in the chemical structures of the substrates and products. To clarify this hypothesis, we identified the site of nucleophilic substitution for 8-oxo-dGDP and ADP-ribose by ^{31}P-NMR measurement of the reaction mixtures in ^{18}O-labeled water. The spectra clearly show that 8-oxo-dGDP is attacked by nucleophilic water at Pβ, whereas ADP-ribose is attacked at Pα. This observation reveals a new concept in enzymology that enzymes do not always catalyze the reaction of substrates with similar chemical structures by using the chemically equivalent reaction site.

References

[1] Zha, M. *et al.* Molecular mechanism of ADP-ribosehydrolysis by human NUDT5 from structural and kinetic studies. *J Mol Biol* **379**, 568-578 (2008).

MS07-P34

Crystal structure of human ppGpp hydrolase

Hye-Yeon Kim[1], Dawei Sun[1] and Young Ho Jeon[1]

[1]*Division of Magnetic Resonance, Korea Basic Science Institute, Ochang 363-883, Korea*
E-mail: hyeyeon@kbsi.re.kr

Bacterial SpoT is a Mn^{2+}-dependent pyrophosphohydrolase to hydrolyze ppGpp to GDP and pyrophosphate, which has also a ppGpp synthetase domain in response to carbon or fatty acid starvation. In this study, recombinant ppGpp hydrolase from Homo sapiens (hMesh1)was expressed in *E. coli*, purified, crystallized and solved its crystal structure. The structure of hMesh1 was determined by SAD method using x-ray data collected from a selenomethionyl-labeled protein crystal. The crystal of hMesh1 was diffracted to 2.0 Å and belonged to the monoclinic space group $P2_1$ with cell dimensions of a=53.92 Å, b=62.42 Å, c=53.94 Å and β=95.3°, which contains two molecules in the asymmetric unit. Overall, hMesh1 is composed of ten α-helices and two β-strands that constitute three subdomains. The helical turn between α3 and α4 contains a conserved HD-box motif found in the superfamily of metal-dependent phosphohydrolases, and coordinates one manganese ion together with helices α2 and α8. This is the first structure of a metazoan SpoT ortholog.

References

[1] Tanis H., Undine M., Horst M., Mike C. and Rolf H., "Conformation antagonism between opposing active sites in a bifunctional RelA/SpoT homology modulates (p)ppGpp metabolism during the stringent response", *Cell*, Vol. 177, No. 1, (2004), pp 57-68.

[2] Irina A., Vsevolod P., Shun-ichi S., Marina N V., Takeshi H., Kozo O., Shigeyuki Y. and Dmitry G V. " Structural basis for transcription regulation by alarmone ppGpp", *Cell*, Vol. 177, No. 3, (2004), pp 299-310.

[3] Lisa U. M., Anne F. and Thomas N., "ppGpp: a global regulator in Escherichia coli", *Trends Microbiol.* Vol. 13, No. 5, (2005), pp236-242.

MS07-P35

Crystal structures of extra cellular dermal glycoprotein from carrot and xyloglucan specific endo-β-1,4-glucanase from *Aspergillus aculeatus*

Takuya Yoshizawa, Hiroshi Hashimoto, Toshiyuki Shimizu, Hisashi Hirano and Mamoru Sato

Graduate School of Nanovioscience, Yokohama City University, 1-7-29 Suehiro-cho, Tsurumi-ku, Yokohama 230-0045, Japan
E-mail: yoshi30@tsurumi.yokohama-cu.ac.jp

Plant cell wall is composed various polysaccharides such as cellulose, hemicellulose and pectin which increase strength of cell wall and maintain plant architecture. Many phytopathogens secrete glucanase to degrade plant cell wall. In response to pathogenic attack, plants produce proteins that inhibit the activity of those glucanases. The extra cellular dermal glycoprotein (EDGP) from carrot is induced by biotic or abiotic stress and inhibits the activity of xyloglucan specific endo-β-1,4-glucanase from *Aspergillus aceuleatus* (XEG). XEG cleaves xyloglucan that is one of hemicellulose cross-linking cellulose microfibrils. Thus, EDGP may play important role in plant defense system.

We progress structural study of EDGP and XEG to realize the inhibition mechanism. Crystals of EDGP and XEG were obtained by hanging drop vapor diffusion method. The crystal of EDGP belongs to space group $P6_2$ with the cell dimensions of $a = b = 130.1$, $c = 44.5$ Å, and $\gamma = 120°$. The structure of EDGP is determined by single isomorphous with anomalous scattering (SIRAS) using I_2-derived crystal prepared by vaporizing iodine labeling (VIL) technique. X-ray diffraction data of native and I_2-derived crystals were collected at SPring-8 beamline BL41XU and Photon Factory (PF) beamline NW12A, respectively. The crystal of XEG belongs to space group $P2_12_12_1$ with the cell dimensions of $a = 62.9$, $b = 79.5$, $c = 80.6$ Å. X-ray diffraction data of native crystals were collected at PF beamline BL17A. The structure of XEG is determined by molecular replacement using the coordinate of Cel12A from *Hypocrea jecorina*. We will discuss the inhibition mechanism by EDGP for the activity of XEG.

MS07-P36

Crystallization and preliminary X-ray analysis of a family 51 glycoside hydrolase, the α-L-arabinofuranosidase from *Thermotoga maritima* MSB8

Arti Baban Dumbrepatil[1, 2], Tae-Yang Jung[2], Jung Mi Park[1], Tae Jib Kim[1] and Eui-Jeon Woo[2]

[1]*Dept.of Food Science & Technology, Chungbuk National University, Chungju, 361-763, Korea*
[2]*Medical Proteomics Research Center, Korea Research Institute of Biosciences and Biotechnology, 111 Gwahango, Yuseong-gu, Daejon 305-806, Korea*
E-mail: artidumbre@gmail.com

The digestion of the plant cell wall requires the concerted action of a diverse repertoire of enzyme activities. Important components of these hydrolase are arabinofuranosidases. α-L-Arabinofuranosidases (AFases; EC 3.2.1.55) are hemicellulases that cleave the gycosidic bond between L-arabinofuranoside side chains and various oligosaccharides. In this study, the first crystallization and preliminary X-ray analysis of the α-L-Arabinofuranosidases from *Thermotoga maritima* MSB8 (TAF), a family 51 glycoside hydrolase, is described. TAF is a hexameric protein consisting of six identical subunits of 484 amino acids and with a calculated molecular weight of 56KDa for each monomer subunit. Purified recombinant protein was crystallized by the sitting-drop method in space group $P2_1$ (unit-cell parameters a=103.710, b=161.538, c=112.602 Å). The crystals diffracted X-rays to a resolution of 3.0 Å. The three dimensional structure of this enzyme, especially with respect to its high thermostability (85~90^{0}C) and varied substrate preferences ranging from arabinan to arabinoxylan is of great interest since it will provide crucial information about substrate binding and specificity of 51 gycoside hydrolase family and basis for the development of industrial production of L-arabinose subsequently.

References

[1] Taylor J; Smith L; Turkenburg P; D'Souza S; Glibert J.and Davies J; "Structural insight into the ligand specificity of a thermostable family 51 arabino-furanosidase,Araf51,from *Clostridium thermocellum*", Biochem J,Vol.395,No.1,(2006),pp 31-37.

[2] Hovel K; Shallom D; Niefind K; Belakhov V; Shoham Y; Baasov T. and Schomburg D; "Crystal structure and snapshots along the reaction pathway of a family 51 α-L-arabinofuranosidase", The EMBO Jrnl,Vol.22,No.19,(2003),pp 4922-4932.

[3] Kaji A. and Tagawa; "Purification, crystallization and amino acid composition of a α-L-arabinofuranosidase from *Aspergillus niger*", Biochim.Biophys.Acta, Vol.207, (1970), pp 456-464.

[4] Miyanaga A;Koseki T;Miwa Y;Mese Y; Nakamura S;Kuno A;Hirabayashi J,Matsuzawa H;Wakagi T; Shoun H. and Fushinobu; "The family 42 carbohydrate-binding module of family 54 alpha-L-arabinofuranosidase specifically binds the arabinofuranose side chain of hemicelluloses", Biochem J,Vol.399,No.3,(2006),pp 503-511.

MS07-P37

Structural and biological investigation of ppGpp hydrolase in metazoa

Dawei Sun[1,3], Gina Lee[3,4], Jun Hee Lee[3], Hye-Yeon Kim[1], Hyun-Woo Rhee[5], Seung-Yeol Park[3], Kyung-Jin Kim[6], Yongsung Kim[3,4], Bo Yeon Kim[7], Jong-In Hong[5], Chankyu Park[3], Hyon E. Choy[8], Jung-Hoe Kim[3], Young Ho Jeon[1,3], Jongkyeong Chung[3,4,9]

[1]*Division of Magnetic Resonance, Korea Basic Science Institute, Chungbuk 363-883, Korea*
[2]*Department of Bio-Analytical Science, University of Science and Technology, Taejon 305-333, Korea*
[3]*Department of Biological Sciences, Korea Advanced Institute of Science and Technology, Taejon 305-701, Korea*
[4]*National Creative Research Initiatives Center and School of Biological Sciences, Seoul National University, Seoul 151-742, Korea*
[5]*Department of Chemistry, Seoul National University, Seoul 151-742, Korea*
[6]*Pohang Accelerator Laboratory, Pohang University of Science and Technology, Pohang 790-784, Korea*
[7]*Korea Research Institute of Bioscience and Biotechnology, Chungbuk 363-883, Korea*
[8]*Department of Microbiology, Chonnam National University Medical College, Kwangju 501-746, Korea*
[9]*Institute of Molecular Biology and Genetics, Seoul National University, Seoul 151-742, Korea*
E-mail: yhjeon@kbsi.re.kr

In response to nutritional limitation, bacteria will trigger stringent response, which is characterized on adopting a physiological progress with primary effect on reduction of protein synthesis and expression of stress-responsible genes. In Escherichia Coli, stringent response was mediated by SpoT and RelA with synthesis and hydrolysis of ppGpp. However, their homologs in metazoans have not been discovered yet. Here, we identified functional SpoT homologs in human and Drosophila (hMesh1 and dMesh1, respectively) and determined their crystal structures. The refined structures contain one active site of ppGpp hydrolysis and highly resemble to bacterial enzyme RelSeq from Streptococcus equisimilis. In addition, it has been shown that Mesh1 proteins can catalyze ppGpp hydrolysis both in vivo and in vitro. Furthermore, Mesh1 antagonized the RelA-overexpressed phenotype and rescued the SpoT-deficient lethality in E. coli, demonstrating the evolutionally conserved function of metazoan SpoT homolog. Finally, Mesh1 null mutant in Drosophila causes retarded body growth, impaired starvation responses and altered metabolic gene expressions. Collectively, these data indicate that metazoan SpoT orthologs not only evolutionarily conserve but also play vital functions in starvation responses.

References

[1] Mechold, U., Cashel, M., Steiner, K., Gentry, D., and Malke, H., "Functional analysis of a relA/spoT gene homolog from Streptococcus equisimilis". *J Bacteriol* , Vol 178 (1996), pp 1401-1411.
[2] Hogg, T., Mechold, U., Malke, H., Cashel, M., and Hilgenfeld, R., "Conformational antagonism between opposing active sites in a bifunctional RelA/SpoT homolog modulates (p)ppGpp metabolism during the stringent response", *Cell*, Vol 117 (2004), pp 57-68.
[3] Kasai, K., Nishizawa, T., Takahashi, K., Hosaka, T., Aoki, H., and Ochi, K., "Physiological analysis of the stringent response elicited in an extreme thermophilic bacterium, Thermus thermophilus",*J Bacteriol*, Vol 188 (2006),pp 7111-7112.
[4] Rhee,H.W., Lee,C.R., Cho, S.H., Song,M.R., and Cashel,M., Choy.,H.E., Seok, Y.J., Hong, J.I.,
[5] "Selective fluorescent chemosensor for the bacterial alarmone (p)ppGpp", *J. Am. Che .Soc,* Vol 130 (2008), pp 784-785.
[6] Potrykus, K., and Cashel, M., "(p)ppGpp: still magical?", *Annu. Rev. Microbiol,* Vol 62 (2008), pp 35-51.

MS07-P38

Structural insight into bacterial flavin containing monooxygenase

Hyo Je Cho and Beom Sik Kang

School of Life Science and Biotechnology, Kyungpook National University, Daegu 702-701, Korea
E-mail: hyoje1124@knu.ac.kr

Flavin-containing monooxygenases (FMOs) catalyze the oxidation at nucleophlic and heteroatom centers which are important for drug, xenobiotic, and endogenous substrate metabolism. A gene from, restricted facultative methylotroph, *Methylophaga* sp. strain SK1 was cloned on *E.coli*. Its expression oxidizes indole to indigo via indoxyl and produced blue pigment indigo. The product of this gene showed similarity to the mammalian FMOs. In the present study, we performed experiment to explain the functional mechanism of FMO from *Methylophaga*. We studied the crystal structures of the wild type as well as protein-cofactor (oxidized $NADP^+$) and mutant protein (Y207S)-substrate (indole) complexes. We found that the wild type bacterial FMO (bFMO) structure was composed of two structural domains, known as small and large domain. Our result showed that the prosthetic group FAD was located at the depressed surface of the active site in the large domain. bFMO needs NADPH as a cofactor in addition to the prosthetic group for its catalytic activity. Oxidized NADP+ complex structure showed a conformational change in the NADPH binding motif. Especially, the side chain of Tyr207 bent back to the base of nicotinamide binding space. In order to find substrate binding structure, we made Tyr207 residue mutant (Y207S). It was found that indole occupied the NADPH binding site through overlapping and stacking on the FAD. Based on our result, it can be concluded that NADP(H) and indole binds at the same position by replacing each other.

References

[1] Choi, H. S., Kim,J. K., CHO, E. H., Kim, Y. C., Kim, J. I., and Kim, S. W., "A novel flavin-containing monooxygenase from *Methylophaga* sp. Strain SK1 and its indigo synthesis in *Escherichia coli*", *Biochem Biophys Res Commun*, Vol. 306, (2003), pp 930-936.

[2] Eswaramoorthy S., Bonanno JB., Burley SK and Swaminathan S., "Mechanism of action of a flavin containing monooxygenase" , *Proc Natl Acad Sci USA*, Vol. 103, No. 26, (2006), pp 9832-9837.

[3] Alfieri A., Malito E., Orru R., Fraaije MW., Mattevi A., "Revealing the moonlighting role of NADP in the structure of a flavin-containing monooxygenase", *Proc Natl Acad Sci USA,* Vol 105, No. 18, (2008), pp 6572-6577.

Asymmetric dimeric structure of ferredoxin-NAD(P)$^+$ oxidoreductase from *Chlorobaculum tepidum*: Implications for binding ferredoxin and NADP$^+$

Norifumi Muraki[1], Daisuke Seo[2], Takeshi Sakurai[2] and Genji Kurisu[1,3]

[1]*Institute for Protein Research, Osaka University, Suita, Osaka 565-0871, Japan*
[2]*Division of Material Science, Graduate School of Natural Science and Technology, Kanazawa University, Kakuma, Kanazawa, Ishikawa 920-1192, Japan*
[3]*Department of Macromolecular Science, Graduate School of Science, Osaka University, Toyonaka, Osaka 560-0043, Japan*
E-mail: gkurisu@protein.osaka-u.ac.jp

Ferredoxin-NAD(P)$^+$ oxidoreductase (FNR) catalyzes the reduction of NAD(P)$^+$ to NAD(P)H with the reduced ferredoxin (Fd) during the final step of the photosynthetic electron transport chain. FNR from the green sulfur bacterium *Chlorobaculum tepidum* (formerly *Chlorobium tepidum*) is functionally analogous to plant-type FNR but shares a structural homology to NADPH-dependent thioredoxin reductase (TrxR). In this study, in order to understand the structural basis for the enzymatic reaction of newly recognized TrxR-like FNRs, we have examined the crystal structure of *C. tepidum* FNR by X-ray crystallography to 2.4 Å resolution [1,2]. Our data reveal that *C. tepidum* FNR retains its structural topology with TrxR but possesses several unique structural features (Figure). *C. tepidum* FNR consists of two functional domains for binding FAD and NAD(P)H that form a homodimer in which the domains are arranged asymmetrically. One NAD(P)H domain is present as the open form, the other with the equivalent NAD(P)H domain as the relatively closed form. We used site-directed mutagenesis on the hinge region connecting the two domains in order to investigate the importance of the flexible hinge. The asymmetry of the NAD(P)H domain and the comparison with TrxR suggested that the hinge motion might be involved in pyridine nucleotide binding and binding of Fd. Surprisingly, the crystal structure revealed an additional C-terminal sub-domain that tethers one protomer and interacts with the other protomer by π-π stacking of Phe337 and the isoalloxazine ring of FAD. The position of this stacking Phe337 is almost identical with both of the conserved C-terminal Tyr residues of plant-type FNR and the active site dithiol of TrxR, implying a unique structural basis for enzymatic reaction of *C. tepidum* FNR.

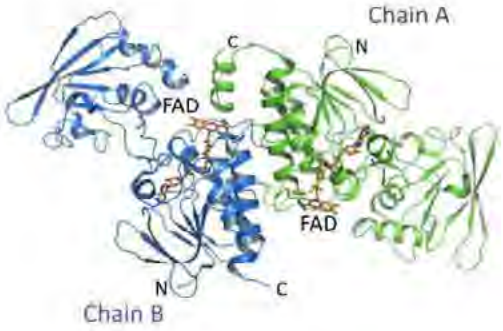

Figure. Over all structure of *C. tepidum* FNR

References

[1] Muraki, N., Seo, D., Shiba, T., Sakurai, T. and Kurisu, G., "Crystallization and preliminary X-ray studies of ferredoxin-NAD(P)$^+$ reductase from *Chlorobium tepidum*", *Acta Cryst. F64*, (2008), p p 186-189

[2] Muraki, N., Seo, D., Shiba, T., Sakurai, T. and Kurisu, G., "Asymmetric Dimeric Structure of Ferredoxin-NAD(P)$^+$ Oxidoreductase from the Green Sulfur Bacterium *Chlorobaculum tepidum*: Implications for Binding Ferredoxin and NADP$^+$", *J. Mol. Biol.*, (2010), in press.

MS07-P40

Crystal structure and functional study of ureidoglycolate dehydrogenase from *Escherichia coli*

Myung-Il Kim, Jeehyun Lee and Sangkee Rhee

Department of Agricultural Biotechnology, Seoul National University, Korea
E-mail: srheesnu@snu.ac.kr

Ureide pathway is a crucial metabolic process in some bacteria and plants to utilize nitrogen in purine, by degrading enzymatically uric acid, a product of purine degradation, into allantoin, which is a common route to both some bacteria and plants. Subsequently, two distinct further catabolic pathways were identified; in plant, allantoin is degraded into glyoxylate, with the release of four-equivalent molecules of ammonia, but in some bacteria four-step enzymatic reactions result in two-equivalent molecules of ammonia, with a conversion of allantoin into glyoxylate and urea. In *Escherichia coli*, ureidoglycolate dehydrogenase (AllD) has been known to catalyze alternative reaction for the last reaction in the bacterial ureide pathway, and produce oxalurate in a NAD(P)-dependent manner, by the oxidation of (*S*)-ureidoglycolate, a substrate for the final reaction. In this study, in order to investigate molecular basis on the reaction mechanism of AllD we are carrying out structural and functional analysis of the enzyme. Further discussion will be presented for the structural features and catalytic mechanism of AllD.

References

[1] Werner A., Romeis T. and Witte C., "Ureide catabolism in *Arabidopsis thaliana* and *Escherichia coli*." *Nat. Chem. Biol*., 6, (2010), 19-21.

MS07-P41

Structural and functional studies of an ureidoglycine-hydrolyzing enzyme from *Arabidopsis thaliana*

Inchul Shin, Woo-Suk Jung, and Sangkee Rhee

Department of Agricultural Biotechnology, Seoul National University, Seoul 151-921, Korea
E-mail: ichul96@snu.ac.kr

Purine is a rich-nitrogen-harboring compound and its degradation is essential for nitrogen recycling in various organisms. In this degradation process, purine is initially degraded into urate, which subsequently enters into the recently identified additional catabolic pathway, the ureide pathway. In this metabolic process, urate is converted into allantoin through three-step enzyme reactions, followed by the formation of allantoate. Allantoate amidohydrolase in plants and some bacteria catalyzes a further conversion of allantoate into ureidoglycine, releasing nitrogen as a form of ammonia. Ureidoglycine produced could face three different fates; (1) formation of glyoxylate and urea in a spontaneous manner, with a release of ammonia, (2) enzymatic conversion into oxalurate by ureidoglycine transaminase in some bacteria, or (3) enzyme-dependent hydrolysis into ureidoglycolate in some bacteria and plant. Recently, an ureidoglycine-hydrolyzing enzyme from *Arabidopsis thaliana* was identified by the aid of bioinformatics and comparative genomics. The enzyme shares high sequence similarity with those of the previously characterized bacterial enzyme, but differs in that plant enzyme contains additional domain at its N-terminus. Currently, we are investigating structural and functional study of ureidoglycine-hydrolyzing enzyme from *Arabidopsis thaliana*. Based on these results, structural and functional features of ureidoglycine hydrolysis will be presented.

References

[1] Werner A. K., Romeis T. and Witte C. P., "Ureide catabolism in *Arabidopsis thaliana* and *Escherichia coli*", *Nat. Chem. Biol*., Vol. 6, (2010), pp 19-21

MS07-P42

Crystal structures of human peroxiredoxin VI in multiple oxidation states

Kyung Hee Kim[1,2], Weon Tae Lee[2] and Eunice EunKyeong Kim[1]

[1]*Life Sciences Division, Korea Institute of Science and Technology, Seoul 136-791, Korea*
[2]*Department of Biochemistry and National Research Laboratory, Yonsei University, Seoul 120-749, Korea*
E-mail: kkhee@kist.re.kr

Peroxiredoxins (Prxs) are redox active cysteine-dependent peroxidases that reduce hydrogen peroxide and alkyl peroxides to water and the corresponding alcohols, respectively. In mammals, six Prxs were identified (Prx I-VI) and they are classified into two groups, 1-Cys Prx and 2-Cys Prx based on the number of conserved cysteine residues. 2-Cys Prx proteins contain conserved cysteines called peroxidatic and resolving cysteine in both the N- and the C-terminal region of protein, while 1-Cys Prx protein has one conserved cysteine (Cys47) in the N-terminal region. 1-Cys Prx protein, also called peroxiredoxin VI, has been widely studied in cells and animal models for protective antioxidant properties such as detoxification of reactive oxygen species (ROS) and protection of the cells from cell death induced by oxidative stress. In peroxiredoxin VI reaction system, the peroxidatic cysteine (Cys47) is oxidized to cysteine sulfenic acid (Cys47-SOH) by H_2O_2, and the sulfenic intermediate gets hyperoxidized to sulfinic acid (Cys47-SO_2H) under the oxidative stress condition. A number of structural and biochemical studies have been carried out, yet the tertiary structure of the reduced and surfinic acid form of peroxiredoxin VI have not been reported. In this study, we present crystal structures of peroxiredoxin VI in three different oxidation states and explain the structural conformation changes upon oxidation.

This work was supported by grants from the Functional Proteomics Center, the 21C Frontier Research & Development Program of the Korea Ministry of Science and Technology, and the Korea Institute of Science and Technology Institutional Program.

References

[1] Choi H.J., Kang SW., Yang CH., Rhee SG and Ryu SE., "Crystal structure of a novel human peroxidase enzyme at 2.0 Å resolution", *Nat. Struct. Biol*., Vol. 5, No. 5, (1998), pp 400-406.
[2] Wood ZA., Schröder E., Robin Harris J and Poole LB., "Structure, mechanism and regulation of peroxiredoxins", *Trends Biochem. Sci*., Vol. 28, No. 1, (2003), pp 32-40.

MS07-P43

Crystal structures of malonyl-CoA-acyl carrier protein transacylase (MCAT) from *Staphylococcus aureus* and *Streptococcus pneumoniae*

Seung Kon Hong[1], Kook Han Kim[1], Joon Kyu Park[1] and Eunice EunKyeong Kim[1*]

[1]*Korea Institute of Science and Technology, Life Sciences Division, Seoul, Korea*
[2]*Department of Bioscience and Biotechnology, Konkuk University, Seoul 143-701, Republic of Korea*
E-mail: biyah@kist.re.kr

The biosynthesis of fatty acids is a fundamental component of the cellular metabolic pathway, since fatty acids are the essential building blocks for membrane phospholipid formation. Since most bacteria and plants synthesize fatty acids using a discrete and highly conserved group of enzymes called the type II fatty acid synthase (FAS II) system that is different from yeast and animal which utilize the type I fatty acid synthase (FAS I), type II FAS system have been receiving enormous attention as possible antibiotic targets. Malonyl-CoA-acyl carrier protein transacylase (MCAT) transfers the malonyl group from malonyl-CoA to holo-acyl carrier protein (ACP), and since malonyl-ACP is a key building block for fatty-acid biosynthesis it is considered as a promising antibacterial target. The crystal structures of MCAT from *Staphylococcus aureus* and *Streptococcus pneumoniae* have been determined at 1.46 and 2.1 Å resolution, respectively. In the *Sa*MCAT structure, the N-terminal expression peptide of a neighboring molecule running in the opposite direction of malonyl-CoA makes extensive interactions with the highly conserved "Gly-Gln-Gly-Ser-Gln" stretch, suggesting a new design platform. Mutagenesis results suggest that the enzymatic activities of the *Spn*MCAT mutants suggest that Ser90 and His199 are the catalytic dyad with Arg115 and Phe198 playing critical roles in catalysis. We believe that these structures provide useful information for the design of novel inhibitors.

This work was supported by grants from the Functional Proteomics Center, the 21C Frontier Research & Development Program of the Korea Ministry of Science and Technology, the Korea Institute of Science and Technology Institutional Program Grant.

References

[1] White S.W., Zheng J., Zhang Y.M., Rock C.O., "The structural biology of type II fatty acid biosynthesis", *Annu. Rev. Biochem*., vol. 74, (2005), pp. 791-831.
[2] Campbell J.W., Cronan J.J., "Bacterial fatty acid biosynthesis: targets for antibacterial drug discovery", *Annu Rev Microbiol*. Vol. 55, (2001), pp. 305-332.

MS07-P44

Characterization and crystallization of perakine reductase, an enzyme involved in monoterpenoid indole alkaloid biosynthesis

Lianli Sun[1,2], Yixin Chen[1], Meitian Wang[3], Santosh Panjikar[4], Joachim Stoeckigt[1,2]

[1]*Institute of Materia Medica, College of Pharmaceutical Sciences, Zhejiang University, 388 Yu Hang Tang Road, Hangzhou, Zhejiang Province, 310058, P.R. China*
[2]*Department of Pharmaceutical Biology, Institute of Pharmacy and Biochemistry, Johannes Gutenberg-University Mainz, Staudinger Weg 5, D-55099 Mainz, Germany*
[3]*Swiss Light Source PX III, Paul Scherrer Institute, CH-5232 Villigen, Switzerland*
[4]*European Molecular Biology Laboratory, Hamburg Outstation Deutsches Elektronen-Synchrotron, Notkestrasse 85, D-22603 Hamburg, Germany*
E-mail: yixinc@163.com

The enzyme Perakine reductase (PR) catalyzes the NADPH-dependent reduction of perakine to raucaffrinoline (Figure). The reaction represents a side-branch of the biosynthetic pathway of the antiarrhythmic alkaloid ajmaline applied in therapy of arrhythmic heart disorders. The 10-step pathway has been elucidated in cell cultures of the Indian medical plant *Rauvolfia serpentina* .

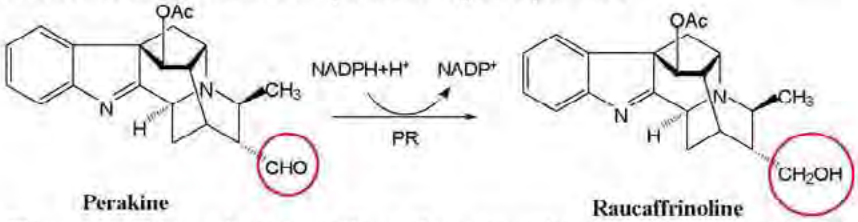

Perakine **Raucaffrinoline**

Figure. Perakine reductase catalyzes the enzymatic reaction from perakine to raucaffrinoline in presence of the reduced cofactor NADPH.

In the past PR was functionally expressed in *Escherichia coli* as the N-terminal His_6-tagged enzyme and was purified to homogeneity. Sequence alignments studies define PR as a novel member of the large aldo-keto reductase (AKR) superfamily. PR [1] exhibits the conserved catalytic tetrad Asp52, Tyr57, Lys84, His126. Site-directed mutagenesis of each of these functional residues to an alanine residue results in > 97.8% loss of enzyme activity. PR represents the first example of the AKR-family which takes part in the biosynthesis of plant – derived monoterpenoid indole alkaloids. In addition to a new esterase, PR significantly extends the *Rauvolfia* alkaloid network to a novel group of alkaloids named peraksine alkaloids. Surprisingly, PR displays also an unusual broad substrate acceptance, reducing small benzaldehyde analogs, medium cinnamic aldehyde derivatives, up to bulky indole alkaloids. The relatively low substrate specificity and delivering de-toxified alcohols from compounds with reactive aldehyde groups may suggest a chemical defence and self-protecting function of PR [2].

Best crystals of methylated His_6-tagged PR were up to now obtained by the hanging-drop vapor-diffusion technique. The crystals diffracted to 2.30 Å. They belong to space group $C222_1$ and one asymmetric unit cell contains one PR molecule. Elucidation of the 3D-structure of PR and its complexes with cofactor NADPH and different substrates are presently under progress.

References

[1] Rosenthal C., Mueller U., Panjikar S., Sun L., Ruppert M., Zhao Y., Stöckigt J., Expression, p urification, crystallization and preliminary X-ray analysis of perakine reductase, a new member of the AKR enzyme superfamily from higher plants. *Acta Crystallographica Section F*, Vol.62, (2006), pp 1286–1289.

[2] Sun L., Ruppert M., Sheludko Y., Warzecha H., Zhao Y., Stöckigt J., Purification, cloning, functional expression and characterization of perakine reductase – the first example from the AKR enzyme family, extending the alkaloidal network of the plant *Rauvolfia*. *Plant Molecular Biology*, Vol. 67, No.5, (2008), pp 455-467.

MS07-P45

Structural analysis of raucaffricine glucosidase, a central enzyme in the alkaloid biosynthetic network of the Indian plant *Rauvolfia*

Liqun Xia[1], Martin Ruppert[2], Meitian Wang[3], Santosh Panjikar[4] and Joachim Stöckigt[1,2]
[1]*Institute of Materia Medica, College of Pharmaceutical Sciences, Zhejiang University, 388 Yu Hang Tang Road, Hangzhou, Zhejiang Province, 310058, P.R. China*
[2]*Department of Pharmaceutical Biology, Institute of Pharmacy and Biochemistry, Johannes Gutenberg University Mainz, Staudinger Weg 5, D-55099 Mainz, Germany*
[3]*Swiss Light Source PX III, Paul Scherrer Institute, CH-5232 Villigen, Switzerland*
[4]*European Molecular Biology Laboratory, Hamburg Outstation Deutsches Elektronen-Synchrotron, Notkestrasse 85, D-22603 Hamburg, Germany*
E-mail: xialiqun2008@yahoo.com.cn

Raucaffricine-*O*-β-D-glucosidase (RG) is an enzyme that takes part in the biosynthesis of monoterpenoid indole alkaloids from the Indian medical plant *Rauvolfia serpentina* , especially for the antiarrhythmic alkaloid ajmaline used to treat heart disorders [1]. Sequence alignment studies show that RG belongs to the glycosyl hydrolase (GH) family 1. Sequence identity of RG is 55% compared to another glucosidase (strictosidine glucosidase, SG) of alkaloid biosynthesis. SG represents the bio-synthetic gateway to the mentioned indole alkaloid family with about 2000 members, some of highly important pharmaceutical activities [2]. The best substrate for recombinant RG is raucaffricine.

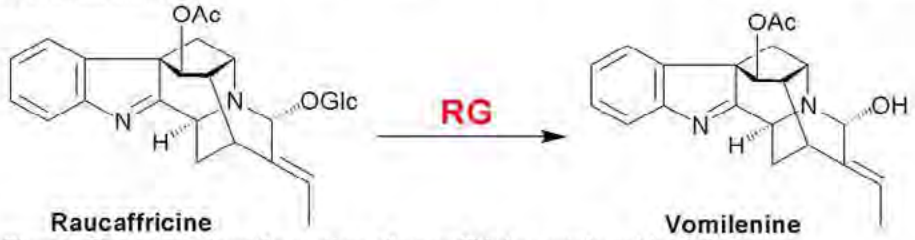

Figure: Enzymatic transformation of raucaffricine catalyzed by RG

The glucosides secologanin and strictosidine at the beginning of the ajmaline biosynthesis pathway are also hydrolyzed by RG, which is in contrast to SG. SG accepts exclusively its natural substrate strictosidine [3]. Site-directed mutagenesis of RG's functional residue Glu-186 to a Gln residue results in >99% loss of enzyme activity. Crystals of RG and its complexes of inactive mutant Glu186Gln (with secologanin and dihydroraucaffricine, respectively) were obtained and survived X-ray measurements at room temperature. Complete data sets were collected to less than 2.5Å. Detailed three-dimensional information describing both, native RG and complexes of inactive mutant of RG, thus providing additional structural characterization and identification of the amino acids that occupy the active site surface of the enzyme. Structural analysis and site-directed mutagenesis experiments demonstrate the essential role of Glu-186 in catalysis. The data presented here will contribute to deciphering the structure-related substrate specificity of raucaffricine glucosidase.

References

[1] Ruppert M., Ma X. and Stöckigt J., "Alkaloid Biosynthesis in Rauvolfia - cDNA Cloning of major Enzymes of the Ajmaline Pathway"; thematic issue "Recent Progress in Alkaloid Chemistry", *Current Organic Chemistry*, Vol. 9, No. 15, (2005), pp 1431-1444.
[2] Barleben L., Panjikar S., Ruppert M., Koepke J. and Stöckigt J., "Molecular Architecture of Strictosidine Glucosidase: The Gateway to the Biosynthesis of the Monoterpenoid Indole Alkaloid Family", *Plant Cell*, Vol.*19*, No. 9, (2007), pp 2886-2897.
[3] Gerasimenko I., Sheludko Y., Ma X. and Stöckigt, J., "Heterologous expression of a Rauvolfia cDNA encoding strictosidine glucosidase, a biosynthetic key to over 2000 monoterpenoid indole alkaloids", *European Journal of Biochemistry*, Vol. 269, No. 8, (2002), pp 2204-2213.

MS07-P46

Drug protein interaction studies of an antiviral agent garcinol targeting HIV-1 protease by *in silico* approach

Prashantha Karunakar[1], Girija C. R[2*], Shalini S[2], Noor Shahina Begum[3] Akheel Ahmed Syed[4]

[1] *Department of Biotechnology and Bioinformatics, Kuvempu University, Shankarghatta, Shivamogga - 577451 Karnataka, India*
[2] *Department of Chemistry, SSMRV College, 4thT Block, Jayanagar, Bangalore - 560041, India*
[3] *Department of Studies in Chemistry, Bangalore University, Central College Campus, Bangalore - 560 001, India*
[4] *Department of Studies in Chemistry, University of Mysore, Manasagangothri, Mysore- 570 006, India*
E-mail : girijashivakumar@rediffmail.com

HIV/AIDS remains the greatest public health and humanitarian challenges in the current world's health sector. For many decades now, millions of lives have been compromised by this disease. HIV-1 protease (HIV-1PR) is an obligatory enzyme in the replication process of the HIV virus. The abundant structural information on HIV-1PR has made the enzyme an attractive target for computer-aided drug design strategies. However, it becomes less effective due to highly resistant new viral strains of HIV, which have multiple mutations in their proteases. Garcinol, a polyisoprenylated benzophenone derivative from *Garcinia indica* fruit rind which has high inhibitory affinity for the HIV-1 protease is examined in this study. Garcinol the inhibitor was docked on to HIV-1PR enzyme using molecular docking program Autodock and binding free energy is calculated using Lamarckian Genetic Algorithm. Inhibitor docked against the enzyme was found to bind with conformational flexibility necessary for exploiting those polar groups providing strong electrostatic interaction with the viral enzyme. The conformation of such molecules will also exploit the interaction geometry along with the molecule size sufficient for spanning the two protease residues to which they will bind making it a good starting point for designing library of garcinol and its analogs as HIV-1 protease inhibitors.

MS07-P47

Structural and functional analyses of W272A and N277A mutant forms of prostacyclin synthase

Yi-Ching Li[1,2], Shu-I Tsai[1], Lee-Ho Wang[3], and Nei-Li Chan[1,2]

[1]*Institute of Biochemistry and Molecular Biology, College of Medicine, National Taiwan University, Taipei 100, Taiwan*
[2]*Institute of Biochemistry, College of Life Sciences, National Chung Hsing University, Taichung City 402, Taiwan*
[3]*Division of Hematology, Department of Internal Medicine, University of Texas Health Science Center at Houston, 6431 Fannin, Houston, TX 77030, USA*
E-mail: li.yiching.li@gmail.com

Prostacyclin synthase (PGIS) plays crucial roles in cardiovascular function by catalyzing an isomerization of prostaglandin H_2 (PGH_2) to prostacyclin, a key bioactive prostanoid known for its potent vasodilation and anti-platelet aggregation activities. Sequence analysis and biochemical characterizations established that PGIS belongs to the P450 enzyme superfamily. Interestingly, unlike other P450s that catalyze O_2- and reductase-dependent mono-oxygenation or hydroxylation reaction, PGIS catalyzes a sterospecific isomerizaton reaction and requires neither O_2 nor any external electron donor for function. To understand how PGIS exhibits its unique enzymatic activity, we have previously determined the crystal structures of the ligand-free and PGH_2 analog U51605-bound PGIS. Structural comparison has lead to the identification of residues in the active site that may be crucial for catalysis. Moreover, we noticed that the side chain of N277 appears to be positioned to form hydrogen-bonding interaction with the C-9 oxygen of substrate PGH_2, likely contributing directly to the cleavage of endoperoxide bond. This hypothesis is consistent with the finding that N277 mutations lower catalytic activity. The position of W272 is also notable among the hydrophobic residues in the active site. With its indole side chain lies parallel to the heme, we originally suspected that W272 might serves as a ceiling in the active site to constrain the spatial position of substrate. To understand the functional significances of these two residues in greater detail, we have determined the crystal structures of the ligand-free and PGH_2 analog U51605-bound forms of N277A and W272A mutant PGIS. The catalytic activities of these two mutant enzymes have also been characterized. These studies have revealed previously unrecognized functions of these two highly conserved residues. Key findings and new insights from this work will be presented in the meeting.

MS07-P48

Structural and functional assay of AtTLP18.3 revealed its novel phosphatase activity involved in repair cycle of photosystem

Hsin-Yi Wu[1], Mao-Sen Liu[1], Tsan-Piao Lin[1], and Yi-Sheng Cheng[1,2]

[1]*Institute of Plant Biology, National Taiwan University, Taipei, Taiwan*
[2]*Department of Life Science, National Taiwan University, Taipei, Taiwan*
E-mail : f92b42016@ntu.edu.tw

AtTLP18.3 is an 18.3 kDa thylakoid lumen protein which can be divided into three segments: a chloroplast transit peptide, a domain of unknown function (DUF477) and a transmembrane α-helix (TMH). The homologs of AtTLP18.3 are highly conserved between eubacteria and photosynthetic plants, and might evolve originally from cyanobacteria. Since the mutants of knock-out or overexpression of AtTLP18.3 don't show observable phenotype, it indicates that this protein may have distinct property with other redundant proteins in chloroplast. Previous report proposed that AtTLP18.3 protein is an auxiliary protein involved in photosystem II (PSII) repair cycle. (Sari et al., 2007; Mulo et al., 2008) It attracted our attention to explore the molecular function of AtTLP18.3 from structural analysis.

In our preliminary result, the gene regulation of AtTLP18.3 had a circadian rhythm, but the protein level showed little rhythm change. A truncated form of AtTLP18.3 without N-terminal transit peptide and C-terminal transmembrane helix was overexpressed and crystallized, it showed an orthorhombic space group $P2_12_12_1$ with unit-cell parameters a=46.9Å, b=49.8Å, c=76.7Å, α=β=γ=90°. Because there are no methionines in AtTLP18.3, two point mutations, L127M and L157M were introduced using site-directed mutagenesis for phasing. Fortunately, the crystals of double mutated AtTLP18.3 are isomorphous to the ones of native protein. The mutant structure was resolved by single-wavelength anomalous dispersion (SAD) method at a resolution of 2.6 Å, and the native structure was resolved at 1.52 Å resolution, accordingly. The folding of AtTLP18.3 comprises of three-layer sandwich from three α-helices in the upper layer, four β-sheets in the middle layer, and two α-helices in the lower layer. It resembled a Rossmann fold. For structural comparison, the coordinates of AtTLP18.3 was submitted to MATRAS database for searching similar folds of proteins with known function. The results showed that various phosphotransferases or phosphatases get high Z-scores to AtTLP18.3. Based on the hints, the enzymatic activity of AtTLP18.3 was confirmed by phosphatase assay using several substrates: *p*NPP, DiFMUP, phosphoserine, and several short phosphopeptides. In conclusion, AtTLP18.3 might act as novel phosphatase to remove the phosphate group for the repair cycle of photosystem.

References

[1] Mulo, P., Sirpio, S., Suorsa, M., and Aro, E.M. (2008). Auxiliary proteins involved in the assembly and sustenance of photosystem II. Photosynthesis Research 98, 489-501.
[2] Sari, S., Allahverdiyeva, Y., Suorsa, M., Paakkarinen, V., Vainonen, J., Battchikova, N., and Aro, E.-M. (2007). TLP18.3, a novel thylakoid lumen protein regulating photosystem II repair cycle. Biochem J 40 6, 415-425.

MS07-P49

Structural characterization of a serpin from the large beetle Ten ebrio molitor and its regulation by heparin

Sun Hee Park, Rui Jiang, Shunfu Piao, Bing Zhang, Eun-Hye Kim, Hyun-Mi Kwon, Xiao Ling Jin, Bok Luel Lee1, and Nam-Chul Ha1

College of Pharmacy and Research Institute for Drug Development, Pusan National University, Jangjeon-dong, Geumjeong-gu, Busan 609-735, Republic of Korea
E-mail: hnc@pusan.ac.kr and brlee@pusan.ac.kr

The Toll signaling pathway, an essential invertebrates' innate immune response, is mediated via serine protease cascade. Once activated, the serine proteases are irreversibly inactivated by serine protease inhibitors (serpins). Recently, we identified three serpin-serine protease pairs that are directly involved in the regulation of Toll signaling cascade in a large beetle, *Tenebrio molitor*. Of these, the serpin SPN48 was cleaved by its target seine protease, Spätzle-processing enzyme, at non-canonical P1 residue of serpin's reactive center loop. To address this unique cleavage, herein, we report the crystal structure of SPN48, revealing that SPN48 exhibits a native conformation of antithrombin, where the reactive center loop is partially inserted into the center of the largest β-sheet of Spätzle-processing enzyme. The crystal structure also shows that SPN48 has a putative heparin binding site that is distinct from those of the mammalian serpins. Ensuing biochemical studies demonstrate that heparin accelerates the inhibition of Spätzle-processing enzyme by a proximity effect in targeting the SPN48. Our finding provides molecular mechanism of how serpins tightly regulate invertebrates' innate immune responses.

References

[1] Rau, J. C., Beaulieu, L. M., Huntington, J. A., and Church, F. C.," Serpins in thrombosis, hemostasis and fibrinolysis.", *J Thromb Haemost* 5 (2007) Suppl 1, 102-115
[2] Gooptu, B., and Lomas, D. A. ," Crystallographic and cellular characterisation of two mechanisms stabilising the native fold of alpha1-antitrypsin: implications for disease and drug design.", *J Mol Biol.* 2009 10;387(4):857-68.
[3] Johnson, D. J., Langdown, J., Li, W., Luis, S. A., Baglin, T. P., and Huntington, J. A.," Crystal structure of monomeric native antithrombin reveals a novel reactive center loop conformation.", *J Biol Chem* (2006) 281(46), 35478-35486
[4] Huntington, J. A., Read, R. J., and Carrell, R. W.," Structure of a serpin-protease complex shows inhibition by deformation.", *Nature* (2000) 407(6806), 923-926
[5] Carrell, R. W., and Owen, M. C.," Plakalbumin, alpha 1-antitrypsin, antithrombin and the mechanism of inflammatory thrombosis.", *Nature* (1985) 317(6039), 730-732
[6] Macfarlane, R. G," An enzyme cascade in the blood clotting mechaniam, and its function as a biochemical amplifier.", *Nature* (1964) 202, 498-499
[7] Walenga, J. M., Petitou, M., Samama, M., Fareed, J., and Choay, J.,"Importance of a 3-O-sulfate group in a heparin pentasaccharide for antithrombotic activity.", *Thromb Res* (1988) 52(6), 553-563
[8] Whisstock, J. C., Pike, R. N., Jin, L., Skinner, R., Pei, X. Y., Carrell, R. W., and Lesk, A. M.,"", *J Mol Biol* (2000) 301(5), 1287-1305

MS07-P50

The crystal structure of hexameric Lon protease: dynamics of the AAA+ module controls access to a sequestered proteolytic chamber

Sun-Shin Cha[1], Young Jun An[1], Chang-Sook Jeong[1], and Sung Gyun Kang[1]

[1]*Marine Biotechnology Research Center, Korea Ocean Research & Development Institute, Ansan 426-744, Republic of Korea*
E-mail: chajung@kordi.re.kr

The ATP-dependent Lon protease has orthologs distributed in all kingdoms of life and is required for survival when cells are subjected to various stress conditions. Lon is a tandem fusion of a molecular chaperone belonging to the AAA+ family and a protease with a serine-lysine catalytic dyad. Here, we report the 2.0 Å resolution crystal structure of the *Thermococcus onnurineus* NA1 Lon (*Ton*Lon). The structure is a three-tiered hexagonal cylinder with a sequestered internal proteolytic chamber accessible through a restricted channel through the AAA+ domains. Conserved axial loops together with an insertion domain containing the membrane anchor comprise a domain positioned on the apical surface of the AAA+ ring that serves as a gate to regulate substrate access to the internal unfolding and degradation chambers. Alternating AAA+ domains in the hexameric ring exist in tight- and weak-binding nucleotide states, displaying different domain orientations and intersubunit contacts, reflective of the ATP hydrolysis-coupled motions driving protein unfolding and translocation. The bowl-shaped proteolytic chamber is contiguous with the chamber formed by the AAA+ domains, and consequently internalized proteins can directly access the proteolytic sites with no further gating restrictions. The structure suggests a model by which Lon can degrade unfolded proteins and small folded proteins or protein subdomains as well.

References

[1] Goldberg AL & John ACS, Intracellular protein degradation in mammalian and bacterial cells. *Annu. Rev. Biochem.* 45:747-803, (1976).
[2] Hershko A & Ciechanover, A The Ubiquitin system for protein degradation. *Annu. Rev. Biochem.* 61:761-807, (1992).
[3] Gottesman S, Proteolysis in Bacterial Regulatory Circuits. *Annu. Rev. Cell Dev. Biol.* 19:565-587, (2003).
[4] Sauer RT, *et al.,* Sculpting the proteome with AAA(+) proteases and disassembly machines. *Cell* 119(1):9-18, (2004).

MS07-P51

X-ray structure of a 3-isopropylmalate isomerase large subunit from *Methanococcus jannaschii*

[1]Eun-Hye Lee, [1]Kwang-Yeon Hwang

[1]*Department of Biotechnology, College of Life Sciences and Biotechnology, Korea University, Seoul 136-701, Korea*
E-mail: kskiss00@korea.ac.kr

Isopropylmalate (IPM) isomerase, the second enzyme involved in leucine biosynthesis, catalyzes the stereospecific isomerization between α-IPM and β-IPM via formation of an intermediate, dimethylcitraconate (1). This enzyme also catalyzes the isomerization between 2-methylmalate and 3-methylmalate, a step involved in isoleucine biosynthesis. IPM isomerase is present in all prokaryotic and several eukaryotic species. This enzyme is consisted with one polypeptide like yeast or two polypeptides like *Methanococcus jannaschii*. Large and small subunits were encoded from genes LeuC and LeuD in *M. jannaschii*, respectively. The active enzyme is heterotetramer consisted of two large and two small subunits (2). IPM isomerase belongs to aconitase family with homoaconitase (2-oxosuberate biosynthesis), aconitase (citric acid cycle). The large subunit is homologous to domain 1,2,3 of homoaconitase and small subunit is homologous to domain4. The IPM isomerase structure wasn't solved yet but small subunit structure from *Pyrococcus horikoshii* was solved (3). Here we report the crystal structure of large subunit of IPM isomerase from *Methanococcus jannaschii*. This resuls will be providing the better understanding of isomerization process of various substrate of IPM isomerase.

References

[1] Drevland R.M., Waheed A., Graham D.E., Enzymology and evolution of the pyruvate pathway to 2-oxobutyrate in Methanocaldococcus jannaschii, J. Bacteriol., 189, (2007), pp 4391-4400.

[2] Jeyakanthan J., Drevland R.M., Gayathri D.R., Velmurugan D., Shinkai A., Kuramitsu S., Yokoyama S., Graham D.E., Substrate Specificity Determinants of the Methanogen Homoaconitase Enzyme: Structure and Function of the Small Subunit, Biochemistry, 49, (2010), pp 2687–2696

[3] Yasutake Y., Yao M., Sakai N., Kirita T., Tanaka I., Crystal structure of the Pyrococcus horikoshii isopropylmalate isomerase small subunit provides insight into the dual substrate specificity of the enzyme, J Mol Biol., 19, 344, 2,(2004), pp 325-33.

MS07-P52

Crystal structure of enonyl-acyl carrier protein reductase (FabI) in complex with NADH and triclosan from *Pseudomonas aeruginosa*

Jeong Hye Lee[1], Ae Kyung Park[1], Ji Ho Moon[2] and Young Min Chi[1]

[1]*Division of Biotechnology, College of Life Sciences, Korea University, Seoul 136-713, Korea*
[2]*Insititute of Life Sciences and Natural Resources, Korea University, Seoul 136-713, Korea*
E-mail: chkasa11@hanmail.net

Enoyl-acyl carrier protein reductase catalyzes the reduction of a trans-2-enoyl-ACP to the fully saturated acyl-ACP in fatty-acid biosynthesis by the ubiquitous fatty acid synthase system. Triclosan is an inhibitor of FabI and helps enhance NADH binding to FabI.

Here we refined a crystal structure of FabI in complex with triclosan and NADH at 1.8 Å resolutions. The X-ray structure showed four molecules in an AU, where the monomer structure comprised of 8 β strands, 7 helices. The inhibitor binds into a hydrophobic pocket which is configurated by hydrophobic residues. Moreover, the closed conformation of the loop helps to bind triclosan tightly. This study will help to find other inhibitors of FabI from Psudomonas aeruginosa which has antibiotics resistance.

References

[1] Heath. R. J., Whiteb. S. W., Rock. C. O., "Lipid biosynthesis as a target for antibacterial agents", Progress in Lipid Research, Vol. 40, Issue. 6, (2001), pp 467 - 497
[2] Qiu. X., Abdel-Meguid. S. S., Jason. S. A., Court. R. I., Smyth. M. G., Payne. D. J., "Molecular basis for triclosan activity involves a flipping loop in the active site", Protein Science, Vol. 8, Issue. 11, (1998), pp 2529 – 2532

MS10-P01

Crystal structure of human transglutaminase 2 in complex with adenosine triphosphate

Byeong-Gu Han[1], Byung Il Lee[1,*]

[1]*Cancer Cell and Molecular Biology Branch, Division of Cancer Biology, Research Institute, National Cancer Center, Goyang, Gyeonggi 410-769, Korea*
E-mail: bilee@ncc.re.kr

Transglutaminase 2 (TG2) is a calcium-dependent multifunctional protein associated with various human diseases. We determined the crystal structure of human TG2 in complex with adenosine triphosphate (ATP). The ATP molecule binds to the previously identified guanosine diphosphate (GDP) binding pocket but has different hydrogen bonds and ion interaction with protein. The four residues Arg476, Arg478, Val479 and Tyr583, all of which are involved in both ATP and GDP binding by hydrogen bonds, might play important roles in the stabilization of TG2 by ATP or GDP. However, Ser482 and Arg580, which are involved in GDP binding, do not form hydrogen bond with ATP. Additionally, we newly discovered an intramolecular disulfide bond between Cys230 and Cys370, which formation might regulate the enzymatic activity of TG2.

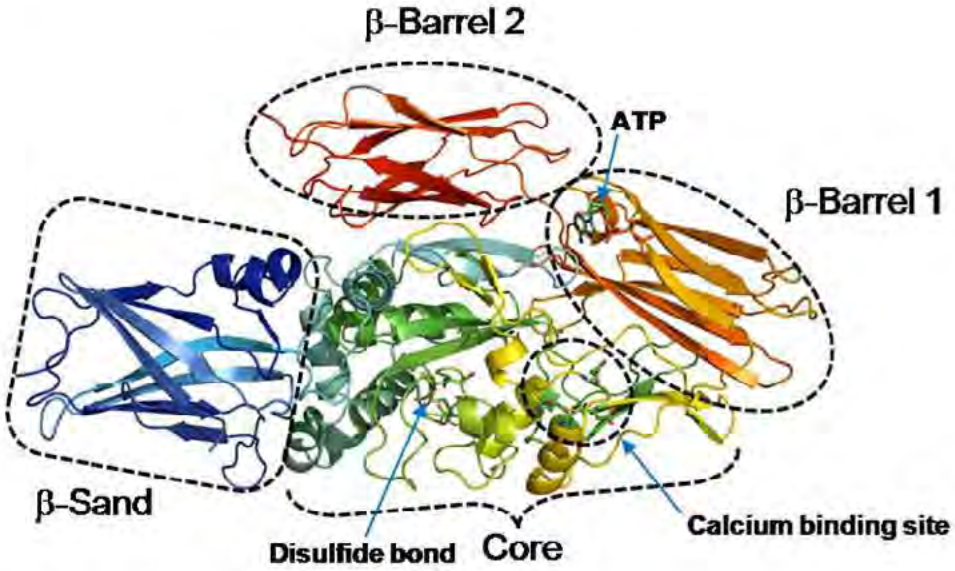

References

[1] Jeon J.H., Cho S.Y., Kim C.W., Shin D.M., Kweon J.C., Choi K.H., Park S.C. and Kim I.G., "GTP is required to stabilize and display transamidation activity of transglutaminase 2", Biochem Biophys Res Commun, Vol. 294, (2002), pp 818-822.

[2] Liu S., Cerione R.A. and Clardy J., "Structural basis for the guanine nucleotide-binding activity of tissue transglutaminase and its regulation of transamidation activity", Proc Natl Acad Sci, Vol. 99, (2002), pp 2743-2747.

[3] Pinkas D.M., Strop P., Brunger A.T. and Khosla C., "Transglutaminase 2 undergoes a large conformational change upon activation", PLoS Biol, Vol. 5, (2007), pp e3270.

[4] Han B.G., Cho J.W., Cho Y.D., Jeong K.C., Kim S.Y. and Lee B.I. "Crystal structure of human transglutaminase 2 in complex with adenosine triphosphate", Int J Biol Macromol, (2010).

MS10-P02

The c-AMP receptor-like protein CLP is a novel c-di-GMP receptor linking cell-cell signalling to virulence gene expression in *Xanthomonas campestris*

Shan-Ho Chou[1,2], Ko-Hsin Chin[1,2], Yen-Chung Lee[1], & Andrew H.-J. Wang[3]

[1] *Institute of Biochemistry, National Chung-Hsing University, Taichung, 40227, Taiwan, ROC*
[2] *National Chung Hsing University Biotechnology Center, National Chung-Hsing University, Taichung, 40227, Taiwan, ROC*
[3] *Institute of Biological Chemistry, Academia Sinica, Nankang, Taipei, Taiwan, ROC*
E-mail: shchou@nchu.edu.tw

C-di-GMP controls a wide range of functions in eubacteria, yet little is known about the underlying regulatory mechanisms. In the plant pathogen *Xanthomonas campestris*, expression of sub-set of virulence genes is regulated by c-di-GMP and also by the CAP-like protein *Xc*CLP, a global regulator in the CRP/FNR superfamily. Here, we report structural and functional insights into the interplay between *Xc*CLP and c-di-GMP in regulation of virulence gene expression. *Xc*CLP bound target promoter DNA with sub-μM affinity in the absence of any ligand. This DNA-binding capability was abrogated by c-di-GMP, which bound to *Xc*CLP with μM affinity. The crystal structure of *Xc*CLP showed that the protein adopted an intrinsically active conformation for DNA binding. Alteration of residues of *Xc*CLP implicated in c-di-GMP binding through modeling studies caused a substantial reduction in binding affinity for the nucleotide and rendered DNA binding by these variant proteins insensitive to inhibition by c-di-GMP. Taken together, the current study reveals the structural mechanism behind a novel class of c-di-GMP effector protein in the CRP/FNR superfamily and indicates that *Xc*CLP regulates bacterial virulence gene expression in a manner negatively controlled by the c-di-GMP concentrations.

References

Chin, K.-H., Lee, Y.-C., Tu, Z.-L., Chen, C.-H., Tseng, Y.-H., Yang, J.-M., Ryan, R. P., McCarthy, Y., Dow, J. M., Wang, A. H.-J. & Chou, S.-H. (2010). The c-AMP Receptor-Like Protein CLP is a Novel c-di-GMP Receptor Linking Cell-Cell Signaling to Virulence Gene Expression in *Xanthomonas campestris*. *J. Mol. Biol.* 396, 646-662.

MS10-P03

Modulating immune function through chemokine binding – Orf virus presents a new twist on an old motif

Kurt L. Krause[1], Rafael Counago[1], Stephen Fleming[2], Andy Mercer[2]
[1]*The Department of Biochemistry, University of Otago, Dunedin. New Zealand*
[2]*The Department of Microbiology and Immunology, University of Otago, Dunedin, New Zealand*
E-mail: kurt.krause@otago.ac.nz

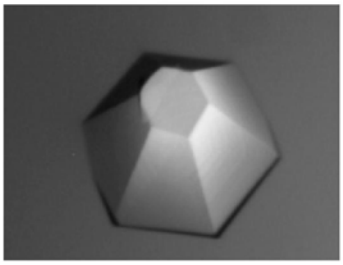

We report the structure of a new class of chemokine binding proteins (CBP) from Orf virus, an important parapoxvirus. CBPs are viral proteins that modulate inflammation by interfering with host chemokine signaling. They bind to their cognate partner with picomolar affinity via an extended beta sandwich structure. The crystals of this protein were challenging to produce and were optimized significantly through the use of additives, like Silver Bullets™. Crystals occupy Space Group $P6_522$ with unit cell parameters of a = b = 75.62 Å, c = 282.49 Å, $\alpha = 90$, $\beta = 90$, $\gamma = 120^{\circ}$. The structure was phased using MAD methodologies and currently the 2.1Å structure is undergoing refinement. Early analysis indicates that it is a member of the β-sandwich family but it is distinct from other family members when superimposed. Additionally the crystal structure is consistent with a physiologic dimer and displays a very broad β sheet on its surface containing contributions from more than ten β strands. The dimeric nature of this CBP appears to be a unique property of its class and may be key in explaining how it is able to bind chemokines from at least two distinct chemokine classes.

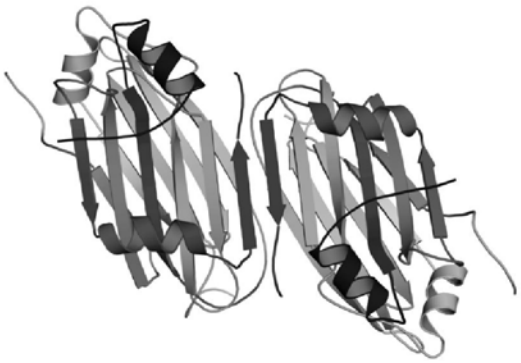

MS10-P04

Structural and functional studies on thiolase from Mycobacterium smegmatis and Mycobacterium tuberculosis

Neelanjana Janardan, M.R.N.Murthy

Molecular Biophysics Unit, Indian Institute of Science, Bangalore-360098, India
E-mail: neela@mbu.iisc.ernet.in

The thiolase family is a widespread group of proteins present in prokaryotes and in three different cellular compartments of eukaryotes. They are ubiquitous enzymes that have important roles in many vital biochemical pathways, including the β-oxidation pathway of fatty acid degradation and various biosynthetic pathways. Thiolases are considered as suitable targets for drug design against pathogenic parasites due to the significant differences in the structure and function of the prokaryotic enzymes when compared to the eukaryotic enzymes. The thiolase reaction mechanism is not yet fully understood.

The present study aims at determining the structure and function of thiolases from several pathogenic organisms including *Mycobacterium tuberculosis*. The structures and functions of these thiolases will be compared with the human counterpart. A bioinformatics search of these genomes with the human thiolase as the probe has revealed that these organisms contain thiolases that might be structurally different from their human counterparts. The genes thus identified were cloned and over-expressesed. Purifictaion, crystallization trials and structure determination trials are underway. Structural and enzymatic studies will be carried out on these thiolases. Attempts will also be made to design suitable inhibitors for these enzymes.

References

[1] Antti M. Haapalainen, Gitte Merilainen and Rik K. Wierenga, The thiolase superfamily: condensing enzymes with diverse reaction specificities.*Biol. Rev.*, 80, (2005), pp. 129–153.

[2] Prasenjit Bhaumik, M Kristian Koski, Tuomo Glumoff, J Kalervo Hiltunen and Rik K Wierenga., Structural biology of the thioester-dependent degradation and synthesis of fatty acids.*Current Opinion in Structural Biology*, 15, (2005), 621–628.

MS10-P05

Crystal structure of the sensor domain of naphthalene chemoreceptor NahY from *Pseudomonas putida*

Truc Kim and Kyeong Kyu Kim

Department of Molecular Cell Biology, Samsung Biomedical Research Institute, School of Medicine, Sungkyunkwan University, Suwon 440-746, Korea
E-mail: kdttruc83@gmail.com

Chemotaxis is one of the most essential abilities of bacteria to effectively and speedily accommodate themselves to environmental changes, characterized by the swimming toward nutrients or fleeing away from poisonous compounds. It involves a complicated signaling network that starts from transmembrane chemoreceptors at one pole of the cell and propagates to the rotary flagellar motor at the opposite side. The abilities of soil bacteria to recognize, move toward, and degrade several pollutant compounds such as polyacromatic hydrocarbon have attracted scientific attention, and the naphthalene chemoreceptor NahY from *Pseudomonas putida* G7 is particularly of interest. The crystal structure of the sensor domain of NahY (exNahY) was determined at 1.79Å resolution by multi-wavelength anomalous diffraction method after substantial crystallization efforts. The exNahY crystal belongs to the orthorhombic space group $P2_12_12_1$, with unit cell parameters of a = 58.68Å, b = 60.62Å, c = 84.90Å, and $\alpha = \beta = \gamma = 120^{\circ}$. The presence of two molecules of similar folding in an asymmetric unit of the unit cell revealed the formation of exNahY dimers. exNahY shares the common fold with the sensor domains of aspartate chemoreceptor, Tar, and serine chemoreceptor, Tsr, which is characterized by the four-helix bundle, although they have divergent amino acid sequences. It was shown by size-exclusion chromatography that the dimerization is triggered by ammonium ions, which was added to crystallization recipe and is abundant in soil environment. Furthermore, isothermal calorimetric analysis revealed specific interactions between the ammonium ion and exNahY. Atomic dissection of the ligand recognition of NahY will not only shed light on the understanding of bacterial chemotaxis, but also will supply an exploitable tool for biodegradation research and synthetic biology.

References

[1] Grimm A.C. and Harwood C.S., "NahY, a catabolic plasmid-encoded receptor required for chemotaxis of *Pseudomonas putida* to the aromatic hydrocarbon naphthalene", *Journal of Bacteriology*, Vol. 181, No. 10, (1999), pp 3310-3316.

[2] Wadhams G.H. and Armitage J.P., "Making sense of it all: bacterial chemotaxis", *Nature Reviews Molecular Cell Biology*, Vol. 5, No. 12, (2004), pp 1024-1037.

[3] Yeh J.I., Biemann H.P., Privé G.G., Pandit J., Koshland D.E. Jr and Kim S.H., "High-resolution structures of the ligand binding domain of the wild-type bacterial aspartate receptor", *Journal of Molecular Biology*, Vol. 262, No. 2, (1996), pp 186-201.

MS10-P06

Crystal structures and binding studies of atovaquone and its derivative with cytochrome bc_1: Molecular basis for drug design

Susanta K. Nayak[1] S. B. Mallik[1], S. P. Kanaujia[2], K. Sekar[2] and T. N. Guru Row[1]

[1]*Solid State and Structural Chemistry Unit, Indian Institute of Science, Bangalore-560012, Karnataka, India*
[2]*Bioinformatics Centre, Indian Institute of Science, Bangalore 560 012, Karnataka, India*
E-mail: susanta@sscu.iisc.ernet.in

Crystal structure of trans-atovaquone (antimalarial drug) [1-2], its new polymorph form and its stereoisomer (cis) along with five other derivatives with different functional groups have been analyzed. Based on the conformational features of these compounds and the characteristics of the nature intermolecular interactions valuable insight into the atomistic details of protein-inhibitor interactions have been derived by docking studies [3]. Comparison with earlier docking studies bring out the importance of the propensity of hydrogen bonded interactions in the binding pocket [4]. The occurrence of C-H···Cl interactions in these systems provides a new pathway for better design. The docking results show that atovaquone and its derivatives have a tendency to form both strong and weak hydrogen bonds and in particular weak hydrogen bond involving chlorine.

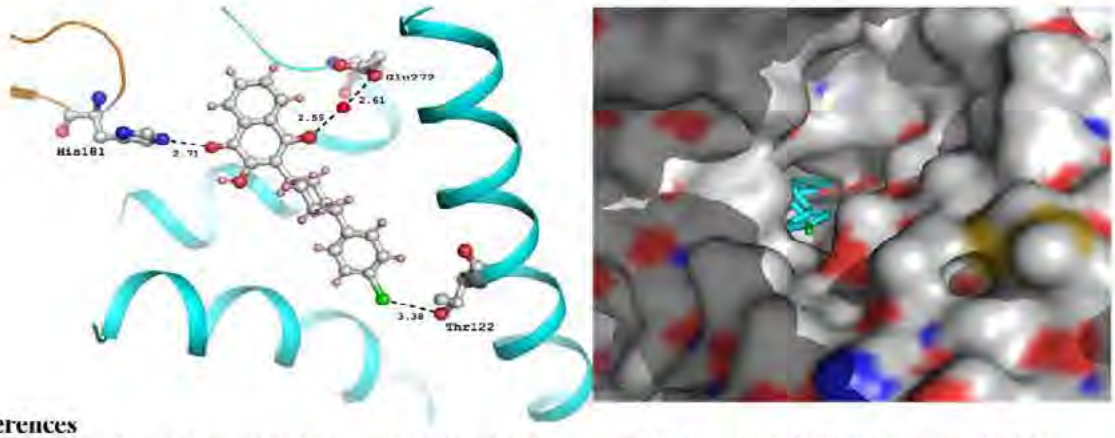

References

[1] Ridley R. and Toure Y. "Malaria Winning the drugs war", *Nature*, Vol. 430, (2004), pp 942-943.
[2] Korsinczky, M., Chen, N., Kotecka, B., Saul, A., Rieckmann, K. and Cheng, Q. "Mutations in Plasmodium falciparum Cytochrome b That Are Associated with Atovaquone Resistance Are Located at a Putative Drug-Binding Site", *Antimicrob. Agents Ch.*, Vol. 44, No. 8, (2000), pp 2100-2108.
[3] Anderson, A. C. "The Process of Structure-Based Review Drug Design", *Chem. Biol.*, Vol. 10 (2003), 787-797 and references therein.
[4] Kessl, J. J., Hill, P., Lange, B. B., Meshnick, S. R., Meunier, B. and Trumpower, B. L. "Molecular Basis for Atovaquone Resistance in Pneumocystis jirovecii Modeled in the Cytochrome bc_1 Complex of Saccharomyces cerevisiae", *J. Biol. Chem.*, Vol. 279, No. 4 (2004), pp 2817-2814 and references therein.

MS10-P07

Structural basis of human p70 ribosomal S6 kinase-1 regulation by activation loop phosphorylation

Sunami T. 1, Byrne N.3, Diehl R.E.3, Funabashi K.2, Hall D.L.3, Ikuta M.1, Patel S.B.3, Shipman J.M.3, Smith R.F.3, Takahashi I.2, Zugay-Murphy J.3, Iwasawa Y.2, Lumb K.J.3, Munshi S.K.3, Sharma S.3

1Department of Chemistry and 2Cancer Research, Tsukuba Research Institute, Banyu Pharmaceutical Company, Limited, Tsukuba, Ibaraki, 300-2611, Japan; 3Global Structural Biology, Merck Research Laboratories, Pennsylvania 19486, U.S.A
E-mail: sunami.tomoko@jaea.go.jp

p70 ribosomal S6 kinase (p70S6K) is a downstream effecter of the mTOR signaling pathway involved in cell proliferation, cell growth, cell-cycle progression, and glucose homeostasis. Several observations suggest a role for p70S6K in cancer, obesity and diabetes. The activation of p70S6K requires multiple phosphorylation events in both the catalytic and autoinhibitory domains (Fig.1.). We initiated structural studies to understand the molecular basis of p70S6K activation. Availability of the structures of the inactive and the active 070S6K would also provide the structural basis for structure guided inhibitor design. The kinase domain of p70S6K1 (p70S6KD) was expressed and purified in both the unphosphorylated (inactive) state and in the 3'-phosphoinositide-dependent kinase-1 (PDK1) phosphorylated (active) state in which Thr-252 of the activation loop is phosphorylated. Unphosphorylated p70S6KD doesn't have activity and phoshorylated p70S6KD is partially activated. Crystal structures were determined as complexes with staurosporine. Unphosphorylated p70S6KD exists in two crystal forms, one in which the p70S6KD exists as a monomer and the other as a domain-swapped dimer. The crystal structure of p70S6KD that is phosphorylated within the activation loop reveals conformational ordering of the activation loop (Fig. 2.). The conformation of the phosphorylation site is consistent with its role in activation. Staurosporine was bound in the catalytic cleft between N and C lobe with three hydrogen bonds to the residues in the catalytic site in both unphosphorylated an phosphorylated states (Fig. 3.). The details of the structures and the insights into the structural basis of the PDK1 induced activation of p70S6K for structure-guided design of specific p70S6K inhibitors will be presented.

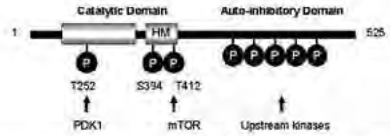

Figure 1. Phosphorylation states of p70S6K1. HM, hydrophobic motif.

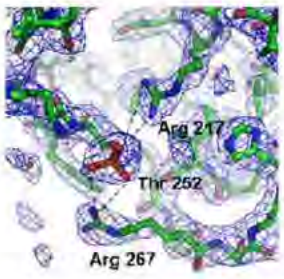

Figure 2. Interaction of Thr(P)-252 with Arg-217 that stabilizes the catalytic loop in the 3'-phosphoinositide-dependent kinase-1-phosphorylated state.

Figure 3. ATP binding pocket of p70S6KD in 3'-phosphoinositide-dependent kinase-1-phosphorylated state of p70S6KD

References

[1] Sunami T., Byrne N.3, Dieh R.E., Funabashi K., Hall D.L., Ikuta M., Patel S.B., Shipman J.M., Smith R.F., Takahashi I., Zugay-Murphy J., Iwasawa Y., Lumb K.J., Munshi S.K., Sharma S.. *J.B.C.*, Vol. 285, 4587-4594.

MS10-P08

Structural studies of TIRAP, an adaptor protein of Toll-like receptor signaling pathway

Yoora Kang, Jungwoo Choe

University of Seoul, Siripdea-gil 13(jeonnong-dong 90), Dongdaemun-gu, Seoul 130-743 Korea
E-mail: yoora195@naver.com

Toll-like receptors (TLRs) can detect a wide variety of invading pathogens by recognizing Pathogen-associated molecular patterns (PAMPs). TLR4 is activated by Lipopolysaccharide (LPS) treatment, leading to activation of NF-κB transcription factor that induces inflammatory responses. TLRs initiate innate immune responses through its intracellular Toll/IL-1 receptor (TIR) domain by interacting with TIR domain containing adaptor protein. TIRAP (also known as Mal) is the one of the adaptor proteins for TLR4 signaling pathway and acts as a sorting adaptor that recruits MyD88 to TLR4 by interacting with the TIR domain of MyD88. It is believed that dimerization of TLR4 ectodomain induced by LPS binding can cause the dimerization of cytosolic TIR domains, serving as a binding surface for the TIR domain of TIRAP. However, the exact mechanism and selectivity of TLR signaling is still uncertain. TIRAP is also known to associate with Phosphatidylinositol-4,5-bisphosphate (PtdIn(4,5)P2) via its N-terminal PIP2 binding site and undergoes various modification including ubiquitination by SOCS-1, phosphorylation by Bruton's kinase and cleavage by caspase-1. Many TIRAP variants are related to various immune diseases like bacteremia, malaria and tuberculosis. Accordingly, the study of crystal structure of TIRAP will reveal how TLR signaling is initiated and how TIRAP is regulated during signaling on the structural basis. Therefore we have attempted to determine the crystal structure of TIR domain of TIRAP to understand how TLR4 signaling is transmitted to downstream signaling. We used *E. coli* expression system to obtain TIRAP proteins with various constructs, and collected x-ray diffraction data for TIRAP TIR domain with a resolution of 3.3 Å.

References

[1] Kristie A. J. and Ashley M., "TIR-containing adaptors in Toll-like receptor signalling", *Cytokine,* Vol 49, (2010), pp 237-244.
[2] Luke A. J. O. and Andrew G. B., "The family of five: TIR-domain-containing adaptors in Toll-like receptor signalling", *Nature Reviews Immunology*, Vol. 7, (2007), pp 353-364.
[3] Luke A. J. O. and Adrian. V. S. H., "A Mal functional variant is associated with protection against invasive pneumococcal disease, bacteremia, malaria and tuberculosis", *Nature genetics*, Vol 39, No 4, (2007), pp 523-528
[4] Tiffany H., Gregory M. B. and Ruslan M., "TIRAP: an adapter molecule in the Toll signaling pathway", *Nature immunology*, Vol 2, No 9, (2001), pp 835-841

MS10-P09

Structural insights into the dual nucleotide exchange and GDI displacement activity of SidM/DrrA

Kwang-Hoon Lee, Hye-Young Suh, Byung-Ha Oh

Department of Biological Sciences, KAIST Institute for the Biocentury, Korea Advanced Institute of Science and Technology, Daejeon 305-701, Korea
E-mail: photon78@kaist.ac.kr

GDP-bound prenylated Rabs, sequestered by GDI (GDP dissociation inhibitor) in the cytosol, are delivered to destined sub-cellular compartment and subsequently activated by GEFs (guanine nucleotide exchange factors) catalysing GDP-to-GTP exchange. The dissociation of GDI from Rabs is believed to require a GDF (GDI displacement factor). Only two RabGDFs, human PRA-1 and *Legionella pneumophila* SidM/DrrA, have been identified so far and the molecular mechanism of GDF is elusive. Here, we present the structure of a SidM/DrrA fragment possessing dual GEF and GDF activity in complex with Rab1. SidM/DrrA reconfigures the Switch regions of the GTPase domain of Rab1, as eukaryotic GEFs do toward cognate Rabs. Structure-based mutational analyses show that the surface of SidM/DrrA, catalysing nucleotide exchange, is involved in GDI1 displacement from prenylated Rab1:GDP. In comparison with an eukaryotic GEF TRAPP I, this bacterial GEF/GDF exhibits high binding affinity for Rab1 with GDP retained at the active site, which appears as the key feature for the GDF activity of the protein.

References

[1] Ingmundson A, Delprato A, Lambright DG, Roy CR (2007) *Legionella pneumophila* proteins that regulate Rab1 membrane cycling. Nature 450: 365–369
[2] Machner MP, Isberg RR (2006) Targeting of host Rab GTPase function by the intravacuolar pathogen *Legionella pneumophila*. Dev Cell 11: 47–56
[3] Machner MP, Isberg RR (2007) A bifunctional bacterial protein links GDI displacement to Rab1 activation. Science 318: 974–977
[4] Murata T, Delprato A, Ingmundson A, Toomre DK, Lambright DG, Roy CR (2006) The *Legionella pneumophila* effector protein DrrA is a Rab1 guanine nucleotide-exchange factor. Nat Cell Biol 8: 971–977
[5] Pfeffer SR, Dirac-Svejstrup AB, Soldati T (1995) Rab GDP dissociation inhibitor: putting Rab GTPases in the right place. J Biol Chem 270: 17057–17059

MS10-P10

Structural study of GTP-sensing pleiotropic transcriptional repressor codY from *Starphylococcus aureus*

Ah reum Han[1], Kyung-Hee Rhee[1], Gye yoon Cho[2], Hosam Ki[2], Kwang Yeon Hwang[1*]

[1,2] *Division of Biotechnology, School of Life Sciences and Biotechnology, Korea University, Anam-Dong, Seongbuk-Gu, Seoul 136-713, Korea*
E-mail : woohut07@korea.ac.kr, chahong@korea.ac.kr

Pleiotropic transcriptional repressor CodY highly conserved in Gram-positive bacteria regulates expression of a hundreds genes directly or indirectly. In pathogenic bacteria like *Listeria, Clostridium, Streptococcus* and *Staphylococcus*, CodY regulates virulence gene expression. In human pathogen *Stapylococcus aureus,* CodY represses genes involved in nitrogen metabolism and regulates synthesis of virulence factor. In addition, SACodY is similar to its homolog in *B. subtilis* related to the proposed GTP binding motif derived from structure and sequence analyses. In order to find structural insights how CodY increasing affinity with DNA in using GTP, we initiated determination of the three-dimensional structure of CodY from *S. aureus* which is composed of 257 amino acids residues (Mr =28755Da). We have overexpressed, purified, and crystallized the SACodY and then conducted a preliminary X-ray crystallographic analysis. The crystal of SACodY belonged to space group $P6_1$, with unit-cell parameters $a = b = 127.015$, $c = 48.929$ Å, a calculated Matthews coefficient of 2.85 $Å^3$ Da^{-1} and two molecules per asymmetric unit. *Refinements of the model structure are* currently in progress and the structural details will be discussed in a poster.

References

[1] Sonenshein, A. L., "CodY, a global regulator of stationary phase and virulence in Gram-positive bacteria.", Curr. Opin. Microbiol. Vol.8, No.2, (2005), pp 203-207.
[2] Pohl, K., Schlink, F. and Wolz, C., "CodY in Staphylococcus aureus: a Regulatory Link between Metabolism and Virulence Gene Expression.", J. Bacteriol. Vol.191, No.9,(2009), pp.2953-2963.
[3] Levdikov, V. M., Blagova, E. and Wilkinson, A. J., "Structural rearrangement Accompanying Ligand Binding in the GAF Domain of CodY from Bacillus subtilis.", J. Mol. Biol. Vol.390, No.5 (2009), pp 1007-1018.

MS10-P11

Structure-function analysis of human L-prostaglandin D synthase bound with fatty acid molecules

Yangyan Zhou [1,2], Neil Shaw[1], Yang Li[1], Yu Zhao[1], Rongguang Zhang[1] and Zhi-Jie Liu[1]

[1] *National Laboratory of Biomacromolecules, Institute of Biophysics, Chinese Academy of Sciences, Beijing 100101, China*
[2] *Graduate University of Chinese Academy of Sciences, Beijing, China*
E-mail: clar007@126.com

Human prostaglandin D synthase (L-PGDS) is a lipocalin type enzyme involved in the metabolism of arachidonic acid and plays a key role in the regulation of sleep, allergy, pain sensation and the development of male reproductive organs. Here, using a combination of crystallographic, biochemical, mutagenesis and kinetic studies, we have gained insights into the mode of ligand binding by human L-PGDS and have identified residues involved in catalysis. Interestingly, structural evidence reveals that two molecules of fatty acids; one molecule each of oleic and palmitoleic acid, bind inside the β barrel. The oleic acid is buried and binds in a highly basic patch in proximity to the catalytically critical Cys65, mimicking the binding of prostaglandin H_2. The palmitoleic acid sits in a relatively neutral region with very few interactions with the protein. Mutating Met64, Leu79, Phe83 or Leu131 to alanine reduced the catalytic efficiency by almost 10-folds, while K59A and Y149A mutations enhanced the catalytic efficiency by more than 2-folds. Met64 seems to function as a kinetic clamp, pushing the thiol group of Cys65 close to the site of nucleophilic attack during catalysis.

References

[1] Urade, Y., and Hayaishi, O. (2000) Prostaglandin D synthase: Structure and function. In Vitamins and Hormones - Advances in Research and Applications, Vol 58 Vol. 58 pp. 89-120, Academic Press Inc, San Diego
[2] Pettipher, R., Hansel, T. T., and Armer, R. (2007) Antagonism of the prostaglandin D2 receptors DP1 and CRTH2 as an approach to treat allergic diseases. Nat Rev Drug Discov 6, 313-325
[3] Qu, W.-M., Huang, Z.-L., Xu, X.-H., Aritake, K., Eguchi, N., Nambu, F., Narumiya, S., Urade, Y., and Hayaishi, O. (2006) Lipocalin-type prostaglandin D synthase produces prostaglandin D2 involved in regulation of physiological sleep. Proceedings of the National Academy of Sciences 103, 17949-17954
[4] Eguchi, N., Minami, T., Shirafuji, N., Kanaoka, Y., Tanaka, T., Nagata, A., Yoshida, N., Urade, Y., Ito, S., and Hayaishi, O. (1999) Lack of tactile pain (allodynia) in lipocalin-type prostaglandin D synthase-deficient mice. Proceedings of the National Academy of Sciences of the United States of America 96, 726-730
[5] Malki, S., Nef, S., Notarnicola, C., Thevenet, L., Gasca, P., Mejean, C., Berta, P., Poulat, F., and Boizet-Bonhoure, B. (2005) Prostaglandin D2 induces nuclear import of the sex-determining factor SOX9 via its cAMP-PKA phosphorylation. Embo J. 24, 1798-1809
[6] Kanaoka, Y., Ago, H., Inagaki, E., Nanayama, T., Miyano, M., Kikuno, R., Fujii, Y., Eguchi, N., Toh, H., Urade, Y., and Hayaishi, O. (1997) Cloning and crystal structure of hematopoietic prostaglandin D synthase. Cell 90, 1085-1095
[7] Urade, Y., and Hayaishi, O. (2000) Biochemical, structural, genetic, physiological, and pathophysiological features of lipocalin-type prostaglandin D synthase. Biochimica et Biophysica Acta (BBA) - Protein Structure and Molecular Enzymology 1482, 259-271
[8] Hoffmann, A., Conradt, H. S., Gross, G., Nimtz, M., Lottspeich, F., and Wurster, U. (1993) Purification and chemical characterization of beta-trace protein from human cerebrospinal fluid - its identification as prostaglandin-D synthase. J. Neurochem. 61, 451-456

MS10-P12

Recombinant fusion protein design for biophysical analysis of integrin subunit dimerization and function

Andrea Francesca M. Salvador, Gabriel N. Valbuena, Lydia Teresa Isabel Salud-Bautista, and Neil Andrew D. Bascos

Protein Structure and Immunology Laboratory, National Institute of Molecular Biology and Biotechnology, University of the Philippines, Diliman. Quezon City, Philippines, 1101
E-mail: ndbascos@up.edu.ph, nadbascos@gmail.com

Integrins provide the principal means for cellular attachment to the extracellular matrix (ECM)[1]. Integrins are made up of subunits that associate as heterodimers on the cell surface[2]. The binding of integrin heterodimers to ECM ligands provide attachment to the ECM as well signals for intracellular processes, thereby "integrating" the intracellular and extracellular environments. The formation of different integrin heterodimer combinations results in different affinities for several ligands as well as variations in intercellular processes signaled[1]. Studies have correlated the formation of different integrin heterodimers with the multiple stages of cancer progression[3] and metastasis[4]. Biophysical analysis of integrin subunit dimerization therefore presents a worthwhile strategy for the progress of cancer treatment. Of the 24 integrin heterodimers identified[5], only three combinations have been successfully crystallized (αVβ3, αIIbβ3 and αXβ1)[2,6,7]. The limited success in crystallization may be attributed to integrin subunit size (~240 kDa/heterodimer), and flexibility[8]. This project aims to increase the efficiency of integrin subunit crystallization by limiting target size and flexibility. Limitations to size and flexibility were designed through the generation of fusion proteins containing only selected integrin subunit domains linked to *fos/jun* leucine zippers. The *Fos/Jun* dimerization domains were included to restrict flexibility, maintain close proximity[9] and facilitate interaction between the expressed subunit domains despite the absence of the rest of the integrin subunit. Genes encoding the functional domains of different integrin subunits were amplified from mammalian cell cultures representing different stages of cancer progression: M4A4, NM2C5, HCT116, A549 (ATCC). Coding sequences for the *Fos* and *Jun* leucine zippers were amplified from these sources as well. Amplicon identities were verified through DNA sequencing. Confirmed amplicons were inserted into cloning plasmids for propagation. Amplicons await transfer into yeast expression plasmids for fusion protein production[10].

References

[1] Giancotti, FG. and Ruoslahti, ER. Integrin Signalling. Science. 1999.285:1028–1032.
[2] Xiong, JP; Stehle, T; Diefenbach, B; Zhang, R; Dunker, R; Scott, D; Joachimiak, A; Goodman, S; and Arnaout, MA. Crystal Structure of the Extracellular Segment of Integrin αVβ3. Science. 2001. 294:339-345.
[3] Shimizu, H; Koyama, N; Asada, M; and Yoshimatsu, K. Aberrant expression of integrin and erbB subunits in breast cancer cell lines. International Journal of Oncology. 2002. 21:1073-1079.
[4] Edlund, M; Miyamoto, T; Sikes, R; Ogle, R; Laurie, GW; Farach-Carson, MC; Otey, CA; Zhau, HE; and Chung, LWK. Integrin Expression and Usage by Prostate Cancer Cell lines on Laminin Substrata. Cell Growth & Differentiatiion. 2001. 12:99-107.
[5] Moschos, Stergios J, Laura M Drogowski, Shelley L Reppert, and John M Kirkwood. "Integrins and Cancer." Oncology (Williston Park, NY) 21, no. 9 (2007): 13-20.
[6] Springer TA, Zhu J, Xiao T, Structural basis for distinctive recognition of fibrinogen gammaC peptide by the platelet integrin alphaIIbbeta3. J Cell Biol. 2008 Aug 25;182(4):791-800
[7] Xie C, Zhu J, Chen X, Mi L, Nishida N, Springer TA. Structure of an integrin with an alphaI domain, complement receptor type 4. EMBO J. 2010 Feb 3;29(3):666-79. Epub 2009 Dec 24. Hynes, Richard O. "Integrins: Versatility, Modulation, and Signaling in Cell Adhesion." Cell 69 (April 1992): 11-25.
[8] Ramirez-Carrozzi, V; Kerppola, T. Dynamics of Fos-Jun-NFAT1 complexes. 2001. Proceedings of the National Academy of Sciences (USA). 98: 4893-4898.
[9] Meta, A; Nakatake, H; Imamura, T; Nozaki, C; and Sugimura, K. High-yield production and characterization of biologically active recombinant aprotinin expressed in Saccharomyces cerevisiae. Protein Expression and Purification. 2009. 66: 22-27.

MS10-P13

Structural study and antibacterial drug design against bacterial blight disease caused by *Xanthomonas oryzae* pv. *Oryzae*

Sampath Natarajan, Thanh Thi Ngoc Doan, Phuong-Thuy Ho Ngo, Jae-Wook Jung, Lin-Woo Kang

Department of Advanced Technology Fusion, Konkuk University, 1Hwayang-dong, Gwangjin-gu, Seoul 143-701, Republic of Korea
E-mail: sams76@gmail.com

Bacterial blight (BB) is a serious and destructive disease caused by *Xanthomonas oryzae* pv. *oryzae* (Xoo); it is prevalent in all over the world specifically in Asian countries, causing huge production losses of rice. Rice is one of the most common staples for human consumption throughout the world. Every year BB is reported to have reduced rice production by as much as 60%. According to a report of the Agricultural Department, BB results in a rice-production loss worth more than 100 million dollars in South Korea alone every year. But till now no effective drugs have been identified and it is essential to develop antibacterial drugs to halt the production losses caused by BB. To initiate the development of antibacterial drugs, the targeted 95 genes are selected from 4538 putative genes responsible for BB disease. The present study is focused to develop the antibacterial drugs.

Xoo malonyl-CoA: acyl carrier protein transacylase (XoMCAT) is one of the essential enzymes targeted for BB disease, encoded by the gene, namely fabD (Xoo0880) which participates in type II fatty acid synthesis (FAS II) to transfer a malonyl group to holo-acyl carrier protein (ACP) to increase the number of two carbons in fatty acid. XoMCAT structure was determined at 2.3Å resolutions with a buffer molecule CHES. Drug screening was carried out by Virtual Library Screening (Molsoft ICM) against Chembridge database containing 492,794 compounds which resulted in 574 compounds against XoMCAT, among which 32 drugs have been identified to be effective against Xoo growth by *in-vitro* biological studies. One of the drugs showed highest Xoo growth inhibition at a concentration of 13µg/mL on the basis of MIC_{50}. Identified drugs are expected to have broad spectrum of antibacterial activity which may be effective against the Type II fatty acid synthesis as well as for bacterial blight disease.

XoMCAT

Ligplot diagram of residues interaction with CHES buffer

MS10-P14

Crystal structure of $_D$-alanine-$_D$-alanine ligase a from *Xanthomonas oryzae* pathovar *oryzae* and its inhibitors from structure-based virtual screening

Thi-Ngoc-Thanh Doan[1], Jin-Kwang Kim[1], Sam Natarajan[1], Yeh-Jin Ahn[2] and Lin-Woo Kang[1]

[1]*Department of Advanced Technology Fusion, Konkuk University, Seoul 143-701, Korea*
[2]*Department of Life Science, College of Natural Sciences, Sangmyung University, Seoul, 110-743, Korea*
E-mail: dtnthanh@gmail.com

$_D$-Alanine-$_D$-alanine ligase (Ddl) catalyzes the formation of $_D$-alanyl-$_D$-alanine dipeptide, an essential bacterial peptidoglycan precursor and it represent an potential target for development new antibacterial drugs. Crystal structure of Ddl chain A from *Xanthomonas oryzae* pathovar *oryzae* (Xoo), causing destructive disease of rice, has been determined at 2.3 Å resolution by molecular replacement method using the template of *Staphylococcus* Ddl (PDB ID: 2I87). The apo enzyme composes three domains that similar to other Ddl structures, in which the active site located at the interface of the first and the third domain. Complex structures of Ddl with ATP (2.1 Å resolution), ADP (2.2 Å) and Ala (2.4 Å) revealed a different orientation of ATP in the active site compared to other Ddls and thus effect on enzyme activity. Since ω-loop is important in substrate binding, XooDdl was switched ω-loop to respective loop from *E.coli* Ddl, *H. pylori* Ddl and resulting enzymes have been characterized. Beside elucidation of enzyme mechanism, the apo structure was applied to ICM program for structure-based virtual screening to find potential inhibitor against this enzyme. Four out of 25 best-ranked compounds showed antibacterial activity and enzymatic inhibitory in micromolar range. Affinity in vitro of XooDdl and two of four compounds were confirmed by NMR[1]. Especially, triplicate in vitro pathogenicity assay showed that one of four compounds was not harmful for rice. This result has promising for develop new inhibitor against this enzyme as well as Xoo.

Keywords: $_D$-alanine-$_D$-alanine ligase, *Xanthomonas*, structuce-based virtual screening, inhibitor

References

[1] Lee et al., "The genome sequence of Xanthomonas oryzae pathovar oryzae KACC10331, the bacterial blight pathogen of rice." Nucleic Acids Res Vol. 33, (2005), pp 577-586
[2] Fan C., Moews P.C., Walsh C.T., and Knox J.R. "Vancomycin Resistance: Structure of D-Alanine:D-Alanine Ligase at 2.3 Å Resolution", Science, Vol. 266, (1994), pp 439-443.

MS10-P15

Structure based design and synthesis of NAmPRTase inhibitors as anticancer agent

Hyung-Seop Youn, Jung-Gyu Lee, Jun Yop An, Kyoung Ryoung Park, Woo Lai San, Youngjin Lee, Won Ju Jeong, Hyun You, Isak Im, Man-Ho Bae, Yong-Chul Kim, and Soo Hyun Eom

Department of Life Science, Gwangju Institute of Science and Technology, Gwangju 500-712, Republic of Korea
E-mail: michaelmyers@gist.ac.kr

Visfatin [pre-B-cell colony-enhancing factor 1 (PBEF) / nicotinamide phosphoribosyltransferase (NAmPRTase)] plays a pivotal role for salvage pathway of nicotinamide adenine dinucleotide (NAD^+) biosynthesis. NAmPRTase has been an attractive target for anticancer agents that induce apoptosis of tumor cells via declining plasma NAD^+ level. In this regards, the small molecule inhibitor FK866 has synthesized and is in Phase II clinical trials at present. In an effort to improve the pharmacokinetic properties of FK866, here we report cell-based and inhibitory activities of structural analogues of FK866 against human NAmPRTase using cell viability and HPLC assay. We also describe structural features of 7, which contains pyrrole group instead of pyridine ring and showed best inhibitory activity in complex with human NAmPRTase. The structure and inhibitory activities indicate that pyridine ring of FK866 is the most effective moiety among various FK866-based inhibitors and there are some possibilities of modification of benzopiperidine group or adding ionic moieties into pyridine ring. Our studies suggest a new strategy for the development of new anticancer agents.

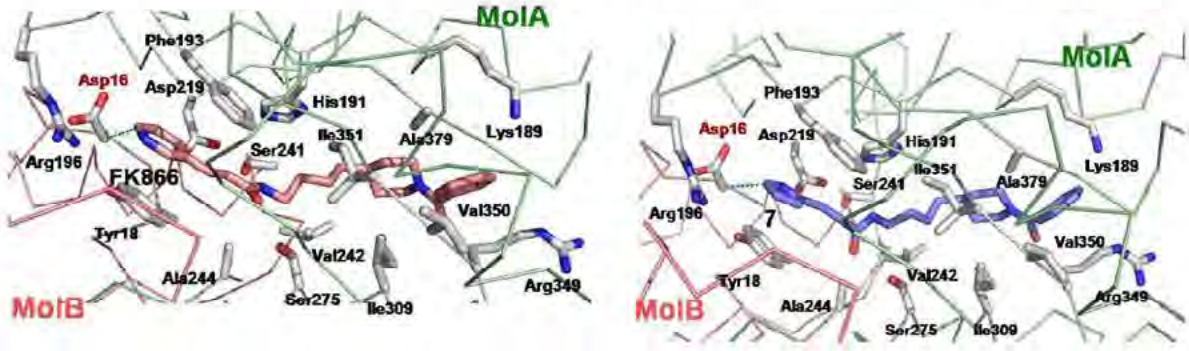

MS10-P16

The structural and pharmacological studies of a dimeric acetylcholine binding protein

Ching-I Anderson Wang, Vu Bach and Richard Lewis

Institute for Molecular Bioscience, the University of Queensland, St. Lucia, Brisbane QLD 4072, Australia
E-mail: a.wang@imb.uq.edu.au

The crystal structures of moluscan acetylcholine binding protein (AChBP) from the snails Lymnaea stagnalis[1] and Aplysia californica[2] are structurally and functionally homologous to the pentameric ligand binding domain of nicotinic acetylcholine receptors (nAChRs). α-Conotoxins isolated from the venom of predatory cone snails have proven to be highly selective inhibitors of specific nAChRs subtypes as well as AChBP. The co-crystal structures of AChBP with α-conotoxins reveal ligand-receptor interactions at binding site between subunits of AChBP [2-5]. Thus these novel venom peptides are valuable probes for nAChR subtype structure-function and the mechanisms of ligand interaction. We have expressed and isolated AChBP in a dimeric form comprising two AChBP subunits instead of five found for the endogenous pentameric state. Interestingly, using a high throughput radioligand binding assay we identified that dimeric AChBP had two distinct binding modes in a ~1:1 ratio. One mode showed affinity characteristic of the pentameric form and a second high affinity interaction with 2–3 orders of magnitude enhanced affinity across a range of peptide toxin inhibitors. We hypothesise that the two subunits that comprising the ligand binding site of dimeric AChBP can exist in two states that maximises ligand-receptor interactions at the high affinity orientation. Dimeric AChBP provides a novel high affinity target that will allow the isolation of low abundance conotoxins from crude venoms not easily detected using conventional assays. In order to study interactions at the high affinity dimeric AChBP conformation, we have collected X-ray diffraction data of the native AChBP dimer at a resolution of 2.6Å and compared this structure with the pentameic form. These results have implications for drug design and nAChR activation mechanisms.

References

[1] Brejc, K.; van Dijk, W. J.; Klaassen, R. V.; Schuurmans, M.; van der Oost, J.; Smit, A. B.; Sixma, T. K. Crystal structure of an ACh-binding protein reveals the ligand-binding domain of nicotinic receptors. Nature 2001, 411, 269-276.

[2] Celie, P. H. N.; Kasheverov, I. E.; Mordvintsev, D. Y.; Hogg, R. C.; van Nierop, P.; van Elk, R.; van Rossum-Fikkert, S. E.; Zhmak, M. N.; Bertrand, D.; Tsetlin, V.; Sixma, T. K.; Smit, A. B. Crystal structure of nicotinic acetylcholine receptor homolog AChBP in complex with an alpha-conotoxin PnIA variant. Nature Structural & Molecular Biology 2005, 12, 582-588.

[3] Ulens, C.; Hogg, R. C.; Celie, P. H.; Bertrand, D.; Tsetlin, V.; Smit, A. B.; Sixma, T. K. Structural determinants of selective alpha-conotoxin binding to a nicotinic acetylcholine receptor homolog AChBP. Proceedings of the National Academy of Sciences of the United States of America 2006, 103, 3615-20.

[4] Hansen, S. B.; Sulzenbacher, G.; Huxford, T.; Marchot, P.; Taylor, P.; Bourne, Y. Structures of Aplysia AChBP complexes with nicotinic agonists and antagonists reveal distinctive binding interfaces and conformations. The EMBO journal 2005, 24, 3635-46.

[5] Dutertre, S.; Ulens, C.; Buttner, R.; Fish, A.; van Elk, R.; Kendel, Y.; Hopping, G; Alewood, P. F.; Schroeder, C.; Nicke, A.; Smit, A. B.; Sixma, T. K.; Lewis, R. J. AChBP-targeted alpha-conotoxin correlates distinct binding orientations with nAChR subtype selectivity. Embo Journal 2007, 26, 3858-3867

MS10-P17

Cloning, expression, crystallization and preliminary X-ray crystallographic analysis of HrcN – an inner membrane ATPase from *Xanthomonas oryzae* pv. *oryzae*

Viet Tan Pham[1], Yeh-Jin Ahn[2], Lin-woo Kang[1]

[1]*Department of Advanced Technology Fusion, Konkuk University, Hwayang dong, Gwangjin-gu, Seoul 143-701, Korea*
[2]*Major in Life Science, College of Natural Sciences, Sangmyung University, 7 Hongji-dong, Jongno-gu, Seoul 110-743, Korea*

E-mail: ptviet79@gmail.com

The type III protein secretion system (TTSS) is a complex organelle in the envelope of many Gram-negative bacteria, it delivers potentially hundreds of structurally diverse bacterial virulence proteins into plant and animal cells to modulate host cellular functions. In *Xanthomonas oryzae* pv. *oryzae* (Xoo) - causes bacterial blight in rice, which is one of the most devastating diseases in rice-cultivating countries – the *Xoo0091 (HrcN)* gene coding for an inner membrane ATPase which hydrolyzes ATP. The conversion of ATP to ADP provides energy for TTSS complex. The *Xoo0091* (*HrcN*) sequence analysis revealed an open reading frame of 1329bp, capable of encoding a polypeptide of 442 amino acid residues with a calculated molecular mass of 47,684Da. This gene was overexpressed in *E.coli* BL21(DE3) and the protein was purified as an active soluble form using Ni-NTA affinity chromatography. The HrcN enzyme was being crystallized in order to elucidate its three-dimensional structure. The results will elucidate the molecular basis of the enzymatic reaction mechanism of HrcN enzyme and will be useful for the design of a potential antibacterial drug against Xoo..

References

[1] Daniela Buttner and ShengYang He, "Type III Protein Secretion in Plant Pathogenic Bacteria", *Plant Physiology*, Vol. 150, (August 2009), pp.1656–1664.
[2] J. Koolman, K. H. Roehm, "Color Atlas of Biochemistry", 2nd edition, Thieme, 2005.
[3] Otwinowski,Z. and Minor, W., "*Methods Enzymol*". 277, (1997), pp. 307–326.
[4] Payne, D. J., Gwynn, M. N., Holmes, D. J. and Rosenberg, M., "*Methods Mol. Biol*". 266, (2004), pp. 231–259.
[5] Sheng Yang He, Kinya Nomura and Thomas S. Whittam, "Type III protein secretion mechanism in mammalian and plant pathogen", *Biochimica et Biophysica Acta*. 1694, (2004), pp. 181–206.
[6] Summers, R. G., Ali, A., Shen, B., Wessel, W. A. and Hutchinson, C. R., "*Biochemistry*". 34, (1995), pp. 9389–9402.

MS10-P18

Molecular basis for recognition of paired immunoglobulin like type2 receptor (PILR) alpha to glycoprotein B (gB) of herpes simplex virus-1 (HSV-1)

OSE Toyoyuki[1], YAMAGUCHI Munechika[2], Jing Wang[3], Kimiko Kuroki[1,2], Shigekazu Tabata[2], Nobuo Maita[2], Seiko Nakamura[2], Mizuho Kajikawa[2], Takeshi Satoh[3], Hisashi Arase[3,4,5], Katsumi Maenaka[1,2,5]

[1]*Faculty of Pharmaceutical Sciences, Hokkaido University*
[2]*Medical Institute of Bioregulation, Kyushu University*
[3]*Research Institute for Microbial Diseases, Osaka University*
[4]*WPI Immunology Frontier Research Center, Osaka University*
[5]*CREST, Japan Science and Technology Agency, Japan*
E-mail: ose@pharm.hokudai.ac.jp

Human Paired Immunoglobulin (Ig) Like type2 Receptors (PILRs) consist of inhibitory (PILR〈) and activating (PILR®) forms with similar extracellular regions, typical for paired receptor families. Recently, human PILRα has been identified as an entry receptor for the surface protein of herpes simplex virus-1 (HSV-1), glycoprotein B (gB), which is a prerequisite for the viral entry. To date, the molecular basis for the PILRα-gB recognition has been poorly understood. We successfully crystallized the extracellular region of human PILRα and determined the 1.4-Å-resolution structure using the iodide—anion derivative crystals by single anomalous dispersion (SAD) method. The structure showed some topological similarity with the Sialic acid binding immunoglobulin like lectin (Siglec) family recognizing a sialic acid, but the putative sugar binding site is conformationally distinctive. Based on this result, the PILRα-gB complex model was constructed. Using *in vitro* binding assay of refolded PILRα protein, the mutagenesis study focusing on the putative gB binding site on PILRα was performed. The result revealed that Arg126, corresponding to the essential R of Siglecs responsible for a sialic acid recognition, has remarkable role in the gB recognition. Furthermore, it was found that the large area around Arg126 is also important for the binding. These results suggested that PILRα harbors a new mode of spontaneous recognition with a sialylated O-glycan and its attached peptide. The PILRα-gB complex has been successfully crystallized and structure determination is in progress. The detail of the interaction between PILRα and gB will be discussed.

MS10-P19

AraC transcription regulator in *Bacillus cereus*

Mi Seul Park[1] and Byung Woo Han[1]

[1]*Department of pharmacy, College of Pharmacy, Seoul National University, Seoul 151-742, Korea*
E-mail: pms323@hotmil.com

Bacillus cereus is in charge of a minority of foodborne illnesses, resulting in severe nausea, vomiting and diarrhea. *Bacillus* foodborne illnesses occur due to survival of the bacterial endospores when food is inappropriately cooked. Transcriptional regulators of the AraC family are widespread among bacteria and regulate genes with diverse functions, ranging from carbon metabolism to stress responses to virulence. AraC family transcriptional regulator found in *Vibrio cholera* regulates toxin-related proteins such as Toxin-coregulated pilus(TCP) and Cholera toxin(CT). In *Bacillus cereus*, AraC family transcriptional regulator is also very important in controlling expression of toxin gene which causes foodborne illnesses. Here we report the crystallographic study of AraC family protein in *B. cereus*.

References

[1] Kotiranta A, Lounatmaa K, Haapasalo M. "Epidemiology and pathogenesis of *Bacillus cereus* f ections". *Microbes Infect* **2** (2): 189–98. (2000)

[2] Turnbull PCB. "*Bacillus*. In: *Baron's Medical Microbiology* ." 4th edition, Barron S et al. eds. Univ of Texas Medical Branch. (1996).

[3] Cristiane C. Frota, K. G. Papavinasasundaram, Elaine O. Davis, M. Joseph Colston "The AraC Family Transcriptional Regulator Rv1931c Plays a Role in the Virulence of *Mycobacterium tuberculosis*." *Infect Immun.*; 72(9): 5483–54869. (2004)

MS10-P20

Crystal structures of murine norovirus RNA-dependent RNA polymerase and its complex with 5-fluorouracil and ribavirin

Intekhab Alam, Ji-Hye Lee, and Kyung Hyun Kim

Department of Biotechnology & Bioinformatics, Korea University, Chungnam 339-700, Korea
E-mail: intekhab@korea.ac.kr

Norovirus, a member of *Caliciviridae* family is the leading cause of viral gastroenteritis worldwide. Bovine and murine norovirus (MNV) are the common infective forms found in animals. The lack of a cellular system to cultivate this virus is the main bottleneck in understanding its replication. Murine norovirus is the only strain of this species that can be propagated in cultured cells. Crystal structures of recombinant RNA dependent RNA polymerase (RdRp) from MNV and its complex with 5-fluorouracil and ribavirin has been determined to 2.5-2.8 Å resolutions. The overall structure has typically similar right hand fold as that of RNA polymerases. Human and MNV RdRp structures with the sequence identity of 59% show essentially identical conformations with r.m.s.d of 1.0 Å. Owing to the high structural similarity of MNV RdRp with other polymerases, our results can successfully be exploited for the design of inhibitors targeting viral RNA polymerases.

References

[1] Rohayem, J., Robel, I., Jager, K., Scheffler, U.&Rudolph, W. Protein-primed and de novo initiation of RNA synthesis by norovirus 3Dpol. J Virol 80, (2006b). pp 7060–7069

[2] Ferrer-Orta, C., Arias, A., Perez-Luque, R., Escarmis,C., Domingo, E. & Verdaguer, N. Sequential structures provide insights into the fidelity of RNA replication. Proc. Natl Acad. Sci. USA, 104, (2007), pp 9463–9468.

[3] Zamyatkin, D. F., Parra, F.,Machin, A., Grochulski, P. & Ng, K. K. Binding of 2′-Amino-2′-Deoxycytidine-5′-Triphosphate to Norovirus Polymerase Induces Rearrangement of the Active Site.J.Biol.Chem. 390, (2008) pp10-16

MS10-P21

Molecular characterization of human influenza virus hemagglutinin

Ki Joon Cho[1], Ji-Hye Lee[1], Seokha Kang[1], Yi Ho Park[1], Jun Young Lee[1], Taslima Gani Khan[1], Joo-Yeon Lee[2], Hee-Bok Oh[2], Chun Kang[2], and Kyung Hyun Kim[1]

[1]*Department of Biotechnology and Bioinformatics, Korea University, Chungnam 339-700, Korea*
[2]*Center for Infectious Diseases, Korea Centers for Disease Control and prevention, Seoul 122-701, Korea*
E-mail: c-azna@korea.ac.kr

Influenza is one of the most important respiratory infectious diseases causing seasonal epidemics or pandemics. A surface glycoprotein hemagglutinin (HA) of influenza virus is of major importance in the primary target of immune response and the primary component of influenza vaccine. Cleavage of the precursor protein HA0 into the subunits HA1 and HA2 by cellular proteases is indispensable for influenza virus infectivity, activating the membrane fusion potential. In this study, individual HA genes from seasonal H1N1 (A/Solomon Island/03/2006) and H3N2 (A/Brisbane/10/2007) vaccine strains and a 2009 pandemic H1N1 (A/Korea/01/2009) isolate were constructed. The recombinant HA proteins were expressed using a baculovirus expression system and purified, which were found to be effective for structural studies. The HA proteins were characterized for thermal stability and proteolytic cleavage which was independent of glycosylation. The influenza A virus HA proteins demonstrated different susceptibility to proteolytic cleavage by proteases and different thermal stability. The crystal structures of both seasonal and pandemic H1N1 HA proteins are compared.

References

[1] Stevens J., Corper A. L., Basler C. F. Taubenberger J. K. Pales P. and Wilson I. A., Structure of the Uncleaved Human H1 Hemagglutinin from the Extinct 1918 Influenza Virus, *Science*, Vol. 303, (2001) pp1866-1870.
[2] Russell R. J., Kerry P. S., Stevens D. J., Steinhauer D. A., Martin S. R., Gamblin S. J. and Skehel J., Structure of Influenza Hemagglutinin in Complex with an Inhibitor of Membrane Fusion, *Proc. Natl. Acad. Sci. USA*, Vol. 105, No. 46, (2008), pp 17736-17741.
[3] Xu R., Ekiert, D. C., Krause J. C. Hai R., Crowe Jr. J. E. and Wilson I. A. Structural Basis of Preexisting Immunity to the 2009 H1N1 Pandemic Influenza Virus, *Science*, Vol. 328, (2010), pp 357-360.

MS10-P22

Comparison of the structures of horse spleen and *Helicobacter pylori* ferritins for iron uptake

Yi-ho Park, Ki Joon Cho and Kyung Hyun Kim

Department of Biotechnology & Bioinformatics, College of Science & Technology, Korea University, Chungnam 339-700, Korea
E-mail: ballanshe@naver.com

Iron is essential for the survival of almost all living organisms and proteins involved in iron metabolism are suggested as the major determinants of virulence. Among those proteins, ferritin plays a role in storage of up to 4,500 irons inside the protein shell. We report here the comparison of the structures of Horse spleen ferritin (HoSF) and *Helicobacter pylori* ferritin (Hpf), which reveals conformational changes for iron uptake. Eukaryotic ferritins are assembled from two types of polypeptide chains (H and L chains) which provide different functions, whereas Hpf has only H (heavy) type of chain and catalyses the first step in iron storage, the oxidation of iron(II). The crystal structures of both ferritins have been solved at resolutions of 1.3-2.1 Å and 2.1-2.6Å as low-iron bound and high-iron bound states, respectively. As the iron content within the protein shell increased, conformational changes have been observed at the 3-fold and 4-fold symmetry channel and nucleation site of proteins. The conformational changes at different iron concentrations show structural evidence of the translocation and binding of Fe ions, which characterizes the difference between bacterial and mammalian ferritins.

References

[1] Cho K. J, Shin H. J, Lee J. H, Kim K. J, Park S, Lee Y. M, Lee C. J, Park S. S, and Kim K. H., "The Crystal Structure of Ferritin from *Helicobacter pylori* Reveals Unusual Conformational Changes for Iron Uptake", *J. Mol. Biol.,* (2009) 390, 83-98

[2] Paul D. H, Stephen J. Y, Alisdair R. F, David M. L, Peter J. A, David W. R, and Pauline M. H., "Comparison of the Three-dimensional Structures of Recombinant Human H and Horse L Ferritins at High Resolution", *J. Mol. Biol.,* (1997) 268, 424-448

MS10-P23

Structural study of aprotinin complexed with a pentapeptide, a conserved sequence responsible for Aβ aggregation

Taslima Gani Khan, Ji-Hye Lee, and Kyung Hyun Kim

Department of Biotechnology & Bioinformatics, Korea University, Chungnam 339-700, Korea
E-mail: taslima@korea.ac.kr

Amyloidosis refers to a variety of conditions in which amyloid proteins are abnormally deposited in organs and/or tissues, of which amyloid A amyloidosis and Alzheimer's Disease are most common. In a previous study of crystal structure of aprotinin (kunitz protease inhibitor) with sucrose octasulfate, Ser-Phe-Phe (SFF) was accidently observed at the monomer-monomer interface, which was further confirmed by cocrystallization. SFF is a conserved sequence found in the N-terminal amyloidogenic region of both human and bovine serum amyloid A (SAA). Likewise, amyloid beta responsible for Alzheimer's disease has conserved hydrophobic core residues, which are crucial for the formation of β-sheet structures. Amyloid precursor protein (APP) also has KPI domain in the N-terminus which has been reported to bind with Aβ fibrils. We therefore gained interest in the structural study of interaction between KPI and Aβ. Crystal structures of aprotinin complexed with a pentapeptide have been determined at 2.6 Å resolution, where the peptide was observed at the monomer-monomer interface in a decameric form of aprotinin. A change in crystal packing with that of native aprotinin is also observed.

References

[1] Jerry P. Melchor and William E. Van Nostrand., "Fibrillar Amyloid b-Protein Mediates the Pathologic Accumulation of Its Secreted Precursor in Human Cerebrovascular Smooth Muscle Cells", *The journal of biological chemistry*, Vol. 275, No. 13, (2000), pp 9782-9791.

[2] Joyce W. Lustbader, *et al.,* "ABAD Directly Links Aß to Mitochondrial Toxicity in Alzheimer's Disease", *Science*, Vol. 304, (2004), pp 448-452.

MS10-P24

Structural basis of the interaction between FAF1 and p97/VCP

Wonchull Kang, Ho Yeon Lee, Men Thi Ngoc Nguyen, Le Thi My Le, and Jin Kuk Yang

Department of Chemistry, College of Natural Sciences, Soongsil University, Seoul 156-743, Korea
E-mail: wonchullk@gmail.com

Fas-associated factor 1 (FAF1) is a multi-functional pro-apoptotic protein involved in Fas-mediated apoptosis, NF-κB signaling, and the ubiquitin-proteasome pathway. Relevant to the ubiquitin-proteasome pathway, FAF1 binds to the N domain of p97/VCP, a molecular chaperone acting in complex with the proteasome, through its C-terminal UBX domain and inhibits the proteasomal protein degradation process. In an effort to elucidate the structural basis of FAF1 function on modulating p97/VCP activity related to the proteasomal protein degradation, we have solved the crystal structure of FAF1 UBX domain in complex with p97/VCP N domain at 2.2 Å resolution. The crystal structure revealed a novel feature of the UBX domain Phe-Pro motif which is the previously known conserved signature of the p97/VCP-binding UBX domains and is actually the key part in the interface. In our high resolution crystal structure of FAF1 UBX – p97/VCP N, the peptide bond between the two key residues, Phe and Pro, adopts a *cis* conformation. In contrast, the peptide between the two key residues has been commonly observed as in the *trans* conformation in all the previously reported structures of UBX domains: the moderate resolution (2.9 Å) crystal structure of p47 UBX – p97/VCP ND1, the NMR structure of p47 UBX, and the NMR structure of FAF1 UBX.

References

[1] Vij, N., " AAA ATPase p97/VCP: cellular functions, disease and therapeutic potential", J. Cell. Mol. Med. Vol. 12, (2008), pp 2511-2518.
[2] Dougan, D. A., Mogk, A., Zeth, K., Turgay, K., and Bukau, B., "AAA+ proteins and substrate recognition, it all depends on their partner in crime", FEBS Lett. Vol. 529, (2002), pp 6-10
[3] Song, E. J., Yim, S. H., Kim, E., Kim, N. S., and Lee, K. J., "Human Fas-associated factor 1, interacting with ubiquitinated proteins and valosin-containing protein, is involved in the ubiquitin-proteosome pathway", Mol. Cell. Biol. Vol. 25, (2005), pp 2511-2524

MS10-P25

Crystal structure of thermostable direct hemolysin from *Vibrio parahaemolyticus*

Hiroshi Hashimoto1, Kumiko Nakahira2, Tsutomu Yamane1, Takashi Fukui2, Kiyohisa Ohnishi2, Toshiyuki Shimizu1, Takeshi Honda3, Mamoru Sato1, Mitsunori Ikeguchi1, Itaru Yanagihara2

[1]*Graduate School of Nanobioscience, Yokohama City University, 1-7-29 Suehiro-cho, Tsurumi-ku, Yokohama 230-0045, Japan*
[2]*Department of Developmental Medicine, Osaka Medical Center for Maternal and Child Health, 840 Murodo-cho, Izumi City, Osaka 594-1101, Japan*
[3]*Department of Bacterial Infections, Research Institute for Microbial Diseases, Osaka University, 3-1 Yamadaoka, Suita, Osaka 565-0871, Japan*
E-mail: hash@tsurumi.yokohama-cu.ac.jp

Thermostable direct hemolysin (TDH) is a major virulence factor of Vibrio parahaemolyticus that causes pandemic foodborne enterocolitis mediated by seafood. TDH exists as a tetramer in solution, and it possesses extreme hemolytic activity. Crystals of TDH were obtained by vapor diffusion method using lithium sulfate as a precipitant. The crystal belongs to space group I4 with unit-cell parameters a = b = 63.0 and c =83 Å. Diffraction data of native and derivative crystals were collected at beamlines SPring-8 BL41XU and Photon Factory AR NW12A, respectively. The crystal structure of TDH was determined by single isomorphous replacement with anomalous scattering of gold derivative by the program SOLVE/RESOLVE and the structure was refined by the programs CNS and REFMAC.

Here, we present the first crystal structure of the TDH tetramer at 1.5 Å resolution. The TDH protomer adopts a beta-sandwich structure composed of ten beta-strands flanked by two helices. The TDH tetramer forms a central pore with dimensions of 23 Å in diameter and approximately 50 Å in depth. The pi-cation interactions between protomers are involved in the tetramer formation and the tetrameric structure is indispensable for hemolytic activity of TDH. Molecular dynamic simulations suggested that water molecules permeate freely through the central and side channel pores. These findings imply a novel hemolysis mechanism by the pore-forming toxin.

References

[1] Yanagihara I., Nakahira K., Yamane T., Kaieda S., Mayanagi K., Hamada D., Fukui T., Ohnishi K., Kajiyama S., Shimizu T., Sato M., Ikegami T., Ikeguchi M., Honda T., Hashimoto H., "Structure and functional characterization of *Vibrio paraheamolyticus* thermostable direct hemolysin", *J. Biol. Chem.*, Vol. 285, No. 21, (2010), pp 16267-16274.

MS10-P26

Crystal structure of hypothetical protein HP0062 from *Helicobacter pylori*

Ae-Ran Kwon

Department of Herbal Skin Care, College of Herbal Bio-Industry, Daegu Haany University, 290, Yugok-Dong, Gyeongsan-Si, Gyeongsangbuk-Do, 712-715, Korea
E-mail: arkwon@dhu.ac.kr

The HP0062 gene encodes a small acidic protein of 86 amino acids with a theoretical pI of 4.6. The crystal structure of hypothetical protein HP0062 from *Helicobacter pylori* has been determined at 1.65 Å by molecular-replacement method. The crystallographic asymmetric unit contains dimer, in which HP0062 monomer folds into a helix-hairpin-helix structure. The two protomers are primarily held together by extensive hydrophobic interactions in an antiparallel arrangement, forming a four helix bundle. Aromatic residues located at *a* or *g* position in the heptad leucine zipper are not major contributor required for HP0062 dimerization but important for the thermostability of this protein.

MS10-P27

Structural analysis of Toll-like receptor 2-activating lipoprotein from *Vibrio vulnificus*

Sangheon Yu[1], Na Yeon Lee[2], Soon-Jung Park[2] and Sangkee Rhee[1]

[1]*Department of Agricultural Biotechnology, Seoul National University, Seoul 151-921, Korea,* [2]*Department of Environmental Medical Biology and Institute of Tropical Medicine, Yonsei University College of Medicine, Seoul 120-752, Korea*
E-mail: shyu@snu.ac.kr

IlpA, a surface protein of the human pathogen *Vibrio vulnificus*, is the first lipoprotein to be characterized in *Vibrio* spp. as a major immunostimulant. Previously, it was characterized that IlpA was subject to lipidation at its N-terminal cysteine residue. The resulting IlpA then activates Toll-like receptor 2 in human cells, and induces overproduction of proinflammatory cytokines closely associated with septic shock in infected individuals. To identify structural features of IlpA, we determined the crystal structure of IlpA at 2.6 Å resolution. Specifically, IlpA consists of two homologous domains, each with α/β topology, similar to the structure of solute-binding protein which is a component of ATP-binding cassette transporter. In fact, binding of L-methionine was observed in the pocket between the two domains, suggesting that IlpA is an L-methionine-binding protein. The structural features of IlpA in this study, along with the immunological properties of IlpA identified previously and other solute-binding proteins, suggest that solute-binding lipoproteins of ATP-binding cassette transporter present at the bacterial cell surface could serve as pathogen-associated molecular patterns to Toll-like receptor 2, causing host immune responses against infection.

Reference

[1] Goo SY., Han YS., Kim WH., Lee KH. and Park SJ., "*Vibrio vulnificus* IlpA-induced cytokine production is mediated by Toll-like receptor 2", *J. Biol. Chem.,* 282**,** (2001), 27647-27658

MS10-P28

Structure of EvpC: A type six secretion system protein from *Edwardsiella tarda*

J. Sivaraman, Chacko Jobichen, Lissa Joseph, Yu-Keung Mok

Department of Biological Sciences, 14 Science Drive 4, National University of Singapore, Singapore 117543
E-mail : dbsjayar@nus.edu.sg

Type six secretion system (T6SS) is a recently identified secretion system used by gram-negative bacteria to inject virulence protein into the host cell to effect the infection (Cascales, 2008; Filloux et al., 2008; Bingle et al., 2008; Pukatzi et al., 2009) . In Edwardsiella tarda the T6SS cluster is named as EVP and it contains 16 different genes which are classified into intracellular apparatus (non-secreted) proteins, secreted proteins and a group of proteins not essential for T6SS. Secretion of Hcp1 (an EvpC homolog) is an essential character of functional T6SS. Here we report the crystal structure of EvpC an Hcp homologue from Edwardsiella tarda refined upto 2.8 Å resolution. EvpC has a loose β-barrel domain with extended loops. The β-barrel consists of 11 anti-parallel β-strands with an α helix located on one side. EvpC can form a hexameric ring with a diameter of 40 Å which is capable of transporting small proteins and ligands. Analytical ultra centrifugation studies on the oligomerisation of this protein showed that EvpC can exist as a dimer and hexamer in solution. Further our structure based mutational studies has identified the critical residues which are important for the function of this protein.

References

[1] Cascales, E. (2008). The type VI secretion toolkit. EMBO Rep 9, 735-741.
[2] Filloux, A., Hachani, A., and Bleves, S. (2008). The bacterial type VI secretion machine: yet another player for protein transport across membranes. Microbiology 154, 1570-1583.
[3] Bingle, L., Bailey, C., and Pallen, M. (2008). Type VI secretion: a beginner's guide. Curr Opin Microbiol 11, 3-8.
[4] Pukatzki, S., McAuley, S., and Miyata, S. (2009). The type VI secretion system: translocation of effectors and effector-domains. Curr Opin Microbiol 12, 11-17.

MS10-P29

In-silico search for putative GmhA binding compounds

Mi-Sun Kim[1], Areum Lim[1], Sarinna Tumapa[2], Sharon peacock[2,3] and Dong Hae Shin[1]

[1]*College of Pharmacy, Ewha Womans University, Seoul 120-750, Korea*
[2]*Faculty of Tropical Medicine, Mahidol University, Bangkok, Thailand*
[3]*Centre for Clinical Vaccinology and Tropical Medicine, Nuffield Department of Clinical Medicine, University of Oxford, Churchill Hospital, Oxford, UK*
E-mail: dhshin55@ewha.ac.kr

Sedoheptulose-7-phosphate isomerase (GmhA) converts D-sedoheptulose-7-phosphate to D,D-heptose 7-phosphate [1]. This is the first step of the biosynthesis pathway of NDP-heptose responsible for a pleiotropic phenotype. This biosynthesis pathway is the target for inhibitors increasing the membrane permeability of Gram-negative pathogens or adjuvants synergistically working with known antibiotics. *Burkholderia pseudomallei* is the causative agent of melioidosis, a serious invasive disease of animals and humans in tropical and subtropical areas. GmhA from *B. pseudomallei* is the antibiotics adjuvant target for melioidosis. The crystal of this enzyme has been solved at 1.9 Å resolution. There is an active pocket where a putative metal binding site is located. To find inhibitors of GmhA, *in-silico* screening with several chemical data bases such as a drug library has been performed. Tens of thousands of chemical compounds have been tested. A number of putative binding compounds were found using FlexX and Surflex-Dock included in the SYBYL software package. Characteristics of these compounds were surveyed and classified to identify binding properties with GmhA.

References

[1] Eidels, L. and Osborn, M. J., "Phosphoheptose isomerase, first enzyme in the biosynthesis of aldoheptose in *Salmonella typhimurium*", *J. Biol. Chem.,* 249, (1974), pp 5642–5648.

MS10-P30

2,3-difluoro-sialic acids as inactivators of influenza neuraminidases

Victor Streltsov[1], Susan Barrett[1], Pat Pilling[1], Stefan B. Hader[2], Patricia Marcé[2], Andrew G. Watts[2] and Jennifer McKimm-Breschkin[1]

[1]*CSIRO, Materials Science & Engineering, 343 Royal Parade, Parkville, 3052, Australia*
[2]*Department of Pharmacy and Pharmacology, University of Bath, BA2 7AY, Bath, United Kingdom*
E-mail: victor.streltsov@csiro.au

Influenza neuraminidase is an enzyme required by the virus to cleave cell-surface sialic acid receptor molecules, a process which facilitates the effective release of newly formed viral particles from the surface of infected cells. As such, inhibitors of influenza neuraminidase such as zanamivir (Relenza®) and oseltamivir (Tamiflu®) are effective for the treatment of influenza. These compounds act as competitive inhibitors and were designed as 'transition-state analogues' and mimic the conformation of DANA [1], itself a potent inhibitor of influenza neuraminidases (K_M 4 μM). Significant drug resistance towards the front line anti-influenza drug oseltamivir has recently been reported, emphasising the need to gain further insight into the mechanisms of the reaction catalysed by the influenza neuraminidase. [2,3].

It has recently been shown that 2,3-difluoro derivatives (fluorine atoms at positions C2 and C3) of sialic acid inhibit the sialidases from *T. cruzi*, *T. rangeli* and *C. perfringens* by forming a stable covalent intermediate [e.g. 4]. These inactivators are anticipated to be less susceptible to drug induced resistance as they target essential catalytic amino acids [5]. However, individual hydrogen-bonding interactions formed between these inactivators and the neuraminidase in both the Michaelis complex and at the transition state remain unclear. We have studied crystal structures of neuraminidase N9 in complex with a series of newly synthesized 2,3-difluoro-*N*-acetyl-neuraminic acid derivatives to probe the importance of individual hydrogen-bonding interactions towards transition-state stabilisation and therefore inhibition of influenza neuraminidases. The X-ray structure showed a clear rotation of the COOH group and loss of fluorine from C2. The ligand sites are populated by the mixtures of 3-fluoro-compounds covalently linked to Tyr406 and theirs defluorinated versions.

References

[1] von Itzstein M., Wu W.-Y., Kok G. B., Pegg M. S., Dyason J. C., Jin B., Phan T. V., Smythe M. L., White H. F., Oliver S. W., Colman P. M., Varghese J. N., Ryan D. M., Wood J. M., Bethell R. C., Hotham V. J., Cameron J. M. and Penn C. R. "Rational design of potent sialidase-based inhibitors of influenza virus replication", *Nature*, 363, (1993), pp 418-423.

[2] Kiso M., Mitamura K., Sakai-Tagawa Y., Shiraishi K., Kawakami C., Kimura K., Hayden F. G., Sugaya N. and Kawaoka Y. "Resistant influenza A viruses in children treated with oseltamivir: descriptive study", *Lancet*, 364, (2004), pp 759-765.

[3] Dharan N. J., Gubareva L. V., Meyer J. J., Okomo-Adhiambo M., McClinton R. C., Marshall S. A., St.George K., Epperson S., Brammer L., Klimov A. I., Bresee J. S., Fry A.M. "Infections with oseltamivir-resistant influenza A(H1N1) virus in the United States". *JAMA*, 301(10), (2009), pp 1034-1041.

[4] Watts, A. G.; Oppezzo, P.; Withers, S. G.; Alzari, P. M.; Buschiazzo, A. J. "Structural and kinetic analysis of two covalent sialosyl-enzyme intermediates on *Trypanosoma rangeli* sialidase", *J. Biol. Chem.*, 281, (2006), pp 4149-4155.

[5] Watts A. G., Withers S. G. "The synthesis of some mechanistic probes for sialic acid processing enzymes and the labeling of a sialidase from *Trypanosoma rangeli*", *Can. J. Chem.*, 82, (2004), pp 1581-1588.

MS10-P31

Crystal structure of GmhA from *Burkholderia pseudomallei*, the causative agent of melioidosis

Mi-Sun Kim[1], Areum Lim[1], Sarinna Tumapa[2], Sharon peacock[2,3] and Dong Hae Shin[1]

[1]*College of Pharmacy, Ewha Womans University, Seoul 120-750, Korea*
[2]*Faculty of Tropical Medicine, Mahidol University, Bangkok, Thailand*
[3]*Centre for Clinical Vaccinology and Tropical Medicine, Nuffield Department of Clinical Medicine, University of Oxford, Churchill Hospital, Oxford, UK*
E-mail: dhshin55@ewha.ac.kr

GmhA from *B. pseudomallei* is the antibiotics adjuvant target for melioidosis. This enzyme is invoved in the first step of heptose biosynthesis pathway [1]. Heptoses are found in the surface polysaccharides of most bacteria, contributing to structures that are essential for virulence and antibiotic resistance. This protein has been cloned, expressed, purified, and crystallized. The synchrotron data were collected to 1.9 Å. The structure was solved by molecular replacement. GmhA crystals grew in the space group $P2_12_12_1$ with four molecules of GmhA in the asymmetric unit. Each GmhA monomer consists of a central five-stranded parallel β-sheet, flanked by five alpha helices, forming a three-layered HβH sandwich architecture. The overall fold is quite similar to the flavodoxin-type nucleotide-binding motif. This enzyme contains a putative metal binding site at the center of its active site. Four of these residues, H64, E68, Q175, and H183, may be required to coordinate a metal ion. Interestingly, a closed form of the enzyme looks catalytically relevant unlike previously reported structures where apo-forms have a characteristic open conformation. A revised mechanism for the action of GmhA is suggested on the basis of this structure.

References

[1] Kneidinger B., Marolda C., Graninger M., Zamyatina A., McArthur F., Kosma P., Valvano M.A. and Messner P., "Biosynthesis pathway of ADP-L-glycero-beta-D-manno-heptose in *Escherichia coli*", *J. Bacteriol.*, 184, (2002), pp 363-369.

MS10-P32

ABIN-1 senses linear ubiquitin chains: structural and biophysical insights

Simin Rahighi[1], Fumiyo Ikeda[2], Masato Kawasaki[1], Ryuichi Kato[1], Ivan dikic[2], Soichi Wakatsuki[1]

[1] *Structural Biology Research Center, Photon Factory, Institute of Materials Structure Science, High Energy Accelerator Research Organization (KEK), Tsukuba, Ibaraki 305-0801, Japan*
[2] *Institute of Biochemistry II and Cluster of Excellence Frankfurt, Goethe University School of Medicine, Theodor-Stern-Kai 7, D-60590 Frankfurt (Main), Germany*
E-mail : Simin@post.kek.jp

The Nuclear Factor-κB (NF-κB) transcription factors are key regulators of numerous basic cellular processes, among them innate immunity, inflammation and malignant transformations. However, unrestrained NF-κB activation is associated with several inflammatory diseases. Therefore, formation and activation of these transcription factors must be tightly regulated. ABIN-1 (A20 binding and inhibitor of NF-κB) has been characterized as one of the negative regulators of NF-κB signaling. Although, this protein is known to function by facilitating A20 (ubiquitin editing protein)-mediated de-ubiquitination of NF-κB pathway regulators, more recent studies attribute ABIN-1 negative regulatory activity to its ubiquitin binding feature. ABIN-1 binds ubiquitin through the AHD-2 (ABIN homology domain-2) also called UBAN (ubiquitin binding in ABIN proteins and NEMO) motif. Previously, we showed that NEMO (NF-κB essential modulator) preferentially binds linear ubiquitin chains via its UBAN motif and this specific binding is essential for regulation of the NF-κB signaling pathway. Here, we provide structural and biophysical evidences that ABIN-1 UBAN motif, also, has higher affinity for linear over other types of ubiquitin chains. The x-ray crystal structures of ABIN-1 in the apo form and in complex with one and two linear diubiquitins are solved in this study. ABIN-1 in the apo form adopts a coiled-coil, homo-dimer structure which provides two symmetrical binding sites for linear diubiquitins. Interestingly, depending on the relative concentration of the two proteins different binding stoichimetries are observed in the crystals. The concentration-dependency of the complex formation by ABIN-1 and linear diubiquitin chains is further examined by ITC (Isothermal Titration Calorimetry) experiments. ABIN-1 UBAN domain recognizes the canonical Ile44 surface and the C-terminal tail of the distal and the newly characterized surface, adjacent to the hydrophobic patch, on proximal ubiquitins. Mutations on the ubiquitin binding surface in ABIN-1 UBAN abolished its inhibitory effects on NF-κB activation. These data explain the specificity of ABIN-1 protein for linear ubiquitin chains and in regulation of NF-κB activation.

MS10-P33

HIV-1 Protease complexed to natural oligopeptide substrates

Amit Das[1], S.C.Bihani[1], V. Prashar[1], J.-L. Ferrer [2] and M.V.Hosur[1]

[1]*Protein Crystallography Section, Solid State Physics Division, Bhabha Atomic Research Centre, Trombay, Mumbai-400085, India*
[2]*LCCP/GSY, Institute de Biologie Structurale, J.-P. Ebel CEA-CNRS-UJF, 41, rue Jules Horowitz, F-380 27 Grenoble Cedex 1, France*
E-mail: amitdas@barc.gov.in, hosur@barc.gov.in

The Human Immunodeficiency Virus type 1 protease (HIV-1 PR) is a virally encoded symmetric homodimeric aspartyl protease that cleaves a series of nine substrate peptide bonds in the viral *gag* and *gag-pol* polyproteins, resulting in functional enzymes and structural proteins, essential for the maturation of the virus. HIV-1 PR is also a rare endopeptidase which can cleave peptides having proline at the cleavage site. Crystal structures of active enzyme and natural substrate(s) complexes are required to understand the mechanism of cleavage to atomic details, which will help in the development of new drugs. We have prepared several complexes of HIV-1 PR with natural oligopeptides and determined high resolution structures of two in-situ substrate/HIV-1 PR complexes, where the peptide bond is transformed to: a tetrahedral intermediate at pH 2.5 [1] and cleaved bi-products at physiological pH 6.2 [2, 3].

In the present study we have complexed HIV-1 PR with a Proline containing substrate (sequence VSFNF*PQITC, * denotes the cleavage site peptide bond) and solved two structures for soaktimes of 24hrs and 72hrs. The data were collected to resolutions 1.74A and 1.0A at ID 14-4 and BM30A beamlines at ESRF. The structures were refined to R-factors 17.9% and 19.2% and R-frees 21.4% and 24.5% respectively. In both complexes, the calculated electron density map suggests the presence of the substrate in active site cavity. The substrate models fitted into the map is interpreted as an in-situ cleaved bi-product complex [NH_2-VSFNF-CO_2H (P product) and NH-PQITC-CO_2H (Q product)]. The Phe residue of the P product is interacting with the outer oxygens of both the catalytic aspartates via hydrogen bonds whereas the Pro residue of the Q product is moved away in both structures. The Pro residue is unable to interact with the catalytic aspartates due to the steric hindrance with its C-delta atom. Contrary to earlier solved complexes, here we find the Q product is the first one to move out of the active site cavity after cleavage in proline containing substrates. The Phe residues superpose within 0.1A whereas the proline residues are separated by more than 1A for 24hrs and 72hrs soaked crystals. The Pro residue interacts with the carboxylate of Phe residue in 24hrs complex but moves further away in the longer soaked complex. Also the carboxylate of the Phe residue moves closer to the catalytic aspartates in the longer soaked complex as compared to the 24hrs soaked complex. These structures reveal the mechanism of cleavage-product release and a different mode of binding for proline containing substrates.

References

[1] Das Amit, Mahale S., Prashar V., Bihani S., Ferrer J.-L. and Hosur M.V., "X-ray snapshot of HIV-1 protease in action: observation of tetrahedral intermediate and its Short Ionic Hydrogen Bond, SIHB with catalytic aspartate", Journal of American Chemical Society, Vol. 132, (2010), pp 6366-6373.
[2] Das Amit, Prashar V., Mahale S., Ferrer J.-L., Serre L. and Hosur M.V., "X-ray structure of insitu HIV-1 protease-product complex: observation of a LBHB between catalytic aspartates", Proceedings of National Academy of Sciences, USA, Vol. 103 , No. 49, (2006), pp 18464-18469.
[3] Bihani S., Das Amit, Prashar V., Ferrer J.-L. and Hosur M.V., "X-ray structure of in-situ HIV-1 protease-product complex", Proteins: Structure, Function and Bioinformatics, Vol. 74, No. 3, (2008), pp 594-602.

MS13-P01

Crystal structure of PPC protein from *Pyrococcus furiosus*

Ji Young Yoon[1], Do Jin Kim[1], Kyoung Hoon Kim[1], Sang Jae Lee[1], Hyoun Sook Kim[1], Jun Young Jang[1], and Se Won Suh[1,2]

[1]*Department of Chemistry, College of Natural Sciences, Seoul National University, Seoul 151-742, Korea*
[2]*Department of Biophysics and Chemical Biology, College of Natural Sciences, Seoul National University, Seoul 151-742, Korea*
E-mail: bandij7@gmail.com

AHL1 (AT-hook Motif and Nucleus Localized protein 1) is a protein localizing at the nuclear matrix and originally identified in *Arabidopsis thaliana*. AHL1 potentially functions as a connection between the nuclear framework and DNA of MAR sequences in interphase nuclei, and covers the chromosomes during mitosis. *A. thaliana* AHL1 (AtAHL1) consists of an AT-hook motif and PPC domain (Plants and Prokaryotes Conserved domain). The AT-hook motif is essential for matrix attachment region(MAR) binding and the hydrophobic region of the PPC is indispensable for nuclear localization. The PPC domain is conserved among AHL1 homologues and also in bacteria and archaea, whereas neither yeasts nor animals has a protein with this domain. The PPC containing proteins in bacteria and Archaea do not have an AT-hook motif. To gain insight into the PPC protein function at the molecular level, we have overexpressed and crystallized PPC protein from *Pyrococcus furiosus*. *Pf*PPC is composed of one α-helix and eight β-strands. In addition, *Pf*PPC forms a trimer. This trimer is maintained by the interactions on the opposite side of the single α-helix in each subunit. Hydrophilic interactions are found in the top and bottom parts, while the hydrophobic interactions are mainly formed in the middle part. Therefore based on our structural study, *Pf*PPC protein has a trimer formation unique to prokaryotes and plants.

References

[1] Fujimoto S., Matsunaga S., Yonemura M., Uchiyama S., Azuma T. and Fukui K., "Identification of a novel plant MAR DNA binding protein localized on chromosomal surfaces.", *Plant Mol Biol.* Vol. 56, No. 2, (2004), pp 225-239.

[2] Lin L., Nakano H,, Nakamura S,, Uchiyama S., Fujimoto S., Matsunaga S., Kobayashi Y., Ohkubo T., Fukui K., "Crystal structure of Pyrococcus horikoshii PPC protein at 1.60 A resolution.", *Proteins.*, Vol. 67, No. 2, (2007), pp 505-507.

MS13-P02

Structural evidence for a dehydrated intermediate in green fluorescent protein chromophore biosynthesis

Sergei Pletnev[1,2], Nadya V. Pletneva[3], Konstantin A. Lukyanov[3], Nadya G. Gurskaya[3], Ekaterina A. Goryacheva[3], Vladimir I. Martynov[3], Alexander Wlodawer[1], Zbigniew Dauter[1] and Vladimir Z. Pletnev[3]

[1]*Macromolecular Crystallography Laboratory, NCI, National Institutes of Health,Argonne, Illinois 60439*
[2]*Basic Research Program, SAIC-Frederick, Argonne, Illinois 60439, USA*
[3]*Shemyakin-Ovchinnikov Institute of Bioorganic Chemistry, Russian Academy of Sciences, 117997 GSP, Moscow V-437, Russia*
E-mail: pletnevs@mail.nih.gov

The acGFPL is the first-identified member of a novel, colorless and non-fluorescent group of green fluorescent protein (GFP)-like proteins. Its mutant aceGFP, with Gly replacing the invariant catalytic Glu-222, demonstrates a relatively fast maturation rate and bright green fluorescence (λex = 480 nm, λem = 505 nm). The reverse G222E single mutation in aceGFP results in the immature, colorless variant aceGFP-G222E, which undergoes irreversible photoconversion to a green fluorescent state under UV light exposure. Here we present a high resolution crystallographic study of aceGFP and aceGFP-G222E in the immature and UV-photoconverted states. A unique and striking feature of the colorless aceGFP-G222E structure is the chromophore in the trapped intermediate state, where cyclization of the protein backbone has occurred, but Tyr-66 still stays in the native, non-oxidized form, with Cα and Cβ atoms in the sp3 hybridization. This experimentally observed immature aceGFP-G222E structure, characterized by the non-coplanar arrangement of the imidazolone and phenolic rings, has been attributed to one of the intermediate states in the GFP chromophore biosynthesis. The UV irradiation (λ = 250–300 nm) of aceGFP-G222E drives the chromophore maturation further to a green fluorescent state, characterized by the conventional coplanar bicyclic structure with the oxidized double Tyr-66 Cα=Cβ bond and the conjugated system of π-electrons. Structure-based site-directed mutagenesis has revealed a critical role of the proximal Tyr-220 in the observed effects. In particular, an alternative reaction pathway via Tyr-220 rather than conventional wild type Glu-222 has been proposed for aceGFP maturation.

MS13-P03

Crystal structure of Tpa1 from *Saccharomyces cerevisiae*, a component of the messenger ribonucleoprotein complex

Hyoun Sook Kim[1], Kyoung Hoon Kim[1], Do Jin Kim[1], Sang Jae Lee[1], Ji Young Yoon[1], Hye Jin Yoon[1], and Se Won Suh[1,2]

[1]*Department of Chemistry, College of Natural Sciences, Seoul National University, Seoul 151-742, Korea*
[2]*Department of Biophysics and Chemical Biology, College of Natural Sciences, Seoul National University, Seoul 151-742, Korea*
E-mail: kobooks@gmail.com

Tpa1 (for *t*ermination and *p*oly*a*denylation) from *Saccharomyces cerevisiae* is a component of a messenger ribonucleoprotein complex at the 3' untranslated region of mRNAs. It comprises an N-terminal Fe(II)- and 2-oxoglutarate-dependent dioxygenase domain and a C-terminal domain. The N-terminal dioxygenase domain of a homologous Ofd1 protein from *Schizosaccharomyces pombe* was proposed to serve as an oxygen sensor that regulates the activity of the C-terminal degradation domain. Members of the Tpa1 family are also present in higher eukaryotes including humans. Here we report the crystal structure of *S. cerevisiae* Tpa1 as a representative member of the Tpa1 family. Structures have been determined as a binary complex with Fe(III) and as a ternary complex with Fe(III) and 2-oxoglutarate. The structures reveal that both domains of Tpa1 have the double-stranded β-helix fold and are similar to prolyl 4-hydroxylases. However, the binding of Fe(III) and 2-oxoglutarate is observed in the N-terminal domain only. We also show that Tpa1 binds to poly(rA), suggesting its direct interaction with mRNA in the messenger ribonucleoprotein complex. The structural and functional data reported in this study support a role of the Tpa1 family as a hydroxylase in the messenger ribonucleoprotein complex and as an oxygen sensor.

MS13-P04

Crystal structure of phosphopantetheine adenylyltransferase from *Enterococcus faecalis* in the ligand-unbound state and in complex with ATP and pantetheine

Hye-Jin Yoon[1], Ji Yong Kang[1], Hyung Ho Lee[2*] and Se Won Suh[1,3*]

[1]*Department of Chemistry, College of Natural Sciences, Seoul National University, Seoul 151-747, Korea*
[2]*Department of Bio & Nano Chemistry, Kookmin University, Seoul 136-702, Korea*
[3]*Department of Biophysics and Chemical Biology, College of Natural Sciences, Seoul National University, Seoul 151-747, Korea*
E-mail: yoonhj@snu.ac.kr

Phosphopantetheine adenylyltransferase (PPAT) catalyzes the penultimate step in Coenzyme A (CoA) biosynthetic pathway. It catalyzes the reversible transfer of an adenylyl group from ATP to 4'-phosphopantetheine (Ppant) to form dephospho-CoA (dPCoA) and pyrophosphate. Previous structural studies revealed how PPATs recognize substrates and products or their analogs. ATP, ADP, Ppant, and dPCoA bind to the same binding site in highly similar manners, while the mode and site of CoA or 3'-phosphoadenosine 5'-phosphosulfate binding are somewhat different. Until now, no structure of any PPAT bound with the pantetheine has been reported. In order to provide further structural information on ligand binding by PPATs, we solved the crystal structure of PPAT from *Enterococcus faecalis* in three forms: (i) the apo form, (ii) a binary complex with ATP, and (iii) a binary complex with pantetheine. The new structural information reported in this study supplements the existing structural data and should be useful for structure-based antibacterial discovery against PPATs.

References

[1] Geerlof A., Lewendon A. & Shaw WV., "Purification and characterization of phosphopantetheine adenylyltransferase from *Escherichia coli*." *J. Biol. Chem.* 274, (1999), pp 27105–27111.
[2] Izard T., "The crystal structures of phosphopantetheine adenylyltransferase with bound substrates reveal the enzyme's catalytic mechanism." *J. Mol. Biol.* 315, (2002), pp 487–495.
[3] Kang JY, Lee HH, Yoon HJ, Kim HS & Suh SW, "Overexpression, crystallization and preliminary X-ray crystallographic analysis of phosphopantetheine adenylyltransferase from *Enterococcus faecalis*." *Acta Crystallogr. sect. F Struct. Biol. Cryst. Commun.* 62, (2006), pp 1131–1133.

MS13-P05

Crystal structures of LacD from *Stapylococcus aureus* and LacD.1 from *Streptococcus pyogenes*: Insights into substrate specificity and virulence gene regulation

Sang Jae Lee[1], Hyoun Sook Kim[1], Do Jin Kim[1], Hye-Jin Yoon[1], Kyoung Hoon Kim[1], Ji Young Yoon[1], and Se Won Suh[1,2]

[1]*Department of Chemistry, College of Natural Sciences, Seoul National University, Seoul 151-742, Korea*
[2]*Department of Biophysics and Chemical Biology, College of Natural Sciences, Seoul National University, Seoul 151-742, Korea*
E-mail: sanzelee@gmail.com

Compared to Class I fructose-1,6-bisphosphate (FBP) aldolases, which catalyze a highly stereo-specific reaction toward FBP only, *S. aureus* LacD was shown to have a broader substrate specificity toward 1,6-bisphosphate derivatives of D-tagatose, D-fructose, D-sorbose, and D-psicose. Two closely-related Class I TBP aldolases in *S. pyogenes*, LacD.1 and LacD.2, are catalytically active but only LacD.1 was shown to be a regulator of global carbon catabolite control. LacD.1 senses nutritional status and regulates the transcription of virulence genes in *S. pyogenes* by associating with RopB, an Rgg family transcription regulator.

In order to provide structural insights into broadened substrate specificity of *S. aureus* LacD and virulence gene regulation by *S. pyogenes* LacD.1, we have determined the crystal structures of both *S. aureus* LacD and *S. pyogenes* LacD.1. Our structures suggest that the substitution of rabbit muscle FBP aldolase E189/S300 and the absence of Y363 in the active sites of *S. aureus* LacD and *S. pyogenes* LacD.1 are the most important determinant for the broader substrate specificity of Class I TBP aldolases as compared to Class I FBP aldolases. The dimerization mode seen in *S. pyogenes* LacD.1 and *S. aureus* LacD is also distinct from that of eukaryotic Class I FBP aldolases. Furthermore, our structural study allows a comparison of the surface features between dimers of *S. pyogenes* LacD.1 and LacD.2, providing a structural insight into the specific interaction of the transcriptional regulator RopB with *S. pyogenes* LacD.1.

MS13-P06

Crystal structure of Hsm3p, an assembly chaperone of the 19S regulatory particle of the proteasome

Sangwoo Kim[1], Tsunehiro Mizushima[1], Yasushi Saeki[3], Keiji Tanaka[3], Koichi Kato[1,4]

[1]*Graduate School of Pharmaceutical Sciences, Nagoya City University, 3-1 Tanabe-dori, Mizuho-ku, Nagoya 467-8603, Japan*
[2]*Laboratory of Frontier Science, Tokyo Metropolitan Institute of Medical Science, Setagaya-ku, Tokyo 156-8506, Japan*
[3]*Department of Biotechnology, Graduate School of Engineering, Nagoya University, Chikusa-ku, Nagoya 464-8603, Japan*
[4]*Okazaki Institute for Integrative Bioscience and Institute for Molecular Science, National Institutes of Natural Sciences, 5-1 Higashiyama, Myodaiji, Okazaki 444-8787, Japan*
E-mail: ksu93@phar.nagoya-cu.ne.jp

The 26S proteasome, is a huge molecular machine with a central role in intracellular protein degradation, consists of a 20S core particle (CP) and two 19S regulatory particles (RPs) composed of ATPase (Rpt) and non-ATPase (Rpn) subunits. Several proteasome-dedicated chaperones are involved in the efficient and correct assembly of the 20S proteasome [1]. Recently, four proteasome-interacting proteins, Nas2/p27, Nas6/gankyrin, Rpn14/PAAF1, and Hsm3/S5b, have been shown to contribute to assembly of the 19S RP [2, 3, 4]. More recently, we determined the crystal structure of yeast Rpn14 at 2.0 Å resolution, which revealed that this chaperone consists of a unique N-terminal domain with unknown function and a C-terminal domain assuming a canonical seven-bladed β-propeller fold [5]. Furthermore, we identified the specific residues of Rpn14 and Rpt6 involved in their complementary charge interaction that is required for the 19S RP assembly. On the other hands, yeast Hsm3p associates with 19S RP via a C-terminal domain of the Rpt1 base subunit. This chaperone is specifically required for the base subcomplex assembly, although mechanistic actions of how it regulates RP assembly remain unclear.

Here, we report the crystal structures of yeast Hsm3p at 2.0 Å resolution, which was determined by the multiwavelength anomalous dispersion (MAD) method using a selenomethionine derivative. Hsm3p consists of 12 tandem HEAT [Huntingtin, elongation factor 3 (EF3), A subunit of protein phosphatase 2A (PP2A), PI3 kinase target of rapamycin 1 (TOR1)] repeats, which has a C-shaped structure consisting entirely of 24 α-helices and connecting loops. While the Rpn14-Rpt6 interaction is primarily characterized by the complementary charge interaction, Hsm3p has no such unique surface properties. Yeast genetics and biochemical studies of the interaction between Hsm3p and Rpt1 are in progress.

References

[1] Murata S., Yashiroda H., Tanaka K., Molecular mechanisms of proteasome assembly, *Nat. Rev. Mol. Cell Biol.* 10, (2009), pp 104–115
[2] Funakoshi M., Tomko R. J. Jr., Kobayashi H., Hochstrasser M., Multiple Assembly Chaperones Govern Biogenesis of the Proteasome Regulatory Particle Base, *Cell* 137, (2009), pp 887–899.
[3] Saeki Y., Toh-E A., Kudo T., Kawamura H., Tanaka K., Multiple Proteasome-Interacting Proteins Assist the Assembly of the Yeast 19S Regulatory Particle, *Cell* 137, (2009), pp 900–913.
[4] Roelofs J., Park S., Haas W., Tian G., McAllister F. E., Huo Y., Lee B. H., Zhang F., Shi Y., Gygi S. P., Finley D., Chaperone-mediated pathway of proteasome regulatory particle assembly, *Nature* 459, (2009), pp 861–865
[5] Kim S., Saeki Y., Fukunaga K., Suzuki A., Takagi K., Yamane T., Tanaka K., Mizushima T., Kato K., Crystal Structure of Yeast Rpn14, a Chaperone of the 19 S Regulatory Particle of the Proteasome, *J. Biol. Chem.* 285, (2010), pp 15159–15166

MS13-P07

A structural genomics approach to the structure determination of macrophage proteins

Kai-En Chen[1], Gautier Robin[1], Justine M. Hill[2], Matthew J. Sweet[1], Stuart Kellie[2], Bostjan Kobe[2] and Jennifer L. Martin[1]

[1]*Institute for Molecular Bioscience, The University of Queensland, Brisbane, Queensland, Australia*
[2]*School of Chemistry and Molecular Biosciences, The University of Queensland, Brisbane, Queensland, Australia*
E-mail: k.chen@imb.uq.edu.au

In the immune system, macrophages are cells differentiated from circulating blood monocytes that represent the first line of defense against pathogen invasion. Macrophages are widely distributed throughout the body and are particularly abundant at the route of pathogen entry. They play a critical role in immune defense by initiating, promoting, preventing, suppressing or terminating immune responses. We established a high-throughput pipeline at the University of Queensland to investigate the structures and functions of novel macrophage proteins [1]. My project began with the selection of 12 novel, biologically interesting and crystallization-feasible targets that were then designed into 96 different constructs. Processing of the 96 constructs was performed in parallel using simple automated applications of ligation-independent cloning, small-scale bacterial expression, small-scale purification and solubility assessment. After processing these 12 targets, I found that 16 constructs of 3 targets (25%) yielded soluble protein. From the three soluble targets, I have spent most time on two proteins BinCARD and Fam96a.

BinCARD (Bcl10 interacting CARD protein) is a CARD-domain containing protein that interacts with Bcl10 to downregulate NF-κB transcription factor activation [2]. Bcl10 is an intracellular signalling protein that also contains a CARD domain. The primary function of Bcl10 is to interact with CARD-domain containing proteins through CARD-CARD interactions to regulate its activity in the NF-κB signalling pathway [3]. The crystal structure of BinCARD solved at 1.5 Å resolution revealed six anti-parallel α-helices, suggesting that this protein is similar to other CARDs of known structures. Before progress toward the interaction study between BinCARD and Bcl10, I also addressed the bottleneck of Bcl10 purification. The challenge was overcome by implementing a matrix-assisted refolding strategy. Approaches to determine the BinCARD and Bcl10 interaction are currently being applied.

Fam96a (family with sequence similarity 96, member a) is a novel DUF59 domain containing protein that belongs to a group of diverse proteins with no function characterised yet. Evidence has shown that exploration of these proteins is an important area for further studies [4]. The crystal structure of Fam96a at 1.8 Å and 2.3 Å resolution revealed two different types of domain swapped-dimer conformation. Interestingly, Fam96a and its homologue Fam96b are the only two DUF59 domain containing proteins to be expressed in mammalian cells. Functional characterization of Fam96a in macrophage is currently being investigated.

References

[1] Puri M, et al., Focusing in on structural genomics: the University of Queensland structural biology pipeline, Biomolecular Engineering, 23, (2006), pp 281-289.
[2] Woo N.H, et al., Inhibition of Bcl10-mediated activation of NF-κB by BinCARD, a Bcl10-interacting CARD protein, FEBS Letters, 578, (2004), pp 239-244.
[3] Ruland J, et al., Bcl10 is a positive regulator of antigen receptor-induced activation of NF-κB and neural tube closure, Cell, 104, (2001), pp 33-42.
[4] Jaroszewski L, et al., Exploration of uncharted regions of the protein universe, PLoS Biology, 7, (2009), pp 1-15.

MS13-P08

Crystal structure of the dimerization domain of human filamin A

Bong-Jin Lee

Research Institute of Pharmaceutical Sciences, College of Pharmacy, Seoul National University, San 56-1, Daehak-dong, Gwanak-Gu, Seoul 151-742, Korea
E-mail: lbj@nmr.snu.ac.kr

By crosslinking actin filaments, filamins play important roles in regulating the dynamics of the actin cytoskeleton which plays a central role in many cell functions such as the maintenance of cell shape, cell division, adhesion, motility, signal transduction and protein sorting. Consistent with this, mutations in human filamin genes are associated with a wide range of developmental abnormalities and defective neuronal migration. And filamins as integrators of cell mechanics and signalling by interacting with transmembrane receptors and cytosolic signaling proteins.

In humans, three filamin isoforms have been identified: filamin A, filamin B, filamin C. Of these, filamin A (FLNa) is the most abundant and widely expressed. Heterozygous null FLNa alleles result in defective neuronal migration causing periventricular heterotopia, while certain FLNa missense mutations cause familial cardiac valvular dystrophy and putative gain-of-function mutations result in a spectrum of congenital malformations generally characterized by skeletal dysplasias.

Human vertebrate filamins are homodimers of two 280kDa subunits, and each subunit contains an N-terminal actin binding domain consisted of two calponin homology domains followed by 24 tandem repeat domains (FLNa1-24) that are interrupted by flexible hinge regions between FLNa15 and FLNa16 and FLNa23 and FLNa24. Dimerization through FLNa24 is crucial for the actin-crosslinking function of filamins.
We report the structure of FLNa domain 24 (FLNa24), and compare the structure with FLNc24 and discuss how dimerization is formed in FLNa24.

MS13-P09

Structural basis for the functional insight of HP0420-homologue from *Helicobacter felis*

Shunfu Piao, Xiao Ling Jin, Bo-Young Yun and Nam-Chul Ha*

**College of Pharmacy and Research Institute for Drug Development, Pusan National University, Jangjeon-dong, Geumjeong-gu, Busan 609-735, Korea*
E-mail: hnc@pusan.ac.kr

Helicobacter pylori infect more than half of the world's population and are considered a cause of peptic ulcer disease and gastric cancer. Recently, hypothetical gene HP0421 was identified in *H. pylori* as a cholesterol α-glucosyltransferase, which is required to synthesize cholesteryl glucosides, essential cell wall components of the bacteria. In the same gene-cluster, HP0420 was co-identified, whose function remains unknown. Here we report the crystal structure of HP0420-homologue of *Helicobacter felis* (HF0420) to gain insight into the function of HP0420. The crystal structure, combined with size-exclusion chromatography, reveals that HF0420 adopts a homodimeric hot-dog fold. The crystal structure suggests that HF0420 has enzymatic activity that involves a conserved histidine residue at the end of the central α-helix. Subsequent biochemical studies provide clues to the function of HP0420 and HF0420.

Reference

[1] Piao S., Jin X.L., Yun B.Y., Kim N., Cho H.S., Fukuda M., Lee H. and Ha N.C. "Crystal structure and functional insight of HP0420-homologue from Helicobacter felis", Biochem Biophys Res Commun, Vol 4, No. 394, (2010), pp 940-6.

MS13-P10

The hexameric structure of AcrA suggests the assembly of a bacterial multidrug efflux pump AcrAB-TolC

Yongbin Xu1,#, Saemee Song2,#, Shunfu Piao1, Hong-Man Kim2, Se-Hoon Sim2, Xiao Ling Jin1, Hyesung Jeon3, Kangseok Lee2,*, and Nam-Chul Ha1,**

1Department of Manufacturing Pharmacy, College of Pharmacy and Research Institute for Drug Development, Pusan National University, Busan 609-735, Republic of Korea
2Department of Life Science (BK21 program), Research Center for Biomolecules and Biosystems, Chung-Ang University, Seoul 156-756, Republic of Korea
3Biomedical Research Center, Korea Institute of Science and Technology, Seoul 136-791, Republic of Korea
E-mail: hnc@pusan.ac.kr

Multidrug resistance caused by export proteins is becoming a serious clinical problem in the antibiotic treatment of bacterial infections. AcrB is a principal multidrug exporter which confers intrinsic drug tolerance to Escherichia coli, and requires outer membrane factor TolC and periplasmic adaptor protein AcrA to form the tripartite AcrAB-TolC pump. However, it remains to be elucidated how the three proteins are assembled in its functional state. In this study, we constructed a tandemly-linked AcrA dimer to reveal the oligomeric state of AcrA, which was as functional as the wild type AcrA in vivo. Subsequent electron microscopic study showed a hexameric model of AcrA, which is similar to the functional homologue MacA hexameric structure that was found in the crystal structures. Our findings support an adaptor-bridging model for the multidrug efflux pumps, which is distinct from a currently prevailing model. Taken together, our observations provide a structural basis for understanding the multidrug resistance of pathogenic bacteria caused by the tripartite multidrug efflux pumps.

MS13-P11

Crystal structure of the MukB hinge domain and its functional implications

Bonsu Ku, Byung-Ha Oh

Department of Biological Sciences, KAIST Institute for the Biocentury, Korea Advanced Institute of Science and Technology, Daejeon 305-701, Korea
E-mail: confuser@kaist.ac.kr

The structural maintenance of chromosomes (SMC) family proteins are core components of multiprotein complexes involved in chromosome organization, including chromosome condensation and sister chromatid cohesion. These proteins share a characterizing V-shaped dimeric structure with two long coiled-coil arms having two ATPase head domains at the distal ends. The hinge domain, located in the middle of the coiled coil, forms the dimer interface. In addition, SMC hinges are reported to play other roles, including serving as a gateway for DNA entry into the cohesin complex. Herein, we report the homodimeric structure of the hinge domain of *Escherichia coli* MukB, a functional homologue of SMC in γ-proteobacter family members. In contrast to SMC hinge of *Thermotoga maritima*, which has a sizable central hole at the dimer interface, MukB hinge forms a constricted dimer interface lacking a hole. Critically, in accordance with the absence of a notable positively charged surface patch, MukB hinge does not interact with DNA. These results suggest that the function of MukB hinge is limited to dimerization of two copies of MukB molecules.

References

[1] Ku B., Lim J.H., Shin H.C., Shin S.Y., Oh B.H., "Crystal structure of the MukB hinge domain with coiled-coil stretches and its functional implications", *Proteins*, Vol. 78, No. 6, (2010), pp 1483-1490.
[2] Woo J.S., Lim J.H., Shin H.C., Suh M.K., Ku B., Lee K.H., Joo K., Robinson H., Lee J., Park S.Y., Ha N.C., Oh B.H., "Structural studies of a bacterial condensin complex reveal ATP-dependent disruption of intersubunit interactions", *Cell*, Vol. 136, No. 1, (2009), pp 85-96.
[3] Gruber S., Arumugam P., Katou Y., Kuglitsch D., Helmhart W., Shirahige K., Nasmyth K., "Evidence that loading of cohesin onto chromosomes involves opening of its SMC hinge", *Cell*, Vol. 127, No. 3, (2006), pp 523-537.
[4] Hirano M., Hirano T., "Opening closed arms: long-distance activation of SMC ATPase by hinge-DNA interactions", *Mol cell*, Vol. 21, No. 2, (2006), pp 175-186.

MS13-P12

Crystal structure and functional characteristics of LmDPK, a novel DNA protection kinase, in *Listeria monocytogenes*

Thao Thi Phuong Duong[1], Sung Wook Kang[1], Truc Dinh Trung Kim[1], Boi Hoa San[1,2] and Kyeong Kyu Kim[1,2]

[1]*Department of Molecular Cell Biology, Samsung Biomedical Research Institute, Sungkyunkwan University School of Medicine Suwon 440-746, Korea*
[2]*Sungkyunkwan Advanced Institute of Nanotechnology, Sungkyunkwan University, Suwon 440-746, Korea*
Email: duong2008@skku.edu

DPK (DNA protection kinase) in *Staphylococcus aureus* was recently identified as a novel histidine kinase with DNA protection activity against reactive oxygen species (ROS). DPK homologues are known in some Gram-positive bacteria belonging to the order Bacillales, and we studied the DPK homolog in *Listeria monocytogenes*, designated as LmDPK. The crystal structure of LmDPK, determined at 1.75 Å resolution, revealed structural similarity to DPK, thereby suggesting functional homology, although they have very limited sequence identity. As inferred from the crystal structure, LmDPK was shown to be autophosphorylated in the presence of ferrous ion and hydroxyl radicals. LmDPK also harbored a DNA protection activity against oxidative damages. These results suggested that the presence of DPK homologues and their biological functions might be general in Gram-positive bacteria.

References

[1] Sung Wook Kang, Kyung min Kim, Hye-yeon Hwang and Kyeong kyu Kim, "A novel DNA protection kinase against oxidative stress in Staphylococcus aureus", 17th East Asian Joint Symposium on Biomedical Research, College of Medicine, National Taiwan University, (2010).
[2] Gray, M. L., and A. H. Killinger, "Listeria monocytogenes and listeric infection". Bacteriol. Rev. Vol. 30, (1966), pp 309-382.
[3] Farber, J.M. and P.I.Peterkin, "Listeria monocytogenes, a Food-Borne pathogen", Micribiol. Rev, Vol. 55, (1991), pp 476-511.
[4] Nair, S., and Finkel, S.E., "Dps protects cells against multiple stresses during stationary phase", J. Bacteriol, Vol. 186, No. 13, (2004), pp 4192-4198.

MS13-P13

Structure mechanism of antigen recognition of the neural cell adhesion molecule L1 protein antibody

Chunhua Wei[1,2,5], Eung Suk Lee[3], Jeong Yi Jeon[1], Seung Jun Kim[4], Young Ho Jeon[2,5], Hyo Jeong Hong[6] and Seong Eon Ryu[1*]

[1]*Proteomics Lab, College of Bio-Engineering, Hanyang University, Seoul 133-791, Korea*
[2]*Bio-Analytical Science, University of Science and Technology, Daejeon 305-333, Korea*
[3]*The Therapeutic Antibody Research Center, Korea Research Institute of Bioscience and Biotechnology, Daejeon 305-806, Korea*
[4]*Medical Proteomics Research Center, Korea Research Institute of Bioscience and Biotechnology, Daejeon 305-806, Korea*
[5]*Division of Magnetic Resonance, Korea Basic Science Institute, Ochang 363-883, Korea*
[6]*Department of Systems Immunology, College of Biomedical Science, Kangwon National University, Chuncheon, Kangwon-Do 200-701, Korea*
E-mail: weichhua02@hotmail.com

The neural cell adhesion molecule L1 (CAML1) protein is a potentially useful diagnostic marker for cancer progression and a candidate for anti-cancer therapy. In the present study we investigated an antibody (A10A3) of the CAML1 protein that has high affinity to the first domain of the N-terminal Ig-like domains. Here, we describe the crystal structure of Fab of A10A3 determined at 1.75 Å resolution. Although the sequence in the light variable chain of Fab of A10A3 is very similar with that of 3BSZ, the loops belong to complementarily determining regions (CDRs) are very different each other. To understand the structural implication of the CAML1, we carried out comprehensive alanine-scanning mutagenesis of all CDRs in A10A3 Fab. The functional mapping of the antigen-binding site contributes to the rotational design for maximal humanization and affinity maturation of the antibody. This is the first structure of CAML1 protein antibody. It will provide a framework for understanding the mechanisms of CAML1 on cancer progression, and may serve as a potential agent for cancer treatment combine with other therapies.

References

[1] Rathjen F.G., Schachner M., "Immunocytological and biochemical characterization of a new neuronal cell surface component (L1 antigen) which is involved in cell adhesion", *EMBO J.*, Vol. 3, No. 1, (1984), pp 1-10.
[2] Hortsch, M., "The L1 family of neural cell adhesion molecules: old proteins performing new tricks", *Neuron*, Vol. 17, No. 4, (1996), pp 587-593.
[3] He Y., Jensen G. J., and Bjorkman P. J., "Cryo-electron tomography of homophilic adhesion mediated by the neural cell adhesion molecule L1", *Structure*, Vol. 17, No. 3, (2009), pp 460-471.
[4] Haspel J., Friedlander D.R., Ivgy-May N., Chickramane S., Roonprapunt C., Chen S., Schachner M., and Grumet M., "Critical and optimal Ig domains for promotion of neurite outgrowth by L1/Ng-CAM", *J. Neurobiol.*, Vol. 42, No. 3, (2000), pp 287-302.
[5] Raveh S., Gavert N., Ben-Ze'ev A., "L1 cell adhesion molecule (L1CAM) in invasive tumors", *Cancer Letters*, Vol. 282, No. 2, (2009), pp 137-145.
[6] Novak-Hofer I., Cohrs S., Grünberg J., Friedli A., Schlatter M.C., Pfeifer M., Altevogt P., Schubiger P.A., "Antibodies directed against L1-CAM synergize with Genistein in inhibiting growth and survival pathways in SKOV3ip human ovarian cancer cells", *Cancer Letters*, Vol. 261, No. 2, (2008), pp 193-204.

MS13-P14

Crystal structure of *Helicobacter pylori* MinE, a cell division topological specificity factor

Jun Yop An[1], Hyung-Seop Youn[1], Jung-Gyu Lee[1], Kyoung-Ryoung Park[1], Lai San Woo[1], Youngjin Lee[1], Won Ju Jeong[1], Gil Bu Kang[1], Hye-Eun Song[1], Mun-Kyoung Kim[1], Jang-Soo Chun[1], Hyesung Jeon[2], and Soo Hyun Eom[1]*

[1]*School of Life Science, Gwangju Institute of Science & Technology (GIST), Gwangju 500-712, Korea*
[2]*Biomedical Research Center, Korea Institute of Science and Technology, Seoul 136-791, Korea*
E-mail: eastway7@gist.ac.kr

In gram negative bacteria, proper placement of the FtsZ ring, mediated by nucleoid occlusion and the activities of the dynamic oscillating Min proteins MinC, MinD and MinE, is required for correct positioning of the cell division septum. MinE is a topological specificity factor that counters the activity of MinCD division inhibitor at the mid-cell division site. Its structure consists of an anti-MinCD domain and a topology specificity domain (TSD). Previous NMR analysis of truncated *Escherichia coli* MinE showed that the TSD domain contains a long α-helix and two antiparallel β-strands, which mediate formation of a homodimeric α/β structure. Here we report the crystal structure of full-length *Helicobacter pylori* MinE and redefine its TSD based on that structure. The N-terminal region of the TSD (residues 19-26), previously defined as part of the anti-MinCD domain, forms a β-strand (βA) and participates in TSD folding. In addition, *H. pylori* MinE forms a dimer through the interaction of anti-parallel βAstrands. Moreover, we observed serial dimer-dimer interactions within the crystal packing, resulting in the formation of a multimeric structure. We therefore redefine the functional domain of MinE and propose that a multimeric filamentous structure is formed through anti-parallel β-strand interactions.

This study was supported by a grant of the Korea Healthcare technology R&D Project, Ministry for Health, Welfare & Family Affairs, Republic of Korea (A092006).

References

[1] Hsieh, C.W., Lin, T.Y., Lai, H.M., Lin, C.C., Hsieh, T.S., and Shih, Y.L., "Direct MinE-membrane interaction contributes to the proper localization of MinDE in E. coli", *Mol Microbiol*, **75**, (2010), 499-512.
[2] Zhou, H., Schulze, R., Cox, S., Saez, C., Hu, Z., and Lutkenhaus, J., "Analysis of MinD mutations reveals residues required for MinE stimulation of the MinD ATPase and residues required for MinC interaction", *J Bacteriol*, **187**, (2005), 629-638.
[3] Suefuji, K., Valluzzi, R., and Ray Chaudhuri, D., "Dynamic assembly of MinD into filament bundles modulated by ATP, phospholipids, and MinE", *Proc Natl Acad Sci USA* , **99,** (2002), 16776-16781.

MS13-P15

Ligand-binding-site prediction program POCASA

MinYao[1], Jian Yu[1], Yong Zhou[1,2], Isao Tanaka[1]

1. Faculty of Advanced Life Science, Hokkaido University, Japan
2. Current address for Zhou: Initiative Research Unit, Advanced Science Institute, RIKEN, Japan
E-mail: yao@castor.sci.hokudai.ac.jp

Identification of ligand binding sites in protein structure is a prerequisite for protein–ligand docking and an important step in structure/fragment-based drug discover (SDDD/FBDD). In this study, we developed a new algorithm, Roll, implemented in a program named POCASA [1], which can predict binding sites by detecting pockets and cavities of proteins with a rolling sphere. To evaluate the performance of POCASA, a test with the same data set as used in several existing methods was carried out. POCASA achieved a high success rate of 77%. A novel function in POCASA is that the pockets could be determined by different probe spheres, which makes it versatile for various ligands and proteins. In addition, the test results indicated that POCASA can predict good 3D shapes of ligand binding sites, which can provide useful information of ligand selection for target protein. A web POCASA is available at http://altair.sci.hokudai.ac.jp/g6/Research/POCASA_e.html

References

[1] Roll: a new algorithm for the detection of protein pockets and cavities with a rolling probe sphere. Jian Yu et al, Bioinformatics 26, 46-52 (2010).

MS13-P16

Structures of enoyl-ACP reductase from *Bacillus cereus*

Su Jin Kim[1,2], Byung Hak Ha[1], Kook-Han Kim[1], Seung Kon Hong[1], Key-Jung Shin[1], Se Won Suh[2] and Eunice EunKyeong Kim[1]

[1]*Life Sciences Division, Korea Institute of Science and Technology, 39-1 Hawolkok-dong, Sungbuk-gu, Seoul, 136-791, Korea*
[2]*Department of Chemistry, College of Natural Sciences, Seoul National University, Seoul 151-747, Korea*
E-mail: sjkim327@kist.re.kr

Enoyl-[acyl carrier protein] reductase (enoyl-ACP reductase; ENR) is a key enzyme in type II fatty-acid synthase that catalyzes the last step in each elongation cycle, therefore, which is an essential enzyme in bacteria. Some pathogens have more than one ENR identified, and *Bacillus cereus* has two ENRs reported, namely FabI and FabL. Here we have determined the crystal structures of FabL from *B. cereus* in the apo and in the $NADP^+$ and indole naphthyridinone inhibitor bound form. The overall structure is almost identical to each other and that of FabI, except three stretches that are disordered in the apo structure get organized as the cofactor and inhibitor bind. The apo structure is found as a dimer in the crystal which agrees with the solution study, while the ternary complex is in its tetramer. The three stretches are important in cofactor and inhibitor binding as well as tetramer formation.

This work was supported by grants from the Functional Proteomics Center, the 21C Frontier Research & Development Program of the Korea Ministry of Science and Technology, and the Korea Institute of Science and Technology Institutional Program.

References

[1] White S.W., Zheng J., Zhang Y.M., Rock C.O., "The structural biology of type II fatty acid biosynthesis", *Annu. Rev. Biochem.*, Vol. 74, (2005), pp 791-831.
[2] Wright H.T., Reynolds K.A., "Antibacterial targets in fatty acid biosynthesis", *Curr. Opin. Microbiol.*, Vol. 10, (2007), pp 447-453.

MS13-P17

PDBj Mine: Design and implementation of relational database interface for Protein Data Bank Japan

Akira R. Kinjo[1], Reiko Yamashita[1], Haruki Nakamura[1]

[1]*Protein Data Bank Japan, Institute for Protein Research, Osaka University, 3-2 Yamadaoka, Suita, Osaka 565-0871, Japan*
E-mail: akinjo@protein.osaka-u.ac.jp

We describe the design and implementation of PDBj Mine, a new database and its interface for Protein Data Bank Japan (PDBj, http://www.pdbj.org/). In PDBj Mine, data are loaded from files in the PDBMLplus format (an extension of PDBML, PDB's canonical XML format, enriched with annotations), which are then served for the user of PDBj via the worldwide web (WWW). We describe the basic design of the relational database and web interfaces of PDBj Mine. The contents of PDBMLplus files are first broken into XPath entities, and these paths and data are indexed in the way that reflects the hierarchical structure of the XML files. The data for each XPath type are saved into the corresponding relational table that is named as the XPath itself. The generation of table definitions from the PDBMLplus XML schema is fully automated. For efficient search, frequently queried terms are compiled into a brief summary tables. Casual users can perform simple keyword search, and "Advanced Search" which can specify various conditions on the entries. More experienced users can query the database using SQL statements which can be constructed in a uniform manner. Thus, PDBj Mine achieves a combination of the flexibility of XML documents and the robustness of the relational database.

MS13-P18

Crystallization and structural analysis of human mitogen-activated protein kinase phosphatase (MAKP) proteins

Song Yi Kim[1,2], A Young kyung [2,3] and Dae Gwin Jeong [2,3]

[1] *Department of Biology, College of Natural Sciences, Chungnam National University, Daejeon 305-764, Republic of Korea*
[2] *Medical Proteomics Research Center, Korea Research Institute of Bioscience and Biotechnology, 52 Eoeun-Dong, Yuseong-Gu, Daejeon, 305-600, Korea*
[3] *Applied Biology, College of Agriculture and life science, University of science and technology, 113 Gwahangno, Yuseong-Gu, Daejeon, 305-333, Korea*
E-mail: syikim@kribb.re.kr

The MAKPs were made up a distinct subgroup of 10 catalytically active enzymes among the larger family of dual-specificity protein phosphatases (DUSP or VHR-like cysteine-dependent protein phosphatases) encoded in the human genome. They all share some common catalytic domain, including an extended conserved HCXXXR motif. They also comprise a family of dual-specificity protein phosphatases that dephosphorylate both phospho-threonine and phospho-tyrosine residues in MAP kinases, including the c-Jun N-terminal protein kinase (JNK)/stress-activated protein kinase (SAPK), the p38 MAPK, and the extracellular signal-related kinase (ERK). Inadequate productions or actions of MAPKs or MAKPs have been associated with diverse human diseases, like cancer, diabetes, and autoimmune diseases. In spite of critical MAKP regulation, the detail understanding of activation mechanism remains not clear so far. For this reason, the crystal structures of MAKP were discussed to unravel various negative regulatory mechanisms to MAPKs. To date, several crystal structure of MAKP family have been solved, which have shown subtle structural differences at residues surrounding active site. Therefore the detailed information of MAKP structures will enable us to verify the interaction between substrates, localization and its mechanism of dephosphorylation. Exactly 7 catalytic domain structure of MAKP out of 10 have been determined but the others still remain unsolved. To provide the structural insight of additional 3 MAKPs, we crystallized them and determined the structure. In addition, the kinetic studies for MAKPs will be followed and after we understood MAKP structures, we will develop how to interact to MAPK and where to localize in MAKP signaling pathways.

References

[1] Stewart, A. E., Dowd, S., Keyse, S. M. & McDonald, N. Q. Crystal structure of the MAPK phosphatase Pyst1 catalytic domain and implications for regulated activation. Nature Struct. Biol. 6, 174–181. (1999)
[2] Camps, M., Nichols, A. & Arkinstall, S. Dual specificity phosphatases: a gene family for control of MAP kinase function. J. Faseb, 14, 6–16. (2000)
[3] Alonso A, Sasin J, Bottini N, Friedberg I, Friedberg I, Osterman A, Godzik A, Hunter T, Dixon J, Mustelin T. Protein tyrosine phosphatases in the human genome. Cell. 117: 699-711. (2004)
[4] Jeong DG, Yoon TS, Kim JH, Shim MY, Jung SK, Son JH, Ryu SE, Kim SJ. Crystal structure of the catalytic domain of human MAP kinase phosphatase 5: structural insight into constitutively active phosphatase. J Mol Biol. 28;360(5):946-55 (2006)
[5] Dae Gwin Jeong, Yoon Hea Cho, Tae-Sung Yoon, Jae Hoon Kim, Seong Eon Ryu, and Seung Jun Kim. Crystal Structure of the Catalytic Domain of Human DUSP5, a Dual Specificity MAP Kinase Protein Phosphatase. PROTEINS. 66:253–258 (2007)
[6] Jeong DG, Jung SK, Yoon TS, Woo EJ, Kim JH, Park BC, Ryu SE, Kim SJ. Crystal structure of the Catalytic domain of human MKP-2 reveals a 24-mer assembly. PROTEINS 15;76(3):763-7 (2009)

MS13-P19

Crystallization of human MST2 SARAH domain

Jinsue Song, Saehae Choi, Il Young Park and Soo Jae Lee

College of Pharmacy, CBITRC, Chungbuk National University, Chungbuk, Korea

The mammalian sterile 20-related kinase 1 and 2 (MST1 and 2) are key components of the Hippo signaling pathway, which is involved in the regulation of a number of diverse cellular process including cell polarization, cell growth and apoptosis. MST2 shares at least two similar pathways with MST1. The first is that MST1 and MST2 can phosphorylate and inhibit AKT activation. In addition, they can activate FOXO3 via phosphorylation. The second is that both proteins can be detected in a complex containing Salvador (hSav). Drosophila MST1/2 homologue Hippo (hpo) bind to and phosphorylates a tumor suppressor protein Sav, which is known to interact with Warts (Wts) protein kinase. MST2 has a stronger stabilizing effect on hSav, and may play a more prominent role in this complex. MST2 has been suggested to participate in the Hpo-Sav-Wts pathway in mammalian cells in a manner dependent on a protein-protein interaction domain, Sav/Rassf/Hpo (SARAH) domain, that is shared by Sav, RASSF, and Hpo. MST2 is involved in the LATS tumor suppressor pathway via complex with hSav, RASSF1A, Nore1 and LATS1, resulting in the phosphorylation of LATS1 and transcription of proapoptotic genes. Here we present the crystallization result of the human MST2 SARAH domain(436-484) in order to provide useful information for interaction with hSav. The SARAH domain(436-484) at the C-terminus of MST2 from *Homo sapiens* has been recombinantly expressed and purified using an *Escherichia coli* expression system. Purified MST2 SARAH domain(436-484) from *Homo sapiens* has been crystallized using the hanging-drop vapour-diffusion technique. The crystals belonged to the space group $P2$, with unit-cell parameters a =62.0 Å, b =119.2 Å, c =62.0 Å, β = 90.5 and the space group $P6_122$, with unit-cell parameters a =54.5 b =54.5 , c =303.1, showed diffraction to 2.7 Å and 2.6 Å resolution, respectively.

MS13-P20

Structural basis for the specialization of Nur, a nickel-specific Fur homologue, in metal sensing and DNA recognition

Young Jun An[1], Chang-Sook Jeong[1], Jung-Ho Shin[2], Jung-Hye Roe[2], and Sun-Shin Cha[1]

[1]*Marine and Extreme Genome Research Center, Korea Ocean Research & Development Institute, Ansan 426-744, Republic of Korea*
[2]*School of Biological Sciences and Institute of Microbiology, Seoul National University, Seoul 151-742, Republic of Korea*
E-mail: gem3@kordi.re.kr

Nur, a member of the Fur family, is a nickel-responsive transcription factor that controls nickel homeostasis and anti-oxidative response in *Streptomyces coelicolor*. Here we report the 2.4 Å resolution crystal structure of Nur. It contains a unique nickel-specific metal site in addition to a non-specific common metal site. The identification of the 6-5-6 motif of the Nur recognition box and a Nur/DNA complex model reveals that Nur mainly interacts with terminal bases of the palindrome on complex formation. This contrasts with more distributed contacts between Fur and the n-1-n type of the Fur binding motif. The disparity between Nur and Fur in the conformation of the S1-S2 sheet in the DNA-binding domain can explain their different DNA-recognition patterns. Furthermore, the fact that the specificity of Nur in metal sensing and DNA recognition is conferred by the specific metal site suggests that its introduction drives the evolution of Nur orthologs in the Fur family.

References

[1] Pennella, M. A., Shokes, J. E., Cosper, N. J., Scott, R. A. & Giedroc, D. P., Structural elements of metal selectivity in metal sensor proteins. Proc Natl Acad Sci U S A, 100, 3713-8, (2003).
[2] Mulrooney, S. B. & Hausinger, R. P., Nickel uptake and utilization by microorganisms. FEMS Microbiology Reviews, 27, 239-261, (2003).
[3] Ahn, B. E., Cha, J., Lee, E. J., Han, A. R., Thompson, C. J. & Roe, J. H., Nur, a nickel-responsive regulator of the Fur family, regulates superoxide dismutases and nickel transport in Streptomyces coelicolor. Mol Microbiol., 59, 1848-58, (2006).
[4] An, Y. J., Ahn, B. E., Roe, J. H. & Cha, S. S., Crystallization and preliminary X-ray crystallographic analyses of Nur, a nickel-responsive transcription regulator from Streptomyces coelicolor. Acta Crystallogr Sect F Struct Biol Cryst Commun, 64, 130-2, (2008).

AsCA2010

The 10th Conference of the Asian Crystallographic Association

ABSTRACTS

Poster Sessions

Area 2. Chemical Crystallography and Materials Science
(MS02, 05, 08, 11, 14)

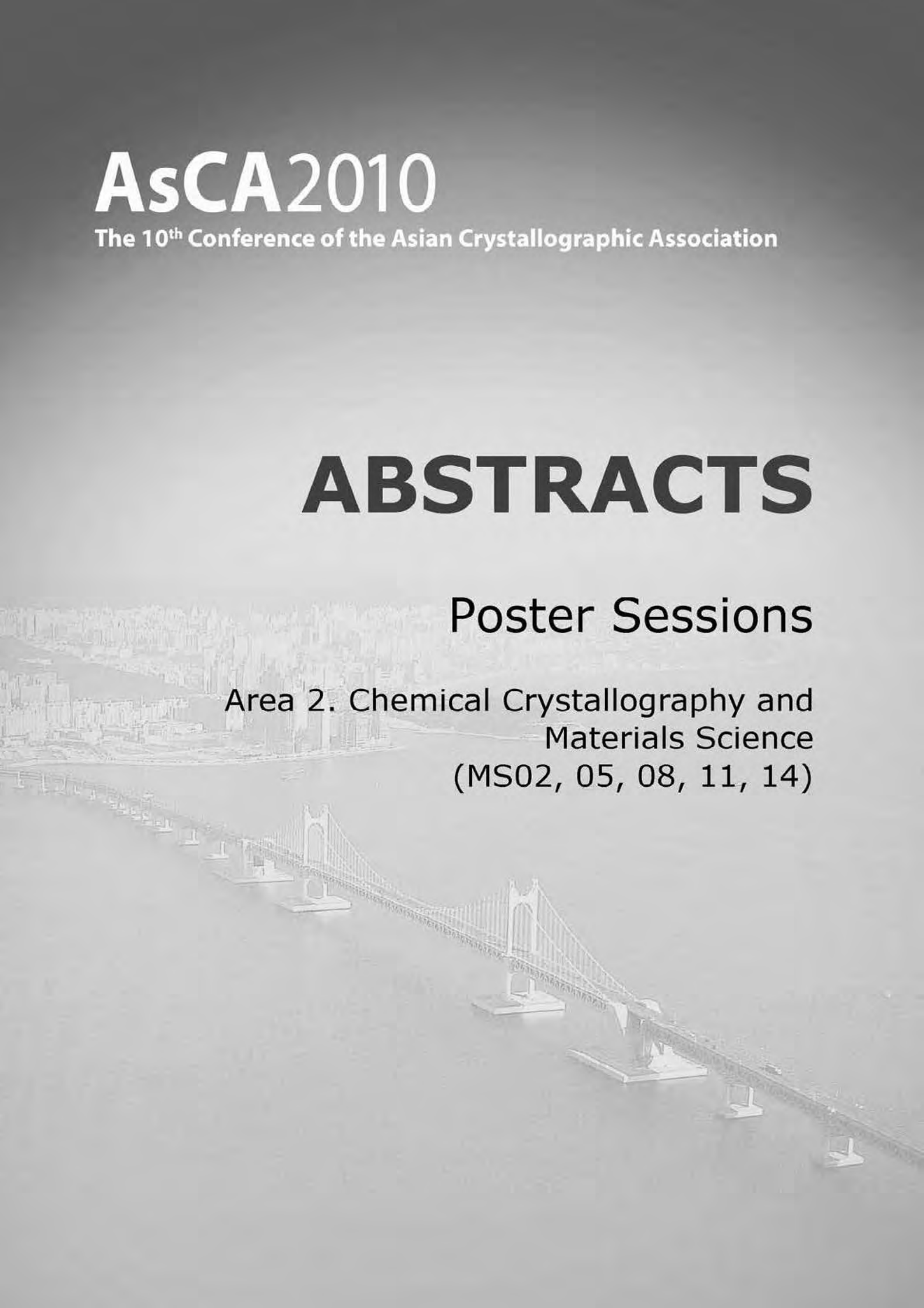

MS02-P01

Metal-organic interpenetrated frameworks based on dipyridyl ligands bearing amide groups

Pei-Chi, Cheng, Jian-Jr Cheng, Ya-Ting Chang and Jhy-Der Chen

Department of Chemistry, Chung-Yuan Christian University, Chung Li, Taiwan, R. O. C.
E-mail: jdchen@cycu.edu.tw

The synthesis and structural characterization of three metal-organic frameworks based on dipyridyl ligands containing amide groups and 1,4-benzenedicarboxylate ligand are reported. The complex [Zn(**L1**)(1,4-BDC)] · H_2O, **1**, which was obtained from the reaction of *N,N'*-di(4-pyridyl)dodecanamide (**L1**) and 1,4-H_2BDC (1,4-H_2BDC = 1,4-benzenedicarboxylic acid) shows an interpenetrating 3-fold framework with a bimodal 4-connected **mog** (moganite) topology, while the two diamondoid complexes [Zn(**L2**)(1,4-BDC)] · H_2O (**L2** = *N,N'*-di(4-pyridyl)adipoamide,[1] **2**, and [Cd(**L**)(1,4-BDC)] · $2H_2O$, **3**, show 8- and 9-fold interpenetrating modes, which belong to IIIa interpenetration with Z_t = 4 and Z_n = 2 and Ia interpenetration with Z_t = 9 and Z_n = 1, respectively. The **L1** ligands in **1** and **2** adopt the AGA *cis* and AAA *trans* conformations,[2] respectively, while the **L2** ligand in **3** adopt the AAGAAAGAA *trans* conformation. All the three complexes show emissions which can be tentatively assigned as $\pi \rightarrow \pi^*$ transitions.

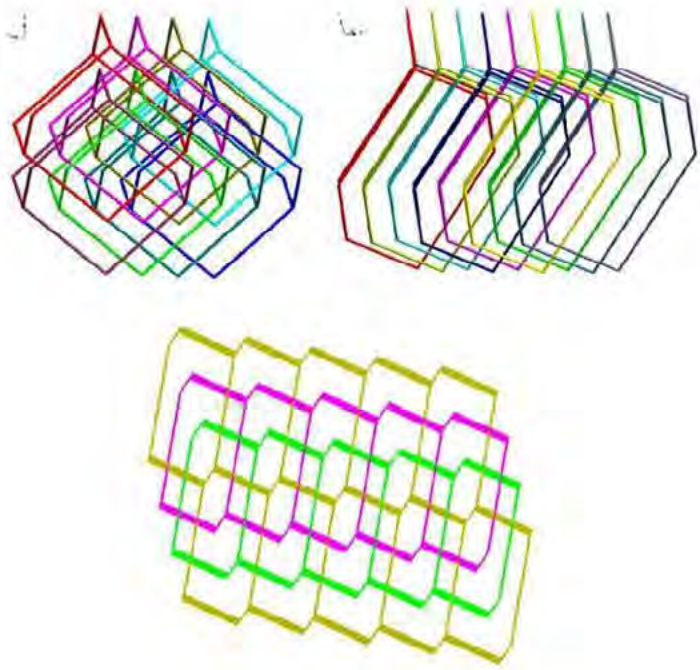

References

[1] Hsu, Y.-F., Lin, C.-H., Chen, J.-D. and Wang, J.-C., A novel interpenetrating diamondoid network f rom self-Assembly of *N,N'*-di(4-pyridyl)adipoamide an copper sulfate: An unusual 12-fold, [6+6] m ode, *Cryst. Growth. Des.*, 8, (2008), 1094-1096.

[2] Hsu, Y.-F., Hu, H.-Li, Wu, C.-J., Yeh, C.-W., Proserpio, D. M. and Chen, J.-D., Ligand isomerism-controlled structural diversity of cadmium(II) perchlorate coordination polymers containing dipyridyladipoamide ligands, *CrystEngComm*, 11, (2009), 168-176.

MS02-P02

Calcium Metal-Organic Frameworks: Synthesis, structural transformations, and sorption properties

Po-Ching Liang,[1] Hsin-Kuan Liu,[1] Chun-Ting Yeh,[1] Chia-Her Lin,[1]* and Vítězslav Zim[2]

[1]*Department of Chemistry, Chung-Yuan Christian University, Chungli 320, Taiwan*
[2]*Joint Laboratory of Solid State Chemistry of the Institute of Macromolecular Chemistry AS CR, v.v.i. and University of Pardubice, Studentská 84, 532 10 Pardubice, Czech Republic*
E-mail: chiaher@cycu.edu.tw

Six new calcium metal-organic frameworks [Ca(BDC)(DMF)(H_2O)] (1), [Ca(ABDC)(DMF)] (2), [Ca_3(BTC)$_2$(DMF)$_2$(H_2O)$_2$]·3H_2O (3), [Ca(H_2DOBDC)(DMF)] (4), [Ca(H_2DOBDC)(DMF)$_2$] (5), and [Ca(H_2DOBDC)$_2$(H_2O)$_2$] (6), (DMF = N,N′-dimethylformamide; BDC = 1,4-benzenedicarboxylate anion; ABDC = 2-aminobenzene-1,4-dicarboxylate anion; BTC = 1,3,5-benzenetricarboxylate anion; H2DOBDC = 2,5-dihydroxyterephthalate anion) were synthesized from calcium ion and aromatic carboxylic acids under solvothermal reactions and microwave-assisted solvothermal reactions. The single crystal structure analysis showed that all complexes display 3D structures containing various inorganic motifs with helical or straight 1D inorganic chains (1–3), pentagonal bipyramidal dimers (4 and 6), or discrete octahedra (5) connected through organic linkers and forming DMF- or water- coordinated neutral frameworks. It is also interesting that both compound 4 and 5 would process a dissolution/reorganization reaction comprises a break and reformation of the Ca–O bond, leading to a destruction/construction structural transformation to a supramolecular isomer, [Ca(H_2DOBDC)$_2$(H_2O)$_2$], with same chemical formula to compound 6. The compounds 1 to 5 were further characterized by TGA, PXRD and UV-vis, IR, and PL spectroscopy. The gas absorption properties were also studied.

References

[1] Liu H. K., Tsao T. H., Zhang Y. T., and Lin, C. H. "The title of the journal paper" Vol. 11, *CrystEngComm*, (2009), pp 1462-1468.

MS02-P03

Synthesis, structure and optical properties of new 4,4'-bipyridine - Intercalated lanthanide sulfates layered framework

Bunlawee Yotnoi[1], Apinus Rujiwatra[1] and Srinivasan Natarajan[2]

[1] *Department of Chemistry, Faculty of Science, Chiang Mai University, Chiang Mai, 50200, Thailand*
[2] *Solid State and Structural Chemistry Unit, Indian Institute of Science, Bangalore, 560012, India*
E-mail: y.bunlawee@gmail.com

Single crystals of $La(SO_4)_2(H_2O)_2(C_{10}H_{10}N_2)_{0.5}$ were synthesized and grown from the reaction between La_2O_3 and 4,4'-bipyridine in sulfuric solution under autogenous pressure generated at 125°C for 24 h. The crystals crystallized in triclinic $P\bar{1}$ with a = 5.03540(10) Å, b = 7.00790(10) Å, c = 16.6321(3) Å, α = 88.50°, β = 87.94°, γ = 75.47°, V = 567.679(17) Å^3 and Z = 2. The La^{III} ions show nine coordination geometry, each of which is bridged to the neighboring ions by the SO_4 anions to form 2D layers, which are intercalated by 4,4'-bipyridine molecules. The 3D networks are then constructed *via* hydrogen bonding interactions. Here, a detailed description of structure and its relation to luminescence and thermal properties are present.

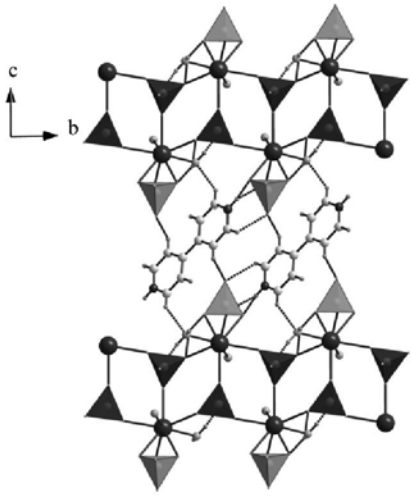

3D structure

References

Bataille, T. and Louer , D., "Two new diamine templated lanthanum sulfates, $La_2(H_2O)_2(C_4H_{12}N_2)(SO_4)_4$ and $La_2(H_2O)_2(C_2H_{10}N_2)_3(SO_4)_6.4H_2O$, with 3D and 2D crystal structures" , *J. Mater. Chem.,* Vol. 12**,** (2002), pp 3487-3493.

Dan, M., Behera, J. N. and Rao, C. N. R., "Organically templated rare earth sulfates with three-dimensional and layered structures" *J. Mater. Chem.*, Vol. 14, (2004), pp 1257-1265.

MS02-P04

X-ray structure of a nickel complex containing 2-aminopyridine and thiocyanate mixed ligands with a 3-dimensional network structure

Masoumeh Tabatabaee,* Saina Saheli

Department of Chemistry, Islamic Azad University Yazd Branch, Yazd, Iran
E-mail: tabatabaee45m@yahoo.com

Pyrimidine derivatives possess considerable biological activity and have been widely used in medicinal and industrial applications. The complexing ability of 2-aminopyrimidine (amp) derivatives with transition metal ions is of great interest. Several transition metal complexes of 2-aminopyrimidine with halide salts, MX_2 (M= Pt, Pd, Cu, Mn, Co and Ni), have been synthesized and their crystal structures reported [1-4]. In continuation of our recent works on aminopyrimidine derivatives [5, 6] and using of 2-aminopyrimidine as neutral ligand [7], in this communication we wish to report our results on the synthesis and characterization of the complex of Ni^{II} with 2-aminopyrimidine and thiocyanate mixed ligands, formulated as $[Ni(amp)_2(SCN)_2(H_2O)_2].2H_2O$ (**1**). 1 crystallizes in the triclinic, space group P-1. The metal ion is hexacoordinated by heterocyclic nitrogen atoms of two 2-aminopyrimidin ligands, two nitrogen atoms of SCN^- ions and two oxygen atoms of two coordinated water molecules Fig 1. The two uncoordinated water molecules occupy suitable positions in the cell. Uncoordinated water molecules are bridged between one complex and adjacent one with strong hydrogen bonds. Extensive O-H...O, O-H...N, O-H...S and N-H... between NH_2 group of 2-minopyrimidine, thiocyanate ions, coordinated and uncoordinated water molecules contribute to the formation of a two-dimensional supramolecular structure (Fig 2).

Fig. 1 General view of 1 in representation of atoms *via* thermal ellipsoids at 50% probability level.

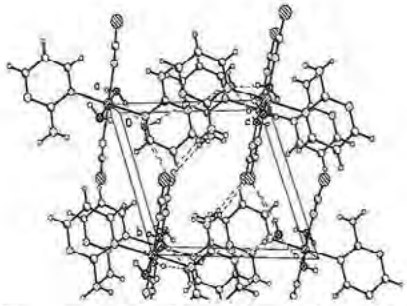

Fig. 2 The fragment of crystal packing of 1 along the crystallographic plane *bc*

References

[1] Ponticelli, G., Spanu, A., Cocco T. and Onnis V. Transition Met. Chem., "palladium(II) and platinum(II),(IV) complexes of 2-aminopyrimidine derivatives", 24, (1999), 370-372.
[2] Prince, B.J., Turnbull, M.M. and Willett, R.D., "Copper(II) halide complexes of 2-aminopyrimidine…", J. Coord. Chem., 56, (2003), 441-452.
[3] Lee, J-H. Lewis, B. Mendes, J. Urnbull, M. & Awwadi, F., "Transition metal halide salts and complexes of 2-aminopyrimidine …", J. Coord. Chem., 56, (2003), 1425-1442.
[4] Masaki, M. E., Prince, B.J. and Turnbull, M.M., "Transition metal halide salts and complexes of 2-aminopyrimidine …", J. Coord. Chem., 55, (2002), 1337-1351.
[5] Tabatabaee, M., Hakimi, F., Roshani, M., Mirjalili, M. and Kavasi, H. R., "1-(2-Pyridyl)-N,N0-dipyrimidin-2-ylmethanediamine", Acta Cryst. E64, (2008), o2112.
[6] Tabatabaee, M., Masoodpour, L., Gassemzadeh M. and Hakimi F., "N,N′-(4-Chlorobenzylidene)dipyrimidin-2-amine", Acta Cryst. E65, (2009), o2979.
[7] Tabatabaee, M., "Diaqua(2-minopyrimidine)(pyridine-2,6-dicarboxylato)Ni(II) monohydrate", Acta Cryst. E66, (2010), m647-m648.

MS02-P05

Structural diversity of four Nd(III)-NDC MOFs based on different secondary building unts (SUBs) showing interesting gas adsorption properties (NDC^{2-} = 2,6-naphthalenedicarboxylate)

Chih-Chieh Wang[1], Ching-Chun Yang[1], Chang-Tsung Yeh[1], and Gene-Hsiang Lee[2]

[1]*Department of Chemistry, Soochow University, Taipei, Taiwan*
[2]*Department of Chemistry, National Taiwan University, Taipei, Taiwan*
E-mail: ccwang@scu.edu.tw

Four lanthanide metal-organic frameworks (LMOFs), $\{[Nd(NDC)_{1.5}(DMF)_2]\cdot 2DMF\cdot H_2O\}_n$ (**1**), $\{[Nd(NDC)_{1.5}(H_2O)_2]\cdot 2DMA\}_n$ (**2**), $\{[Nd_2(NDC)_3(DMA)(H_2O)_2]\cdot 3DMA\}_n$ (**3**), and $\{[Nd(NDC)(NO_3)(DMA)_2]\}_n$ (**4**) (NDC^{2-} = 2,6-Naphthalenedicarboxylate; DMF = dimethylformamide, DMA = dimethylacetamide), based on Nd(III)–NDC bridges, have been synthesized and structural characterized by single-crystal X-ray diffraction method. In compound **1**, each Nd(III) ion is nine-coordinate bonded to nine oxygen atoms of five NDC^{2-} ligands and two DMF molecules. Two Nd(III) ions are bridged by six NDC^{2-} ligands with three different coordination modes, bis-chelating, tetramonodentate, and bischelating/bismonodentate, to generate a $[Nd_2(COO)_6]$ dinuclear moiety, which serves as an octahedral secondary building unit (SBU) to produce a 3D open-framework coordination polymer. In **2**, each Nd(III) ion is eight-coordinate bonded to eight oxygen atoms of five NDC^{2-} ligands and two water molecules. The Nd(III) ions are bridged by four tetramonodentate and one bis-chelating NDC^{2-} ligands with a square-pyramidal building unit to produce a 3D triangle MOF. In **3** and **4**, the Nd(III) ions are bridged by four NDC^{2-} ligands with tetramonodentate coordination mode to generate a $[Nd_2(COO)_4]$ dinuclear moiety, which serves both as square paddle-wheel building unit to produce a 3D open-framework and 2D layered-framework MOFs for **3** and **4**, respectively. The TGA measurements show that all of the four Nd(III)–NDC MOFs exhibit high thermo-stability and keep their crystalline forms up to about 400 °C. The sorption isotherm of N_2 and H_2 at 77 K shows a type-I profile for **1** and **2**, and their surface area has been determined by using the BET equation.

Syntheses, structures and photoluminescence properties of hexanuclear gold(I)-silver(I) mixed metal complexes

Hiroko Fujioka, Yoshiki Ozawa, and Koshiro Toriumi

Department of Material Science, University of Hyogo, 3-2-1 Kouto, Kamigori-cho, Hyogo 678-1297, Japan
E-mail: ri09n018@stkt.u-hyogo.ac.jp

Hexanuclear metal complexes of Cu(I) or Ag(I), having a d^{10} electron configuration, give strong red or green photoluminescence under UV irradiation. [1] Six metal atoms are located in an octahedral arrangement linked by iminiothiolato ligands, constructing a wheel-like structure (Fig.1). Their emission properties are assigned to a transition from a triplet cluster-centered excited state (^{3}CC) which consists of in-phase s/p orbitals of six metal atoms. [1] On the triplet photoexcited state, the metal core has been expected to be contracted. Recently, we have reported the single crystal structure analysis of $[Cu_6(Et\text{-}pyt)_6]$ (**1**) (Et-pyt$^-$ = 6-ethylpyridinethiolato) under photoirradiation, in which the direct observation of the shrinkage of the metal cluster core has been demonstrated. [2] On the other hand, there are few reports for such integrated coordination compounds of Au(I). Here, we report new hexanuclear mixed-metal complexes $[Ag_4Au_2(Et\text{-}pyt)_4X_2]$ (X= Cl(**3**), Br(**4**), I(**5**)) including Au(I) synthesized by the metal exchange reaction with the silver complex $[Ag_6(Et\text{-}pyt)_6]$ (**2**).

The complex **3** was obtained as a pale yellow solid from a chloroform solution of **2** reacted with AuCl(tht) (tht = SC_4H_8). The X-ray structure analysis reveals that the complex consists of four Ag(I) and two Au(I) linked by four Et-pyt ligands, constructing an octahedral cluster (Fig. 2). The Au(I) atoms are located on diagonal vertexes of the octahedron. Two Cl atoms are bridged adjacent two Ag(I) atoms in the equatorial position. The whole molecule takes D_2 symmetry. The bromo- or iodo-bridged analogues (**4**, **5**) were also obtained by reacting with AuBr(tht) or AuI, respectively. These complexes **3**, **4**, **5** give orange emission under UV light (365nm) irradiation in the crystalline state (Fig. 3). The emission maxima (575 nm for **3**, **4** and 625 nm for **5**) are slightly longer than that in the Ag_6 complex **2**.

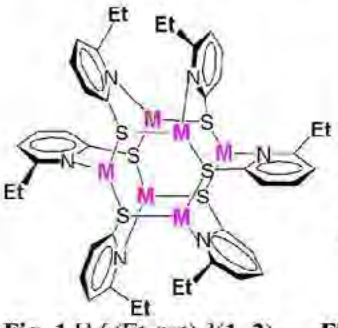

Fig. 1 $[M_6(Et\text{-}pyt)_6]$(**1**, **2**).

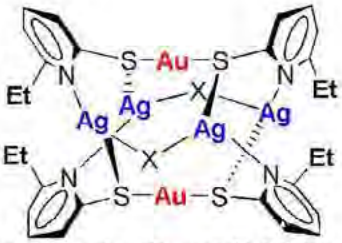

Fig. 2 $[Ag_4Au_2(Et\text{-}pyt)_4X_2]$(**3**–**5**).

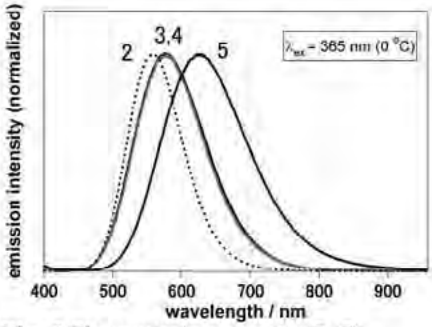

Fig. 3 Photomission spectra (**2**–**5**).

References

[1] Xie H., Kinoshita I., Karasawa T., Kimura K., Nishioka T., Akai I., Kanemoto K., "Structure Study and Luminescence Thermochromism in Hexanuclear 6-Methyl-2-Pyridinethiolato Copper(I) Crystals." *J. Phys. Chem. B*, Vol. 109 No. 19,(2005), pp 9339-9345.

[2] Ishida T, Kimura K., Ozawa Y., Mitsumi M., Toriumi K., "Synthesis and crystal structure analysis at photoexcited state of hexanuclear Cu(I) and Ag(I) 6-ethylpyridine-2-thiolato complexes.", Symposium of Coord. Chem. Soc. Jpn., Kanazawa, Japan, Vol. 58, 3Bb-10, (2009).

MS02-P07

Functional cyclobutane derivatives for metal organic frameworks

Goutam Kumar Kole, Geok Kheng Tan, Lip Lin Koh and Jagadese J. Vittal

[1]*Department of Chemistry, National University of Singapore, 3 Science Drive 3, Singapore-117543, Singapore*
E-mail: goutam@nus.edu.sg

Metal-organic frameworks (MOFs) constructed from multidentate ligands have emerged as an important class of materials for various potential applications in sorption, separation, ion exchange, catalysis, sensor technology and drug delivery. Aromatic polycarboxylic acids have been proven to be potential class of ligands for the designed synthesis of robust coordination polymers with interesting framework topologies by tuning their sizes and shapes. Herein, we employ the photochemical [2+2] cycloaddition reaction to generate functional cyclobutane derivatives with desired geometry as novel ligands for synthesizing MOFs.

Crystal engineering principles have been exploited to generate a series of molecular salts of *trans*-4,4'-stilbenedicarboxylic acid (H_2SDC) and *trans*-3-(4-pyridyl)-acrylic acid (4-PA) where we have achieved the parallel orientations of the photoreactive double bonds prior to dimerization. The detailed synthetic strategy to access *rctt*-1,2,3,4-tetrakis-(4'-carboxyphenyl)-cyclobutane (TCCB) in quantitative yield via green-mechanochemical route using organic amines with H_2SDC and the possible relation with the chain lengths of the diamines have been described. The crucial role of anions present in the molecular salts of asymmetric olefins like 4-PA have been explored for the stereoselective synthesis of such cyclobutane derivatives. Two possible parallel orientations for asymmetric olefins like 4-PA, *viz.* '*head-to-head*' and '*head-to-tail*' were successfully achieved by tuning the anions present in the molecular salts. The possible cation – cation repulsion in the *head-to-head* orientation is balanced and stabilised by cation – anion interactions of bisulphate and sulphate anions, on the other hand, the *head-to-tail* orientation is stabilised by cation-π (carbonyl) interactions. The photochemical [2+2] cycloaddition reaction of the ground sample of the sulphate-bisulphate salt of 4-PA took place quantitatively after reorganization of C=C double bonds. All the cyclobutane derivatives are synthesized for the first time *via* environmentally benign green route and in quantitative yields. The structures (with framework topology) of the MOF and co-crystal obtained from TCCB would be elaborately discussed in the presentation.

References

[1] Kole G. K., Tan G. K. and Vittal J. J., "Anion-Controlled Stereoselective Synthesis of Cyclobutane Derivatives by Solid-State [2 + 2] Cycloaddition Reaction of the Salts of trans-3-(4-Pyridyl) Acrylic Acid", *Org. Lett.*, Vol. 12, No. 1, (2010), pp 128-131.

[2] Kole G.K., Koh L. L., Lee S. Y., Lee S. S. and Vittal J. J. "A new ligand for metal–organic framework and co-crystal synthesis: mechanochemical route to *rctt*-1,2,3,4-tetrakis-(4'-carboxyphenyl)-cyclobutane" *Chem. Commun.*, Vol. 46, (2010), pp 3660-3662.

[3] Kole G. K., Cairns A. J., Eddaoudi M. and Vittal J. J., "The Solvent-free porous framework resulted from 3D entanglement of 1D zigzag coordination polymer", *New J. Chem.*, Vol. 34, (2010), Advance Article, DOI: 10.1039/c0nj00217h

[4] Kole G. K., Tan G. K. and Vittal J. J., "Crystal engineering studies on the salts of *trans*-4,4'-stilbenedicarboxylic acid in the context of solid state [2+2] cycloaddition reaction" *CrystEngComm*, Manuscript accepted for publication.

Stepwise synthesis of charged and neutral 2-D networks via 1-D silver(I) coordination polymer based on bis(4-pyridylmethyl) sulfide

Ki-Min Park[1], Joobeom Seo[1], Suk-Hee Moon[2], Jagadese J. Vittal[1,3] and Shim Sung Lee[1]

[1]*Department of Chemistry and WCU Center for NanoBio Chemical Materials, Gyeongsang National University, Jinju 660-701, South Korea*
[2]*Subdivision of Food Science, Kyungnam College of Information and Technology, Busan 616-701, South Korea*
[3]*Department of Chemistry, National University of Singapore, 3 Science Drive 3, Singapore 117543, Singapore*
E-mail: kmpark@gnu.ac.kr

For the advances of controlled engineering of solid-state structures with large and potentially useful cavities or channels, much effort has focused upon the use of rationally designed ligand system and coordination characteristics of the metal ions. More subtle effects on the topological configuration such as anion control are also receiving renewed attention. Thus, it is desirable to be able to prevent interpenetration when we need, and be able to generate the structure with the useful cavities or channels. The approach we have used to generate the anticipative open frameworks is a stepwise increment of the dimension via two step synthesis.

To achieve our stepwise-reaction strategy, we have investigated the effect of anion in the coordination environment of 1-D silver(I) coordination polymer precursors based on bis(4-pyridylmethyl)sulfide **L**, as well as the versatility of bridging ligands such as 4,4'-bipyridine (**bpy**) and terephthalate ($\mathbf{tp}^{2-}$) on the stepwise synthesis of the higher dimensional open frameworks with neutral or positive charge.

Herein, we report the stepwise synthesis and structural characterization of 2-D coordination polymer frameworks with positive charged or neutral cavities. First, reactions of bis(4-pyridylmethyl)sulfide (**L**) with silver salts (**1**: nitrate and **2**: perchlorate) afforded the respective double-stranded 1-D chains $[Ag(\mathbf{L})NO_3]_n$ (**1**) and $\{[Ag_2(\mathbf{L})_2](ClO_4)_2\}_n$ (**2**) both of which are stabilized by face-to-face π-π interactions. In this case, the silver(I) center in the nitrato complex **1** shows four-coordinated distorted tetrahedral geometry, whereas that of the perchlorato complex **2** exhibits a distorted trigonal planar geometry. The difference of these structures indicates that the coordination ability of the anions have important effects on the silver(I) coordination environments. Interestingly, the perchlorato 1-D complex **2** allows the further reactions with bridging ligands such as 4,4'-bipyridine (**bpy**) and terephthalate ($\mathbf{tp}^{2-}$) to give a 2-D positive-charged network $\{[Ag_2(\mathbf{L})_2(\mathbf{bpy})]\cdot(ClO_4)_2\cdot C_6H_6\}_n$ (**3**) and a 2-D neutral network $\{[Ag_2(\mathbf{L})_2(\mathbf{tp})]\cdot 2DMSO\cdot 6H_2O\}_n$ (**4**), respectively. The nitrato 1-D complex **1**, however, showed no reactivity with the bridging ligands in the same condition. The results show that the replacement of anion by the bridging ligand in the coordination sphere of the 1-D precursor plays crucial roles in determining the reactivity for the synthesis of higher dimensional open frameworks.

2-D positive-charged network of **3** $\{[Ag_2(\mathbf{L})_2(\mathbf{bpy})]\cdot(ClO_4)_2\cdot C_6H_6\}_n$

Ladder type network of **2** $\{[Ag_2(\mathbf{L})_2](ClO_4)_2\}_n$

2-D neutral network of **4** $\{[Ag_2(\mathbf{L})_2(\mathbf{tp})]\cdot 2DMSO\cdot 6H_2O\}_n$

MS02-P09

Networking of O_2S_2-macrocycle with silver perchlorate into 1-D and 2-D coordination polymers: Kinetic and thermodynamic products

So Young Lee[1], Jong Hwa Jung[1], Ki-Min Park[1], Jagadese J. Vittal[1,2] and Shim Sung Lee[1]

[1]*Department of Chemistry and WCU Center for NanoBio Chemical Materials, Gyeongsang National University, Jinju 660-701, S. Korea.*
[2]*Department of Chemistry, National University of Singapore, 3 Science Drive 3, Singapore 117543, Singapore*
E-mail: sslee@gnu.ac.kr

We have been interested in the assembly of supramolecular architectures based on the exocoordination of thiacrown system because the sulfur donor is expected to favor binding toward soft metal ions in an exocyclic mode.[1,2] In this work[3], the solvent-dependent double-stranded 1-D coordination polymer $[Ag_2\mathbf{L}_2(ClO_4)_2]_n$ (**1**) and another 1-D polymer $\{[Ag_2\mathbf{L}_2(CH_3CN)]\cdot 2ClO_4\}_n$ (**2a**) with the shape of a vertically halved tube were obtained in the reactions of a 16-membered O_2S_2-macrocycle **L** with silver(I) perchlorate in DCM/MeOH and CH_3CN, respectively. Time-dependent crystallization experiments unambiguously show that **2a** is a kinetic product and transforms into a thermodynamically more stable $[Ag\mathbf{L}ClO_4]_n$ (**2b**) with a 2-D square-grid structure.

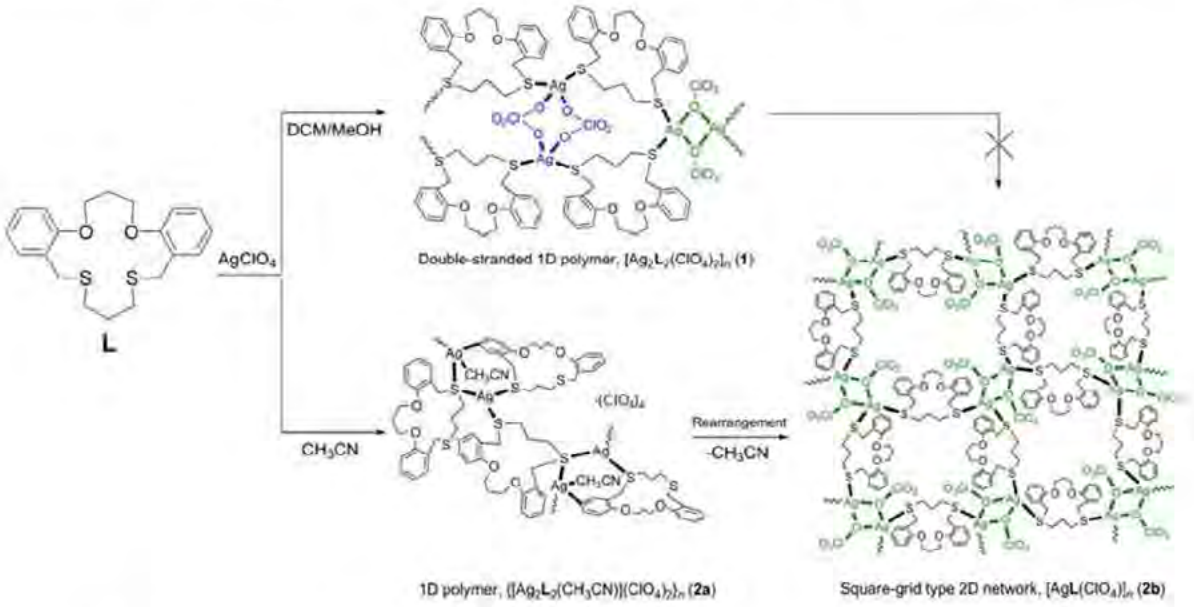

References

[1] Park, S., Lee S. Y., Lee S. S., "Discrete mercury(II) complexes, one-dimensional and palladium-mediated two-dimensional silver(I) coordination polymers of NS_2-macrocycle: synthesis and structural characterization", Inorg. Chem. Vol. 49, (2010), pp 1238-1244.

[2] Lindoy L. F., Meehan G. V., Vasilescu I. M., Kim H. J., Lee J.-E., Lee S. S., "Transition and post-transition metal ion chemistry of dibenzo-substituted, mixed-donor macrocycles incorporating five atoms", Coord. Chem. Rev., Vol. 254, (2010), pp 1713-1725.

[3] Lee S. Y., Jung J. H., Vittal J. J., Lee S. S., "The solvent-dependent networking of O_2S_2-macrocycle with silver perchlorate into 1-D and 2-D coordination polymers", Cryst. Growth Des., Vol. 10, (2010), pp 1033-1036.

MS02-P10

Synthesis of 4d–4f heterometallic coordination framework by postsynthetic modification

Young Ok Jang and Soon W. Lee

Department of Chemistry (BK21), Sungkyunkwan University, Natural Science Campus, Suwon 440-746, Republic of Korea
E-mail: kurtcobain35@nate.com

Complex $\{[Eu_2(L)_6(H_2O)_4]\cdot[Eu_2(L)_4(H_2O)_8](NO_3)\}$ (**1**) was prepared from $Eu(NO_3)_3$ and a flexible multidentate ligand (L = 3-pyridinepropionic acid) under microwave heating conditions. A novel 4*d*–4*f* (Ag–Eu) coordination polymer, $\{[EuAg(L)_2(H_2O)_3](NO_3)_2(H_2O)_4\}$ (**2**), could be prepared by the postsynthetic modification, in which complex **1** was treated with $AgNO_3$. The flexible multidentate ligand (L) possesses two potential linking groups: a pyridyl group (a soft group) and a carboxylate group (a hard group). Interestingly, complex **1** contains two dimers; one is a neutral species and the other is an ionic species. In complex **1**, carboxylates of ligands are bound to europium ions, but the pyridyl nitrogen atoms remain non-coordinated. Polymer **2** is a 3-dimensional heterometallic coordination framework, whose monomer unit consists of one Eu^{3+} ion, one Ag^{+} ion, two ligands, three aqua ligands, and two counterions. Consistent with our expectation on the basis of the hard–soft and acid–base concept, the hard Eu^{3+} ions are coordinated to the carboxylate oxygen atoms, and the soft Ag^{+} ion is coordinated to the pyridyl nitrogen atoms. The Eu···Eu distances are 4.1369 (2) and 4.0991 (2) Å.

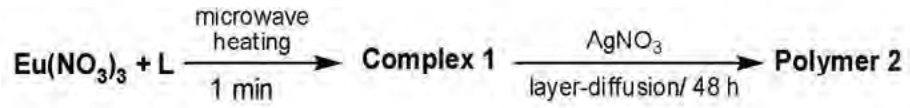

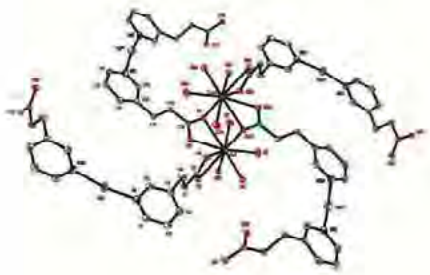

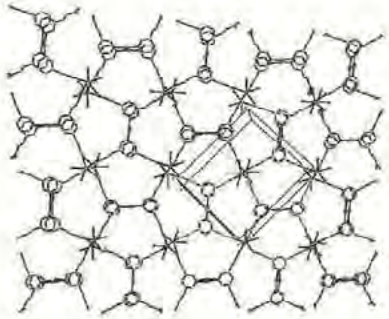

References

[1] Cahill C. L., de Lill D. T. and Frisch M., "Homo- and heterometallic coordination polymers from the f element", *CrystEngComm*, 9, (2007), 15–26.

[2] Wang Z. and Cohen S. M., "Postsynthetic modification of metal–organic frameworks", *Chem. Soc. Rev.*, 38, (2009), 1315–1329.

MS02-P11

Reactivity of RhCp* complexes containing labile ligands toward potential linking ligands containing terminal thiophene or furan rings: preparation and structures of $[Cp^*Rh(L^1)Cl_2]$, $[Cp^*Rh(\eta^2\text{-}NO_3)(L^1)](OTf)$, and $\{[Rh(L^2)]\cdot(OTf)\}_\infty$ [L^1 = 1,2-bis((thiophen-2-yl)methylene)hydrazine); L^2 = 1,2-bis((furan-2-yl)methylene)hydrazine]

Kyung-Eun Lee and Soon W. Lee

Department of Chemistry (BK21), Sungkyunkwan University, Natural Science Campus, Suwon 440-746, Korea
E-mail: hoyi21236@skku.edu

Rhodium(III)–Cp* complexes containing labile ligands, $[Cp^*RhCl_2]_2$, $[Cp^*Rh(\eta^2\text{-}NO_3)(OTf)]$, and $[Cp^*Rh(OH_2)_3](OTf)_2$, reacted with potential linking ligands [L^1 = (2-thiophene)–CH=N–N=CH–(2-thiophene); L^2 = (2-furan)–CH=N–N=CH–(2-furan)] to give two molecular compounds, $[Cp^*Rh(L^1)Cl_2]$ (**1**) and $[Cp^*Rh(\eta^2\text{–}NO_3)(L^1)](OTf)\cdot CH_2Cl_2$ (**2**·CH_2Cl_2), and one organometallic coordination polymer, $\{[Rh(L^2)]\cdot(OTf)\}_\infty$ (**3**). Whereas one imine nitrogen atom within the ligand is coordinated to the Rh metal in compounds **1** and **2**, both nitrogen atoms are bound to two neighboring Rh metals in compound **3** to lead to a 1-D chain polymer.

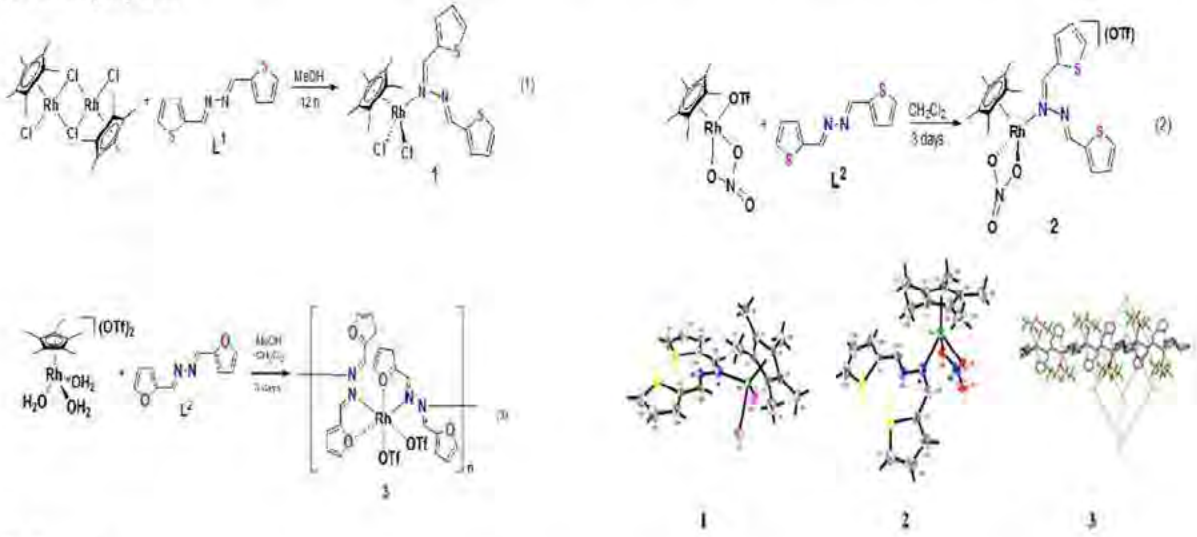

References

[1] Swiegers G. F. and Malefetse T. J., "Classification of coordination polygons and polyhedra according to their mode of self-assembly", *Coord. Chem. Rev.*, 225, (2002), 91–121.

[2] Wang J.-Q., Ren C.-X. and Jin G.-X., "Synthesis and Structural Charaterization of Macrocyclic Half-Sandwich Rhodium(III) and Iridium(III) complexes Bearing Bipyridyl Derivatives and Terephalate", *Organometallics*, 25, (2006), 74–81.

[3] Varshavsky Y. S., Cherkasova T. G., Galding M. R., Khrustalev V. N., Podkorytov I. S., Gindin V. A., Smirnov S. N. and Nikol'skii A. B., "Heterometallic cyanide-bridged complexes containing $Rh^{I}Ru^{II}Rh^{I}$ triad: NMR data on exchange reactions and ligand effect transmission", J. Organomet. Chem., 694, (2009), 2917–2922.

MS02-P12

Tailored thermal expansion in Metal-Organic Frameworks

Yue Wu[1], Cameron J. Kepert[1]

[1]*School of Chemistry, The University of Sydney, NSW 2006, Australia*
E-mail: wu@chem.usyd.edu.au

Metal-organic framework (MOF) chemistry provides the opportunity to make crystalline solids with an unprecedented level of structural and functional control. Previously, designing solid materials for a particular coefficient of thermal expansion has been extremely difficult. Our previous research has demonstrated that the dynamic behavior of certain structural motifs common to a wide range of MOFs also counteract the usual positive thermal expansion of chemical bonds.[1,2] This work suggests a new route whereby the thermal expansion properties of a material may be controlled chemically, through the structural versatility of MOFs.

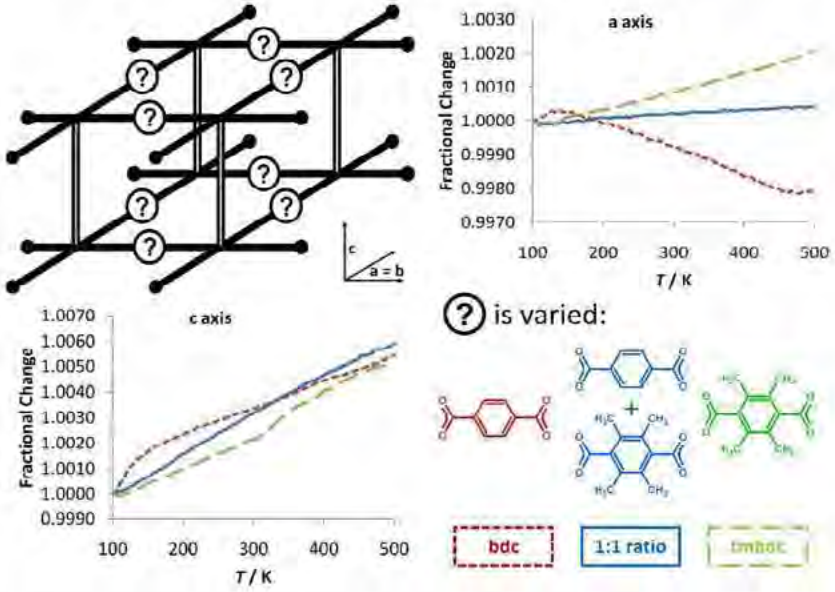

Figure 1. The unit cell thermal behavior of a framework with varying ligands

Here we look at a series of isotopological, tetragonal frameworks. They are composed of square grid sheets formed by 1,4-benzenedicarboxylates linked through dimetal-tetracarboxylate 'paddlewheels', forming the a-b plane. The sheets are pillared by diazo[2.2.2]bicyclooctane (dabco) through the paddlewheel axial site, along the c axis. We show that by varying the carboxylate ligand, the thermal expansion of the framework in the a-b plane may be positive or negative (see fig. 1). Moreover, by making a mixing ligand framework, a near-zero thermal expansion can be achieved. It is also shown that thermal expansion in the c-axis is almost independent of the carboxylate ligands used. We deduce possible mechanisms for the behavior observed based on our previous research into the negative thermal expansion of MOFs bearing the paddlewheel motif.

References

[1] Wu Y., Kobayashi A., Halder G. J., Peterson V. K., Chapman K. W., Lock N., Southon P. D., Kepert C. J., "Negative Thermal Expansion in the Metal-Organic Framework Material Cu-3(1,3,5-benzenetricarboxylate)(2)" *Angew. Chem. Int. Ed.*, Vol. 47, No. 46, (2008) pp 8929 – 8932

[2] Peterson V. K., Kearley G. J., Wu Y., Ramirez-Cuesta A.J., Kemner E., Kepert C. J., "Local Vibrational Mechanism for Negative Thermal Expansion: A Combined Neutron Scattering and First-Principles Study" *Angew. Chem. Int. Ed.*, Vol. 49, No. 3, (2010) pp 585-588

MS02-P13 – Cancelled

Structurally responsive flexible PCPs to sorption of guests and ligand substitutions

Joobeom Seo,[1] Ryotaro Matsuda,[1,2] Charlotte Bonneau[1] and Susumu Kitagawa[1,2,*]

[1]*ERATO Kitagawa Integrated Pores Project, Japan Science and Technology Agency (JST), Kyoto, Japan*
[2]*Institute for Integrated Cell-Material Sciences, Kyoto University, Kyoto, Japan*
E-mail: joobeomi@gmail.com

One of the advantages of porous coordination polymers (PCPs) or metal organic frameworks (MOFs) compared to the other microporous compounds such as zeolites or activated carbons reside in the opportunity to control the pore surface properties through the functionalization of the organic ligands.[1] In addition, PCPs with flexible structure can undergo several types of dynamic structural transformations resulting in high selectivity for guest inclusion, hysteretic sorption, stepwise guest uptake and gate-opening type adsorption behaviors.[1] Therefore, the design of pore properties utilizing flexible motifs or functional organic components is of importance to obtain PCPs with desirable functions. In this presentation, we will introduce two topics in the characterization of structural transformations of flexible PCPs upon sorption of guest molecules.

In the first topic, a 3D pillared-layer coordination polymer, $\{[Cd_2(pzdc)_2\mathbf{L}(H_2O)_2]\cdot 5(H_2O)\cdot(CH_3CH_2OH)\}_n$ (**1**; pzdc = 2,3-pyrazinedicarboxylic acid; **L** = 2,5-bis(2-hydroxyethoxy)-1,4-bis(4-pyridyl)benzene) will be introduced.[2] Compound **1** shows i) a rotatable pillar bearing ethylene glycol side chains acting as a molecular gate with locking/unlocking interactions triggered by guest inclusion between the side chains and ii) framework flexibility with slippage of the layers (Figure 1a). We have demonstrated how these characteristics have direct consequences on the selective, stepwise adsorption and gate-opening behaviors of the framework for various guest molecules.

The second topic concerns 2-fold interpenetrated PCPs. A series of 4-pyridine terminated ditopic pillar ligands with varying functional substituents on the central phenyl ring were synthesized and incorporated into 2-fold interpenetrated frameworks to understand the ligand substitution effects on the structural transformations and guest adsorption properties. The frameworks clearly show reversible structural transformations in response to the removal and rebinding of guest molecules (Figure 1b). The characterization of the framework deformations has provided valuable insights for the understanding of the stepwise or gate-opening type adsorption behaviors of gases on the frameworks.

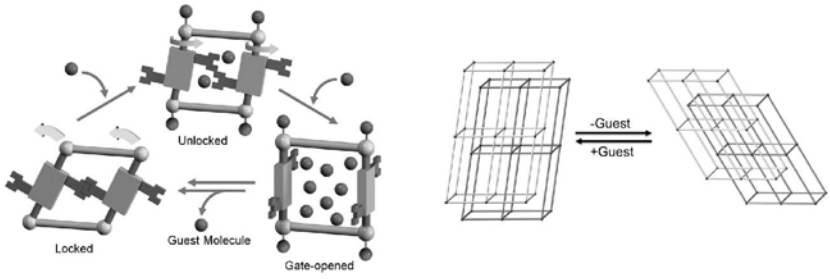

Figure 1. Schematic representations of the structural transformations for (a) a 3D pillared-layer coordination polymer **1** and (b) a series of 2-fold interpenetrated frameworks.

References

[1] S. Kitagawa and R. Matsuda, "Chemistry of Coordination Space of Porous Coordination Polymers", *J. Coord. Chem. Rev.*, 251, (2007), 2490.

[2] J. Seo, R. Matsuda, H. Sakamoto, C. Bonneau and S. Kitagawa, "A Pillared-Layer Coordination Polymer with a Rotatable Pillar Acting as a Molecular Gate for Guest Molecules", *J. Am. Chem. Soc.*, 131, (2009), 12792.

MS02-P15

Solvothermal synthesis and structures of templated and hybrid solids in the imidazole manganese vanadate system

Kittipong Chainok[1,2], Herman H-Y. Sung[1], Ian D. Williams[1]

[1]*Department of Chemistry, Hong Kong University of Science and Technology, Hong Kong*
[2] *Department of Chemistry, Rangsit University, Phathumtani, Thailand*
E-mail: chwill@ust.hk

The solvothermal synthesis and X-ray crystal structures of six new manganese vanadate phases incorporating imidazole ligands or counterions are reported. The system clearly demonstrates how product types are dependent on temperature, time, pH and stoichiometry. Two organo-templated open-frameworks of formula $[ImH][Mn_3(OH)_2(V_4O_{13})]$ **1** and **2** (shown below) are formed between 110−160°C with lower imidazole ratios. These contain 10-membered ring channels housing imidazolium counterions and have mixed Mn^{II}–Mn^{III} valences. The structures are stable to 200°C and loss of guest molecules. Other 2D hybrid phases are typically formed using higher imidazole ratios and at lower temperatures, these include $[Mn_2(Im)_8(V_4O_{12})]$ **3** containing cylotetravanadate rings and $[ImH][Mn(Im)_3(V_3O_9)]$ **4**. in which $(VO_3)n$ chains are cross-linked by $Mn(Im)_2$ and $Mn(Im)_4$ units. An analog of **3** $[Mn_2(Im)_6(dmso)_2(V_4O_{12})]$ **5** was also formed from dimethylsulfoxide. Compounds **1-5** contain octahedral Mn and tetrahedral V ions, but another hybrid solid $[Mn_2(Im)_3(V_4O_{12})]$ **6** was found to contain both square-pyramidal and octahedral Mn^{II} centers and 5-coordinate bipyramidal vanadium, underscoring the structural diversity possible in the system.

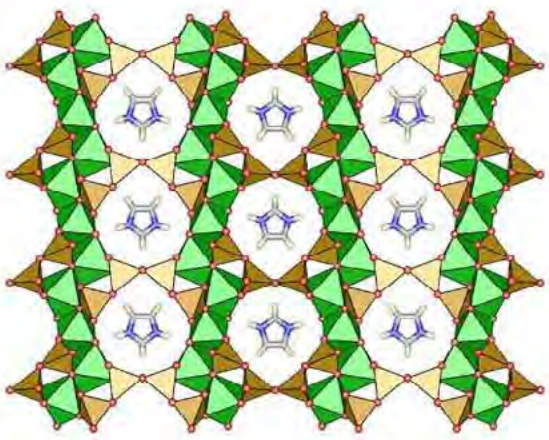

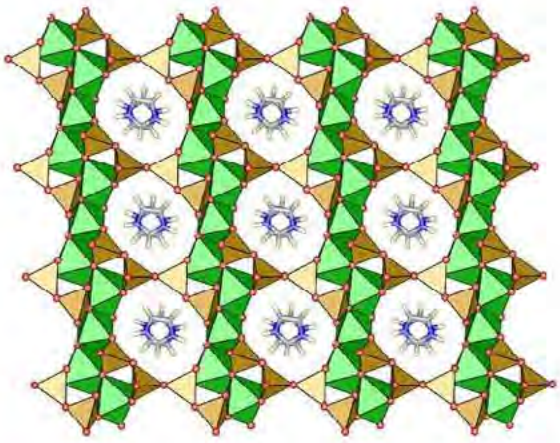

MS05-P01

Supramolecular assemblies of 1,2,4,5-cyclohexanetetracarboxylic acid with various aza-donor compounds

Manish Raut[1] and V. R. Pedireddi[2]

[1]*Solid State and Supramolecular Structural Chemistry Unit, Division of Organic Chemistry, National Chemical Laboratory, Dr. Homi Bhabha Road, Pune 411 008, India*
[2]*School of Basic Sciences, Indian Institute of Technology, Bhubaneswar 751 013, India*
E-mail: md.raut@ncl.res.in

A supermolecule is an organized entity that is created by the association of two or more chemical species held together by intermolecular forces such as hydrogen bonds, van der Waals forces, coordination bonds, halogen bonds, etc.[1] As the carboxylic acid moiety represents the most widely studied functional group within the realm of supramolecular synthesis, we have carried out co-crystallization of 1,2,4,5-cyclohexanetetracarboxylic acid (**1245CTC**) with various aza donor compounds like 4,4'-bipyridine, 2,2'-bipyridine, 1,2-*bis*(4-pyridyl)ethane, 1,2-*bis*(4-pyridyl)ethene, phenazine, 1,10-phenanthroline, 4,7-phenanthroline, etc., to study the affinity of the polycarboxylic acids in molecular recognition.[2,3] The complexes, thus, obtained have been characterized by single crystal X-ray diffraction method and the structural analysis reveal the formation of exotic supramolecular assemblies in the form of host-guest type networks, sheets, interpenetrated ladders, etc. Packing arrangement for the representative examples are shown in Figure 1. The structural features of these assemblies would be illustrated in detail in poster presentation.

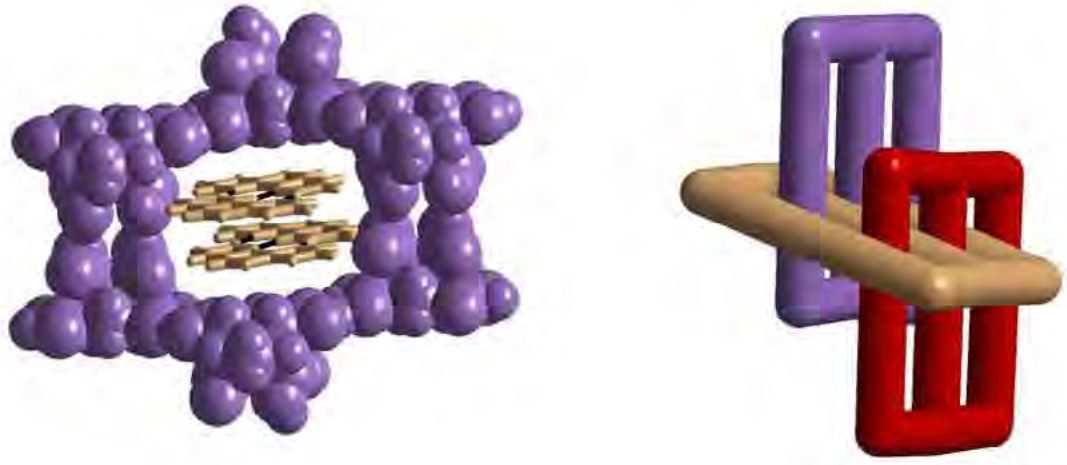

(a) (b)

Figure 1: Supramolecular assemblies formed by 1,2,4,5-cyclohexanetetracarboxylic acid with 1,10-phenanthroline and (b) 4,4'-bipyridine (schematic representation).

References

[1] Lehn J. -M., "Supramolecular Chemistry: Concepts and Perspectives"; VCH: Weinheim, (1995).
[2] Arora, K. K.; Pedireddi, V. R., "A Rational Study of Crystal Engineering of Supramolecular Assemblies of 1,2,4,5-Benzenetetracarboxylic Acid" J. Org. Chem. Vol. 68, No. 24, (2003), pp 9177-9185.
[3] Arora, K. K.; Talwelkar, M. S., Pedireddi, V. R., "Supramolecular synthesis of some molecular adducts of 4,4'-bipyridine N,N'-dioxide" New J. Chem. Vol. 33, No. 1, (2009), pp 57-63.

MS05-P02

Unusual C--H...π interactions in the structure of 3,4,5-trimethoxy -*N*-*p*-tolylbenzamide

Jim Simpson[1] and Aamer Saeed[2]

[1] *Department of Chemistry, University of Otago, P.O. Box 56, Dunedin 9054, New Zealand*
[2] *Department of Chemistry, Quaid-i-Azam University, Islamabad 45320, Pakistan*
E-mail : jsimpson@alkali.otago.ac.nz

3,4,5-Trimethoxy-*N*-*p*-tolylbenzamide (I) is a benzanilide derivative derived from *p*-toluidine and 3,4,5-trimethoxybenzoyl chloride. The crystal packing is predictably influenced by strong N—H...O hydrogen bonds, augmented by C—H...O contacts generating $R^2_1(6)$ ring motifs and forming chains of molecules down the *a* axis [1]. These chains are further reinforced by C—H...π interactions involving the methyl groups of a methoxy substituent. Chains are linked in a head-to-tail fashion by an additional weak C—H...O contact and other C—H...π interactions building the three dimensional network. An unusual feature of the packing in this structure is the extensive contribution of C—H...π interactions, involving two hydrogen atoms from each of the methyl groups of the 3- and 5- methoxy substituents.

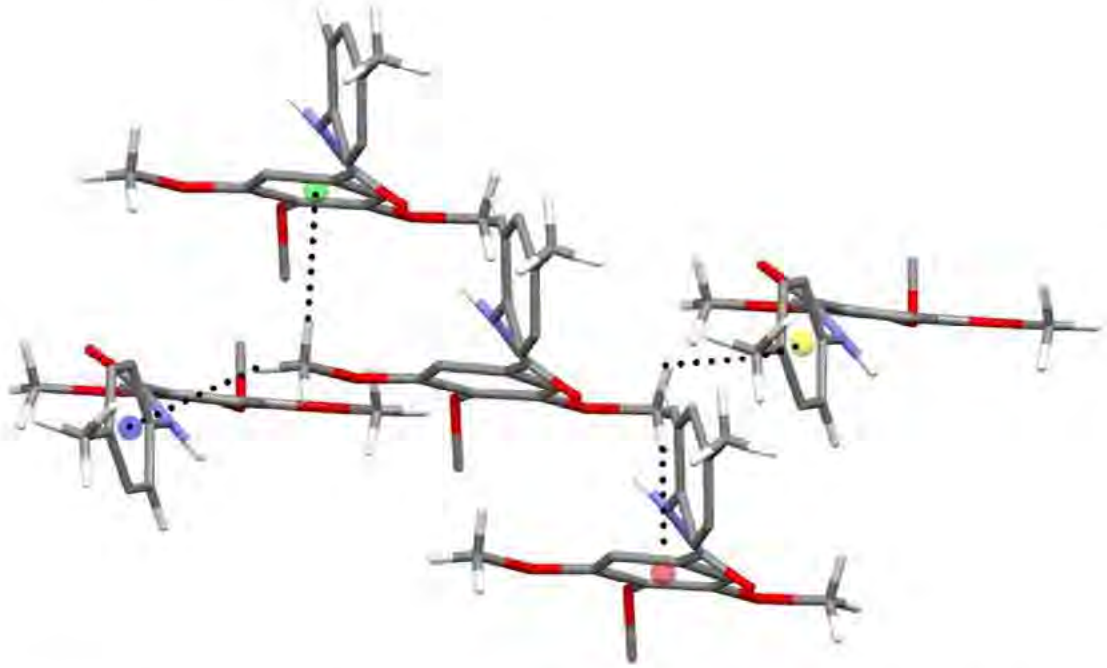

References

[1] Bernstein, J., Davis, R. E., Shimoni, L. and Chang, N.-L. (1995). *Angew. Chem. Int. Ed. Engl.* **34**, 1555—1573.

MS05-P03

Using water as a design element in crystal engineering. Host-guest compounds of hydrated 3,5-dihydroxybenzoic acid

Sunil Varughese and Gautam R. Desiraju

Solid State and Structural Chemistry Unit, Indian Institute of Science, Bangalore 560 012, India
E-mail: s.varughese@yahoo.co.uk

The inclusion of water in organic and metal organic crystals is of fundamental and practical importance and is not comparable to the inclusion of other solvents of crystallization.[1-4] In this regard, a series of hydrated host-guest compounds of 3,5-dihydroxybenzoic acid were prepared and analyzed. The acid molecules make a hexagonal arrangement and the water molecules, occupying the peripheries of the hexagonal voids, act as "hooks" to connect the guest molecules with the host-framework via hydrogen bonding. Thus, molecules with diverse functionalities, such as ester, nitrile, formyl, ketone, sulfoxide and alcohol, were employed for the study. By choosing guest molecules with a certain size and containing good hydrogen bond acceptors, we were able to anticipate reasonably well the formation of nearly isostructural host-guest hydrates. While the acid exhibits a similar conformation (*syn-anti*) and makes hexagonal arrangements, the structural diversity is introduced by the nature, size and arrangement of the guest molecules in the voids. Further to the guest stabilization, water acts as a good mediator of effective crystal packing and also determines the topology of the host framework. The role of water is both extensive and consistent that the question arises as to whether water is really a host or a guest in these structures. The structural intricacies and the role of water in the structure directing role will be discussed.

References

[1] Ludwig R., "Water: From Clusters to Bulk", *Angew. Chem., Int. Ed.* Vol. 40, No. 10, (2001), pp 1808-1827.
[2] Jeffrey G. A., "*An Introduction to Hydrogen Bonding*", Oxford: New York, (1997), pp 135-152.
[3] Wells, A. F. "*Structural Inorganic Chemistry*", 5th Edition, Clarendon: Oxford, (1984), pp 668.
[4] Desiraju G. R., "*Crystal Engineering: The Design of organic Solids*" Elsevier, Amsterdam, (1989), pp 138-142.

MS05-P04

Investigation of the crystal structure of mixed $(Rb_{1-x}Tl_x)H_2PO_4$ by neutron diffraction

In-Hwan Oh[1], Kwang-Sei Lee[2], Martin Meven[3] and Gernot Heger[4]

[1]*Neutron Science Division, KAERI, 1045 Daedeokdaero, Yuseonggu, Daejeon 305-353, Korea*
[2]*Department of Nano Systems Engineering, Inje University, Gimhae 621-749, Korea*
[3]*FRM-II, Technische Univesität München, Lichtenbergstr.1, Garching D-85747, Germany*
[4]*Institut fuer Kristallographie, RWTH Aachen, Jaegerstr.17-19, Aachen D-52056, Germany*
E-mail: oh1905@kaeri.re.kr

In the present work we investigate RDP-TDP mixed crystals by neutron diffraction. RbH_2PO_4 (RDP) and TlH_2PO_4 (TDP) belong to the KDP (KH_2PO_4) structure family of $A(H,D)_2PO_4$-type (A = K^+, Rb^+, Tl^+, Cs^+, etc), which is well known for its crucial hydrogen bonded ferroic behavior.. RbH_2PO_4 (RDP) and TlH_2PO_4 (TDP) show distinct room temperature crystal structures despite of the same ionic radii (1.47 Å) of Tl^+ and Rb^+. While the paraelectric RDP (isotypic to KDP) shows a three-dimensional network of hydrogen bonded PO_4-groups with tetragonal symmetry, the monoclinic structure of the ferroelastic TDP is characterized by a two-dimensional network. Their disordered H-distributions have been studied in detail [1,2]. Highly perfect RDP-TDP mixed crystals were grown from aqueous solution. For $(Rb_{0.51}Tl_{0.49})H_2PO_4$ a full crystal structure analysis was performed at room temperature based on diffraction data up to $(\sin\theta/\lambda) = 0.827 Å^{-1}$ at HEiDi, FRM-II, Germany. $(Rb_{0.51}Tl_{0.49})H_2PO_4$ crystallizes in the monoclinic space group $P2_1/a1$ with a = 14.4281(1) Å, b = 4.543(5) Å, c = 6.400(9) Å, and β = 91.77(9)°. The crystal structure is isotypic to TDP with a H-disordering in the O-H···O hydrogen bonds. This result matches well with NQR-investigations [3], where it was suggested that the mixed crystals $(Rb_{1-x}Tl_x)H_2PO_4$ show no phase transition at low temperatures for $0.2<x<0.8$ and also confirmed our former neutron findings [4]. Compared to the previous investigation on $Rb_{0.46}Tl_{0.54}H_2PO_4$ [4], no noticeable difference was observed except concerning the hydrogen bonds. In the crystal structure, there are three symmetry independant H-atoms. Two of them are disordered, whereas one H-atom is already ordered at room temperature. The difference in chemical composition is not so big. However, the hydrogen bond angles, especially for the disordered hydrogen atoms show significant changes. It could be very interesting to investigate the RDP-TDP mixed crystals more systematically and as a function of temperature in order to better understand the role of the lone-pair electrons of the Tl^+ ions for the phase stability and to follow the disorder behavior of the hydrogen atoms.

References

[1] Oh, I. H., Mattauch, S., Merz, M. and Heger, G., "Structural phase transition and hydrogen ordering of TlH_2PO_4 at low temperature", Acta Cryst. B62, (2006), pp 719-728.
[2] Mattauch, S., Heger, G., and Michel, K. H., "High resolution neutron and x-ray diffraction studies as a function of temperature and electric field of the ferroelectric phase transition of RDP", Cryst. Res. Technol. Vol. 39, (2004), pp. 1027-1054.
[3] Seliger, J. and Zagar, V., "Nuclear-quadropole double – resonance study of the solid solution $Rb_{1-x}Tl_xH_2PO_4$", Physical Review B52, (1995), pp 1070-1077.
[4] Oh. I. H., Mattauch, S., Heger, G. and Lee Cheol Eui, "Neutron diffraction study of a $Rb_{0.5}Tl_{0.5}H_2PO_4$ single crystal", Journal of the Physical Society of Japan, Vol. 77, (2008), pp 094602.

Crystal and molecular structure of tris(tert-butyl-3-butanoato) gallium

S. Brahma [a], S.A.Shivashankar [a] T.Narasimhamurthya [a] Vasu [b]

[a] *Materials Research centre, IISc., Bangalore560012, India*
[b] *Vivekananda Degree College, Malleshwaram wes tBangalore-560055, India*
E-mail: sanjaya@mrc.iisc.ernet.in

The use of metal-organic (MO)complexes as precursors for chemical vapour deposition (CVD) for thin films. In the title compound an Gallium complex, the ligand has methyl terminal group on both sides The structure determination of this complex a possible MOCVD precursor has been a part of our ongoing research. The structure is solved using direct methods. The cell parameters are a = 9.3419Å, b = 17.1340Å, c = 20.0290Å, α = 71.985°, β=79.928°, γ= 82.196° and Z = 2. The coordination geometry is essentially octahedral. The Ga-O bond lengths range from 1.951 to 1.967Å due to electron delocalization with in the chelate ring and the O-Ga-O bond angles with in the chelate rings vary from 91° to 92°. In the compound Ga atom is coordinated by the ketone O atoms of three bidentate ligands forming an octahedral geometry. The six-membered chelate rings are planar each are perpendicular to each other. Molecular structure is stabilized by intra-molecular interactions with keto O atoms with chelate rings. Solvent bi-pyridine is forming inter-molecular hydrogen bonding with the chelate ring. Interesting results will be presented at the conference.

Corresponding author : tate_rao@mrc.iisc.ernet.in

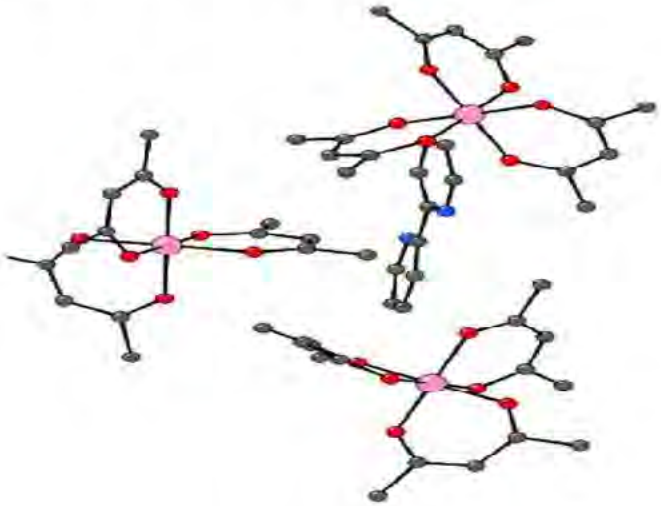

References:

[1] S. Brahma, et al., "*Acta Cryst.* (2008)". C64, m140-m143
[2] G. M. Neelgund, et.al., "*Acta Cryst.* (2007)". C63, m74-m76

MS05-P06

Molecular structure of fluorescent copper(II) complexes with anti cancer activity

Vedavati G. Puranik[1], Satish Bhat[2], Anupa Kumbhar[2], Huissain Heptullah[3] and Ayesha Khan[3]

1Centre for Materials Characterization, National Chemical Laboratory, Pune- 411 008, India
2Department of Chemistry, University of Pune, Pune-411 007; India
3Institute of Bioinformatics and Biotechnology, University of Pune, Pune-411 007, India
E-mail: vg.puranik@ncl.res.in

In recent years there has been a rapid expansion in research and development of novel metal-based anticancer drugs to improve clinical effectiveness, to reduce general toxicity and to broaden the spectrum of activity [1-2]. Most of the reported metal-based anticancer compounds [3-4] are not intrinsically fluorescent, so they need to be modified with a fluorescent tag in order to be visualized within the cell. This approach has been found to be useful in studying the cellular responses of several fluorescent platinum(II) complexes. In the present work we have synthesized fluorescent ligand, 2-(1-naphthyl)imidazo[4,5-f][1,10]phenanthroline (NIP) which on complexation with Cu(II) make the complexes fluorescent so that we can monitor the cell penetration, distribution and efflux mechanisms of these fluorescent compounds when incubated with cancer cell lines using fluorescence spectroscopy. The compounds were tested for their anticancer activity on a panel of cisplatin-sensitive and cisplatin-resistant cell lines. These complexes bind to DNA by intercalation

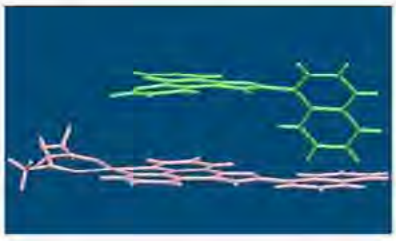

Fig-1

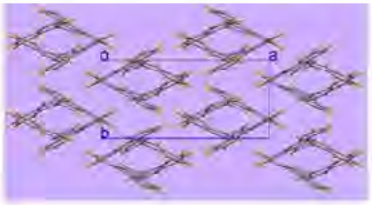

Fig-2

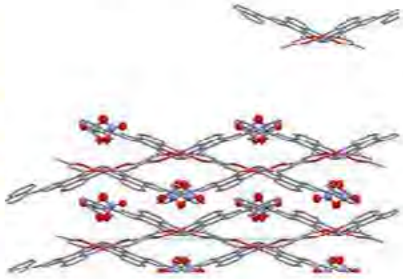

Fig-3

Ligand molecule belongs to the monoclinic space group $P2_1/c$, inwhich the naphthalene ring is at an angle to phenanthroline ring in the ligand while in the Cu complex the molecule is planar Fig-1. When it forms a Cu complex, naphthalene ring rotates through 49.43 ° to form hydrogen bonds with lattice nitrates. NIP shows diamond like packing arrangement when viewed down c axis Fig-2. Two of the complex molecules pack in such way to form butterfly like structure Fig-3. In each cationic molecule, two of the planar ligands are held together by π-π interactions while the NO_3 anion connects the symmetry related molecules via C-H…O and C-H…N interactions.

References

[1] Cusumano M., Pietro M., GiannettoA, and Vainiglia P.A.
[2] J.Inorg. Biochem. 99 (2005) 560–565
[3] Norde´n B., Lincoln P., Kerman B.A.,Tuite E., Metal Ions in Biological Systems,
[4] Sigel A., Sigel H.(Eds.), vol. 23, Marcel Dekker, New York, 1996.
[5] Wu J.Z., Yuan L.
[6] J. Inorg. Biochem. 98 (2004) 41–45.
[7] Baruah H., Bierbach U.
[8] J. Biol. Inorg. Chem. 9 (2004) 335–344.

MS05-P07

The relevance of unconventional hydrogen bonding in the polymerization and assembly of polydiacetylene DCHD

Bagautdin Bagautdinov[1], Kunihisa Sugimoto[1], Sono Sasaki[1], Fumiko Yoshida[2], Che-Hsiu Shih[3], Jungeun Kim[1], Hiroshi Tanaka[4], Kohji Tashiro[5] and Masaki Takata[1,2,3]

[1]*SPring-8/JASRI, 1-1-1 Kouto, Sayo-cho, Sayo-gun, Hyogo 679-5148, Japan*
[2]*RIKEN SPring-8 Center, Harima Institute, 1-1-1 Kouto, Sayo-cho, Sayo-gun, Hyogo 679-5148 Japan*
[3]*The University of Tokyo, Tokyo, 153-8902, Japan*
[4]*Shimane University, Matsue, Shimane 490-8504, Japan*
[5]*Toyota Technological Institute, Tempaku, Nagoya 468-8511 Japan*
E-mail: bagautdi@spring8.or.jp

In this work, we specifically address the polymerization of 1,6-di(N-carbazolyl)-2,4-hexadiyne (DCHD) and the role of bonding and nonbonding interactions in polymer formation and stabilization. For this we carried out a high brilliance SPring-8 (Hyogo, Japan) synchrotron X-ray study of monomer and polymer DCHD in the temperature range from 20 to 350 K. Given that the polymerization reaction is interplay of the monomer and polymer lattices, a comparative analysis of the structures allows us to uncover important insight into the structural machinery controlling formation and stability of polymer DCHD. For advance details, we examined the structures on a charge density level using maximum entropy method (MEM) upgraded for mapping of electron density jointly with electrostatic potential, electric field and atomic polarization [1,2]. It allows us to expose the nature of bonded and nonbonded interactions forming the structures. Based on MEM maps viewed the hydrogen bonds as bridges with covalent, electrostatic, and dispersive components, it was found that crystalline polymer DCHD mainly determined by network of unconventional >C−H···π bonds between sidechain >C−H and π-electron of the triple bond (C≡C) segment of nearby backbone as well as amongst the interlayer carbazolyl rings packed in a herringbone motif. In the monomer form, >C−H···π(C≡C) link carbazolyl ring to the triple bond segments of the nearby monomers. The arrangement of the inter-monomer H-bonds is changed from the low-temperature trifurcated (four-centered) to the bifurcated (three-centered) at temperatures above 140 K. It is well known that DCHD above 140 K is both thermal and γ–ray solid-state polymerizable [3]. Present detailed structures distinguished that trifurcated H-bonds stabilize monomers providing additional conformational constraints which apparently prevent twist of monomer rods to the reactive state. Thermal fading of the additional constraint results in non-planar bifurcated H-bond arrangement which may accommodate the "monomer rods" to "polymer backbone" switch. In the end resulted polymer phase, the backbones strengthened by linear (two-centered) H-bonds. Thus, in the DCHD system unconventional >C−H···π interactions of trifurcated and linear geometries direct the structural stability for the monomer and polymer forms, respectively, while bifurcated one triggers the solid-state monomer-to-polymer reactivity.

References

[1] Takata, M., "The MEM/Rietveld method with nano-applications - accurate charge-density studies of nano-structured materials by synchrotron-radiation powder diffraction", Acta Cryst. A, Vol. 64, (2008), pp. 232-.245.
[2] Tanaka, H., Kuroiwa, Y. & Takata, M., "Electrostatic potential of ferroelectric PbTiO3: Visualized electron polarization of Pb ion", Phys. Rev. B, Vol. 74, (2006), pp.172105-1-172105-4.
[3] Enkelmann, V., "Structural aspects of the topochemical polymerization of diacetylenes", Adv. Polym. Sci., Vol. 63, (1984), pp. 91–136.

MS05-P08

Crystal engineering of hydroxybenzoic acids. Influence of solvent in the synthon diversity and crystal packing

SeethaLekshmi Sunil and T. N. Guru Row

Solid State &Structural Chemistry unit, Indian Institute of Science, Bangalore 560 012, India
E-mail: seetha208@yahoo.co.uk

Systematic analysis of intermolecular interactions formed between various molecular building units is an interesting topic in the area of crystal engineering.[1] Although the acid-pyridine interactions are well known in literature, the studies pertaining to triazines are relatively rare. Melamine is an interesting candidate due to its symmetry and the availability of several hydrogen bond donor and acceptor functionalities. Further, it is an important compound from the industrial and economical perspective. The recognition patterns of melamine with a series of substituted hydroxybenzoic acids have been studied with the assumption that the OH and COOH groups can make a cooperative influence in the recognition process and results in diverse synthons and supramolecular architectures. All these complexes form solvated assemblies and the solvent of crystallization plays an important role in the structure stability. The molecular adducts exhibit a co-crystal-salt continuum and the formation of the salts cannot be predicted on the basis of ΔpKa values, as most of the molecular candidates have similar pKa values.[2] The synthon diversity and the crystal packing in terms of intermolecular interactions provide useful inputs for crystal design.

References

[1] Desiraju G. R., *Crystal Engineering. "The Design of Organic Solids"*, Elsevier, Amsterdam, (1989).

[2] Hathwar, V. R., Pal, R. and Guru Row, T. N., "Charge Density Analysis of Crystals of Nicotinamide with Salicylic Acid and Oxalic Acid: An Insight into the Salt to Cocrystal Continuum" *Cryst. Growth Des.* Vol. 10, (2010), (DOI:10.1021/cg100457r).

MS05-P09

Crystal structure of 7, 8-dimethyl-4-bromomethylcoumarin

Ramakrishna Gowda[1], K.V Arjuna Gowda[2], Mahantesha Basanagouda[3], Manohar V. Kulkarni[3].

[1]*Department of Physics, Govt. College for Women, Kolar - 563 101, Karnataka, India*
[2]*Department of Physics, Govt. First Grade College, K.R Pura, Bangalore-560 036, Karnataka, India*
[3]*Department of Chemistry, Karnatak University, Dharwad-580 003, Karnataka, India*
E-mail: arjunagowda@indiainfo.com

Coumarins are a class of naturally occurring oxygen heterocycles which have been found to exhibit wide ranging biological activities [1-3] through its innumerable derivatives. Structural studies on coumarins have been focused on their solid state photochemical dimerization [4], hydrogen bonding [5], mode of packing [6], molecular self assembling [7] and photo physical properties [8]. Introduction of bromine has resulted in formation of hydrates, intermolecular hydrogen bonding, eclipsed conformation observed in 3-bromocoumarin [9], 6-bromo-3-acetylcoumarin [10] and 3-bromoacetylcoumarin [11] respectively. 3-Bromophenyl-6-acetoxymethyl-coumarin-3-carboxylates have been found to exhibit potential anticancer and antitumor activity [12]. Crystals suitable for diffraction studies were grown by slow evaporation technique using acetic acid as a solvent.

The crystals of the compound crystallize in monoclinic with space group *C*2/c having 8 molecules in the unit cell of dimensions crystal system a = 18.5025 (14), b = 9.8785 (7), c = 13.1639 (10) Å and β = 118.908 (2) ^{0}.

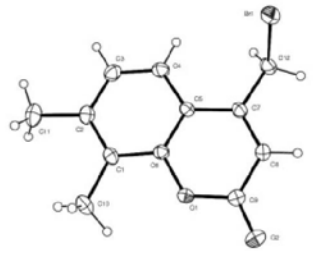

The data was collected using ω and φ scan mode. 14710 measured reflections of which 3610 independent reflections and 2516 reflections with $I > 2\sigma$ (I). With absorption correction: multi-scan. The structure was solved using Wingx software package and the model was refined by the full-matrix least-square method. The refinement was continued till the final R = 0.04, R_w = 0.116, The title compound is cyclic planar but it is less aromatic in nature due to absence of continuous delocalization of pi electrons around the coumarin ring skeleton. A bond length of deviation is observed at C1-C10 (1.495 (3) A°). This is due to the bonding of sp^2 (C1) - sp^3 (C10) hybridization.

References

[1] Kulkarni M.V, Kulkarni G.M, Lin C.H, Sun C.M (2006) *Curr. Med Chem.*, Vol 13, pp 2795.
[2] Fylaktakidou KC, Hadjpavlou D, Litinas KE, Nicolaides DN (2004) *Curr,Pharm Design* Vol. 10, pp 3813.
[3]. Neyts J, Clercq ED, Singha R, Chang YH, Das AR, Chakraborty SK, Hong,SC, Tsay SC, Hsu MH, Hwu JR (2009) *J Med Chem* 5 Vol. 2, pp 1486.
[4] Gnanaguru K, Ramasubbu N, Venkatesan K, Ramamurthy V (1985) *J Org,Chem* Vol. 50, pp 2337.
[5] Munshi P, Row T. N. G (2005) *J Phys Chem* A Vol. 109, pp 659.
[6] Gavuzzo E, Mazza F (1974) *Acta Cryst B* Vol. 30, pp:1351,
[7] Murthy JN, Venkatakrishnan P, Singh AS (2003) *Cryst Eng Comm* Vol. 5, pp 507.
[8] Katerinopoulos HE (2004) *Curr Pharm Des* Vol. 10, pp 3835.
[9] Gaultier J, Hauw C (1965) Acta Cryst C, pp 19:927,
[10] Kokila MK, Puttaraja, Kulkarni MV, Shivaprakash NC (1996) *Acta Cryst,* Vol. C52, pp 2078.
[11] Puttaraja, Vasudevan KT, Kulkarni MV (1991) *Acta Cryst* Vol. C47, pp 774,
[12] Kempen I, Papapostolou D, Thierry N, Pochet L, Counerotte S, Masereel B, Foidart J-M, Reboud-Ravaux M, Noel A, Pirotte B (2003) Br J Can Vol. 88, pp 1111.

MS05-P10

The unusual phase behaviour of $Sr_2TiSi_2O_8$ and structurally related compounds

Patryck Allen[1], Siegbert Schmid[1]

[1]*School of Chemistry, The University of Sydney, NSW 2006, Australia*
E-mail: patryck.allen@sydney.edu.au

The Fresnoite $A_2TiM_2O_8$ (A = Ba, Sr; M = Si, Ge) structure type is one of several possible alternatives currently being investigated to replace PZT and other lead-based piezoelectric materials because of their potential to exhibit excellent piezoelectric response coefficients [1-2]. Understanding the underlying structural chemistry of these materials is critically important to developing new materials with optimised physical properties that are comparable to or better than the current lead-based piezoelectrics.

The $Ba_2TiSi_2O_8$, $Ba_2TiGe_2O_8$, and $Sr_2TiSi_2O_8$ family members are structurally well characterised [3-6]. Recent research efforts have been directed towards the study of incommensurate modulations in these structures using quantitative high resolution transmission electron microscopy and rigid unit mode analysis [7-8] It has been shown that the specific modulated structures and physical properties are highly dependent on the ratio of ionic radii of the atoms on the A and M sites [3, 9].

Variable temperature synchrotron powder X-ray and electron diffraction data from $Sr_2TiSi_2O_8$ provide previously unreported evidence of unusual phase behaviour between 125 – 1273 K. Electron diffraction data confirm that two incommensurately modulated $Sr_2TiSi_2O_8$ phases coexist at room temperature. Observation of the position of the satellite reflections in $Sr_2TiSi_2O_8$ electron diffraction patterns at elevated temperatures suggests that the minor (tetragonal $P4bm$) phase completely converts into the major (orthorhombic $Cmm2$) phase on heating above 480 K.

Recently collected variable temperature X-ray and electron diffraction data will also be presented for the previously unreported compositions $Sr_2TiSi_{1.0}Ge_{1.0}O_8$, $Sr_2TiSi_{1.8}Ge_{0.2}O_8$, $Sr_2TiSi_{1.6}Ge_{0.4}O_8$, discussing the changes in the incommensurate phases at elevated temperatures when minor substitutions are made for strontium and silicon in the $Sr_2TiSi_2O_8$ structure. Additionally, physical property measurements including dielectric constants and piezoelectric response coefficients of selected compositions will be presented and discussed in terms of the potential application of these compounds as commercial electronic materials.

References

[1] Halliyal A., Bhalla A. S., Markgraf S. A., and Cross L. E., *Ferroelectrics*, 62, (1985), pp 27-38.
[2] Asahi T., Osaka T., Kobayashi J., Abrahams S. C., Nanamatsu S., and Kimura M., *Phys. Rev. B*, 63, 9, (2001), pp 1-13.
[3] Höche T., Russel C., and Neumann W., *Solid State Comm.*, 110, 12, (1999), pp 651-656.
[4] Höche, T., Neumann, W., Esmaeilzadeh, S., Uecker, R., and Russel, C., (2002) *J. Solid State Chem.*, **166**, (1), pp 15-23.
[5] Höche T., Esmaeilzadeh S., Uecke R., Lidin S., and Neumann W., *Acta Cryst. B*, 59, (2003), pp 209-216.
[6] Markgraf S., Halliya A., Bhalla A. S., Newnham R. E., and Prewitt C. T., *Ferroelectrics*, 62, 1-2, (1985), pp 17-26.
[7] Bindi L., Dusek M., Petricek V., and Bonazzi P., *Acta Cryst B.*, 62, (2006), pp 1031-1037.
[8] Withers R. L., Tabira Y., Liu Y., and Höche T., *Phys. Chem. Minerals* 29, 9, (2002), pp 624-632.
[9] Markgraf S. A., Randall C. A., and Bhalla A. S., *Ferroelectrics Lett. Sect.*, 11, 5, (1990), pp 99-102.

MS05-P11

Supramolecularly aggregated coordination solids containing 4-CNpy ligand

Sanchay Jyoti Bora[1] and Birinchi Kumar Das

Department of Chemistry, Gauhati University, Guwahati 781014, Assam, India
E-mail: sanchay.bora@gmail.com

Ligand systems containing electron donor and acceptor sites lead to supramolecular aggregation, and in this context 4-cyanopyridine (4-CNpy) containing an electron-withdrawing nitrile group as the acceptor and the pyridyl nitrogen as the donor represents a suitable candidate. The supramolecular behavior of a few coordination solids containing 4-CNpy ligands have been studied. The metal compounds of formulation $[M(H_2O)_3(SO_4)(4\text{-}CNpy)_2].H_2O$ [M = Ni (**1**) and Co (**2**)], $[Ni(fum)(H_2O)_2(4\text{-}CNpy)_2]$ (**3**) [fum = fumarate] and $[Cu_2(OAc)_4(4\text{-}CNpy)_2]$ (**4**) have been synthesised. In **1** and **2**, the neutral complexes along with the uncoordinated H_2O molecules are glued together preferentially into inverse bilayers by non-covalent interactions including unique interlayer interactions between antiparallel nitrile groups. Hartree-Fock and DFT calculations indicate the interactions to be energetically significant. The unit cell similarity index (Π) value of 0.0046 for these two compounds suggests their isostructural behaviour. Compound **3** consists of nearly octahedral Ni^{2+} centers bridged by bidentate fumarato ligands to form a one-dimensional chain extending approximately in crystallographic *c*-axis. These chains form intermolecular hydrogen bonds to assemble into supramolecular layers. Compound **4** has the familiar lantern-type structure where the distorted square pyramidal coordination environment of copper(II) consists of equatorial carboxyl O- atoms of acetato and axial N- atom of 4-CNpy ligands. The unique supramolecular interactions are also operative in these structures as well.

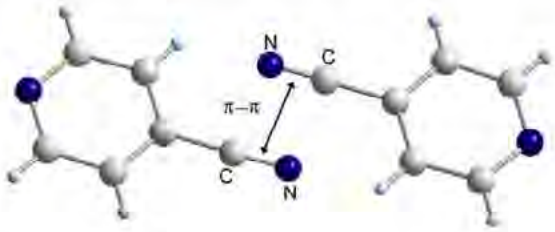

References

[1] Das B. K., Bora S. J., Bhattacharyya M. K. and Barman R. K., "Inverse bilayer structure of mononuclear Co(II) and Ni(II) complexes of type $M(H_2O)_3(SO_4)(4\text{-}CNpy)_2$", *Acta Cryst.*, Vol. B56, (2009), pp 467-473.

[2] Das B. K. and Barman R. K., "Tetrakis (-acetato-*O,O'*)bis[(4-cyanopyridine-*N*) copper(II)]", *Acta Cryst.*, Vol. C57, (2001), pp 1025-1026.

[3] Fábián L. and Kálmán, A., "Volumetric Measure of Isostructurality", *Acta Cryst.*, Vol. B55, (1999), pp 1099-1108.

[1]Present address: *Department of Chemistry, Pandu College, Guwahati 781012, Assam, India*

MS05-P12

Reinvestigation of structure-composition relationship in Na_xWO_3

Tapas Debnath[1], Claus H. Rüscher[2], Altaf Hussain[1]

[1]*Department of Chemistry, University of Dhaka, Dhaka -1000, Bangladesh*
[2]*Institut für Mineralogie, Leibniz Universität Hannover, 30167 Hannoveer, Germany*
E-mail: tapasnet@yahoo.com

Systematic reinvestigation of Na_xWO_3 solid-solution series reveal coexisting phases of cubic perovskite tungsten bronze (PTB_c), tetragonal tungsten bronze (TTB), and tetragonal perovskite tungsten bronze (PTB_t) in the range of $0.15 \leq x \leq 0.4$, which has been quantified by Rietveld refinement of XRD data. Pure PTB_t and orthorhombic perovskite tungsten bronze (PTB_o) appear for $x = 0.1$, and 0.05, respectively. Structural studies for single phase PTB_c Na_xWO_3 show that all compositions in the range of $0.4 < x < 0.9$ can uniquely be refined using space group Im-3. The linear increase in lattice parameters with increasing x in PTB_c Na_xWO_3 is explained by increasing W-O bond length, suggesting an x independent tilt of about 3° of the WO_6 octahedra. For the PTB_t phase it is shown that the puckering effect, i.e. the off centering of W along c-axis, is insufficient to explain the structure. Additionally the WO_6 octahedra show a tilt around the c axis, which is consistent with space group P4/ncc.

Ordering in intercalated Co atoms and electron density distributions of layered compounds Co_xTiS_2

Ken-ichi Ohshima and Takuro Kawasaki

Institute of Materials Science, University of Tsukuba, Tsukuba 305-8573, Japan
E-mail: ohshima@bk.tsukuba.ac.jp

Titanium disulphide TiS_2 has the 1T-CdI_2-type structure, which has the space group $P\bar{3}m1$ with a trigonal symmetry. Most atoms and organic molecules can be intercalated in the van der Waals gap of TiS_2. In particular, intercalation compounds M_xTiS_2 (M=3d transition metal) have been examined, because of their characteristic physical properties depending on guest species M and composition *x*.

From a structural point of view, it is interesting that interlayer lattice parameter *c* of Mn_xTiS_2 increases markedly and that of Co_xTiS_2 and Ni_xTiS_2 decreases with increasing of composition *x*.[1)] The present authors have recently studied both the nature of chemical bonding from the electron density distribution (EDD) obtained by the maximum entropy method (MEM)[2)] and atomic arrangements of the guest atoms in Mn_xTiS_2[3)] and Ni_xTiS_2[4)], respectively. Further, both a detailed structural study on the ordering behavior and disordering process in intercalated Ni atoms of Ni_xTiS_2 have been performed with using single-crystal X-ray diffraction and *in situ* X-ray diffraction techniques.

In this study, a structural study of layered compounds CoxTiS2 (x=0.26, 0.43, and 0.57) by X-ray diffraction analysis has been performed to investigate both the ordered atomic arrangement and disordering behavior of intercalated Co atoms, and the nature of the chemical bond from the electron density distribution (EDD) obtained by the maximum entropy method. The 2ax2ax2c superstructure of the Co atoms is observed for x=0.26 and 0.57, and disappears at 510 and 550 K, respectively. On the other hand, √3ax√3ax2c superstructure of the Co atoms is observed for x=0.43, and disappears at 610 K. It is understood that the type of the transition is second-order-like. The overlapping of the EDD between Co and S atoms & Ti and S atoms are clearly seen, which are corresponding to the covalent bonding in the van der Waals gap layer and in the TiS_2 one. It is expected that the nature of covalent bonding between Co and S atoms causes decreasing of the interlayer distance.

References

[1] Inoue M., Hughes H.P. and Yoffe A.D., "The electronic and magnetic properties of the 3d transi tion metal intercalates of TiS2", *Adv. Phys.*, Vol. 38 (1989), pp 565-604.
[2] Sakata M. and Sato M., "Accurate structure analysis by the maximum-entropy method", *Acta Crystallogr.* A, Vol. 46, No.4, (1990), pp 263-270.
[3] Kawasaki T. and Ohshima K., "X-ray structural analysis of layered compoundsMn_xTiS_2", *J. Phys. Soc. Jpn.*, Vol. 77, No. 5, (2008), pp 054601-1~-5.
[4] Kawasaki T. and Ohshima K., "Ordering in intercalated Ni atoms and electron density distribution s of layered compounds Ni_xTiS_2", *J. Phys. Soc. Jpn.*, Vol. 78, No. 10, (2009), pp 104603-1~-8.

Synthesis, structure and ionic conductivity in scheelite type $Li_{0.5}Ce_{0.5-x}Ln_xMoO_4$ (x = 0 and 0.25, Ln = Pr, Sm): A fast lithium-ion conductor

Dipankar Saha, Giridhar Madras, Aninda J. Bhattacharyya and T. N. Guru Row

Solid State and Structural Chemistry Unit, Indian Institute of Science, Bangalore 560 012, India
E-mail: s.dipankar@sscu.iisc.ernet.in

Development of solid electrolytes with fast lithium ion conductivity is one of the key areas of current research due to their demand in laptop, computer, cellular phone, digital camera and electric vehicles [1-3]. These solid electrolytes possess several advantages over already commercialized lithium ion batteries using organic liquid electrolytes. The advantages are essentially with regard to safety issues such as leakage, corrosion, inflammability. Solid electrolyte of scheelite type lithium ion conductors have also attracted interest particularly for lithium battery operation at high temperature (300 -600) °C [4]. Scheelite type solid electrolytes, $Li_{0.5}Ce_{0.5-x}Ln_xMoO_4$ (x = 0 and 0.25, Ln = Pr, Sm) have been synthesized using a solid state method. Their structure and ionic conductivity (σ) were obtained by single crystal x-ray diffraction and ac-impedance spectroscopy respectively. X-ray diffraction studies reveal a space group of $I4_1/a$ for $Li_{0.5}Ce_{0.5-x}Ln_xMoO_4$ (x = 0 and 0.25, Ln = Pr, Sm) Scheelite compounds. The un-substituted $Li_{0.5}Ce_{0.5}MoO_4$ showed high lithium ion conductivity $\sim 10^{-5}$–10^{-3} $\Omega^{-1}cm^{-1}$ in the temperature range (300-700) °C ($\sigma = 2.5\times10^{-3}$ $\Omega^{-1}cm^{-1}$ at 700 °C). The substituted compounds showed lower conductivity compared to the unsubstituted compound. High ionic conductivity is attributed to the layered structure of $Li_{0.5}Ce_{0.5-x}Ln_xMoO_4$ (x = 0 and 0.25, Ln = Pr, Sm), which allows fast conducting pathways for the lithium ion.

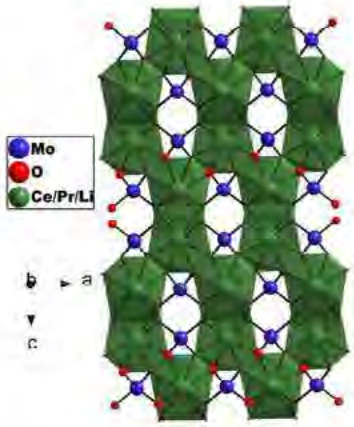

References

[1] Minami T., Tatsumisago M., Wakihara M., Iwakura C., Kohjiya S. and Tanaka, I., *"Solid State Ionics for Batteries"*, Springer, (2005).

[2] Tarascon J. M. and Armand, M., "Issues and challenges facing rechargeable lithium batteries", *Nature*, Vol. 414, (2001), pp 359-367.

[3] Aono H., Imanaka H. and Adachi G. Y., "High Li+ Conducting Ceramics", *Acc. Chem. Res.*, V ol. 27, (1994), pp 265-270.Robertson A. D., West A. R. and Rithie A. G., "Review of crystall ine lithium-ion conductors suitable for high temperature battery applications", *Solid State Ionics*, Vol. 104, (1997), pp 1-11

MS05-P15

Polymorphism in benzyl alcohol: An *in situ* cryocrystallographic study

Ranganathan Sathishkumar, Susanta K. Nayak, and T. N. Guru Row

Solid State and Structural Chemistry Unit, Indian Institute of Science, Bangalore, 560 012, India
E-mail: sathishkumar@sscu.iisc.ernet.in

In situ cryocrystallography techniques have been successfully applied to the determination of the crystal structures of compounds which are liquids at room temperature [1]. Further, using this technique it is possible to analyze intermolecular interactions of molecular species without the influence of solvent participation either as promoter for crystal growth or as incorporated solvatomorph. Benzyl alcohol is a liquid at room temperature crystallizes when subjected to *in situ* cryocrystallization at 150K. The crystals belong to a monoclinic space group $P2_1$ with a = 5.8581 Å, b = 4.8779Å, c = 10.7636 Å, β =91.70, Z'= 1and V=307.44 Å^3. The structure is stabilized by a conventional O-H···O hydrogen bond [2] resulting in a chain along the b-axis with a surrogate (sp^3) C-H···π interaction as shown in the figure (1a). The carbon atoms in the phenyl ring show large thermal parameters suggesting a possible disorder. On cooling the same crystal to 90K additional reflections appears indicating a polymorphic modification. Indeed, the structure is monoclinic $P2_1$, but with Z'=2 and with a = 11.5742 Å, b = 4.8263Å, c = 11.9660 Å, β =115.86 and V=601.4 Å^3, disorder disappears, however the inter molecular interactions remains the same as shown figure (1b).

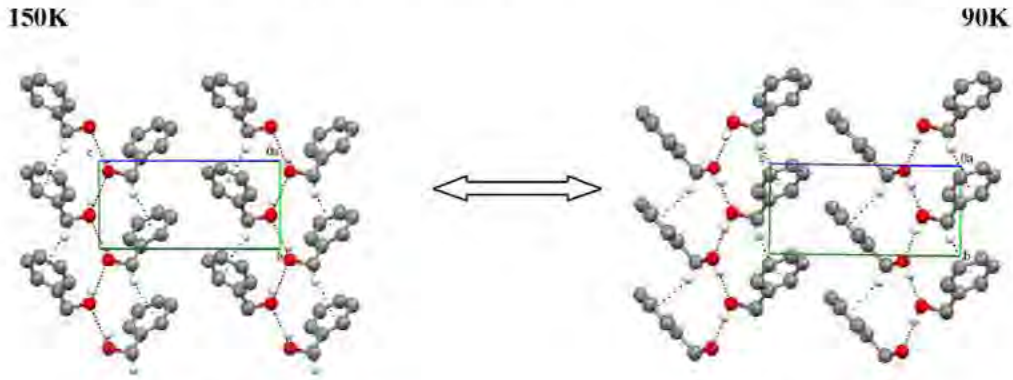

Figure (1a)

Figure(1b)

References

[1] Chopra D., and Guru Row T. N., "In situ Cryocrystallization: Pathways to Study Intermolecul ar Interactions", *J. Ind. Ins. Sci.*, Vol. 87, (2007), pp 167-211.

[2] Nishio M., Umezawa Y., Honda K.,Tsuboyama S and Suezawa H., " CH/π hydrogen bonds in organic and organometallic chemisty", *CrystEngComm*, Vol.11, (2009), pp 1757-1788 and refer ences therein.

MS05-P16

Crystal structure and semi-empirical quantum chemical calculation of 3-dibromoacetyl-2H-1-benzopyran-2-one

S.Shalini[1], C. R. Girija[1*] T.V.Venkatesha[2] and M.M.Jotani.[3]

[1]*Chemistry Research Centre, SSMRV Degree College, 4th T Block, Jayanagar, Bangalore -560 041, India*
[2]*Department of Chemistry, Jnana Sahyadri, Kuvempu University, Shankargatta-577 451, India*
[3]*Department of Physics, Bhavan's Sheth R. A. College of Science, Khanpur, Ahmedabad-380 001, Gujarat, India*
E-mail : girijashivakumar@rediffmail.com

Coumarins are an important class of organic compounds with vast structural diversity and they find useful applications in synthetic chemistry, medicinal chemistry and photo chemistry. Several substituted coumarin derivatives find application in the dye industry and have been used to develop laser dyes.

In view of its importance and to understand the weak interactions which control the packing of molecular moieties and their significance in crystal engineering we have established the crystal structure of 3-Dibromoacetyl-2H-1-benzopyran-2-one commonly known as 3-Dibromoacetylcoumarin. The compound crystallizes in triclinic space group P-1 with the crystal parameters as: a = 7.1868(2) Å, b = 8.9689(3) Å, c = 9.7126(3) Å, α = 69.005(2), β = 85.990(2) ° , γ = 71.155(2) V=552.41(3) $Å^3$, Z = 4, D_x = 2.080 Mg m^{-3} and μ = 7.323 mm^{-1}. The structure is solved by direct method using SIR92 program and refined by full matrix least square on F^2 using SHELXL-97 program to a final value 0.0282 for 2257 reflections with I > 2 σ (I). The crystal structure is stabilized by intermolecular C-H…O hydrogen bonds forming $R^2_2(12)$ graph-set motif as well as some π-π stacking interactions. The Semi-empirical Quantum Chemical Calculations were performed on the refined parameters using MOPAC2009 program to optimize the structure with Parameterization Model 6 (PM6) approximation. The minimizations were terminated at r. m. s. gradient of less than 0.01 KJ-mol^{-1} $Å^{-1}$ providing heat of formation equal to -63.51 Kcal for the molecule in the asymmetric unit. The ionization potential, dipole moment and self consistency field (SCF) factor are calculated as 10.076 eV, 6.367 Debye and 46 respectively. The geometry optimization using MOPAC2009 result HOMO- LUMO energies as -10.076 and -1.951 eV respectively.

Key Words: Coumarins, Hydrogen bonds, Weak interactions, MOPAC calculations.

MS05-P17

Influence of interstitial defects on the concentration of cation vacancies

Anatoly M. Sazonov[1], Viktor V. Onufrienok[2], Anatoly V. Chzhan[3]

[1-3]*Department of Mineralogy, Siberian Federal University, Krasnoyarsk, Russia*
E-mail: anatoly.sazonov@yandex.ru

Synthetic pyrrhotites (Fe_nS) not containing interstitial atoms in the crystal structure and natural pyrrhotites of the "Blagodatny" mine containing interstitial point defects have been investigated in the stable phase. As a result of comparison of the crystal structure and the phase composition of the synthesised samples with natural pyrrhotites the influence of the inclusion atoms on the concentration of cation vacancies has been established. The purpose of the work: to study the phase composition of iron sulphides with the ratio x = S/Fe (1.00 <x <1.20.) in some decades after high-temperature synthesis. To compare the results of the research done on synthetic pyrrhotites not containing interstitial atoms, with natural pyrrhotites with various interstitial atoms in crystal structure. To study the influence of interstitial defects on the sulphur and iron ratio in samples, and also on the concentration of cation vacancies in crystal structure. As the result of the X-ray research of structure and phase composition as of initial samples, so of those ones sustained within 29 years, all possible stable phase compositions of pyrrhotite have been established. It has been determined that FeS, $Fe_{0.975}S$, $Fe_{0.950}S$, $Fe_{0.909}S$, $Fe_{0.875}S$ can be stable compositions. There was not and could not be any impurity in the structure of these pyrrhotites. Let us mention that directly after synthesis pyrrhotites formed a homogeneous sequence almost along the whole composition sequence FeS - Fe_7S_8 which corresponds to the references' data. As the result of the research of 31 series of pyrrhotites from the "Blagodatny" mine it has been established that besides cation vacancies all of them have dot interstitial defects of various elements in the crystal structure. First of all these elements are Ni, Cu, Co, Zn, Ag, and the gold grade in the rock thus reached 31,5 g/t. In stable pyrrhotites not containing dot interstitial defects the maximum S/Fe ratio is about 1.15 while this ratio for pyrrhotites of the "Blagodatny" mine reaches 1.179. Though such ratio of sulphur and iron is possible for synthetic metastable pyrrhotites, they change the phase composition with time depending on external conditions (for example, a pyrite, monocline pyrrhotite and szomolnokite are formed). Nevertheless there is no doubt that the pyrrhotite of the "Blagodatny" mine with the ratio S/Fe =1.179 is stable as well. This can be explained only by the fact that cations of other metals occupy not only vacant cation positions, but also replace Fe ions in the points of the crystal lattice. Let us note that if interstitial cations occupy only vacant cation positions S/Fe ratio could not change. Thus only the number of vacant cation positions in the crystal structure would change. Conclusions**:** interstitial cations influence the number of vacant positions in the crystal structure of pyrrhotite. When comparing concentration of cation vacancies in the structure of pyrrhotite and gold grade in the rock the tendency of gold increase at the increase of cation vacancies in samples was observed. This dependence is not linear and its nature is complicated, however, the tendency for gold increase in samples at the increase of cation vacancies is evident.

MS05-P18

From coordinates to chemistry: 'decifering a cif'

Dr. Colin R. Groom, Dr. Jason C. Cole and Dr. Aurora J. Cruz-Cabeza

CCDC, 12 Union Road, Cambridge, CB2 1EZ, United Kingdom
E-mail: groom@ccdc.cam.ac.uk

Whilst it is often straightforward to model atomic positions into electron density calculated from crystallographic experiment, it can be quite difficult to appreciate the precise *chemical* details of a structure. This is a challenge we have faced for over forty-five years and which now presents itself over a hundred times a day: Given the contents of a cif, create a chemically searchable database entry.

This presentation will focus on the tools the CCDC has developed to unlock the knowledge contained in over half a million crystal structures in the Cambridge Structural Database to aid in the interpretation of newly deposited coordinates. We have taken a probabilistic approach to enable the reliable assignment of '*chemistry*' to the hugely diverse ranges of molecules for which we now have structures; this represents a step change in our ability to interpret crystal structures

MS05-P19

Photochromic property control using acid-base type co-crystal formation of salicylideneaniline derivatives

Kohei Johmoto, Sekine Akiko , and Hidehiro Uekusa

Department of Chemistry and Materials Science, Graduate School of Science and Engineering, Tokyo Institute of Technology, Tokyo 152-8551, Japan
E-mail: johmoto@chem.titech.ac.jp

Salicylideneaniline (SA) derivatives are a well-known solid-state photochromic substance that changes the color from yellow to red by UV irradiation and red to yellow by visible light irradiation or heat. The yellow to red color change is explained as a tautomerism from the enol (yellow) to the cis-keto intermediate form followed by conformational change to the trans-keto form (red) via the pedal motion. This photochromic property is known to relate to its molecular conformation in the crystal, i.e., a photochromic SA derivative has non-planar conformation and non-photochromic one is planar.

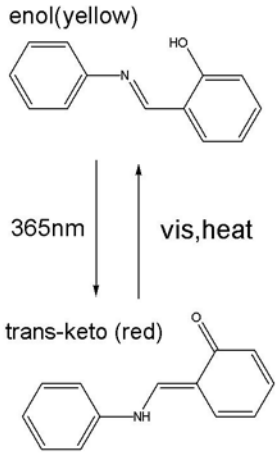

Scheme: photochromism of SA

In order to control the photochromic property of SA derivative via the control of their molecular conformation, co-crystal formation strategy by using acid-base type strong intermolecular interaction was employed and the co-crystal structures were compared. With nine different base molecules, ten acid-base type co-crystals were obtained for N-salicylidene-3-carboxyaniline (H3C). Among these co-crystals, six (include H3C crystal) are photochromic, and the other five are non-photochromic. The dihedral angle between two rings in the H3C molecule ranges from 6 to 49 degrees. The dihedral angles in these photochromic co-crystals are more than about 27 degrees, in contrast those in non-photochromic co-crystals are less than about 27 degrees.

These results clearly show that it is possible to control a SA derivative's photochromic property via conformation control by the co-crystal formation, and the dihedral angle threshold of photochromic property is about 27 degrees in this SA derivative (H3C).

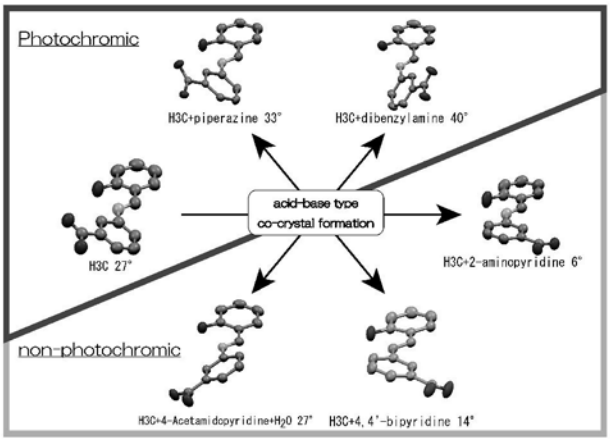

Fig. : The conformational controls of H3C by using acid-base type co-crystal ormation

Detailed comparison on temperature dependence of XANES spectra for $PbTiO_3$, $ATiO_3$ and A_2TiO_4 compounds (A = Mg, Ca, Sr,Fe)

Tomotaka Nakatani[1], Tatsuya Hiratoko[1], Maki Okube[2], Takashi Takeda[3], Kei-ichiro Murai[4] and Akira Yoshiasa[1]

[1]*Graduate School of Sciences and Technology, Kumamoto University, Kumamoto 860-8555, Japan*
[2]*Materials and Structures Labo. Tokyo Institute of Technology, Yokohama 226-8503, Japan*
[3]*National Institute for Materials Science, Tsukuba, Ibaraki 305-0044, Japan*
[4]*Facultyl of Engineering, Tokushima University, Tokushima 770-8506, Japan*
E-mail: 101d8071@st.kumamoto-u.ac.jp

Ti k-edge X-ray absorption near edge structure (XANES) spectra of PbTiO3 and various titanates such as $ATiO_3$ (perovskite- and ilmenite-type structure, A=Mg,Ca,Sr,Ba,Pb) and A_2TiO_4 (spinel-type structure, A=Mg,Fe) were measured at various temperatures up to 1100 K. The composition, local structure and temperature dependence of XANES spectra was investigated especially on the phase transition. Ti atoms are located in TiO_6 octahedral sites for the all samples. The measurements of Ti k-edge XANES spectra were carried out in transmission mode at beam line BL-7C and BL-12C of the Photon Factory in KEK, Tsukuba. X-ray absorption measurements in the temperature range from 18K to 1100K were made under a helium atmosphere. Ti k-edge XANES spectra change largely with different compositions, while the temperature dependence of XANES spectra is small in the each compound even if undergoing structural phase transition. Perovskite-type ATiO3 compounds reveal several phase transitions. $SrTiO_3$ and $PbTiO_3$ perovskite undergo structural phase transition in the temperature ranges in this study, $SrTiO_3$; rhombohedral-tetragonal-cubic, $PbTiO_3$; tetragonal-cubic. Weak but distinct changing of the XANES spectra was observed near phase transition point. These structural transitions of perovskite are caused mainly by rotation and distortion of TiO_6 octahedron. Pre-edge feature and local structure around Ti atom is little changing by rotation of octahedron. The distinct changing of pre-edge XANES spectra was observed at some transition points. Five pre-edge peaks can be identified: pp(a) 4.9667eV, pp(b) 4.9687eV, pp(c) 4.9727eV, pp(d) 4.9747eV and pp(e) 4.9796eV. The temperature dependence for each pre-edge peaks is largely different in temperature and local structure [1]. The electronic state of the absorber atom is reflected in the XANES spectra. The different XANES spectra show the different electronic structure of the Ti-O bounds in each compound [1]. The electronic state of Ti reflects a chemical bond with oxygen and also with the A site atoms via oxygen atoms. XANES spectra are reflected in electronic state of the absorption atom. Even if the Ti atom for these titanates has the same coordinates and valence electrons in TiO_6 octahedron, the oxygen atoms around Ti have different electronic state and orbitals affected by the A site atoms. The different behaviors of the pre-edge intensity suggest that the increase and decrease of X-ray absorptivity at various temperatures is fluctuated by the hybridized orbital proportion and local symmetry.

References

[1] Hashimoto T., Yoshiasa A., Okube M., Okudera H. and Nakatsuka A., "Temperature dependence o f XANES spectra for $ATiO_3$, A_2TiO_4, and TiO_2 compounds with structural phase transitions", *The American Institute of Physics,Conf. Proc.* Vol.882 AIP Melville, NY, (2007) pp. 274-276.

Temperature dependence of XANES spectra for $BaTiO_3$, $SrTiO_3$ and TiO_2 with structural phase transitions

Tatsuya Hiratoko[1], Tomotaka Nakatani[1], Maki Okube[2], Akihiko Nakatsuka[3], Kei-ichiro Murai[4] and Akira Yoshiasa[1]

[1]*Graduate School of Sciences and Technology, Kumamoto University, Kumamoto 860-8555, Japan*
[2]*Materials and Structures Labo. Tokyo Institute of Technology, Yokohama 226-8503, Japan*
[3]*Department of Advanced Material Science and Engineering, Yamaguchi University, Yamaguchi 775-861, Japan*
[4]*Facultyl of Engineering, Tokushima University, Tokushima 770-8506, Japan*
E-mail: 074s3092@st.kumamoto-u.ac.jp

Ti K-edge X-ray absorption near edge structure (XANES) spectra of BaTiO3, SrTiO3 perovskite and TiO2 rutile and anatase were measured at various temperatures. The composition, structure and temperature dependence of XANES spectra was investigated especially on the phase transition. Synthesized TiO2 rutile (99.999%), SrTiO3 perovskite (99.99%), and BaTiO3 perovskite (99.99%) were used and identified by X-ray diffraction. The appropriate amount of fine powder sample and boron nitride powder was mixed and pressed into pellet of <0.2 mm I thickness and 10.0 mm in diameter. All samples had edge-jumps with 0.7 ($\Delta\mu d$), where μ is the linear absorption coefficient and d is the thickness. The measurements of Ti k-edge XANES spectra were carried out in transmission mode at beam line BL-7C and BL-12C of the Photon Factory in KEK, Tsukuba. X-ray absorption measurements in the temperature range from 18K to 1000K were made under a helium atmosphere.

The XANES spectra for TiO2 are largely different between anatase and rutile structure, although these two compounds have the same composition. Five pre-edge peaks can be identified: pp(a) 4.9667 eV, pp(b) 4.9687 eV, pp(c) 4.9727 eV, pp(d) 4.9747 eV and pp(e) 4.9796 eV. Ti K-edge XANES spectra change largely with different compositions, while the temperature dependence of XANES spectra is small in each compound even if undergoing structural phase transition. Perovskite-type ATiO3 compounds reveal several phase transitions. SrTiO3 and BaTiO3 perovskite undergo several structural phase transitions in the temperature ranges in this study, SrTiO3; rhombohedral-tetragonal-cubic, BaTiO3; trigonal-orthorhombic-tetragonal-cubic, the distinct changing of pre-edge XANES spectra was observed near transition points. Ti atoms are located in TiO6 octahedral sites for the all samples. These structural transitions of perovskite are caused mainly by rotation and distortion of TiO6 octahedron. The temperature dependence for each pre-edge peak is largely different in temperature and local structure [1]. The electronic state of the absorber atom is reflected in the XANES spectra. The different XANES spectra show the different electronic structure of the Ti-O bounds in each compound [1]. The electronic state of Ti reflects a chemical bond with oxygen and also with the A site atoms via oxygen atoms. Even if the Ti atom for these titanates has the same coordination number and valence electrons in the TiO6 octahedron, the oxygen atoms around Ti have different electronic state and orbital hybridization affected by the A site atoms.

References

[1] Hashimoto T., Yoshiasa A., Sugahara M., Okube M., Okudera H. and Nakatsuka A., "Temperature dependence of XANES spectra for ATiO3, A2TiO4 and TiO2 compounds with structureal phase transitions.", *The American Institute of Physics,Conf. Proc.* Vol.882 AIP Melville, NY, (2007) pp. 428 -430.

[2] Itie J.P., Couzinet B., Polian A., Flank A.M. and Lagarde P., "Pressure-induced disappearance o f the local rhombohedral distortion in $BaTiO_3$." *Europhysics Letters,* Vol. 74, (2006) pp. 706-71 1

Local structure analysis of tektites by Fe K-edge XAFS spectroscopy

Takahiro Furuta[1], Ling Wang[1], Maki Okube[2], Takashi Takeda[3], Hiroki Okudera[4] and Akira Yoshiasa[1]

[1]*Graduate School of Sciences and Technology, Kumamoto University, Kumamoto 860-8555, Japan*
[2]*Materials and Structures Labo. Tokyo Institute of Technology, Yokohama 226-8503, Japan*
[3]*National Institute for Materials Science, Tsukuba, Ibaraki 305-0044, Japan*
[4] *Graduate School of Science and Technology, Kanazawa University, Kanazawa 920-1192, Japan*
E-mail: yoshiasa@sci.kumamoto-u.ac.jp

Tektite is natural glass and formed as large meteorites impact at the Earth's surface. Local structure of Fe in tektite was studied by X-ray absorption fine structure (XAFS) spectroscopy. We have carried out Fe K-edge XAFS measurements to get information about the local structure and chemical state of Fe in many species with different locality, size and color in tektites such as Hainanite, Indochinite, Philippinite, Australite, Bediasite and Moldavite. XAFS spectra near the Fe K-edge in tektite and iron minerals have been measured in transmission mode and in fluorescence made using Lytle-type or 19-elements SSD detector at PF BL-12C of Photon Factory in the National Laboratory for High Energy Physics, Japan [1]. Clear EXAFS (Extended X-ray Absorption Fine Structure) oscillations were observed for tektite. For local structure analysis, we carried out the parameter fitting with an analytical EXAFS formula expressed by a cumulant expansion up to third order term, and determined the radial distribution around iron, precise local Fe-O bonds, EXAFS Debye-Waller factors and effective pair potentials $V(u)=\mathbf{a}u^2/2+\mathbf{b}u^3/3!$ for Fe-O bond in tektite, FeO wustite [2,3], Fe3O4 magnetite, γ-Fe2O3 maghemaite,α-Fe2O3 hematite have been investigated by the XAFS technique. XANES spectra are quite sensitive to the three-dimensional atomic configuration around X-ray absorbing atoms and oxidation state of iron. The XANES spectra of Fe-K edge in tektites are clearly different from those in natural minerals. The chemical shift of threshold energy in XANES spectra between tektite and FeO was observed. The chemical shift is depending on changing oxidation state of Fe like Fe2+ and Fe3+. The threshold E0 energies shift to lower energy with decreasing oxidation states. All samples for tektite show the valence of Fe is completely divalent state (Fe^{2+}), though Fe ions have both trivalent and divalent state in many iron minerals in terrestrial conditions [2,3]. We have found some tektite with 4-, 5- and 6-fold coordinated Fe. This study indicates that the local structure of Fe should be changed in the impact event and the following stage. Tektites splashed to the space and travelled in several kinds of process and routes, which lead to different temperature and pressure history. Local structure of Fe should be related with the temperature, pressure, quenching rate, sizes of impact meteorite and size of falling melts. As a result, there are some difference in the bonding structure of Fe atoms and arrangements of neighboring oxygen

References

[1] Sakai S., Yoshiasa A., Arima H., Okube M., Numako C. and Sato T., "XAFS study of As in K-T boundary clay", *The American Institute of Physics,Conf. Proc.* Vol.882 AIP Melville, NY, (2007) pp. 274-276.

[2] Yoshiasa A., Sugiyama K., Sakai S., Isobe H., Sakamoto D., Ota K., Arima H. and Takei H.." Synthesis of Single Crystal $(Mg_{1-x}Fe_x)_{1-\delta}O$ (x=0.001-1.00) Solid-solution and Electrical Conduction mechanism at High Temperature and Pressure" *Journal of Crystal Growth,* Vol. 311, (2009) pp. 974-977

[3] Yoshiasa A., Ohtaka O., Sakamoto D., Andrault D., Fukui H. and Okube M. "Pressure and compositional dependence of electric conductivity in the $(Mg_{1-x}Fe_x)_{1-\delta}O$ (x=0.01-0.40) solid-solution" *Solid State Ionics,* Vol. 180, (2009) pp. 501-505

MS05-P23

H/D effect in a room temperature ionic liquid: *N*, *N*-diethyl-*N*-methyl-*N*-(2-methoxyethyl) ammonium tetrafluoroborate

Hiroshi Abe[1], Yusuke Imai[1], Takahiro Takekiyo[2] and Yukihiro Yoshimura[2]

[1]*Department of Materials Science and Engineering, National Defense Academy, Yokosuka 239-8686, Japan*
[2]*Department of Applied Chemistry, National Defense Academy, Yokosuka 239-8686, Japan*
E-mail: ab@nda.ac.jp

Room temperature ionic liquids (RTILs) are organic salts, which consists simply of a cation and an anion. Almost zero vapor pressure and nano-heterogeneity are representative features of the RTILs. The nano-heterogeneity is divided into polar and non-polar regions. The RTILs are regarded as environmentally friendly 'green chemistry' for recycling system. Utilizing the almost zero vapor pressure, CO_2 separation is developed for industrial applications. Recently, complicated phase behaviors in *N*, *N*-diethyl-*N*-methyl-*N*-(2-methoxyethyl) ammonium tetrafluoroborate, [DEME][BF_4]-water system were reported [1]. Simultaneous X-ray diffraction and differential scanning calorimetry can determine the phase diagram precisely.

Systematically, crystal structures of [DEME][BF_4]-H_2O, CH_3OH, C_2H_5OH and C_6H_6 mixtures were examined [2, 3]. Particularly in 0.9 mol % H_2O, anomalous twin-related domains, two kinds of superstructures and their volume contraction occurred unexpectedly. By introducing a sublattice with an equivalent sublattice constant, the twin-related domains, two kinds of superstructures, and the volume contraction at 0.9 mol % H_2O are well explained. Average distance between water molecules at 1 mol% coincides with the sublattice constant. In the same manner with a ferroelectric material, we perform the H/D exchange of water in order to clarify hydrogen bonding in quite a small amount of water. By substituting D_2O for H_2O fixing at 1 mol%, the above anomalies disappeared gradually [4]. Moreover, crystallization temperature is decreasing with increasing D.

H/D effect as geometrical is well known in the ferroelectric materials. 'Proton-mediated covalent bonding (PMCB)' is an idea to interpret the experimental results. PMCB as attractive interaction is realized by quantum delocalization of proton. In [DEME][BF_4]-1 mol% H_2O, we deduce that anomalous crystallization is derived from the 'on-centering' proton as shown in Fig. 1(a). Hence, 1 mol% water network is enhanced by PMCB. On the other hand, 'off-centering' deuteron disturbs the network (Fig. 1(b))

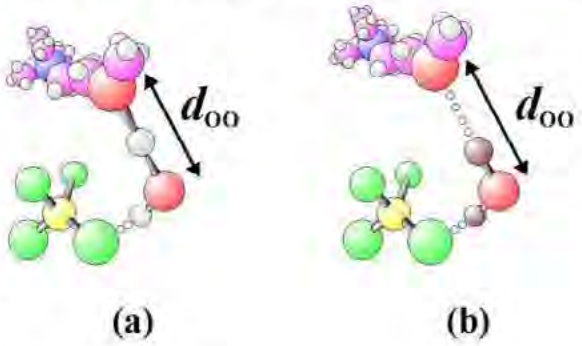

Fig.1 A bonding scheme of (a) H_2O and (b) D_2O in crystal. The atomic distance between oxygens, d_{OO}, varies depending on the interaction.

References

[1] Abe H., Yoshimura Y., Imai Y., Goto T. and Matsumoto H., "Phase Behavior of Room Temperature Ionic Liquid-H_2O Mixtures: *N*, *N*-diethyl-*N*-methyl-*N*-2-methoxyethyl ammonium tetrafluoroborate", *Journal of Molecular Liquids*, Vol. 150, (2009) pp 16-21.

[2] Imai Y., Abe H., Goto T., Yoshimura Y., Kushiyama S. and Matsumoto H., "Orientational Ordering of Crystal Domains in Ionic Liquid Based Mixtures", *Journal of Physical Chemistry B*, Vol. 112, (2008) pp 9841-9846.

[3] Imai Y., Abe H. and Yoshimura Y., "X-ray Diffraction Study of Ionic Liquid Based Mixtures", *Journal of Physical Chemistry B*, Vol. 113, (2009) pp 2013-2018.

[4] Abe H., Imai Y., Takekiyo T. and Yoshimura Y., "Deuterated Water Effect in a Room Temperature Ionic Liquid: *N*, *N*-Diethyl-*N*-Methyl-*N*-2-Methoxyethyl Ammonium Tetrafluoroborate", *Journal of Physical Chemistry B*, Vol. 114, (2010) pp 2834-2839.

MS05-P24

A Combined experimental and theoretical charge density study of di-chromium complex with a Cr-Cr quintuple bond

Lai-Chin Wu[1], Chia-Wei Hsu[2], Yu-Chun Chuang[1] Gene-Hsiang Lee[1], Yi-Chou Tsai[2], Yu Wang[1]*

[1]*Department of Chemistry, National Taiwan University, Taipei, Taiwan*
[2]*Department of Chemistry, National Tsing Hua University, Hsinchu, Taiwan*
E-mail: d92223012@ntu.edu.tw

A combined experimental and theoretical study on a quintuple bonded di-chromium complex, $Cr_2(dipp)_2$ (dipp- = (Ar)NC(H)N(Ar) and Ar = 2,6-*i*-Pr_2-C_6H_3) is performed. Two dipp ligands are bridged between two Cr metal ions; each Cr metal is coordinated to two N atoms of the ligands in a linear fashion. The Cr metal is in a low covalent and low coordination number condition, which stabilizes a multiple bond formation. Indeed it gives the shortest Cr-Cr bond distance of 1.7484(1) Å. The bond characterization of such a quintuple bond in the complex is undertaken both experimentally by high resolution single-crystal X-ray diffraction and theoretically by density functional calculation based on the experimental geometry. Bond characterizations of the complex will be presented in terms of topological properties; Fermi-hole function, electron localization function (ELF), source function (SF) and natural bonding orbital (NBO) analysis. The electron density at the Cr-Cr bond critical point is 1.70 e/Å^3; a quite high value for a metal-metal bond. The Cr-Cr quintuple bond is confirmed with one σ, two π and two δ interactions by NBO analysis and Fermi hole function. The MOs also illustrate that five bonding orbitals are predominantly contributed from the 3*d* orbitals of Cr(I) metal ion. The effective bond order from NBO analysis is 4.40. Detail comparison between experiment and theory will be given.

MS05-P25

In situ observation of crystal structure of $BaTiO_3$-based ceramics under high electric field

Hisanori Ohkubo[1], Chikako Moriyoshi[1], Fumiko Yoshida[1], Yoshihiro Kuroiwa[1], Noriyuki Inoue[2] and Takafumi Okamoto[2]

[1]*Department of Physical Science, Hiroshima University, Kagamiyama, Higashi-Hiroshima, Hiroshima 739 -8526, Japan*
[2]*Murata Manufacturing Co., Ltd., Nagaokakyo, Kyoto 617-8555, Japan*
E-mail: hisanori-ohkubo@hiroshima-u.ac.jp

A broad variety of $BaTiO_3$-based ceramics is developed as a dielectric for multilayer ceramic capacitors (MLCCs). To satisfy requirements for the lower dielectric loss and lower microphonics, rare-earth and Mg ions co-substituted $BaTiO_3$ are proposed as candidates for the dielectrics, which enable us to suppress various problems involved in applying the dielectric properties of pure $BaTiO_3$ to MLCCs. The temperature dependence of permittivity can be improved by increasing the contents of rare-earth and Mg ions, although the Curie temperature (T_C) is significantly decreased. We have recently revealed that Gd is the most effective rare-earth element for suppressing insulation degradation for applied voltage and temperature stress among $BaTiO_3$-based ceramics. In this paper, we report *in situ* crystal structure analysis of $(Ba_{0.94}R_{0.06})(Ti_{0.97}Mg_{0.03})O_3$ (BGTM) under variations in electric field and temperature using a sample fabricated based on a MLCC. The electric-field-induced lattice strain and atomic displacement are demonstrated in the environments realizing the electric device operating.

Powder diffraction experiment was carried out using the large Debye-Scherrer camera installed at BL02B2 in SPring-8. The energy of X-rays was 35 keV (λ = 0.35 Å) to establish the transmission geometry. The phase transition temperature T_C = 293 K was confirmed by the simultaneous measurements of the diffraction patterns and the dielectric constants. The crystal structures were measured in the temperature range of 295 K - 400 K in the paraelectric phase, and the applied electric field up to 300 kV/cm.

The tetragonal distortion was detected for the ceramic grains arranged in electric field, which was significant as the temperatures were approaching T_C. The lattice strain was increased with increasing the electric field, and saturated above 100 kV/cm at 300 K. The displacement of the *B*-site ions showed a similar variation as the lattice strain. These results give clear evidence that the lattice strains observed in the paraelectric phase are attributed to the displacements of the constituent ions in the electric field.

MS05-P26

Nanoporous structures as a brand-new type of color conversion phosphor for solid-state lighting-LEDs

Pei-Ci Jhang and Sue-Lein Wang

Department of Chemistry, National Tsing Hua University, Hsinchu, Taiwan 30013, R.O.C.
E-mail: ggcc1740@yahoo.com.tw

This research reports the determination of an extraordinary crystal structure, NTHU-7[1], which was crystallized from a green solvent, a challenging preparative way of synthesis and contributing a great significance to the discovery of a new type of nanoporous materials. NTHU-7 is the first metal phosphite material exhibiting distinct photoluminescence with unprecedented organic-inorganic hybrid nanotubular structures, each individual nanotubule is built from four strains of $[Ga_2(HPO_3)_2]$ four-ring (4R) ribbons connected via four oxalate groups to form 16R aperture window at the tubule opening. The hybrid nanotubule has an external diameter of 16.3 Å and internal diameter of 8.0 Å, similar to the double-walled CNT. Compared with general color conversion phosphors of inorganic material with condensed structures, an entirely different synthesis method is used in our study to prepare a brand-new type of color conversion phosphor. We firstly used ionothermal reaction containing choline-based deep-eutectic solvent (DES) which is environmentally friendly green solvent with biodegradable and versatility to prepare the novel color conversion phosphor, NTHU-7. Unlike commercialized or developed color conversion phosphors with extrinsic emissions that originate from emitting activators doped into condensed host lattices,[2] the activator-free NTHU-7 could intrinsically emit intense yellow-green light under the excitation of NUV and blue light. The underlying origin of such unforeseeable yellow emission has been previously observed in two interesting nanoporous metal phosphates prepared by our group, NTHU-4[3] and NTHU-6[4] yet without decisive explanations. Owing to the discovery of NTHU-7, we are able to make experimental inquiry on NTHU-7 and its analogues to unveil an answer to the fundamental emission mechanism. Phosphors that are currently under development for LEDs include four major categories based on condensed hosts of metal oxides, metal sulfides, metal nitrides, and alkaline-earth metal oxonitrides. All the phosphors in these categories are extrinsic phosphors with emissions activated by dopants through a known fundamental emission mechanism. Now, with the discovery of NTHU-7 we can firmly establish the fifth category: nanoporous MPO-based phosphors. The new phosphors are intrinsic and considered all-inclusive because of the integrity of activator (defect or disorder), sensitizer (organic template), and host (nanoporous structure) in nature. Fabrication of near-white and green LEDs by coating lanthanide-free phosphors on GaN and InGaN chips was firstly achieved with NTHU-7. This brand-new type of color conversion phosphor has wide excitation range in the NUV and visible region, a rare and commendable characteristic compared to commercialized phosphors like YAG:Ce.

References

[1] Jhang P. C., Yang Y. C., Lai Y. C., Liu W. R., Wang S. L., "A Fully Integrated Nanotubular Yellow-Green Phosphor From An Environmentally Friendly Eutectic Solvent" *Angew. Chem. Int. Ed.* Vol. 48 (2009), pp 742-745..

[2] Kitai A., "*Luminescent Materials and Application*", 1st edition, Wiley, (2008).

[3] Liao Y. C., Lin C. H., Wang S. L., "Direct White Light Phosphor: A Novel Porous Zinc Gallophosphate with Tunable Yellow to White Luminescence" *J. Amer. Chem. Soc.*, Vol. 127 (2005), pp 9986-9987.

[4] Yang Y. C., Wang S. L., "Intrinsic Yellow Light Phosphor: An Organic-Inorganic Hybrid Gallium Oxalatophosphate with Hexameric Octahedral Ga6(OH)4O26 Cluster", *J. Am. Chem. Soc.*, Vol. 130 (2008), pp 1147-1148.

MS05-P27

Preparation and characterization of a metformium salt of monoprotonated decavanadate

Aungkana Chatkon and Kenneth J. Haller

School of Chemistry, Institute of Science, Suranaree University of Technology, Nakhon Ratchasima 30000 Thailand
E-mail: achatkon@hotmail.com

The biological activity of decavanadate complexes has been intensively studied *in vivo* as insulin mimetics and they have been shown to have synergistic interactions with other biologically active small molecules [1]. Metformin is a biguanide derivative which is commonly used in the form of the hydrochloride salt as an oral hypoglycemic drug to treat type 2 diabetes mellitus. In this study, we report a compound of metformium decavanadate synthesized from V_2O_5, $C_4H_{11}N_5{\cdot}HCl$, and H_2O in molar ratio of 1.2:1:555 (pH about 5) by refluxing at 60°C for 15 hours followed by keeping the solution at RT for one month to give yellow crystals.

The novel compound was characterized by X-ray diffraction, SEM/EDX, FTIR, and thermal analysis. The EDX spectrum indicates presence of vanadium. The IR spectrum has a strong peak at 961 cm^{-1} that can be assigned to υ(V=O), strong bands at 844, 743 and 589 cm^{-1} characteristic of υ(V–O) and δ(V–O–V), and a weak band at 836 cm^{-1} attributed to υ(V–OH) protonated decavanadate [2,3]. The bands at 3360, 3346, 1691, 1645, (1498 & 1469), 1421, and 1067 cm^{-1} typical of $\upsilon_{as}(NH_2)$, $\upsilon(^{+}NH_2)$, υ(C=N), δ_{as}(NCN), υ(CN), $\upsilon(CH_3)$, and $\rho(NH_2)$ of metformium ion respectively [4]. The broad band at 3517 cm^{-1} can be assigned to H_2O in the compound, consistent with nine water molecules corresponding to 9.47% (calc. 9.15%) weight loss observed below 140°C by thermogravimetric analysis (TGA).

References

[1] Yraola F., García-Vicente S., Marti L., Albericio F., Zorzano A. and Royo M., "Understanding th e mechanism of action of the novel SSAO substrate $(C_7H_{10}N)_6V_{10}O_{28}{\cdot}2H_2O$, a prodrug of peroxov anadate insulin mimetics", *Chem. Biol. Drug Des.*, Vol. 69, No. 6, (2007), pp 423-428.

[2] Wery A. S. J., Gutiierrez-Zorrila J. M., Luque A. and Roman P., "Influence of protonation on crystal packing and thermal behaviour of tert-butylammonium decavanadates", *Polyhedron*, Vol. 15, No. 24, (1996), pp 4555-4564.

[3] Kasuga N. C., Umeda M., Kidokoro H., Ueda K., Hattori K. and Yamaguchi K., "Four novel solid-state supramolecular assemblies constructed from decavanadate salts and decamethylcucur bit[5]uril", *Cryst. Growth Des.*, Vol. 9, No. 3, (2009), pp 1494-1498.

[4] Spectral Database for Organic Compounds (SDBS): http://riob01.ibase.aist.go.jp/sdbs/cgi-bin/direc t_frame_top.cgi

Structural phase transition without accompanied spin transition of complex *t*-{Fe(abpt)$_2$[N(CN)$_2$]$_2$}

Chou-Fu Sheu[1], Yu-Chun Chuang[1], Yi-Hung Liu[2], Hwo-Shuenn Sheu[3], Yu Wang[1*]

[1]*Department of Chemistry, National Taiwan University, Taipei, 10617 Taiwan*
[2]*Instrumentation Center, National Taiwan University, Taipei, 10617 Taiwan*
[3]*National Synchrotron Radiation Research Center, Hsinchu, 30076 Taiwan*
E-mail: hiav8d.tw@gmail.com

A reversible crystal-to-crystal structural phase transition is found in one of the polymorphs (**A**) of complex *t*-{Fe(abpt)$_2$[N(CN)$_2$]$_2$} (abpt = 4-Amino-3,5-bis(pyridin-2-yl)-1,2,4-triazole). The crystal at 25 K remains unchanged as triclinic space group $P\bar{1}$ from that of the ambient temperature, but with different cell parameters: a = 8.7960(6), b = 8.8110(9), c = 10.1020(7) Å, α = 94.146(8)°, β = 93.296(6)°, γ = 114.460(7)°, V = 707.48(10) Å^3. Thermal-dependent powder x-ray diffraction reveals a first order phase transition with transition temperature, $T_{1/2}$, at 270 K, which coincides with the change in cell parameters monitored by single crystal diffraction experiment. The molecular geometry before and after phase transition does display significant differences on the orientation of the axial ligand, [N(CN)$_2$], illustrated in figure below, where two molecules, one at 25K (open bond) and the other at 300K (close bond), are superimposed. With the coordinated nitrogen N3 as a pivot, the dicyanoamide is shift toward the direction of uncoordinated pyridyl ring of abpt at low temperature phase, the uncoordinated terminal nitrogen N9 of [N(CN)$_2$]$^-$ is found to be shifted by as far as 1.57 Å. However the Fe-N bond distance and the octahedron distortion parameters around Fe indicate that Fe remains at high spin state even after the phase transition which is in accord with the observed temperature-dependent magnetic measurement.

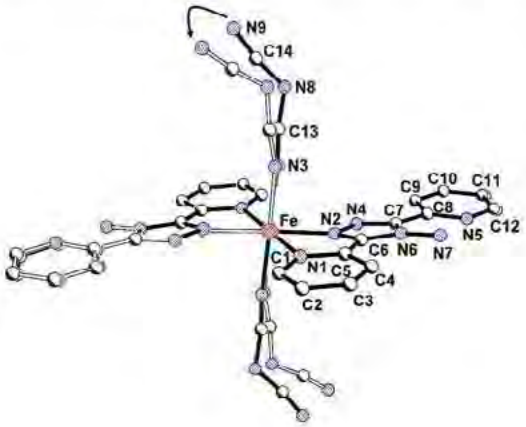

References

[1] Sheu, C. F., Pillet, S., Lin, Y. C., Chen, S. M., Hsu, I. J., Lecomte, C. and Wang, Y., "Magnetostructur al Relationship in the Spin-Crossover Complex *t*-{Fe(abpt)$_2$[N(CN)$_2$]$_2$}: Polymorphism and Diso rder Phenomenon", *Inorg. Chem.*, 47, (2008), pp 10866-10874.

[2] Pillet, S., Lecomte, C., Sheu, C. F., Lin, Y. C., Hsu, I. J., Wang, Y., "Light induced modulate d structure of the spin crossover compound {Fe(abpt)$_2$[N(CN)$_2$]$_2$}", *J. Phys.: Conf. Ser.*, 21, (2 005), pp 221-226.

[3] Moliner, N., Gaspar, A. B., Munoz, M. C., Niel, V., Cano, J., Real, J. A., "Light- and Thermal-Induced Spin Crossover in {Fe(abpt)$_2$[N(CN)$_2$]$_2$}. Synthesis, Structure, Magnetic Properties, and High-Spin ↔ Low-Spin Relaxation Studies", *Inorg. Chem.*, 40, (2001), pp 3986-3991.

MS05-P29

Electronic structures and luminescence properties of double activated $YTaO_4:Eu^{3+},Tb^{3+}$ and $YNbO_4:Eu^{3+},Tb^{3+}$ phosphors

M. Nazarov[1], Do Young Noh[1], A. Zhbanov[2], and Yong-Gu Lee[2]

[1]*Department of Materials Science and Engineering, Gwangju Institute of Science and Technology, 1 Oryong-dong, Buk-gu, Gwangju 500-712, Republic of Korea*
[2]*Department of Mechatronics, Gwangju Institute of Science and Technology, 1 Oryong-dong, Buk-gu, Gwangju 500-712, Republic of Korea*
E-mail: nazarov@gist.ac.kr

Yttrium tantalate ($YTaO_4$) and yttrium niobate ($YNbO_4$) doubly doped by Eu^{3+} and Tb^{3+}, were investigated using X-ray diffraction, X-ray excitation luminescence, and first-principles quantum-mechanical calculations in order to study their structural and luminescent properties. We found that the incorporation of the rare earth ions (5% mol concentration of Eu^{3+} and Tb^{3+}) into M'-$YTaO_4$ structure and into M-$YNbO_4$ structure did not change the basic structure significantly, but increased the unit cell volume according to Vegard's law. The total energy, electronic band structure, and density of states calculations (DOS) are performed via the full potential linear-augmented plane wave approach, as implemented in the WIEN2K code, within the framework of density functional theory. The exchange correlation energy of electrons is described in generalized gradient approximation (GGA96) to calculate the total energy, band structure and DOS (Fig.1)

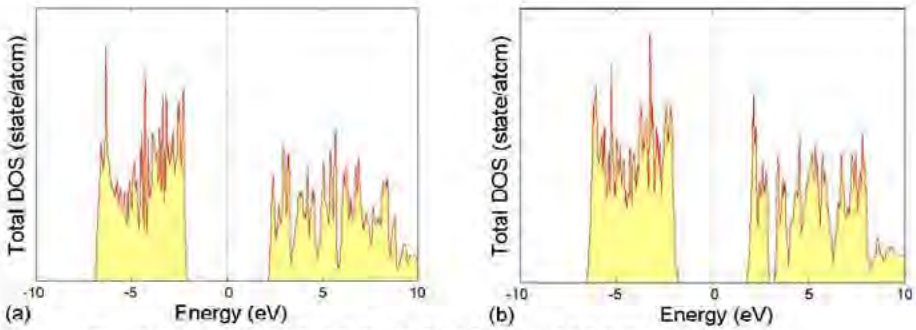

Fig. 1. Total DOS of $YTaO_4:Eu^{3+}Tb^{3+}$(a) and $YNbO_4:Eu^{3+}Tb^{3+}$ (b)

When rare earth ions such as Eu^{3+} and Tb^{3+} are incorporated simultaneously to partially substitute the yttrium ions from the host crystalline lattice, Eu^{3+} and Tb^{3+} emission centers are created. In this case, the luminescence can be red-shifted toward longer wavelengths, and both emission centers might contribute to the overall luminescence. The doubly activated M'-$YTaO_4$ structure shows the better luminescence compared with M-$YNbO_4$. The incorporation of these 2 activators into the host crystalline lattice substituting the yttrium ions seems to efficiently enhance the charge-transfer process for the M'-$YTaO_4$ structure, where the average Ta-O distances are smaller in M' structure than Nb-O distances in M structure. Under X-ray excitation, it is quite reasonable to assume that the excitation energy is absorbed first by the host lattice, which involves the transition between 4d-like states of Y and 2p-like states of O. The absorbed energy may then be transferred to TaO_4^{-3} and NbO_4^{-3} groups and at last transferred to the Eu^{3+} and Tb^{3+} emission centers. This assumption is confirmed by calculation the electronic band structure and density of states. The charge-transfer gaps between Ta-O and Nb-O are clearly shown in Fig. 1. The valence band (left) consists of mainly the O 2*p* orbital and the conduction band (right) of the T a and Nb 4*d* orbital. The band gaps are estimated as 4.2 eV and 3.6 eV, correspondingly, which agrees well with our experimental results. Synthesized double activated tantalate and niobate phosphors with improved luminescence properties can berecommended as good candidates for different applications including LED and X-ray intensifying screens.

MS05-P30

Reversible phase transition in a new polymeric zinc metavanadate, $[Zn(Im)_4][V_2O_6]$

Samroeng Krachodnok[1], Kenneth J. Haller[1] and Ian D. Williams[2]

[1]*School of Chemistry, Institute of Science, Suranaree University of Technology, Nakhon Ratchasima 300 00 Thailand*
[2]*Department of Chemistry, Hong Kong University of Science and Technology, Hong Kong*
E-mail: dsk4610137@live.com

A new polymeric zinc metavanadate, $[Zn(Im)_4][V_2O_6]$ was successfully synthesized from hydrothermal reaction of $Zn(OAc)_2{\cdot}2H_2O$, V_2O_5, imidazole, and H_2O in the mole ratio of 1:1:9:222 at 110 °C for 2 days (~96% yield, based on V). DSC measurements show that this compound undergoes a reversible first-order phase transition at ~279 K (endothermic) and at ~275 K (exothermic) with a hysteresis of 4 K. The structure was determined by single crystal X-ray diffraction at 100 (2) K, ordered phase (D_{calc} = 1.809 Mg m^{-3}) and 293 (2) K, disordered phase (D_{calc} = 1.776 Mg m^{-3}) (the space group is triclinic *P*–1 at both temperatures). The structure contains anionic polymeric chains of corner-sharing VO_4 tetrahedra separated by discrete $[Zn(Im)_4]^{2+}$ cations. At 100 K the chains are ordered with every fourth μ-O atom lying on an inversion center, and the second and sixth μ-O atoms ordered on positions alternating up and down along the chain propagation axis, placing two $[V_2O_6]^{2-}$ units and two crystallographically independent $[Zn(Im)_4]^{2+}$ cations in the asymmetric unit. The geometries of the cations are distorted tetrahedra, with one angle significantly different (N11–Zn–N31 of 112.7(3)° and 120.4(3)°, respectively). As the temperature is increased, the alternating up-down positions of the chains of the ordered structure, disorder, creating additional inversion centers at the second and sixth μ-O atom positions of the 100 K structure, thereby cutting the unit translation in the chain direction in half, consequently cutting the cell volume in half, and transforming into a disordered structure. The cations also reorient and rearrange, the N11–Zn–N31 angle of the single independent cation becomes 118.1(1)°.

A three-dimensional supramolecular network formed by interconnecting the cations to anions through four strong N–H···O hydrogen bond interactions at 100 K, whereas two additional bifurcated H23···O8/O8B and H33···O7/O7B hydrogen bond with their distances become slightly lengthened and shortened as a respond to increasing temperature. Its network stability is reinforced by fourteen weak C–H···O hydrogen bond interactions at 100K, whereas twelve weak interactions related at 293 K, which loosing two weak interactions of C12A–H12A···O7A and C35–H35···O2. When considering the intercation interactions along the *c* axis that can be divided into two parts, (i) they related on polymeric anionic propagations, two are parallel and two are tilted *ff* N–H···π hydrogen bond interactions whereas observed only two parallel *ff* N–H···π interactions at 293 K, that is the answer the question why N11–Zn–N31 angle is significantly different; (ii) they occupied in between the anions, each six-fold aryl embrace interconnected their neighbors formed two different motif types of *ef* C–H···π hydrogen bond interactions, –2 *ef*–no *ef*–2 *ef*–4 *ef*– motif at 100 K whereas –2 *ef*–4 *ef*– motif at 293 K, depend on the Zn···Zn distances, ~ 5.6, ~5.8, and ~6.8 Å correlated to none, four, and two *ef* C–H···π hydrogen bond interactions, respectively.

References

[1] Chen L.-Z., Zhao H., Ge J.-Z., Xiong R.-G. and Hu H.-W., "Observation of deuteration effect in co-crystal system: hexamethylenetetraminium 3,5-dinitrobenzoate hemideuterated water", *Crys t. Growth Des.*, Vol. 9, No. 9, (2009), pp 3828-3831.
[2] Ye H.-Y., Chen L.-Z. and Xiong R.-G., "Reversible phase transition of pyridinium-3-carboxylic acid perchlorate", *Acta Cryst. Sect. B*, Vol. 66, No. 3, (2010), pp 387-395.

Study of intermolecular interactions in two imidazo[2,1-b] [1,3,4] thiadiazoles

M.K. Kokila[1], G. N. Anil Kumar[2] Subhas S. Karki[3], R.Vinaya Kumar[3] and M. V. Kulkarni[4]

[1]*Department of Physics, Bangalore University, Bangaluru-560056, India*
[2]*Department of hysics, M.S. Ramaiah Institute of Technology, MSRIT Post, Bangaluru-560 054, India*
[3]*Department of Pharmaceutical Chemistry and Pharmacology, KLES College of Pharmacy, 2nd Block, Rajajinagar, Bangaluru 560 010, India*
[4]*Department of Studies in Chemistry, Karnatak University, Dharwad -570 001, India*
E-mail: drmkkokila@gmail.com

The generation of engineered interactions between preselected constituent blocks of molecular assemblies is an emerging area in crystal engineering. In crystal structures the packing of the molecules mainly depend on the symmetry of the lattice and intermolecular interactions which drive the molecules to assemble together.[1] In addition to conventional hydrogen bonding weak interactions were also extensively studied and utilized in designing variety of molecules of specific interest. Some of the steering forces that have been recognized are halogen–halogen interactions[2], charge transfer, electrostatic forces, pi–pi stacks[4]. In view of these we attempted to study the role of weak interactions in aryl substituted imidazo[2,1*b*][1,3,4]thiadiazoles with an intention of understanding the role of interactions involving halogens[5].

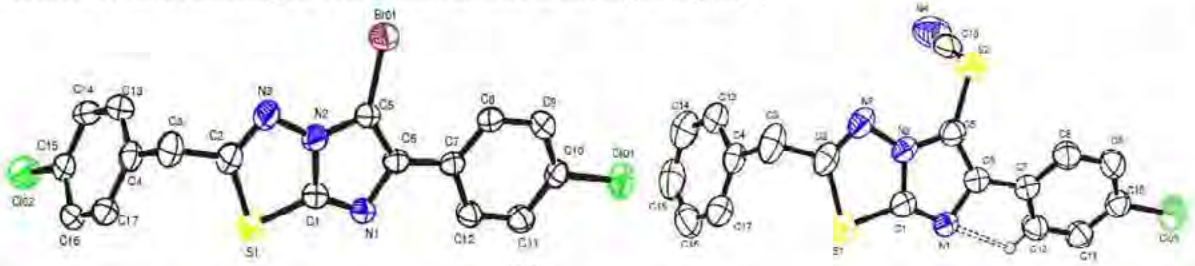

(II)

In the present study, we have analyzed the crystal and molecular structures of 5-bromo-2-(4-chlorobenzyl)-6-(4-chlorophenyl)imidazo[2,1*b*][1,3,4]thiadiazole $C_{17}H_{10}N_3$ Br Cl_2 S (I), and 2-benzyl-6-(4-chlorophenyl) imidazo[2,1-*b*][1,3,4]thiadiazol-5-ylthiocyanate C_{18} H_{11} N4 Cl S_2(II). Compound (I) crystallizes under Orthorhombic , *Pbcn* spacegroup where as (II) crystalized under Monoclinic, $P2_1/c$ spacegroup. The final R-factor is 0.039 for both (I) and (II).

In (I), the chlorobenzyl and chlorophenyl rings were twisted at 86.06^0 and 15.11^0 respectively from the planar imidazothiadiazole moiety. But, in (II), the benzyl and chlorophenyl rings were twisted at 62.92^0 and 31.7^0 respectively. In both (I) & (II), molecular structures were stabilized by intermolecular Cl ... π, π – π interactions and C –H ... N hydrogen bonds. The detailed structural aspects and discussion on modes of packing will be presented and discussed.

References

[1] T.N. Guru Row: Hydrogen & Fluorine in crystal Engineering, Coordination Chemistry Reviews 183 (1999) 81–100.
[2] T. Steiner, G. R. Desiraju, Distinction between the weak hydrogen bond and the van der Waals interaction.Chem. Commun. 1998, 891 – 892.
[3] Motohiro Nishio, Yoji Umezawa, Kazumasa Honda, Sei Tsuboyamad and H. Suezawae CH/π hydrogen bonds in organic and organometallic chemistry, Cryst Eng Comm,2009,11,1757 -88.
[4] G. N. Anilkumar, M. K. Kokila, Puttaraja, S. S. Karki M. V. Kulkarni 6-(4-Chlorophenyl) imidazo[2,1-b][1,3,4]thiadiazole-2-sulfonamide, Acta Cryst. (2006). E62, o2014–o2016.

MS05-P32

Stereospecific metal bonding to cytosine in the tipodal tris(2-aminoethyl)amine (tren)-ligand system: Crystal structure of $[\{Cu(tren)\}_2(cytosinato)]\cdot(ClO_4)_3\cdot 0.5H_2O$

M.S. Rahman[1] and K. Aoki[2]

[1] *Department of Chemistry, University of Dhaka, Dhaka-1000, Bangladesh*
[2] *Department of Materials Science, Toyohashi University of Technology, Toyohashi 441-8580, Japan*
Email : shahid_du_ch@yahoo.com

Stereospecific interligand interactions, involving hydrogen-bonding, electrostatic repulsion, and steric constraint, could affect the base- and site-specific metal bonding to nucleic acid bases. To verify this hypothesis, we introduced a tris(2-aminoethyl)amine (tren)-ligand system, where tren bears three primary amine groups that could function as hydrogen-bonding donors only. The reaction between tren, Cu^{2+} and cytosine was undertaken under alkaline conditions to give a ternary tren–Cu^{2+}–cytosine complex, $[\{Cu(tren)\}_2(cytosinato)](ClO_4)_3\,0.5H_2O$, whose crystal structure was determined by X-ray diffraction. The complex crystallizes in the space group $P2_1/n$ with a = 18.662(2) Å, b = 11.467(2) Å, c = 15.827(4) Å , β = 98.94(2)°, V = 3346(1) Å^3, and Z = 4. In the structure of the $[\{Cu(tren)\}_2(cytosinato)]^{3+}$ cation, two tren-capped Cu^{2+} ions bind to a cytosinate anion, one through the deprotonated N(1) with the formation of an N(tren)–H···O(2) hydrogen bond, and the other through both the ring N(3) and the exocyclic O(2) of the base, forming a four-membered chelate ring. The significance of intramolecular interligand interaction as a factor that affects metal-binding sites on cytosine is emphasized.

Structures and bonding modes of tetra-bonded hypervalent oxygen compounds

Etsuko Tomiyama[1], Kengo Yoshida[1], Masanobu Uchiyama[1], Yohsuke Yamamoto[2] and Daisuke Hashizume[3]

[1]*Advanced Elements Chemistry Research Team, RIKEN, Saitama 351-0198, Japan*
[2]*Department of Chemistry, Hiroshima University, Hiroshima 739-8526, Japan*
[3]*Advanced Technology Support Division, RIKEN, Saitama 351-0198, Japan*
E-mail: etomiyama@riken.jp

Hypervalent compound of second raw elements is rarely reported although the structure and bonding mode give valuable information on reaction intermediate. Oxygen atom, in particular, has no vacant valence orbital to accept electrons, therefore, the formation of hypervalent bonds is more difficult than those of boron and carbon atoms. Recently, probable candidates of hypervalent tetra-bonded oxygen compounds, **1** and **2**, were synthesized with the B–O–S contacts on the anthracene architecture. Now, we report the structures of these molecules and discuss the bonding modes.

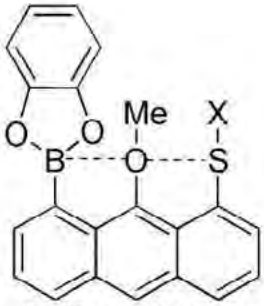

1: X = phenyl
2: X = cyclohex

In **1**, the anthracene moiety is planer, and S, O and B atoms on 1, 9 and 8 positions, respectively, are on the same plane within 0.3 Å.(Fig. 1) The distances are 2.88 and 2.48 Å for O1–S1 and O1–B1, respectively, indicating the formation of the O–B and O–S hypervalent bonds. The conformation around anthracene–SPh bond is *s-trans* (C12–C13–S1–C22 = 6°), and the angle of C22–S1–O1 is almost linear (168°). This geometry prefers donation of the lone pair on the O1 to the S1 to form the O1–S1 bond.

The structure of **2** is considerably different from **1**.(Fig. 2) The anthracene moiety is not planar, the benzene ring bonded to the S atom deviates from the plane formed by the remaining atoms in the anthracene moiety. The S1 atom is also deviated from the anthracene plane by 0.6 Å. The O1–S1 and O1–B1 distances are significantly different from those of **1**; the corresponding distances are 2.97 and 2.34 Å for O1–S1 and O1–B1, respectively. The angle of S1–C13–C14 (124°) is considerably larger than that of **1** (120°). The most remarkable structural difference is found on the conformation around the C13–S1 bond. The torsion angle of C12–C13–S1–C22 is 117°, thus the relative orbital arrangement of the S1 atom against the O1 atom is different from those of **1**. The arrangement leads to different bonding mode on the O1–S1 bond from that in **1**. To clarify the detailed bonding modes of the hypervalent O–B and O–S, we performed theoretical calculations.

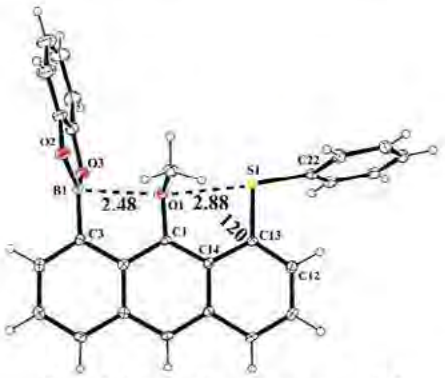

Fig. 1 Molecular Structure of **1**.

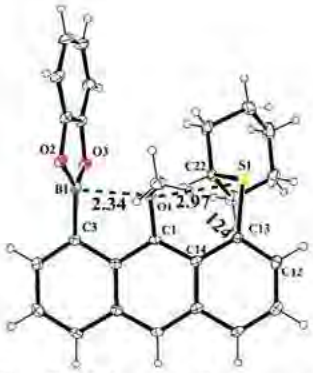

Fig. 2 Molecular Structure of **2**.

MS05-P34

Synthesis, structures, photophysical characterization and OLED applications of some multifunctional cyclometalated iridium metallophosphors containing 9-phenylcarbazoles

Wai-Yeung Wong, Ching-Shan Lam and Cheuk-Lam Ho

Department of Chemistry, Hong Kong Baptist University, Waterloo Road, Hong Kong
E-mail: rwywong@hkbu.edu.hk

Since there is an upsurge of research interest in the development of high-performance organic light-emitting diodes (OLEDs), iridium(III) complexes containing aryl-substituted 2-[3-(*N*-phenylcarbazolyl)]pyridine molecular framework are presented here. These complexes are thermally stable solids and highly efficient electrophosphors. The optical, structural, electrochemical, photo- and electrophosphorescence traits of these iridium phosphors have been studied in terms of the electronic nature of the ligands. Due to the propensity of the electron-rich carbazolyl group to facilitate hole injection/transport, the presence of such a moiety can increase the highest occupied molecular orbital levels and improve the charge balance in the resulting complexes relative to the parent metallophosphor with 2-phenylpyridine ligands. Electrophosphorescent OLEDs with outstanding device performance can be fabricated based on these materials. The work can be extended to realizing high-efficiency white light OLEDs.

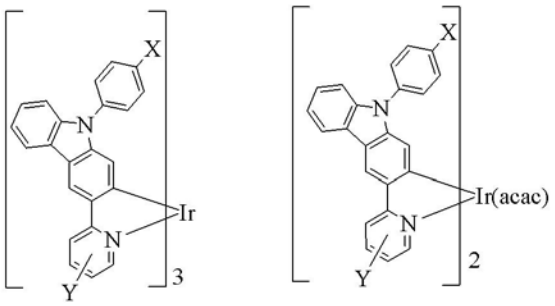

Acknowledgement: The work was supported by the Hong Kong Research Grants Council (HKBU202709).

References

[1] Wong W.-Y., Ho C.-L., Gao Z.-Q., Mi B.-X., Chen C.-H., Cheah K.-W., Lin Z., *Angew. Chem.Int. Ed.*, 45, (2006), 7800-7803.
[2] Ho C.-L., Wang Q., Lam C. S., Wong W.-Y., Ma D., Wang L., Gao Z.-Q., Chen C.-H., Cheah K.-W., Lin Z., *Chem. Asian J.*, 4, (2009), 89-103.
[3] Wong W.-Y., Ho C.-L., *J. Mater. Chem.*, 19, (2009), 4457-4482 (a Feature article).

Concerted disorder through the hydrate region of tricyclic acyclovir : $C_{11}H_{13}N_5O_3 \cdot 2H_2O$

Montha Meepripruek[1,2] and Kenneth J. Haller[1]

[1]*School of Chemistry and* [2]*School of Biochemistry, Institute of Science, Suranaree University of Technology, Nakhon Ratchasima 30000, Thailand*
E-mail: montha_mee@hotmail.com

Tricyclic acyclovir, 3-[(2-hydroxyethoxy)-methyl]-6-methyl-3*H*-imidazolo[1,2-*a*]purin-9(5*H*)-one, has been reported as the dihydrate, and the complex hydrogen bond network of water and tricyclic acyclovir molecules suggested to be related to the solvation of the molecules in solution [1]. The $Z = 2$ structure contains four independent solvent water molecules, forming an $(H_2O)_8$ cluster through a strong hydrogen bond (d[O···O] = 2.81 Å) between two water molecules across an inversion center. Three of the independent water molecules are ordered while the inversion center requires one hydrogen atom in the fourth to be statistically disordered. The second disordered hydrogen position is a strong donor to the 2-hydroxyl group of the side chain of one independent molecule of tricyclic acyclovir.

The hydroxyl group in turn relates to an equivalent group on the next molecule through a strong hydrogen bond (d[O···O] = 2.67 Å) across another inversion center requiring statistical disordering of the hydroxyl hydrogen atom. The result of the hydrogen atom disorders is concerted chains propagating in opposite directions as shown in Figure 1, which differ only in the placement of the hydrogen atoms.

The $(H_2O)_8$ clusters shown in Figure 2 are essentially perpendicular to the chains just described and create a 2D network with both independent tricyclic acyclovir molecules, using strong O–H···O water-water and water-drug, and O–H···N water-drug interactions.

Reference

[1] Suwińska, K., Golankiewicz, B., and Zielenkiewicz, W., "Water molecules in the crystal structure of tricyclic acyclovir", *Acta Cryst. Sect. C*, Vol. 57, (2001), pp 767-769.

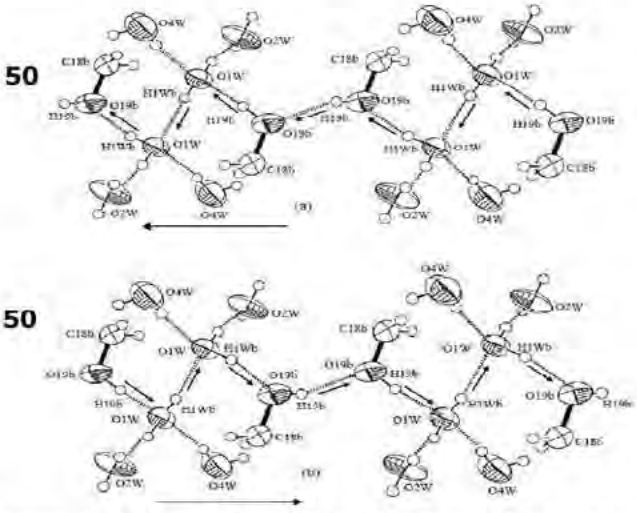

Figure 1. Chains of concerted H-bonds of the statistically disordered O1W and O19b hydrogen atoms. In (a) all

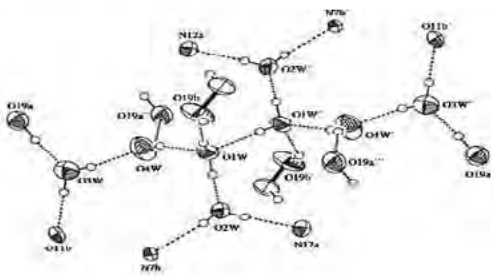

Figure 2. The water molecules form an $(H_2O)_8$ cluster surrounded by ten tricyclic

Stability of clopidogrel bisulfate (PLAVIX), an antiplatelet drug, under elevated conditions

Nongnuj Muangsin[1], Chuttree Phurut[1] and Thapong Teerawatananon[1]

[1]*Department of Chemistry, Faculty of Science, Chulalongkorn University, Bangkok, 10330, Thailand*
E-mail: nongnuj.j@chula.ac.th

Stability of drugs towards heat, moisture, oxidation and light is an important topic of great practical interest in pharmaceutical field, and any degradation will usually adversely affect the therapeutic activity of the drug. Clopidogrel (PLAVIX) or methyl(+)-(S)-α-(2-chlorophenyl)-4,5,6,7-tetrahydrothieno[3,2-c]pyridine-5-acetate hydrogen sulfate is a potent oral antiplatelet agent often used in the treatment of diseases related to coronary artery, peripheral vascular and cerebrovascular. Clopidogrel bisulfate (CPL^+ HSO_4^-) exists in many polymorphic forms (Form I to VII). Only Form I and II are used in pharmaceutical formulation. Therefore, in this work, we investigated the stability of clopidogrel Form I under extreme conditions; high pressure and high temperature using hydrothermal method, in the present and without water. We have found that CPL^+ is stable under these extreme and dry conditions and the hydrogen sulfate counter ion undergoes chemical reaction with the solvent used. For example, clopidogrel isopropylsulfate was obtained when using isopropyl alcohol as a solvent. In the present of water, clopidogrel is decomposed to brown viscose jelly. This phenomenon is also the same when clopidogrel is in a base condition. The mechanism of clopidogrel degradation is under investigation in our laboratory.

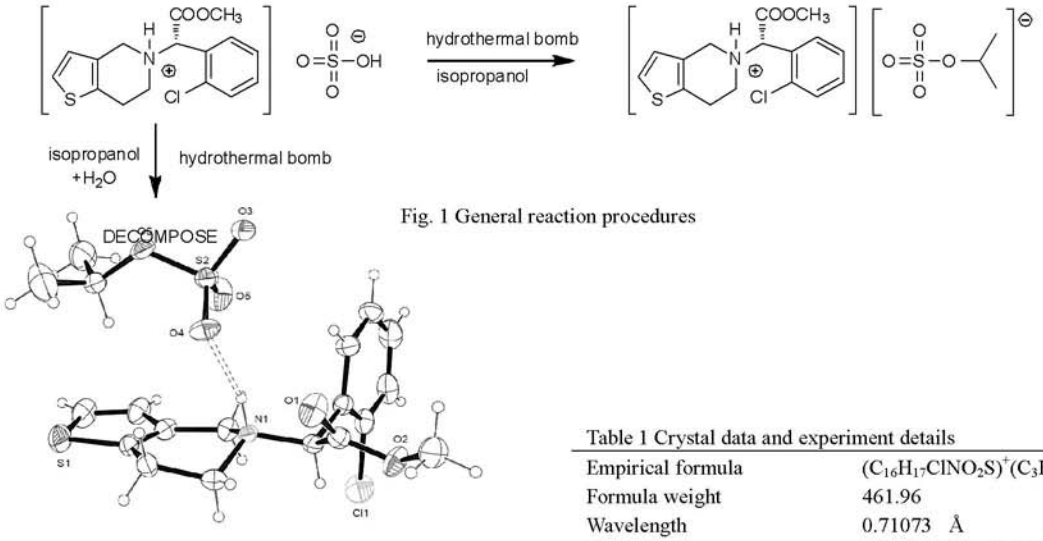

Fig. 1 General reaction procedures

Fig. 2 The molecular structure of the title compound, showing 50% probability displacement ellipsoids. Hydrogen bonds are shown as dashed lines

Table 1 Crystal data and experiment details

Empirical formula	$(C_{16}H_{17}ClNO_2S)^+(C_3H_7OS)^-$
Formula weight	461.96
Wavelength	0.71073 Å
Crystal system, space group	orthorhombic, $P2_12_12_1$
Unit cell dimensions	a = 8.2710(8) Å
	b = 13.281(1) Å
	c = 20.075(2) Å
Volume	2205.2(4) Å^3
Z, Calculated density	4, 1.391 g/cm^3
Absorption coefficient	0.397 mm^{-1}
Reflections collected / unique	8130 / 2456 [*R*(int) = 0.0588]
Data / restraints / parameters	2456 / 0 / 262
Goodness-of-fit on F^2	1.019
Final R indices [$I>2\sigma(I)$]	*R*1 = 0.0519, *wR*2 = 0.1191
R indices (all data)	*R*1 = 0.1110, *wR*2 = 0.1443

References

[1] Koradia V., Chawla G. and Bansal AK. "Qualitative and quantitative analysis of clopidogrel bisulphate polymorphs", *Acta. Pharm.* 54, 3, (2004), pp. 193-204.

[2] Agrawal H., Kaul N.K., Paradkar A.R. and Mahadik K.R. "Stability indicating HPTLC determination of clopidogrel bisulphate as bulk drug and in pharmaceutical dosage form", Talenta, 61, 5, (2003), pp. 581-589.

MS05-P37

Successive volume expansion observed in a small-pore zeolite

Yongjae Lee,* Yongmoon Lee, Dong-Hoon Seoung

Department of Earth System Sciences, Yonsei University, Seoul 120-749, Korea
E-mail: yongjaelee@yonsei.ac.kr

While an ever-expanding variety of zeolites with a wide range of framework topology is available, it is desirable to have a way to tailor the chemistry of the zeolitic nanopores for a given framework topology and provide controlled access to the interior for selective sorption and separation. With this respect, both framework and nonframework cation substitution have been extensively attempted to over 190 zeolitic materials reported so far and attributed to the plethora of zeolite science and technology.[1] Most recent example of this is the synthesis of PST-1, a framework Ga-substituted analogue of natrolite, which is shown to be selective for small molecules such as H_2 and He.[2] On the other hand, nonframework cation substitution can be achieved relatively easily via post-synthesis modification, and the exchanged cations exert different selectivity towards foreign molecules as a combined effect of modified coordination chemistry and framework distortion/relaxation.[3] This is, however, subjected to the ability of a zeolitic framework to allow the kinetic migration of exchanging cations into the pores and channels. Specially, small-pore zeolites have been known to show very limited cation exchange capacity, and natrolite and its related analogues have been such examples, into which both cation and water access are hindered at normal conditions.[4] Here we show that fully K-exchanged and subsequently Rb-, and Cs-exchanged natrolites can be prepared under modest conditions from natural Na-natrolite and exhibit successive volume expansions by 10%, 15.7%, and 18.5%, respectively. This constitutes the largest, ever-reported volume expansion observed in zeolites and occurs by converting the elliptical channels into progressively circular ones. The step-wise changes in the nanopore volume and shape thus demonstrate the simplest, yet most dramatic means to tailor the selectivity of zeolitic nanopores and promises novel applications of this class of small-pore zeolites.

References

[1] Baerlocher C, McCusker LB, & Olson DH (2007) *Atlas of Zeolite Framework Types* (Elsevier, Amsterdam) 6th Ed.
[2] Shin J, *et al.* (2009) PST-1: A Synthetic Small-Pore Zeolite that Selectively Adsorbs H2. *Angew.Chem. Int. Ed.* 48:1-4.
[3] Barrer RM (1982) *Hydrothermal Chemistry of Zeolites* (Academic Press, London).
[4] Dyer A & Faghihian H (1998) Diffusion in heteroionic zeolites: part 1. Diffusion of water in heteroionic natrolites. *Micropor. Mesopor. Mater.* 21:27-38.

MS05-P38

Structural comparison of tetrapodal and bipodal host inclusion compounds with amine base

Fumiaki Sano, Akiko Sekine, Hidehiro Uekusa

Department of Chemistry and Materials Science, Tokyo Institute of Technology, 2-12-1 Ookayama, Meguro-ku, Tokyo, 152-8551, Japan
E-mail:sano.f.ab@m.titech.ac.jp

Tetrapodal and axis-wheel type compound, 1,4-di[bis(4'-hydroxyphenyl)methyl]benzene (TXP) ; Fig.1, is well recognized host molecule to form inclusion compound with many small organic molecules. This inclusion host has two guest catching pockets around the molecule, one is between two adjacent phenol groups and the other is beside the central benzene ring. Also, in some case, the host framework is formed to have guests in the cavity space. In this study, in order to elucidate the characteristics of the TXP inclusion crystals with amines and related compound, their crystal structure were analyzed and compared with corresponding bisphenol-A (Fig.2) inclusion crystals. Bisphenol-A is a bipodal smaller host compound, which would have only one pocket between two phenols.

TXP-ethylenediamine (TXP-EN) inclusion crystal was obtained by recrystallization from ethylenediamine solution. X-ray structure analysis showed that it crystallize in triclinic space-group $P\bar{1}$ (a =11.476(4), b =11.675(4), c =12.739(4) Å, α=72.454(5), β=83.898(6), γ=86.164(6) °). In the crystal, two TXPs and ENs are on different center of symmetry and also one more EN molecule is in an asymmetric unit forming 1:2 inclusion crystal. These EN molecules hydrogen bond to OH group of TXPs and forming a hydrophilic layer parallel to the *ab*-plane between TXP layers (Fig.3). Two of three independent EN molecules situate in pockets formed by the central benzene ring and two apart phenol groups, however, the remaining one EN is in a cavity space surrounded by four phenol groups. The pocket of two adjacent phenols is not observed due to host molecule packing.

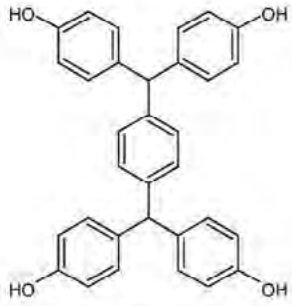

Fig. 1

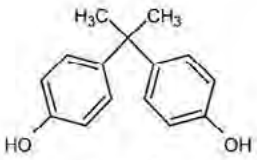

Fig. 2

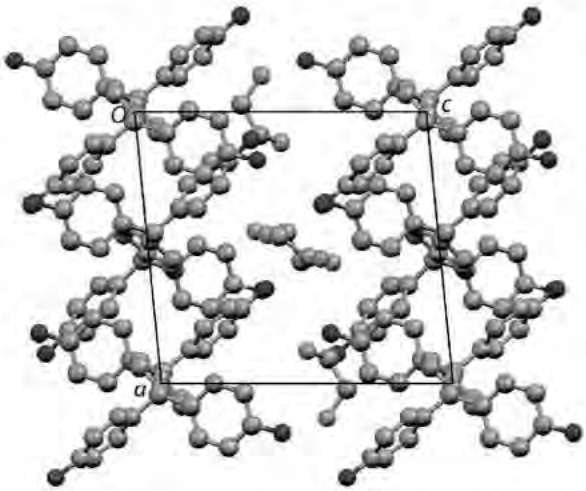

Fig. 3 The crystal structure of TXP-ethylenediamine viewed along the *b*-axis

Structural evolution of stoichiometric praseodymium silicate oxyapatite, $Pr_8Sr_2Si_4O_{26}$

Terutoshi Sakakura[1], Minami Kamoshita[1], Jun Wang[1] and Nobuo Ishizawa[1]

[1] *Ceramic Research Laboratory, Nagoya Institute of Technology, Tajimi 507-0071, Japan*
E-mail: 16513301@stn.nitech.ac.jp

Since the rare-earth bearing oxyapatites were found to have relatively high oxide-ion conductivities at moderate temperatures, attention has been drawn on their applications to the gas-sensing devices and electrolytes for solid oxide fuel cells. For the enhancement of the conductivity, structural differences among various rare-earth oxyapatites and the estimation of the migration pathways have also been studied energetically. For example, Ali *et al.* (2008) examined the nuclear and electron density distribution of the nonstoichiometric and oxygen-excess $La_{9.69}(Si_{5.70}Mg_{0.18})O_{26.37}$, using the maximum-entropy methods-based powder pattern fitting, and confirmed the presence of interstitial O atoms. [1] On the other hand, Okudera *et al.* (2004) revealed no such O atoms even at high temperatures in $Nd_{9.33}Si_6O_{26}$ through the *in-situ* single-crystal X-ray diffraction experiment. [2]

We first synthesized single crystals of stoichiometric $Pr_8Sr_2Si_4O_{26}$ by the self-flux method using $SrCl_2$. The structure was determined at approximately 23, 300, 500,700 and 900 °C, using the *in-situ* single-crystal X-ray diffraction technique. The crystal was found to have the apatite-type structure with the centrosymmetric space group $P6_3/m$. In the structure, the 4f and 6h Wyckoff positions are available for the rare-earth and alkaline earth elements. Population analysis suggested that the 4f site is shared by Sr and Pr with almost equal probability while the 6h site is almost 100% occupied by Pr. This indicates that structure become unstable if the equilateral triangle composed of Pr^{3+} at 6h sites along the hexagonal channel is disturbed by substitution with aliovalent cation like Sr^{2+}. No interstitial sites were found for oxide anions at all temperatures. The thermal ellipsoid of O4 at the centre of the Pr triangle was 3-times prolate along the *c*-axis at room temperature, and no significant temperature dependency was observed for its prolateness. Details of the structural evolution will be given in the presentation.

References

[1] Ali, R., Yashima, M., Matsushita, M., Yoshioka, H., Ohoyama, K., Izumi, F., "Diffusion Path of Oxide Ions in an Apatite-Type Ionic Conductor $La_{9.69}(Si_{5.70}Mg_{0.30})O_{26.24}$", *Chem. Mater.*, 20, (2008), pp5208-5208.

[2] Okudera, H , Yoshiasa, A , Masubuchic , Y . , Higuchi , M , Kikkawa , S . , " Temperature dependence of structural parameters in oxide-ion-conducting $Nd_{9.33}(SiO_4)_6O_2$: single crystal X-ray studies from 295 to 900K", *Journal of Solid State Chemistry*, 177, (2004), pp4451–4458

MS05-P40

Crystal structure and magnetic behaviors of novel lanthanide(III) carboxylate compounds

Hsiu-Mei Lin[1,2], Jen-Yun Wu[1], Pei-An Hsiung[2], Chi-Rung Lee [3], and I-Jui Hsu [4]

[1]*Institute of Bioscience and Biotechnology, National Taiwan Ocean University, Keelung, Taiwan 20224, R.O.C.*
[2]*Department of Life Science, National Taiwan Ocean University, Keelung, Taiwan 20224, R.O.C.*
[3]*Department of Chemical and Materials, Minghsin University of Science and Technology, Xinfeng Hsinchu 30401, Taiwan R.O.C.*
[4]*Department of Molecular Science and Engineering, National Taipei University of Technology, Taipei, Taiwan 10608, R.O.C.*
E-mail: hmlin@mail.ntou.edu.tw

The novel lanthanide complexes, $[Ln(\mu_1\text{-tzbc})(\mu_2\text{-tzbc})(OH)(H_2O)_4]_2$ (Ln = Nd, Eu, and Tb; tzbc = tetrazole benzylcarboxylate), have been synthesized under hydrothermal conditions. Based on the x-ray diffraction data, all of them are isostructures. In each isolated molecule complex, there is one inversion center inside the molecule, so that the asymmetric unit consists of one metal (Ln^{3+}) coordinated by four H_2O, one OH^-, and two tzbc ligands. One of the tzbc ligand is bonded to one metal ion as μ_1 mode, and the other is coordinated to two lanthanide ions by μ_2 bridging mode. The magnetic measurements of all the three complexes display quite interesting results due to the different $4f^n$ configurations. In Tb complex, the distance between two Tb ions is 5.109Å, and the $\chi_M T$ is *ca.* 23 $cm^3mol^{-1}K$ from 300K to 25K and then decreased to *ca.* 11.5 $cm^3mol^{-1}K$ as temperature decreased to 2K. However, in Nd complex, the distance between two Nd atoms is 5.062Å, and the $\chi_M T$ is *ca.* 3 $cm^3mol^{-1}K$ at 300K and this value is decreased to *ca.* 1.5 $cm^3mol^{-1}K$ as temperature down to 2K, which is close to one free ion contribution. Moreover, magnetic phenomenon displayed by the Eu complex indicates that the ground term is no longer as theoretical prediction of $^7F_0$. In addition, the interactions with DNA of these complexes will also be discussed in this presentation.

References

[1] Li Y., Zheng F.-K., Liu X., Zou W.-Q., Guo G.-C., Lu C.-Z., Huang J.-S. "Crystal Structure and Magnetic and Luminescent Properties of a Series of Homodinuclear Lanthanide Complexes wi th 4-Cyanobenzoic Ligand", *Inorganic Chemistry*, Vol. 45, No. 16, (2006), pp 6308–6316.

[2] Dalguebonne C., Kerbellec N., Guillou O., Bunzil J. C., Gumy F., Catala L., Mallah T., Audebra nd N., Gerault Y., Bernot K., Calvez G. "Structure and Luminescent Properties of Micro- ND Nanosized Particles of Lanthanide Terephthalate Coordination Polymers", *Inorganic Chemistry*, Vol. 47, No. 9, (2008), pp 3700–3708.

Structural and electronic properties of tetrahedral fullerenes and diamond-like fullerene crystals

Alexander Zhbanov[1,2], Yong-Gu Lee[1], Ching-Tarng Liang[2] and Yia-Chung Chang[2]

[1]*Department of Mechatronics, Gwangju Institute of Science and Technology, 1 Oryong-dong, Buk-gu, Gwangju 500-712, Republic of Korea*
[2]*Research Center for Applied Sciences, Academia Sinica, 128, Section 2, Academia Road, Nankang, Taipei 115, Taiwan*
E-mail: azhbanov@gist.ac.kr

For fullerenes of tetrahedral symmetry, systematization based on fullerene cage geometry is suggested. The technique is based on the description of the mutual arrangement of pentagons. The geometry of all possible tetrahedral fullerenes has been determined. The smallest tetrahedral fullerenes are shown in Fig.1. The initial geometrical characteristics of fullerenes have been calculated by Tersoff-Brenner model. The semiempirical tight-binding method was used for optimization of geometry and estimation of stability for insulated tetrahedral fullerenes. Structural, cohesive, elastic, and electronic properties are predicted as well as theoretical x-ray diffraction spectra for diamond-like fullerene crystals are derived.

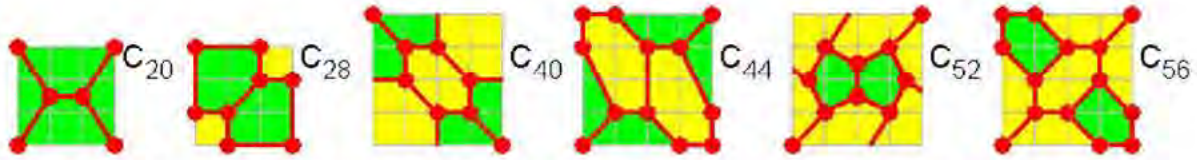

Fig. 1. Schematic projection of the first smallest tetrahedral fullerenes on to the cubic face

The electron levels for insulated fullerenes and electronic band structure for crystals are performed via first principles full potential linearized augmented plane-wave (LAPW) density functional theory, as implemented in the WIEN2k [1] code and a full-potential linearized augmented Slater-type orbital (LASTO) method, LASTO code [2]. The optimized lattices for several diamond-like fullerene crystals are shown in Fig.2.

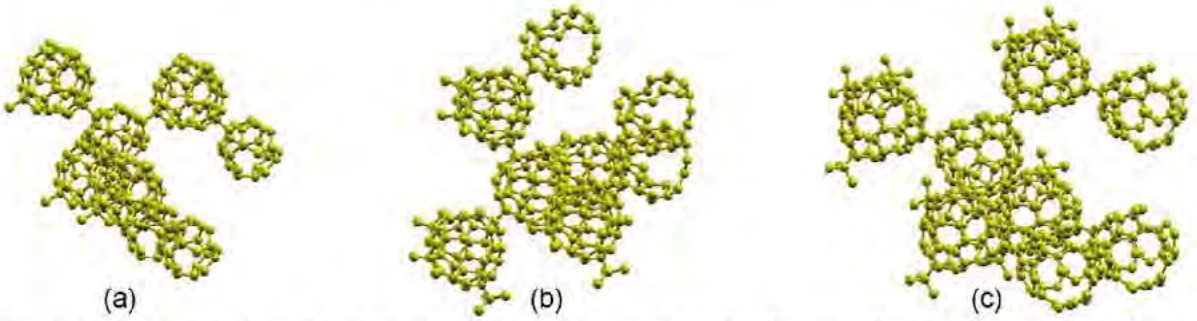

Fig. 2. Optimized lattices for diamond-like fullerene crystals: C_{28}+C_{40} (a), C_{44}+C_{44} (b), and C_{56}+C_{56} (c) hyperdiamond.

References

[1] Blaha P., Schwarz K., Madsen G.K.H., Kvasnicka D. and Luitz J., "*WIEN2k, An Augmented Plane Wave Plus Local Orbitals Program for Calculating Crystal Properties*", Vienna university of Technology, (2001)

[2] Chang Y.-C., James R.B. and J. W. Davenport J.W., "Symmetrized-basis LASTO calculations of defects in CdTe and ZnTe", *Physical Review B*, Vol. 73, (2006), 035211, 11 pp.

Crystal structures of bipyridine-copper(II) complexes as anticancer agents

A.Kaewthong [1], M..Sukwattanasinitt [2], N. Muangsin[1]

[1]*Research Centre for Bioorganic Chemistry, Department of Chemistry, Faculty of Science, Chulalongkorn University, Bangkok, 10330, Thailand.*
[2]*Organic Synthesis Research Unit, Department of Chemistry, Faculty of Science, Chulalongkorn University, Bangkok, 10330, Thailand*
E-mail: AWAT_GOLF@HOTMAIL.COM

In the present, cancer is the leading cause of death. Platinum and transition metal coordination complexes, for example cisplatin are an effective anticancer drug, but it has side effects and easily excreted from the body. Therefore, bipyridine (bpy) transition complexes have been developed as potential antitumor agents. In this work, a series of bpy–copper(II) complexes have been dev eloped and their cytotoxic activities have been assessed as new anticancer agents. However, their c ytotoxic mechanisms are still unclear. To investigate their possible mechanisms, the DNA binding affinity by UV-titration and fluorescence spectroscopy, thermal denaturation (TM) analysis and X-ray crystallography were determined. The preliminary results showed that the copper complexes beari ng one bpy unit have the most potential cytotoxic activity. They may be further developed as new anticancer agents, however, more compounds have to be performed. Our groups have still investigated for more derivatives and studied on other possible mechanisms.

References

[1]. Karanadh, P.; Leech, D. "Improved synthesis of 4,4`-diamino-2,2`-bipyridine from 4,4`-dinitr2,2`-bipyridine-N,N'-dioxide", *Tetrahedron Letters* , 45, (2004), pp 121-123.
[2]. Lo,Y.C.; Ko,T.P.; Su,W.C.; Su,T.L.; Wang, A.H.J. "Terpyridine–platinum(II) complexes are effective inhibitors of mammalian topoisomerases and human thioredoxin reductase 1", *J.Inorg.Biochem*, 103, (2009), pp 1082-1092.

Cu $(L_1)_n (L_2)_m$

Where L_1 = 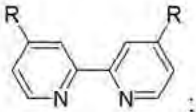

; R=H, NH_2

L_2 = Cl^-, SO_4^{2-} or OAc^-

n, m = integral number;

n = 0, 1 or 2

m = 4-n or 6-n

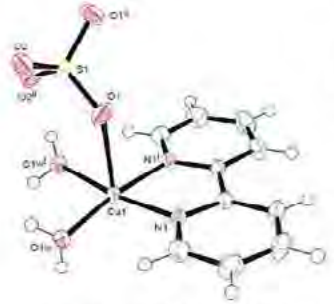

$[Cu(bpy)(H_2O)_2]SO_4$

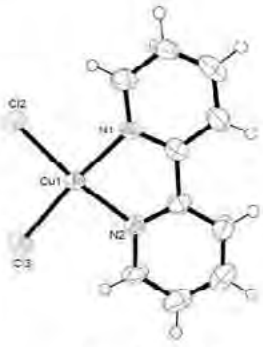

$[Cu(bpy)Cl_2$

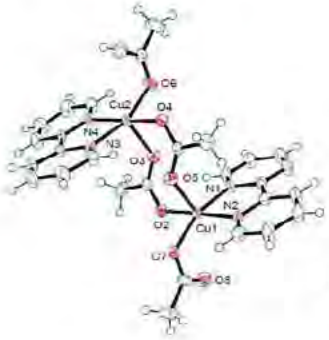

$Cu(bpy)(OAc)_2$

MS05-P43

Visualisation and characterisation of voids in molecular crystals

Mark A. Spackman[1], Michael J. Turner[1], Joshua J. McKinnon[1] and Dylan Jayatilaka[1]

[1]*School of Biomedical, Biomolecular and Chemical Sciences, University of Western Australia, Perth, Australia*
E-mail: mark.spackman@uwa.edu.au

We are undertaking further software development with *CrystalExplorer* [1] to characterize and visualize voids in molecular crystals, with the aim of eventually mapping properties such as the electrostatic potential and electric field on the surfaces and inside the voids. As a first step we have recently implemented a novel approach to mapping voids based on isosurfaces of the procrystal electron density (the sum of spherical atoms, or the crystallographer's usual independent atom model). This is a very simple - and much more realistic - alternative to conventional approaches that represent atoms and probe molecules as hard spheres with van der Waals radii. It can be used successfully to locate and visualise void space in crystalline materials, as well as readily compute surface areas and volumes of the voids. The method is quite general, computationally rapid, and capable of locating and characterising all "empty" space in molecular crystals, not just the larger cavities and channels.
Figure 1 illustrates examples of void surfaces for three metal-organic frameworks (MOFs). For HKUST-1 [2] (sometimes referred to as Cu-BTC), the 0.0003 au isosurface of the procrystal electron density yields a surface area of 2606 $m^2 g^{-1}$ and a pore volume of 0.53 $cm^3 g^{-1}$, values that compare favourably with recent experimental estimates from N_2 adsorption isotherms (surface areas of 2175 $m^2 g^{-1}$ (Langmuir) and 1507 $m^2 g^{-1}$ (BET) and a pore volume of 0.75 $cm^3 g^{-1}$ [3].

To date we have applied this approach to the visualisation and quantitative characterisation of voids in crystals of hydrophobic dipeptides, MOFs, covalent organic frameworks (COFs), zeolites, electrides, and in investigating the effect of pressure on molecular crystals. The focus in these applications is on a comparison with existing computational methods, as well as with the results from various experimental techniques that provide independent estimates of volumes and surface areas of void space and porosity. The presentation will summarize these results, and highlight how this simple electron density function can be used to advantage to explore cavities, cages and channels in crystalline materials.

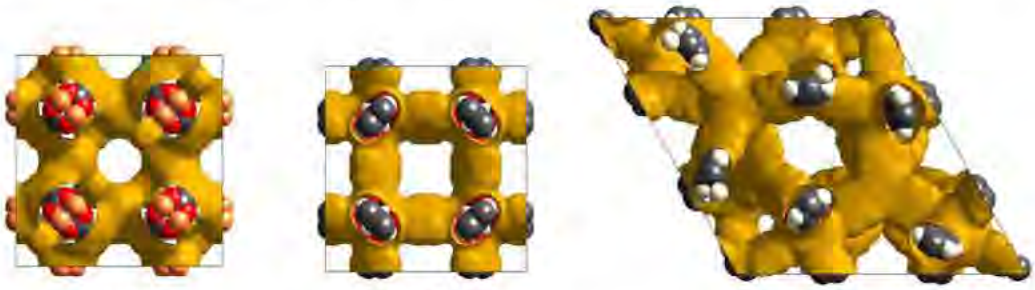

Figure 1. Void surfaces (isosurfaces of the procrystal electron density at 0.0003 au) for three MOFs.

References

[1] S. K. Wolff, D. J. Grimwood, J. J. McKinnon, M.J. Turner, D. Jayatilaka, M. A. Spackman, CrystalExplorer 2.2, (2010) University of Western Australia (http://hirshfeldsurface.net/CrystalExplorer).
[2] S.S.-Y. Chui, S.M.-F. Lo, J.P.H. Charmant, A.G. Orpen and I.D. Williams, Science, 1999, 283, 1148-1150.
[3] J.L.C. Rowsell and O.M. Yaghi, J. Am. Chem. Soc., 2006, 128, 1304-1315.

The position determination of H/D in the protonated and deuterated LaFeAsO1-yHx

Junrong Zhang[1], Chul-Ho Lee[2], Shuki Torii[1], Masao Yonemura[1], Toru Ishigaki[3], Teguh Panca Putra[1], Ping Miao[1], Takashi Muroya[1], Ryoko Tomiyasu[1], Takashi Kamiyama[1]

[1]*Institute of Materials Structure Science, High Energy Accelerator Research Organization, 203-1 Shirakata, Tokai, Ibaraki 319-1106, Japan*
[2]*National Institute of Advanced Industrial Science and Technology, Central 2, 1-1-1 Umezono, Tsukuba, Ibaraki 305-8568, Japan*
[3]*Ibaraki University, Ibaraki Quantum Beam Research Center, Shirakata 162-1, Tokai, Ibaraki 319-1106, Japan*
E-mail: jrzhang@post.kek.jp

A family of protonated and deuterated FeAs-based superconductors[1] (LaFeAsO1-yH/Dx) was studied. The magnetization and resistivity measurements exhibit a very large enhancement of superconducting transition temperature (Tc ~ 35 K) by H/D-doping, while the maximum Tc of an oxygen-deficient compound is 28 K[2]. We suppose that H doping might lead to the structural changes and suppress antiferromagnetic order. So the key point is the position of hydrogen atoms.

Neutron scattering has been carried out at neutron powder diffractometer SuperHRPD @J-PARC, which has the world highest resolution of $\Delta d/d = 0.03\%$. Rietveld refinement (by Z-Rietveld) and Maximum Entropy Method (by Z-MEM) are utilized to perform the structure solution and determine the position of H. The results show that the occupancy of H/D is far lower than the nominal content. By the analysis of the difference of H- and D-doped data, Hydrogen is supposed to be located at 2c-site and bonded to oxygen. The bond length is 0.9802 A.

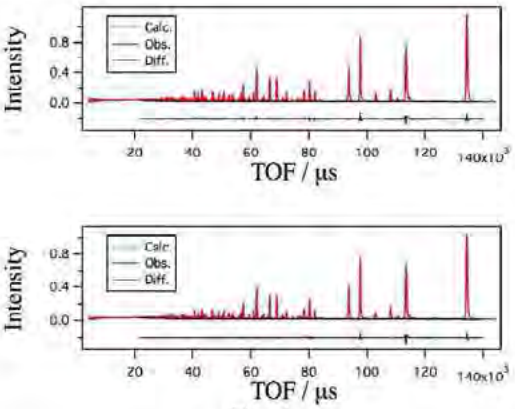

Fig. 1

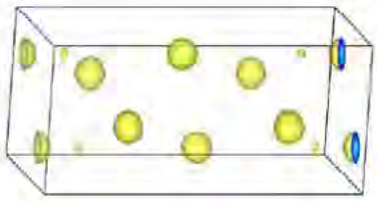

Fig.2

Fig. 1 upper: Observed and calculated neutron scattering patterns of LaFeO0.55H0.55, lower: Observed and calculated neutron scattering patterns of LaFeO0.55D0.55.
Fig.2 The 3D plot of nuclear density distribution of LaFeO0.55H/D0.55 from MEM analysis.

References

[1] Y. Kamihara, T. Watanabe, M. Hirano, and H. Hosono, J. Am. Chem. Soc. 130, 3296 (2008).
[2] Chul-Ho Lee, A. Iyo, H. Eisaki et.al, J. Phys. Soc. Jpn. 77, 083704 (2008).

High-temperature single-crystal X-ray diffraction study on the decarbonation of $FeCO_3$

J. Wang [1], T. Sakakura [1], N. Ishizawa [1] and H. Eba [2]

[1]*Department of Frontier materials, graduate School of Engineering, Nagoya Institute of Technology, Tajimi 507-0071, Japan*
[2]*Department of Chemistry and Energy Engineering, Tokyo City University, Tokyo 158-8557, Japan*
E-mail: wang_jun@crl.nitech.ac.jp

Siderite ($FeCO_3$) is commonly found in hydrothermal veins, and considered as potential CO_2 mineral trapping. A use of Fe/CO_2 fuel cells for CO_2 mitigation has been examined. [1] The decarbonation of the $FeCO_3$ product is important in a view point of carbon monoxide retrieval as a carbon resource. The present study was undertaken to unveil the evolution of siderite structure associated with the decarbonation. Single-crystals of $FeCO_3$ were grown by the hydrothermal method. Diffraction data at various temperatures were taken with the Smart Apex II single-crystal X-ray diffractometer. An interesting behavior was observed for the changes in unit cell dimensions as a function of time. Immediately after raising the crystal temperature, the *a*-length in the hexagonal setting of the rhombohedral cell expanded superfluously, and then shrank gradually towards an equilibrium point as a function of time. No such time dependency was observed for the changes in *c*-length. The time necessary for a complete relaxation of cell dimensions depended on the heat program, while it took typically 3 days when the sample was heated rapidly from the room temperature to 250 °C. The structural change which occurs during the relaxation period was investigated by the single-crystal diffraction data collected every 6 hours, as will be discussed in the presentation. Above *circa* 300 °C, crystals of $FeCO_3$ commenced decomposition into iron oxides: one iron oxide was identified as hematite (α-Fe_2O_3) while the another was presumably maghemaite (γ-Fe_2O_3) or magnetite (Fe_3O_4). The topotaxial orientation relationships of the iron oxides with respect to $FeCO_3$ were studied from various reciprocal sections reconstructed from the frame data.

Reference

[1] Rau, G. H., "Possible use of Fe/CO_2 fuel cells for CO_2 mitigation plus H_2 and electricity prod uction", *Energy Conversion and Management* **45** (2004), pp 2143–2152.

MS05-P46

Model complexes of the active center in nitrite reductase

Yasushi Kai[1], Kazue Ohmi[1], Haruka Teranishi[1], Tsuyoshi Inoue[2], Sinnichiro Suzuki[3], Akiko Minami[3] and Kazuya Yamaguchi[3]

[1]*Department of Environmental and Biological Chemistry, Fukui University of Technology, Fukui 910-8505, Japan*
[2]*Department of Applied Chemistry, Graduate School of Engineering, Osaka University, Osaka 565-0871, Japan*
[3]*Department of Chemistry, Graduate School of Science, Osaka University, Osaka 560-0043, Japan*
E-mail: kai@fukui-ut.ac.jp

To get some structural information about the active center of nitrite reductase, a series of model complexes have been synthesized. In the enzyme[1], two types of copper active centers are included. Among which, type 2 copper is considered to act as the metal center of the reduction of nitrite ion (NO_2^-) to nitric oxide (NO). The type 2 copper is coordinated by three histidine residues and a water. To mimic the active center of nitrite reductase, a series of complexes containing a tridentate aromatic amine compound [bis(2-pyridylmethyl)amine, bpa] in the absence and presence of nitrite ion have been synthesized. The nitrite ion reduction activities of a series of complexes were measured and compared with those molecular structures determined by X-ray diffraction method. By the introduction of heavy substituent in Y, the stereo of N atom becomes rigid. The molecular structure of CubpaEtNO_2 (X=H, Y=Et) reflects a typical structure in this series of complexes (Fig.1).

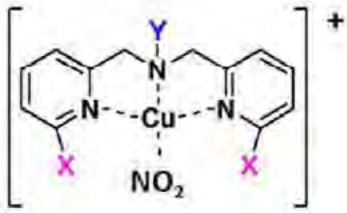

Cubpa Complexes

The copper atom is hexa co-ordinated with three N atoms from bpa ligand, two O atoms from nitrite ion, and an O atom from perchlorate ion. The substituent of N2 and O2 of nitrite ion locate on the same side of nearly planar bpa ligand and opposite from the perchlorate ion.

The coordination modes of two O atoms in nitrite ion are quite different. The bond distance of Cu-O1 is 1.985(1)Å and that of Cu-O2 is 2.521(1)Å. On the other hand, the bond distance of N4-O1 is 1.298(2) Å and that of N4-O2 is 1.230(2) Å. Therefore, the coordination scheme of nitrite ion to copper atom is drawn as the one shown below.

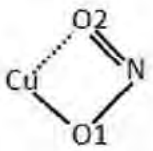

The molecular structures of this series of complexes will be compared and discussed from the viewpoints of reduction activity and chemical properties.

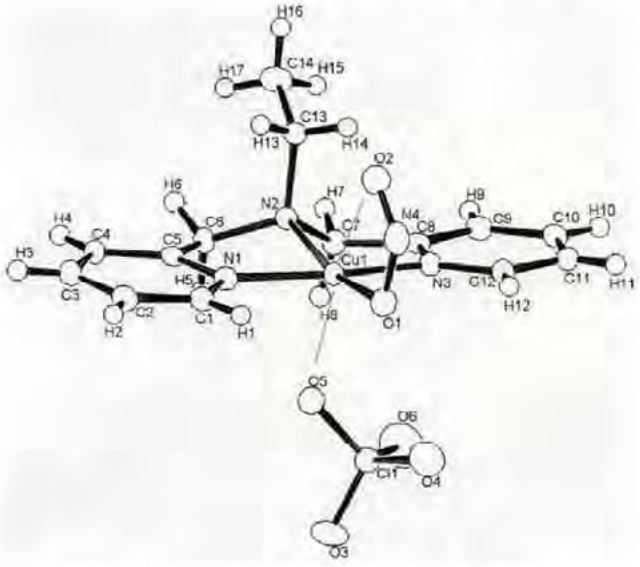

Fig. 1 Molecular Structure of CubpaEtNO_2

References

[1] Masaki Nojiri, Yong Xie, Tsuyoshi Inoue, Takahiko Yamamoto, Hiroyoshi Matsumura, Kunishige Kataoka, Deligeer, Kazuya Yamaguchi, Yasushi Kai, and Shinnichiro Suzuki, "Structure and function of a hexameric copper-containing nitrite reductase.", *Proc. Natl. Acad. Sci. USA*, 104, 4315-4320 (2007)

New pentanary thiophosphates, $A_x(Ta_{1-y}Ti_y)PS_5$ (A =K, Rb, Cs): A systematic approach toward new mixed-metallic phases

Kyoung-hee Kim, Jae-min Yu and Hoseop Yun

Division of Energy Systems Research and Department of Chemistry, Ajou University, Suwon 443-749, Korea
E-mail: hsyun@ajou.ac.kr

New mixed-metallic thiophosphates, $K_{0.47}Ta_{1-x}Ti_xPS_5$(x=0.46), $Rb_{0.5}Ta_{1-x}Ti_xPS_5$(x=0.56), and $Cs_{0.69}$ $Ta_{1-x}Ti_xPS_5$(x=0.59) have been synthesized with the reactive halide fluxes and structurally characterized by single-crystal X-ray diffraction techniques. The structure of $A_xTa_{1-y}Ti_yPS_5$ is built up from the dimeric $[M_2S_{10}]$ units composed of edge-sharing $[MS_6]$ (M=Ta or Ti) octahedra. These units are linked by sharing common edges with four tetrahedral $[PS_4]$ groups yielding a two-dimensional layer. These layers are stacked on top of each other to create van der Waals gaps and the alkali metal ions reside in this space. Electrons are transferred from the alkali metals to the mixed Ta/Ti atoms and the stoichiometry of the phases can be controlled systematically with the use of the difference of electropositivities and sizes of each alkali metal. Eventually the amount of alkali metals restricts the composition of the metals. In this presentation, the relationship between the Ta^{5+}/Ti^{4+} ratios and the stoichiometry of alkali metals will be discussed as will the chemistry of the related thiophosphates. The title compounds exhibit absorption band gaps of 1.7eV~1.8eV and these phases can be classified as semiconductors.

References

[1] Gutzmann A., Näther C. and Bensch W., Z. Anorg. Allg. Chem. 2005, 631, 524-529

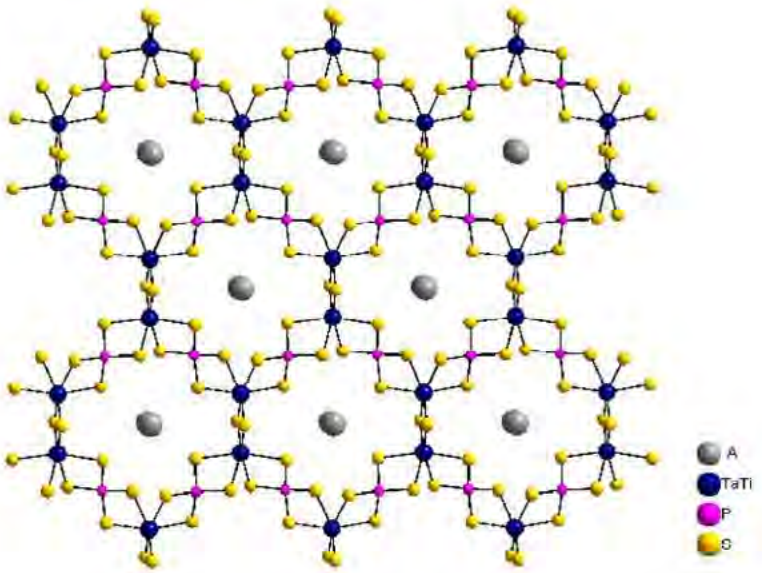

Gradual intermetallic bond formation controlled by alkali metals in quinternary metal thiophosphates, $A_y(Ta_xM_{1-x})PS_6$ (A=K,Rb; M= Ti, Zr)

Sojeong Park, Eunsil Lee, Hoseop Yun

Department of Energy Systems Research and Department of Chemistry, Ajou University, Suwon 443-749, Korea
E-mail: hsyun@ajou.ac.kr

The new quinternary metal thiophosphates, $A_y(Ta_xM_{1-x})PS_6$ (A=K, Rb; M=Ti, Zr) have been synthesized with the use of reactive alkali metal halide fluxes and structurally characterized by single crystal X-ray techniques. The structure of the title compounds are closely related to that of the previously reported $TaPS_6$[1], which serves as a host structure in the title compounds. The host structure is composed of intertwined right- and left-handed helices and the framework has empty channels, where alkali metal cations reside. The electronic structure calculations of the framework indicate that the low-lying electron acceptor level should be the empty d orbitals of the transition metals. When the guest ions are inserted to the empty channels, the electrons released by alkali metals are transferred to the metal sites. As a result, the intermetallic bond start to form and the bond strength can be controlled gradually by the amount of alkali metals and the characteristics of each constituent metal ion. In this presentation synthetic efforts using various alkali metals for new mixed-metallic phases as well as the relationship between the amount of alkali metal ions and the intermetallic bond strength will be discussed.

References

[1] Fiechter, S.; Kuhs, W.F.; Nitsche, R. Acta Crystallogr. 1980, *B36*, 2217

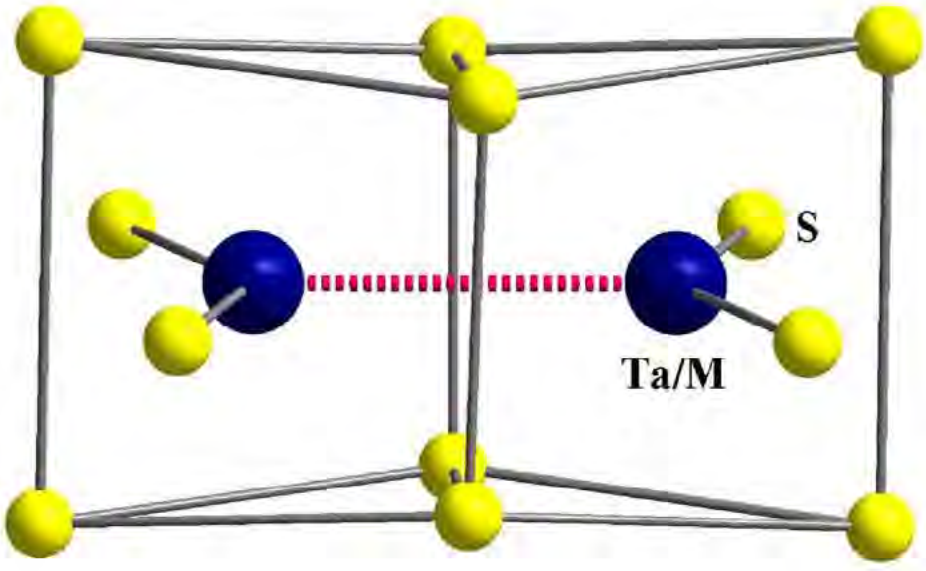

MS05-P49

Effect of 3*d* transition metal substitution on crystal structure in LaO*M*As (*M* = Mn, Fe, Ni, Zn) by high-energy synchrotron radiation powder diffraction

Shozo Hiramoto[1], Satoshi Yasuda[1], Chikako Moriyoshi[1], Fumiko Yoshida[1], Yoshihiro Kuroiwa[1], and Koichi Takase[2]

[1]*Department of Physical Science, Hiroshima University, Kagamiyama, Higashi-Hiroshima, Hiroshima 739 -8526, Japan*
[2]*Department of Physics, College of Science and Technology, Nihon University, Kanda-Surugadai, Chiyoda-ku, Tokyo 101-8301, Japan*
E-mail: s-hiramoto@hiroshima-u.ac.jp

Lanthanide oxyarsenide LaOMAs, where M is 3d transition metal ion, has recently attracted much attention since superconductivity of F-doped LaOFeAs was discovered. The LaOMAs compounds have a layered structure with the space group of $P4/nmm$ (tetragonal). The M-As layer alternates with the O-La layer along the c-axis. In the M-As layer, each M is surrounded by As atoms, which form edge-shared tetrahedra around the M sites. Similarly the La atoms form tetrahedron around the O atom in the O-La layer. The electric properties of the LaOMAs system depend on M: for example, metallic for M = Fe and Ni, and semiconducting for M = Mn and Zn. To investigate the origin of such a difference from the crystal structure, the electron charge density analysis is useful because it helps us to understand chemical bonding nature in crystal. In this study, we derive the crystal structures of LaOMAs (M = Mn, Fe, Ni, and Zn) at the charge density levels to discuss the difference in the electronic properties.

The high-energy synchrotron radiation powder diffraction experiment was performed using a large Debye-Scherrer camera with an imaging plate installed at BL02B2 in SPring-8. The wavelength used was λ = 0.5 Å (E = 25 keV). The diffraction patterns were obtained at 300 K. The structure parameters and electron charge density distributions were derived using the maximum entropy method (MEM)/ Rietveld method.

No significant structural difference was found in the La-O layer. In the M-As layer, on the other hand, clear differences were observed. The tetrahedra composed by M and As in the metallic compounds are compressed along the c-axis, whereas those in the semiconducting ones are slightly elongated along the c-axis. It was revealed that the chemical bonding between M and As is more covalent in the metallic compounds than in the semiconducting compounds. These results are consistent with the experimental fact that the conducting nature is more apparent in the Fe-As or Ni-As layer. It is presumed that 3d electrons are localized and produce ionic chemical bonding in the semiconducting compounds.

Triplet biradical states of dibromo and dichloro mononuclear polypyridine iridium(III) complexes

Naokazu Yoshikawa[1], Shinichi Yamabe[2], Nobuko Kanehisa[3], Tsuyoshi Inoue[4], Hiroshi Takashima[1] and Keiichi Tsukahara[1]

[1]*Department of Chemistry, Nara Women's University;* [2] *Department of Chemistry, Nara University of Education;* [3]*Division of Electrical, Electronic and Information Engineering, Osaka University;* [4]*Department of Applied Chemistry, Graduate School of Engineering, Osaka University*
E-mail: naokazuu@dream.com

Emission and electronic properties of eight Ir^{3+} centered polypyridine complexes were studied systematically. A crystal structure of $[IrBr_2(phen)_2]PF_6$ was obtained by the X-ray diffraction study, where phen is 1,10-phenanthroline. The computed geometry is in good agreement with the experimental one. Those in the triplet biradical states were also determined computationally to investigate the source of emission spectra. Two geometric isomers of $[IrX_2(bpy)_2]^+$ and $[IrX_2(phen)_2]^+$ (Fig 1) and the isomerization transition states were obtained with X = Cl and Br. For the dichloro complexes, triplet-biradical isomers have nonequivalent bpy and phen ligands through the Jahn-Teller geometric distortion. It is suggested that strong emission arises from the asymmetric spin density distributions.

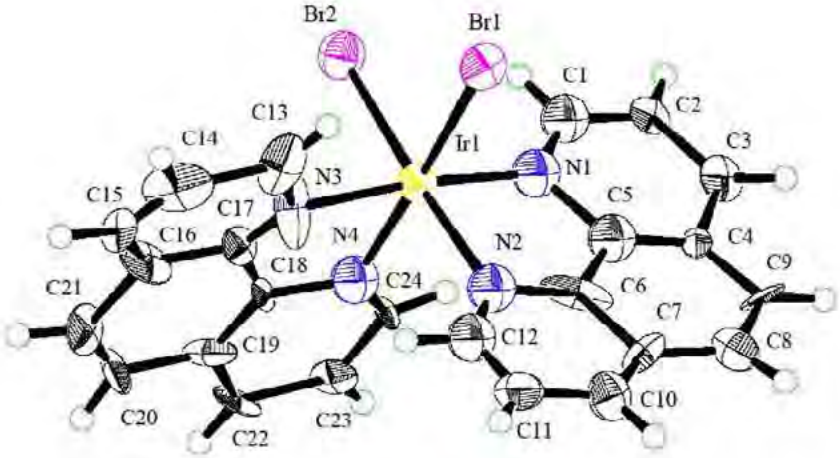

Fig 1

References

[1] Terki R., Simoneau L. -P. and Rochefort A., "Tailoring the Photoluminescence Properties of Io nic Iridium Complexes", *J. Phys. Chem. A*, Vol. 113, No. 3, (2009), pp 534-541.

MS05-P51

Phase transitions of tetraalkylammonium salts of decavanadates containing 1,4-dioxane molecules

Tatsuhiro Kojima[1], and Tomoji Ozeki[1]

[1]*Department of Chemistry, and Department of Chemistry & Materials Science, Tokyo Institute of Technology, O-okayama, Meguro-ku, Tokyo152-8551, Japan*
E-mail: tkojima@chem.titech.ac.jp

Phase transitions is closely related with the intermolecular interactions in the crystalline state. Long alkyl chains adopt various conformations and packed so as to achieve closest packing in the crystals. Unlike functional groups, they show relatively weak interactions with surrounding molecules. Therefore, when a crystal containing long alkyl chains is cooled, conformation of some of the chains may change. In order to reveal the relationship between phase transition and intermolecular interaction in the crystal structure, we investigated the detail of phase transition of the crystals which contain decavanadate and tetraalkylammonium cation. Herein we report the three crystals which show phase transition depending on the temperature, [(C5H11)4N]2[H4V10O28](C4H8O2)3 (1), [(C6H13)4N]2[H4V10O28](C4H8O2)4 (2), and [(C7H15)4N]2[H4V10O28](C4H8O2)8 (3).

These three crystals were obtained by recrystallization of [(C5H11)4N]3[H3V10O28], [(C6H13)4N]3[H3V10O28], [(C7H15)4N]3[H3V10O28] from the mixed solvents of 1,4-dioxane and water. All the crystals contain the tetraprotonated decavanadate that donate hydrogen bonds to four 1,4-dioxane molecules. When cooled from 293K to 123K, (1) and (2) showed phase transition from monoclinic P21/n, 11.1341(2)/ 20.6109 (3)/ 17.9373 (4)/ 90/ 105.9920(7)/ 90, Volume 3957.0 to monoclinic P21/c, 18.1891 (2)/ 20.5002 (2)/ 22.0170 (3)/ 90/ 112.0153 (5)/ 90, Volume 7611.1 and from tetragonal I41/a, 38.8749(12)/ 38.8749(12)/ 12.4443(9)/ Volume 18806.5, to monoclinic C2/c 53.8043(8)/ 12.3166(2)/ 36.8334(8)/ 90/ 133.093(2)/ 90 / Volume 17824.5, respectively. On the other hand, (3) showed unique behavior. When cooled rapidly it did not show phase transition, but when cooled slowly it showed phase transition from monoclinic P21/c, 16.6577(2)/ 19.2730(2)/ 18.9407(2)/ 90/ 92.227(10)/ 90, Volume 6076.2 to monoclinic Cc, 32.3738(3)/ 38.2015(4)/ 18.8169(2)/ 90/ 91.6169(10)/ 90, Volume 23262.1. Single crystal X-ray structure determinations of (1) and (2) revealed that the change between the structure of the room temperature phase and that of the low temperature phase was associated only with the conformational change of methyl- or ethyl-group. On the other hand, the structural change in the crystal of (3) was relatively large. The buthyl-group changed its conformation and swapped its position with a 1,4-dioxane molecule, which does not have any hydrogen bond. The mobility of the swapped 1,4-dioxane can be also evidenced by the fact that the crystal of (3) is unstable in the air at room temperature. Therefore, the flexibility of tetrahepthyl ammonium cation and the mobility of 1,4-dioxane seem to facilitate the phase transition.

Two silver(I) complex structure in a single crystallization: flexible metallacyclodimer vs helical channel network

Chi Won Kim[1], Eun Ji Kim[1] and Ok-Sang Jung[1]

[1]*Department of Chemistry, College of Natural Sciences, Pusan National University, Pusan 609-735, Korea*
E-mail: kimchiwon@pusan.ac.kr

Studies on the self-assembly of $AgClO_4$ with 1,2-bis(dimethyl(4-pyridyl)silyl)ethane (L) were carried out. The slow diffusion of an organic solution of L into an aqueous solution of $AgClO_4$ affords two different single crystalline solids, block and thin plate crystals. The block crystal consists of metallacyclodimers of the composition $[Ag(L)]_2(ClO_4)_2$ whereas the thin plate crystal consists of unique ligand-induced helical channel networks of $[Ag_2(L)_3](ClO_4)$. The block and thin plate crystals form in a ratio of 1 : 9, respectively, in a mixture of water and ethanol, but the ratio is depending on solvents and concentrations. Furthermore, the block crystals have two significantly different metallacyclodimers in a unit cell, presumably owing to the flexible 26-membered cyclodimer including flexible a transannular argentophilic interaction. Such subtle effects may be ascribed to the existence of a variety of eclipsed, gauche, or anti- conformations of L.

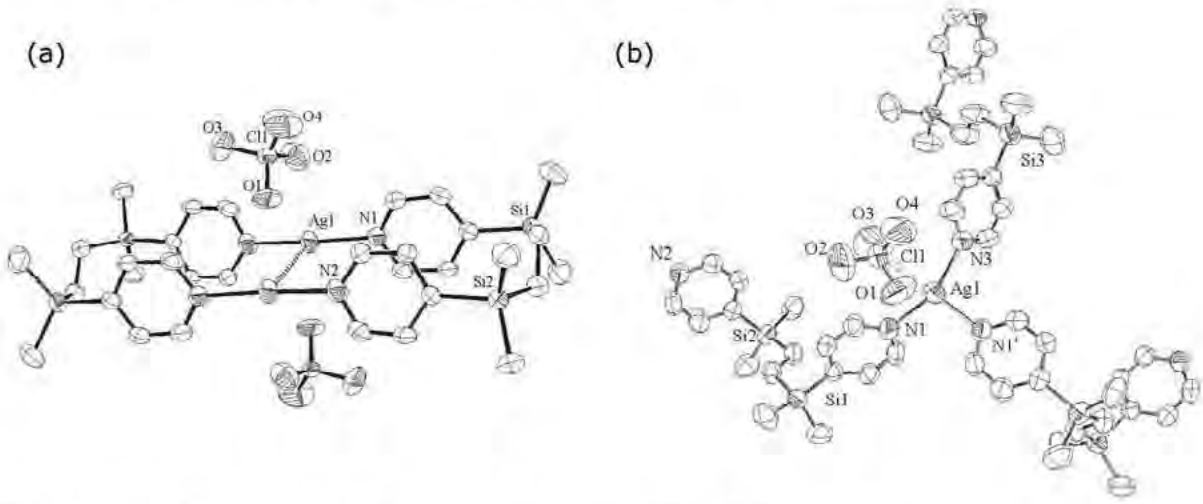

Figure 1. Crystal structures of (a) metallacyclodimer and (b) helical channel network

References

[1] Batten S.R., Robson R., *Angew. Chem., Int. Ed.* Vol. 37, (1998), pp 1460-1494.
[2] Steel P.J., *Acc. Chem. Res.* Vol. 38, No. 4, (2005), pp 243-250.
[3] Mahmoudkhani A.H., Shimizu G.K.H., *Inorg. Chem.* Vol. 46, No. 5, (2007), 1593-1602.

MS05-P53

Fine competition and control among argentophilic, electrostatic, and π···π interactions in a molecular chair

Jungmin Ahn, Ok-Sang Jung

Department of Chemistry, College of Natural Sciences, Pusan National University, Busan , Korea
E-mail: jamtyzz@pusan.ac.kr

The reaction of AgX (X^- = $NO3^-$, $ClO4^-$, and $CF3SO3^-$) with 1,3-bis(3-pyridyl)tetramethyldisiloxane (L) at room temperature affords 20-membered metallacyclodimers, [Ag(L)]2(X)2. For the macrocyclodimer, fine competition among argentophilic, electrostatic, and π···π interaction exists. The macrocyclodimer is a unique molecular chair that tunes a transannular argentophilic interaction via the bite size of counteranions. In order to reversibly control the argentophilic interaction, anion exchange has been accomplished. The anion exchangeability is depending on the water-solubility rather than the electrostatic interaction between silver(I) and anions.

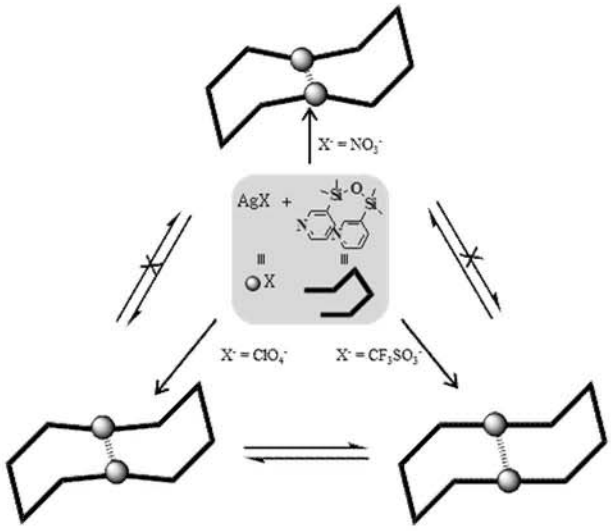

Microwave-assisted preparation of an europium complex: $[Eu(NO_3)_2(H_2O)_3(L)_2]\cdot(NO_3)(H_2O)$ {L=2-(4-pyridylium)ethanesulfonate, $(4\text{-pyH})^+–CH_2CH_2–SO_3^-$}

Zhen Nu Zheng and Soon W. Lee

Department of Chemistry (BK21), Sungkyunkwan University, Natural Science Campus, Suwon 440-746, Korea
E-mail: zhennv@skku.edu

A novel europium complex, $[Eu(NO_3)_2(H_2O)_3(L)_2]\cdot(NO_3)(H_2O)$ {L = 2-(4-pyridylium)ethanesulfonate, $(4\text{-pyH})^+–CH_2CH_2–SO_3^-$}, was prepared from europium nitrate pentahydrate and ligand L in H_2O under microwave heating conditions. In this complex, the europium metal is coordinated to nine oxygen atoms. The pyridyl nitrogen is protonated in such a way that the coordinated ligand has an NH^+ (4-pyridyl) positive end and an SO_3^- negative end; that is, the ligand L is a zwitter ion. In the following figures, the left one is a molecular structure, in which the atoms with the suffix "A" are generated by the crystallographic inversion operation. The right one is a packing diagram, in which dotted lines indicate hydrogen bonds.

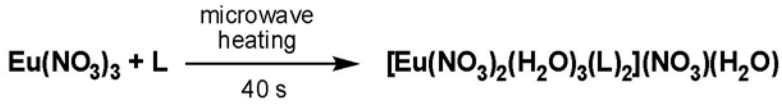

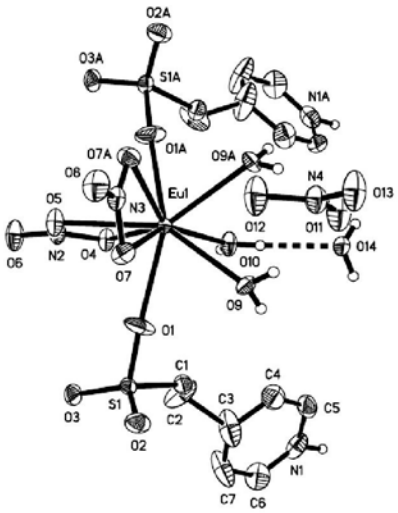

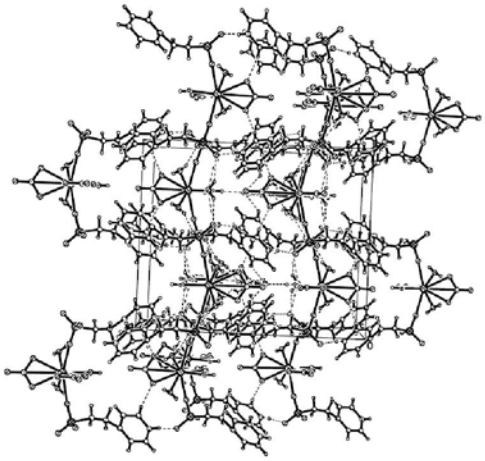

References

[1] Zhang J., Li Z., Wen Y., Kang Y., Cheng J. and Yao Y., "Syntheses and structure of two novel Ag(I) complexes: [μ_3-2-(4-pyridyl)ethanesulfonato-*N*,*O*,*O*']-aqua-silver(I) and melamine-[2-(4-pyridyl)ethanesulfonato-*N*]-silver(I)", *J. Mol. Struct.*, 697, (2004), 185–189.

[2] Cahill C. L., de Lill D. T. and Frisch M., "Homo- and heterometallic coordination polymers from the f element", *CrystEngComm*, 9, (2007), 15–26.

A terbium dimer bridged by (imidazol)benzoic acid: $[Tb(NO_3)_3(OMe)(ibaH)]_2$[iba = 4-(1H-imidazol-1-yl)benzoic acid]

Yeong-MinJung and Soon W. Lee

Department of Chemistry (BK21), Sungkyunkwan University, Natural Science Campus, Suwon 440-746, Korea
E-mail: upym@nate.com

A novelbridged terbium dimer was prepared from terbium nitrate pentahydrate ($Tb(NO_3)_3{\cdot}5H_2O$) and 4-(1*H*-imidazol-1-yl)benzoic acid under solvothermal conditions. In the title complex,two 9-coordinate Tb metals are linked by the (imidazol)benzoate ligand, in which the imidazol nitrogen is protonated. The Tb metal is coordinated to nine O atoms from three η^2-NO_3^-,one OMe^-, and two protonatedbis(monodentate) (imidazol)benzoic acid ligands to form a distorted tricappedtrigonal prismatic core. The N2–H and O2–H protons in the ligand participate in intermolecular hydrogen bonds. This terbium compound will be further studied for so-called "postsynthetic modification"to prepare novel compounds including 3*d*–4*f* coordination polymers [1,2].

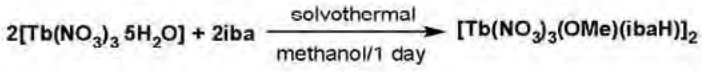

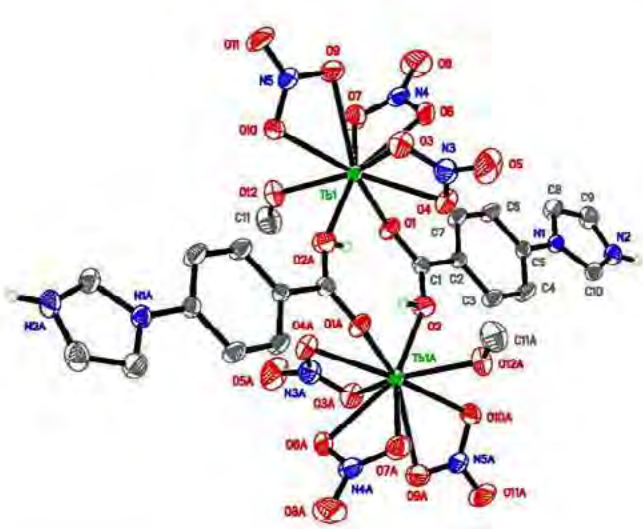

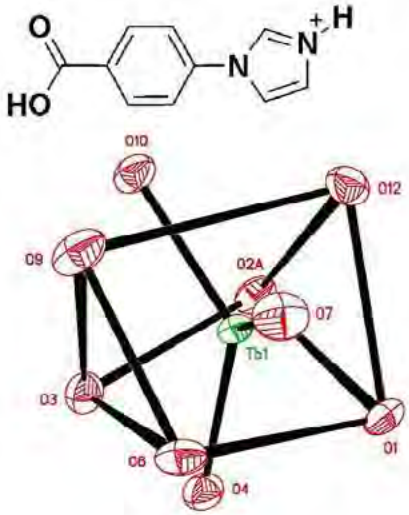

References

[1] Wang Z. and Cohen S. M., "Postsynthetic modification of metal–organic frameworks", *Chem. Soc. Rev.*, 38, 5, (2009), 1315–1329.

[2] Gadzikwa T., Farha O. K., Mulfort K. L., Hupp J. T., Nguyen S. T., "A Zn-based, pillared paddlewheel MOF containing free carboxylic acids via covalent post-synthesis elaboration",*Chem. Commun.*, 25, (2009), 3720–3722.

MS05-P56

Crystal and molecular structure of 5-bromo-1H-indole-2,3-dione

S.Shylaja [a]. K.B.R.Varma [a] T.Narasimhamurthy [a] Vasu [b]

[a] *Materials Research centre, IISc., Bangalore560012, India*
[b] *Vivekananda Degree College, Malleshwaram west Bangalore-560055, India*
E-mail: tate_rao@mrc.iisc.ernet.in

Indole derivatives have been found to exhibit antibacterial and antifungal and antitumor activities. Halogenated indole derivatives exhibit marked antimicrobial activities. Some of the indole alkaloids extracted from plants possess interesting cytotoxic, antitumor or antiparasitic properties.

The indole ring is planar, with maximum deviation for C_1 0.041(2)Å . The N-C distances are not equal due to conjugation in the ring system. The oxygen atoms O_1 deviated from the indole ring by 0.421(2)Å. The Phenyl ring is coplanar with the indole ring. The crystal structure is stabilized by weak C-H…O interactions running along crystallographic *c*-axis generating a chain described by $C_2^2(6)$. In additions to this, a short inter-molecular contact is observed between atom O_2 and symmetry related atom N_1 at x, y +1, z. Interesting results will be discussed at the conference.

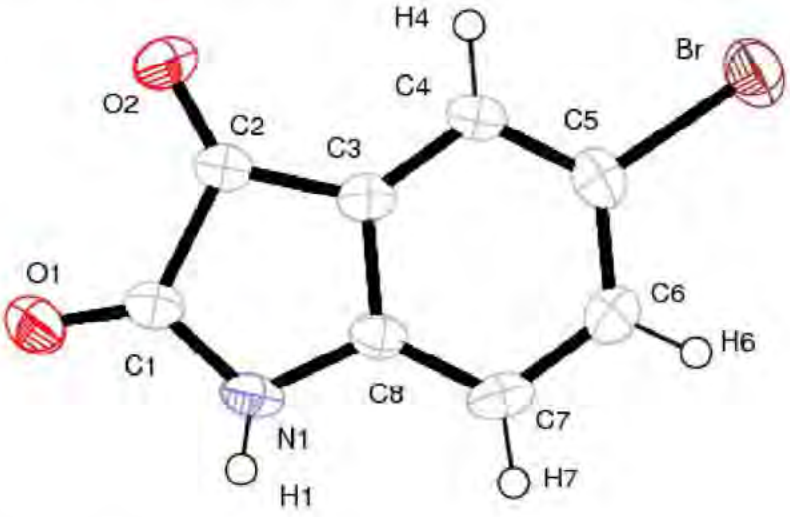

References

[1] A. V. Kurkin, etal, Acta Cryst. (2008). E64, o1448.

MS05-P57

Progress in using short wavelength radiation for chemical crystallography

T. Samtleben[1], J. Graf[1], B. Hasse[1], J. Wiesmann[1], C. Michaelsen[1], F. Fabbiani[2], T. Schulz[3], D. Stalke[3], H. Ott[4]

[1]*Incoatec GmbH, Geesthacht, Germany*
[2]*GWZ, University of Goettingen, Germany*
[3]*IAC, University of Goettingen, Germany*
[4]*Bruker AXS GmbH,Karlsruje, Germany*
E-mail: samtleben@incoatec.de

Combining synthetic multilayer mirrors with microfocus X-ray sources (rotating or stationary target) has become a standard with in-house X-ray sources for single crystal diffraction as well as a number of applications in powder diffraction. The maximum angle of incidence at which a multilayer mirror reflects is significantly smaller for higher energy radiation, such as Mo-K_α or Ag-K_α radiation than it is for Cu-K_α radiation. This is why synthetic multilayer mirrors traditionally have been used for Cu-K_α radiation or softer wavelengths. Modern deposition technology, however, allows for the reproducible production of high quality multilayer mirrors with smaller *d*-spacing. In consequence these mirrors reflect higher energy radiation at larger angles of incidence. Combined with the latest generation of microfocus sealed tubes this provides new high-performance low-power X-ray sources for shorter wavelengths.

We will present selected results on the use of these low-power consumption, high-performance sources for Mo-K_α and Ag-K_α radiation in small molecule and high-pressure crystallography.

Molecular structure of 2-amino-N (2-fluorophenyl)-4, 5, 6, 7-tetra hydro-1-benzothiophene-3-carboxamide

M. K. Kokila[1], K. Chandra Kumar[2] J. Saravanan[3] and M. V. Kulkarni[4]

[1]*Department of Physics, Bangalore University, Bangaluru-560056, India*
[2]*Department of Engineering Physics, H.K.B.K. College of Engineering, Bangaluru-560045 India*
[3]*Department of Pharma chemistry, PES College of Pharmacy, Bangaluru-560050 India*
[4]*Department of Studies in Chemistry, Karnatak University, Dharwad -570 001, India*
E-mail: drmkkokila@gmail.com

Hydrogen bonds are considered as strongest design elements in crystal engineering. However halogens are also utilized widely to design molecules. Among halogens the interactions involving organic fluorine is of more interest [1]. It has been shown that fluorine does not readily accept hydrogen bonding and hence fluorine behaves differently from chlorine and bromine[2]. In view of these we designed and investigated crystal structures of halogenated thiophenes [3] which are found to exhibit broad spectrum of biological activities.

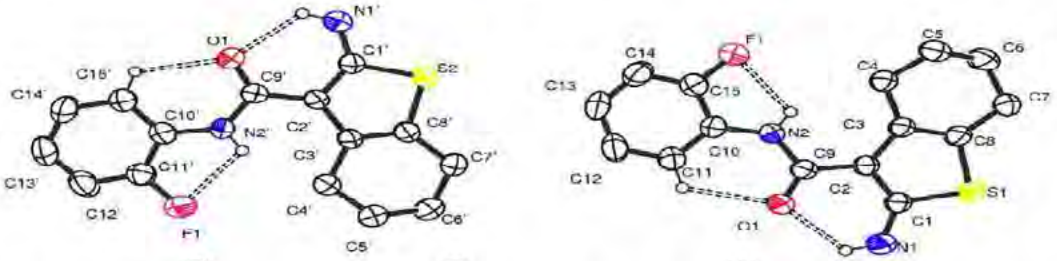

(B) (I) (A)

The three dimensional intensity data of the compound 2-amino-N (2-fluorophenyl)-4, 5, 6, 7-tetrahydro-1-benzothiophene-3-carboxamide (I) were collected using Bruker Smart CCD diffractometer using graphite monochromated MoKα radiation. The compound $C_{15}H_{15}FN_2OS$, crystallizes under Triclinc system, P1 space group, a = 9.052(15) Å, b = 9.066(15)Å, c = 9.582(15) Å, α = 106.02(5), β = 106.32(3) and γ = 103.53(4)°, V = 682.6(19) $Å^3$, Z = 2, D = 1.41 Mg m^{-3}. The data of the compound were corrected for LP factors and used for the structure solution. The structure was solved by direct methods using SIR92 program and refined using full matrix least-squares on F^2 to an R value of 0.037 using SHELXL-97 program.

In the asymmetric unit there are two independent molecules A and B. The conformation of the cyclohexene ring is same in both molecules A & B. The dihedral angles between the thiophene moiety and the 2-florophenyl ring are 5.31(5) Å and 5.41(4) Å in A and B respectively. The molecule is conformationally locked by intra-molecular hydrogen bonds of the type N-H…O and C-H…O forming six membered rings. There is an intra-molecular C-H…F interaction forming a five membered ring. The packing arrangement of molecules in the unit cell shows inter-molecular hydrogen bonding of the type N-H…O and C-H…F interactions stabilizes the crystal structure which links the molecules into chains running parallel to the c-axis.

References

[1] T.N. Guru Row: *Hydrogen & Fluorine in crystal Engineering*, Coordination Chemistry Reviews 183 (1999) 81–100.
[2] Howard J.A.K., Hoy V.J., O'Hagan, & Smith G.T.(1996). Tetrahedron, 52, 12613-12622.
[3] K. Chandra Kumar, M. K. Kokila, Puttaraja, J. Saravanan, S. Mohan, *2-amino-N-(2-methoxy phenyl) 4, 5, 6, 7-tetrahydro-1-benzothiophene-3-carboxamide*, Acta Cryst E (2007) E63, o3009.

MS05-P59

Synthesis, structures and characterization of organotin complexes derived from 3,5-di-*tert*-butyl-4-hydroxybenzyl alcohol

S. M., Lee,[1] H. Mohd. Ali [1] and K. M. Lo[1]

[1]*Department of Chemistry, Faculty of Science, University of Malaya, Malaysia*
E-mail: smlee@um.edu.my

Organotin complexes comprises of an important class in organometallic chemistry in view of its structural diversity and biological activity. Among these compounds, organotin carboxylates have drawn considerable attention attributed to its significant important anti-tumor properties. Although the structures of organotin carboxylates are closely related in the solid state form, there is a clear progression from monomeric species to inifinite polymeric chains. In the present studies, a series of organotins were prepared from 2-(3,5-di-*tert*-butyl-4-hydroxybenzyl)sulfanyl acetic acid and 3,5-di-*tert*-butyl-4-hydroxybenzyl)sulfanylethanehydrazine Schiff base ligands. The complexes were characterized by various spectroscopic methods including IR, NMR spectroscopies. The X-ray structures of the crystalline complexes were reported. The presence of the two bulky *tert*-butyl on the phenyl ring prevents any intermolecular or intramolecular hydrogen bonding interation involving the hydroxy group.

References

[1] Tiekink, E. R. T., "Structural chemistry of organotin carboxylates: a review of the crystallographic literature", Appl. Org. Chem. 5, (1991), pp. 1–23.
[2] Yehye, W. A., Ariffin, A. & Ng, S. W., "2-[(3,5-Di-tert-butyl-4-hydroxybenzyl)sulfanyl]-N'-isopropylideneacetohydrazide", Acta Cryst. E65, (2009), pp. o730.

MS05-P60

Structure-property relationships in phosphous-based nanoporous metal oxides

Sue-Lein Wang

Department of Chemistry, National Tsing Hua University, Hsinchu, Taiwan 30013, ROC
E-mail: slwang@mx.nthu.edu.tw

Interest in organic-inorganic hybrid nanoporous materials has spiked recently due to the emerging discovery of new structures and interesting new properties. The system of organically templated phosphous-based metal oxides especially stood out over the past ten years for its remarkable structural porosity and intriguing optical property. Our recent study on metal phosphates/phosphites made several breakthroughs on creating novel structures, discovering new chemistry and intriguing property.[1-6] NTHU-4, a 14-membered-ring channel structure of zinco gallium phosphate, is the first metal-activator-free yellow and white-light phosphors; NTHU-6, the first oxalatophosphate with hexameric octahedral Ga-O cluster that emit bright yellow light; NTHU-7, the first organically templated gallium oxalatophosphite with unprecedented nanotubular structure, is a yellow-green phosphor. All these can be used as color-conversion phosphor for LEDs. Following NTHU-2, we successfully prepared an organo-metallophosphate, NTHU-8, which exhibits a three-dimensional hybrid framework containing nanometer-sized channels with intriguing bimodal porosity. The unique adsorption property grants NTHU-8 potential in application of hydrogen storage. In addition, our latest study on a novel layered zinc phosphate, NTHU-9, revealed a unique metal-activator-free orange phosphor with dual photo-generated properties, photoluminescence and photochromism. Structural features and distinct properties of these novel open-framework materials will be presented and discussed.

References

[1] Liao, Y. C.; Lin, C. H.; Wang, S. L."Direct White Light Phosphor: A Novel Porous Zinc Gallophosphate with Tunable Yellow to White Luminescence" *J. Amer. Chem. Soc.*, Vol. 127 (2005), pp 9986-9987.

[2] Yang, Y. C.; Wang, S. L. " Intrinsic Yellow Light Phosphor: An Organic-Inorganic Hybrid Gallium Oxalatophosphate with Hexameric Octahedral Ga6(OH)4O26 Cluster", *J. Am. Chem. Soc.*, Vol. 130 (2008), pp 1147-1148.

[3] Jhang, P. C.; Yang, Y. C.; Lai, Y. C.; Liu, W. R.; Wang, S. L. "A Fully Integrated Nanotubular Yellow-Green Phosphor From An Environmentally Friendly Eutectic Solvent" *Angew. Chem. Int. Ed.* Vol. 48 (2009) , pp 742-745.

[4] Huang, S. H.; Lin, C. H.; Wu, W. C.; Wang, S. L. "Network Topology Of A Hybrid Organic Zinc Phosphate With Bimodal Porosity And Hydrogen Adsorption" *Angew. Chem. Int. Ed.* Vol. 48, (2009), pp 6124-6127.

[5] Liao, Y. C.; Liao, F. L.; Chang, W. K.; Wang, S. L. "A Zeolitic Organo-Metallophosphate Hy brid Material with Bimodal Porosity" *J. Amer. Chem. Soc.*, Vol. 126 (2004), pp 1320-1321.

[6] Jhang, P. C.; Chuang, N. T.; Wang, S. L. "Layered Zinc Phosphates with Photoluminescence and Photochromism: Chemistry in Deep Eutectic Solvents" *Angew. Chem. Int. Ed.* Vol. 49 (2010), pp 4200-4204.

MS05-P61

Crystal morphological study on the solubility limits of synthetic Al-substituted goethite

Fei Wu[1, 2], Peter Smith[2], Bill Richmond[1], Franca Jones[1], Kate Wright[1],

[1] *Department of Chemistry, Curtin University, GPO Box U1987, Perth 6845, Australia*
[2] *CSIRO Light Metals Flagship, Parker Centre, CSIRO Minerals, Perth, Australia*
E-mail: Fei.Wu2@postgrad.curtin.edu.au

This study has examined the crystal structure of synthetic Al-substituted goethites and the relationship between the Al substitution and unit cell parameters. We have also attempted to establish the limit of Al for Fe substitution in the formation of Al-goethites based on XRD and TEM analysis.

Aluminium substituted goethites were synthesised by ageing of coprecipitated $Fe(NO_3)_3$ and $Al(NO_3)_3$ in KOH solution at 70°C [1]. The effects of aluminium substitution on the crystal morphology of the solid solution were studied by XRD and TEM (Fig. 1&2). The particle size decreases with the increase of aluminium substitution (Fig. 2). Elemental analysis suggests that Al for Fe substitution is limited since only a portion of the available aluminium was incorporated in the goethite structure. The strain in the goethite structure, caused by the smaller Al^{3+} ion incorporation could contribute to the substitution limit for aluminous goethite [2]. A more complicated mechanism is expected for the formation of the diaspore-goethite solid solution. Thermal analysis results show two endothermic peaks at ~75°C and ~290°C for synthetic Al-goethite, which are attributed to the loss of surface-absorbed water and the dehydroxylation of Al-goethite respectively. The temperature for the latter peak increased with increasing Al substitution.

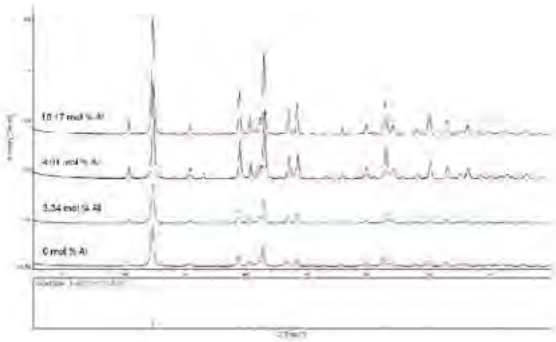

Figure 1. XRD patterns of Al-goethite samples

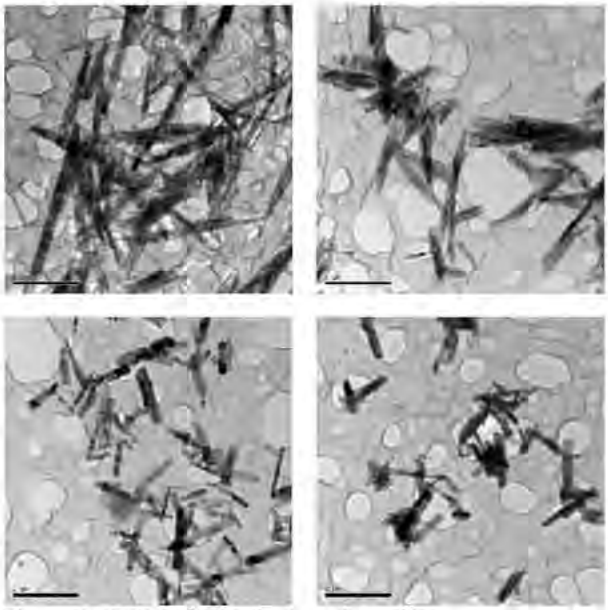

Figure 2. TEM of Al substituted goethite
(Al substitution: top left: 0 %; top right: 3.34 %; bottom left: 8.01%; bottom right: 10.0%. Bar=1μm)

References

[1] Schwertmann, U. and Cornell, R. M., "*Iron Oxides in the Laboratory: Preparation and Chara cterization*", 2nd edition, Weinheim, Wiley-VCH, (2000).

[2] Sudaka, C., Subbanna, G. N. et al., "Effect of cationic substitutents on particle morphology of goethite and the magnetic properties of maghemite derived from substituted goethite", *Journal of Material Science*, Vol. 39, No. 13, (2004), pp 4271-4286.

Influence of cation vacancies on the phase composition of iron sulphides 29 years after synthesis

Viktor V. Onufrienok[1], Anatoly M. Sazonov[2]

[1-2]*Department of Mineralogy, Siberian Federal University, Krasnoyarsk, Russia*
E-mail: VOnufriynok@yandex.ru

There was studied the dependence of the phase composition on the sulphur-iron ratio in the pyrrhotite (FenS) samples after being synthesized at 1273 K and kept in the atmosphere at room temperature for 29 years. The iron sulfides with S/Fe ratio from 1.0 up to 2.0 have been obtained. The crystal structure of iron sulfides as directly after synthesis, so after air storage were investigated using the X-ray analysis method. The samples obtained after air storage contained goethite FeO(OH), czomolnokite {Fe(SO4)(H2O)}, pyrite FeS2, troilite FeS, smythite Fe8S9 and pyrrhotite with the phase composition Fe1-nS (1C - hexagonal pyrrhotite) and Fe7S8 (4C - monoclinia pyrrhotite).

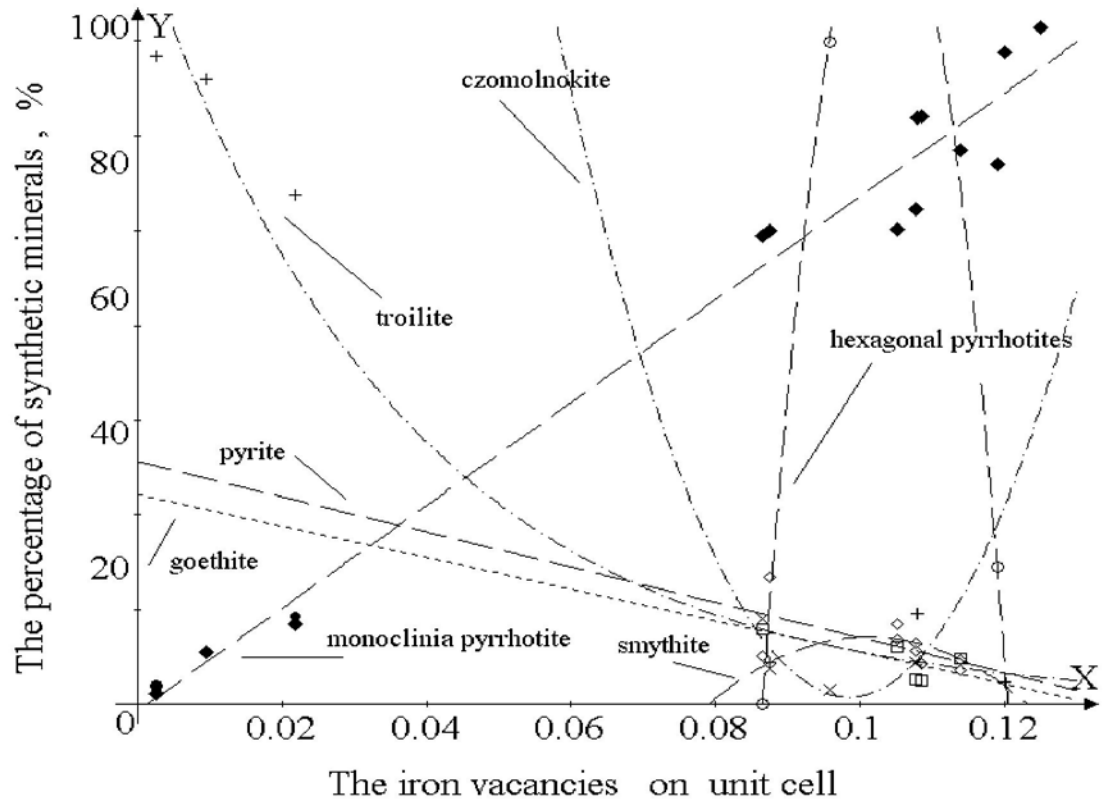

Fig.1. The diagram of phase ratio of the synthetic iron sulphides.

The purpose of the work: to study influence of cation vacancies on the phase composition of iron sulphides 29 years after synthesis.Conclusions: 1) The area of the pyrrhotites' homogeneous samples in the stable phase has been determined. The single-phase samples (according to the results of the X-ray research) correspond to the structures. 2) The diagram of phase ratio of the pyrrhotites sustained isothermally in the atmosphere of the Earth for 29 years has been offered.

The crystal structure of a new dioxo-molybdenium(VI) complex of a tridentate Schiff base ligand

Iran Sheikhshoaie[1], Niaz Monadi[1], Helen Stoeckli-Evans[2]

[1] *Department of Chemistry, Shahid Bahonar University of Kerman, Kerman, Iran*
[2] *Institute of Physics, University of Neuchâtel, Rue Emile-Argand 11, 2009 Neuchâtel, Switzerland*
E-mail: i_shoaie@yahoo.com

A new dioxo-molybdenum (VI) complex [MoO2 (L)(H2O)] has been synthesized, using 2-((E)-(2-hydroxypropylimino)methyl)-4-methoxyphenol as tridentate ONO donor Schiff base ligand (H2L) and MoO2(acac)2 [Scheme 1] by usual method[1].. A Triclinic space group P-1 was determined by X-ray crystallography from single-crystal data of this complex. Suitable crystals of this complex were obtained as yellow plates. The intensity data were collected at 233K (-40°C) on a Stoe Mark II-Image Plate Diffraction System [2] and using MoKα graphite monochromatic radiation. Image plate distance 130 mm, Tω rotation scans 0 - 180° at Φ 0°, and 0 - 55° at Φ 90°, step Δω = 1.5°, exposures of 7 mins per image, 2θ range 1.76 - 52.59°, dmin – dmax = 23.107 - 0.802 Å. The structure was solved by Direct methods using the program SHELXS-97 [2]. The refinement and all further calculations were carried out using SHELXL-97 [3]. The crystal structure of this metal complex is shown in Figure 1.

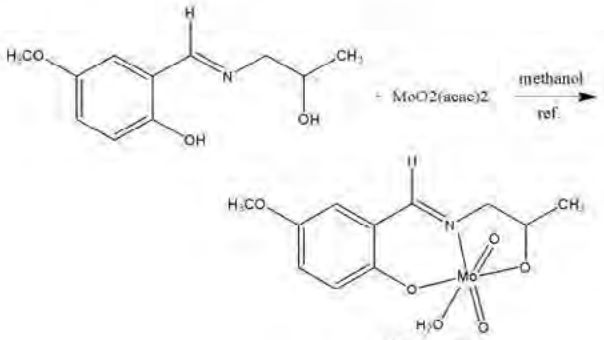

Scheme 1

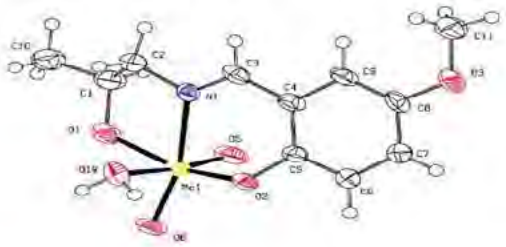

Fig. 1

References

[1] Sheikhshoaie I., Rezaeifard A., Monadi N., Kaafi S., *Polyhedron* (2009), 28, pp 733–738.
[2] Stoe & Cie. *X-Area V1.52 & X-RED32 V1.48 Software*, (2009), Stoe & Cie GmbH, Darmstadt, Germany.
[3] Sheldrick, G. M., *Acta Cryst.*, (2008), A64, pp 112-122.

Synthesis, crystal structure, and fluorescence property of chalcone derivatives

Thawanrat Kobkeatthawin[1, 2], Suchada Chantrapromma[2] and Hoong-Kun Fun[3]

1Department of Chemistry and Center of Excellence for Innovation in Chemistry, Faculty of Science, Prince of Songkla University, Hat-Yai, Songkhla 90112, Thailand
2Crystal Materials Research Unit, Department of Chemistry, Faculty of Science, Prince of Songkla University, Hat-Yai, Songkhla 90112, Thailand
3X-ray Crystallography Unit, School of Physics, Universiti Sains Malaysia, Penang, 11800 USM, Malaysia
E-mail: kul_atom@hotmail.com

Two chalcone derivatives namely, (E)-1-(4-chlorophenyl)-3-[4-(diethylamino)phenyl]prop-2-en-1-one (1) and (E)-1-(4-bromophenyl)-3-[4-(diethylamino)phenyl]prop-2-en-1-one (2) were synthesized by aldol condensation. Their structures were established on the basis of 1H-NMR, FT-IR and UV-Vis spectroscopy and single-crystal X-ray structure determination. Both compounds crystallize out in monoclinic system with space group P21/c. Under UV light, compounds 1 and 2 exhibited strong fluorescence emission at λem 529 and 526 nm, respectively, when was excited at 435 nm in CHCl3.

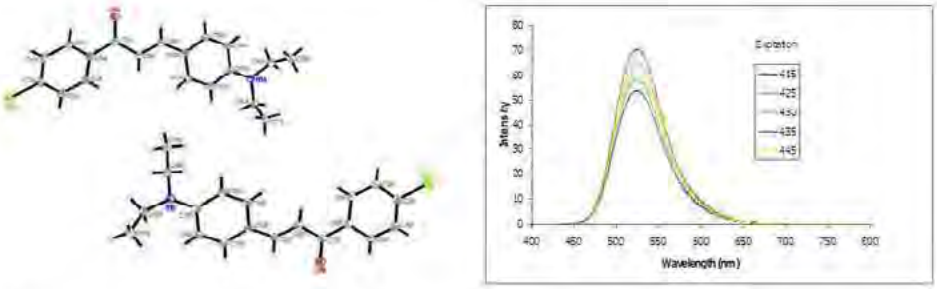

Fig 1. The crystal structure and emission spectra of compound 1.

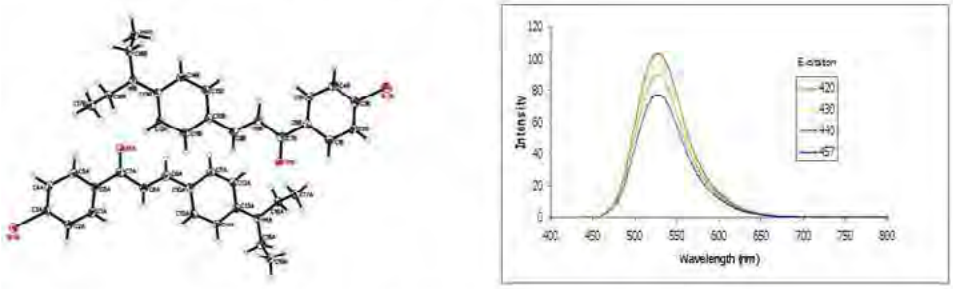

Fig 2. The crystal structure and emission spectra of compound 2.

References

[1] Jun Z., Zhicheng X., Yanil W., Shaomin S. and Chuan D., "Spectral properties of intramolecular charge transfer fluorescence probe 1-keto-2-(*p*-dimethylaminobenzal)-tetrahydronaphthalene", *Spectrochimica Acta Part A*, Vol.70, (2008), pp 888-891.

[2] Hidehiro K., Gen-ichi K. and Kazuhiko M., "Synthesis and photoluminescence of π-extended fluorine derivatives: the first example of a fluorescent solvatochromic nitro-group-containing dye with a high fluorescence quantum yield", *Tetrahedron Letters*, Vol. 51, (2010), pp 181-184.

[3] Vladimire T., Martina P., Miroslava S. and Pal P., "Some fluorescence properties of dimethylaminochalcone and its novel cyclic analogues", *Spectrochimica Acta Part A*, Vol. 74, (2009), pp 1242-1246.

MS05-P65

Partial resolution of racemic Cu(I) complex via crystallization

Michael Y. Chiang[1], Jing-Yun Wu[2]

[1]*Department of Chemistry, National Sun Yat-sen University, Kaohsiung, Taiwan.*
[2]*Department of Applied Chemistry, National Chi Nan University, Puli, Nantou County, Taiwan*
E-mail: michael@facmail.nsysu.edu.tw

Chiral resolution is a most desired process in organic synthesis, especially when medical implication is involved. Most racemic compounds form racemic crystals. Spontaneous resolution of the racemic compounds into conglomerate crystals—crystal contains only one of the two enantiomers—is rare. Ever since Louis Pasteur demonstrated the spontaneous resolution of sodium ammonium tartrate by crystallization of the two enantiomers, people have been trying to apply this method with only limited success. The laws governing the spontaneous separation are still not fully understood, except perhaps the recognition of weak intermolecular interactions to be one important key factor behind the laws.

In attempts to synthesize and study the reactivity of some copper iminophosphine complexes, we accidentally observed a conglomerate crystal formation from the racemic Cu (I) complex. The racemic Cu (I) complex (Figure 1) crystallized into two different crystal forms in the THF/hexane solution. One crystal form is centric with both R and S enantiomers crystallized pair-wise. The other crystal form is non-centric with solely one form packed in helical fashion. This is a significant observation since the later form represents spontaneous resolution of the racemic Cu (I) complex. Both crystal structures are examined in detail and the different interactions within their solid structures are discussed.

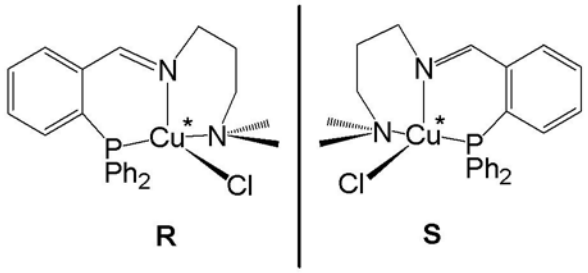

Figure 1. Structure of R and S enantiomers of Cu (I) [P,N,N] complex

References

[1] Van't Hoff J. H., "*The Arrangement of Atoms in Space*", 2nd edition, translated and edited by E iloart A., Longmans, Green, and Co., London, (1898), p. 46.
[2] Lennartson A. and Hakansson M., "Diphenyldipyridinezinc(II): partial spontaneous resolution of an organometallic reagent", *Acta Cryst.* C65, (2009), m205-m207.

Disordering of the $[NbOF_5]^{2-}$ anions in centrosymmetric structures of $(C_2H_6NO_2)_2[NbOF_5]$, $(C_3H_8NO_2)_2[NbOF_5]\cdot 2H_2O$, $[Sn_2F_2][NbOF_5]$, $K_4[Sb_2F_8][NbOF_5]$ and $Mn[NbOF_5]\cdot 4H_2O$

Andrey V. Gerasimenko, Ivan A. Tkachenko, Ruven L. Davidovich, Tamara F. Antokhina, Evgeny B. Merkulov
Institute of Chemistry, Far East Branch, Russian Academy of Sciences, Vladivostok, Russia
E-mail: gerasimenko@ich.dvo.ru

The interest in the compounds of transition metals with distorted coordination polyhedra is caused by their extreme importance at designing materials with structure-dependent properties. The metals of the above type include niobium whose atom is displaced in the $[NbOF_5]^{2-}$ anion along the Nb=O bond in the O atom direction. The present communication is devoted to studies of disordering of the $[NbOF_5]^{2-}$ complex ion in centrosymmetric structures of $(C_2H_6NO_2)_2[NbOF_5]$ (I) (space group $P2_1/c$), $(C_3H_8NO_2)_2[NbOF_5]\cdot 2H_2O$ (II) (space group $P\bar{1}$), $K_4[Sb_2F_8][NbOF_5]$ (III) (space group $P\bar{1}$), $[Sn_2F_2][NbOF_5]$ (IV) (space group $P2_1/n$), α-$Mn[NbOF_5]\cdot 4H_2O$ (V) (T= 153K, space group $P2_1/c$) and β-$Mn[NbOF_5]\cdot 4H_2O$ (VI) (T=297 K, space group C2/m).

Originally, the structures (I-VI) were solved for the Nb atoms located in the inversion centres and the F1 and O1 atoms occupying the same position. At this stage, the niobium atoms had significant thermal displacements along the Nb—F1/O1 bonds (Fig. 1a), while the Nb—F1/O1 bond lengths had the values of 1.91 ÷ 1.93 Å almost equal to average values of axial bond lengths Nb=O and Nb—F in ordered structures. It was established on the basis of the analysis of the anisotropic displacement parameters of atoms and difference electron-density syntheses that the Nb atoms were displaced from the inversion centers along the Nb—F1/O1 bonds in the O atoms direction. Refinement of the structures with the Nb atoms split positions (рис. Fig. 1b) resulted in satisfactory anisotropy of niobium atoms and geometric parameters of $[NbOF_5]^{2-}$ anions comparable to those in ordered structures: (bond lengths) Nb=O from 1.75 up to 1.81 Å; Nb—F_{ax} from 2.03 up to 2.09 Å; Nb—F_{eq} from 1.92 up to 1.97 Å. To sum up, in the structures (I-V) the Nb, O and F atoms in the *trans*-position relatively to the O atom are disordered in regard to inversion centers, while disordering is of a static character.

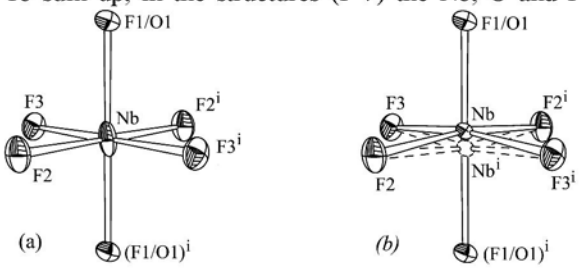

Figure 1. Overall view of the $[NbOF5]^{2-}$ anion in I-VI structures showing the elongated displacement ellipsoids of the Nb atoms when situated on the inversion centre (a) and the disordered displacement of the Nb atoms from the inversion centre (b) [Symmetry code: (i) -x, -y,-z.]

In the crystals $Mn[NbOF_5]\cdot 4H_2O$, a phase transition was found in the temperature range from 282 up to 296 K. During the phase transition, a unit cell (α-phase) transforms into a C-centered one (β- phase). The transition into the β-phase is accompanied by splitting of all ligand positions near the Nb and Mn atoms into two equally probable ones. In our opinion, the reason for such a splitting consists in addition of dynamic disordering to the regular positional disordering of the α-phase, i.e. at temperatures higher than that of the phase transition one can observe abrupt changes of the orientation of Nb- and Mn-octahedra on two most probable positions, while the phase transition belongs to the type "order-disorder".

The authors thank the Russian Foundation for Basic Research (project No. 08-03-00355) for financial support.

MS05-P67

Crystal structure and microwave dielectric properties of indialite

H. Ohsato[1,2], A-Y. Kim[3], T. Sakakura[4], N. Ishizawa[4], C-I. Cheon[3], and J-S. Kim[1]

[1]*Dept. of Semiconductor and Display Engineering, BK21 Graduate School, Hoseo University, 165 Sechul-ri, Baebang-myeon, Asan-si Chungnam 336-795, Korea*
[2]*Department of Research, Nagoya Research Institute, 1-13 Yotsuya-dori, Chikusa-ku, Nagoya 464-0819, Japan*
[3]*Dept. of Material Science and Engineering, Hoseo University, 165 Sechul-ri, Baebang-myeon, Asan-si Chungnam 336-795, Korea*
[4]*Material Science and Engineering, Nagoya Institute of Technology, Gokiso-cho, Showa-ku, Nagoya 466-8555, Japan*
E-mail: ohsato@naa.att.ne.jp

Recently, the utilizable frequency region for wireless communication has been expanded to millimeter wave, because of shortage of frequency resource, and request high speed and high data transfer rate. Personal area network (PAN) using non-condense high speed digital wireless telecommunications system, and radar for car anti-collision system are required high Q, low ε_r and temperature stable millimeter wave dielectrics. Silicates are candidate for millimeter wave dielectrics, because of low er and high Q. Indialite (Mg2Al4Si5O18) is a kind of silicates, which is high temperature form of cordierite. Millimeter wave dielectric properties of cordierite are low dielectric constant: ε_r = 6.2, high Q: Qf = 39,900 GHz, and temperature stable of resonate frequency: TCf = -24 ppm/°C.

The millimeter wave dielectric property of Ni-doped cordierite was improved the Qf from 39,900 to 90,600 GHz. The crystal structure of Ni-doped cordierite has a tendency to change to the indialite with high symmetry. The ordered $(AlSi)_6O_{18}$ ring of cordierite deformed to disorder ring. It's confirmed by the volume sizes of SiO_4 and AlO_4 tetrahedra, and covalency between Si-O and Al-O bonds based on the crystal structure analysis.

In this study, indialite single crystals with hexagonal prism grown from melts are analyzed crystal structure, and relationships among the crystal structure and the millimeter wave dielectric properties are discussed.

References

[1] Ohsato H., "Microwave Materials with High Q and Low Directric Constant for Wireless Communications", *Mater. Res. Soc. Symp. Proc.* Vol.833, (2005), pp55-62.
[2] Terada M., Kawamura K., Kagomiya I., Kakimoto K., and Ohsato H., "Effect on Ni substitution on the microwave dielectric properties of cordierite", *J. Euro. Ceram. Soc.*, Vol.**27**, *No.3, (2007),* pp 3045-3148.
[3] Ohsato H., Kagomiya I., Terada M., and Kakimoto K., "Origin of Improvement of Q Based on High Symmetry Accompanying Si-Al Disordering in Cordierite Millimeterwave Ceramics", *J. Euro. Ceram. Soc.*, Vol. **30**, (2010), pp 315-318.

Novel anticancer agents: synthesis, crystal structures, cytotoxic activities, DNA-binding studies and topoisomerase II inhibitory of the sulfonyl containing 6-deoxyclitoriacetal derivatives

Thapong Teerawatananond[1], Nattaya Ngamrojnavanich[1], Narongsak Chaichit[2], and N. Muangsin[1]

[1]*Research Centre for Bioorganic Chemistry, Department of Chemistry, Faculty of Science, Chulalongkorn University, Bangkok 10330, Thailand*
[2]*Department of Physics, Faculty of Science and Technology, Thammasat University, Patumthani 12120, Thailand*
E-mail: Thapong_sthc@hotmail.com

6-Deoxyclitoriacetal **(1)** has been identified to have a good cytotoxic activity against various types of human carcinoma, possibly due to its ability to intercalate with DNA as evidenced *in vitro* assay [1]. The sulfonate derivatives of 6-deoxyclitoriacetal were synthesized to enhance its cytotoxic activities as novel anticancers [2,3]. Screening of these compounds for cytotoxic activity has shown that tosylate derivative **(4)** was more potent and selective than commercial doxorubicin hydrochloride. X-ray structures and their cytotoxic activities have considerably revealed that the not only a bent-shaped structure but also the suitable functional groups at C11 play an important role in increasing their cytotoxicities. Additionally, the sulfonate derivatives were evaluated their ability to inhibit topoisomerase II activity. They had potentially inhibited the topoisomerase II more 70% inhibition. Finally, we studied the DNA-binding affinity of 6-deoxyclitoriacetal and its sulfonate derivatives based on UV-Visible spectroscopic techniques [4].

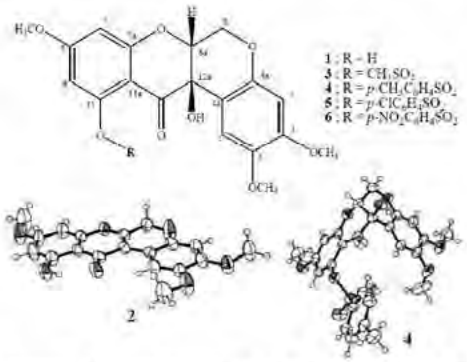

Figure 1 Chemical structures of 6-deoxyclitoriacetal and its derivatives, ORTEP drawing of X-ray structures of dehydrated of 6-deoxyclitoriacetal (**2**) and tosylate derivative (**4**).

Compound	Structure	%Topoisomerase II inhibition	Anticancer (IC_{50} (μg/mL))		
			KB	MCF7	NCI-H187
Doxorubicin	Bent	-	2.01	42.52	0.03
Stemonal	Planar	-	Inactive	Inactive	Inactive
1	Bent	87	13.28	23.65	3.12
2	Planar	71	Inactive	Inactive	Inactive
3	Bent	100	24.98	17.36	6.48
4	Bent	87	0.02	Inactive	0.02
5	Bent	Not inhibition	46.77	Inactive	0.41
6	Bent	Not inhibition	Inactive	Inactive	0.59

Keywords: 6-deoxyclitoriacetal, structure-activity, sulfonate derivatives, cytotoxic activity and topoisomerase II

References

[1] Roengsumran S., Khorphueng P., Chaichit N., Jaiboon-Muangsin N., Petsom A., "Crystal structure of 6-deoxyclitoriacetal, $C_{19}H_{18}O_8$", *Z. Kristallogr. NCS*, 218, (2003), 105-106.

[2] Chimsook P., Teerawatananond T., Ngamrojnavanich N., Chaichit N., Muangsin N., "12a-Hydroxy-2,3,9-trimethoxy-12-oxo-6,6a,12,12a-tetrahydrochromeno[3,4-*b*]chromen-11-yl-4-methylbenzene sulfonate", *Z. Kristallogr. NCS*, 225, (2010), 374-376.

[3] Teerawatananond T., Chaichit N., Muangsin N., "Co-crystal structure of 11-hydroxy-2,3,9-trimethoxy-6*H*-chromeno[3,4-*b*]chromen-12-one and 11-hydroxy-2,3,9-trimethoxy-chromeno[3,4-*b*]chromene-6,12-dione", *J. Chem. Cryst.*, 40, (2010), 591–596.

[4] Teerawatananond T., Ngamrojnavanich N., Sompornpisut P., Chaichit N., Muangsin N., "Structure-cytotoxicity relationship of 6-deoxyclitoriacetal and its sulfonate derivatives based on X-ray crystallography", *Manuscript in preparation for publication in Journal of Bioorganic & Medicinal Chemistry.*

MS05-P69

Pressure-induced hydration and cation migration in a potassium -exchanged natrolite

Dong-Hoon Seoung, Yongmoon Lee, Yongjae Lee*

Department of Earth System Sciences, Yonsei University, Seoul 120-749, Korea
E-mail: sdh@yonsei.ac.kr

Natrolite ($Na_{16}Al_{16}Si_{24}O_{80}$-$16H_2O$) is one of the small pore zeolites that is built from cross-linked T_5O_{10} chain to form helical 8-ring channels along the c-axis. Within the natrolite channel, sodium cations and water molecules are orderly distributed in an 1:1 ratio. It is been known that under hydrostatic pressure, the channel water content of sodium-natrolite increases abruptly by 50% near 1 GPa and by 100% above 1.2 GPa. We have recently prepared a fully potassium-exchanged natrolite (K-NAT, $K_{15.2}Al_{16}Si_{24}O_{80}$-$14H_2O$) and found K-natrolite exhibits ca. 10% expanded unit cell volume at ambient conditions via reversed and statistically distributed potassium cations and water molecules, compared to the original Na-natrolite. In order to understand comparative high pressure chemistry of natrolite as a function of nonframework cation, high-pressure synchrotron X-ray powder diffraction was performed at beamlines 5A at PLS (Pohang Light Source) and X14A at NSLS (National Synchrotron Light Source). Under hydrostatic conditions mediated by pure water as pressure-transmitting medium, K-NAT exhibits volume discontinuities involving ca. 3.8 % expansion near 1 GPa and ca. 2.2 % contraction above 2.5 GPa. Preliminary result from Rietveld refinements suggests that the expansion near 1 GPa is due to pressure-induced hydration, whereas the contraction above 2.5 GPa is via cation and water redistribution within the channel toward an ordered fashion as observed in the superhydrated Na-NAT.

MS05-P70

Raman spectral and X-ray diffraction of CO_2 absorption Into natrolite under high-pressure

Dan Liu[1], Zhenxian Liu[2], Yongjae Lee[1]*

[1]*Department of Earth System Sciences, Yonsei University, Seoul 120-749, Korea*
[2]*Geophysical Laboratory, Carnegie Institution of Washington, Washington DC 20015, USA*
Email: YongjaeLee@yonsei.ac.kr

Zeolite minerals have their unique physical and chemical properties due to their typical structure, which composed of corner connected networks of (Al, Si)O_4 tetrahedra, yielding cavities and channels, occupied by extra–framework charge balancing metal cations and water molecules. In recent years, there many researchers investigated their usage as selective adsorbents in gases purification processes. In order to understand the adsorption of small gas CO_2 on zeolite, we have carried out a comprehensive investigation of the adsorbents of carbon dioxide on natrolite by micro-Raman spectroscopy and x-ray diffraction under high temperature and high pressure. We found the breathing mode of elliptical channel display a relatively large redshift around 0.6 GPa and 90℃ using CO_2 as a pressure medium, which implied the expansion of the natrolite framework. At the same time, new Raman peaks start to appeared in the patterns. On the basis of the structural refinement of XRD data, the natrolite shows an abrupt volume expansion near 1.4 GPa and 110℃, which is in good agreement with our Raman results. These anomalous behaviors indicate the preferential absorption of CO_2 into the natrolite channel.

MS05-P71

Structures of herbal compounds: 5-hydroxy substituted flavones

Krishnaiah M, Ravi Kumar R and Jagadeesh Kumar N.

Department of Physics,Sri venkateswara University, Tirupati, 517502 India
E-mail: profkrishnaiah.m@gmail.com

Flavonones have recognized spasmolytic, expectorant, antiulcer, liver-protecting and antimicrobial properties [1]. Flavones are a class of flavonoids with the phenyl substituent in position 2 of the benzo-pyrone ring. The title compounds: 5-hydroxy 7,8,2'-rimethoxy flavone (I); 5-hydroxy-7-2'-6'-trimethoxy flavone (II) and 5,2'-Dihydroxy-7-methoxyflavanone (III) were isolated from the whole plant of Andrographis echioides Nees (Acanthaceae), an erect herb widely distributed in the dry districts of tropical India and Sri Lanka [2]. The leaf juice of the plant is used as a remedy for fevers [3]. The study of the leaves leads to the isolation of the flavones, dihydroechioidinin, echioidinin, ethioidin, skullcapflavone 1,21-O methyl ether and skullcapflavone 1,21-O glucoside [4,5]. The structure determination of the title compounds , (I)(II) &(III), were undertaken as a part of our ongoing structure–activity study aimed at designing more active compounds, and in order to study the conformational features of the compounds.

Crystal data:

(I) 5-hydroxy 7,8,2'-rimethoxy flavone compound (C18H16O6), crystallizes in triclinic system with P-1 space group. The cell parameters are a = 7.602(2), b = 8.7563(10), c = 11.642(3)Å , α=5.252(16), β = 84.838(12), γ = 78.469(14)° and V = 754.6(3) Å3. The structure has a final R1 = 0.0315 & wR2 = 0.0883.

(II) 5-hydroxy-7-2'-6'-trimethoxy flavone compound (C18H16O6), crystallizes in Monoclinic system with P 21/c space group. The cell parameters are a = 11.003(7), b = 11.015(7), c = 13.734(9) Å, β = 113.159(10)°, and V = 1530.4(17) Å3. The structure has a final R1 = 0.0372 & WR2 = 0.0918.

(III) 5,2'-Dihydroxy-7-methoxyflavanone compound (C16 H14 O5), crystallizes in Monoclinic system with P 21/c space group. The cell parameters are a = 10.1961(10), b = 7.5600(8) , c = 18.243(2), β= 105.59(2)°, and V=1354.5(2) Å3. The structure has a final R1 = 0.0638 & wR2 = 0.1559.

Fig I

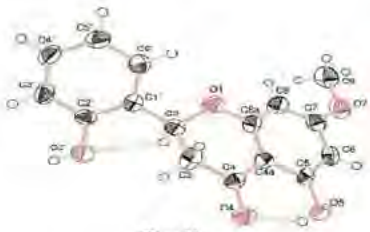

Fig:II

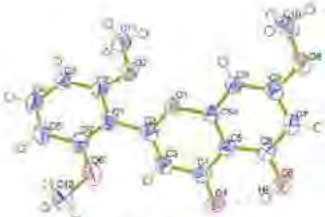

Fig:III

The hydroxyl group at C5 has a gauche arrangement with respect to the H5–O5–C5–C4a giving rise to a strong intramolecular contact between the H atom of the O5 hydroxyl group and carbonyl atom, O4 . This leads to the formation of a pseudo-six-membered ring comprising of atoms O4, C4, C4a, C5, O5 and H5. Intermolecular hydrogen bonds 1) C6–H6…O5 links the molecules into layers. Within the layer, every molecule is linked by Intermolecular hydrogen bonds and are stabilized by π–π interactions.

References

[1] Gabor M The pharmocology of Benzopyrone Derivatives and Related compounds Budapest: A kademiai-Kiado (1986).

[2] Gamble JS; Flora of the presidency of Madras. Botanical Survey of India, Calcutta., vol 2 (1956) P. 1051.

[3] Kirtikar KR, Basu BD; Indian medicinal plants,vol 3. periadical express, New Delhi (1975). pp188 4-1886.

[4] Govindachari T R, Parthasarathy PC, Pai B R & Subramanyam P S, Tetrahedron, 21 (1965) 263 3, 3715.

[5] Jayaprakasam B, Damu A G, Gunasekhar D, Phytochemistry, (1999) 1-3.

Crystal chemical screening of the ICSD for discovery of materials with high Li^+ mobility

Matthew Sale and Maxim Avdeev

Bragg Institute, Australian Nuclear Science and Technology Organisation (ANSTO), New Illawarra Road, Lucas Heights, NSW, Australia
E-mail: mts@ansto.gov.au

The Inorganic Crystal Structure Database (ICSD) contains crystallographic information for 4,000+ Li-containing materials. Only a small proportion of these structures have been experimentally studied to determine their Li-ion conductivity as direct electrochemical measurements for such a large number of materials are not feasible. We employ economical computational methods to identify compounds with certain crystal structural pre-requisites for more detailed studies by more accurate theoretical and experimental methods.

We implement the Bond Valence Sum energy map method to test whether a crystal structure possesses infinite ion-conduction pathways suitable for Li+ transport. An example of such maps is shown in Fig. 1. As a result we have identified a number of materials which show promise as good Li+-conductors. The details of the analysis and discussion of crystal structural features of the identified materials will be presented.

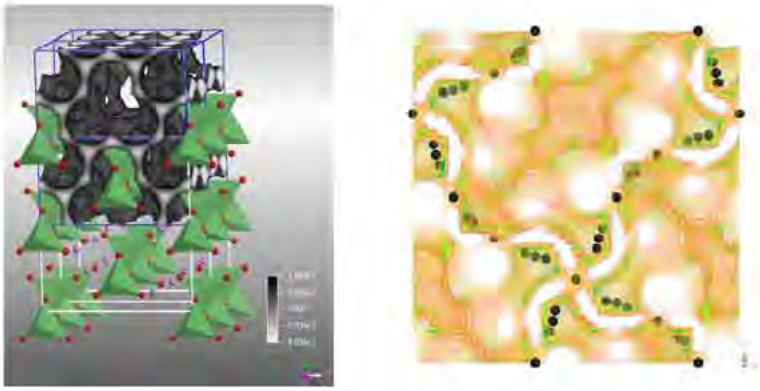

Fig 1. Above are shown examples of BVS energy maps which show infinitely connected pathways, an important prerequisite to Li-ion conductivity. In both diagrams, the shaded areas indicate likely positions of Li-ions. Observe the correlation between the experimentally measured location of the partially occupied Li-ions (black dots in right picture) and the BVS predicted locations.

Capture of hydroxyl group (OH) cationic vacancies in structures of the Pyrrhotite

Alexander G. Nikiforov [1], Viktor V. Onufrienok[2], Anatoly V. Chzhan[3]

[1-3]*Department of Mineralogy, Siberian Federal University, Krasnoyarsk, Russia*
E-mail: VOnufriynok@sfu-kras.ru

In consequence with the research of minerals of the ocean floor the interest to the connections the structure of which includes hydroxyl group (OH) has increased.

Samples for research were prepared using the method of dry synthesis by sintering settlement amount of components in vacuum in quartz ampoules at temperature 1000°C with a various mode of cooling. Samples were synthesised in 1979 in the laboratory of L.V. Kirensky Institute of Physics (Krasnoyarsk). After synthesis the samples were maintained at the room temperature (~ 25°C) in atmospheric conditions until the repeated X-ray analysis. In 2008 the samples were studied again in the laboratory of the X-ray analysis of Siberian Federal University .

The purpose of the work: determination of pyrrhotites structure changes when hydroxyl group (OH) is introduced into it.

Results:
1. Metastable pyrrhotites were resolving into goethite {FeO(HO)}. In proximity stoichiometric FeS the maintenance of a goethite was maximum (x=1.04). At increase in parity S/Fe the maintenance of a goethite exponentially fell down. For example, for x = 1.105 it comprised of already 6.62 % .
2. The contents of a czomolnokite was marked by largest extremum for x=1.48 and comprised of 56.13 %. Percentage of this phase decreased both with increase x, and with its reduction. For example, for x = 1.66 czomolnokite in samples percentage 11.65 %, and for x=1.158 - comprised of 6.19 %.
3. The maximum percentage hydroxyl group (OH) reached compound of 10.79 % for x=1.48. Thus together with czomolnokite the phase hydronium was fixed also. With reduction x the maintenance of hydroxyl group (OH) in samples also decreased to value 1.7 (x = 1.158), and then increased to value of 3.74 % (x=1.04). As this takes place to the right of a minimum the phase rhomboclase together with czomolnokite was fixed, and at the left - the phase parabutlerite was fixed in unison with goethite.
4. The phase rozenite was fixed in proximity a minimum with rather high maintenance of sulphur in samples (x=1.73). Percentage hydroxyl group (OH) in this case comprised of 4.25 %.

Automation in single crystal X-ray diffraction (SC-XRD)

Bernd Hinrichsen[1], Martin Adam and Joerg Kaercher[2]

[1]*Bruker AXS GmbH, Östliche Rheinbrückenstr. 49, 76187 Karlsruhe, Germany*
[2]*Bruker AXS Inc. E. Cheryl Parkway 5465 Madison, WI 53711-5373, USA*
E-mail: bernd.hinrichsen@bruker-axs.de

Automation has greatly improved speed, quality and reliability for a wide range of analytical instruments. It has lead to lower costs per sample on one hand and released the scientist from routine work on the other. Recently we developed a software tool (*XPRESSO*), which is capable of running an entire diffraction experiment and analysis autonomously. It is available as an integral part of the *APEX2* software suite. *XPRESSO* represents a milestone in experimental automation hitherto only reached by the SMART X2S, the first ever fully automated desktop diffractometer. Automation in SC-XRD will allow for both: opening the method for a broader range of applicants, who will benefit from the method's analytical power and reduce the workload on crystallographers allowing them to focus on crystallographically more challenging samples.

The methodology of the crystallographic engine will be described in detail. Examples of structures[1,2] solved using this approach will be presented.

Figure 1: The molecule of Co(dpdpm)(NO3)2, automatically solved with the X2S[1].The hydrogen bonds to neighbouring molecules are shown as dotted lines.

References

[1] Shaw J. L., Noll B. C., "[Diphenyldi(pyrazol-1-yl)methane]-dinitratocobalt(II)", Acta Cryst. E, Vol. 66, (2010), m140.
[2] Ivanova B. B., Spiteller M., "Noncentrosymmetric Crystals with Marked Nonlinear Optical Properties", J. Phys. Chem. A, Vol. 114, No. 15, (2010), pp 5099-5103.

MS05-P75

Making the most of a SuperNova diffractometer equipped with both Mo and Cu micro-focus sources, an Atlas detector and AutoChem

Zoltán Gál, Alexandra Griffin and Oliver Presly

Agilent Technologies XRD (formerly Oxford Diffraction)
E-mail: zoltan.gal@agilent.com

The advent of dual wavelength X-ray diffractometers (like the **Gemini** platform first introduced in 2005) brought the one-click convenience of choosing the radiation used on a sample per sample basis to the home laboratory. In practice, this meant that routine structure determinations of an organometallic sample (most typically using Mo Kα) could be easily followed by determining the absolute configuration of a light atom (C,H,N,O) crystal (most typically done with Cu Kα) without the need to spend several hours or days in order to reconfigure the instrument.

Further improvements in both the source and detector technologies over the last few years meant, that the performance of the dual wavelength *micro-focus* instruments (such as the **SuperNova Atlas** system first launched in 2008) afforded a dramatic jump in throughput as well as pushed the limits of what is possible to achieve with in-house measurements.

Examples that clearly showcase the capabilities of this instrument will be presented including a complete and automated structure determination in under 10 minutes from mounting to cif file creation, a high-resolution charge density measurement, the determination of the absolute configuration of a purely hydrocarbon-based crystal as well as establishing the presence of a bound ligand in a protein sample – all using the same hardware setup controlled by CrysAlis^{Pro}.

Keywords: crysalis pro, absolute configuration, charge density, protein diffraction, autochem

Photoinduced rearrangement of *N*-chlorinated acetanilides and benzanilides to chloroaromatic amides in the solid state: Inverted relative stability of Π_N and Σ_N amidyl radicals

Panče Naumov[1], Yildiray Topcu[1], Mirjana Eckert-Maksić[2], Fabijan Pavošević[2], Manoj Kochunnoonny[1] and Zoran Glasovac[2]

[1]*Graduate School of Engineering, Osaka University, 2–1 Yamada-oka, Suita 565–0871, Osaka, Japan*
[2]*Rudjer Bošković Institute, Bijenička 54, HR–10000 Zagreb, Croatia*
E-mail: npance@wakate.frc.eng.osaka-u.ac.jp

When solid *N*-chloroacetanilide (**1a**) is exposed to UV light, or even to unfiltered natural sunlight, it undergoes a solid-to-solid photoreaction, whereupon *p*-chloroacetanilide (**1d**) is obtained in very high yield (see the Scheme).[1] During the reaction, following photolysis of the N—Cl bond, a chlorine atom from the *N*-chloroamide group of each molecule is transferred to an aromatic ring of an adjacent molecule within the undulated head-to-tail hydrogen bonded molecular ribbons.

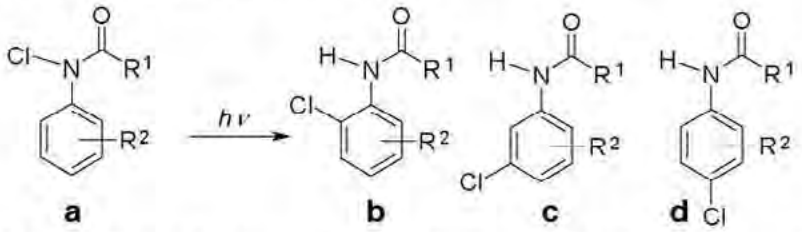

Label	R^1	R^2
1	Me	H
2	Me	*o*-Me
3	Me	*m*-Me
4	Me	*p*-Me
5	Ph	H
6	Me	2,4,6-*t*-Bu
7	Ph	2,4,6-*t*-Bu

Scheme. Photoinduced rearrangement of substituted *N*-chloroanilides and benzanilides.

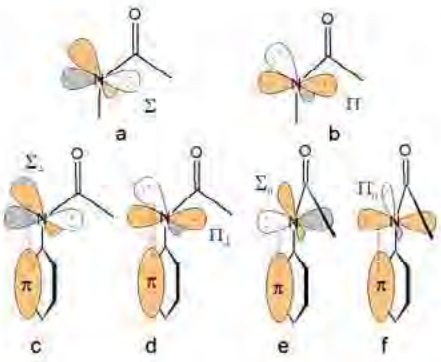

Figure (left). Simplified schematic representation of orbital interaction of the Σ_N (a, c, e) and Π_N (b, d, f) states of simple aliphatic (a, b) and aromatic (c–f) *N*-centered amidyl radicals.

On a series of seven substituted *N*-chlorinated acetanilides and benzanilides (Scheme) we demonstrate here that this photoinduced reaction is a new, more general solid-state rearrangement, by means of which UV-excited *N*-chloroaromatic amides are converted into chloroaromatic amides *via* amidyl (acylaminyl) radical intermediates. Although the Π_N state of the acyclic amidyl radicals is usually preferred over the Σ_N configuration, stabilization by aromatic conjugation and steric constraints decrease significantly the Π–Σ gap in these intermediates, leading to equal probability of the unpaired electron for population of both available orbitals.[2] Extensive theoretical calculations of the relative Π–Σ energies of the photoinduced *cis* and *trans*-amidyl radicals indicate that they are produced by photolysis of the sterically overcrowded *N*-chlorinated acetanilides and benzanilides which can exist as Σ_N radicals in the solid state.

References

[1] Naumov, P., Sakurai, K., Tanaka, M. and Hara, H., J. Phys. Chem. 2007, B111, 10373–10378.
[2] Muchall, H. M., Werstiuk, N. H. and Lessard, J., J. Mol. Struct. (Theochem) 1999, 469, 135–142.
[3] Glover, S. A., Goosen, A., McCleland, C. W. and Schoonraad, J. L., J. Chem. Soc. Perkin Trans. II 1986, 645–652.

Topochemical limits for solid-state photoreactivity by fine tuning of the π---π interactions

Shi-Yao Yang, Panče Naumov and Shunichi Fukuzumi

Graduate School of Engineering, Osaka University, 2–1 Yamada-oka, Suita, Osaka 565–0871, Japan
E-mail: npance@wakate.frc.eng.osaka-u.ac.jp

By utilizing a series of six solid forms of a single planar dicarboxylic acid as a low-dimensional supramolecular entity able for self-templation (Figure), in this work we assessed in great detail the effect of several structural factors on photodimerization reactivity.[1] The results showed that the distance between the reactive olefinic bonds (d) has comparably greater effect on the yield and distribution of the products than either of the slippage (q_2) or inclination (q_3) of the bond planes relative to each other. Although semi-quantitatively, the decreasing trend of the photochemical yield corresponds well with the increasing bond separation. From the present set of structures, it was concluded that all *parallel* double bonds separated to ≤ 4.0165 Å are reactive. Bonds with d slightly larger than this value may be, but are not necessarily reactive. The inactivity is facilitated by relative twisting of the bonds ($q_1 \neq 0$). On the basis of the semi-quantitative correlations for the photoreactive forms, and the similarity of the yields of forms F and E, the distance between the olefinic bonds in form F whose structure could not be determined, is predicted as ≥ 4.01 Å. The reactivity is also affected by the charge (neutral or ionic) of the reacting molecule and specific intermolecular interactions in which the reactive functionality participates. This first report on the solid-state photochemistry of the bisstyrylbenzene moiety demonstrates, in much more direct and quantitative way than it has been established before, the effect of subtle structural factors on the reactivity for photodimerization of double bonds in crystalline state.

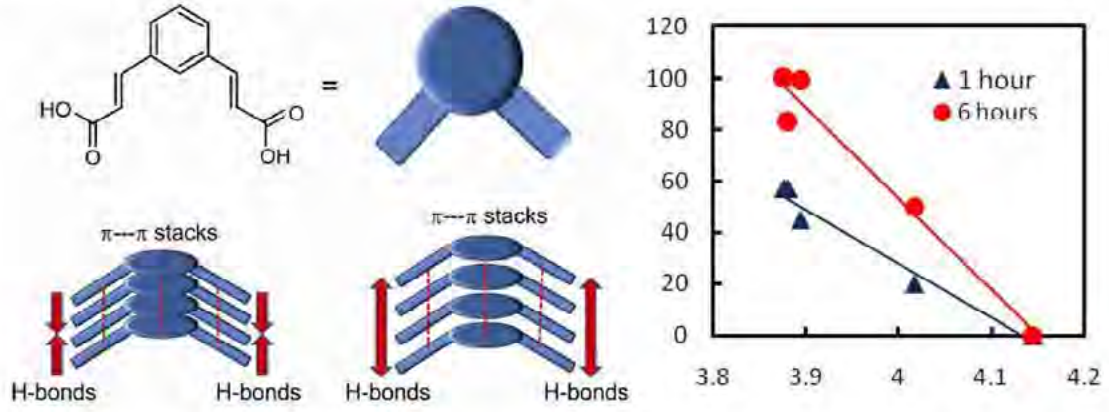

Figure. Left: Schematic of the control over the weak interaction (π–π stacking) by employing strong interaction (hydrogen bonding) in a self-templated bisstyrylbenzene moiety. Right: Dependence of the dimerization yield (y axis, in %) from the NMR data on the π–π stacking distance (x axis, in Å) after 1 hour and 6 hours from the onset of the UV irradiation.

Reference

[1] Yang, S.-Y., Naumov, P. and Fukuzumi, S., "Topochemical Limits for Solid-State Photoreactivit y by Fine Tuning of the π-π Interactions", *J. Am. Chem. Soc.* **2009**, *131*, 7247—7249.

MS05-P78

Different complexation behavior of a proton transfer compound obtained from 2,9-dimethyl-1,10-phenanthroline and 4-hydroxy-pyridine-2,6-dicarboxylic acid with Cr(III), Co(III), Ni(II) and Cu(II)

Janet Soleimannejad[1], Hossein Aghabozorg[2]

[1]*Department of Chemistry, Faculty of Science, Ilam University, Ilam, Iran*
[2] *Faculty of Chemistry, Islamic Azad University, North Tehran Branch, Tehran, Iran*
E-mail: Janet_Soleimannejad@yahoo.com

Different aspects of proton transfer have been widely studied [1-3]. In recent years, we have been interested in synthesis of proton transfer compounds and study of their behavior with metal ions [4-6]. The title compounds, (dmpH)[Cr(chelH)$_2$]·3H$_2$O, **1**, [Co(chelH$_2$)(chelH)]·dmp·4H$_2$O, **2**, (dmpH)[Ni(chelH)$_2$]·4H$_2$O, **3** and [Cu(chelH)(dmp)]·3H$_2$O, **4** (dmp is 2,9-dimethyl-1,10-phenanthroline and chelH$_3$ is chelidamic acid or 4-hydroxypyridine-2,6-dicarboxylic acid) were obtained by one-pot reaction of 2,9-dimethyl-1,10-phenanthroline and 4-hydroxypyridine-2,6-dicarboxylic acid with corresponding salts in aqueous solution. The compounds were fully characterized and their structures were determined by X-ray crystallography. The compounds **1**, **2** and **3** are similar in coordination sphere around the metal ions, with some differences between protonation sites of chelidamate ion and the charge of complex, but compound **4** is essentially different. The compounds **1, 2** and **3** are six coordinated, but **4** is five coordinated. In comparison, the compounds **1**, **2**, and **3** contain (chelH)$^{2-}$ coordinated to Cr(III), Ni(II) and Co(II) to form an anionic complex and dmp species as a counterion and water molecules in the crystal structure, but **4** differently has both (chelH)$^{2-}$ and dmp species coordinated to Cu(II) forming a neutral complex with water molecules in the crystal structure. There are various O–H···O, O–H···N and N–H···O hydrogen bonds found in the structures.

References

[1] R. Glaser and M. Lewis, *Org. Lett.*, 1(1999), 273.
[2] C. Gong and J. M. J. Fréchet, *Macromolecules*, 33(2000), 4997.
[3] H. E. Zimmerman and Jie Cheng, *Org. Lett.*, 7(2005), 2595.
[4] H. Aghabozorg, F. Ramezanipour, B. Nakhjavan, J. Soleimannejad, J. Attar Gharamaleki, and M. A. Shari, *Cryst. Res. Technol.*, 42(11)(2007), 1137-1144.
[5] J. Soleimannejad, H. Aghabozorg, F. Manteghi and S. Najafi, *Acta Cryst.*, E65(2009) m761-m762.
[6] J. Soleimannejad, H. Aghabozorg , S. Hooshmand, M. Ghanbari, F. Manteghi and M. Shamsipur, *J. Iran. Chem. Soc.*, 7(2)(2010), 405-418.

MS08-P01

Comparison with three H-, Si- and C-based giant materials on the various planetary materials

Yasunori Miura

Faculty of Science, Yamaguchi University, Yoshida, Yamaguchi, 753-8512, Japan
E-mail: yasmiura@yamaguchi-u.ac.jp

Introduction: The H (hydrogen), Si (silicon) and C (carbon) elements are the most abundant elements from elemental abundances based on Si (106) at the Solar System, mineral crust and life materials, respectively. There are few reports on structure and compositional comparison of giant molecules H, Si and C on water- Earth and water-less planetary bodies, which is main purpose of the present paper [1, 2, 3]. H-based giant molecules: H-bearing materials of water, vapor and ice are the most significant state changes for active planet and human activity. However, water molecule (H2O) and hydroxyl ion (OH), respectively, are mainly referred to life activity for water-planet Earth, which are investigated by the molecules of the spectral analyzers (Infra-Red and Raman etc.). It is very difficult to form water molecules on the water-less space and planetary bodies due to sources of O (oxygen) isolated, though the H element is main production of any space from nuclear fusion of star in the Sun. Therefore, continuous collisions on the rocky materials of Si-O (silicate) composition are required by dynamic impact process. Si-based giant materials of silica: Tetrahedral structure of silica (SiO4) shows various changes in solid replacements to silicate minerals (from olivine to feldspar) on Earth's rocks. At high temperature and pressure conditions, the bulk structure by the X ray-powder diffraction shows quartz silica pattern with different calculated density as giant silica structure with foreign elements and remnants of high critical conditions found at impact materials (such as shocked quartz) and burned materials in industry (fly ashes of coal ashes and glass slag). C-based giant molecules: Carbon-bearing giant molecules are changed at three states of carbon dioxides in vapor and liquid, and graphite and diamond in solid states. After high temperature and pressure conditions, the bulk structure by the X ray-powder diffraction shows graphite carbon pattern with different calculated density as giant carbon structures with foreign elements and remnants of high critical conditions. Recent technique can produce micro-diamonds by impact condition from carbon-bearing materials at every places, which is main problems for minor or major crystalline structure by spectral studies of the IR or Raman method. Amorphous carbon is amorphous in major but tiny crystalline grains in minor structure, which is main difficulty to identify a diamond for many papers. In-situ SEM electron microscopic observation: In order to identify the bulk carbon and silica structures with various "different compositions without the X-ray diffraction" , the Field-Emission Scanning Electron Microscopy (FE-SEM) are applied in this study to elucidate aggregates of nano-particles for carbon-rich or silica-rich particles for X-ray bulk minerals of quartz silica and graphite carbons. Summary: X-ray powder diffraction indicates average mineral structures of giant molecules, whereas in-situ SEM observation indicates aggregates of nano-particles with remained at previous critical conditions. These differences are considered to be caused by material changes at three states (vapor-liquid-solid) to produce various progressive changes through critical conditions.

References

[1] Miura Y., Complex texture and structure of shocked quartz mineral with graphite grain. *Acta Cry st.* (IUCR), 2008, 64, 55.

[2] Miura Y., Shocked carbonate minerals formed by natural and artificial impact processes, *Frontiers in Mineral Sciences 2007* (Univ. of Cambridge, UK), 223-223.

[3] Miura Y., Evidence for shock wave effect of meteoritic impact. *Shock Waves Journal* (Springer-Verlag), 1, 35-41.

MS08-P02

Local structure of Co-based additives in $LiBH_4$ + $LiNH_2$ system

Takashi Asano[1,2], Daiju Matsumura[2], Yuka Okajima[2], Hai-Wen Li[3], Shin-ich Orimo[3], Hikaru Terauchi[1], Isao Takahashi[1] and Yasuo Nishihata[2]

[1]*School of Science and Technology, Kwansei-Gakuin University, Sanda 669-1337, Japan*
[2]*Japan Atomic Energy Agency, 1-1-1 Koto, Sayo, Hyogo 679-5148, Japan*
[3]*Institute for Materials Research, Tohoku University, Sendai 980-8577, Japan*
E-mail: cyk28483@kwansei.ac.jp

Hydrogen is the favored energy carriers for the future society, because it has high energetic power and only produces water by combustion. Considering the utilization of hydrogen as the mobile application, it becomes important to exploit a novel hydrogen-storage method with minimum risks. Promising materials for that purpose are light-weight complex hydrides, since they have a high storage capacity per unit volume. $LiBH_4$ + $LiNH_2$ system is one of the high capacity hydrogen storage systems. Mixture of $LiBH_4$ and $LiNH_2$ can form a stable compound. Recently, it has been reported that a doping of $CoCl_2$ decreases the dehydrogenation temperature of mixture of $LiBH_4$ and $LiNH_2$ [1].

In order to understand the reaction mechanism and the influence of $CoCl_2$ additive, we have performed x-ray absorption fine structure (XAFS) spectroscopy at the Co *K*-edge. Moreover, we have also used dispersive XAFS equipment which consists of a curved crystal and a position sensitive detector, with a simultaneous measurement of quadrupole mass spectroscopy (QMS).

The sample of $LiBH_4$ + $LiNH_2$ + 5wt% $CoCl_2$ was prepared by ball milling for 2 h. We observed the XAFS spectra for the milled sample and the dehydrogenated sample as shown in Figures 1 and 2. With the analysis of the extended energy region of the spectra, it is deduced that the Co atoms form a mixed structure of metal and boride phase at 298-473 K for the milled sample. At 673 K, the amount of the boride phase is increased, which is connected to the increase of the peak at 7727 eV. A large metal Co particle is formed at 873 K with a complete different structure of XAFS spectra. The dehydrogenated sample shows a similar structural change with the milled sample as temperature increases. However, the amount of the transformation is not as large as the milled sample undergoes. These results may indicate that the structural transformation of the Co metal phase influences the decrease of the dehydrogenation temperature for the $LiBH_4$ + $LiNH_2$ system.

References

[1] Tang W. S., Wu G., Liu T., Wee A. T. S., Yong C. K., Xiong Z., Hor A. T. S., Chen P., "Cobalt-catalyzed hydrogen desorption from the $LiNH_2$–$LiBH_4$ system", *Dalton Transactions*, No. 18, (2008), pp 2395-2399.

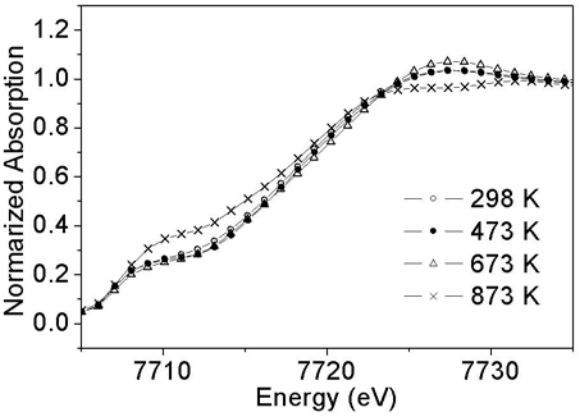

Figure 1. XAFS spectra for the milled samples.

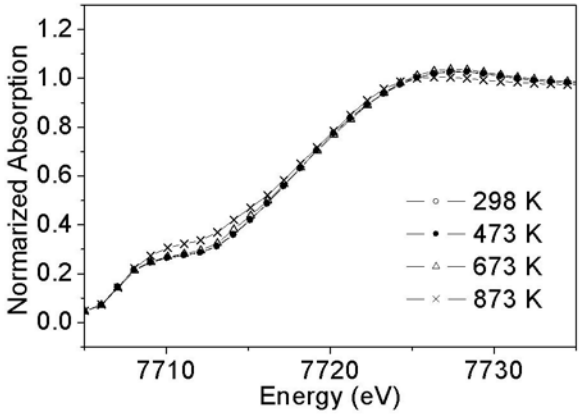

Figure 2. XAFS spectra for the dehydrogenated samples.

Molecular dynamics simulations of structure and dynamics of organic molecular crystals

Alexandra Nemkevich[1], Hans-Beat Bürgi[2], Mark A. Spackman[1] and Ben Corry[1]

[1]*School of Biomedical, Biomolecular and Chemical Sciences, University of Western Australia, Perth, Australia*
[2]*Laboratory of Crystallography, University of Berne, Berne, Switzerland*
E-mail: nemkea01@uwa.edu.au

Atomic vibrations and reorientations of part or all of a molecule affect a broad range of bulk crystal properties. Most of our knowledge of this motion in crystals comes from various kinds of diffraction, solid state NMR, IR and Raman experiments, but molecular dynamics (MD) provides an alternative method of investigating motion in crystals. It provides direct information on the displacements, types of motion and frequencies of such processes. However, it is still difficult to assess the reliability of MD simulations at reproducing the dynamics aspects of molecules in crystals. We have begun to address this question by examining how well classical MD simulations reproduce structure and dynamics in a sample of organic molecular crystals.

Model compounds covering a range of polarity and flexibility have been simulated using GAFF, CHARMM22, OPLS and MM3 force fields. Results for molecular and crystal structure and thermal motion, including molecular reorientations and internal rotations, have been compared between force fields and with experimental data. The MM3 force field does not perform well in condensed phase simulations, while GAFF, CHARMM and OPLS perform similarly. Molecular and crystal structures are generally reproduced well, with a few exceptions. Atomic displacement parameters (ADPs) are generally underestimated and, although on the order of experimental values, have a relative error of up to 50%. Examples of molecular reorientation and internal rotation observed in the simulations include in-plane reorientations of benzene, methyl rotation in alanine, decane, and isopropylcyclohexane, pyramidal inversion of nitrogen in amino groups and rotation of amino groups around the C-N bond. Frequencies of such dynamic processes were calculated, as well as thermodynamic properties for reorientations in benzene and alanine.

We conclude that MD simulations can be used for qualitative analysis, while quantitative results should be taken with caution. It is important to compare the simulations with as many experimental quantities as available before using them to study or quantify crystal properties not available from experiment.

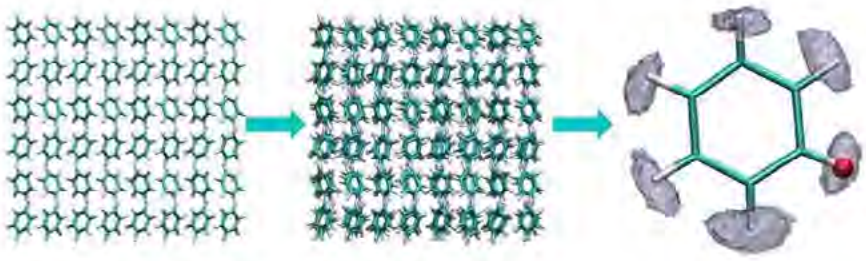

Figure 1. Schematic representation of the simulations. Left to right: the crystal structure of benzene; a snapshot from a CHARM22 simulation at 218 K; probability isosurfaces for a single hydrogen atom.

MS08-P04

Crystal structure of new cobaloxime complex with photochromic azobenzene derivatives as axial base ligand

Hiroki Yamagiwa1, Akiko Sekine2 and Hidehiro Uekusa 2

1Department of Chemistry, Tokyo Institute of Technology, Tokyo, 152-8551, Japan
2Department of Chemistry and Materials Science, Tokyo Institute of Technology, Tokyo, 152-8551, Japan
E-mail: yamagiwa.h.aa@m.titech.ac.jp

It has been reported that β-cyanoethyl cobaloxime complex isomerizes to α-cyanoethyl one by the photoirradiation of visible light in the crystalline-state. On the other hand, azobenzene is well-known for its photochromic reaction: it reversibly isomerizes from trans- to cis-azobenzene. In order to control the reactivity of photochromism by changing the environment in the crystalline-state, we investigated new β-cyanoethyl cobaloxime complexes with azobenzene derivatives as axial base ligands.

(β-cyanoethyl)(4-aminoazobenzene)cobaloxime was synthesized. Two pseudo-polymorphic single crystals, solvate 1 and unsolvate 2, were obtained from methanol solution (methanol:water = 6:1) and ethanol, respectively. The structures were determined by single crystal X-ray analysis. The crystallographic data are (1): a =16.4674(4) Å, b =10.0509(2) Å, c =32.1190(6) Å, β =95.810(1) °, V =5288.78(6) Å3, monoclinic, space group: P21/c, Z=8, R1= 0.045, (2): a =23.341(3) Å, b =6.5350(7) Å, c =16.9110(19) Å, = 91.508(6) °, V=2578.6(5) Å3, monoclinic, space group: P21/c, Z= 4, R1= 0.054. In the crystal of 1 (Fig. 1), two cobaloxime complexes, molecule A and molecule B, with one crystal water and one methanol molecule are present in the asymmetric unit. The coordinated 4-aminoazobenzenes are planar, and have trans conformation in both A and B. The conformation of -cyanoethyl group of molecule A is oriented parallel to the cobaloxime plane, while that of molecule B is oriented perpendicular to the cobaloxime plane. The cobaloxime molecules are connected each other by hydrogen bond via solvent water and methanol. For 2, there is one independent molecule. The 4-aminoazobenzene is also planar, and has trans conformation. The conformation of -cyanoethyl group is oriented perpendicular to the cobaloxime plane.

The crystalline-powder cobaloxime complexes were irradiated with each of UV and visible light to examine the photochromic reaction of 4-aminoazobenzene and photoisomerization of -cyanoethyl group in crystals 1 and 2. The change of UV-vis and IR spectra for 1 was observed by the preliminary measurement.

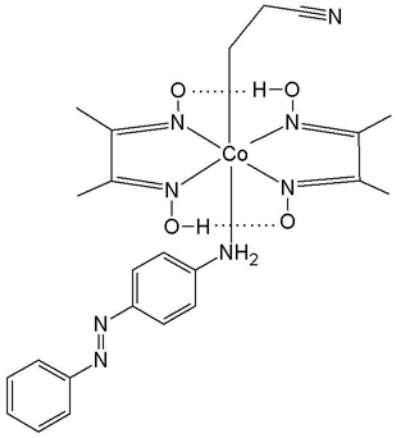

Scheme 1. (β-cyanoethyl)(4-aminoazobenzene)-cobaloxime complex

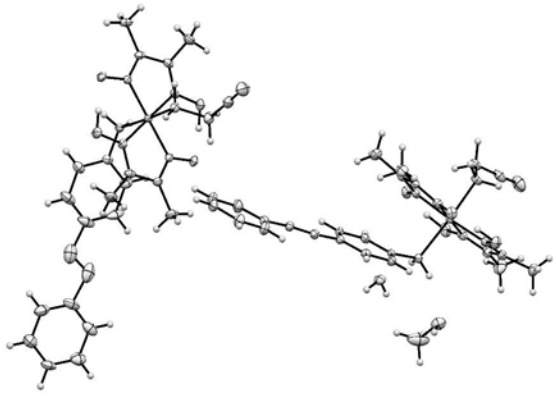

Fig.1 Molecular structure of 1

MS08-P05

Controllable photochromism in hybrid type cobaloxime complex

Akiko Sekine[2], Sayaka Ina[2], Hiroki Yamagiwa[1], Kohei Johmoto[2] and Hidehiro Uekusa [2]

[1]*Department of Chemistry, Tokyo Institute of Technology, Tokyo, 152-8551, Japan*
[2]*Department of Chemistry and Materials Science, Tokyo Institute of Technology, Tokyo, 152-8551, Japan*
E-mail: asekine@chem.titech.ac.jp

Photochromic materials have attracted attention over recent years. In order to create new materials that have dynamically controllable photochromism, we designed new hybrid type cobaloxime complexes with photochromic compounds. In such crystals, it is expected that photochromism changes dynamically associating with crystalline-state photoisomerization of cobaloxime complexes. In this study, (1)salicylideneaniline and (2) azobenzene derivatives are used as photochromic compounds. For (1), crystalline-state photochromism is expected because conformational change of salicylideneaniline is small during the photochromic reaction. On the other hand, for (2), it is expected that the phorochromism occur effectively by controlling the reaction cavity in the crystal, although conformational change of the azobenzene derivative is large.

(β-cyanoethyl)(*N*-(3,5-di-*tert*-butylsalicylidene)-4-aminopyridine)cobaloxime(Co-SAP) and (β-cyanoethyl)(4-aminoazobenzene)cobaloxime for (1) and (2), respectively, were successfully synthesized. For Co-SAP, two pseudo-polymorphic single crystals, unsolvate **1** and diethylether solvate **2,** were obtained from diethylether solutions and their structures were characterized by single crystal X-ray diffraction analyses. The dihedral angle of phenyl rings of SAP are 87.7(2)° in crystal **1** and 58.8 (2)° and 37.8(2)° in crystal **2**, which are larger than that of salicylideneaniline crystal. This is excpected to be more photoreactive in both crystals **1** and **2** than in salicylideneaniline crystal. In the photoreactivity measurement of **1,** the SAP part displayed the photochromism upon UV irradiation as indicated by the color change from yellow to orange in the solid state. Also, after the photoisomerization of the cobaloxime part occurred upon visible light irradiation, the photochromism of the SAP part was also observed by UV light, however, the lifetime of colored species became significantly shorter. It would be explained that the reaction cavity around the SAP part was modified by solid state photoisomerization reaction of alkyl group of the cobaloxime complex. In this study, further relationship between the structure dependent photochromic reactivity of SAP and isomerizaion of cobaloxime complex in the crystalline state is investigated.

Table 1. Crystal data

crystal	**1**	**2**
a / Å	8.8424(5)	12.4914(18)
b / Å	12.1719(6)	16.480(2)
c / Å	16.6623(8)	19.481(2)
α / Å	109.0140(10)	69.184(3)
β / Å	95.903(2)	89.726(3)
γ / Å	103.593(2)	71.056(3)
V / Å^3	1616.29(14)	3517.7(8)
Space Group	P-1	P-1
Z	2	4
R	0.0550	0.0682

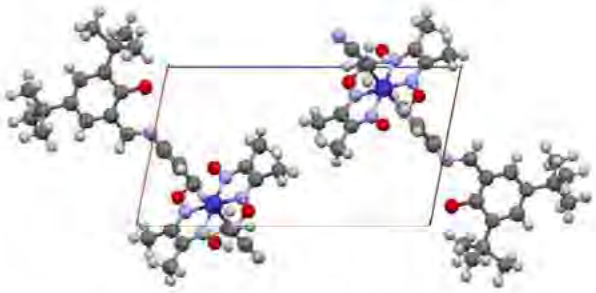

Fig.1 Crystal structure of **1**

MS08-P06

Dehydration induced color switching of isophthalic acid crystal

Aya Sakon[1], Akiko Sekine[1], Hidehiro Uekusa[1]

[1] *Tokyo Institute of Technology, Japanese, 2-12-1 Ookayama, Meguro-ku, Tokyo, 152-8551, Japan*
E-mail: sakon.a.aa@m.titech.ac.jp

Structural transformation by dehydration / hydration process often causes physicochemical property change, so the phenomenon is important in the field of materials science, such as pharmaceuticals. Especially, among such changes, the color switching is interesting because of its application for sensing materials or optical information storage devices.

In this study, crystal color switching caused by the dehydration / hydration structural transformation of 5-aminoisophthalic acid is reported. The colorless hemihydrate crystal transformed to a new yellow crystalline phase when heated to 140°C, and it returned to original hemihydrate phase when subjected to high humidity condition. The new yellow phase was identified as unsolvated crystal by TG/DTA measurement. Interestingly, the dehydration process with color switching also proceeded when the hemihydrate crystal was exposed to acetonitrile or ethanol vapor, thus indicating this reversible structure and color-switching phenomenon is a kind of "vapochromism".

The single crystal of the unsolvated phase was obtained by recrystallization from methanol. The X-ray structural analysis showed that it crystallized in the orthorhombic space group *Pbcn* with cell parameters a =3.6585(3), b =14.7575(12) and c =14.6863(11)Å. The crystal structure has hydrogen bonded one-dimensional chain structure along the c-axis via carboxyl group dimer motif. In the crystal, two aromatic rings are parallel with the distance of 3.34Å indicating π-π interaction. This intermolecular interaction would explain the yellow color of the crystal. In the hemihydrate crystal, the molecule exists as a zwitter ionic form (COO^- and $NH3^+$) caused by carboxylic H transfer to amino N, so it does not forming carboxyl group dimer for the carboxylate group.

It is noteworthy that the proton transferring zwitter ion formation and the rearrangement of hydrogen bonding network were also occurred during the dehydration / hydration reversible structural transformation.

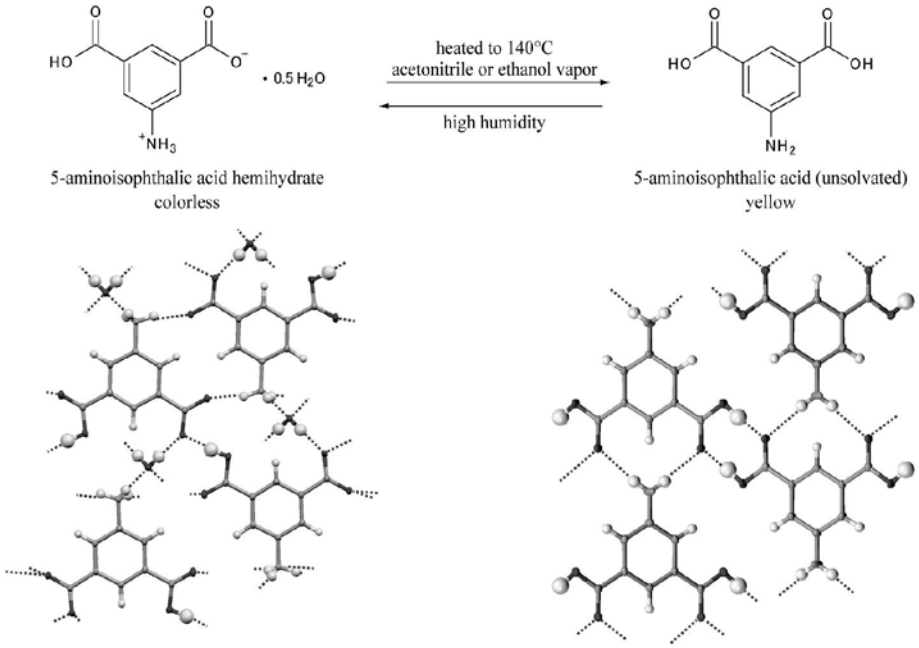

Hydration and dehydration transformation of sodium naproxen pseudopolymorphs

Takashi Miyamoto[1], Akiko Sekine[1], Hidehiro Uekusa[1]

[1] *Tokyo Institute of Technology, Japanese, 2-12-1, Oookayama, Meguro-ku, Tokyo, 152-8551, Japan*
E-mail: miyamoto.t.aa@m.titech.ac.jp

Hydrated forms of API (Active Pharmaceutical Ingredient) is often used for pharmaceutical products. Their hydration and dehydration transformation are important in the field of pharmaceutical science because the hydration/dehydration induces crystal structure changes which largely affect on the chemical and physical properties. Sodium Naproxen ((S)-6-Methoxy-α-methyl-2-naphthaleneacetic Acid Sodium Salt, Fig.1) is widely used as nonstereoroidal anti-inflammatory drug (NSAID). It is known that depending on recrystallization process or environmental conditions, sodium naproxen has five pseudopolymorhs, i.e., one anhydrous form (ASN), one monohydrated form (MSN), two dihydrated forms (DSN, CSN), and one tetrahydrated form (TSN).

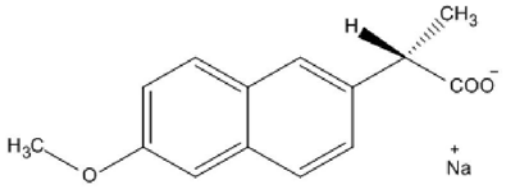

(Fig.1) sodium naproxen

In order to clarify the hydration/dehydration process of sodium naproxen from structural points of view, the crystal structures of pseudopolymorphs were analyzed and compared. Among them, the most hydrated form, TSN, is attractive because it is the starting crystal to transform to different low hydrated crystals. In this study, hydration and dehydration behavior of tetrahydrated sodium naproxen is investigated through the crystal structure analysis.

The crystal structure of tetrahydrated form (TSN) was determined by single crystal X-ray diffraction analysis. The crystal structure of TSN has triclinic system with space group $P1$ (a = 7.091(3) Å b = 11.132(5) Å c = 20.645(9) Å α = 82.208(9)° β = 81.989(9)° γ = 89.884(9)°) and contains four independent sodium cations, naproxen anions and sixteen water molecules in the asymmetric unit. In the crystal, hydrophilic layer structures composed of sodium cations and water molecules are formed parallel to the *ab*-plane and layers of naproxen anions are stacked on them (Fig.2). Among sixteen water molecules, fourteen of them have interactions with sodium cations and the others are situated beside the Na^+/H_2O layer without interactions to the sodium cations. It is interesting that the oxygen atoms of carboxyl group have no direct interaction with sodium cations in contrast to ASN and MSN. The hydration environment of sodium cations is found to reflect the hydration number of each pseudopolymorphs. The numbers of Na-O (COO^- and H_2O) interactions for ASN, MSN, and TSN are four, five, and six for each sodium cations, respectively. In their structures, the inserted water molecules by hydration process mainly contribute to the separation of naproxen anion and Na^+. To complete isolated Na^+/H_2O layer in which all sodium cations are in six coordinated environment.

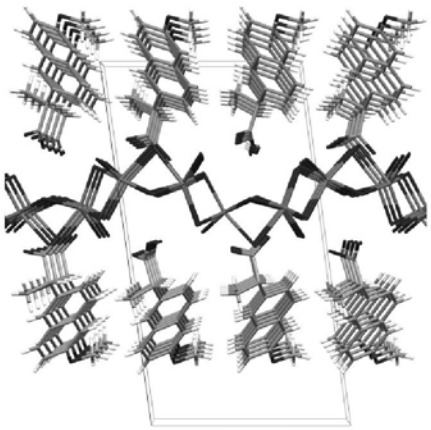
(Fig.2) the crystal structure of tetrahydrated form of sodium naproxen

Single crystal structure analyses of photo-excited states of photoluminescent hexanuclear d^{10} metal complexes

Yoshiki Ozawa[1], Toru Ishida, Kimihiro Kimura and Koshiro Toriumi
Department of Material Science, University of Hyogo, 3-2-1 Kouto, Kamigori-cho, Hyogo 678-1297, Japan
E-mail: ozawa@sci.u-hyogo.ac.jp

Hexanuclear metal complexes of Cu(I) or Ag(I) $[M_6(pyt)_6]$ (M = Cu, Ag; pyt^- = pyridinethiolato) (Fig. 1) give intense luminescence under UV illumination in the solid-state. The nature of the emission has been assigned to a triplet multi-metal cluster-centered (^{3}CC) transition state like as in the halogen bridged Cu(I) tetranuclear cubane-like cluster complexes. [1,2] On the photo-excited state, the metal-cluster core is expected to be shrunk because of an electron migration to a bonding-character CC orbital (Fig. 2). To figure out the photo-emission process by direct observation of the molecular distortion, we have performed single crystal X-ray structure analyses at the photo-excitation states.

Single crystal X-ray diffraction experiments under photo-irradiation were performed at the SPring-8 BL02B1 station. A single crystal of copper(I) complex with the ethyl-pyridinethiole ligand $[Cu_6(Et\text{-}pyt)_6]$ (Et-pytH=6-ethylpyridine-2-thione) was mounted on the vacuum camera at 25 K was used for X-ray diffraction data collection under UV laser (325/442 nm, 0.03/0.1 W) irradiation. Photo-difference Fourier syntheses at the section of the triangle Cu_3 plane perpendicular to the virtual 3-fold axis of the molecule show that two of three Cu atoms move toward to the remaining Cu atom (Fig. 3). This indicates that the contraction of Cu-Cu atomic distance will occur at the photo-excitation state resulting in shrinkage of the metal cluster core. We have also performed the same experiments for the silver complex $[Ag_6(Et\text{-}pyt)_6]$. The observed peaks and holes of charge densities in the photo-difference Fourier maps are similar to that in the Cu crystal, although their amplitude is below the significant levels.

Fig. 1

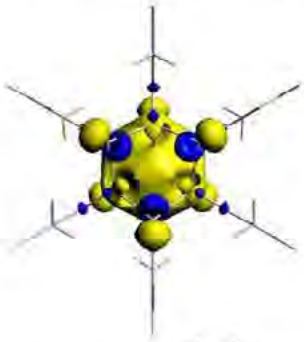

Fig. 2

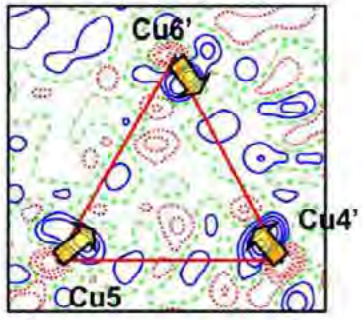

Fig. 3

Fig.1 Structure of $[M_6(Et\text{-}pyt)_6]$(M = Cu, Ag). **Fig. 2** Unoccupied CC orbital by DFT calculation. **Fig. 3** Photo-diffrence Fourier map in the section of the plane including three Cu atoms. Arrows indicate possible shift directions of the metal atoms under the photoirradiation.

References

[1] Xie H., Kinoshita I., Karasawa T., Kimura K., Nishioka T., Akai I., Kanemoto K., "Structure Stu dy and Luminescence Thermochromism in Hexanuclear 6-Methyl-2-Pyridinethiolato Copper(I) Cry stals," *J. Phys. Chem. B*, Vol. 109 No. 19,(2005), pp 9339-9345.

[2] Ford P. C., Vogler A., "Photochemical and Photophysical Properties of Tetranuclear and Hexanuclear Clusters of Metals with d^{10} and s^2 Electronic Configurations", *Acc. Chem. Res.* Vol. 26, (1993), pp 220-226.

MS08-P09

Selective pseudo-polymorphic transformation pathways of organic crystalline materials established using powder X-ray diffraction analysis

Kotaro Fujii[1], Yasunari Ashida[1], Hidehiro Uekusa[1], Fang Guo [2], Kenneth D.M. Harris[2]

[1] *Department of Chemistry and Materials Science, Tokyo Institute of Technology, Japan*
[2] *School of Chemistry, Cardiff University, Cardiff CF10 3AT, Wales, UK*
E-mail : *fujii.k.aa@m.titech.ac.jp*

Pseudo-polymorphic transformations (desolvation, solvation and solvent exchange) are very important phenomena in the field of material science because of their potential to improve and/or control the solid-state properties of the target materials. However, such transformations have not been completely understood because of the difficulty to obtain the structural information of the resulted phase which is mainly caused by the disintegration of the single crystalline form of the parent phase during the transformations. In such cases, the crystal structure determination from the powder X-ray diffraction data is clearly most powerful technique and we have succeeded to reveal several phenomena by using this strategy.[1-3]

Recently, the methanol solvate crystalline phase (**M**) of benzene-1,2,4,5-tetracarboxylic acid was found to selectively transform into two different phases, hydrate phase (**H**) under the presence of atmospheric water vapor and non-solvate phase (**N**) under the absence of atmospheric water vapor.[4] In order to reveal the mechanistic aspects on the selective transformation, the crystal structures of the phase **M** and **N** were determined by the single and powder X-ray diffraction analysis, respectively (crystal structure of **H** is known). All crystal structures have sheet like structure and the observed structural similarities clearly explain the facile transformation from phase **M** into **H** or **N**. Interestingly, phase **M** (1.55 g cm^{-3}; –180 °C) has significantly lower density than those of **H** (1.67 g cm^{-3}; –113 °C) and **N** (1.63 g cm^{-3}; 27 °C). This fact can be explained from the loosely packed methanol molecules which make a large methanol channel in phase **M** and the methanol molecules may easily release through this channel with the final outcome of the transformation is altered by the presence of the atmospheric water.

References

[1] S. Hirano, S. Toyota, F. Toda, K. Fujii, H. Uekusa, *Angew. Chem. Int. Ed.*, 2006, 45(36), 6013.
[2] K. Fujii, Y. Ashida, H. Uekusa, S. Hirano, S. Toyota, F. Toda, Z. Pan, K. D.M. Harris *Cryst. Growth Des.*, 2009, **9**, 1201.
[3] K. Fujii, H. Uekusa, N. Itoda, G. Hasegawa, E. Yonemochi, K. Terada, Z. Pan, K. D.M. Harris, *J. Phys. Chem. C*, (2010), 114(1), 580.
[4] K. Fujii, Y. Ashida, H. Uekusa, F. Guo, K. D.M. Harris, *Chem. Comm.*, (2010), 46(24), 4264.

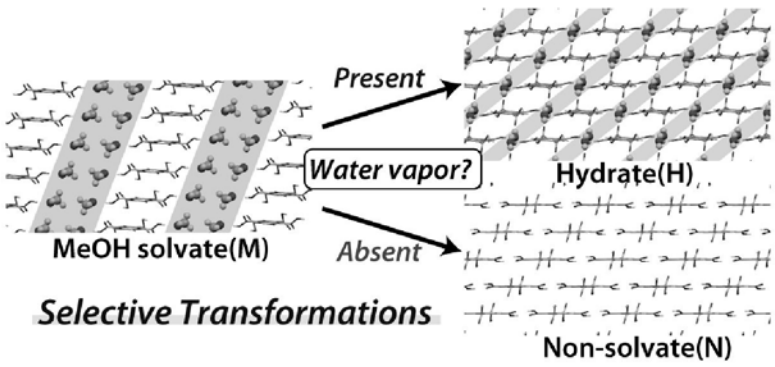

MS08-P10

New insights into molecular mechanisms of photoinduced and thermally induced effects in crystals

Panče Naumov

Department of Material and Life Science, Graduate School of Engineering, Osaka University, 2–1 Yamada-oka, Suita, Osaka, Japan
E-mail: npance@wakate.frc.eng.osaka-u.ac.jp

Understanding of the physicochemical processes in thermally active or photoactive materials requires detailed knowledge of the molecular mechanism of the related changes in their structures. During the last several years, in our laboratory we have employed several X-ray diffraction (XRD) techniques in combination with other analytical (microscopic, spectroscopic and thermoanalytical) methods to study, at atomic-scale resolution, the structural (molecular and supramolecular) perturbations which can be induced in a variety of small-molecule crystalline materials by utilizing light excitation, changes in temperature, or other external stimuli. The XRD techniques which we usually employ in such studies including steady-state or time-resolved X-ray single crystal/powder photodiffraction (photocrystallography) and variable-temperature (XRD). The results have provided direct insight into the structures of unstable species and dynamic solid-state phenomena, including electronic transitions.
In this talk, our recent results with these techniques applied on several solid-state systems which are of importance for electronics/spintronics, nanotechnology, medical or bioanalytical applications will be summarized. In particular, the results include photodimerizations[1,2], gradual/sharp phase transitions[3-6], thermosalient (jumping) effects[3], photomechanical effects[2], solid-state rearrangements[6-10], unstable biological molecules[11], photomagnetization effects and photoinsuced phase transitions of persistent organic radicals[6], unstable radical transients[8] or uncommon radical states[10], photochromic[12] and thermochromic[13-15] slid-state species, very unstable crystals[16], and other systems.

References

[1] Yang, S.-Y., Naumov, P. and Fukuzumi, S., *J. Am. Chem. Soc.* **2009**, *131*, 7247.
[2] Naumov, P., Kowalik, J., Solntsev, K. M., Baldridge, A., Moon, J.-S., Kranz, C. and Tolbert, L. M., *J. Am. Chem. Soc.* **2010**, *132*, 5845.
[3] Skoko, Z., Zamir, S., Naumov, P. and Bernstein, J., submitted for publication.
[4] Naumov, P., Sakurai, K., Asaka, T., Belik, A. A.;, Adachi, S., Takahashi, J. and Koshihara, S., *Chem. Commun.* **2006**, *14*, 1491.
[5] Naumov, P., Sakurai, K., Asaka, T., Belik, A. A., Adachi, S., Takahashi, J. and Koshihara, S., *Inorg.Chem.* **2006**, *45*, 5027.
[6] Naumov, P., Hill, P. J., Sakurai, K., Tanaka, M. and Ariga, K., *J. Phys. Chem.* **2007**, A*111*, 6449.
[7] Naumov, P., Makreski, P. and Jovanovski, G., *Inorg. Chem.* **2007**, *46*, 10624.
[8] Naumov, P., Sakurai, K., Tanaka, M. and Hara, H., *J. Phys.Chem.* **2007**, B*111*, 10373.
[9] Naumov, P., Makreski, P., Petrusevski, Gj., Runcevski, T. and Jovanovski, G. submitted.
[10] Naumov, P., Topcu, Y., Eckert-Maksić, M., Pavošević, F., Kochunnoonny, M. and Glasovac, Z., submitted.
[11] Naumov, P., Ozawa, Y., Ohkubo, K. and Fukuzumi, S., *J. Am. Chem. Soc.* **2009**, *131*, 11590.
[12] Naumov, P., Yu, P. and Sakurai, K., *J. Phys. Chem.* **2008**, A*112*, 5810.
[13] Naumov, P., Lee, S. C., Ishizawa, N., Jeong, Y. G., Chung, I. H. and Fukuzumi, S., *J. Phys. Chem.* **2009** A*113*, 11354.
[14] Naumov, P., Ishizawa, N., Wang, J., Pejov, Lj. and Lee S. C., submitted.
[15] Naumov, P., Nukui, A., Sakurai, K, Tanaka, M., et al. *Chem. Commun.* **2007**, *4*, 347.
[16] Petrusevski, Gj., Naumov, P., Jovanovski, G. and Bogoeva-Gaceva, G. *ChemMedChem* **2008**, *3*, 1377.

MS08-P11

The origin of solid-state thermochromism of polycyclic overcrowded enes: A Hundred-year old mystery resolved

Panče Naumov[1], Nobuo Ishizawa[2], Jun Wang[2], Ljupčo Pejov[3] and Sang Cheol Lee[4]

[1]*Graduate School of Engineering, Osaka University, 2-1 Yamada-oka, Suita, Osaka 565-0871, Japan*
[2]*Ceramics Research Laboratory, Nagoya Institute of Technology, Tajimi, Gifu 507-0071, Japan*
[3]*Ss. Cyril and Methodius University, Arhimedova 5, MK-1001 Skopje, Macedonia*
[4]*Kumoh National Institute of Technology, Gumi 730-701, Korea*
E-mail: npance@wakate.frc.eng.osaka-u.ac.jp

From the first report of the thermochromism of the solutions of bianthrone (**2**, Figure 1) by Meyer in 1909,[1,2] to later observations using crystalline overcrowded polycyclic aromatic enes (PAEs), there has been continual interest in this phenomenon by organic chemists. Despite the extensive theoretical treatment given to the *in vacuo* models, a scientific explanation for the interplay among the twisting, folding and bending (Figure 2) in the evolution of the high-temperature (HT) thermochromic forms of crystalline overcrowded PAEs has remained unresolved for a century.

We report herein the crystal structures of the indanedione **1** (2-(thioxanthen-9-ylidene)indane-1,3-dione) and bianthrone **2** (Figure 1) determined at temperatures up to the melting point with a genuine setup for *in situ* single-crystal HT XRD. Surprisingly, the results showed the solid-state thermochromic change of the PAEs **1** and **2** is not a result of switching between different conformations. Instead, the change of the excited-state potential surface appears to be a dynamic effect, and was identified as a result of the large molecular distortions due to increased thermal atomic oscillations. The excited-state calculations (Born-Oppenheimer molecular dynamics (BOMD) simulations, followed by TD-DFT calculations on selected snapshots from the equilibrated BOMD trajectories) substantiated the results, and confirmed that the solid-state thermochromism is effected by modification of the excited-state potential energy surface instigated by strong thermal oscillations. Moreover, the HT electronic spectra indicated that the thermochromism of crystalline PAEs is not an entirely reversible phenomenon, and that more than one molecular mechanism is necessary to account for the color change of different PAEs.

References

[1] Meyer, H. Über neue Reduktions- produkte des Anthrachinons. *Ber. Dtsch. Chem. Ges.* **1909**, *42*, 143–145.
[2] Meyer, H. Über neue Derivate des Anthrachinons (erste Mitteilung über Zweikernchinone). *Monatsh. Chem.* **1909**, *30*, 165–177.

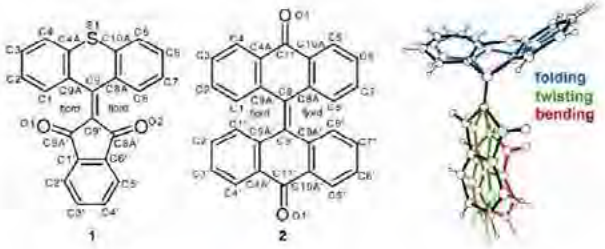

Figure 1. Chemical structures, with atom labeling, of the PAEs **1** and **2**. Right: schematic representation of the folding, twisting and bending of PAEs, exemplified with portions of **1** and exaggerated for clarity.

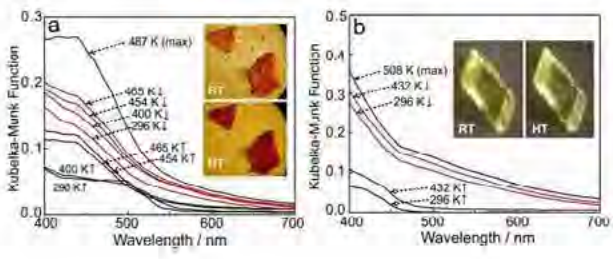

Figure 2. Temperature effects on the reflectance UV-visible spectra and single crystals of **1** (a) and **2** (b) induced by heating (black curves, ↑) and cooling (red curves, ↓) (rate: 2 K/min for **1** and 5 K/min for **2**).

MS08-P12

New type of dual solid-state thermochromism: Modulation of intramolecular charge transfer by intermolecular $\pi-\pi$ interactions, kinetic trapping of aci-nitro group and reversible molecular locking

Panče Naumov[1], Sang Cheol Lee[2], Nobuo Ishizawa[3], Young Gyu Jeong[2], Ihn Hee Chung[2] and Shunichi Fukuzumi[1]

[1]*Graduate School of Engineering, Osaka University, 2–1 Yamada-oka, Suita, Osaka 565–0871, Japan*
[2]*Kumoh National Institute of Technology, Gumi 730–701, Korea*
[3]*Ceramics Research Laboratory, Nagoya Institute of Technology, Tajimi, Gifu 507–0071, Japan*
E-mail: npance@wakate.frc.eng.osaka-u.ac.jp

On heating above room temperature, some crystalline polymorphs of the 1,3-bis(hydroxyalkylamino)-4,6-dinitrobenzenes (BDB*n*, *n* = 2 – 5) exhibit "dual" thermochromism: *gradual* color change from yellow to orange at lower temperatures, and *sharp* color change from orange to red at higher temperatures. These two thermochromic changes are related to different solid-state processes: the *gradual* thermochromic change is related to decreased distance and weakened π–π interactions between the stacked benzene rings, whereas the *sharp* thermochromic change is assigned to intramolecular transfer of one amino proton, whereupon the aci-nitro form is thermally populated.[1]

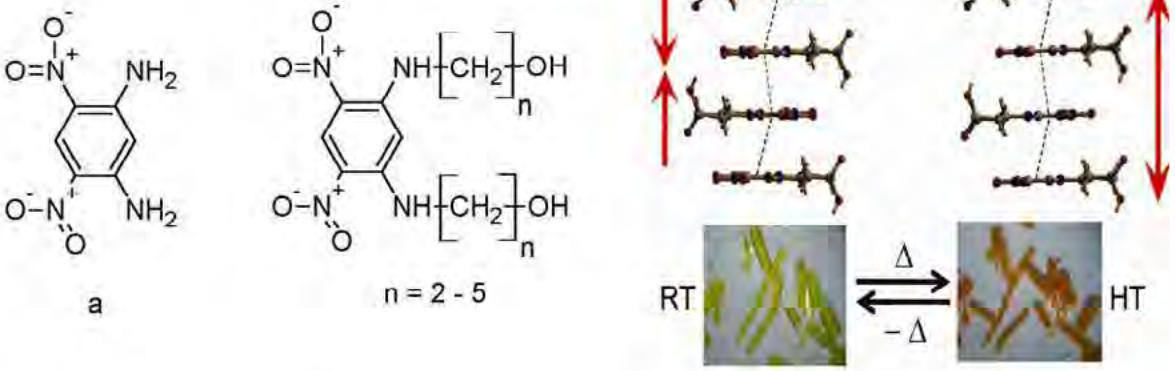

Reference

[1] Naumov, P., Lee, S. C., Ishizawa, N., Jeong, Y. G., Chung, I. H. and Fukuzumi, S., "New Type of Dual Solid-State Thermochromism: Modulation of Intramolecular Charge Transfer by Intermolecular π–π Interactions, Kinetic Trapping of Aci-Nitro Group and Reversible Molecular Locking", *J. Phys. Chem.* **2009**, A*113*, 11354—11366.

MS11-P01

Room temperature ferromagnetism in pure CdSe and CdSe:Ni nanorods

Sanjeev Kumar[1], Sunil Kumar[2], NK Verma[2]

[1]*University College of Engineering, Punjabi University, Patiala – 147 002, India*
[2]*School of Physics and Materials Science, Thapar University, Patiala – 147 004, India*
E-mail: sanjeev04101977@gmail.com

We report here room temperature ferromagnetism in CdSe and Ni-doped CdSe nanorods. Pure and 3% Ni-doped CdSe nanorods are synthesized by using low temperature solvothermal process. X-ray diffractogram (XRD) depicts the wurtzite (hexagonal) structure of the CdSe nanorods. The XRD peaks shift to larger angles with Ni substitution in CdSe nanorods. From Transmission Electron Microscopy (TEM) analysis, it is found that the average diameter of the CdSe nanorods is about 4-5 nm having lengths of about 50 nm. Magnetic studies are made by using Superconducting Quantum Interference Device (SQUID). The room temperature ferromagnetic behaviour has been shown by both pure CdSe as well as Ni-doped CdSe nanorods.

References

[1] Beaulac R., Archer P.I., Oshsenbein T., Gamelin D.R., Mn^{2+}-doped CdSe quantum dots: new i norganic materials for spin-electronics and spin-photonics" *Advanced Functional Materials*, 18, (2008), 3873-3891.

[2] Singh S.B., Limaye M.V., Date S.K., Gokhale S., Kulharni S.K., "Iron substitution in CdSe na noparticles: magnetic and optical properties" *Physical Review B*, 80, (2009) 235421-8.

MS11-P02

Doping effects of multiferroic $BiFeO_3$ ceramics

Jun-Ki Hong[1,2], Jin-Ho Joo[2] , J.-G. Park[3], Seongsu Lee[1]

[1]*Neutron Science Division, Korea Atomic Energy Research Institude (KAERI), Daejeon, 305-353, Korea*
[2]*School of Advanced Materials Science and Engineering, SungKyunKwan University, Suwon, Gyeonggi, 440-746, Korea*
[3]*Department of Physics and Astronomy, Seoul National University, Seoul, 151-747, Korea*
E-mail: whoaussy@naver.com

Multiferroics, materials combining multiple order parameters, offer an exciting way of coupling phenomena such as electronic and magnetic order. The coexistence of different order parameter permits potential applications in information storage, spintronics, and magnetic or electric field sensors. The perovskite $BiFeO_3$(BFO) is known to be antiferromagnetic below the Neel temperature of 640K and ferroelectric with a high Curie temperature of 1100K. According to the previous doping studies of BFO, it is likely that non-stoichiometry and second-phase formation are the factors responsible for leakage current in BFO. It has been suggested that oxygen nonstoichiometry leads to valence fluctuations of Fe ions in BFO, resulting in high conductivity. To reduce the large leakage current of BFO, one attempt is to make donor-doped BFO compounds.

In this study, we try to generate the single phase multiferroric material with ferromagnetic property at room temperature. $Bi_{0.9}Ba_{0.1}Fe_{(1-X)}Mn_{(x)}O_3$ ceramics have been fabricated by a solid-state reaction method. The crystal and magnetic structure are studied using x-ray diffraction (XRD) and neutron powder diffraction. The XRD data shows the single phase crystal structure similar with un- doped BFO. With increasing Mn doping concentration, the MH data indicates the enhancement of ferromagnetic component. We will discuss the magnetic and electric property change of doped BFO polycrystalline to realize the multiferroric single crystal with combining ferromagnetic and ferroelectric.

References

[1] S.-W. Cheong and M. Mostovoy, "Multiferroics: a magnetic twist for ferroelectricity", Nat. Mater. 6, 13-20 (2007).
[2] Seongsu. Lee et al., "Single ferroelectric and chiral magnetic domain of single-crystalline $BiFeO_3$", Phys. Rev. B 78, 100101 (2008).
[3] Sosnowska, I. et al., "Spiral magnetic ordering in bismuth ferrite", J. Phys. Solid State Phys.15,4835-4846(1982)

Magnetic and dielectric properties of multiferroic $YMn^{4+}(Mn_{1-x}T_x)^{3+}O_5$ (T = Ga and Fe)

Hiroyuki Kimura[1], Kenta Yamazaki[1], Yuma Sakamoto[1], Mamoru Fukunaga[1], Yukio Noda[1], Nobuyuki Abe[1], Taka-hisa Arima[1] and Haruhiro Hiraka[2]

[1]*Institute of Multidisciplinary Research for Advanced Materials, Tohoku University, Sendai 980-8577, Japan*
[2]*Institute of Material Research, Tohoku University, Sendai 980-8577, Japan*
E-mail: kimura@tagen.tohoku.ac.jp.

YMn2O5 is famous for showing a colossal magnetoelectric effects. Since ferroelectric phase in this material arises concomitantly at the magnetic phase transition, it was believed that the electric polarization is driven by Mn4+ and Mn3+ spins. YMn2O5 involves edge-shared Mn4+O6 octahedral chain running along c-axis, and a pair of Mn3+O5 pyramids bridging Mn4+O6 chains. In this configuration, the cycloidal Mn4+ spin structure in bc-plane can give the electric polarization due to antisymmetric exchange between neighbored spins expressed by $\dot{S}_i \times \dot{S}_j$. On the other hand, zig-zag antiferromagnetic (AF) chain in ab-plane may also produce the electric polarization by symmetric exchange striction between neighbored spins with $\dot{S}_i \cdot \dot{S}_j$ interaction. To clarify which exchange interaction ($\dot{S}_i \times \dot{S}_j$ and $\dot{S}_i \cdot \dot{S}_j$) is essential for the ferroelectricity in this system, we substituted non-magnetic Ga and magnetic Fe ions for magnetic Mn ion in YMn2O5. Substitution by Ga3+ dilutes effective Mn3+ spins, which makes the magnetic interaction in zig-zag AF chain weakened. On the contrary, Fe3+ ion has S = 5/2 spin in high-spin-state, which can builds up the zig-zag AF interaction effectively.

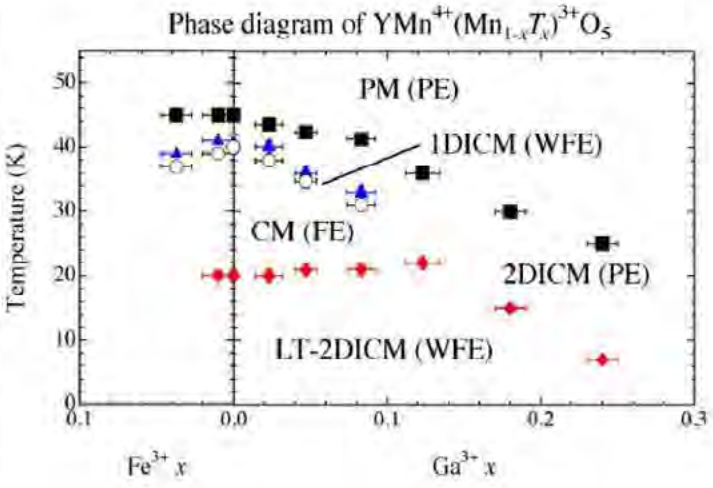

Figure: Dielectric and Magnetic phase diagram of $YMn^{4+}(Mn_{1-x}T_x)^{3+}O_5$ (T = Ga and Fe).

Figure shows the dielectric and magnetic phase diagram as a function of Ga3+ and Fe3+ substitution, determined by neutron magnetic diffraction and dielectric measurements. The phase diagram shows that the dilution of Mn3+ spins suppresses the intermediate commensurate magnetic (CM) phase where the large electric polarization arises (FE phase). On the contrary, the incommensurate magnetic phase at the lowest temperature (LT-2DICM phase) survives in higher Ga3+ concentration, where the weak electric polarization arises (WFE). Upon Fe3+ substitution, LT-2DICM phase becomes immediately unstable and completely disappears at Fe3+ x = 0.04. These results indicate that the ferroelectricity in this system comes from both $\dot{S}_i \cdot \dot{S}_j$ and $\dot{S}_i \times \dot{S}_j$ interactions, the former is given by zig-zag AF chain involving Mn3+ spins and the latter is given by the cycloidal Mn4+ spin structure which is hardly affected by the dilution of Mn3+ spins.

Role of interlayer electrostatic interaction in superconductivity of $LaFeAsO_{1-x}F_x$

J.Kim[1,2], T.Sawada[3], K.Sugimoto[1,2], K.Kato[1,2], M.Ishikado[4], S.Shamoto[4], A.Fujiwara[1], M.Takata[1,2,3]

[1] *Japan Synchrotron Radiation Research Institute, 1-1-1 Kouto, Sayo-cho, Sayo-gun, Hyogo 679-5198, Japan*
[2] *RIKEN SPring-8 Center, Harima Institute, 1-1-1 Kouto, Sayo-cho, Sayo-gun, Hyogo 679-5148, Japan*
[3] *Graduate School of Frontier Sciences, University of Tokyo, Chiba-ken 277-8561, Japan*
[4] *Japan Atomic Energy Research Institute, 4-49 Muramatsu, Tokai-mura, Naka-gun, Ibaraki 319-1184, Japan*
E-mail: kimj@spring8.or.jp

Since the discovery of high-T_c (26 K) superconductivity in F-doped LaFeAsO, $LaFeAsO_{(1-x)}F_x$ [1], various efforts of material scientists have been attracted to the enhancement of T_c under high physical pressure as well as chemical pressure by F doping. They found that T_c increases to 43 K under external pressure of 3 GPa [2]. The replacement of La with other rare earth elements, such as Ce, Pr, Nd, Sm, Gd, has also driven the T_c up to 55 K at ambient pressure [3]. In those studies, the hypothesis relating superconductivity to the layered structure of $LaFeAsO_{(1-x)}F_x$ has been suggested as a scenario in which, the FeAs layer is responsible for the superconductivity and the distortion of the $FeAs_4$ tetrahedron plays an important role in superconductivity [4]. Detailed relation between local structure and superconductivity, however, has not been clarified yet.

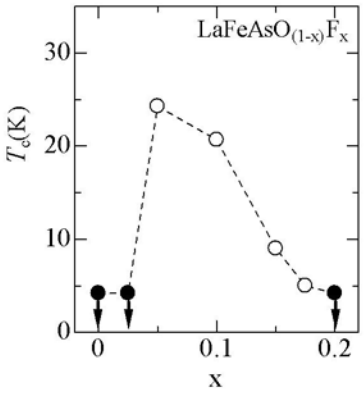

Fig 1. Doping concentration x dependence of T_c in the $LaFeAsO_{(1-x)}F_x$

In this study, we unveiled the effect of local structure of $LaFeAsO_{(1-x)}F_x$ on T_c for x = 0 - 0.2: T_c varies depending on the x and shows a maximum value of 24.3 K at x = 0.05 as shown in Fig. 1. For precise structural analysis, we have measured high quality synchrotron powder X-ray diffraction data at SPring-8, and carried out the charge density study by MEM/Rietveld method [5]. The electrostatic-potential distribution, which visualizes more effectively phenomena in crystal [6], could be extracted from our high quality charge density map. We have found from the analysis that significant specific feature of electrostatic potential between the FeAs and LaO layers for the sample showing the maximum T_c (x = 0.05). In the talk, the evolution of electrostatic potentials around FeAs layer upon F doping and its key role in superconductivity will be discussed.

References

[1] Yoichi Kamihara, *et al.*, "Iron-Based Layered Superconductor $La[O_{1-x}F_x]FeAs$ (x = 0.05−0.12) with T_c = 26 K", J. Am. Chem. Soc. **130** (2008) pp. 3296-3297.
[2] Hironari Okada, *et al.*, "Superconductivity under High Pressure in LaFeAsO", J. phys. Soc. Jpn. **77** (2008) pp. 113712-113716.
[3] J. Karpinski *et al.*, "Single crystals of $LnFeAsO_{1-x}F_x$ (Ln = La, Pr, Nd, Sm, Gd) and $Ba_{1-x}Rb_xFe_2As_2$: Growth, structure and superconducting properties", Physica C: Supercon. **469**(2009) pp. 370-380.
[4] C.H. Lee *et al.*, "Effect of Structural Parameters on Superconductivity in Fluorine-Free $LnFeAsO_{1-y}$ (Ln = La, Nd)", J. Phys. Soc. Jpn. **77** (2008) pp. 083704, 4pages.
[5] M. Takata *et al.*, "The Influence of the Completeness of the Data Set on the Charge Density Obtained with the Maximum-Entropy Method", Acta Cryst. A **52** (1996) pp. 287-290.
[6] H. Tanaka, *et al.*, "Electrostatic potential of ferroelectric $PbTiO_3$: Visualized electron polarization of Pb ion", Phys. Rev. B. **74** (2006) pp. 172105, 4pages.

X-ray magnetic circular dichroism study of $La_{1-x}Ba_xCoO_3$ at Co *K* absorption edge

Hiroaki Morii[1], Takuya Yasue[1], Maki Okube[1], Takeshi Ohno[1], Takayasu Hanashima[1,2] and Satoshi Sasaki[1]

[1]*Materials and Structures Laboratory, Tokyo Institute of Technology, Yokohama 226-8503, Japan*
[2]*Photon Production Laboratory, Kusatsu 525-0055, Japan*
E-mail: morii.h.aa@m.titech.ac.jp

Undoped $LaCoO_3$ has a broad peak of the magnetic susceptibility around T = 90 K. The rhombohedrally distorted perovskite has been recognized to have an intermediate-spin state (IS; $t_{2g}^5e_g^1$, S = 1) for the Co^{3+} 3*d* configuration [1-2]. When La^{3+} is partially substituted by divalent cation such as Sr^{2+}, Ba^{2+} or Ca^{2+}, the substitution is expected to introduce holes into Co-O bonds. The compositional-dependent study for $La_{1-x}Ba_xCoO_3$ has suggested that the rhombohedral *R*-3*c* phase becomes cubic at x = 0.4, being ferromagnetic in the range $0.2 \leq x < 0.5$ and metallic at x = 0.5 [3]. The existence of an intermediate spin state has been demonstrated in half-doped $La_{0.5}Ba_{0.5}CoO_3$ which is coupled to the Jahn-Teller effect [4,5]. There is a report that $La_{1-x}Ba_xCoO_3$ shows a spin-glass behavior in the range $x < 0.2$ and a ferromagnetic order for larger x with a saturation of T_c (≈ 200 K) [6].

X-ray magnetic circular dichroism (XMCD) is indispensable to examine the magnetic and electronic state of Co in $La_{1-x}Ba_xCoO_3$, because in the soft X-ray region the spectra at the Co *L* edge closely overlaps with those at the Ba *M* edge. Powder crystals of $La_{1-x}Ba_xCoO_3$ were synthesized from appropriate molar mixtures of Co_2O_3, La_2O_3 and $BaCO_3$. The mixtures were ground in an agate mortar, prepared in an aluminum crucible, and heated up to 1273 K and maintained for 36 hours. The products were ground again and heated at 1373 K for 60 hours and quenched. X-ray powder diffraction measurements were performed to confirm a single phase for each. The compounds of x = 0, 0.175, 0.2, 0.23, 0.25, 0.28, 0.3, 0.35 and 0.4 were examined by SQUID and X-ray measurements. XMCD experiments were carried out with the Co *K* absorption edge in the BL-6C of Photon Factory, where Si(111) double-crystal monochromator and diamond(001) phase retarder were used to produce circularly polarized X-rays of $3^{(H)}$ x $2^{(V)}$ mm^2. The powder samples were mounted on several sheets of transparent tape, which were set between ionization chambers in the Faraday arrangement with a pair of rare-earth magnets.

The XMCD and XANES spectra were obtained from the absorption data with the right and left circularly polarized X-rays. XMCD reflects the local spin and orbital polarization of the final states at the inner core absorption edges. By the Ba substitution for La, negative and positive XMCD peaks were clearly observed around E = 7.719 and 7.723 keV of the threshold and main edge, respectively, suggesting the existence of intermediate-spin states of Co^{3+} and Co^{4+}. The presentation will compare with the previous results for $La_{1-x}Sr_xCoO_3$ [7] and discuss the electronic and magnetic state of Co ions.

References

[1] Raccah, P. M. and Goodenough, J. B., *J. Appl. Phys.*, Vol. 39, (1968), pp 1209-1210.
[2] Korotin, M. K., Ezhov, S. Y., Solovyev, I. V., Anisimov, V. I., Khomskii, D. I. and Sawatzky, G. A. , *Phys. Rev. B*, Vol. 54, (1996), pp 5309-5316.
[3] Patil, S. B., Keer, H. V. and Chakrabarty, D. K., *Phys. Status Solidi A*, Vol. 52, (1979), pp 6 81-686.
[4] Fauth, F., Suard, E. and Caignaert, Y., *Phys. Rev. B,* Vol. 65, (2001), pp. 060401-1-4.
[5] Wang, J., Wang, Z. D., Zhang, W. and Xing, D. Y., *Phys. Rev. B*, Vol. 66, (2002), pp 064406 -1-5.
[6] Kriener, M., Zobel, C., Reichl, A., Baier, J., Cwik, M., Berggold, K., Kierpel, H., Zabara, O., Freimuth, A. and Lorenz, T., *Phys. Rev. B*, Vol. 69, (2004), pp 094417-1-7.
[7] Hanashima, T., Azuhata, S., Yamawaki, K., Shimizu, N., Mori, T., Tanaka, M. and Sasaki, S., *Jpn. J. Appl. Phys.*, Vol. 43, (2004), pp 4171-4178.

Propeller-like thermal vibration of molecules in ferroelectric molecular crystal CCl_3CONH_2

Chikako Moriyoshi and Yoshihiro Kuroiwa

Department of Physical Science, Hiroshima University, Kagamiyama, Higashi-Hiroshima, Hiroshima 739-8526, Japan
E-mail: moriyosi@sci.hiroshima-u.ac.jp

Trichloroacetamide CCl_3CONH_2 (abbreviated as TCAA) is an organic compound of a molecular crystal with monoclinic structure. Two independent TCAA molecules (molecule A and B) exist in the crystal and connected by N-H•••O hydrogen bonds to form a dimer. TCAA undergoes two successive phase transitions at T_C = 355 K and T_0 = 358 K on heating. The space group of TCAA is $P2_1$ below T_C and $P2_1/c$ above T_0. The *D-E* hysteresis loops, which indicate the ferroelectric activity of TCAA, were observed below T_C [1,2]. In this study, we examine the temperature variation of thermal motion of molecules in the TCAA crystal in the ferroelectric phase by analyzing X-ray diffraction intensities from a single crystal.

Single crystals of TCAA were grown by slow cooling the ethanol solution. A spherical sample was made from the grown crystal and used in the diffraction measurements. The diffraction intensities were collected using a four-circle diffractometer with MoKα radiation. Above $T_m \sim 370$ K, the diffraction intensities diminish, so that the TCAA crystal was melt or sublimated. Structural parameters were determined by the iterative least-squares method, and the electron charge density distribution was analyzed by the maximum entropy method (MEM). Rotational disorder was observed only in the molecule B below T_C. Three Cl ions in the molecule B have two equilibrium sites, respectively. The ratio of the occupancies of two sites was 7:3 and almost unchanged below T_C. In the paraelectric phase above T_0, the molecules A and B become equivalent and the ferroelectricity is lost by appearance of inversion symmetry. Both molecules show the violent rotational disorder, as if 'the propeller of CCl_3' was spinning round on the C-C bond axis. We suppose that such rotational disorder enhances the repulsion force between the dimers to give rise to the melting of the crystal above T_m.

References

[1] Kamishina Y., Akishige Y., and Hashioto M., "Ferroelectric Activity on Organic Crystal Trichl oroacetamide", *J. Phys. Soc. Jpn.*, Vol. 60, No. 7, (1991), pp 2147-2150
[2] Akishige Y. and Kamishina Y., "Weak Ferroelectricity on Organic Crystal Trichloroacetamide", *J. Phys. Soc. Jpn.*, Vol. 70, No. 10, (2001), pp 3124-3128.

MS11-P07

The structural characterization and magnetic interactions in doped rare-earth manganites

Wiqar Hussain Shah

Department of Physics, college of Science, King Faisal University, Hofuf, 31982, Saudi Arabia

The aim of my research is to identify fundamental mechanisms responsible for structural phase transitions in doped rare-earth manganites and to present new theoretical and experimental studies on the subject. Local structural changes due to the influence of chemical pressure or temperature, like, doping, atomic rearrangements, ordering effects, the behavior of defects and the formation and dynamics of domain walls and transformation as well as kinetic phenomena will be presented. We also intend to identify improved tools to analyses and to better understand the structural behavior of some doped rare-earth manganites at the bulk as well as at the nano-scale by different theoretical techniques. The aim of this presentation is to discuss new developments at the interface of X-ray diffraction and absorption spectroscopy and Synchrotron radiations. The spectrum of contrast mechanisms includes among others absorption, x-ray fluorescence, small angles neutron scattering, coherent scattering due to Fresnel diffraction (phase contrast) and Bragg diffraction.

MS14-P01 - Cancelled

MS14-P02 - Cancelled

MS14-P03

Mapping the strain field of chemically treated surface of semiconductor crystals using X-ray Bragg-surface diffraction

Y. W. Tsai[1], C. H. Chu[1], S,-C. Weng[1], Y.-Z. Zeng[1], H.-Y. Chen[1], Y.-H. Yan[1], O. N. Zarubina[2], G. M. Mokrousov[2], and S.-L. Chang[1, 3]

[1]*Department of Physics, National Tsing Hua University, Hsinchu, Taiwan, R.O.C. 300*
[2]*Department of Chemistry, Tomsk State University, Tomsk, Russia*
[3]*National Synchrotron Radiation Research Center, Hsinchu, Taiwan, R.O.C. 300*
E-mail: g943322@alumni.nthu.edu.tw

Recent study indicates that three-beam Bragg-surface diffraction (BSD) is capable of measuring the small lattice distortion of a crystal substrate in a thin film/crystal sample system. This method is now applied to investigate stain distribution of chemically treated surface of semiconductor crystals. Two sample systems are investigated: GaAs[001] and InAs[111] crystals. Chemical treatments of these samples were prepared in liquid environments. Dissolution of samples was done by selective mechanism at which there was an increase of vacancy concentration in the near-surface layer of gallium and indium for GaAs and InAs, accordingly. The three-beam (002)/(111) BSD for GaAs at 9 keV and the (222)/(-131) BSD for InAs at 10 keV are used for this study, where (002) for GaAs and (222) for InAs are symmetric Bragg reflection, while (111) for GaAs and (-131) for InAs are the surface diffraction. During the experiments, the diffraction images of surface reflections are recorded on a charge coupled device (CCD) with high spatial resolution ($20 \times 20 \mu m^2$), which provide the information of the lattice parameter variation of the crystals studied. The strain analysis shows that the sensitivity of lattice parameter is about $\Delta a/a = 10^{-4}$ for GaAs and $\Delta a/a = 5 \times 10^{-5}$ for InAs.

Protein cages provide a platform of cell-permeable and biocompatible imaging probe in living cells

Seung-Hye Choi,[1,2] Kuiwon Choi,[1] Ick Chan Kwon,[1] Kwang Yeon Hwang,[2] and Hyung Jun Ahn[1,*]

[1] *Biomedical Science Center, Korea Institute of Science and Technology, South Korea*
[2] *Division of Biotechnology, Korea University, South Korea*
E-mail: hjahn@kist.re.kr

Caged proteins are macromolecules exhibiting a self-assembled nanoplatform that can be used for detection of biomolecule. We present here the strategy to image apoptotic cells using a nanoplatform of caged protein. For that purpose, cage protein was genetically modified to have two abilities, real-time imaging of apoptosis and cellular uptake. A high ratio of target peptides to cage formed from self-assembling of cage subunits resulted in increase of fluorescence signals per a probe particle, and our cage probe was well cell-permeable and exceedingly biocompatible. We demonstrated that cage probe was specifically cleaved by effector caspase in cell-free conditions, and also finally apoptotic events were imaged real-timely in living cells. Our strategy provides an application to imaging and sensing of other specific protease activities.

We mainly focus on small heat shock protein (Hsp), of which subunit is genetically engineered to have two abilities, real-time imaging of apoptosis and cell-permeability. For that purpose, both of Asp-Glu-Val-Asp (DEVD) motif, of which the N-terminus is cleaved by the effector caspases [1], and hexahistidine motif are respectively incorporated to the C-terminal end of cage subunit (Fig. 1). Self-assembling of cage subunits forms spatially well-defined nanoparticles with a high ratio of DEVD substrate to cage, which results in multiplication of imaging signals per a probe particle (Fig. 2). Our engineered cage probe is exceedingly biocompatible since it is based on a protein platform, whereas the inorganic or polymer-based imaging probes may be cytotoxic to cells or living organs. In the present studies, hexahistidine motif, which is usually designed to be used for protein purification, imparts high degree of cell-permeability to protein cages. Our engineered cage protein is specifically cleaved by effector caspase in cell-free conditions, and also visualizes apoptotic events real-timely in living cells (Fig. 2).

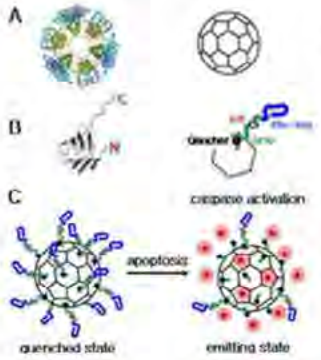

Fig. 1

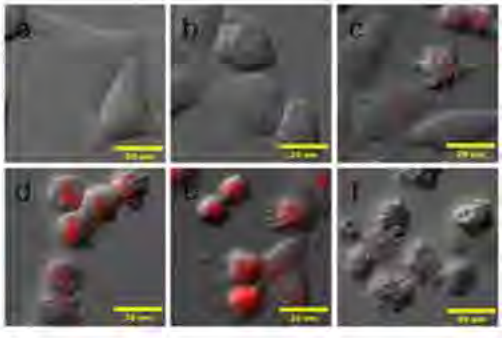

Fig. 2

Fig. 1. Self-assembled Hsp cage in molecular structure represent a sphere nanoplatform.
Fig. 2. Visualization of activation of effector caspase in TRAIL-treated HeLa cells.

References

[1] Bullok K, Piwnica-Worms DJ. *J. Med. Chem.* **2005**, 48, 5404-5407.

MS14-P05

Long-range-order and short-range-order structures of Co-doped Y_2O_3 nanocrystals

Y. L. Soo[1,2], T. S. Wu[1], C. S. Wang[1], S. L. Chang[1], T. S. Chan[2], C. A. Hsieh[2], and J. F. Lee[2]

[1]*Department of Physics, National Tsing Hua University, Hsinchu 30013, Taiwan*
[2]*National Synchrotron Radiation Research Center, Hsinchu, Taiwan*
E-mail: soo@phys.nthu.edu.tw

Long-range-order and short-range-order structures of Co-doped Y_2O_3 nanocrystals have been probed by x-ray powder diffraction (XRD) and extended x-ray absorption fine structure (EXAFS) techniques, respectively. These samples were prepared by polyol method followed by thermal annealing at different temperatures from 300°C to 900°C. The XRD data show a progressive transition of crystal structure from amorphous to that of bulk Y_2O_3 as the annealing temperature increases. The annealing-temperature-dependent changes of nanoparticle size were also revealed by the XRD results using Scherrer equation. Local structures surrounding Y atoms in the Y_2O_3 host and the Co dopant atoms were determine by Y and Co K-edge EXAFS, respectively. Combining the XRD and EXAFS analyses, we conclude that thermal annealing can drive the Co atoms located on interstitial sites inside the nanoparticles towards the particle surface while enlarging the size and improving the crystal structure of the host nanoparticles. As the annealing temperature increases, the saturation magnetization of the samples obtained from superconducting quantum interference device (SQUID) measurements also increases. The increase of saturation magnetization can be attributed to the increase of Co atoms on the particle surface where increased number of oxygen vacancies leads to enhanced saturation magnetization in the high-temperature-annealed samples.

MS14-P06

Nano-particle formation by Pd complex deposited on polystyrene thin films

Koyasu Naoki, Ohshima Yuji, Koiso Naohiro, Terauchi Hikaru, Hashimoto Takeji, and Takahashi Isao

Faculty of Science and Technology, Kwansei Gakuin University, Gakuen 2-1, Hyogo Japan
E-mail: nakky72@gamil.com

Oxide layers on the surface of catalytic metal nanoparticles often reduce the catalytic activity. Coagulation of nanoparticles occurring especially at high temperatures is also a crucial problem for the efficiency as catalysts because of the substantial reduction of effective surface region. Recently, the possibility of health risks of nanoparticles and threats to the environment has been argued. In order to solve the above-mentioned problems, novel nanoparticle-embedding techniques that are compatible for safety and economic efficiency must be exploited, where we can manufacture a nanoparticle-embedded matrix with optimal spatial distribution, arrangement and number density of nanoparticles. Pd is a technologically important rare metal for its high chemical performance as catalyst and promising applications as a hydrogen storage material. Hashimoto et. al. showed that by using microphase separation of block copolymer a 3D striped structure consisting of Pd nanoparticles can be formed after thermal decomposition of a Pd compound [1]. In the present study, we investigate a thermally evolved structure of Pd nanoparticles spread on the surface region of polystyrene ultrathin films with combination of surface-sensitive X-ray diffraction and several microscopic techniques. The Pd complex was evaporated in a low vacuum chamber onto the polystyrene films spincoated on Si(100). After the evaporation, in situ measurements of X-ray reflectivity (XR) and grazing incidence X-ray diffraction (GIXD) were performed at high temperatures to determine the structure parameters on nanoparticles. Atomic force microscopy and confocal laser scanning microscope were used for the ex situ observation in real space.

References

[1] T. Hashimoto, et al., Polymer 50 (2009) 2696-2705.

MS14-P07

Interfacial structure of polystyrene/polyhydroxybutyrate two-layer film revealed by X-ray diffraction

K. Nozaki, K. Ishimoto, J. Takemoto, C. Yang, X. Sun, K. Shimizu, H. Terauchi, and I. Takahashi

Faculty of Science and Technology, Kwansei Gakuin University, Sanda 669-1337, Japan
E-mail: aoj22680@kwansei.ac.jp

A lot of polymers with excellent properties are ubiquitously utilized in modern society as a form of ultrathin films, e.g., coating, foams, paints and adhesion bonds. In many applications, ultrahigh performance peculiar to polymer multilayer films has been eagerly sought and developed. Physical properties of interfaces are especially of importance in organic devices, since they deeply rely on electrical properties like carrier mobility at metal/polymer interfaces, polymer/polymer interfaces, polymer/semiconductor interfaces, etc. Therefore, it is very important to understand the structure and morphology of polymer interfaces which correlate directly with physical properties. In the present study, we investigate an interfacial structure and morphology of polymer thin layers with X-ray diffraction. We prepared two-layer thin films consisting of glass-forming atactic polystyrene (PS) and semicrystalline biodegradable polyhydroxybutyrate (PHB), because we are specially interested in the development of interfacial morphology associated with glass transition and crystallization of each layer. A PS layer was spincoated on Si(100) followed by the spincoating of PHB layer. Both X-ray reflectivity (XR) and grazing incidence X-ray diffraction (GIXD) showed some anomalous variation occurring around the glass transition temperature of PS and crystallization temperature of PHB. In order to enhance the diffracted X-ray from the interfacial region, we made a sample in which Indium nanoparticles were evaporated onto the PS surface before the PHB deposition. Such a sandwiched sample also showed an interesting variation in XR giving us the detailed morphological change at this interface.

MS14-P08

Surface structure and morphology of PEG/PEO blends thin film: composition and temperature dependence study

Yoshiki Kurokawa, Hideaki Takahashi, Hikaru Terauchi, Isao Takahashi and Katsumi Shimizu

School of Science and Technology, Kwansei Gakuin University, Sanda, Hyogo 669-1337, Japan
E-mail: shimizu@kwansei.ac.jp

Polyethylene glycol (PEG) and polyethylene oxide (PEO) are widely used industrial materials because the properties inherent in PEG and PEO such as biocompatibility, lubricating ability and water solubility are required for general industrial products as well as for cosmetic and medical products. These two polymers are known to exhibit different physical properties and composed of the same monomeric structure ($-CH_2-CH_2-O-$) with different molecular weight: PEG for below 50,000 g/mol and PEO for above 50,000 g/mol. The crystalline structure and phase morphology in PEG and PEO give a direct impact on their final properties. Hence, it is critical to control the formation of the higher-order structure; blending is often used for that purpose. The previous studies on the morphologies and their kinetics in polyolefin blends have demonstrated a controllable phase structure and morphology, even though the monomeric structural similarity between two polymers is rather high [1,2]. As most structural and morphological studies of polymer blends deal with the polymers composed of different monomeric structures, little attention has been paid toward a possibility for controlling the material properties using polymers with a monomeric structural similarity.

In this report, we focus on PEG/PEO blend thin film for exploring a possibility to control the surface structure and morphology with the same kinds of polymers with a different molecular weight. For attain that purpose, a specular X-ray reflectivity (XR) measurement, grazing incidence X-ray diffraction (GIXD) experiment and atomic force microscopy (AFM) observation were carried out. The polymers, PEG and PEO were purchased from Polymer Source Inc., and the characteristics of these polymers including a number averaged molecular weight (M_n) and polydispersity (M_w/M_n) are: PEG (M_n = 10,500 g/mol, M_w/M_n = 1.08) and PEO (M_n = 380,000 g/mol, M_w/M_n = 1.3). The thin film samples were prepared by spin-coating (at 4,500 rpm for 40 sec) with aqueous solution onto Si(100) substrate capped with the natural silicon oxide. The specular XR and GIXD were observed using a high resolution diffraction system with a stationary cupper anode X-ray tube (Smart Lab system, Rigaku Co., Ltd.). The X-ray beam was monochromated using a multilayer miller for using a CuK_α radiation (wavelength λ = 1.5418 Å). The AFM images were recorded using a Nanopice (Seiko Instruments Inc.) with a damping mode. At room temperature, the surface morphology did not show any significant composition dependence in the PEO-rich components (Fig.1(a)), however in the PEG-rich components, we observed a partial dewetting (Fig.1(b)), which was consistent with the XR results. The composition dependence of the integrated Bragg intensity revealed an anisotropic crystalline structure. The temperature dependence study will be presented combined with the composition dependence study at room temperature.

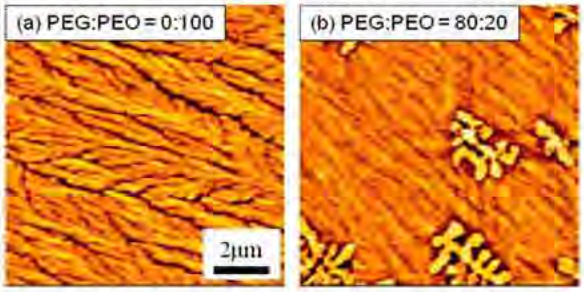

Figure1 AFM image of PEG/PEO blend

Reference

[1] Shimizu K., Wang H., Wang Z., Matsuba G., Kim H. and Han C. C., "Crystallization and pha se separation kinetics in blends of linear low-density polyethylene copolymers", *Polymer*, Vol. 45, No. 21, (2004), pp 7061-7069.

[2] Matsuba G., Shimizu K., Wang H., Wang Z. and Han C. C., "Kinetics of phase separation and cr ystallization in poly(ethylene-ran-hexene) and poly(ethylene-ran-octene)", *Polymer*, Vol. 44, No. 24, (2003), pp 7459-7465.

Glass transition and thermal expansion of ultrathin polystyrene films: An X-ray reflectivity study at various heating/cooling rates

Chunming Yang, Shunsui Matsuura, Kiyoaki Inoue, Kohei Ishimoto, Naoki Koyasu, Hikaru Terauchi, and Isao Takahashi

Faculty of Science and Technology, Kwansei Gakuin University, Sanda 669-1337, Japan
E-mail: yangchunming@126.com

Glass transition is a phenomenon between a liquid state and a glass state, which usually occurs upon rapid cooling. The signature of glass transition is experimentally observed as a break in physical properties (e.g., volume and enthalpy) or a sudden change in their derivative (e.g., thermal expansivity and heat capacity). In confined glassy polymer thin films considered as a good example of quasi two-dimensional system, linear thermal expansion coefficient of the film can be a measure of glass transition temperature (T_g). The T_g in polystyrene (PS) films decreased with decreasing thickness revealed by ellipsometry, while the linear thermal expansion in glass state α_{glass} was reported to increase with decreasing thickness [1-3]. Enhanced mobility in surface region which is supported by the increase in α_{glass} has been ascribed to be an origin of the reduced T_g in ultrathin glassy films. However, in another ellipsometric study [4] as well as positron annihilation lifetime spectroscopy [5] and X-ray reflectivity (XR) [6], α_{glass} seems to be independent of the film thickness or even shows a tendency of a decrease with decreasing thickness, which was accompanied by the reduction of T_g.

In the present study, we perform precise measurements on XR of thin PS films under various scanning rates (heating rate: 0.50°C/min, 0.05°C/min and 0.01°C/min; cooling rate: 0.50°C/min and 0.01°C/min). Atactic PS thin layers on Si substrates were prepared by spin-coating method. Before the XR measurements, samples were annealed above bulk glass transition temperature for 12 hours. Thickness of the films ranged from 4 nm to 70 nm. The results show that α_{glass} is independent of the thickness or slightly decreased with decreasing thickness at the faster scanning rate (0.50°C/min, 0.05°C/min), while α_{glass} increases with decreasing thickness at an ultraslow heating rate of 0.01°C/min. It indicated that the linear thermal expansion coefficient does not only depend on the thickness but a function of scanning rate.

References

[1] J.L. Keddie, R.A.L. Jones, and R.A. Cory, "Size-dependent depression of the glass transition temperature in polymer films", *Europhys. Lett.* 27 (1994) 59.
[2] S. Kawana and R. A. L. Jones, "Character of the glass transition in thin supported polymer film s", *Phys. Rev. E* 63 (2001) 021501.
[3] L. Singh et al., "Influence of molecular weight and film thickness on the glass transition temper ature and coefficient of thermal expansion of supported ultrathinpolymer films", *Thin Solid Films*, 449 (2004) 231.
[4] S. Kim et al., "Confinement effects on glass transition temperature, transition breadth, and expan sivity: Comparison of ellipsometry and fluorescence measurements on polystyrene films", *Eur. Phys. J. E* 30 (2009) 83.
[5] DeMaggio G B et al., "Interface and Surface Effects on the Glass Transition in Thin Polystyrene Films", *Phys. Rev. Lett.* 78 (1997) 1524.
[6] T. Miyazaki, K. Nishida, and T. Kanaya, "Thermal expansion behavior of ultrathin polymer films supported on silicon substrate" *Phys. Rev. E*, 69 (2004) 061803

Structure analysis of hydroxyapatite nano-crystals by electron powder diffraction

Kyung Song, Jin-Gyu Kim and Youn-Joong Kim

Division of Electron Microscopic Research, Korea Basic Science Institute, Daejeon 305-333, Korea
E-mail: ksong@kbsi.re.kr

X-ray crystallography has very well adapted to the structure analysis of large single crystals. With the trend in research and application toward materials on the nanometer scale, however, X-ray diffraction reaches its limits for structure solution because of its insufficient intensity data. Electron crystallography can be a powerful tool for the structure determination of the nano-sized materials. The electron interactions with matter are about 10^6 times stronger than the ones observed with X-ray. Nevertheless, up to now electron crystallography is still difficult and time consuming task compared to X-ray crystallography because of its inherent problems. The dynamical effects of electron diffraction are the most serious problem for structure solving. As a solution for this problem, the precession electron diffraction technique is a very useful to get intensities of all reflections closer to kinematical condition by decreasing the dynamical behavior of electron diffraction [1].

In this study, we present a structure solution of hydroxyapatite nano-crystals (ALDRICH) using electron diffraction. Crystal structure of hydroxyapatite ($Ca_5(PO_4)_3(OH)$) has a hexagonal system (a=9.417(2) Å, c=6.875(2) Å) and its space group is $P6_3/m$ (#176) symmetry [2].

To judge the quality of the structure refinement with the electron diffraction technique, we have obtained the reflection data using conventional electron powder diffraction (EPD) and precession election diffraction (PEPD). As a result of structure refinement by Rietveld analysis, the reliability factors of the EPD data were R_p=19.7% and R_{wp}=21.8%, as compared to R_p=6.62% and R_{wp}=8.85% for X-ray powder diffraction. On the other hand, the reliability factors of the PEPD data were R_p=16.0% and R_{wp}=17.4%, which improved the EPD refinement results. In order to enhance the structure reliability, we carried out additional experiments employing variable microscopic conditions (condenser lens aperture, exposure time, camera length, specimen cooling, and CCD detector). Finally, we obtained further improved refinement results, R_p=11.2% and R_{wp}=12.6%. It is expected, therefore, that PEPD technique has great potential to overcome the present limitations of X-ray crystallography for structure determination of nano-sized crystalline materials.

References

[1] Vincent R., Midgley P.A., "Double conical beam-rocking system for measurement of integrated electron diffraction intensities", *Ultramicroscopy*, Vol. 53, (1994), pp 271-282.
[2] Hughes J.M., Cameron M., Crowley K.D., "Structural variation in natural F, OH, and Cl apatites", *American Mineralogist*, Vol. 74, (1989), pp 870-876.

Symmetry determination of Ag_2Te nanowire using electron diffraction

Jin-Gyu Kim[1], Sang-Gil Lee[1], Kyung Song[1], Juneho In[2], Bongsoo Kim[2], Youn-Joong Kim[1]

[1]*Division of Electron Microscopic Research, Korea Basic Science Institute, Daejeon 305-333, Korea*
[2]*Department of Chemistry, KAIST, Daejeon 305-701, Korea*
E-mail: jjintta@kbsi.re.kr

Electron diffraction is a useful method for determining the crystal structure of nano-sized materials over limitations of X-ray diffraction techniques. There are, however, some difficulties in using electron diffraction. The most serious problem is the dynamical scattering effects by strong interaction between electron beam and specimen. As a solution for this problem, the precession electron diffraction technique, first developed by Vincent and Midgley, has been investigated to get intensities of all reflections closer to kinematical condition [1]. We have determined the crystal symmetry of silver telluride (Ag_2Te) nanowire (NW) using electron diffraction technique. Ag_2Te is an attractive material that exhibits thermoelectricity, structural phase transitions, and magnetoresistance (MR) and a good candidate for thermoelectric devices semiconductor switches, and magnetic sensors [2]. We have grown freestanding Ag_2Te NWs on a sapphire substrate by the vapor transport method and performed HRTEM imaging (Fig. 1(a)) to analyze the growth direction of Ag_2Te NW through comparing with the JCPDS cards.

In order to determine the crystal symmetry, firstly, we have obtained tilt series electron diffraction from an Ag_2Te nanowire using conventional selected electron diffraction technique to determine the cell parameters. As a results, the cell parameters (a = 8.17 Å, b = 4.42, c = 8.31 Å, β = 113.7°) were determined by 3D reconstruction method in reciprocal space (Fig. 1(b)). In addition, we have tried the 3D symmetry determination (= space group) of Ag_2Te NW using precession electron diffraction technique.

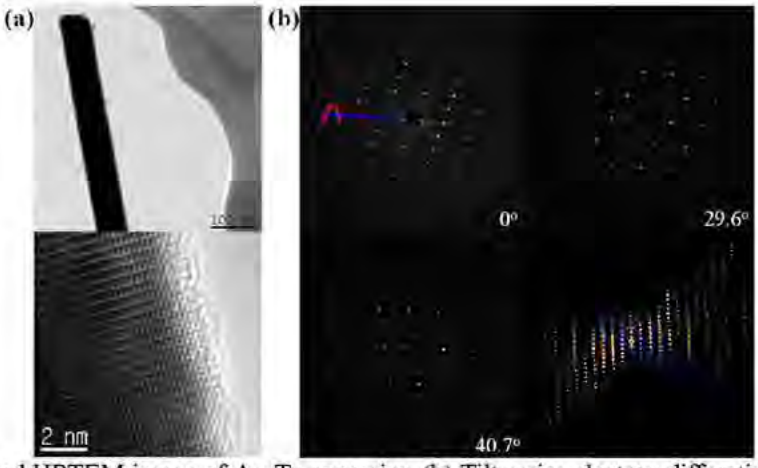

Fig. 1. (a) BF image and HRTEM image of Ag_2Te nanowire. (b) Tilt series electron diffraction patterns obtained from (a) and reciprocal space of Ag_2Te nanowire by 3D reconstruction.

References

[1] Vincent R. And Midgley P.A. "Double conical beam-rocking system for measurement of integrated electron diffraction intensities", *Ultramicroscopy*, 53, (1994), pp 271–282.
[2] Li F., Hu C, Xiong Y., Wan B, Yan W, and Zhang M. "Phase-transition-dependent conductivity and thermoelectric property of silver telluride nanowires", *J.Phys. Chem. C*, 112, (2008), pp 16130-16133.

Development for X-ray crystal structure analysis of a surface-shallow layer and its application to the epitaxial crystals of halogen-bridged platinum(II,IV) complexes

Hiroaki Yamanaka,[1,2] Daisuke Yamashita,[1] Aki Takazaki,[1] Minoru Mitsumi,[1] Yoshiki Ozawa,[1] Koshiro Toriumi,[1] and Osami Sakata[2]

[1]*Department of Material Science, University of Hyogo, Kouto 3-2-1, Kamigori-cho, Ako-gun, Hyogo 678 -1297, Japan*
[2]*Japan Synchrotron Radiation Research Institute / SPring-8, Kouto 1-1-1, Sayo-gun, Hyogo 679-5198, Japan*
E-mail: rk09e004@stkt.u-hyogo.ac.jp

Chemical and physical phenomena that happen in a shallow layer of a crystalline material such as photo-induced chemical reaction and lattice distortion at the crystal boundary of epitaxial crystals should be elucidated more clearly if three-dimensional structure of the crystal surface layer up to 1 μm in depth could be determined by a depth-resolved X-ray diffraction technique. This new diffraction method could be achieved by measuring many diffraction intensities and by exactly controlling the X-ray penetration depth.

Epitaxial crystals of the halogen-bridged mixed-valence platinum(II,IV) complexes were made, and the structure analyses on the surface region were tried. The surface film crystal of the chloro-bridged platinum(II,IV) complex (**1**) was successfully crystallized from its supersaturated solution on the (001) plane of the bromo-bridged platinum(II,IV) base crystals (**2**) which was isomorphous to (**1**) with slightly different cell dimensions. The X-ray diffraction experiments were performed using the multi-axis diffractometer at SPring-8 BL13XU. The epitaxial crystal of (**1**) that grows up on the substrate of (**2**) by thickness less than 4 μm was investigated.

Out-of-plane reflections were measured using 8 keV X-ray for a grazing incident angle of 0.1°~2.0°. Three pairs of 02*l* reflections observed on the two-dimensional diffraction image are shown in Fig. 1. Each two neighboring Bragg spots were assigned to those from the surface film crystal of (**1**) and the substrate of (**2**), respectively. This suggests that the epitaxial film crystal is just a single crystal with its orientation being almost the same as the substrate crystal. The intensity ratios of the film crystal to the substrate become larger as incident angle decrease.

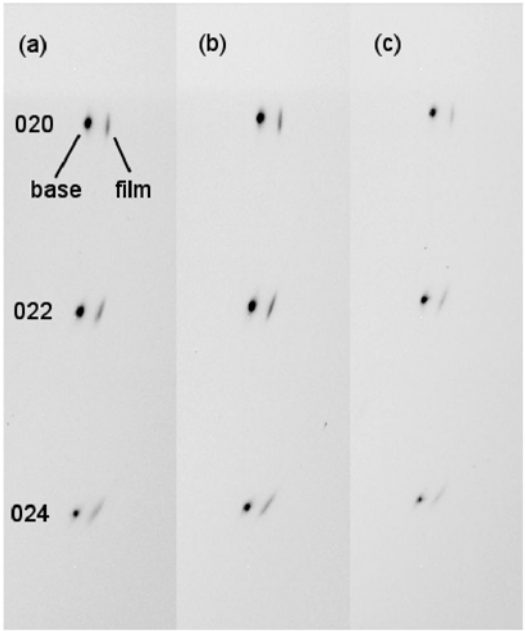

Fig. 1 Two-dimensional diffraction images for the epitaxial crystal. Incident angles are (a) 0.1°, (b) 0.3°and (c) 0.5°, respectively.

MS14-P13

One-pot synthesis and application of magnetite containing meso porous carbon *via* organic-organic self-assembly

Sang-Wook Chu, Sung Soo Park, Jeong Hun Shin and Chang-Sik Ha*

Department of Polymer Science and Engineering, Pusan National University, Busan 609-735, Korea
E-mail: ipris2000@pusan.ac.kr

We synthesized highly ordered and magnetic nanoparticles containing mesoporous carbon using organic-organic self-assembly method *via* one-pot synthesis process. Metal ion contents in mesoporous carbon were controlled from 1.0 to 10 wt% (to weight of the added resol precursor). With the content of Fe below 2.5 wt%, the mesostructures of magnetite containing mesoporous carbons were well retained with 2-D hexagonal symmetry at 700 °C, while the mesostructures were collapsed with the content above 5.0 wt% Fe. The mesostructures of the mesoporous carbons were characterized by synchrotron small angle X-ray scattering (Pohang Accelerator Laboratory, Korea) as well as nitrogen sorption behaviors and tranmission electron microscopy. With the increase of Fe content from 1.0 to 2.5 wt%, the particle sizes of magnetite in mesoporous carbon were increased from 10.2 to 18.6 nm after carbonization at 700 °C in Ar flow. The particle sizes of magnetite in mesoporous carbon with 1.0 wt% Fe content were increased from 6.1 to 27.8 nm after carbonization at various temperatures from 600 to 900 °C. With the increase of Fe content 1.0 wt% to 10 wt% in magnetite containing mesoporous carbon, BET surface area and pore size were decreased 635.4 to 199.9 m^2g^{-1} and 36.0 to 25.7 Å, respectively. The saturation magnetization value of magnetite containing masoporous carbon with 1.0 wt% iron (1 wt% Fe-FDU-15) after carbonization at 700 °C was 7.7 $emug^{-1}$. We demonstrated the usefulness of these composites for the immobilization of drug (Ibuprofen) and proved their easy manipulation by means of an external magnetic field.

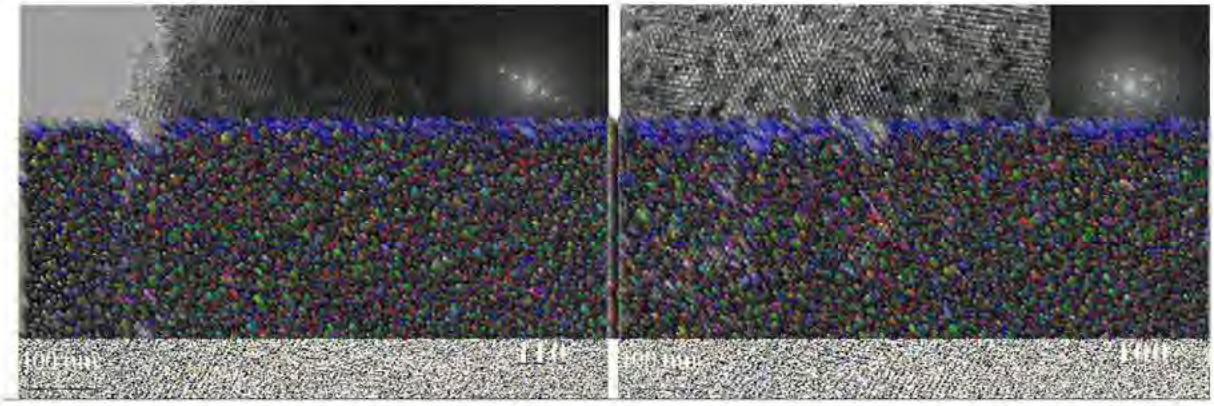

Figure 1. TEM images of 1 wt% Fe-FDU-15.

References

[1] Meng Y., Gu D., Zhang F., Shi Y., Cheng L., Feng D., Wu Z., Chen Z., Wan Y., Stein A. and Zhao D., "A Family of Highly Ordered Mesoporous Polymer Resin and Carbon Structures from Organic-Organic Self-Assembly", *Chem. Mater.*, Vol. 18, No. 18, (2006), pp 4447-4464.

[2] Zhai Y., Dou Y., Liu X., Tu B. and Zhao D., "One-pot synthesis of magnetically separable ordered mesoporous carbon" *J. Mater. Chem.* Vol. 19, No. 20, (2009), pp 3292-3300.

[3] Lee J., Jin S. M., Hwang Y., Park J. G., Park H. M. and Hyeon T., "Simple synthesis of mesoporous carbon with magnetic nanoparticles embedded in carbon rods", *Carbon*, Vol. 43, No. 12, (2005), pp 2536-2543.

[4] Park I.-S., Choi M., Kim T.-W. and Ryoo R., "Synthesis of magnetically separable ordered mesoporous carbons using furfuryl alcohol and cobalt nitrate in a silica template" *J. Mater. Chem.*, Vol. 16, No.33, (2006), pp 3409-3428.

MS14-P14

Adsorption behavior of amino acids on periodic mesoporous organosilicas (PMOs)

Jeong Hun Shin, Sung Soo Park, Sang-Wook Chu and Chang-Sik Ha*

Department of Polymer Science and Engineering, Pusan National University, Busan 609-735, Korea
E-mail: hoonya00@nate.com

Amino acids are of great importance in many fields, including solid-phase peptide synthesis and production of pharmaceutical and agrochemical compounds and biomedical sensors. These applications generally require amino acids to be placed in the form of well-ordered layers on the surface of solid by adsorption. Periodic mesoporous organosilicas (PMOs) have remarkable features, such as large surface area, tunable pore size, and modifiable surface properties. These features make PMOs a very promising adsorbent for amino acid.

In this study, we prepared periodic mesoporous organosilica (PMO) materials from 4,4-bis(triethoxysilyl)biphenyl, 1,4-bis(triethoxysilyl)benzene and bis[3-(trimethoxysilyl)-propyl amine as precursors and investigated on their adsorption behavior of various amino acids as a guest material. The mesostructures of the PMOs were characterized by synchrotron small angle X-ray scattering (Pohang Accelerator Laboratory, Korea) as well as nitrogen sorption behaviors and tranmission electron microscopy.

We carried out adsorption studies of various amino acids on the PMOs under various conditions such as different kinds of PMOs as absorbents, various concentration of amino acids and pH. For amino acids, we tested glycine, L-lysine, and isoleucine. Adsorption of various amino acids on PMOs. have been characterized by UV-vis spectroscopy using the ninhydrin reaction. The adsorption behavior was strongly dependent on the isoelectric point and hydrophobicity of PMO as well as the hydrophobicity of an amino acid.

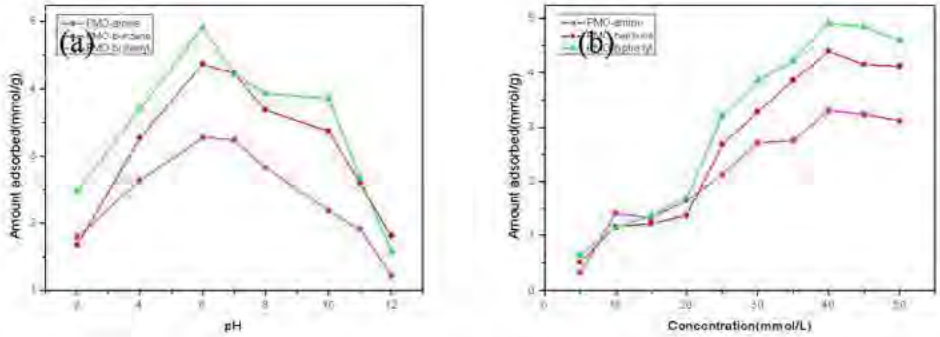

Figure 1. The amount of isoleucine adsorbed on PMOs as a function of (a) pH of solution and (b) concentration.

References

[1] Deng F., Sun Y., Gao Q., Xu Y., Wu D. and Shen W., "Amino Acid Adsorption on Mesoporous Material: Influence of Types of Amino Acids, Modification of Mesoporous Materials, and Solution Conditions", *Journal of Physical Chemistry B*, Vol. 112, No. 7, (2008), pp 2261-2267.

[2] Sun S.-W., Lin Y.C., Weng Y.M. and Chen M.J., "Efficiency improvements on ninhydrin method for amino acid quantification", *Journal of Food Composition and Analysis*, Vol. 19, No. 2-3, (2006), pp 112-117.

[3] Park M.N., Park S.S., Selvaraj M., Zhao D. and Ha C.-S., "Hydrophobic mesoporous materials for immobilization of enzymes", *Microporous and Mesoporous Materials*, Vol. 124, No. 1-3, (2009), pp 76-83.

First-principles calculation of dielectric function for graphite, graphene, and carbon nanotubes

Alexander Zhbanov and Yong-Gu Lee*
Department of Mechatronics, Gwangju Institute of Science and Technology, 1 Oryong-dong, Buk-gu, Gwangju 500-712, Republic of Korea
E-mail: azhbanov@gist.ac.kr, lygu@gist.ac.kr

We performed density-functional theory (DFT) analysis of the structural, electronic, and optical properties of graphite, graphene, and carbon nanotubes. Calculations of the dielectric function and optical absorption were performed under light polarized parallel and perpendicular to the tube axis or the graphene plane. The computations were performed using the full potential linear-augmented plane wave approach as implemented in the WIEN2k [1] code. First-principles calculation has shown quite good agreement with experimental data for graphite as shown in Fig.1. We studied insulated nanotubes of different chirality and a bundle of nanotubes. We can see the displacement of peaks for different structures such as graphene and carbon nanotubes (see Fig. 2).

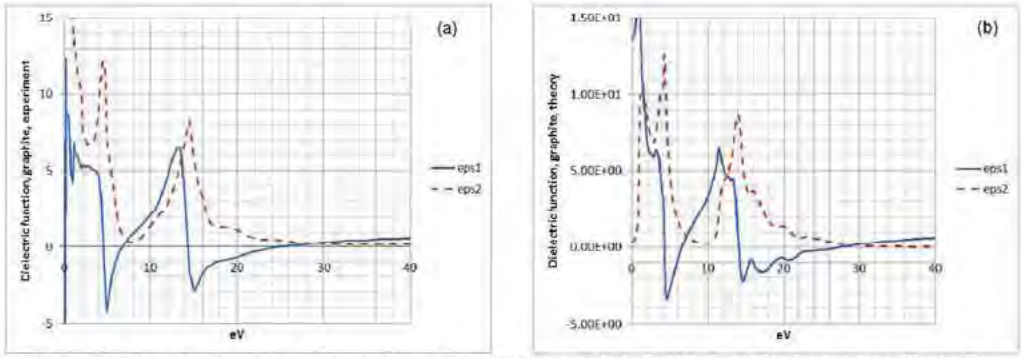

Fig. 1. Dielectric function of graphite: (a) experimental data [2] and (b) *ab initio* calculation

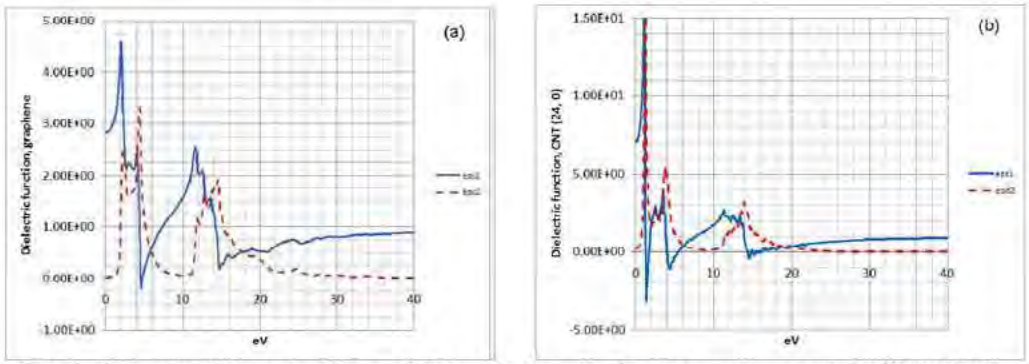

Fig. 2. First-principles calculation of dielectric function for (a) graphene and (b) CNT(24,0)

Acknowledgments: This research was supported by a grant from the institute of Medical System Engineering (iMSE) in the GIST, Korea and by the Research Center for Biomolecular Nanotechnology at GIST, Korea.

References

[1] Blaha P., Schwarz K., Madsen GK.H., Kvasnicka D. and Luitz J., "*WIEN2k, An Augmented Plane Wave Plus Local Orbitals Program for Calculating Crystal Properties*", Vienna university of Technology, (2001)
[2] Borghesi A., and Gulzzetti G. "Graphite (C)." *Handbook of Optical Constants of Solids II*, Academic Press, (1991), pp 449-460.

MS14-P17

Synthesis of biocompatible and mechanically compatible Ti based solid material for implant prototyping

A. A. Shaikh[a], S. Dudziak[c], O. Meier[c] and T. M. Gesing[b]

[a]*Department of Chemistry, University of Dhaka, Dhaka 1000, Bangladesh*
[b]*Department of Crystallography, Institute of Geosciences, University of Bremen, Germany*
[c]*Laser Zentrum Hannover e. V. Hollerithallee 8, 30419 Hannover, Germany*
E-mail: aftab74@yahoo.com

Because of their excellent biocompatibility, superior corrosion resistance, high specific strength and low density, Ti based materials have been extensively used as implants for artificial hard-tissue replacement. It is found that the Young's modulus of pure Ti (110 GPa) is relatively low compared to other conventional implant materials (210 GPa for stainless steel). Although Ti has comparably low Young's modulus, still there is a huge difference in elasticity between the Ti implant and its surrounding tissues. However, critical problems arisen by the mismatch of Young's modulus between implant and surrounding tissues are still unsolved. An alternative to improve the mechanical property mismatch is to reduce elastic modulus of pure Ti by introducing pores, thereby minimizing stress shielding effect between implant and bone where inserting. We have developed a number of biocompatible foaming agents which allows a laser induced Ti foaming without leaving the toxic degradation products in the Ti matrix. The generated porous samples were analysed regarding the total porosity, the location and the size and shape of pores by taking optical and electron micrographs together with micro-CT imaging and analysis. The porous Ti structure with maximum total porosity of 57.0% has been generated in this laser induced foaming process. The porous Ti sample with this amount of porosity is predictable to reduce the stiffness of pure Ti material. Therefore, the produced porous material with higher elasticity could be the potential candidate for hard tissue replacement.

MS14-P18

Analysis of electron diffraction patterns from bone minerals

Chang-Yeon Kim[1], Tae-Hoon Jeon[1], Eun-Kyung Kim[1], Hyosun Lim[1], Seung-Won Nam[2], Kyung Song[3], Sang-Gil Lee[3], Woomi Yang[3], Jun-Ho Jeong[3], Jong-Man Jeong[3], Jin-Gyu Kim[3], Hwanuk Kim[3] and Youn-Joong Kim[1,3]

[1]*Graduate School of Analytical Science and Technology, Chungnam National University, Daejeon 305-764, Korea*
[2]*Department of Bioscience and Biotechnology, Chungnam National University, Daejeon 305-764, Korea*
[3]*Division of Electron Microscopic Research, Korea Basic Science Institute, Daejeon 350-333, Korea*
E-mail: cykim28@gmail.com

Bone is a composite material composed of apatite, collagen and water. Up to 65% of bone is made up of apatite and it influences the strength of bone [1]. Hydroxyapatite (HAp) is one of the main inorganic phases of bone and its ideal chemical formula is $Ca_5(PO_4)_2OH$. This research used transmission electron microscopes (TEM) to study microstructures and atomic structures of bones, focused on quantitative analysis of electron diffraction patterns of bone minerals presented in nanometer scale. 100 ~ 200 nm width of collagen fibrils were observed from TEM specimens of cortical bones and HAp was a nano-sized inorganic phase which can be found among the collagen fibrils (Fig. 1). Electron diffraction patterns (EDP) of HAp was quite distinct from conventional EDP of nano-sized crystalline materials, showing arc-shaped reflections of (002) and (004) planes together with circle-shaped reflections from other planes. HAp belongs to $P6_3/m$ in space group and has a screw axis along the c-axis, which gives rise to systematic extinctions of (001) and (003) reflections.

In order to perform quantitative structure analysis of bone minerals, we separated the inorganic phases from the organic matrix and applied texture electron pattern analysis and electron precession techniques. Variations in structures of bone minerals from different parts, ages and species of bones were also investigated.

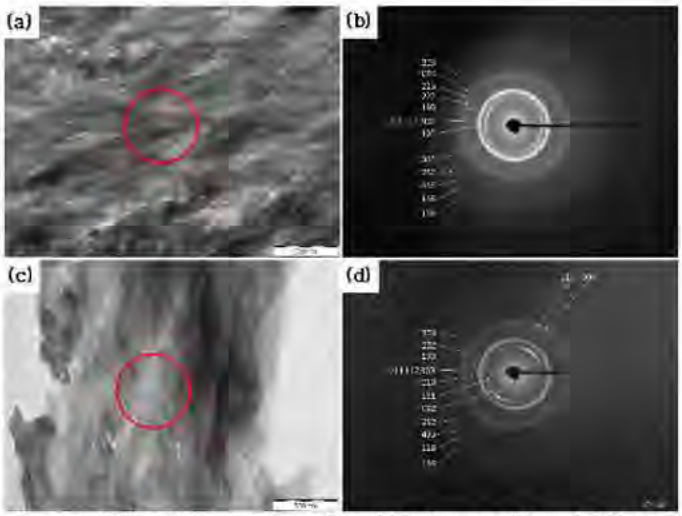

Fig. 1. TEM images and electron diffraction patterns of a rabbit femur ((a) and (b)) and a chicken femur ((c) and (d)).

References

[1] Olszta M., Cheng X., Jee S., Kumar R., Kim Y., Kaufman M., Douglas E. and Gower L., "Bone structure and formation: A new perspective", Materials Science and Engineering R, Vol. 58, (2007), pp 77-116.

MS14-P19

Synthesis and characterization of Sb_2S_3 & Sb_2Se_3 nanorods via complex decomposition by hydrothermal method

Abdolali Alemi, Younes Hanifehpour Firouzsalari

Department of Inorganic Chemistry, Faculty of Chemistry, University of Tabriz, Iran
E-mail: alemi.aa@gmail.com

Recently, metal chalcogenides have attracted considerable attention due to their proven and potential applications in electronic, optical and superconductor devices. Among these materials, antimony sulfide and antimony selenide are kind of semiconductors with interesting high photosensitivity and high thermoelectric power. They are layer-structured direct band gap semiconductor with orthorhombic crystal structure.Sb_2S_3 and Sb_2Se_3 has been extensively investigated for its special applications as a target material for microwave devices, television cameras, rechargeable storage cell, and various optoelectronic devices. In a typical procedure, 0.4 g CS_2, 0.6 g EDTA and 1 g NaOH were added to 50 ml distilled water and stirred well for 20 min at room temperature. Then, 1 mmol of $SbCl_3$ was added to above mixture and the mixture was transferred into a 100 ml Teflon-lined autoclave .The autoclave was sealed, maintained at 180° C for 48 h and cooled at room temperature,naturally. The black precipitate was filtered and washed with dilute chloride acid and water.

Also, we used dimethyl diselenium and $SbCl_3$ as raw materials with the same route in synthesizing of Sb_2Se_3 nanorods. Typical XRD patterns of the as-prepared Sb_2S_3 and Sb_2Se_3 are shown in Fig1a and 1b. All the peaks in the Fig.1a can be indexed to an orthorhombic phase with lattice parameters a=11.22 Å, b=11.28 Å and c=3.84Å ,are consistent with the values reported for single crystals of Sb_2S_3 (JCPDS card File:42-1393). Fig.1b can be attributed to the orthorhombic phase of Sb_2Se_3 with lattice parameters a=11.62 Å, b=11.76 Å and c=3.95Å (JCPDS card File:72-1184).

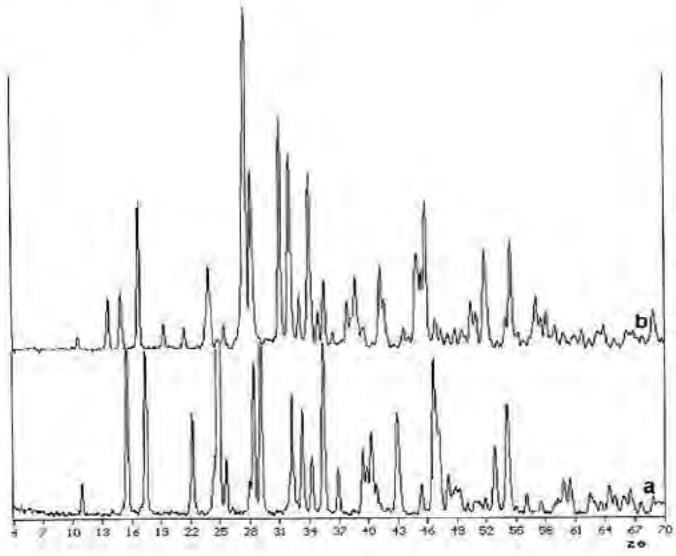

Figure1.XRD patterns of the as-prepared Sb_2S_3 (a) and Sb_2Se_3 (b) at 180° C and 48 h.

References

[1] Han Q., Chen J., Lu J., Yang X., and Wang X., "preparation and characterization of belt like Sb_2Se_3 crystals", Materials Letters, Vol.62, (2008),pp2050-2052

[2] Wang D., Song C., Fu X., and Li X., "Growth of one-dimentional Sb_2S_3 and Sb_2Se_3 crystals with straw-tied-likearchitectures",Journal of Crystal Growth,Vol.281,(2005),pp611-615

[3] Shen G., Chen D., Tang K., Jiang X., and Qian Y., "A rapid ethylendiamine-assisted polyol ro ute to synthesize Sb_2E_3 (E=S,Se) nanowires", Journal of Crystal Growth ,Vol.252,(2003),pp350-354.

MS14-P20

Preparation & characterization of Ho^{3+} doped Sb_2Te_3 nanoplates by hydrothermal method and investigation of optical properties

Abdolali Alemi, Younes Hanifehpour Firouzsalari

Department of Inorganic Chemistry, Faculty of Chemistry, University of Tabriz, Iran
E-mail: alemi.aa@gmail.com.

Binary compounds such as Sb2Te3 and its alloys are thermoelectric materials with small band gap and layered crystalline structures. These materials have investigated for direct conversion of thermal energy to electric energy and they specially are using for electronic refrigeration. In this research work the new HoxSb2-xTe3 based nano-plates materials were synthesized by a hydrothermal co-reduction method. Tellurium (1 mmol), and NaOH (0.6g) were added to distilled water (60 mL), and then NaBH4 (0.5g) and SbCl3 and Ho2O3 with stoichiometric molar ratio were added and the mixture was transferred to a 100 mL Teflon-lined autoclave. The autoclave was sealed, maintained at 180 °C for 48 h and then cooled to room temperature. The black precipitate obtained was filtered and washed with ethanol and water. The powder X-ray diffraction pattern shows the HoxSb2-xTe3 crystals belong to the rhombohedral phase with calculated lattice parameters a=4.264 Å and c=30.458Å(Fig.1).

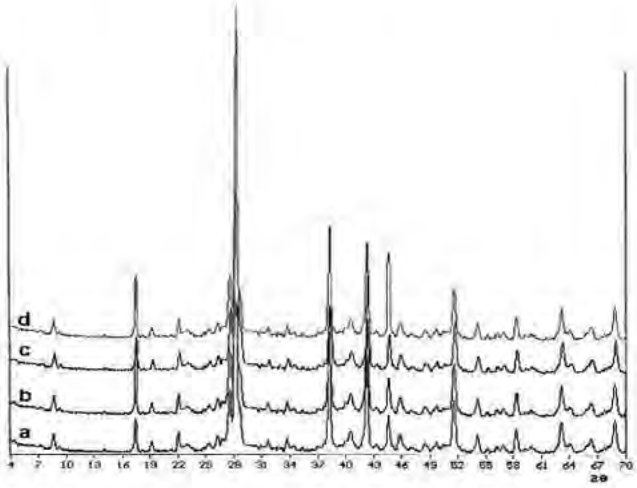

Figure1. XRD patterns of Sb1.90Ho0.1Te3 (a: x =0.00, b: x = 0.02, c: x = 0.05, d: x = 0.10).

Powder XRD patterns indicate that the HoxSb2-xTe3 crystals with x = 0 - 0.1 are isostructural with hexagonal Sb2Te3. The cell parameter c decreases for Ho3+ upon increasing the dopant content (x), while a slightly increases. Changes in lattice parameter could be related to the radius of Ho3+ cations. SEM images show that doping of the Holmium ions in the lattice of Sb2Te3 generally results in nano-plates materials. Emission spectroscopy reveals mainly intense electronic transitions of the Ho3+ ions from excited to ground state of Ho3+.

References

[1] Shi W., Zhou L., Song S., and Zhang H., "Hydrothermal Synthesis and Thermoelectric Transport Properties of Impurity-Free Antimony Telluride Hexagonal Nanoplates", Advanced Materials, Vol.20,(2008),pp1892-1897.

[2] Chim T. and Chun B.,"Microstructure and thermoelectric properties of n- and p- type Sb2Te3 alloys by rapid solidification processes", Journal of alloyes and compounds, Vol.437, (2007),pp225-230.

[3] Ji H., Zhao X.,.Zhang Y., Lu B. and Ni H. ," solvothermal synthesis and thermoelectric properties of lanthanum contained Bi-Te and Bi-Se-Te alloys", Materials letters,Vol.59,(2005),pp 682-685.

P14-21

Collecting complete 3D electron diffraction data using the automatic rotation method

Sven Hovmöller, Peter Oleynikov, Daliang Zhang, and Xiaodong Zou

Structural chemistry, Stockholm University, 10691 Stockholm, Sweden
E-mail: sven.hovmoller@mmk.su.se

Atomic structures of crystals < 1μm^3 can only be solved by electron crystallography. The most complicated zeolites and quasicrystal approximants that have been solved were by electron diffraction (ED) and electron microscopy (EM). Yet, there are still obstacles preventing electron crystallography from being as widely used as X-ray diffraction.

One problem is the uncertain quality of ED and EM, due to multiple scattering of electrons; even in very thin (< 20 nm) samples. This problem is less severe when the crystal is not viewed along a main crystal axis or a main diagonal. Electron precession reduces multiple diffraction and makes the diffracted intensities more reliable i.e. kinematical.

Another problem of electron crystallography has been that it can only be done by highly skilled and well trained persons. Also, it is virtually impossible to collect complete 3D ED or HRTEM data considering all the diagonal views that are needed for complex structures. This is in great contrast to for example X-ray powder diffraction, where you just put a powder sample into an instrument and it collects the data. There is a strong demand for automatic and simple methods for collecting high-quality complete 3D ED data. Such data can be collected either by dedicated hardware, such as the DigiStar from NanoMegas or digitally by collecting a very large number of diffraction patterns, taken every 0.1° or 0.05°.

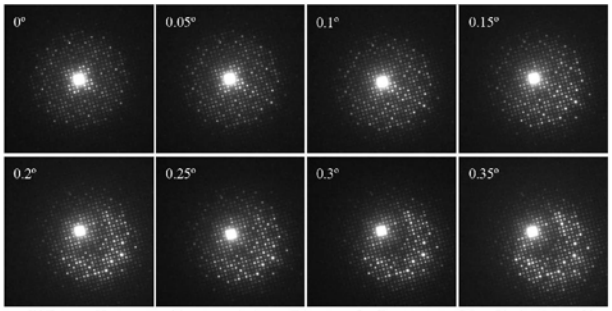

Part of high precision beam tilt series performed by the rotation method. The electron beam was tilted slowly away from the [001] zone axis at 0°, while the direct beam was kept at the same position.

In order to collect complete 3D ED data, the crystal has to be rotated continuously with respect to the electron beam, by about 90° (less for highly symmetric crystals but more for crystals with low symmetry). We have developed the digital electron rotation method, where complete 3D diffraction data to 1 Å resolution or even higher is collected. This has become possible because the modern electron microscopes and CCD cameras are computer controlled.

The rotation steps must be < 0.1° if reflections with resolution higher than 1.0 Å are to be collected. Only then are they sampled finely enough. Such an accuracy of rotation cannot be reached by the goniometer, but it is possible using the beam tilt. We collect series of 80 frames at 0.05° intervals, covering a total of 4° rotation by automatic beam tilt control. Then we tilt the goniometer by 3.5° (allowing some overlap between series) and start a new series etc. The whole data set, with some 2000 frames may be collected within one hour.

Reference

Zhang,D.L., Hovmöller,S., Oleynikov,P. and Zou,X.D. Collecting 3D electron diffraction data by the rotation method. Z. Kristallogr. 225 (2010) 94–102.

AsCA2010

The 10th Conference of the Asian Crystallographic Association

ABSTRACTS

Poster Sessions

Area 3. Chemical Crystallography and Materials Science (MS03, 06, 09, 12, 15)

Area 4. Other Areas (MS17)

Site preference and electron-density distribution of Fe ions in magnetite by X-ray resonant and non-resonant scattering

Takuya Yasue[1], Yuhei Kaneko[1], Maki Okube[1] and Satoshi Sasaki[1]

[1]*Materials and Structures Laboratory, Tokyo Institute of Technology, Yokohama 226-8503, Japan*
E-mail: yasue.t.aa@m.titech.ac.jp

Magnetite Fe_3O_4 has the crystal structure of inverse-spinel type, where only Fe^{3+} ions occupy the tetrahedral A sites and Fe^{2+} and Fe^{3+} ions equally occupy the octahedral B sites [1-3]. Various physical properties of magnetite such as metallic behavior, mixed valence and electron hopping are subject to the cation distribution between two kinds of sites. It was also reported in X-ray absorption experiments that the pre-edge peak of magnetite originates from the atoms in the A sites [4-6]. It is interesting to pinpoint the electrons of specific atoms by extracting the X-ray intensity by resonant scattering from the total scattered intensity. For example, the position of 1*s* electrons can be estimated from the *shell structure factors* due to the X-ray resonant scattering (XRS) at an absorption edge [7]. On the other hand, the difference-Fourier series in X-ray diffraction can provide a mean for the location of bonding 3*d* electrons, by subtracting out the electron density of all atoms in the crystal structure. Thus, the electron-density analysis has developed to make use of the intensity difference between resonant and non-resonant X-ray scattering. In this study, we have focused on the site-specific study for the electron-density distribution associated with the 1*s* and 3*d* states of Fe atoms.

Synchrotron experiments at the Fe *K* absorption edge were performed at the BL-6C beamline of the Photon Factory using a conventional Rigaku AFC5 four-circle diffractometer. In order to compensate the intensity for the polarization effect, the incident beam was converted through a transmission-type X-ray phase retarder to circularly polarized X-rays with a synthetic single crystal of (001) diamond. A spherical crystal of 0.13 mm in diameter was used for the intensity measurements in the range $2\theta \leq 90°$. The wavelengths corresponding to positive and negative XMCD peaks at Fe *K* pre edge were selected as λ = 1.7442 Å (E = 7.1082 keV) and λ = 1.7438 Å (E = 7.1098 keV), respectively. On the information at the off-peak position of the pre edge, the intensity data were measured at λ = 1.7449 Å (E = 7.1051 keV). Least-squares calculation and difference-Fourier synthesis were performed with the softwares of RADY and FRAXY, respectively.

The conventional difference-Fourier synthesis was first made based on the calculation with the Fourier coefficients $|F_{obs}(\boldsymbol{k})|$ as electron density $\rho_{obs}(\boldsymbol{r})$ and $|F_{calc}(\boldsymbol{k})|$ as $\rho_{calc}(\boldsymbol{r})$. The XRS effect in crystal structure factors measured on a pre-edge peak "A" makes it possible to perform a difference-Fourier synthesis for targeting only resonant electrons The difference in the electron density can be given as $\Delta\rho(\boldsymbol{r}) = V^{-1}\Sigma\Sigma\Sigma\{|F_{obs}{}^{A}(\boldsymbol{k})| - |F_{obs}{}^{off}(\boldsymbol{k})|\}\exp\{2\pi i\phi_{calc}(\boldsymbol{k})\}\exp(-2\pi i\boldsymbol{k}\cdot\boldsymbol{r})$, where the termination effect of Fourier series is automatically corrected. Based on the electron-density distribution of bonding 3*d* and resonant 1*s* electrons, the site preference of Fe ions in magnetite will be discussed.

References

[1] Verwey E. J. W. and de Boer, J. H., *Rec. Trav. Chim. Pays-Bas*, Vol. 55, (1936), pp 531-540.
[2] Bauminger, R., Cohen, S. G., Marinov A., Ofer, S. and Segal, E., *Phys. Rev.*, Vol. 122, (1961), pp 1447-1450.
[3] Sasaki, S., *Acta Crystallogr. B*, Vol. 53, (1997), 762-766.
[4] Maruyama, H., Harada, I., Kobayashi, K. and Yamazaki, H., *Physica B*, Vol. 208-209, (1995), pp 760-762.
[5] Saito, F., Toyoda, T., Mori, T., Tanaka, M., Hirano, K. and Sasaki, S., *Physica B*, Vol. 270, (1999), pp 35-44.
[6] Matsumoto, K., Saito, F., Toyoda, T., Ohkubo, K., Yamawaki, K., Mori, T., Hirano, K., Tanaka, M. and Sasaki, S., *Jpn. J. Appl. Phys.*, Vol. 39, (2000), pp 6089-6093.
[7] Sasaki, S. and Tsukimura, K., *J. Phys. Soc. Jpn.*, Vol. 56, (1987), pp 437-440.

MS03-P02

Accurate determination of local structural properties by X-ray absorption fine structure

Sang-Wook Han

Department of Physics Education, Chonbuk National University, Jeonju 561-756, Korea

Long range atomic orderings can be measured with x-ray diffraction (XRD) while local structural properties can be described by extended x-ray absorption fine structure (EXAFS). EXAFS can detect the local structural properties around a selected element, including atomic bond lengths, disorders, coordination numbers, and species of atoms. EXAFS measurements do not require crystal structures. Therefore, EXAFS can be applied for crystals, amorphous, and mixed phased matters. Furthermore, EXAFS does not dependent on the phase of a material, such as solid, liquid, and gas. We will introduce the EXAFS technique, comparing with XRD in detail. We will demonstrate EXAFS studies of the structural properties of nanomaterials, including nanoparticles, nanorods, and nanotubes, which are difficult to be determined by XRD.

MS03-P03

Structure of transmembrane pore reconstructed by anomalous X-ray diffraction

Ming-Tao Lee[1,2], Shiuan-Shiaou Wu[1], Wei-Yu Lin[1], Yi-Ting Sun[1, 3]

[1]*Scientific Research Division, National Synchrotron Radiation Research Center, Hsinchu 30076, Taiwan R.O.C.*
[2]*Department of Physics, National Central University, Jhongli 32001, Taiwan R.O.C.*
[3]*Institute of Molecular Medicine, National Tsing Hua University, Hsinchu 30013, Taiwan R.O.C.*
E-mail: mtlee@nsrrc.org.tw

We determined the structure of the melittin-induced transmembrane pore by X-ray diffraction. The multibilayer sample on substrate was prepared in full hydration. The peptide-to-lipid ratio, P/L, of the melittin-lipid mixtures were in the condition where pores were present, as established previously by neutron in-plane scattering in correlation with oriented circular dichroism. At low hydration levels, the interbilayer distance shortened and caused the membrane pores to become long-ranged correlated and form a periodically ordered lattice of rhombohedral symmetry. Here we used the multiwavelength anomalous dispersion (MAD) method to solve the phase problem for a rhombohedral phase of a phospholipid with brominated chains and performed multiwavelength anomalous diffraction at the bromine K edge. We found the melittin-induced pores were at least partially framed by a lipid monolayer. Evidence suggests that the pore structure is of the toroid type different from the barrel-stave type induce by alamethicin.

MAX200x and max80 high-pressure/high-termperature experiments from Helmholtz Centre Potsdam, GFZ German Research Centre for Geosciences at DESY, German Electron synchrotron

Christian Lathe, Hans Joachim Mueller and Joern Lauterjung

Helmholtz Centre Potsdam, GFZ German Research Centre for Geosciences, Telegrafenberg, 14407 Potsdam, Germany
E-mail: christian.lathe@gfz-potsdam.de

For geoscientists, material scientists, physicists and chemists it is very important to study the samples under extreme conditions. It is necessary to use in-situ X-ray diffraction experiments at synchrotron beamlines because of the high intensity and the broad energy range to figure out the stability of minerals under high pressure and temperature, the determination of bulk moduli, the thermal expansion, phase diagrams, and the behaviour of kinetic measurements.

The first apparatus in Europe was installed in 1992 at HASYLAB, MAX80, a single-stage multi-anvil system. MAX80 allows in-situ diffraction studies in conjunction with the simultaneous measurement of elastic properties up to 12 GPa and 2000 °C [1]. This very successful experiment is used by over forty scientist groups from the whole high pressure community all over the world and is supported by the Helmholtz Centre Potsdam.
Today new materials and the use of high brilliant synchrotron sources allow constructing double-stage multi-anvil systems for X-ray diffraction to reach much higher pressures. The newly designed high-flux hard wiggler (HARWI-II) beamline is an ideal X-ray source for this kind of experiments at the MAX200x. The MAX200x is operated in the double-stage compression mode, in which the first stage is the DIA-type apparatus with six anvils and the second stage consists of eight anvils.

Either tungsten carbide or cubic boron nitride is used for the second stage anvils. This system has a capability of generating pressures up to 25 GPa and temperatures of 2000 °C by a resistance furnace [2]. This experiment is operated since 2006 by Helmholtz-Centre Potsdam, GFZ, German Centre for Geosciences and is used by more than ten groups from different countries every year. An important issue, not only for geoscientists, is to obtain the thermoelastic properties of materials, that means the bulk modulus and the thermal expansion. These values can be calculated due to the changes of the unit-cell-parameters of the sample under different pressure and temperature conditions.

References

[1] Peun T., Lauterjung J., Hinze E., "*High pressure and high temperature investigations on intermetallic compounds using energy-dispersive X-ray powder diffraction.*" - Nuclear Instruments and Methods in Physics Research Section B: Beam Interactions with Materials and Atoms Volume 97, Issues 1-4, Pages 483-486, (1995).

[2] Lathe C., Müller H.J., Schilling F.R., Reichmann H.J., Lauterjung J., "*HARWI-II: A New High Pressure Beamline Equipped with a Large-Volume Press, MAX200x.*" - Synchrotron Radiation in Natural Science Vol. 5, No 1-2, pp. 111-114, (2006).

MS03-P05

Environmental structural analysis of hydrolytic condensed oxides with complex structure

Reiko Murao, Kazumasa Sugiyama

Institute for Materials Research, Tohoku University, Sendai 980-8577, Japan
E-mail: r_murao@imr.tohoku.ac.jp

Hydrolytic condensed oxide materials frequently indicate complex structural features and unique thermal properties, which depend on their preparative conditions. To clarify the mechanism of the hydrolytic condensation together with physic-chemical properties of obtained materials, it is important to understand the so-called middle range ordering composed of local structural units. Extended X-ray absorption fine structure (EXAFS) is a powerful method to analyze the local coordination environment of specific elements. On the other hand, the radial distribution function (RDF) obtained by the X-ray diffraction provides the useful structural information on the middle-range ordering. In particular, anomalous X-ray scattering (AXS) measurements can provide the environmental-RDF around a specific element. This paper demonstrates some selected examples of structural studies for synthetic and natural hydrolytic condensed oxides by the combination of AXS and EXAFS analyses. As an example, Fig.1 shows ordinary RDFs for various ZrO_2-SiO_2 gels prepared by precipitating sols of oxy-zirconium salts and tetra-ethoxysilane (TEOS) into alkali solvents. Only from the dried gel prepared from the sol by refluxing aqueous solution of the $ZrO(NO_3)_2$ and TEOS mixture, zircon ($ZrSiO_4$) can be crystallized by the low temperature annealing at 1150 °C [1]. Differences in correlations around 3 Å and 4 Å appear to indicate the structural features of the amorphous precursor related to the formation of zircon at low temperatures. Structure of natural chrysocolla ($CuSiO_3 \cdot 1.4H_2O$) and synthesized $Cu(OH)_2$ micro-crystallite analyzed by the AXS technique will be also discussed. The AXS measurement at the Cu-*K* absorption edge serves a unique environmental information around Cu, which allows us to discuss the linkage structure of coordination polyhedra $Cu(O,OH)_6$.

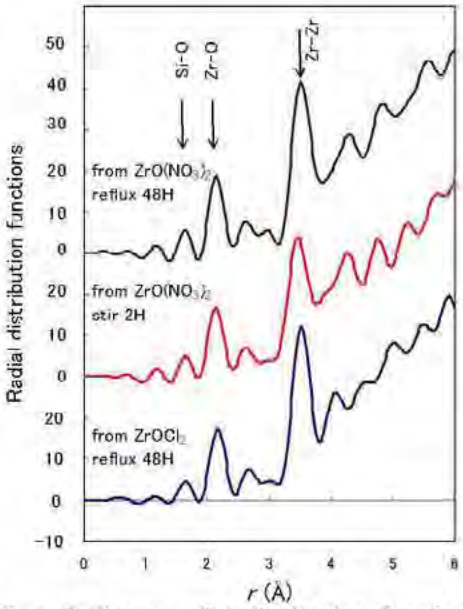

Fig.1 Ordinary radial distribution function $4\pi r^2\rho(r)$ for Zr-Si-O dried gels condensed from mixture of TEOS and oxy-zirconium salts.

References

[1] Veytizou C., Quinson J.F., Jorand Y., "Preparation of zircon bodies from amorphous precursor powder synthesized by sol-gel processing", *J. Eur. Cera. Soc.*, Vol. 22, (2002), pp 2901-2909.

MS03-P06

Development of a micro-strip detector for high-energy XRD

TAGUCHI Takeyoshi[1], MATSUSHITA Kazuyuki[1], Maciej Kachel[2], Robert Szczygiel[2] and Pawel Grybos[2]

[1]*Rigaku Corporation, 3-9-12 Matsubara-cho, Akishima-shi, Tokyo, Japan*
[2]*AGH University of Science and Technology, Krakow, Poland*
E-mail: takey@rigaku.co.jp

A micro-strip detector has become almost a standard detector for in-house X-ray diffractometry [1]. It significantly reduces the data acquisition time to compare with the conventional scan with a point detector such as a scintillation counter or a proportional counter. However, its detective quantum efficiency (DQE) becomes low as the incident X-ray energy gets high since a thin (a few hundred micron) silicon is usually used as a sensor. On the other hand, the number of the applications using high energy X-ray (> 15keV) has been increasing and a strip detector which has high DQE at high energy region is demanded. We have been developing a micro-strip detector with high DQE at high energy[2]. Some examples will be shown.

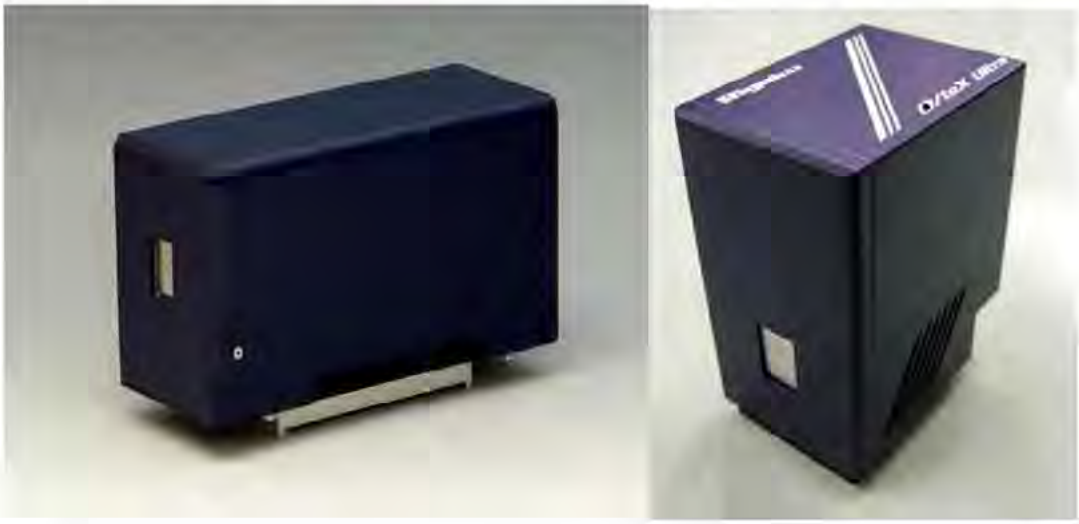

References

[1] Szczygiel R., Grybos P., Maj P., Tsukiyama A., Matsushita K. and Taguchi T., IEEE Transacti ons on Nuclear Science, Vol. 56, 2, (2009), pp 487-495.
[2] Kachel M., Grybos P., Szczygiel R., and Taguchi T., "SXDR64 – Low noise ASIC for Si and CdTedetectors", to be submitted to *Proc.of iWoRiD 2010*, MRC Laboratory of Molecular Biolog y, Cambridge, U.K.(2010)

Structural study of $Zr_{50}Cu_{40}Al_{10}$ and $Zr_{50}Ni_{40}Al_{10}$ amorphous alloys by anomalous X-ray scattering coupled with reverse Monte-Carlo simulation

Toru Kawamata[1], Y. Yokoyama[1] and K. Sugiyama[1]

[1]*Institute for Materials Research, Tohoku Uiversity. Katahira 2-1-1, Aoba-ku, Sendai, 980-8577, Japan*
E-mail: kawamata@imr.tohoku.ac.jp

The physicochemical properties of Zr-based amorphous alloys are affected by kinds of solute elements and their concentrations. The formation ability of a glassy phase is strongly enhanced by the addition of Al in the cases of binary Zr-Cu and Zr-Ni systems [1]. We carried out the AXS-RMC analysis of ternary amorphous alloys in order to discuss the structural role of Al. AXS-RMC analysis is a combinatorial analysis of anomalous X-ray scattering (AXS) method and reverse Monte-Carlo (RMC) simulation, and this new analytical method is suggested to be one of the most powerful techniques for discussing the fine structures of disordered materials [2].

Ordinary and environmental radial distribution functions (RDFs) of $Zr_{50}Cu_{40}Al_{10}$ amorphous alloy obtained by the AXS analysis are shown in Fig. 1. Although the structural information on six atomic pairs of Zr-Zr, Zr-Cu, Zr-Al, Cu-Cu, Cu-Al and Al-Al are included in the ordinary RDF, the environmental RDF around Zr can be explained by a harmony of three pair correlations of Zr-Zr, Zr-Cu and Zr-Al, only. The environmental-RDF around Cu is similarly employed for obtaining the structural information for three atomic pairs of Cu-Cu, Cu-Zr and Cu-Al. These environmental-RDFs allow us to discuss structural features of amorphous alloys in details and present results indicate that the environmental structure around Zr is obviously modified by the introduction of Zr-Al pairs. As shown in Fig.2, similar discussion can be possible to make for the Ni case and the obtained RDF data for the Zr-Ni-Al system show the preferred correlation for the Zr-Al pairs, which serve the structural change around Zr. Further structural details induced by the addition of Al in the binary Zr-Cu and Zr-Ni amorphous alloys could be obtained by AXS-RMC analysis. The overall preference of icosahedron-like local structural units are confirmed around Zr. This structural feature appears to have no concentration dependence of Al addition. In the presentation, we will report topological features of the detailed three-dimensional structural models of the amorphous alloys.

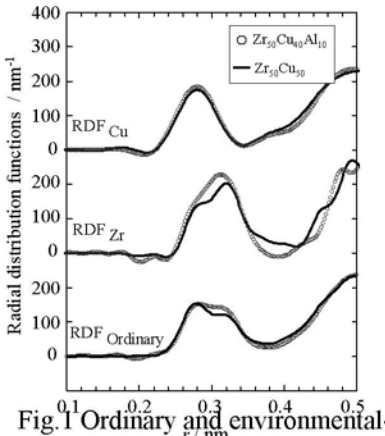

Fig.1 Ordinary and environmental-RDFs for $Zr_{50}Cu_{50}$ and $Zr_{50}Cu_{40}Al_{10}$ amorphous alloys.

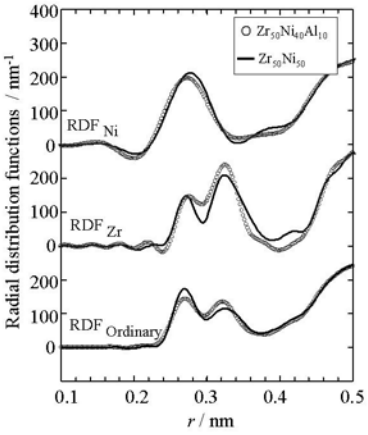

Fig. 2 Ordinary and environmental-RDFs for the $Zr_{50}Ni_{50}$ and $Zr_{50}Ni_{40}Al_{10}$ amorphous alloys.

References

[1] Xing L.Q., Ochin P. and Bigot J., "Effects of Al on the glass-forming ability of Zr-Cu based alloys" *Journal of Non-Crystalline Solids,* Vol. 205-207, (1996), pp 637-640.

[2] Kawamata T., Yokoyama Y., Saito M., Sugiyama K. and Waseda Y., "Structural study of $Zr_{50}Cu_{50}$ amorphous alloy by anomalous X-ray scattering coupled with reverse Monte-Carlo simulation" *Material Transactions,* (submitted for publication.)

MS03-P08

High brilliance laboratory sources for small x-ray beams

T. Samtleben, C. Michaelsen, B. Hasse, J. Wiesmann, U. Heidorn, S. Kroth, F. Hertlein

Incoatec GmbH, Max-Planck-Strasse 2, 21502 Geesthacht, Germany
E-mail: samtleben@incoatec.de

In our talk we give an overview on current developments of our high brilliance microfocus source, the IμS, for diffractometry in the lab. The IμS consists of a 30 W air-cooled sealed tube with a small anode spot below 40 μm. It is available with Cu, Mo, Ag or Cr radiation. The attached multilayer optics shapes the beam in two directions. Focussing of the beam is as possible as collimating. We explain the unique features of the X-ray source and the design, production and characterization of the multilayer optics. Beam parameters like monochromaticity, flux, brilliance and divergence demonstrate the quality of the IμS.

Selected examples of applications show the benefit of the new microfocus solutions, especially in combination with modern detector technology. The IμS can be combined with all types of 2-dim detectors, like image plates or CCD's. Furthermore, it can be used to upgrade older equipment as well as being a fully integrated component in a modern diffractometer.

We will be showing the following applications, to name but a few:
- texture measurements of high-temperature-superconducting thin films, in order to optimize technically relevant parameters
- grazing incidence small angle scattering of multilayer films in order to compare deposition processes
- structure measurements of crystals at non ambient high-pressure conditions
- temperature-induced phase transitions of an organic semiconductor material
- spatially resolved stress analysis of welding-seams at iron-containing „real" automotive parts

Synchrotron radiation beamline for macromolecular assemblies at SPring-8 operated by the Institute for Protein Research (BL44XU)

Eiki yamashita[1], Masato Yoshimura[1,2], Mamoru Suzuki[1], Kazuya Hasegawa[3], Yukito Furukawa[3], Toru Ohata[3], Takashi Kumasaka[3], Go Ueno[4], Masaki Yamamoto[4], Shinya Yoshikawa[5], Tomitake Tsukihara[1,5] and Atsushi Nakagawa[1]

[1]*Institute for Protein Research, Osaka University, 3-2 Yamadaoka, Suita, Osaka 565-0871, Japan*
[2]*Taiwan NSRRC, Taiwan Beamline Office at SPring-8, 1-1-1 Kouto, Sayo-cho, Sayo-gun, Hyogo 679-5148, Japan*
[3]*JASRI/SPring-8, 1-1-1 Kouto, Sayo-cho, Sayo-gun, Hyogo 679-5198, Japan*
[4]*RIKEN/SPring-8, 1-1-1 Kouto, Sayo-cho, Sayo-gun, Hyogo 679-5148, Japan*
[5]*Graduate School of Life Science, University of Hyogo, 3-2-1 Kouto, Kamigori-cho, Ako-gun, Hyogo 678-1297, Japan*
E-mail: atsushi@protein.osaka-u.ac.jp

Biological macromolecular assemblies play significant roles in many biological reaction systems, such as energy transfer, protein synthesis, signal transduction, molecular motors and so on. Detailed understanding of the functions of the macromolecular assemblies requires information derived from three-dimensional atomic structures. X-ray crystallography is one of the most powerful techniques to determine the three-dimensional structures of macromolecular assemblies at atomic level. It is usually be known that biological macromolecular assembles are difficult to be crystallized or grown to larger size crystals. In addition, the unit cells of these crystals are quite large. Because of these features of the crystals of biological macromolecular assemblies, it is usually very difficult to obtain good diffraction data. The difficulties of diffraction data collection of biological macromolecular assembles are as follows; extremely weak diffraction power, narrow space between diffraction sports, x-ray radiation sensitive etc. High brilliance and highly paralleled synchrotron radiation from the undulator is an extremely powerful tool for diffraction data collection from macromolecular assembly crystals with large unite cell.

The Institute for Protein Research (IPR) of Osaka University is operating a beamline for crystal structure analysis of biological macromolecular assemblies at SPring-8 (BL44XU). This beamline is designed to collect high quality diffraction data from biological macromolecule assembly crystals with large unit cells. The light source of this beamline is a SPring-8 standard type in-vacuum undulator. Liquid nitrogen cooled double crystal monochromator and horizontal focusing mirror are used as the optical components. A high precision diffractometer combined with a specially designed large image-plate detector, DIP6020, and a high performance CCD detector, MX-225HE, is installed. BSS (Beamline Scheduling Software), which is SPring-8 protein crystallography beamline standard GUI, is installed to unify user operation throughout protein crystallography beamlines in the SPring-8. Diffraction data from crystals of large nucleoprotein complex, Vault, with large unit cell (over 700 angstrom) has successfully been collected higher than 3.5 Å resolution [1]. Present status and the future plan of the beamline will be discussed.

References

[1] Tanaka H., Kato K., Yamashita E., Sumizawa T., Zhou Y., Yao M., Iwasaki K., Yoshimura M. and Tsukihara T., "The Structure of Rat Liver Vault at 3.5 Angstrom Resolution", *Science*, Vol. 323, No. 5912, 384-388 (2009).

MS03-P10

Data processing software for a new TOF single crystal neutron diffractometer "iBIX" at J-PARC

Takashi Ohhara[1], Katsuhiro Kusaka[2], Takaaki Hosoya[2], Kazuo Kurihara[1], Taro Yamada[2], Katsuaki Tomoyori[2], Takeshi Yokoyama[2], Yuki Onishi[2], Ichiro Tanaka[2], Nobuo Niimura[2], Toshiya Otomo[3], Jiro Suzuki[3] and Takeshi Nakatani[1]

[1]*Japan Atomic Energy Agency (JAEA), Tokai, Ibaraki 319-1195, Japan*
[2]*Ibaraki University, Hitachi, Ibaraki 316-8511, Japan*
[3]*High Energy Accelerator Research Organization (KEK), Tsukuba, Ibaraki 305-0801, Japan*
E-mail: ohhara.takashi@jaea.go.jp

For a single crystal diffractometer, a data processing software which extracts a HKLF list from raw data is one of the most important components. We have developed a new data processing software, named "STARGazer", for a new TOF single crystal neutron diffractometer, "IBARAKI Biological Crystal Diffractometer (iBIX)", which is constructed at Materials and Life-science Facility (MLF) of J-PARC.

STARGazer has several functional components; 1) making histogram data from raw event data, 2) peak search from the raw data, 3) determination of the UB matrix, 4) finding the Bravais lattice, 5) refinement of the UB matrix, 6) calculate the intensities of all Bragg reflections, and 7) data visualization. The algorithms of crystallographic fundamental functions of those components referred the algorithms of program ISAW, which is a data processing software package developed on Argonne National Laboratory. In addition, STARGazer has some additional functions optimized for the measurement of protein crystals on the iBIX; real-space indexing technique to find UB matrix, refinement of the detector position simultaneously in UB matrix refinement, and finding the Bragg reflections which are overlapping with neighboring reflections. In the near future, a function to deconvolute the overlapping Bragg reflections will be added.

We have already collected and processed neutron diffraction dataset of ammonium bitartrate, glutamic acid and some crystals of organic molecules. The obtained cell parameters agreed with the known values and positions of hydrogen atoms are reasonable. In this presentation, we will show the feature of STARGazer and also show the results of neutron structure analyses of the organic molecules by iBIX.

MS03-P11

Development of a new beamline dedicated to low energy SAD experiments at the Photon Factory

Naohiro Matsugaki[1], Yusuke Yamada[1], Leonard M.G. Chavas[1], Masahiko Hiraki[1], Masato Kawasaki[1], Ryuichi Kato[1], Noriyuki Igarashi[1], Atsushi Koyama[1], Shigeru Yamamoto[1], Kimichika Tsuchiya[2], Tatsuro Shioya[2], Tomohiro Aoto[2], Hideki Maezawa[1], Seiji Asaoka[2], Hiroshi Miyauchi[2], Toshihiro Tahara[2], Yasunori Tanimoto[2] and Soichi Wakatsuki[1]

[1]*Institute of Materials Structure Science, High Energy Accelerator Research Organization (KEK), Japan*
[2]*Accelerator Laboratory, High Energy Accelerator Research Organization (KEK), Japan*
E-mail : naohiro.matsugaki@kek.jp

Recent advances in SAD (single anomalous dispersion) phasing techniques facilitate to solve macromolecular crystal structures using sulfurs or phosphors, which are naturally included in macromolecules but emit quite weak anomalous signals. The method would be quite useful in solving membrane proteins or macromolecular complexes, for which heavy atom or selenomethionine derivative crystals are difficult to prepare. The Structural Biology Research Center at the Photon Factory has developed a new microfocus beamline dedicated to SAD experiments with sulfurs and phosphors under the national project 'Targeted Proteins Research Program'. The beamline is designed to take full advantage of a low energy X-ray beam at around 4keV to enhance anomalous signals from light atoms. The light source is an in-vacuum short gap undulator optimized at around the energy with the fundamental harmonics. The vacuum section of the beamline has only one beryllium window, followed by a diffractometer equipped with a helium cryostream and a specially designed helium chamber to minimize the attenuation of the lower energy beam. Simple optics (a cryo-cooled channel-cut monochromator and bimorph KB focusing mirrors) are adapted to deliver well-focused beam with a good stability.

The beamline has been opened to users from May 2010. The focused beam size (FWHM) at the sample position is 70 um (H) x 10 um (V), and the measured beam intensity is in the order of 10^{10} photons/sec on the area of 10 um square. In the presentation, the current status of the beamline and the first results of SAD experiments are reported.

MS03-P12

SENJU: A new time-of-flight single crystal neutron diffractometer at J-PARC

Takuro Kawasaki[1], Kenichi Oikawa[1], Itaru Tamura[1], Takashi Ohhara[1], Koji Kaneko[1], Hiroyuki Kimura[2], Ryoji Kiyanagi[2], Miwako Takahashi[3], Tamiko Kiyotani[4], Masatoshi Arai[1], Yukio Noda[2], and Ken-ichi Ohshima[3]

[1]*Japan Atomic Energy Agency, 2-4 Shirane, Shirakata, Tokai, Ibaraki, 319-1195, Japan*
[2]*Institute of Multidisciplinary Research for Advanced Materials, Tohoku University, 2-1-1 Katahira, Aoba-ku, Sendai, Miyagi, 980-8577, Japan*
[3]*Institute of Materials Science, University of Tsukuba, 1-1-1 Tennodai, Tsukuba, Ibaraki, 305-8573, Japan*
[4]*Showa Pharmaceutical University, 3-3165 Higashi-Tamagawagakuen, Machida, Tokyo, 194-8543, Japan*
E-mail: kawasaki.takuro@jaea.go.jp

SENJU is a new single crystal diffractometer for spallation neutron source in Materials and Life Science Experimental Facility (MLF) at Japan Photon Accelerator Research Complex (J-PARC). It is currently under construction and is scheduled to be complete by spring 2011. The diffractometer is designed to perform diffraction experiment under various environmental conditions, and the crystal and magnetic structure of materials whose lattice constants up to 50 Å will be studied. SENJU also shed light on the superlattice reflection or diffuse scattering in the reciprocal lattice space to analyze the local structures as well as phase transitions of the materials. Measurement using small sample, less than 1.0 mm^3, will be realized. A poisoned decoupled moderator was selected to measure peak profiles of Bragg reflection and intensity distributions of superlattice reflection or diffuse scattering with good accuracy. At the beginning, the diffractometer will have 31 two-dimensional scintillation detectors to observe the wide area of reciprocal lattice space by one measurement. Various sample environments will be provided, such as cryogenic cooling and magnetic field.

The Australian Synchrotron: research opportunities now and into the future

Kia S. Wallwork[1], Chris Glover[1], Nigel Kirby[1], Tom Caradoc-Davies[1], and Ian Gentle[1]

[1]*Australian Synchrotron, 800 Blackburn Road, Clayton, Vic. 3168, Australia*
E-mail: kia.wallwork@synchrotron.org.au

The Australian Synchrotron (AS), which began operation in 2007, offers user access to 9 beamlines and is open to researchers throughout Australasia and the wider international community. Of these operating beamlines, 5 are directly relevant to crystallographic applications, including: macromolecular and micro- crystallography (MX1 and MX2, respectively); powder diffraction (PD); X-ray absorption spectroscopy (XAS); and small- and wide-angle X-ray scattering (SAXS/WAXS). Together these instruments allow examination of a variety of problems including measurement of short and long range atomic order, and the determination of bond lengths and atomic oxidation states in bulk materials.

The MX1 and MX2 beamlines provide remote and on-site control of protein and small-molecule crystallography experiments. The MX2 beamline accommodates protein samples of size greater than 5x5x5 μm^3 and small molecule crystals less than 1x1x1 μm^3. Samples on both beamlines can be loaded by hand or by robot and are held under cryogenic conditions throughout the experiment. The micro-crystallography beamline also features a 30x30 μm^2 beam size, user selectable collimating apertures, and user-selectable energy changes allowing for multiple wavelength anomalous dispersion measurements on micro-crystals.

The powder diffraction beamline is a versatile instrument which facilitates a wide variety of experiments, from phase identification and quantification to structure elucidation and micro-structural analyses. With the Mythen-II detector at its heart the beamline is capable of acquiring relatively high resolution *in situ* diffraction data; data from LaB_6 show FWHM of (111) reflection of 0.0012°. A wide selection of sample stages and ancillaries are available to users, as is the option to use one's own sample environment. Samples mounted in capillaries and on flat plates can be examined and the accessible temperature range is 80-2570 K.

The XAS beamline is a high-flux wiggler-based beamline for XANES and EXAFS (X-ray absorption near-edge spectroscopy and extended X-ray absorption fine structure) measurements for elements where $Z > 20$ (Ca). The beamline utilizes a 100-element Ge detector and is optimized for fluorescence measurements of dilute systems (currently down to ~1 micro molar). A small focused beam spot (0.2 x 0.5 mm^2) enables measurements with *in situ* sample environments. These techniques compliment powder diffraction measurements, affording information about oxidation state which provides additional detail to studies of crystallographic structure.

The small- and wide-angle scattering beamline provides transmission and grazing incidence SAXS measurements on solids, liquids and surfaces, and in many cases simultaneous semi-1D WAXS analysis. High photon intensity and Pilatus detector systems allow fast data acquisition at up to 10's of frames per second. High signal to background allows analysis of very weakly scattering samples such as dilute protein solutions (in some cases as low as 0.1 mg/mL). Automated data acquisition and rapid sample alignment also provides for high through-put studies, up to a few thousand samples per day. The end station is highly flexible and able to accommodate a vast range of sample environments for *in situ* studies. This presentation will highlight the capabilities of the above selection of AS beamlines and will also outline planned developments on those beamlines.

MS03-P14

Introduction of 6B beamline at Pohang Accelerator Laboratory in Korea for the small molecule X-ray crystallography

Dohyun Moon

Beamline Division, Pohang Accelerator Laboratory, Pohang, Kyungbook 790-784, Korea
E-mail: dmoon@postech.ac.kr

The 6B beamline at Pohang Accelerator Laboratory (PAL) in Korea has been designed to operate in the photon-energy range of 6~17.5 keV (2.0 ~ 0.71Å) based on a bending magnet light source. It is dedicated to single crystal crystallography with material and biological samples. This beamline consists of three optical components, a collimating mirror, Si(111) double crystal monochromator (DCM) in order to tune the X-ray photon energy, and a toroidal focusing mirror. The photon flux at the sample position is 10^{11} photons/s, an energy resolution is 10^{-4}, and beam size is 250 μm^2 The experiment station is equipped with high speed and high sensitivity of an ADSC Quantum Q210 area detector containing a 210mm^2(4096 x 4096 pixel) detection area, high accuracy air-bearing one-axis goniometer, a cryojet for cooling sample using a liquid nitrogen its controlled 90~400K range, a helijet for extremely low temperature achievement using a liquid helium its 9K temperature, and a scintillation fluorescence detector. The conveniences for users are provided such as high resolution microscopy with DSLR photo system, high performance data processing server with HKL2000, movable hood, variety tools for mounting crystals and so on. Operation of this beamline was started from year 2001 as a first synchrotron crystallography in Korea and supported supramolecule and small molecule user from year 2009. Most of the beamline users constitute small molecule users nowadays. The status of beamline, equipments and several fabrication techniques will be presented on this poster.

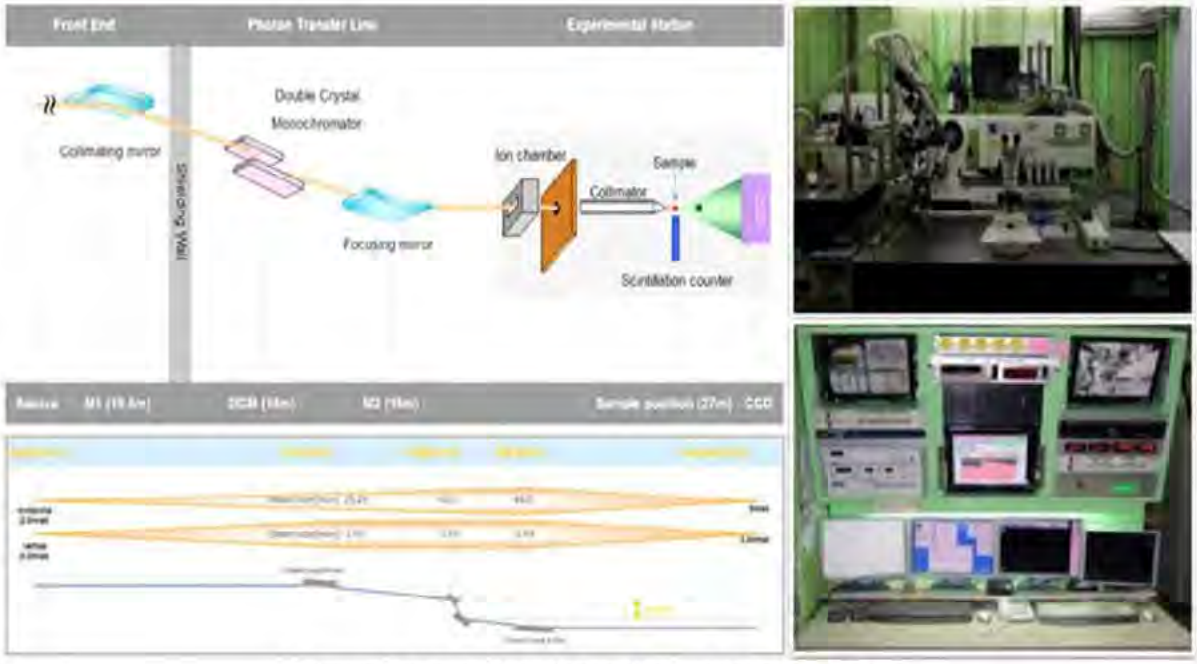

Schematic view of the 6B beamline and experiment space.

MS03-P15

A simulation report of a single crystal diffractometer using an image plate for nano-bio research

Sang Jin Cho[1], Tae Sung Yoon[2] Chang Hee Lee[3], Shin Ae Kim[4], Ji Yong So[5], Kyong-Pyo Kim[6]

[1,3,4,5,6]Neutron Science Division, Korea Atomic Energy Research Institute, 1045 Daedeok-daero, Yuseong-gu, Daejeon, 305-353, Rep. of Korea
[2] Korea Research Institute of Bioscience and Biotechnology, Gwahak-ro 111 Yuseong-gu, Daejeon, 305-806, Rep. of Korea
E-mail: sjcho@kaeri.re.kr

Recognizing the increasing R&D need for nano-bio structures involving Hydrogen Atoms, a project entitled 'Development of a Single Crystal Diffractometer Using Neutron Image-Plate for Nano-Bio Research' started in May this year. A single crystal diffractometer is to be installed at HANARO and the relevant instruments of the project will be opened to general users in early 2012. For this project, a simulation of beam line as precedent work is indispensable to optimize the layout of the instruments while considering the scientific and engineering aspects, for example, determination of monochoromator type & crystal plane, adding neutron guides as a beam path, space for the image plate and its heavy shielding and so on. It was decided to use a Ge(311) crystal as a monochromator and supermirror guides on the beam path to increase the neutron flux. In this paper simulation results at various positions for neutron beam flux and its divergence will be described.

MS03-P16

The first neutron structure analysis of biological macromolecule with IBARAKI Biological Crystal Diffractometer -iBIX- in J-PARC

Katsuhiro Kusaka[1], Taro Yamada[1], Takaaki Hosoya[1], Takashi Ohhara[2], Kazuo Kurihara[2], Ichiro Tanaka[1] and Nobuo Niimura[1].

[1]*Frontier Research Center for Applied Atomic Sciences, Ibaraki University, Tokai, Ibaraki 319-1195, Japan*
[2]*J-PARC Center, Japan Atomic Energy Agency, Tokai, Ibaraki 319-1195, Japan*
E-mail: kusakats@mx.ibaraki.ac.jp

Since 2004, Ibaraki prefecture has constructed the TOF neutron biological diffractometer (IBARAKI Biological Crystal Diffractometer: iBIX) at BL03, in Material and Life Science Facility in J-PARC. The diffractometer is designed to cover samples that have their cell edges up to around 135 Å with a resolution up to 1.2 Å (biological macromolecules) and to 0.7 Å (organic compounds).

In 2008, the basic part of the instrument of iBIX, including 14 detectors (a two dimensional detector which consists of ZnS:Ag/$^{10}B_2O_3$ scintillators with a wavelength shift fiber system, and the total solid angle of the detector system: 9%) has been completed to prepare for diffraction experiment. Since the end of December in 2008, iBIX bas been opened for users. Neutron diffraction datasets of several organic compounds of the known structure have been collected by using the iBIX and molecular structures obtained from the analysis agreed with the reported structures.

We have tried to collect the first TOF neutron diffraction dataset of a protein crystal by using iBIX in order to estimate the performance and characteristics of iBIX. The selected crystal for the purpose is ribonuclease A soaked in heavy water. The crystal volume was 4.7 mm^3. The cell parameters were a=30.4 Å, b=38.6 Å, c=53.4 Å, b=105.8° in a monoclinic form, respectively. Measurement conditions are as follow: the accelerator beam power: 120kW, the pulse repetition: 25Hz, the range of wavelengths: 1.5~4.5 Å (the 1st frame), 4.2~7.5 Å (the 2nd frame), the number of measurement settings: 100 settings (1st frame: 67settings, 2nd frame: 43 settings), the exposure time: 5 hours/setting (the 1st frame), 1 hour/setting (the 2nd frame), the total amount of measurement time for full dataset: 17 days.

The data reduction (to extract a HKLF list from raw data) was carried out by using a new data processing software "STARGazer" which we have developed for TOF neutron diffraction data. At present, the data reduction of almost all of the first frame data set was finished and consequently the tentative HKLF list was obtained. The completeness of Bragg reflections is about 80% of 1.9 Å resolution. The first structure refinement was carried out with this tentative intensity dataset. We have succeeded in obtaining the reasonable structure after the first structure refinement with tentative data by comparing with the already-reported structure [1]. In future we will proceed the reduction of the remaining data (of the 2nd frame) and try to improve the resolution (less than 1.8 Å) and accuracy of intensity data. We will report the results of the further structure refinement with the final processed data in the conference.

References

[1] Yagi D., Yamada T., Kurihara K., Ohnishi Y., Yamashita M., Kuroki R., Tanaka I. and Niimura N., "A neutron crystallographic analysis of phosphate-free ribonuclease A at 1.7 Å resolution" *Acta Cryst* D**65**, (2009), pp 892-899.

Highest brilliance X-ray sources for home lab instrumentation – from solid target anode to liquid metal jet micro-focus

Martin Adam[1], Arnt Kern[1], Christoph Ollinger[1], Carsten Michaelson[2], Till Samtleben[2]

[1]*Bruker AXS GmbH, Oestliche Rheinbrueckenstrasse 49, D 76181 Karlsruhe, Germany*
[2]*Incoatec GmbH, Max-Planck-Str. 2, 21502 Geesthacht, Germany*
E-mail: info@bruker-axs.de

For a wide variety of x-ray applications the depth of accessible information is limited by the brilliance of the x-ray source. Recent break throughs in x-ray source technology push the limits further. Over the years rotating anode based systems became a standard in x-ray diffraction. The latest generation offers an increased brilliance combined with reduced maintenance costs. At the same time microfocus sealed tube systems like the ImS enable for air-cooled, hot x-ray sources with almost no power consumption. Current developments are focusing on sources using liquid metal jet targets (e.g. a Gallium alloy) instead of fast spinning solid metal targets. These in-house sources will make power loads of the order of 500 kW/mm^2 possible. Operated a focal spot sizes below 20 microns at an x-ray energy of 9.2 keV the way for applications with a brilliance comparable to bending magnet sources in a home-lab instrument is paved.

Combining the sources with state-of-the-art multilayer mirrors, allows to transport the brilliance, enabling highest flux-densities at the sample suitable for e.g. diffraction and scattering investigations on very small samples or with very high spatial resolution.

During the course of the presentation dedicated data will discuss the potential of such sources integrated into a laboratory x-ray diffraction instrument.

MS03-P18

New X-ray imaging cameras give insight into X-ray source characteristics

Licai Jiang[1], Hugh Garvey[1], Nick Grupido[1], Bodo Ehlers[1], Bonglea Kim[1], Ladislav Pina[2], Martin Horvath[2]

[1]*Rigaku Innovative Technologies, Inc., 1900 Taylor Road, Auburn Hills, MI 48326*
[2]*Rigaku Innovative Technologies Europe, s.r.o., Novodvorska 99, 142 21 Prague 4, Czech Republic*
E-mail: licai.jiang@rigaku.com

Advances in microfocus x-ray sources and synchrotron beamlines have resulted in smaller, better defined x-ray beams. Characterizing such beams is an important and sometimes difficult task. In this paper, Rigaku will present results from two recently developed cameras allowing the characterization of x-ray image features from instruments and synchrotrons, where the feature size can be on the order of microns. One new camera, the Xsight™ Micron, has been used to characterize the beam coming from a microfocus x-ray source with a new, high-precision graded multilayer optic based on Rigaku's Arc)Sec™ technology. The second camera, Xsight™+, shows dramatic improvement in laboratory instrument alignment and setup time. We will show the advantages of using a high-resolution imaging detector for the alignment of x-ray instruments, especially when using small, well-defined beams. We will also show how these cameras can help with synchrotron and other x-ray sources.

MS06-P01

Morphological structures of a polymethacrylate diblock copolymer bearing POSS moieties probed by grazing incidence X-ray scattering

Byungcheol Ahn[1], Sangwoo Jin[1], Tomoyasu Hirai[2], Yecheol Rho[1], Sungmin Jung[1], Kwang-Woo Kim[1], Samdae Park[1], Jin Chul Kim[1], Wonsang Kwon[1], Junman Choi[1], Dong Min Kim[1], Jungwoon Jung[1], Kyungtae Kim[1], Mihee Kim[1], Yong-Gi Ko[1], Masa-aki Kakimoto[2], Padma Gopalan[3], Teruaki Hayakawa[2,*], Moonhor Ree[1,*]

[1] *Department of Chemistry, Center for Electro-Photo Behaviors in Advanced Molecular Systems, BK School of Molecular Science, Division of Advanced Materials Science, Pohang University of Science & Technology, Pohang, 790-784, Republic of Korea*
[2] *Department of Organic and Polymeric Materials, Tokyo Institute of Technology, 2-12-1-S8-36 O-okayama, Meguro-ku Tokyo 152-8552, Japan*
[3] *Department of Materials Science and Engineering, University of Wisconsin-Madison, Madison, Wisconsin 53706*
E-mail: ree@postech.edu

The morphological structures in thin films of a diblock copolymer of methyl methacrylate and polyhedral oligomeric silsesquioxane (POSS) functionalized methacrylate (PMMA-*b*- PMAPOSS) with a volume ratio of 13/87 were investigated in detail by using synchrotron grazing incidence small and wide-angle X-ray scattering (GISAXS and GIWAXS). In addition, its thermal properties were studied. Thin films of this diblock copolymer were found to undergo phase-separation during solvent-annealing with carbon disulfide and post thermal annealing. To quantitatively analyze the scattering data, GISAXS and GIWAXS formulas were derived and applied. Our detailed analysis found that cylinders of PMMA blocks are induced to form in the diblock copolymer films by solvent-annealing and are hexagonally packed in the PMAPOSS matrix, in which the cylinders are oriented vertically with respect to the film plane. In the solvent-annealed films, both the PMMA cylinders and the PMAPOSS matrix are featureless, i.e., amorphous. However, the post thermal annealing process induces aggregation of the POSS moieties, which results in the formation of crystals with an orthorhombic lattice unit cell. These crystals were found to consist of PMAPOSS block chains in a helical conformation in which the molecular PMAPOSS cylinders are aligned in the film plane. The formation of these crystals is induced by the ordering ability of the POSS moieties. The crystals were found to melt above 190 °C during heating and subsequent cooling. In contrast, the hexagonally packed structure of the PMMA cylinders in the solvent-annealed and post thermally annealed films was found to be retained during the heating and the subsequent cooling. In addition, the scattering analysis provides detailed structural parameters. The 2D GISAXS and GIWAXS patterns were reconstructed from the determined structural parameters by using the derived scattering formulas, and found to be in good agreement with the experimental patterns. Moreover, a model for the structure of the films of the diblock copolymer is proposed.

MS06-P02

Nanoporous conducting polymer thin films generated from ionic interaction block copolymers templates

Yecheol Rho[1], Ayumi Takahashi[2], Tomoya Higashihara[2,*], *Byungcheol Ahn*[1], Samdae Park[1], Jin Chul Kim[1], Dong Min Kim[1], Jungwoon Jung[1], Wonsang Kwon[1], Kyungtae Kim[1], Mihee Kim[1], Yong-Gi Ko[1], Sungmin Jung[1], Junman Choi[1], Moonhor Ree[1,*], and Mitsuru Ueda[2,*]

[1] *Department of Chemistry, Center for Electro-Photo Behaviors in Advanced Molecular Systems, BK School of Molecular Science, Division of Advanced Materials Science, and Polymer Research Institute, Pohang University of Science & Technology (POSTECH), Pohang 790-784, Republic of Korea*
[2] *Department of Organic and Polymeric Materials, Graduate School of Science and Engineering, Tokyo Institute of Technology, 2-12-1-H-120, O-okayama, Meguro-Ku, Tokyo, 152-8552, Japan*
E-mail: ree@postech.edu

A series of well-defined aniline-chain-end-functionalized regioregular poly (3-hexylthiophene)s (P3HT-NH_2) and sulfo-chain-end-functionalized polystyrene (PS-SO_3H) have been prepared based on quasi-living Grignard metathesis and living anionic polymerization, respectively. Block copolymers via ionic interaction, (P3HT-NH_3^+)- *b*-(PS-SO_3^-)s, were successfully synthesized, simply by blending P3HT-NH_2 with PS-SO_3H in toluene. The thermal and optical properties of the block copolymers were investigated by differential scanning calorimetry (DSC) and ultraviolet-visible (UV-vis) spectroscopy. The self-assembly behavior of the (P3HT-NH_3^+)-*b*-(PS-SO_3^-) thin film was observed by atomic force microscopy (AFM) and transmission electron microscopy (TEM). In addition, grazing incidence X-ray scattering (GIXS) analysis found the microphase separation of P3HT-NH_3^+ and PS-SO_3^- domains as well as the packing behavior of P3HT-NH_3^+ segments in block copolymer thin films. By exploiting the pH-sensitive ionic interaction, the PS-SO_3^- domains were selectively etched with ethyl acetate/triethylamine, cleaving the ionic interaction between P3HT-NH_3^+ and PS-SO_3^- segments, to obtain the target nanoporous P3HT-NH_2 films. The porosity of the films was confirmed by AFM, scanning electron microscopy (SEM) and GIXS analyses.

MS06-P03

Effect of C_{60} fullerene on the duplex structure of i-motif DNA with complementary DNA in solution

Byungcheol Ahn[1], Mihee Kim[1], Kyeong Sik Jin[1], Su Ryon Shin[2], Yecheol Rho[1], Kyungtae Kim[1], Sungmin Jung[1], Seon Jeong Kim[2,*] and Moonhor Ree[1,*]

[1]*Department of Chemistry, National Research Laboratory for Polymer Synthesis and Physics, Pohang Accelerator Laboratory, Center for Electro-Photo Behaviors in Advanced Molecular Systems, BK School of Molecular Science, Division of Advanced Materials Science, and Polymer Research Institute, Pohang University of Science & Technology, Pohang 790-784, Republic of Korea*
[2]*Center for Bio-artificial Muscle and Department of Biomedical Engineering, Hanyang University, Seoul 133-791, Republic of Korea*
E-mail: ree@postech.edu

The structural effects of fullerene on i-motif DNA were investigated by characterizing the structures of fullerene-free and fullerene-bound i-motif DNA, in the presence of cDNA in solutions of varying pH, using circular dichroism and synchrotron small-angle X-ray scattering. To facilitate a direct structural comparision between the i-motif and duplex structures in response to pH stimulus, we developed atomic scale structural models for the duplex and i-motif DNA structures, and for the C_{60}/i-motif DNA hybrid associated with the cDNA strand, assuming that the DNA strands are present in an ideal right-handed helical conformation. We found that fullerene shifted the pH-induced conformational transition between the i-motif and the duplex structure, possibly due to the hydrophobic interactions between the terminal fullerenes and an internal TAA loops in the DNA strand. The hybrid structure showed a dramatic reduction in cyclic hysteresis.

MS06-P04

Molecular organization of laterally tethered rod-coil molecules

Dong-Je Hong[1,2], and Myongsoo Lee[2]

[1]*Department of Chemistry, Yonsei University, Seoul 120-749, Korea*
[2]*Center for Supramolecular Nan-Assembly, Department of Chemistry, College of Natural Sciences, Seoul National University, Seoul 151-747, Korea*
E-mail: aquadj@yonsei.ac.kr

Rod-coil systems consisting of rigid rod and flexible coil segments are excellent candidates for creating well defined supramolecular structures via a process of spontaneous organization. Recently, we have synthesized series of structurally T-shaped rod-coil molecules with various volume fractions relative to molecular weight. The rod-coil molecules consist of penta-*p*-phenylene conjugated rod segments connected to poly (propylene oxide) (PPO) and 1st generation ethylene oxide dendrimer segments laterally attached through an imidazole linkage. The rod-coil molecules based on lateral linear chains self assembly into layered structures in which the rod segments are organized with different molecular packing in rod layer plane. The rod segments are organized parallel to each other to form different sublayers within rod layers to roll up into filled or tubular scrolls[1] depending on volume fraction. However, molecules with laterally grafted dendritic chain self assemble into spiral 2D columnar structures[2] in which the rod segments showed similar molecular packing with molecules in stepped column structures[3]. The supramolecular structural variation can mainly be attributed to the variation of aromatic rod length and cross-sectional area of coil segments. Insight into the mechanism of scroll formation is provided by observation of intermediate structures kinetically trapped by quenching from the melt and by computer simulation. These results demonstrate that rational design of a self-assembling molecule based on a laterally tethered rod building block allows stable nanostructures to be produced.

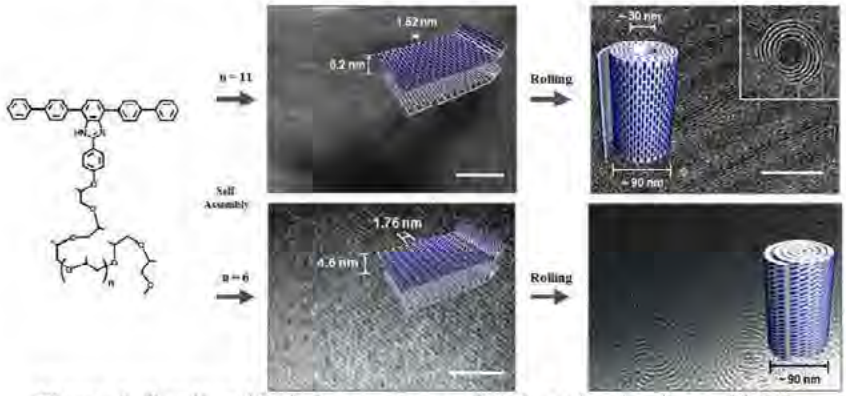

Figure 1. Scroll and Tubular structures of T-shaped rod-coil amphiphiles.

References

[1] Dong-Je H., Eunji L., Haemi J., Jeong-kyu L., Wang-Cheol Z., Trung D. N., Sharon C. G. and Myongsoo L., "Solid-State Scrolls from Hierarchical Self-Assembly of T-Shaped Rod–Coil Molecules", *Angewandte Chemie International Edition*, Vol. 26, (2009), pp 1664-1668.

[2] Dong-Je H., Eunji L., and Myongsoo L., "Self-Organized Spiral Columns in Laterally Grafted Rods.", *Chemical Communications*, Vol. 1, No. 1, (2010), pp 4896-4898.

[3] Dong-Je H., Eunji L., Jeong-kyu L., Wang-Cheol Z., Minwoo H., Eunji S. and Myongsoo L., "Stepped Strips from Self-Organization of Oligo(p-phenylene) Rods with Lateral Dendritic Chains.", *Journal of the American Chemical Society*, Vol. 130, (2008), No. 43, pp 14448-14449.

MS06-P05

Microstructure of PLA-PEG block copolymer aqueous solutions as studied by small angle X-ray scattering

Hye-Jin Jeon, Yeon Hung Oh, Hak Seung Jeong, Woon Bo Shim, Hyun Hoon Song

Department of Advanced materials, Hannam University, Daejeon 305-811, S. Korea
E-mail: hj9594@hnu.kr

Modern plastics industry has evolved due to development of polymer materials with superior characteristics and features. They are used more than 100 million tons. Polymers in the past consider the durability for the environment has been produced. Therefore, most of the commercial plastics are semi permanent. Thus, environmental pollution became a problem. In recent years, environmental conservation with biotechnology and life extension related research is growing. In particular, biodegradable polymer spotlighted as an important material has processibility, practicality, stability, affordability, and environmental aspects are very superior. Accordingly, biodegradable polymer that has been studied with much interest in the past few decades. Polyesters including poly(lactic acid) (PLA), poly(glycolic acid) (PGA), poly(lactic-co-glycolic acid) (PLGA) that have had extensive clinical use as FDA-approved materials for resorbable sutures, pins, screws, and staples1-3. Especially PLA can be applied to drug delivery material, artificial skin and so on. PLA has been combined with a hydrophic poly(ethylene glycol) (PEG) segment to produce an amphiphilic copolymer structure. Polyether, PEG has been also used as a source of hydrophilicity because of its outstanding physicochemical and biological properties including solubility in water and in organic solvents, non-toxicity and bioresorbability4. The biodegradable rate and hydrophilicity of this kind of biodegradable poly(ester-ether) may be controlled by adjusting the mole ratio of hydrophobic segments and sequence distribution of segments. In recent years many efforts have been made in synthesis of PLA-PEG diblock copolymer. PLA-PEG diblock copolymers will self-assemble spontaneously in water into a spherical micelle of a few hundred molecules which has a core of densely packed hydrophobic PLA block and a dense PEG brush shell which radiates from the core5,6. And they occur sol-gel transition by various concentration and temperature. However, the variation of microstructure during the phase transition has not been reported. Therefore, in this work, PLA-PEG diblock copolymer was synthesized. The aqueous solutions of the synthesized block copolymers with different concentrations were prepared and their sol-gel transitions with the detailed microstructures accompanying the transition were examined by the small angle X-ray scattering. Amphiphilic PLA-PEG diblock copolymers with various block lengths were synthesized by ring opening bulk polymerization. The aqueous solutions of the synthesized block copolymers indicate sol-gel transition by variation of concentration and temperature. Small angle X-ray scattering measurements were based on the transition temperature and the concentration. As a result, the sample prepared using a PEG (Mw = 1900), distance was gradually increase at below transition temperature. Because broken physical crosslink of between micelles. Micelles will be independent and random. At this time, changes to the sol state. Furthermore, exceeded a critical temperature, distance was rapidly increases. PEG is lose gradually hydrophilicity by temperature rise. So, the aggregation and collapse that occur in micelles. And sample of using a PEG (Mw = 5000) also broken physical crosslink of between micelles. However, even though the temperature rise, micelles does not occur collapse because chain length longer than PEG (Mw 1900) and the strong hydrophilicity also. Instead, PEG shell will be contraction. In addition, even though the temperature more rises, micelles will be only aggregation.

References

[1] Kwon, G. S.; Kataoka, K. *Adv. Drug Deliv. Rev.*, 1995, 16, 295.
[2] Torchilin, V. P. J. *Controlled Release,* 2001, 73, 137.
[3] Jones, M.; Leroux, *J. Eur. J. Pharm. Biopham.*, 1999, 48, 101.
[4] Zhu, Z.; Xiong, C.; Zhang, L.; Yuan, M.; Deng, X. *European Polymer Journal.* 1999, 35, 1821.
[5] Gao, Z.; Eisenberg, A. *Macromolecules,* 1993, 26, 7353.
[6] Waton, G; Michels, B.; Zana, R. *Macromolecules,* 2001, 34, 907

MS06-P06

Surface-induced columnar structures of discotic liquid crystals in thin films

Hyo-Sik Kim[1], Sung-Min Choi[1], Brian D. Pate[2] and Po Gyu Park[3]

[1]*Dept. of Nuclear and Quantum Eng., Korea Advanced Institute of Science and Technology, Daejeon, 305-701, Korea*
[2]*Dept. of Physics, Central Michigan University, Mount Pleasant, MI 48859, USA*
[3]*Division of Physical Metrology, Korea Research Institute of Standards and Science, Daejeon, 305-340, Korea*
E-mail: itsmine11@kaist.ac.kr

Columnar discotic liquid crystals (DLCs), which provide high one-dimensional charge-carrier mobility, have attracted considerable interest for their potential applications in organic electronic and optoelectronic devices such as field effect transistors and photovoltaics. Typically, a DLC molecule consists of a rigid disc-like aromatic core with flexible aliphatic side chains. The DLC can exist in various phases such as nematic, columnar hexagonal, or rectangular phases depending on its thermodynamic state.[1] In the columnar phase, the overlap of delocalized π-orbitals of neighboring aromatic cores provides excellent charge-carrier mobility along the columnar axis.[2] For many practical applications, therefore, it is essential to fabricate a thin film of uniaxially oriented and highly ordered columnar structure of DLCs over a macroscopic area of substrate.

Typically, the structures and orientations of thin films on substrates are strongly influenced by interfacial interactions at film-substrate interface which propagate across the film thickness.[3] Therefore, the surface energy of substrates are often modified to fabricate the self-assembly of molecules with desired orientations. In the case of block copolymers in a lamellar phase, it has already been shown that the preferential orientation of domains (parallel or perpendicular to the substrate) depends on the interfacial energy between substrate and polymer segment, and typically, the degree of ordering of the lamellar structures decreases with film thickness. It is also expected that the ordering of columnar structures of DLCs on substrates is influenced by the film thickness, affecting the performance of DLC devices. In this study, the structures of magnetically aligned DLC, cobalt (n-decylthio)porphyrazine, thin films on octadecyltrichlorosilane(OTS)-functionalized substrates, with various film thickness ranging from 49 to 845 nm, are investigated by the grazing-incidence small angle X-ray scattering (GISAXS) which is a very powerful technique for investigating the internal structures of thin films (Figure).

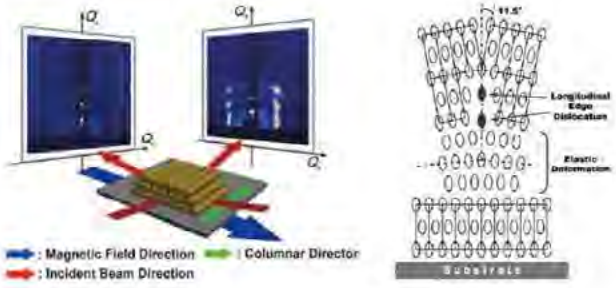

References

[1] Kumar S., "Self-organization of disc-like molecules: chemical aspects", *Chem. Soc. Rev.*, Vol. 35 (2006), pp 83-109.
[2] Schouten P. G., Warman J. M., de Haas M. P., Fox M. A., Pan H.-L., "Charge migration in supramolecular stacks of peripherally substituted porphyrins", *Nature*, Vol. 353 (1991), pp 736-737
[3] Russell T. P., Coulon G., Deline V. R., Miller D. C., "Characteristics of the surface-induced orientation for symmetric diblock PS/PMMA copolymers", *Macromolecules*, Vol. 22 (1989), pp 4600-4606

Fabrication of highly ordered SWNT superstructures in a polymeric system

Changwoo Doe[1], Hyung-Sik Jang[1], Tae-Hwan Kim[1], Steven R. Kline[2], and Sung-Min Choi[1]

[1]*Department of Nuclear and Quantum Engineering, Korea Advanced Institute of Science and Technology, Daejeon, 305-701, Republic of Korea*
[2]*NIST Center for Neutron Research, Gaithersburg, Maryland 20899-6102, USA*
E-mail: sailorpluto@kaist.ac.kr

Fabrication of highly ordered arrays of single-walled carbon nanotubes (SWNTs) has received great interest for a wide range of potential applications. Here, highly-ordered SWNT superstructures which shows thermally switchable pattern between one- and two- dimensional arrays are fabricated by cooperative self-assembly of non-covalently functionalized SWNTs and a PE6200 (PEO10.5-PPO30-PEO10.5)/water system[1]. The non-covalently functionalized isolated SWNTs are fabricated by in-situ polymerization of micelles [2,3]. Small angle x-ray scattering (SAXS) measurements show that when the PE6200/water system is in an isotropic phase, two-dimensional hexagonal arrays of SWNTs are formed by depletion attraction, and when the PE6200/water system is in a lamellar phase, one-dimensional lattices of SWNTs intercalated in the polar regions of the polymeric lamellar structure are formed by entropically driven segregation and two-dimensional depletion attraction. These two highly ordered SWNT superstructures are thermally reversible, following the temperature-dependent phase behavior of the PE6200/water system.

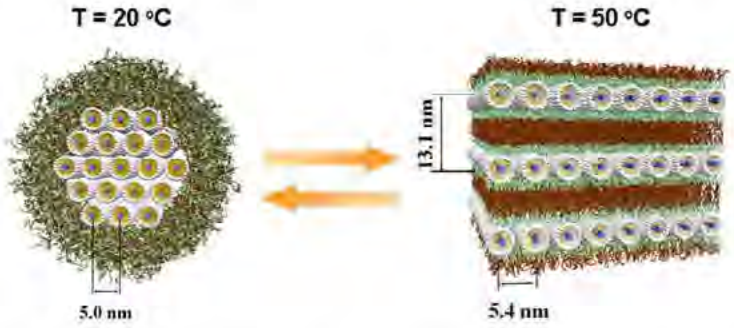

Figure 1. Hexagonal array of p-SWNTs formed by depletion attraction in PE6200/water at low temperature and one-dimensional lattices of p-SWNTs intercalated in the polar region of polymeric lamellar structure (PE6200/water).

References

[1] C. Doe, H.-S. Jang, T.-H. Kim, S. R. Kline, and S.-M. Choi, "Thermally Switchable One- and Two-Dimensional Arrays of Single-Walled Carbon Nanotubes in a Polymeric System", *J. Am. Chem. Soc.*, Vol. 131, No. 45, (2009), pp 16568-16572.

[2] T.-H. Kim, C. Doe, S.R. Kline, and S.-M. Choi, "Water-Redispersible Isolated Single Wall Carbon Nanotubes Fabricated by in-situ Polymerization of Micelles", *Adv. Mater.*, Vol. 19, No. 7, (2007), pp 929-933.

[3] T.-H. Kim, C. Doe, S.R. Kline and S.-M. Choi, "Organic Solvent-Redispersible Isolated Single Wall Carbon Nanotubes Coated by In-situ Polymerized Surfactant Monolayer", *Macromolecules*, Vol. 41, No. 9, (2008), pp 3261-3266.

MS06-P08

Highly ordered self-assembly of negatively charged nanorods and cationic liposomes

Tae-Hwan Kim[1], Shin-Hyun Kang[1], Changwoo Doe[1], Jihyun Yu[1], Jun-Bo Sim[1], Jehan Kim[2], Steven R. Kline[3], and Sung-Min Choi[1]

[1]*Department of Nuclear and Quantum Engineering, Korea Advanced Institute of Science and Technology, Daejeon, 305-701, Republic of Korea*
[2]*Beamline Research Division, Pohang Accelerator Laboratory, Pohang University of Science and Technology, Pohang, Gyeongbuk, 790-784, Republic of Korea*
[3]*NIST Center for Neutron Research, Gaithersburg, Maryland 20899-6102, USA*
E-mail: hunny@kaist.ac.kr

Though self-assembly of 1D nanoparticles into highly ordered superstructures has been of great interest as a route toward materials with new functionalities, the phase behavior of 1D nanoparticles interacting with surrounding materials, which is the key information to design self-assembled superstructures, has not been fully exploited yet. Reported is a phase diagram of the negatively charged nanorod and cationic liposome (CL) complexes in water. It is exhibited that they self-assemble into three different highly ordered superstructures, the intercalated lamellar, the doubly intercalated lamellar, and the centered rectangular structures depending on the $d_{spacing}/d_{rod}$ ratio, which depends on the particle curvature and electrostatic interaction [1]. Negatively charged rodlike nanoparticles with various radii (cRODn) were synthesized by copolymerization of polymerizable surfactants, n-alkyltrimethylammonium 4-vinylbenzoate (CnTVB, n = the number of carbon in alkyl chain), which form wormlike micelles in water, and the anionic hydrotropic salt, sodium 4-styrenesulfonate (NaSS) [2]. The CLs were prepared by extruding a 5:5 (mass ratio) mixture of univalent cationic lipid, dioleoyltrimethylammoniumpropane (DOTAP), and zwitterionic lipid, dioleoylphosphatidylcholine (DOPC), through 200 nm Nucleopore filters. The new phase diagram can be used to understand and design new highly ordered self-assemblies of 1D nanoparticles in soft matter and may provide new novel routes for scalable production of ordered 1D nanoparticle composites with new functionalities.

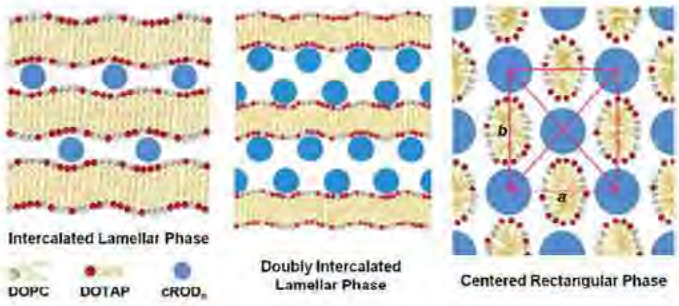

Figure 1. Three different phases formed by negatively charged 1D nanoparticles and CLs

References

[1] T.-H. Kim, S.-H. Kang, C. Doe, J. Yu, J.-B. Sim, J. Kim, S. R. Kline, and S.-M. Choi, "Highly Ordered Self-Assembly of 1D Nanoparticles in Phospholipids Driven by Curvature and Electrostatic Interaction", *J. Am. Chem. Soc.*, Vol. 131, No. 21, (2009), pp 7456-7460.

[2] T.-H. Kim, S.-M. Choi, and S.R. Kline, "Polymerized Rodlike Nanoparticles with Controlled Surface Charge Density", *Langmuir*, Vol. 22, No. 6, (2006), pp 2844-2850

MS06-P09

Synchrotron grazing incidence wide-angle X-ray scattering analysis on molecular aggregation structure of full- or semi-aromatic polyimide films

Byungcheol Ahn[1], Junji Wakita[2], Sangwoo Jin[1], Tae Joo Shin[1], Yecheol Rho[1], Samdae Park[1], Jin Chul Kim[1], Wonsang Kwon[1], Dong Min Kim[1], Jungwoon Jung[1], Kyungtae Kim[1], Mihee Kim[1], Yong-Gi Ko[1], Sungmin Jung[1], Junman Choi[1], Moonhor Ree[1,*], Shinji Ando[2,*]

[1]*Department of Chemistry, Pohang Accelerator Laboratory, Center for Electro-Photo Behaviors in Advanced Molecular Systems, BK School of Molecular Science, Division of Advanced Materials Science, and Polymer Research Institute, Pohang University of Science and Technology, Pohang 790-784, Korea*
[2]*Department of Chemistry and Materials Science, Tokyo Institute of Technology, Ookayama, Meguro-ku, Tokyo 152-8552, Japan*
E-mail: ree@postech.edu

The intermolecular aggregation structures of fully aromatic polyimides (Ar-PIs) prepared from pyromillitic dianhydride and those of semialiphatic polyimides (Al-PIs) from 4,4'-diamino- cyclohexylmethane were characterized by GIWAXS technique. The aggregation structures of both Ar- and Al-PI thin films formed on Si substrates were identified as a mixture of ordered domain and amorphous matrix. For Ar-PIs with glass transition temperatures (*Tg*) higher than the imidization temperature (*Ti*), the aggregation structures are significantly influenced by the three-dimensional structures of the PI chain. Rodlike molecular structures with high planarity are prerequisites for the growth of ordered domains of Ar-PIs, whereas an Ar-PI having a bent and nonplanar structure exhibits the highest amorphous characteristics. In addition, the bulky -CF3 groups in the diamine moiety increase the interchain distance in the ordered domains. For Al-PIs with *Tg*s lower than *Ti*, the degree of interchain ordering was higher than those of Ar-PIs, but was decreased significantly by decreasing *Tg*s. This is due to the vigorous motion of PI chains during thermal imidization

MS06-P10

Self-assembled brush polymers with glycine derivatives and its biocompatibility

Yecheol Rho, Jungwoon Jung, Gahee Kim, Samdae Park, Hyunchul Kim, Jin Chul Kim, Dong Min Kim, Byungcheol Ahn, Wonsang Kwon, Kyungtae Kim, Mihee Kim, Yong-Gi Go, Sungmin Jung, Junman Choi, Sejin Son, Won Jong Kim, Moonhor Ree

Department of Chemistry, Center for Electro-Photo Behaviors in Advanced Molecular Systems, BK School of Molecular Science, Division of Advanced Materials Science, and Polymer Research Institute, Pohang University of Science & Technology (POSTECH), Pohang 790-784, Republic of Korea
E-mail: ree@postech.edu

We have synthesized brush polymers with various glycine derivatives as the end groups of their long alkyl bristles. The polymers are thermally stable up to 170–210 °C and form good quality films through conventional spin- or dip-coating and subsequent drying. Interestingly, the thin films of these brush polymers exhibit different molecular multi-layer structures that arise through the efficient self-assembly of the bristles with glycine derivative end groups. These brush polymer films have hydrophilic surfaces and exhibit some water sorption. The extent of the water sorption by these films depends upon the nature of the glycine derivatives in the bristle end. These films not only repel fibrinogen molecules and platelets from their surfaces, but also have high resistance to bacterial adherence. Moreover, the films were found to provide conducive surface environments for the successful anchoring and growth of HEp-2 cells, and to exhibit excellent biocompatibility in mice. These brush polymers have potential uses in biomedical applications including medical devices, especially blood contacting devices such as catheters, stents, blood vessels, and biosensors, due to their enhanced biocompatibility and the reduced possibility of post-operative infection

MS06-P11

Structures characterization of star polystyrenes with varying numbers of arms through synchrotron X-ray scattering

Yecheol Rho[1], Sangwoo Jin[1], Tomoya Higashihara[2], Samdae Park[1], Jin Chul Kim[1], Dong Min Kim[1], Jungwoon Jung[1], Byungcheol Ahn[1], Sungmin Jung[1], Wonsang Kwon[1], Kyungtae Kim[1], Mihee Kim[1], Yong-Gi Ko[1], Junman Choi[1], Moonhor Ree[1,*] and Akira Hirao[2,*]

[1] *Department of Chemistry, Center for Electro-Photo Behaviors in Advanced Molecular Systems, BK School of Molecular Science, Division of Advanced Materials Science, and Polymer Research Institute, Pohang University of Science & Technology (POSTECH), Pohang 790-784, Republic of Korea*
[2] *Polymeric and Organic Materials Department, Graduate School of Science and Engineering, Tokyo Institute of Technology, H-127, 2-12-1, Ohokayama, Meguro-ku Tokyo 152-8552, Japan*
E-mail: ree@postech.edu

We have synthesized well-defined multiarmed star polystyrenes, with 6, 9, 17, 33, and 57 arms, and studied their molecular shapes and structural characteristics in a good solvent (tetrahydrofuran at 25 °C) and in a theta (Θ) solvent (cyclohexane at 35 °C) by small-angle X-ray scattering (SAXS) using a synchrotron radiation source. Analysis of the SAXS data provided a detailed characterization of the molecular shapes, including the contributions of the blob morphology of the arms, the radius of gyration, the paired distance distribution, the radial electron density distribution, and the Zimm−Stockmayer and Roovers g-factor, for the multiarmed star polystyrenes. In particular, the molecular shapes of the star polystyrenes were found to change from a fuzzy ellipsoid, for the 6-armed polystyrene, to a fuzzy sphere, for the 57-armed polystyrene, with an increasing number of arms. The ellipsoidal character of the star polystyrenes with fewer arms may originate from the extended anisotropically branched architecture at the center of the molecule. The arms of the star polystyrenes were found to be more extended than those of the linear polystyrenes. Furthermore, the degree of chain extension in the arms increased with the number of arms.

MS09-P01

A fast and fully automated solution for Lipidic Cubic Screening (LCP) using mosquito LCP

Joby Jenkins, Patricia Edwards, Rob Lewis and Joanne Franklin

TTP Labtech Ltd, Melbourn Science Park, Melbourn, Royston, Herts, SG8 6EE, UK
E-mail: joby.jenkins@ttplabtech.com

Membrane proteins such, as G-protein coupled receptors, are known to be much more difficult to purify and crystallise than soluble proteins due to their native environment within the lipid bilayer of the cell membrane. As a result aqueous solutions are unsuitable for their reconstitution as they require lipids or detergents to retain their structural integrity.

The *in meso* crystallisation technique revolutionised the process of crystallising membrane proteins. This method utilises highly viscous lipid mesophases to contain the membrane proteins for crystallisation. However, there are a number of technical difficulties associated with the LCP method which makes this process difficult to perform and challenging to automate.

One problem is the viscous nature of the lipids which can be almost solid at room temperature. As a result the addition of protein to the lipid and subsequent reconstitution can be hard to achieve. In addition, the accurate dispensing of LCP, required for efficient miniaturisation, and the precise positioning of drops required for efficient imaging of membrane crystals present two other challenges.

TTP LabTech has solved this problem by developing mosquito® LCP, a dedicated instrument that offers a fully automated solution to LCP screening. This instrument offers fast throughput, high precision and unrivalled reproducibility. Here we describe the benefits of the instrument and how the renowned and reliable positive displacement tip technology ensures that the LCP screening preparation is performed to the highest standard with the minimum amount of effort.

macroSNAP: A computer program for comparing and clustering protein structures

Christopher Gilmore, Gordon Barr, Wei Dong, Adrian Lapthorn and Stuart MacKay

Department of Chemistry, University of Glasgow, Glasgow G12 8QQ, Scotland, UK
E-mail: chris@chem.gla.ac.uk

We have developed two computer programs:
1. PolySNAP [1] which compares and clusters powder patterns and 1-d spectroscopic data.
2. dSNAP [2] which is a tool for clustering hits from the Cambridge Structural Database.

We have adapted these procedures into a program, macroSNAP, for comparing and clustering protein structures with associated, interactive visualisation tools. It works as follows:
1. A set of protein structures is mined from the PDB.
2. The programs SSM or Theseus are used to perform a pair-wise superposition of each of the protein structures. The matching statistics are used to generate a correlation matrix, and a similarity matrix, **s**.
3. Using **s**, we carry out hierarchical cluster analysis. The results are presented as a dendrogram.
4. Metric multidimensional scaling (MMDS) is also used to generate a three-dimensional space in which each protein is represented by a single point in a 3-d box of unit dimensions.
5. The cut level, represented by the solid horizontal line in the dendrogram (see figure), is calculated, thus defining the number of discrete clusters. The cut level is interactive, and can be altered by the user.
6. Displays of superposed structures ca be performed using a COOT interface.

As an example, 47 aaRs crystal structures were mined from the PDB, and clustered using macroSNAP.
As expected, they are separated into two distinct clusters:
1. The class I aaRSs (green) have a Rossman fold and have the parallel beta-strands core.
2. The class II aaRSs (red) have a unique fold made up of antiparallel β-strands.

The outlier (yellow) is not an aaRS structure but an unrelated human IgG-Fc immunoglobulin.

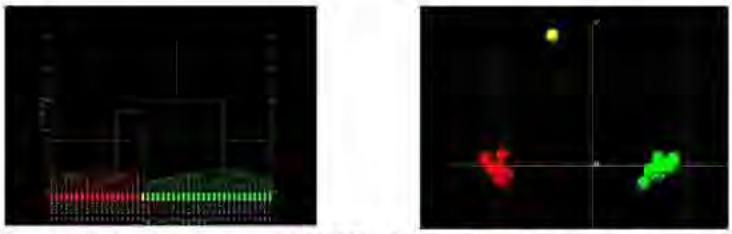

Figure: A dendrogram and MMDS plot for 47 aaRs crystal structures.

macroSNAP is available free of charge to all non-profit organizations.(www.chem.gla.ac.uk/snap/)

References

[1] Barr, G., Dong, W. and Gilmore, C.J., "PolySNAP3: a computer program for analysing and visualizing high-throughput data from diffraction and spectroscopic sources", *J. Appl. Cryst.*, Vol 42, (2009), pp 965-974.
[2] Barr, G., Dong, W., Gilmore, C.J., Parkin, A. and Wilson C.C., "dSNAP: a computer program to cluster and classify Cambridge Structural Database searches", *J. Appl. Cryst.*, Vol 38, (2005), pp 833-841.

MS09-P03

Automated crystal centering by use of UV LED

Leonard M.G. Chavas[1], Yamada Yusuke[1], Masahiko Hiraki[1], Noriyuki Igarashi[1], Naohiro Matsugaki[1] and Soichi Wakatsuki[1]

[1] *Structural Biology Research Center – Photon Factory, High Energy Research Organization (KEK), 305-0801 Tsukuba-shi Oho 1-1, Japan*
E-mail: leonard.chavas@kek.jp

The continuously increasing demand for synchrotron beam-time, both from academic and industrial users, is a direct outcome of the exponential growth of macromolecular crystallography. Fully automated procedures at every level of the experiments are being implemented at all synchrotron facilities, allowing the screening of a profusion of sample crystals for more and more projects. However, the sample recognition and centering in the X-ray beam represents one of the major obstacles to achieving such automation.

Several independent algorithms have been developed to achieve crystal recognition and centering. The most popular method relies on pattern recognition of the loop encircling the crystal (1). Ideal for high-throughput data collections, this frequently used routine has the advantage to allow the screening of plenty of samples in a timely and efficient manner. Nevertheless, when dealing with crystals of small sizes or shifted from the loop center, it suffers from a lack of precision. Other techniques include diffraction-based analysis crystal centering (2), increase of crystal-to-surrounding contrast by differential lights (3), X-ray fluorescence (4) and UV-fluorescence recognition (5).

UV-based crystal centering takes advantage of the capacity of UV-light to specifically react with aromatic residues present in proteins or with DNA base pairs. Although very efficient, a well-known side effect of illuminating biological samples with strong UV-sources resides in the damages induced on the irradiated samples (6). In the present study, the effectiveness of a softer UV-light for crystal centering, by taking advantage of low power LED sources was investigated. Detailed analysis will be done on the impact of such UV-light source on the irradiated sample. Finally, it will be shown how the use of UV LED can represent a low-cost solution for non-damaging crystal centering with high specificity.

References

[1] Muchmore S.W., Olson J., Jones R., Blum M., Greer J., Merrick S.M., Magdalinos P. and Nienaber V.L., "Automated crystal mounting and data collection for protein crystallography", *Structure*, 8, (2000), pp R243-R246.
[2] Song J., Mathew D., Jacob S.A., Corbett L., Moorhead P. and Soltis S.M., "Diffraction-based automated crystal centering", *J. Synchrotron Rad.*, 14, (2007), pp 191-195.
[3] Lavault B., Ravelli R.B. and Cipriani F., "C3D: a program for the automated centring of cryocooled crystals", *Acta Crystallogr. D Biol. Crystallogr.*, 62, (2006), pp 1348-1357.
[4] Karain W.I., Bourenkov G.P., Blume H. and Bartunik H.D., "Automated mounting, centering and screening of crystals for high-throughput protein crystallography", *Acta Crystallogr. D Biol. Crystallogr.*, 58, pp 1519-1522 (2002).
[5] Pohl E., Ristau U., Gehrmann T., Jahn D., Robrahn B., Malthan D., Dobler H. and Hermes C., "Automation of the EMBL Hamburg protein crystallography beamline BW7B", *J. Synchrotron Rad.*, 11, (2004), pp 372-377.
[6] Nanao M.H. and Ravelli R.B.G., "Phasing macromolecular structures with UV-induced structural changes", *Structure*, 14, (2006), pp 791-800.

MS09-P04

Improved technologies for high-resolution X-ray crystallography

H. Tanaka[1], M. Sato[2], K. Inaka[3], N. Furubayashi[3], S. Takahashi[1], B. Yan[1], A. Higashiura[4], M. Suzuki[4], S.-Y. Park[5], Y. Higuchi[6], Y. Yoshimura[2] and A. Nakagawa[4]

[1]*Confocal Science Inc., Chiyoda, Tokyo 101-0032, Japan*
[2]*Japan Aerospace Exploration Agency, Tsukuba, Ibaraki 305-8505, Japan*
[3]*Maruwa Foods and Biosciences Inc., Yamatokoriyama, Nara 639-1123, Japan*
[4]*Osaka University, Suita, Osaka 565-0871*
[5]*Yokohama City University, Yokohama, Kanagawa 230-0045, Japan*
[6]*University of Hyogo, Ako, Hyogo 678-1297*
E-mail: tahakah@confsci.co.jp

Japan Aerospace Exploration Agency (JAXA) launched more than 300 kinds of protein samples to a microgravity environment for crystallization in JAXA-GCF and JAXA-NGCF projects, which started in 2003[1]. At the beginning, we emphasized the development of technologies for crystal quality improvement in space, but afterwards, we realized that a series of technologies, from a preparation of protein sample to a three-dimensional structural analysis, were essential for efficient usage of high-quality diffraction data. To obtain these technologies, the "International Space Station applied research partnership program" started in 2004, the leader of which was Professor Nakagawa in Osaka University, cooperated with JAXA for the joint research, in collaboration with the University of Hyogo, Yokohama City University, Maruwa Foods and Biosciences Inc., and Confocal Science Inc. In the program, we developed;

a protein purification system. The purity of the protein was indexed by SDS-PAGE, Native-PAGE and/or DLS.

an optimization method of salt concentration in a crystallization solution of polyethylene glycol as a precipitant for efficient crystallization.

a theory of crystallization condition optimization which accelerates the effectiveness of the microgravity environment.

a remodeled beamline which was specialized for obtaining high resolution X-ray diffraction data set.

a data collection and a refinement methods of high resolution X-ray diffraction data set[2].

a high-pressure cryo-cooling system to reduce the usage of cryoprotectant[3].

These series of technologies are mandatory for high-resolution crystallography and positively work for the efficient usage of microgravity crystallization.

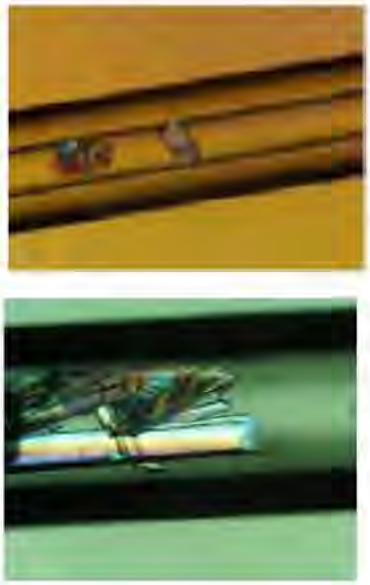

Fig. High-quality crystals of H-protein (0.69 Å) (upper) and Alpha-amylase (0.79 Å)(lower)

We thank the Japan Synchrotron Radiation Research Institute (JASRI) for access to and user support at the synchrotron facilities at SPring-8, Harima, Japan.

References

[6] Sato, M., Tanaka, H., Inaka, K., Shinozaki, S., Yamanaka, A., Takahashi, S., Yamanaka, M., Hirota, E., Sugiyama, S., Kato, M., Saito, C., Sano, S., Motohara, M., Nakamura, T., Kobayashi, T., Yoshitomi, S. and Tanaka, T., "JAXA-GCF project - High-quality protein crystals grown under microgravity environment for better understanding of protein structure", *Microgravity Sci.Technol.*, **18**, (2006) 5-10.

[7] Higashiura, A., Kurakane, T., Matsuda, M., Suzuki, M., Inaka, K., Sato, M., Kobayashi, T., Tanaka, T., Tanaka, H., Fujiwara, K. and Nakagawa, A., "High-resolution X-ray crystal structure of bovine H-protein at 0.88 Å resolution", *Acta Cryst.*, D66, (2010) 698-708.

[8] Kim, C.U., Kapfer, R. and Gruner, S.M., "High-pressure cooling of protein crystals without cryoprotectants", *Acta Cryst.*, D61, (2005) 881-890.

High-quality protein crystal growth experiment (JAXA PCG) on board the Japanese Experiment Module 'Kibo' in the International Space Station

M. Sato[1], H. Tanaka[2], K. Inaka[3], N. Furubayashi[3], S. Sano[1], S. Takahashi[2], B. Yan[2], E. Hirota[2], T. Ichikawa[4], S. Shinozaki[4], M. Shirakawa[1] and Y. Yoshimura[1]

[1]*Japan Aerospace Exploration Agency, Tsukuba 305-8505, Japan*
[2]*Confocal Science Inc., Tokyo 101-0032, Japan*
[3]*Maruwa Foods and Biosciences Inc., Nara 639-1123, Japan*
[4]*Japan Space Forum, Tokyo 100-0004, Japan*
E-mail: sato.masaru@jaxa.jp

Japan Aerospace Exploration Agency (JAXA) has started new protein crystallization experiments, the "High-Quality Protein Crystal Growth Experiment (JAXA PCG)" in the Protein Crystallization Research Facility (PCRF) onboard the Japanese Experiment Module 'Kibo' (JEM) in the International Space Station (ISS) since July, 2009, and is planning to perform six space experiments, twice a year, until 2012. Based on previous experiences of more than 300 kinds of protein crystallization in space in JAXA-GCF and JAXA-NGCF projects onboard the Russian Service Module in the ISS from 2003 to 2008[1], JAXA achieved a user-friendly support system which could help researchers to take part in the project easily, and accumulated know-how to make full use of microgravity environment for growing high-quality crystals. At present, the protein samples for the third flight of JAXA PCG experiment was launched from Baikonur Cosmodrome in Kazakhstan in the beginning of September and will be landed from ISS in the end of November, 2010. Russian and Malaysian researchers as well as Japanese researchers of academics, industries and national projects participate in the experiments. New users from the other countries are very welcome.

In our presentation, we introduce the unique concept of JAXA PCG and brief report of crystallization and X-ray diffraction analysis of proteins in our project.

We thank ESA and Prof. J.-M. Garcia-Ruiz and the members of his laboratory in CSIC-University of Granada for the usage of GCB and their helpful advices when we started our project in 2002. And we thank the Federal Space Agency of Russia and RSC Energia for the usage of the Russian Service Module and the Russian transportation system, Progress and Soyuz space vehicles.

References

[1] Sato, M., Tanaka, H., Inaka, K., Shinozaki, S., Yamanaka, A., Takahashi, S., Yamanaka, M., Hirota, E., Sugiyama, S., Kato, M., Saito, C., Sano, S., Motohara, M., Nakamura, T., Kobayashi, T., Yoshitomi, S. and Tanaka, T., "JAXA-GCF project - High-quality protein crystals grown under microgravity environment for better understanding of protein structure", *Microgravity Sci.Technol.*, **18**, (2006) 5-10.

Analyses of X-ray damage on the oxidized form of high-potential iron-sulfur protein at ultra-high resolution

Yu Hirano, Hiraku Ohno, Hideyuki Jonotsuka, Kazuki Takeda and Kunio Miki

Department of Chemistry, Graduate School of Science, Kyoto University, Sakyo-ku, Kyoto 606-8502, Japan
E-mail: yuu@kuchem.kyoto-u.ac.jp

Crystallographic analyses at ultra-high resolution (d < 1.0 Å) are required for determining positions of hydrogen atoms or visualizing outer shell electrons. Such structural information is important for understanding protein functions. Especially in electron transfer proteins, orientations of bound waters affect redox potentials and outer shell electrons are directly related to the redox activities. However, X-ray damage has been investigated at medium (1.5-3 Å) resolutions until now. These studies reported only significant effects on protein structures, such as cleavage of disulfide bonds or removal of carboxyl groups of asparatic or glutamic acid side chains. Therefore, evaluation of X-ray damage at ultra-high resolution is necessary for elucidating structural changes upon the electron transfer reactions. We have studied crystal structures of high-potential iron-sulfur protein (HiPIP) from the thermophilic purple bacterium *Thermochromatium tepidum*[1-3]. Influences of X-ray irradiation were analyzed in the reduced form of HiPIP at 0.7 Å resolution. Effects of X-rays appeared as reduction of electron densities of hydrogen atoms and as increases of average *B* factors of the protein and the [Fe_4S_4] cluster. We could collect the best data set in which X-ray damage was greatly reduced using attenuated X-rays.

Recently, we successfully crystallized the oxidized form of HiPIP, and collected diffraction data at 0.7 Å resolution with high energy X-rays (31 keV) at the beamline BL41XU of SPring-8. The serial data sets were collected at the same position of the crystal in order to investigate the influences of X-rays in the oxidized form of HiPIP, which is thought to be more sensitive to X-rays than the reduced form. Results of the structure analysis will be discussed at the meeting.

References

[1] Nogi T., Fathir I., Kobayashi M., Nozawa T. and Miki K., "Crystal structures of photosynthetic reaction center and high-potential iron-sulfur protein from *Thermochromatium tepidum*", *Proc. Natl. Acad. Sci. USA*, 97, (2000), 13561-13566.

[2] Liu L., Nogi T., Kobayashi M., Nozawa T. and Miki K., "Ultra-high resolution structure of high-potential iron-sulfur protein from *Thermochromatium tepidum*", *Acta Crystallogr. D*58, (2002), 1085-1091.

[3] Takeda K., Kusumoto K., Hirano Y. and Miki K., "Detailed assessment of X-ray induced structural perturbation in a crystalline state protein", *J. Struct. Biol.*, 169, (2010), 135-144.

MS09-P07

Towards efficient crystallization screening using high performace UV fluorescence imaging

Jian Xu[1] and Michael Willis[1]

[1]*Rigaku Automation, 5999 Avenida Encinas, Suite 150, Carlsbad, CA 92008, USA*
E-mail: Jian.Xu@rigaku.com

With the advent of modern imaging technologies and crystallization automation tools, researchers are able to rapidly create hundreds and thousands of experiments. Screening through those images in order to identify the protein crystal leads can be a time consuming and daunting task. Visible images can often show objects that require further examination. Micro crystals hidden in the precipitation of the crystallization drops as well as distinguishing protein crystals from salt crystals are particularly challenging for visible light imaging. UV fluorescence imaging allows researchers to screen through thousands of images much more rapidly and reliably, as they can simply look for the resulting fluorescence objects detected on the CCD and depicted in the image itself. Rigaku introduces the Minstrel HT UV™, custom engineered to meet the increased demand for a high-throughput ultraviolet and visible crystal imaging and protein crystal monitoring system. We have focused our research and development efforts and the combined knowledge of experts in optics, photochemistry, illumination, and automation to develop a custom solution that provides the highest sensitivity, the highest optical resolution, and the least photo damage to a protein sample. The optimal balance of high resolution and depth of field for the crystallographic application seamlessly images hanging drop, sitting drop, and microbatch experiments for all UV suitable plates. Collaborating with scientists in both academic and industrial communities, we have employed this new technology on crystallization screening of several real world protein samples. The results from the collaboration will be presented, illustrating an improved efficiency of identifying protein crystal leads from screening.

MS09-P08

The high-pressure cryocooling for supramolecular crystals: in the case of Rice Dwarf Virus

Akifumi Higashiura[1], Masaru Sato[2], Koji Inaka[3], Masaki Shirakawa[2], Yoshinori Yoshimura[2], and Atsushi Nakagawa[1]

[1]*Institute for Protein Research, Osaka University,Osaka 565-0871, Japan*
[2]*Japan Aerospace Exploration Agency, Ibaraki 305-8505, Japan*
[3]*Maruwa Foods and Biosciences, Inc., Nara, 639-1123, Japan*
E-mail: hgsur-a@protein.osaka-u.ac.jp

In recent years, macromolecular X-ray crystallography has been advanced significantly by the use of high-brilliance synchrotron beams, high-performance and high-precision large area detectors, and data-reduction programs and any other improvements. To avoid the radiation damage from high-brilliance X-ray beams, the cryo-cooling method has been also developed. In most cases, the crystals need to move or replace the harvesting solution to the cryo-protectant solution, and the condition of cryo-protectant solution is determined through a trial and error process. To overcome the problem of cryo-protectant, the high pressure cryocooling was developed. In this method, a protein crystal is picked up by a cryoloop and pressurizing the crystal to 200 MPa in He gas, cooling under high pressure and releasing the pressure. After that the quality of X-ray diffraction from the high-pressured crystal was improved [1].

Rice dwarf virus (RDV) is a member of the genus *Phytoreovirus* in the family *Reoviridae* and causes rice dwarf disease in Asian countries. RDV was crystallized by the vapor diffusion method using low density PEG solution as a precipitant [2], and the atomic structure was determined at 3.5 Å resolution by X-ray crystallography [3]. In the data collection, RDV crystals were mounted in glass capillary tubes filled with mother liquor because the crystal was sensitive to environmental changes. As the data collection was carried out at room temperature and the crystals were easily damaged by X-ray irradiation, more than 120 crystals were used for the structure determination. The resolution of RDV was relatively high in supramolecular crystal structures (The crystal belongs to the space group of I 222, with cell dimensions of a=770, b=795, c=814 Å), however the structure inside the core particle was not able to modeled.

To clarify the inner structure of RDV we have tried to improve the quality of the crystal and the resolution of X-ray diffraction. For the X-ray data collection using synchrotron radiation in cryo-temperature we adapted the high pressure cryo-cooling method to the RDV crystals.

References

[1] Kim CU, Kapfer R and Gruner SM., "High-pressure cooling of protein crystals without cryoprotectants.", Acta Cryst. D, 61, (2005), pp 881-890.
[2] Mizuno H., Kano H., Omura T., Koizumi, M., Kondoh M. and Tsukihara T., "Crystallization and preliminary X-ray study of a double-shelled spherical virus, rice dwarf virus.", J. Mol. Bio l., 219(4), (1991), pp 665-669
[3] Nakagawa A., Miyazaki N., Taka J., Naitow H., Ogawa A., Fujimoto Z., Mizuno H., Higashi T., Watanabe Y., Omura T., Cheng R.H. and Tsukihara T., "The atomic structure of rice dwarf virus reveals the self-assembly mechanism of component proteins", Structure, 11(10), (2003), pp 1227-1238

MS09-P09

Fluorescence-based screening for soluble human proteins by POET in baculovirus-infected insect cells for structural studies

Song-ying Ouyang, Neil shaw, Zhi-Jie Liu

National Lab of Biomacromolecules, Institute of Biophysics, Chinese Academy of Sciences, Beijing, 100101, China
E-mail: ouyangsy@moon.ibp.ac.cn

Production of structure-grade soluble proteins in substantial quantities takes a critical role in protein structure research. Unfortunately, this has been impeded because a variety of proteins were found insoluble, unstable or can not be purified in bacterial expression system. Baculovirus expression vector system is a eukaryotic expression system and thus uses many of the protein modification, processing, and transport systems present in higher eukaryotic cells and usually provide very high levels of foreign gene production. The baculovirus/insect cell expression system is a very attractive and powerful tool for the production of heterogeneous gene products, especially expression of recombinant eukaryotic proteins. This article describes an improved pooled open reading frame (ORF) expression technology (POET) that uses recombinational cloning and Liquid Chromatography Tandem mass spectrometry (LC/MS) to identify proteins that yield high levels of soluble, purified protein expressed in insect cells. Twenty-two human gene ORFs/fragments were subcloned into baculovirus expression vector and positive recombinant bacmids were constructed, purified, and transfected into Sf9 insect cells. After bulk expression and purification, 2 proteins were identified as soluble protein with higher expression level. By using this improved POET method described here allows the expression characteristics of proteins to be quickly determined in only once experiment in baculovirus expression system.

References

[1] W.K. Gillette, D. Esposito, P.H. Frank, M. Zhou, L.R. Yu, C. Jozwik, X. Zhang, B. McGowan, D.M. Jacobowitz, H.B. Pollard, T. Hao, D.E. Hill, M. Vidal, T.P. Conrads, T.D. Veenstra, J.L. Hartley, Pooled ORF expression technology (POET): using proteomics to screen pools of open reading frames for protein expression. *Mol Cell Proteomics* 4 (2005) 1647-1652.

[2] T. Waybright, W. Gillette, D. Esposito, R. Stephens, D. Lucas, J. Hartley, T. Veenstra, Identification of highly expressed, soluble proteins using an improved, high-throughput pooled ORF expression technology. *BioTechniques* 45 (2008) 307-315.

MS09-P10

Hematin-hematin self-association in hemozoin by X-ray powder diffraction and X-ray absorption spectroscopy

Victor Streltsov[1,4], Ruben Dilanian[2,4], Nectarios Klonis[4,5] Eric Hanssen[3,4,5], Harry Quiney[2,4] and Leann Tilley[4,5]

[1]*CSIRO, Materials, Science & Engineering, 343 Royal Parade, Parkville, 3052, Australia*
[2]*School of Physics,* [3]*Bio21 Molecular Science and Biotechnology Institute and* [4]*ARC Centre of Excellence for Coherent X-ray Science, The University of Melbourne, Vic., 3010, Australia*
[5]*La Trobe Institute of Molecular Science, La Trobe University, Melbourne, 3086, Australia*
E-mail: victor.streltsov@csiro.au

Plasmodium falciparum is the causative agent of the most severe form of malaria in humans. As part of its complex life cycle, the parasite invades, grows, and multiplies within the red blood cells of its host. The parasite engulfs packets of hemoglobin from the host cell cytoplasm using a cytostome and transports the hemoglobin to an acidic digestive vacuole. In this acidic environment the hemoglobin is digested by the action of a series of proteases, and the prosthetic group, heme (ferroprotoporphyrin IX, FP-Fe(II)), is oxidized to hematin (ferriprotoporphyrin IX, FP-Fe(III)) before undergoing a process of biocrystalization to form the malaria pigment, hemozoin.

Hemozoin formation is essential for FP-Fe(III) detoxification in the parasite; it is the main target of quinoline antimalarials and can modulate immune and inflammation responses. To gain further insight into the likely mechanisms of crystal formation and hemozoin reactivity, we have purified hemozoin from *P. falciparum* and solved the crystal structure at a resolution of 2.4 Å using X-ray powder diffraction data [1]. The analysis confirms that the structures of hemozoin and β-hematin are very similar, as suggested previously [2,3). There is nevertheless a clear indication of heterogeneity in the Fe-O coordination in hemozoin. This leads to a greater disorder in the crystal packing of hemozoin than in synthetic β-hematin, which may reflect differences in the mechanisms that lead to crystal formation in these materials. Our analysis of the structural units that comprise the crystal allow us to propose a new model for the formation of hemozoin involving π-π dimers as the nucleation unit. Previous structural studies of β-hematin have assumed that the nucleating unit for the formation of β-hematin and hemozoin is a μ-Pr dimer.

In support of our model, we have conducted an X-ray absorption spectroscopy (XAFS) study of aggregated FP-Fe(III) in suspension and confirmed that self-associated hematin-hematin does not contain substantial levels of μ-Pr dimers. The crystallization may be initiated by the formation of a π-π stacked dimer that subsequently converts to the β-hematin dimeric unit (μ-Pr) as suggested in (4). Hemozoin can be considered to be a crystal composed of π-π dimers stabilized by iron-carboxylate linkages. We have also demonstrated that highly purified hemozoin has a general peroxidase activity and is capable of catalyzing lipid peroxidation. These findings have implications for understanding the immunomodulatory effects of hemozoin and its interaction with antimalarial drugs.

References

[1] Klonis N., Dilanian R., Hanssen E., Darmanin C., Streltsov V., Deed D., Quiney H. and Tilley L. "Hematin-hematin self-association states involved in the formation and reactivity of the malaria p arasite pigment, hemozoin", *Biochemistry*, 49, (2010), pp 6804–6811.
[2] Bohle, D. S., Dinnebier, R. E., Madsen, S. K. and Stephens, P. W. "Characterization of the produ cts of the heme detoxification pathway in malarial late trophozoites by X-ray diffraction", *J. Bio l. Chem.*, 272, (1997), pp 713–716.
[3] Pagola, S., Stephens, P. W., Bohle, D. S., Kosar, A. D. and Madsen, S. K. "The structure of mala ria pigment β-haematin", *Nature*, 404, (2000), pp 307–310.
[4] Egan, T. J. "Haemozoin formation", *Mol. Biochem. Parasitol.*, 157, (2008), pp 127–136.

MS09-P11

Automating microseeding protein crystallography set-ups using Mosquito®

Joby Jenkins, Rob Lewis & David Smith

TTP Labtech Ltd, Melbourn Science Park, Melbourn, Royston, Herts, SG8 6EE, UK
E-mail: joby.jenkins@ttplabtech.com

Crystallising proteins, required for structure determination by X-ray diffraction, is a difficult and labour-intensive task. One of the many challenges facing the protein crystallographer is growing crystals of sufficient size and quality to successfully determine the protein's structure (this typically requires crystals of around 100-300 μm). For structure-based drug design a further challenge is being able to generate a sustainable crystal system capable of producing liganded structures iteratively to support active chemistry. Microseeding, where small crystals are crushed and suspended in a slurry of crystallisation buffer to produce new nucleation sites, is a recognised technique to improve crystal quality as well as promote the growth of larger, single crystals. However, it requires experimentation with varying concentrations of solutions to achieve successful results and as a manual process this can be very consuming.

One approach to increase the speed and efficiency of microseeding set-ups is through the automation of the seeding process. However, this is not a simple process because of the problems that crystallisation robots have with dispensing low volumes. The mosquito® liquid handler (TTP LabTech) is ideally suited to automating the complex set-ups required for microseeding due to its ability to perform multiple aspirations and dispenses with each pipette and the precise handling of nanolitre volumes of solutions, regardless of their viscosity. Here we describe an automated approach to setting up microseeding protocols in 96-well plates using mosquito.

MS09-P12

Getting the most out of your synchrotron

Joseph D. Ferrara, Colin Acheson, Keith Crane, Angela Criswell, Pierre Le Magueres, Bret Simpson

Rigaku Americas Corporation, 9009 New Trails Drive, The Woodlands, TX 773381, USA
E-mail: joseph.ferrara@rigaku.com

X-ray diffraction data collection at synchrotron beam lines is an essential tool for crystallographers to solve protein crystal structures. The characteristics of the X-ray beam: high intensity, low divergence, very small size, and tuneable wavelength are features required for anomalous diffraction phasing methods, high-resolution structure refinements and data collection on weak and difficult samples. In addition, the proliferation of synchrotron beam lines in many countries and the increased availability of beam time has made synchrotron facilities accessible to virtually every crystallographic laboratory in the world. To use the synchrotron most effectively, it is absolutely essential that crystallographers arrive prepared with samples whose quality and cryo-conditions have been previously tested and optimized at home. To address this, Rigaku has developed new instruments that will help researchers screen large numbers of samples in their own lab and recover those suitable for synchrotron data collection. In this work we will present:

The UV crystallization imaging systems from the Minstrel family, combining a UV light source with a visible light source in order to quickly detect protein crystals in crystallization drops and distinguish them from salt or detergent crystals.

The new ScreenMachine, a simple and self-contained X-ray diffractometer optimized for fast and easy screening of crystal candidates at home.

The automatic sample changer ACTOR, which can reliably mount and dismount a large number of samples without user intervention.

MS09-P13

High-end solution for in-house protein crystallography

Martin Adam[1], Marianna Biadene[1], Matt Benning[2], Vernon Smith[1]

[1]*Bruker AXS GmbH, Karlsruhe, Germany*
[2]*Bruker AXS Inc, Madison, WI, USA*
E-mail : info@bruker-axs.de

Recent advances in optics and the introduction of microfocus rotating anode generators have provided a remarkable increase in the performance of home laboratory X-ray systems. When combined with an ultra sensitive CCD detector, these systems can produce data comparable to that collected at synchrotron beamlines. This enhanced system performance can increase productivity and maximize flexibility when dealing with challenging projects, reducing the reliance on synchrotron sources. The advanced capabilities of these solutions allows for a number of experiments which are not feasible on many currently installed systems including:

data sets suitable for in-house SAD phasing
high quality, high-resolution data sets with resolution better than 1.2 Å
x-ray exposure time of less than a minute for complete data collection

We will present data on crystals of a number of number of proteins to demonstrate the exciting capabilities of a high-end systems such as the X8 PROTEUM (figure 1).

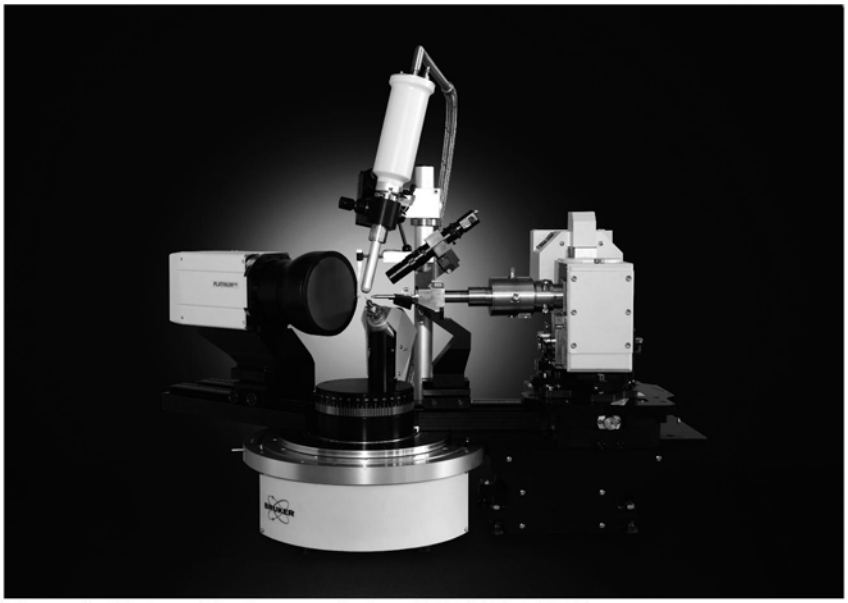

Figure 1: High-end In-house solution (X8 PROTEUM)

MS12-P01

Crystallization of catalytic domain of human MAP kinase phosphatise 5 for neutron diffraction experiments

Simranjeet Singh Sekhon[1, 2], Elena Magay[1] and Tae-Sung Yoon[1, 2]

[1]*Medical Proteomics Research Center, Korea Research Institute of Bioscience and Biotechnology, 111 Gwahangno, Yuseong-gu, Daejeon 305-806, Korea*
[2]*Bio-Analytical Science Major, University of Science and Technology, 111 Gwahangno, Yuseong-gu, Daejeon 305-806, Korea*
E-mail: simran@kribb.re.kr

Neutrons penetrate deeply in the biological materials and the enhanced visibility of hydrogen atoms from water, substrates and proteins enables direct determination of protonation state, and helps to provide a more complete picture of atomic structure. Structural biology could not be fully benefited from neutron diffraction studies because of its requirement of 'big' crystals to compensate the weak flux of available neutron sources. Even the most advanced neutron source still requires protein crystals of size >0.1~1.0mm^3 [1]. To obtain large crystals, we investigated various seed crystallization conditions, and also determined the phase diagram to identify the best conditions for growing the seed crystals.

The catalytic domain of human MAP Kinase Phosphatase 5 (MKP5c) of which crystal structure was solved by x-ray diffraction method [2] was selected for this study because its unit-cell size is suitable to existing neutron diffraction beam-lines [1]. MKP5c was purified and concentrated to 20mg/ml in 20 mM HEPES (pH 7.0) as final buffer. Using 24-well Linbro plate, we obtained 0.3mm size crystals in the longest dimensions by sitting-drop vapor-diffusion method, initiated by mixing equal volume of the 20mg/ml protein and the reservoir solution containing 24%PEG 3350. However, we observed that by increasing the reservoir volume from 500µl to 2.5ml using one-well organ-dish at high protein concentration (100~140 mg/ml) in sitting-drop resulted in bigger seed crystals of sizes 0.5~0.6mm in the longest dimensions. The purified MKP5c protein was concentrated to 50mg/ml and phase diagram was investigated by batch method varying protein and crystallizing agent concentration, and the three zones: i) under-saturation zone, ii) meta-stable zone, and iii) nucleation zone were determined [4]. By inserting seed crystals in the meta-stable zone of the phase diagram and continuously "feeding" these crystals with growing protein solution, we have obtained 0.87mm size crystal in the longest dimensions. We are repeatedly "feeding" the seed crystals to achieve size >0.1~1.0mm^3 suitable for neutron diffraction experiments.

References

[1] Blakeley M.P., Langan P., Niimura N., and Podjarny A., "Neutron crystallography: opportunities, challenges, and limitations", *Current Opinion in Structural Biology,* (2008)18, pp 593-600.
[2] Jeong D.G., Yoon T.S., Kim J.H., Shim M.Y., Jung S.K., Son J.H., Ryu S.E., and Kim S.J., "Crystal structure of the catalytic domain of human MAP Kinase Phosphatase 5: structural insight into constitutively active phosphatase", *Journal of Molecular Biology*, (2006)360, pp 946-955.
[3] Chayen N.E., "Comparative studies of protein crystallization by vapor-diffusion and microbatch techniques", *Acta Cryst.* D54,(1998), pp 8-15.
[4] Asherie N., "Protein crystallization and phase diagrams" *Methods* 34, (2004), pp 266-272

MS12-P02

Growing lysozyme crystals for neutron diffraction beamlines

Elena Magay[1] and Tae-Sung Yoon[1,2]

[1]*Medical Proteomics Research Center, Korea Research Institute of Bioscience and Biotechnology, 111 Gwahangno, Yuseong-gu, Daejeon 305-806, Korea*
[2]*Bio-Analytical Science, University of Science and Technology, 111 Gwahangno, Yuseong-gu, Daejeon 305-806, Korea*
E-mail: elena@kribb.re.kr

Neutron protein crystallography beamlines have been emerging with the introduction of new detectors and high-flux neutron sources although they still require protein crystals of which volumes are larger than 0.1~1.0 mm^3 [1] for diffraction experiments or much bigger ones for the tests of beamlines. Hen-egg white lysozyme (HEWL) has been extensively studied during the past decades as a model system for protein crystal growth (PCG) studies. In spite of the commercial availability and the easiness of crystallization, PCG studies on HEWL have rarely reported to exceed 1 *mm* in length by widely used PCG techniques such as vapor-diffusion or batch methods although its crystallization in a concentration of $NiCl_2$ gradient was reported to 'reproducibly' produce crystals of 4 *mm* in length within 10 days [2]. Aiming to obtain large test crystal of HEWL for neutron diffraction beamline(s) which are under construction and testing in Korea, we found that the $NiCl_2$-concentration gradient method [2,3] could be the easiest way to obtain the desired crystals. However, we also found that obtaining such a size crystal depended on the commercial sources of HEWL. In this work, we provide an improved method based on our own application of $NiCl_2$-concentration gradient method.

PCG trials were conducted at 23°C on HEWLs available from *Sigma* (USA) and *Seikagaku* (Japan), which were prepared at 50 mg/ml in the 50mM Na acetate buffer (pH 4.5). All protein solutions were filtrated through 0.22 μm Sartorius filter. Powders of $NiCl_2$ (1g) were put into the bottom of a vertically held test tube of 100 mm in length, upon which an aqueous solutions of HEWL was carefully applied [2]. The salt was dissolved within a few hours and started to diffuse upwards. The 'crystal hanger' represents *Hampton* capillaries which are attached on a *Hampton* cover-slip and inserted into the test tube sealed by grease. Control PCGs without 'crystal hanger' and test PCGs with 'crystal hanger' of varying the number of inserted capillaries (1~5) of different diameters (0.1~1.5mm) and with different amount of protein applied (60~400mg) were performed. In both control and test PCGs, crystals started to grow only in a region of 15 ~ 40 mm from the bottom of the test tube. In the control PCGs of Sigma, many small crystals were distributed upon the wall of test tube and no single crystal exceeded 1 *mm* in length. In the test PCGs of Sigma, crystals grew up to 2~3 mm in length. In the control PCGs of Seikagagu, a few crystals of 3~4 mm in length were obtained after two weeks. We observed that many crystals appeared around the capillaries in all test PCGs. The 'best' yield of big crystals was in the test PCG with three capillaries of 1.0 mm in diameter. The amount of supplied protein solution did not contribute in any significant manner. We found that the inserted capillaries induced the nucleation around them and suppressed the nucleation on the wall of tubes. Hence we obtained HEWL crystals of 2~4 *mm* in length regardless of its commercial sources.

References

[1] Blakeley M.P., Langan P., Niimura N., and Podjarny A., "Neutron crystallography: opportunities, chal lenges, and limitations", *Current Opinion in Structural Biology,* (2008) 18, pp 593-600.
[2] Ataka M. and Katsura T., "A large single crystal of the tetragonal form of lysozyme can be grown in a concentration gradient of NiCl2", JAERI-Memos (1992). 92-213, p 61.
[3] Tachibana M., Kobayashi Y., Shimazu T., Ataka M., Kojima K. "Growth and mechanical properties of lysozyme crystals", Journal of Crystal Growth (1999). 198/199, 661-664.

MS12-P03

Controlling the coordination numbers of lanthanoid atoms by the use of multidentate polyoxometalate ligands

Tomoji Ozeki,[1] Yusuke Kato and Takahiro Shimono[1]

[1]*Department of Chemistry and Materials Science, Tokyo Institute of Technology, 2-12-1-H-63, O-okayama, Meguro-ku, Tokyo 152-8551, Japan*
E-mail: tozeki@cms.titech.ac.jp

Coordination numbers of lanthanoid atoms is an important factor dominating the efficiencies of the lanthanoid-containing luminescent materials since the overtones and harmonics of the O–H stretching mode play essenitial roles in the quenching of the luminescence. Lacunary polyoxometalates that serve as rigid multidentate oxygen donorligands are good candidates for modifying the coordination geometries of the lanthanoid cations. We have examined its influence by analyzing the structures of the complexes where lanthanoid cations (*Ln* = La, Ce, Pr, Nd, Smand Eu) are incorporated into the lacunary site of $[\alpha_2\text{-}P_2W_{17}O_{61}]^{10-}$ Dawson type polyoxometalate.

Single crystal X-ray diffraction of La, Pr, Nd, Sm and Eu derivatives were carried out by using synchrotron radiations. Single crystal structures were classified into two types, either of which has lanthanoid atoms incorporated into the lacunary site of $[\alpha_2\text{-}P_2W_{17}O_{61}]^{10-}$ and *not* incorporated into the lacunary sites, serving as counter-cations sitting outside the polyoxometalate ligands. The latter links polyoxometalate ligands into one-dimensional extended structures. The coordination number of the lanthanoiod cations incorporated into the lacunary site of $[\alpha_2\text{-}P_2W_{17}O_{61}]^{10-}$ is 9 for La and 8 for the other lanthanoid elements, while those for the free Ln^{3+} cations are 9 for all these compounds. These differences result in the geometries of the extended structures. Effect of the structure hindrance and the nature of polyoxometalate ligands on the coordination numbers and the mechanisms as to how the differences in the coordination numbers result in the differences in the extended structures will be discussed.

MS12-P04

The fascinating world of tautomers and their crystal structures

Dr. Aurora J. Cruz-Cabeza , Dr. Jason C. Cole and Dr. Colin R. Groom

CCDC, 12 Union Road, Cambridge, CB2 1EZ, United Kingdom
E-mail: cruz@ccdc.cam.ac.uk

Although tautomerism is a well-known phenomenon in organic chemistry, it appears to have been largely forgotten within a solid state context. In the context of pharmaceutical materials, the identification and characterisation of tautomers of drug molecules in the solid state could have important intellectual property and commercial implications. This has been illustrated by the late identification of new tautomers of well-known pharmaceutical molecules such as barbituric acid, omeprazole, ranitidine, sulfasalazine or irbesartan. A better understanding of the phenomenom of tautomerism in the solid state is fundamental… and timely!

This presentation will take us through *the fascinating world of tautomers* in crystal structures. We will present our recent work on the generation and identification of tautomers in the Cambridge Structural Database (CSD). We will provide a classification of tautomers as observed in their crystal structures, their frequency of observation and will illustrate the fine balance between tautomers stability and intermolecular interactions. We will rationalize the effect of the crystalline environment on the observation of tautomers and their predictability.

MS12-P05

Crystal engineering of rare-earth (Sm, Gd) molybdates based on organic linkers

Dinesh Kumar and A. Ramanan

Department Chemistry, I.I.T.Delhi, Hauz Khas, New Delhi-110016, India
E-mail: aramanan@chemistry.iitd.ac.in

Crystal engineering of metal organic solids is of contemporary interest due to its potential applications in the areas of magnetism, catalysis, sensor and gas storage. Our objective is to explore the crystallization of these solids from aqueous solution (ambient, hydrothermal and solvothermal) and establish a link between molecular species aggregating in the solution and the supramolecular interactions observable in the solid state. For this purpose we have adopted a retrosynthetic analysis[1-3] by examining related crystal structures reported in the database and implement a synthetic protocol to rationally design new solids. In this poster we present our preliminary reports on the synthesis and characterization of rare-earth molybdates in the presence of EDTA.

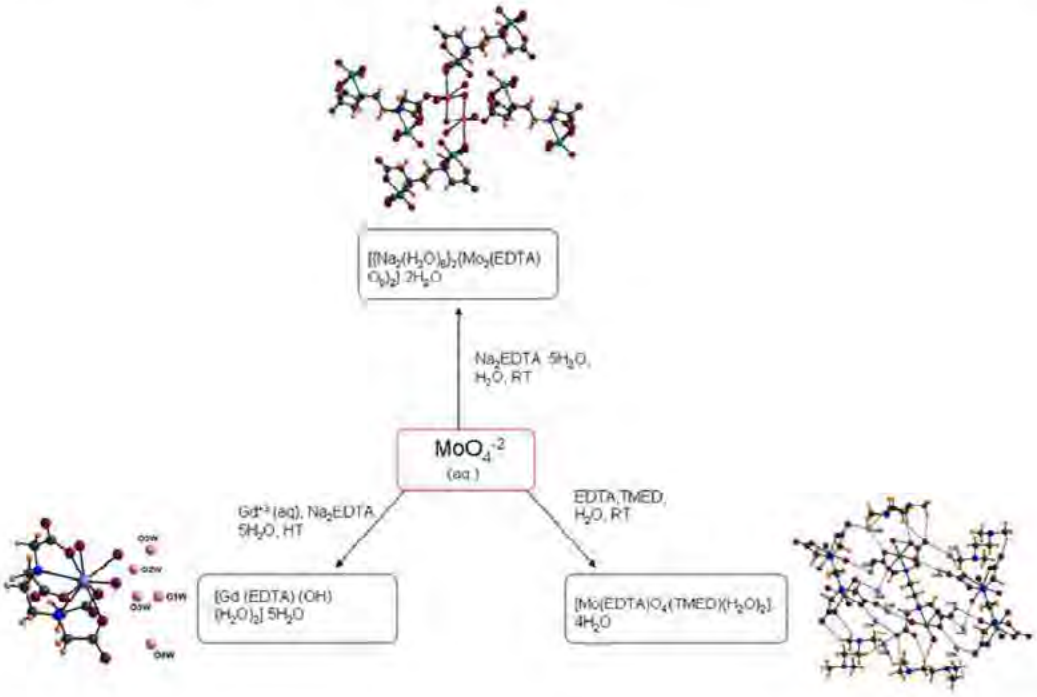

References

[1] Singh M, Thomas J and Ramanan A, "Understanding Supramolecular Interactions Provides Clu es for Building Molecules into Minerals and Materials:a Retrosynthetic Analysis of Copper-Bas ed Solids" *Aus. J. Chem.*,63, 565-572.

[2] Thomas J. and Ramanan A., "Growth of copper pyrazole complex based phosphomolybdates. Supramolecular interactions dictate nucleation of a crystal", *Cryst. Growth & Des.*, 8, 2008, 3 390-3400.

[3] Pavani K. et al., "The Hydrothermal Synthesis of Transition Metal Complex Templated Octamo lybdates", *Eur. J. Inorg. Chem.*, 2007, 568-578.

[4] Thomas J. and Ramanan A., "Growing crystals from solution: By design or by default?", *Curr. S ci.*, 93, 2007, 1664-1667.

Protein crystallization with synthetic zeolite molecular sieves as hetero-epitaxic nucleants

Michihiro Sugahara, Yuko Kageyama-Morikawa and Naoki Kunishima

Protein Crystallography Research Group, RIKEN SPring-8 Center, 1-1-1 Kouto, Sayo-cho, Sayo-gun, Hyogo 679-5148, Japan
E-mail: msuga@spring8.or.jp

Protein crystallization is still a major bottleneck in structural biology. Although the sparse matrix crystallization screening is widely used in protein X-ray crystallography, coarse and unadjustable samplings of this screening often fail in obtaining high quality of crystals especially in the case of proteins with poor crystallizability. To increase the success rate of protein crystallization, we previously developed an advanced crystallization method using molecular sieves (MS) as hetero-epitaxic nucleants by which a directed crystal nucleation on the material surface occurred in a variety of proteins (Figure) [1]. In this work, the hetero-epitaxic nucleant method using MS was applied to the sparse-matrix crystallization screening of xylanase from *Trichoderma longibrachiatum* as a test protein, which provided faster formation of larger single crystals with better diffraction quality as compared with the conventional screening. In many cases, MS induced crystal formation under the conditions that did not provide any protein crystal using the conventional crystallization method without MS. Importantly, the structure of the MS-dependent new crystal form revealed a synergistic effect of MS and zinc ion. In current protein crystallography, available sample amount for crystallization trials is limited especially when the expression level of the target protein is low. In such cases, a minimum set of sparse matrix crystallization screening in the presence of MS may be the most effective way to achieve the diffraction quality of protein crystals.

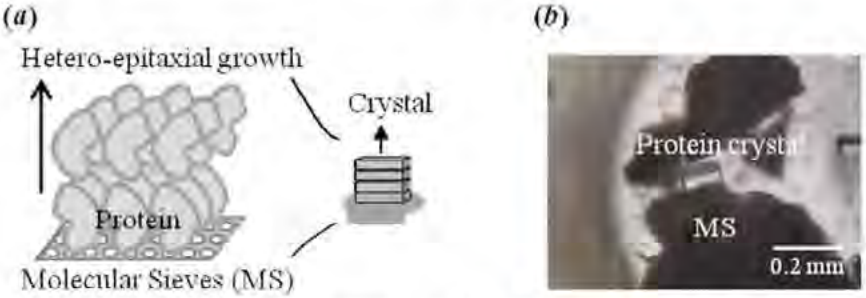

Figure (*a*) Schematic diagram of hetero-epitaxic nucleant for protein crystallization. (*b*) Photograph of protein crystals from MS.

References

[1] Sugahara M., Asada Y., Morikawa Y., Kageyama Y. and Kunishima N., "Nucleant-mediated prote in crystallization with the application of microporous synthetic zeolite", *Acta Crystallogr.* D64, (2 008), pp 686–695.

MS12-P07

Crystal packing analysis of nonmolecular solids – A retrosynthetic approach

Monika Singh and Dinesh Kumar and Arunachalam Ramanan

Department of Chemistry, Indian Institute of Technology Delhi, New Delhi 110016, India
E-mail: aramanan@chemistry.iitd.ac.in

Crystal engineering deals with understanding the growth of crystalline solids (molecular and nonmolecular) from solution in terms of recognizable supramolecular interactions. Analysis of such interactions between molecules (organic, inorganic, metal complex) are more obvious as the solid is held together only by weak forces. However, influence of nonbonding interactions in the formation of nonmolecular or extended solids is less obvious due to the occurrence of ionic, covalent or coordinate bonding in one or more dimensions. This presentation will discuss how the concept of synthons, supramolecular synthons and tectons can be employed to interpret the crystal packing of nonmolecular solids in terms of aggregation followed by condensation of chemically reasonable molecules in the solution preceding nucleation of a crystal. Such an approach provides chemical insights into the architecture of a crystal as well as predictive components to design new materials.

References

[1] Singh M., Thomas J. and Ramanan A., "Understanding supramolecular Interactions provides clues for building molecules into minerals and materials: A retrosynthetic analysis of copper based solids", *Aus. J. Chem.,* Vol. 63, (2010), pp 565-572.
[2] Thomas J. and Ramanan A., "Growth of copper pyrazole complex templated phosphomolybdates: Supramolecular interactions dictate nucleation of a crystal", *Crystal Growth & Design,* Vol. 8, (2008), pp 3390-3400.
[2] Thomas J. and Ramanan A., "Growing crystals from solution: By design or by default", *Current Science* Vol. 93, (2007), pp 1664-1667.
[3] Upreti S. and Ramanan A., "Role of nonbonding interactions in the crystal growth of phenazinediamine tetrahydrate: New insights into the occurrence of 2D water layers in crystal hydrates", *Crystal Growth & Design,* Vol. 7, (2007), pp 966-971.
[4] Ramanan A. and Whittingham M.S., "How molecules turn into solids: The case of metal organic frameworks", *Crystal Growth & Design*, Vol. 6, (2006), pp 2419-2421

MS12-P08

Desktop alchemist™: A high precision fine screen maker to automate crystallization optimization

Jian Xu[1] and Michael Willis[1]

[1]*Rigaku Automation, 5999 Avenida Encinas, Suite 150, Carlsbad, CA 92008, USA*
E-mail: Jian.Xu@rigaku.com

Optimization of crystallization conditions is a critical and time-consuming step in the macromolecular crystallization process. Optimization requires a controllable, reproducible and fast method to refine crystallization conditions in chemical and physical space from an initial screening and to prove that these conditions are viable to yield crystals of x-ray diffraction quality. The number of variables to be considered in an optimization design process can be considerably large, which often limits the number of experiments to be explored. Rigaku introduces the Desktop Alchemist™ fine screen maker, a cost effective and easy to use automation tool for complex optimization. Built upon the industry standard Alchemist™ platform, but with a compact footprint, the Desktop Alchemist offers the ability to dispense reagents from ethanol to 100% glycerol with unsurpassed accuracy and precision, ensuring reproducible results without wasting any expensive chemicals. Non-contact dispensing with Tapper™ technology in conjunction with the patented BirdFeeder™ assembly eliminates cross-contamination since no tubing, pump, or washing is necessary. 26 chemical stocks can concurrently be available to set up experiments on most standard SBS screen plates as well as on Linbro/VDX plates. We will report the results from our precision studies on dispensing chemical stocks of various viscosities, demonstrating that a very viscous solution such as 50% PEG8000 can be dispensed in 1 µl with a total CV of less than 2%.

MS12-P09

Growth and study of optical properties of polycrystalline and single crystals of CdI_2

Alka garg and Anita

Department of Physics, Gargi College, Siri Fort Road, New Delhi 110049, India
E-mail: alkagargi67@yahoo.com

CdI_2 powder was pelletized and subjected to annealing at appropriate temperatures to prepare polycrystalline CdI_2. Also single crystals of CdI_2 were grown using solution method .Both the single crystals and polycrystalline material of CdI_2 were characterised through XRD to ascertain the crystalline nature of the sample [1]. Both were subjected to UV spectroscopy for studying the transmittance over the wavelength range 200-900nm.From analysis of the absorption coefficient, the fundamental absorption can be determined. Optical band gap has been determined for both polycrystalline and single crystals. Results were compared in view of their grain sizes [2].

References

[1] Trigunayat G.C., "A survey of phenomenon of polytypism in crystals"Solid State Ionic, Elsevier Science Publishers B.V.(1991).
[2] Tyagi Pankaj and Vedeshwar A.G., "Grain size dependent optical bandgap of CdI_2 films", Bull. Mater. Sci, vol.24, No. 3,(June 2001), pp 297-300.

MS12-P10

In-situ diffraction: a powerful tool for studying undisturbed crystals in crystallization droplets

Tadeusz Skarzynski

Agilent Technologies XRD (formerly Oxford Diffraction)
E-mail: tadeusz.skarzynski@agilent.com

Protein crystals are usually difficult to grow and can suffer damage on their way from the crystallization drop to the X-ray beam. The damage may be caused by manual handling, change of environment during harvesting, adverse effects of cryo-protection solutions and the dramatic change of temperature due to cryo-cooling. Traditional X-ray experiments to test crystals take time and effort and are often inconclusive.

Characterization of protein crystals with X-rays *in-situ*, without needing to extract them from the crystallization plate, allows establishing a "base line" for crystal quality and evaluating resolution limits before crystals are subjected to any manipulation. The testing of crystals in crystallization plates also allows quickly distinguishing between salt and protein crystals, test harvesting, soaking and cryoprotectant conditions and selecting the best crystals for data collection.

We will show how the *in-situ* testing using the Agilent Technologies **PX Scanner** system for home labs can be used as a powerful tool providing valuable feedback for macromolecule crystallization. Initial trials of using the in-situ diffraction to detect ligand and heavy-atom binding will be presented as well.
Keywords: crystallization process, X-ray methods, in-situ diffraction

Gel crystallization of calcium-lead hydroxyapatite, MHAP (M = Ca^{2+} and/or Pb^{2+})

Oratai Saisa-ard and Kenneth J. Haller

School of Chemistry, Institute of Science, Suranaree University of Technology, Nakhon Ratchasima 30000 Thailand
E-mail: Oratai_phasai@yahoo.com

Calcium hydroxyapatite ($Ca_5(PO_4)_3(OH)$, CaHAP) is the main component of mammalian hard tissues such as bones and teeth. The structure belongs to space group $P6_3/m$ and has ability to accept ionic substituents in both anionic and cationic sites. Ca^{2+} can be replaced by various divalent cations such as Cd^{2+}, Sr^{2+}, and Pb^{2+}, PO_4^{3-} can be replaced by AsO_4^{3-} and VO_4^{3-}, and OH^- can be replaced by F^- and Cl^-. The Ca^{2+} atoms are located on two different sites; *h* sites, mirror planes at z = 1/4 and 3/4, and *f* sites, 3-fold axes at (1/3, 2/3, z) and (2/3, 1/3, z), as shown in Figure 1. Pb^{2+} can accumulate in bone causing a bone disease known as osteoporosis. A recent study [1] has shown the interesting result of dissolution of solid CaHAP and precipitation of isostructural lead hydroxyapatite (PbHAP) when CaHAP is placed in a solution containing Pb^{2+}. In addition Pb^{2+} can substitute in both *h* and *f* sites of CaHAP structure, but the *h* site is preferred [2]. Structural study of MHAP (M = Ca^{2+} and/or Pb^{2+}) is important to understanding the stability and ionic equilibria of this material, and the incorporation of M^{2+} into stable apatite structures.

Bond valence calculations are used to rationalize the unusual interatomic bond parameters reported in the PbHAP structure determined from powder X-ray diffraction data [3]. Gel crystallization was used to prepare larger crystals of MHAP due to its inherent advantages in controlling nucleation and crystal growth rates by changing the composition and density of the gel medium. The FT-IR spectrum of the product exhibits the $\nu(PO_4)$ and $\delta(PO_4)$ band in the 919-1046 and 518-600 cm^{-1} regions, respectively, and ν(OH) at 3555 cm^{-1} indicating presence of phosphate and hydroxyl groups in the product. EDX results demonstrate the presence of Pb^{2+} or Ca^{2+} in the samples consistent with the experimental stoichiometries.

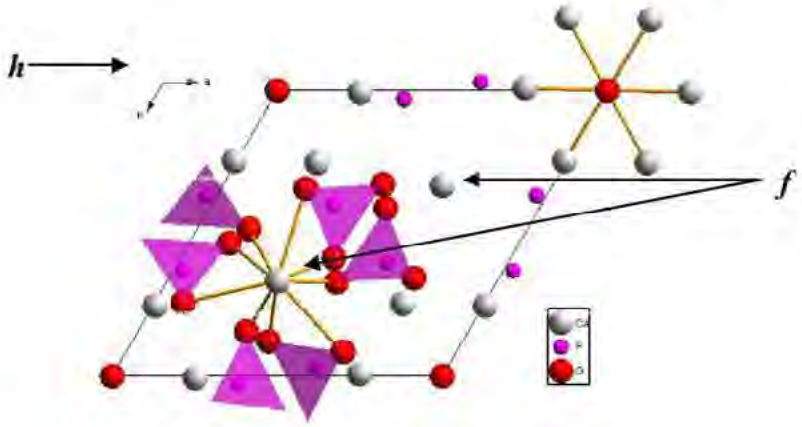

Figure 1. Representation of Ca, O, and P atoms in CaHAP structure projected on the *ab* plane.

References

[1] Mavropoulos E., Rocha C. C. N., Moreira C. J., Rossi M. A., and Soares A. G. "Characterization of phase evolution during lead immobilization by synthetic hydroxyapatite" *Mater. Charact.*, Vol. 53, (2004), 71-78.

[2] Zhua K., Yanagisawa K., Shimanouchi R., Ondaa A., Kajiyoshi K. "Preferential occupancy of metal ions in the hydroxyapatite solid solutions synthesized by hydrothermal method" J. Eur. Ceram. Soc., Vol. 26, (2006), 509–513.

[3] Barinova A. V., Lusvardi G., Menabue L., and Saladini M., "Crystal structure of synthetic hydroxylpyromorphite $Pb_5(PO_4)_3(O H)$" *Kristallografiya*, Vol. 43, (1998), 224-227.

Ab inito structure analysis of solid-state photodimerized methoxyazachalcone from powder diffraction data

Hisashi Konaka[1], Yoko Tokugawa[2] and Shinji Yamada[2]

[1]*Application & Software Development Department, X-ray Analysis Division, Rigaku Corporation, 3-9-12, Matsubara-cho, Akishima-shi, Tokyo 196-8666 Japan*
[2]*Department of Chemistry, Faculty of Science, Ochanomizu University, 2-1-1, Otsuka, Bunkyo-ku, Tokyo 112-8610 Japan*
E-mail: konaka@rigaku.co.jp

The solid-state photodimerization of alkens has received considerable attention in synthetic organic photochemistry because it can afford products unobtainable in solution reaction.[1] Despite its significant synthetic potential, controlling the crystal packing modes is generally a difficult issue. Recently, it has been reported that the cation-π interaction between the pyridinium ring and an aromatic ring serves as a powerful tool to arrange 4`-methoxy-4-azachalcone hydrochloride (**1**•HCl) in a head-to-tail fashion, the photolysis of which resulted in a *syn* head-to-tail dimer (**2**•2HCl) with excellent stereoselectivities and quantitative yields in the crystalline state.[2]

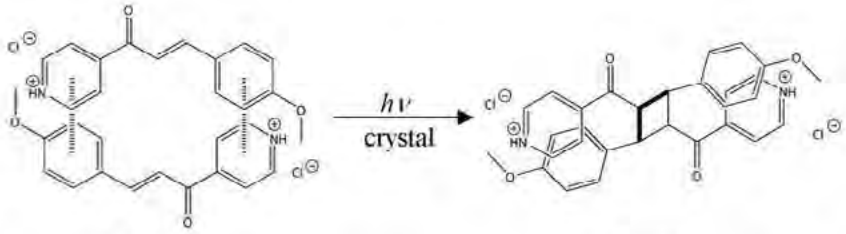

2 **1**•HCl **2**•2HCl

In this study, the crystal structure of **2**•2HCl was clarified without recrystallization using *ab initio* structure determination from laboratory X-ray powder diffraction data as shown in Fig 1.
As a result of analysis, the photo-irradiated powder consisted of dimerized **2**•2HCl (42%) and unreacted **1**•HCl (58%), and another dimer (*anti* isomer or head-to-head isomer) was not included. Experimental and structure analysis details will be reported in this presentation.

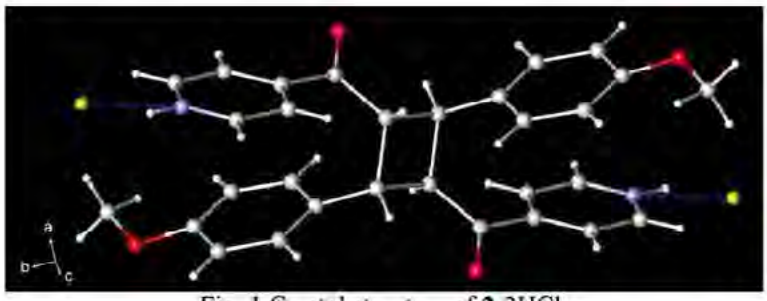

Fig. 1 Crystal structure of **2**•2HCl.

References

[1] Hasegawa M. *Chem. Rev.* 83, 507 (1983).
[2] Ramamurty V. and Venkatesan K. *Chem. Rev.* 87, 433 (1987).
[3] Toda F. *Acc. Chem. Res.* 28, 480 (1995).
[4] Gamlin J. N., Jones R., Leivovich M., Patrick B., Scheffer J. R. and Trotter J. *Acc. Chem. Res.* 29, 203 (1996).
[5] Tanaka K. and Toda F. *Chem. Rev.* 100, 1025 (2000).
[6] Yamada S. and Tokugawa Y. *J. Am. Chem. Soc.* 131, 2098 (2009).

MS15-P02

Effect of pH on zinc oxide crystallographic structure

Sanjeev Gautam[1], I. J. Lee[2] and Keun Hwa Chae[1]

[1]*Nano Analysis Center, Korea Institute of Science and Technology (KIST), Seoul 136-791, S. Korea*
[2]*Pohang Accelerator Laboratory, Pohang University of Science and Technology (POSTECH), Pohang 791-784, S. Korea*
E-mail: sgautam71@kist.re.kr

Zinc oxide has a wide range of applications in the functional devices, catalysts, pigments, optical materials, cosmetics, nanostructure varistors, UV absorbers, gas sensors and industrial additives [1]. Different methods for production of ZnO nano-morphology have already been investigated [1-3]. In this paper we report the crystal structure of Zinc Oxide nano-crystals synthesized by hydrothermal process by variation of precursor pH. High resolution x-ray diffraction (HRXRD) measurements are done at 10B XRS KIST-PAL beamline of Pohang Light Source (PLS), Korea with storage energy 2 GeV and maximum current 200 mA. The crystal structure is studied by using the PowderX [4] and Fullprof [5] simulations. Examination of the composition and morphology of materials produced, reveal the presence of wurtzite single-crystalline phase, which is further investigated through Reitveld refinement [5]. The effect of pH is studied on the value of aspect ratio, and found to vary with an increase in the pH of the precursor solution. The ZnO nanostructures with various morphologies have potential applications in catalyst carrier, chemical sensors and optoelectronic nanodevices.

References

[1] Hingorani, S., Pillai, V., Kumar, P., Mutani, M.S. and Shah, D.O., "Microemulsion mediated s ynthesis of zinc-oxide nanoparticles for varistor studies", *Mater. Res. Bull.*, Vol. 28, (1993) pp 1303.
[2] El-Shall, M.S., Gravier, D., Pernisz, U. and Baraton, M.I. "Synthesis and characterization of n anoscale zinc oxide particles: I. Laser vaporization/condensation technique", *Nanostruct. Mater.*, Vol. 6, (1995), pp 297
[3] Lin, H.M., Tzeng, S.J., Hsiau, P.J. and Tsai, W.L., "Electrode effects on gas sensing propertie s of nanocrystalline zinc oxide", *Nanostruct. Mater.*, Vol. 10, (1998), p.465.
[4] Dong C "Powderx: Windows-95-based program for powder x-ray diffraction data processing", *J App l Cryst.*, Vol. 32, (1999), pp 838.
[5] Rodriguez-Carvajal, "Recent advances in magnetic structure determination by neutron powder di ffraction", *Physica B*, Vol. 192 (1993) pp 55-69.

MS15-P03

Structures differ from sodium and potassium urate crystals

Hwo-Shuenn Sheu, Wei-Ju Shi, and Wei-Tsung Chuang

National Synchrotron Radiation Research Center, Hsinchu 30076, Taiwan

Uric acid is an important metabolite in biologies. It is known as a principal endogenous danger signal released from injured cells and reconginized as a danger signal from dying mammalian cells found by Y. Shi *et al* [1] recentely. The most important urate salt is maybe Monosodium urate monohydrate (MSU), which has been considered response for gout disease since 1960's. The crytstal of Potassium urate is speculated to isomorphous of MSU for a long time. It is only very recentely that Schorn *et al* [2] investegated Sodium and Potassium urate crystals differ in their inflammatory potential. They use of immunofluorescence, immunogold labelling and crystal morphology studies, find that albumin was shown to interact preferentially with the {110} faces of MSU crystals, that is the planes of the incipient crystal exposing sodium cation layers. Synchrotron powder diffraction patterns of Potassium urate crystals reveal quite different from that of MSU. In this study, we have solved the crystal structure of Potassium urate by using synchrotron powder diffraction data and simmulation annealing method. MSU crystalizes in Triclinic space group with unit cell parameters of a=10.8739(5), b=9.4859(3), c=3.55781(9)Å, alpha=95.363(4), beta=99.411(5), and gamma=97.060(4)°, and Potassium urate crystalizes slightly different in Triclinic with a=3.5611(9), b=10.227(3), c=10.920(3)Å, alpha=115.54(3), beta=94.38(4), and gamma=92.36(3)°. The slightly difference in crystal packing and morphorlogy between Sodium and Potassium urate crystals maybe cause their ability differ in gout disease. We will discuss the detail crystal structural differences between Sodium and Potassium urate in this report.

Reference

[1] Y. Shi, J. E. Evans and K. L. Rock, "Molecular identification of a danger signal that alerts t he immune system to dying cells", Nature **425**, 516-521 (2003).

[2] C. Schorn, C. Janko, L. Munoz, C. Schulze, M. Strysio, G. Schett, and M. Herrmann, Sodium an d potassium urate crystals differ in their inflammatory potential, Autoimmunity 42(4): 314–316 (2 009).

MS15-P04

Diffraction vector approach and new detector for two-dimensional X-ray diffraction

Bob B. He

Bruker AXS Inc. 5465 East Cheryl Parkway, Madison, WI 53711, USA
E-mail: bob.he@bruker-axs.com

The two most important developments in two-dimensional x-ray diffraction are area detectors for collecting 2D diffraction patterns and algorithms in analyzing 2D diffraction patterns [1]. Recent advances in area detectors, particularly the one based on the MikroGap technology, and the diffraction vector approach in 2D data analysis are discussed with experimental examples in phase identification, stress measurement, texture analysis and grain size determination.

Two-dimensional diffraction pattern contains information in a large solid angle. The 2D image can be described by the diffraction intensity distribution in both 2θ and γ directions. Unit diffraction vector is used in the data analysis of the 2D diffraction pattern. The unit diffraction vector for all the pixels in the 2D pattern can be calculated in the laboratory coordinates. The data analysis requires the unit diffraction vector to be expressed in the sample coordinates, which can be obtained by vector transformation. For the Eulerian geometry with three sample rotation angles (ω, ψ, ϕ), the transformation is given by:

$$\begin{bmatrix} h_1 \\ h_2 \\ h_3 \end{bmatrix} = \begin{bmatrix} -\sin\omega\sin\psi\sin\phi - \cos\omega\cos\phi & \cos\omega\sin\psi\sin\phi - \sin\omega\cos\phi & -\cos\psi\sin\phi \\ \sin\omega\sin\psi\cos\phi - \cos\omega\sin\phi & -\cos\omega\sin\psi\cos\phi - \sin\omega\sin\phi & \cos\psi\cos\phi \\ -\sin\omega\cos\psi & \cos\omega\cos\psi & \sin\psi \end{bmatrix} \begin{bmatrix} -\sin\theta \\ -\cos\theta\sin\gamma \\ -\cos\theta\cos\gamma \end{bmatrix}$$

The unit vector expressed in the sample coordinate can then be used to derive fundamental equation for many applications or data corrections. The fundamental equation for stress analysis, for instance, is given by the scalar product of the strain tensor ε_{ij} with the unit vector $\{h_1, h_2, h_3\}$:

$$\varepsilon^{\{hkl\}}_{(\gamma,\omega,\psi,\phi)} = \varepsilon_{ij} \cdot h_i \cdot h_j$$

where $\varepsilon^{\{hkl\}}_{(\gamma,\omega,\psi,\phi)}$ is the measured strain from 2D pattern. For texture analysis, the pole figure angles (α,β) are given by pole mapping equations:

$$\alpha = \sin^{-1}|h_3| = \cos^{-1}\sqrt{h_1^2 + h_2^2} \quad \text{and} \quad \beta = \pm\cos^{-1}\frac{h_1}{\sqrt{h_1^2 + h_2^2}} \quad \begin{cases} \beta \geq 0^\circ & if \quad h_2 \geq 0 \\ \beta < 0^\circ & if \quad h_2 < 0 \end{cases}$$

The diffraction unit vector is also used in polarization correction, absorption correction and effective volume calculation for crystal size evaluation by γ-profile analysis.

The VÅNTEC-500 area detector, based on proprietary MikroGap technology, achieves high resolution and low detector noise with a very high dynamic range by combining the advantages of a gaseous detector with the new resistive anode micro-design. It is designed and optimized for the two-dimensional x-ray diffraction system for analytical applications in various materials research, such as nanotechnology, thin films, polymers, metals, biomaterials, forensics and process control. The detector features a large active area and a tapered geometry which makes it possible to capture diffraction patterns in a large solid angle and to access high diffraction angles. The combination of the high sensitivity, low noise, high count rate, and high resolution makes it the technology of choice for laboratory diffractometer for many applications, especially for stress and texture analysis.

References

[1] Bob He, *Two-dimensional X-ray Diffraction*, John Wiley & Sons, (2009).

MS15-P05

Comparision of crystallite shape ellipsoid in various polymers

H Somashekarappa[1], R Gopalakrishne Urs[2], V Annadurai[3], S S Mahesh[4], and R Somashekar[5]

[1]*Department of Physics, Yuvaraja's College, University of Mysore, Mysore, India*
[2] *Department of Physics National Institute of Engineering, Mysore, India*
[3] *Department of Physics Sambram Institute of Technology, Bangalore, India*
[4] *Department of Physics Cambridge Institute of Technology, Bangalore, India*
[5] *Department of Studies in Physics, University of Mysore, Manasagangotri, Mysore, India*

We have carried out line profile analysis of X-ray data recorded from various polymers/polymerblends/fibres like Silk, Cotton, HPMC, Chitosan, SBS etc.. For this purpose we have used in-house Whole Powder Pattern Fitting (WPPF) developed by us. The results obtained are correlated with the physical properties to establish the structure-property relation between these polymers/fibres.

MS15-P06

Using crystallographic knowledge to ease powder structure solution using DASH

Dr. Jason C. Cole, Dr. Colin R. Groom , Dr. Aurora J. Cruz-Cabeza

CCDC, 12 Union Road, Cambridge, CB2 1EZ, United Kingdom
E-mail: cole@ccdc.cam.ac.uk

DASH is a program for direct space solution of powder diffraction patterns. The program uses a Simulated Annealing algorithm to search configurational space to generate trial crystal structures with a view to finding a solution that fits well to the observed powder pattern. Good fits can then be refined using standard techniques leading to a structural solution.

Recently, DASH has been adjusted to allow direct use of torsion angle distributions from the CSD. It is known that limiting search space to likely regions greatly increases the chance of finding a correct solution in direct space programs. Previous implementation of DASH contained the ability for a user to limit search space by making judgments on the likely search regions based on torsion angle distributions from the CSD. This, however, involved significant user intervention and judgment. To improve this, a new protocol called 'Mogul Distribution Biasing' has been developed to allow direct usage of torsion angle distributions for solution purposes. Results show that the new method performs well, allowing solution of complex structures with more than 20 degrees of freedom in a significantly quicker time than with unrestrained searching.

MS15-P07

The importance of Mn(III) in phase transition of some Mn perovskites

T. Y. Tan and B. J. Kennedy

School of Chemistry, The University of Sydney, NSW 2006, Australia
E-mail: ttan6692@uni.sydney.edu.au

The complex interplay between charge, spin and orbital ordering in Mn Perovskites results in such oxides displaying complex, and potentially technologically important electronic and magnetic properties, not the least of which is the Giant Magnetoresistance Effect. High-resolution powder synchrotron X-ray diffraction was performed on Mn perovskites of the type $Ca_{0.8-x}Sr_xNd_{0.2}Mn_{1-y}Cr_yO_3$ in order to establish the effect of Cr substitution for the Mn on crystallographic structure and on phase transformation behavior in complex perovskite manganites. The introduction of Nd^{3+} onto the perovskite A-sites induces partial reduction of the Mn on the perovskite B-site. The amount of the Jahn-Teller Mn^{3+} character can also be controlled by partially replacing the Mn with Cr. Variable temperature diffraction studies of the two series $Ca_{0.4}Sr_{0.4}Nd_{0.2}Mn_{1-x}Cr_xO_3$ and $Ca_{0.2}Sr_{0.6}Nd_{0.2}Mn_{1-x}Cr_xO_3$ with $x = 0.1$ and 0.2 will be described. High temperature diffraction measurements show that the tetragonal oxides $Ca_{0.2}Sr_{0.6}Nd_{0.2}Mn_{1-x}Cr_xO_3$, with *I4/mcm* symmetry apparently transform, directly to the cubic structure. In contrast, increasing the magnitude of the tilts through the addiction of Ca in $Ca_{0.4}Sr_{0.4}Nd_{0.2}Mn_{1-x}Cr_xO_3$ stabilizes an orthorhombic structure and a more complex sequence of phase transition is observed, namely *Pbnm* ↔ *I4/mcm* ↔ *Pm3m*.

References

[1] Kennedy, B.J., et al., "Structural characterisation of the perovskite series SrxCa1-x-yNdyMnO3: Influence of the Jahn-Teller effect." Journal of Solid State Chemistry, 2009. 182(10): p. 2858-2866.

[2] Howard, C.J. and M.A. Carpenter, "Octahedral tilting in cation-ordered Jahn-Teller distorted perovskites - a group-theoretical analysis." Acta Crystallographica Section B-Structural Science, 2010. 66: p. 40-50.

Crystal structural change by guest sorption/release processes of the macrocyclic boronic ester investigated by laboratory powder X-ray diffraction analysis

Kotaro Fujii[1,3], Hidehiro Uekusa[1,3], Yuji Kikuchi[2,3], Hiroki Takahagi[2,3], Kosuke Ono[2,3], and Nobuharu Iwasawa[2,3]

[1] *Department of Chemistry and Materials Science, Tokyo Institute of Technology, Japan*
[2] *Department of Chemistry, Tokyo Institute of Technology, Japan*
[3] *CREST, Japan Science and Technology Agency*
E-mail: fujii.k.aa@m.titech.ac.jp

Recently, diboronic acid and racemic tetrol(**1**) are found to form a self-assembled macrocyclic boronic ester in the presence of appropriate guest molecules.[1] These types of macrocyclic compounds attract many interest because they can be used as a host molecule to absorb and store several types of guest molecules. Recently, the toluene inclusion crystal of the macrocyclic boronic ester (**2**) was found to form one dimensional stacking of **2** along the *b*-axis with an infinite one dimensional toluene channel. It is interesting to explore the crystal structure of the guest-free apohost, in order to investigate whether the crystal can retain its one dimensional tunnel structure, which has enough size to absorb guest molecules, after the guest release. However, **2** tends to incorporate guest molecules during the recrystallization processes and the apohost crystal can only be obtained by guest release process, such as heating of the sample, which usually results to form micro-crystalline powders. Obviously, the crystal structure determination from powder X-ray diffraction data is an essential tool to establish the crystal structure of the apohost. In this study, the apohost of **2** was determined from the laboratory powder X-ray diffraction data and the structural change by guest sorption and release processes were investigated.
The powder X-ray diffraction data of the toluene inclusion crystal of **2** and the apohost crystal of **2**, which was obtained by heating of the toluene inclusion crystal, are significantly different as shown in the figure. However, interestingly, the apohost structure, determined from the laboratory powder X-ray diffraction data, was found to retain its crystal packing even after the guest release. The apohost has one dimensional stacking of **2** along the *b*-axis forming the one dimensional guest free tunnel. This tunnel is expected to absorb the guest molecules easily and, in fact, the apohost crystal readily absorbs the toluene molecules, when the toluene vapor was applied to the solid apohost, and it transforms into the toluene inclusion crystal within 20 min.

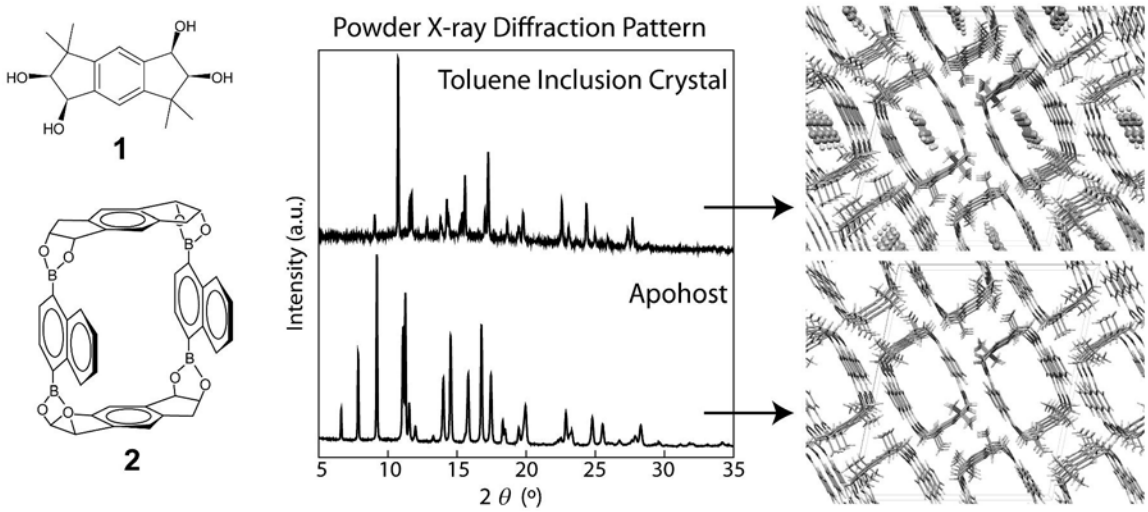

Reference

[1] N. Iwasawa, H. Takahagi, *J. Am. Chem. Soc.*, 2007, 129, 7754-7755

Status report on super high resolution powder diffractometer at J-PARC

Shuki Torii[1], Masao Yonemura[1], Teguh Panca Putra[1], Junrong Zhang[1], Miao Ping[1], Takashi Muroya[1], Ryoko Tomiyasu[1], Takahiro Morishima[3], Setsuo Sato[1], Hidenori Sagehashi[1], Toru Ishigaki[2], Yukio Noda[3], Takashi Kamiyama[1]

[1] *High Energy Accelerator Research Organization, KEK Tokai Campus, 203-1 Shirakata, Tokai, Naka, Ibaraki 319-1106, Japan*
[2] *Ibaraki University, Ibaraki Quantum Beam Research Center, 162-1 Shirakata, Tokai, Naka, Ibaraki 319-1106, Japan*
[3] *Tohoku University, 2-1-1 Katahira, Aoba-ku, Sendai 980-8577, Japan*
E-mail: torii@post.kek.jp

The first neutron was produced successfully from a spallation neutron source in Japan Proton Accelerator Research Complex (J-PARC) at the end of May of 2008. Super High Resolution Powder Diffractometer, SuperHRPD, located at about 100 m from a thin side of a decoupled poisoned moderator achieved the world best resolution $\Delta d/d = 0.035\%$. In the summer of 2009, we installed a new SuperHRPD chamber, which was produced by a small and medium-sized enterprise group, JSS, in Ibaraki prefecture to improve S/N, and to achieve better resolution as well as intensity. The new chamber consists of a vacuum sample chamber with capacity of about 1 m3, and gas-filled scattering banks around it. In the design concept of a new chamber, a detector solid angle is increased, d-range / Q-range is expanded and also choices of high-intensity mode and high-resolution mode are implemented by varying incident collimations. To cover this large detector solid angle, about 1500 one-dimensional 3He position-sensitive detectors (PSDs) of 1/2 inch in diameter were installed in the backward bank, 90 degree bank, and low-angle bank, which consists of 320, 192 and 192 PSD(s), respectively. The on-beam commissioning of the new SuperHRPD was completed in autumn, and general users began to use this new chamber.

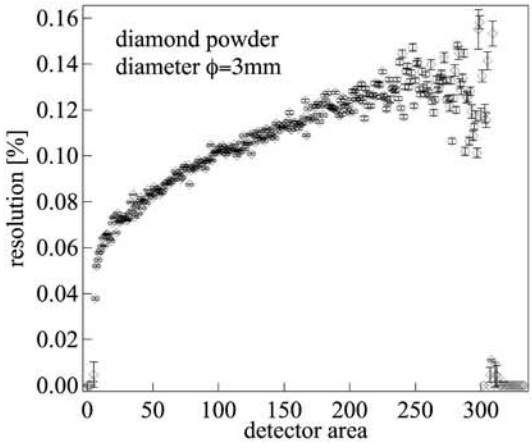

Fig.1 left : A new SuperHRPD chamber was installed in Summer of 2009. Right: A detector range dependency of the resolution. When the value of the horizontal axis is larger, a scattering angle of detector area becomes smaller.

MS15-P10

Research and developments at the Australian synchrotron powder diffraction beamline

Kia S. Wallwork[1], Qinfen Gu[1] and Justin A. Kimpton[1]

[1]*Australian Synchrotron, 800 Blackburn Road, Clayton, Vic. 3168, Australia*
E-mail: kia.wallwork@synchrotron.org.au

The ability to relate the properties of a material with its crystal structure is arguably the most valuable capability of powder diffraction research. Routinely in the natural world, and in the synthetic materials chemistry arena, poly-crystalline materials are readily produced that have interesting and/or important properties. To further understand the manner in which materials or minerals are formed, processed, and/or used it is often necessary to accurately identify the constituent phases and the crystal structure(s) of those phases.

By its very nature powder diffraction allows such examination of natural minerals and functional materials alike. It permits the study of bulk materials and provides a robust alternative for structural characterization when single crystals cannot be found. Examples may include *in situ* study of reaction mechanisms, the study of crystal chemistry, phase identification, and the trend of physical and/or magnetic properties with crystal structure.

Synchrotron powder X-ray diffractometry further enhances powder diffraction-based studies by affording greatly improved angular and energy resolution enabling superior, more reliable data analysis. In addition, the synchrotron experiment benefits from the greater flux (X-ray) density delivered by the source, thereby allowing the examination of smaller samples, with excellent signal to noise, in much faster time-frames than conventional laboratory diffraction experiments. The ability to set-up the experiment station and to tune the X-ray wavelength according to the composition of the sample and the requirements of the experiment are also important considerations of synchrotron-based experiments.

This presentation highlights the value of synchrotron X-ray diffractometry through the examination of a variety of practical and applied uses of powder diffraction, including the development of energy storage materials and the examination of mineralogical processing.

In situ powder X-ray diffraction for gas adsorption on ordered mesoporous materials

Keiichi Miyasaka[1], Norihiro Muroyama[2], Kyoungmin Jung[1], Yoshiki Kubota[3] and Osamu Terasaki[1,2]

[1] *Graduate School of EEWS, Korea Advanced Institute of Science and Technology, South Korea*
[2] *Structural Chemistry, Stockholm University, Sweden*
[3] *Graduate School of Science, Osaka Prefecture University, Osaka, Japan*
E-mail: keii@kaist.ac.kr

Since their discovery in the early 1990s, mesoporous materials[1] have attracted a lot of attention due to various potential applications based on the periodic arrangement of easily tunable mesopores. The pore structure information is essential for understanding the properties of porous media as well as their usage in applications. Gas adsorption isotherm is perhaps the most commonly used in laboratories everyday for characterizing the pore structures. However, the analyses on isotherm data include assumptions such as geometrical model of pores and various interaction parameters fitted from standard isotherms to express the fluid state. We present *in situ* synchrotron powder XRD studies for gas adsorption on ordered mesoporous materials for characterizing the pore structure and fluid state.[2,3] The *in situ* synchrotron powder XRD experiments were performed at a synchrotron radiation facility SPring-8 (BL02B2), Japan, and the experimental data have been analyzed by maximum entropy method and analytical modeling method based on continuous electron density distribution for representing the silica solid wall and the fluid adsorbed on the wall. This diffractometric approach allows us to investigate the precise pore structure of mesoporous materials as well as to monitor the fluid growth on the mesopores. The modeling of the pore structure and the fluid state is first developed, and then the approach is applied to typical mesoporous materials: 2-dimensional MCM-41[1] (plane group *p6mm*), 3-dimensional SBA-16 (space group *Im*-3*m*) and MCM-48 (*Ia*-3*d*). This gives a possibility to reconcile isotherm and diffraction experiments for the future studies on characterizing mesoporous materials.

References

[1] C. T. Kresge, M. E. Leonowicz, W. J. Roth, J. C. Vartuli, J. S. Beck, *Nature* **1992**, 359, pp 710.
[2] N. Muroyama, A. Yoshimura, Y. Kubota, K. Miyasaka, T. Ohsuna, R. Ryoo, P. I. Ravikovitch, A. V. Neimark, M. Takata, O. Terasaki, *J. Phys. Chem. C* **2008**, 112, pp 10803.
[3] K. Miyasaka, A. V. Neimark, O. Terasaki, *J. Phys. Chem. C* 2009, 113, 791.

X-ray diffraction analysis of carbon extracted from a fruit like fullerene

B. Mallick[1], Sonam Narayan[2], Suraj Patra[2], Ashmaa Parvin[2], K. B. Sahu[3], B. Mishra[4] and S. Sahu[1]

[1]*Institute of Physics, Bhubaneswar, India*
[2]*Department of Physics, Spintronic Technology & Advance Research, Bhubaneswar, India*
[3]*Department of Mechanical Engg., Spintronic Technology & Advance Research, Bhubaneswar, India*
[4]*Department of Chemistry, Spintronic Technology & Advance Research, Bhubaneswar, India*
E-mail: bmallick_iopb@scientist.com

A special type of tree was discovered. The tree species was rarely found in different parts of Orissa. The shape of the fruits of the above tree was made up of single/multiple spheres. The surface of the fruit is just like the fullerene and is shown in Fig. 1. Carbon was extracted from the above fruit, simply by burning the fruit at 500 °C in an ordinary oven. X-ray diffraction of the extracted carbon powder was carried out using Bruker AXS, next-generation D8 ADVANCE™ X-ray diffractometer. The diffraction data obtained was compared with the structure of the C_{60}. The complete structural study is under progress. The detail analysis of the results will be reported in the full paper.

Fig. 1. Fruit like Fullerene

References

[1] Krätschmer W., Fostiropoulas K., and Hufman R.., "Evidence for the presence of the C_{60} molecule", *Chem. Phys. Lett*, Vol. 170, (1990), pp 167-170.
[2] Chen X., Yamanaka S., Sako K., Inoue Y., and Hufman R., "First single-crystal X-ray structural refinement of the rhombohedral C_{60} polymer", *Chem. Phys. Lett*, Vol. 356, (2002), pp 291-297.
[3] Scanlon J. C., and Ebert L. B., "X-ray diffraction study of fullerene soot", *J. Phys. Chem*, Vol. 97, (1993), pp 7138-7140.

Development of defect perovskites for use as cathode materials in lithium ion batteries

William R. Brant and Siegbert Schmid

School of Chemistry, The University of Sydney, Sydney NSW 2006, Australia
E-mail: wbra4691@uni.sydney.edu.au

The development of new high capacity cathodes is becoming increasingly important as currently used materials reach their critical energy density limit. Defect perovskite structures such as $Li_{3x}La_{0.67-x}TiO_3$ and $Li_{3x}La_{0.33-x}NbO_3$ are an alternative due to their high ionic conductivity, structural flexibility and high intercalation limits [1-2]. However, in order to further develop the properties of defect perovskites, a thorough understanding of the structural changes, which occur during lithium intercalation and how these affect the electrochemical properties, is essential. Due to the different scattering factors for X-rays and neutrons, particularly for lithium, neutron scattering techniques are extremely useful for the precise structural study of these materials.

We have previously synthesised the perovskite structures $Sr_{0.8}Ti_{0.6}Nb_{0.4}O_3$ (STN) and $Li_{0.18}Sr_{0.66}Ti_{0.5}Nb_{0.5}O_3$ (LSTN) (see figure below), both composed of lighter components than $Li_{3x}La_{0.33-x}NbO_3$. While STN intercalated only a small amount of lithium via chemical means, LSTN readily intercalated lithium. Neutron studies of LSTN before and after chemical lithium intercalation provided significant insight into the structural behaviour of lithium during the initial intercalation process. STN intercalated up to 0.2 mol of lithium per formula unit electrochemically. Again LSTN was able to intercalate a larger amount of lithium electrochemically. Further ex-situ neutron studies have revealed the structural changes, which occur at the end of the intercalation process. While surprisingly STN undergoes very little structural change on intercalation LSTN appears to experience octahedral rotations, which lead to a lower symmetry structure.

This contribution will address the structural changes, which occur in LSTN during chemical and electrochemical intercalation and in STN during electrochemical intercalation. The observed structural changes provide significant insight into the origins of many of the observed electrochemical properties such as specific capacity, reversibility and ionic conductivity.

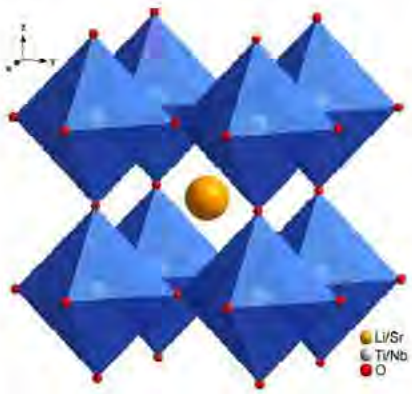

Figure: Cubic perovskite unit cell with Ti^{4+}/Nb^{5+} surrounded by six O^{2-} anions creating a three dimensional network inside which Sr^{2+} or Li^{+} are located

References

[1] Y. Inaguma; C. Liquan; M. Itoh; T. Nakamura, "High Ionic Conductivity in Lithium Lanthanum Titanate", *Solid State Commun.*, Vol. 86 No. 10, (1993), pp 689-693.

[2] A. Nadiri; G. Le Flem; C. Delmas, "Lithium Intercalation in $Ln_{1/3}NbO_3$ Perovskite-Type Phases (Ln = La, Nd)", *J. Solid State Chem.*, Vol. 73, (1988), pp. 338 - 347.

Stacking faults in $Ca_4B_2B'O_9$-type layered brownmillerites

H. Krüger[1,2], T. R. Welberry[1], J. D. Fitz Gerald[3], R. L. Withers[1] and S. Stöber[4]

[1]*Research School of Chemistry, Australian National University, Canberra, ACT 0200,* [2]*Institute of Mineralogy and Petrography, University of Innsbruck, Austria,* [3]*Research School of Earth Sciences, Australian National University, Canberra,* [4]*Faculty of Geosciences, Martin Luther University of Halle-Wittenberg, Germany*
E-mail: hannes.kruger@anu.edu.au

In a structural study of calcium ferrite phases for cement clinkers, we synthesised crystals of a structure-type described as an intergrowth between the brownmillerite (BM) and the K_2NiF_4-type structure [1]. Single crystals were grown using a flux-method and contain three-valent *B* (Fe, Al) and four-valent *B'* cations (Mn, Ti). The unit cell contains two BM-like O-T-O blocks, hence we propose the term *layered brownmillerites* for this structure-type. The structure adopts space group *Amma* with a=5.3, b=26.7, c=5.5 Å, in which the two BM blocks are linked by the centring vector, and the tetrahedral chains show disorder of two possible configurations. However, the diffraction pattern reveals strong diffuse rods along b^*, which occur at $h\ k\ l{+}½$ ($h{\neq}0$). The doubling of c is caused by an alternating sequence of different orientations in the tetrahedral chains. In this new unit cell (c doubled), the old *A*-centring vector becomes [0, ½, ±¼]. The two possible shifts along c^* (fig. 1) affect mostly the tetrahedral layers, which exhibit stacking faults. The rest of the structure basically retains the old lattice. High-resolution transmission electron microscopy reveals the stacking faults. Images recorded along the [102] zone axis (fig. 2) give a high contrast for the different chain configurations [2, 3]. The dotted lines represent the tetrahedral layers. A projection of the [0, ½, ½] direction (straight line) helps to identify stacking faults (see staggered line). The rods of diffuse scattering show strong variations of intensity. In order to reveal the structural reasons, a computer simulation was performed using a random stacking sequence. Additionally, small shifts (parallel to a) of the atoms in close proximity of the chains, were introduced into the model. The sign of the shifts are opposite for the two different chain configurations. Calculated diffraction patterns [4] (fig. 3, right) are in good agreement with the X-ray diffraction data (fig. 3, left).

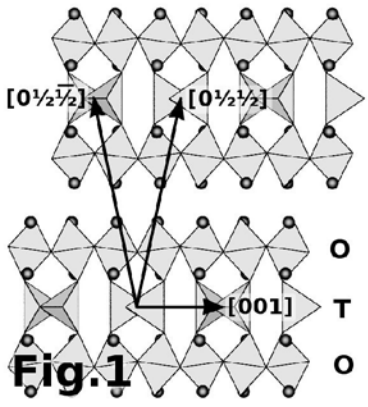

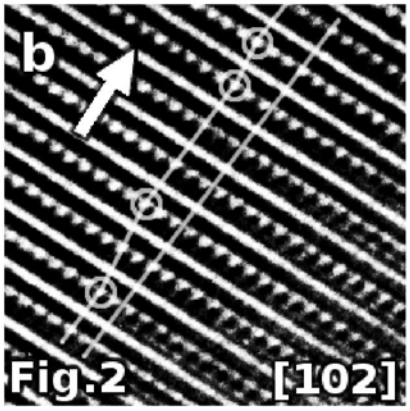

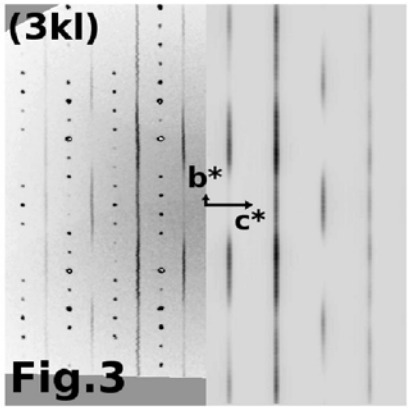

References

[1] Barrier, N., Pelloquin, D., Nguyen, N., Giot, M., Boure, F. and Raveau, B., *Chem. Mater.*, Vol. 17, (2005), pp 6619-6623
[2] D'Hondt, H., Abakumov, A. M., Hadermann, J., Kalyuzhnaya, A. S., Rozova, M. G., Antipov, E. V. and Tendeloo, G. V., *Chem. Mater.*, Vol. 20, (2008), pp 7188-7194
[3] Krekels, T., Milat, O., Tendeloo, G. V., Amelinckx, S., Babu, T. G. N., Wright, A. J. and Greaves, C., *J. Solid State Chem.*, Vol. 105, (1993), pp 313-335
[4] Butler, B. D. and Welberry, T. R., *J. Appl. Crystallogr.*, Vol. 25, (1992), pp 391-399

MS17-P02

Enhancement of the ν_4 band in heme at NIR laser enhancement attributed to supramolecular interactions

Ratchadaporn Puntharod[1,2], Bayden R. Wood[3], and Kenneth J. Haller[1]

[1] *School of Chemistry, Institute of Science, Suranaree University of Technology, Nakhon Ratchasima 30000, Thailand*
[2] *Department of Chemistry, Faculty of Sciences, Maejo University, Chiangmai 50290, Thailand*
[3] *Centre for Biospectroscopy, School of Chemistry, Monash University, Victoria 3800, Australia*
E-mail: ratchada_aim@hotmail.com

The resonance Raman enhancement of the oxidation state marker band (ν_4 at ~1375 cm^{-1}) for the iron(III) porphyrins, Fe(TPP)Cl, $[Fe(TPP)]_2O$, Fe(OEP)Cl, and $[Fe(OEP)]_2O$ has been investigated by using 413, 514, 633, 782, and 830 nm excitation laser sources. Only $[Fe(OEP)]_2O$ shows the minimum enhancement of the ν_4 band when exciting with 782 and 830 nm. X-ray crystallographic results show the stereochemistry of the hemes are similar with a five-coordinate square-pyramidal geometry and high-spin iron(III) ion. The bond lengths of Fe–N and Fe–axial ligands including the displacement of Fe atom out of the porphyrin plane and distance of porphyrin-porphyrin plane in Fe(OEP) as well as the dihedral angles and delocalized π-system of Fe(TPP) are normal and do not provide an explanation for this unusual observation. The supramolecular interactions have been investigated as a possible reason to understand the enhancement of the ν_4 band at near infrared laser excitation. The most significant difference among these hemes is the number of intermolecular interactions leading to the hypothesis that the enhancement of the ν_4 band is primarily a result of the supramolecular interactions.

References

[1] Scheidt W. R.; Michael M. G., "Structure of monoclinic choloro(meso-tetraphenylporphyrinato) iron(III)", *Acta Cryst. C*, Vol. 45, (1989), pp 1214-1216.

[2] Swepston P. N.; Ibers J. A., "Redetermination of the structure of μ-oxo-bis[5,10,15,20-tetraphenylporphyrinato)iron(III)] at 122 K, $[Fe_2O(C_{44}H_{28}N_4)_2]$", *Acta Cryst. C*, Vol. 41, (1985), pp 671-673.

[3] Senge M. O., "Chloro(2,3,7,8,12,13,17,18-octaethylporphyrinato)iron(III)", *Acta Cryst. E*, Vol. 61, (2005), pp m399-m400.

[4] Cheng B.; Hobbs J. D.; Debrunner P. G.; Erlebacher J.; Shelnutt J. A.; Scheidt W. R., "An unusual near-eclipsed porphyrin ring orientation in two crystalline forms of (μ-oxo)bis[octaethyl-porphyrinato)iron(III)]. Structural and molecular mechanics studies", *Inorg. Chem.*, Vol. 34, (1995), 102-110.

MS17-P03

Recombinant fusion protein design for biophysical analysis of integrin subunit dimerization and function

Andrea Francesca M. Salvador, Gabriel N. Valbuena, Lydia Teresa Isabel Salud-Bautista, and Neil Andrew D. Bascos

Protein Structure and Immunology Laboratory, National Institute of Molecular Biology and Biotechnology, University of the Philippines, Diliman, Quezon City, Philippines, 1101
E-mail: ndbascos@up.edu.ph, nadbascos@gmail.com

Integrins provide the principal means for cellular attachment to the extracellular matrix (ECM)[1]. Integrins are made up of subunits that associate as heterodimers on the cell surface[2]. The binding of integrin heterodimers to ECM ligands provide attachment to the ECM as well signals for intracellular processes, thereby "integrating" the intracellular and extracellular environments. The formation of different integrin heterodimer combinations results in different affinities for several ligands as well as variations in intercellular processes signaled[1]. Studies have correlated the formation of different integrin heterodimers with the multiple stages of cancer progression[3] and metastasis[4]. Biophysical analysis of integrin subunit dimerization therefore presents a worthwhile strategy for the progress of cancer treatment. Of the 24 integrin heterodimers identified[5], only three combinations have been successfully crystallized (αVβ3, αIIbβ3 and αXβ1)[2,6,7]. The limited success in crystallization may be attributed to integrin subunit size (~240 kDa/heterodimer), and flexibility[8]. This project aims to increase the efficiency of integrin subunit crystallization by limiting target size and flexibility. Limitations to size and flexibility were designed through the generation of fusion proteins containing only selected integrin subunit domains linked to *fos/jun* leucine zippers. The *Fos/Jun* dimerization domains were included to restrict flexibility, maintain close proximity[9] and facilitate interaction between the expressed subunit domains despite the absence of the rest of the integrin subunit. Genes encoding the functional domains of different integrin subunits were amplified from mammalian cell cultures representing different stages of cancer progression: M4A4, NM2C5, HCT116, A549 (ATCC). Coding sequences for the *Fos* and *Jun* leucine zippers were amplified from these sources as well. Amplicon identities were verified through DNA sequencing. Confirmed amplicons were inserted into cloning plasmids for propagation. Amplicons await transfer into yeast expression plasmids for fusion protein production[10].

References

[1] Giancotti, FG and Ruoslahti, ER. Integrin Signalling. *Science*. 1999.285:1028–1032.
[2] Xiong, JP; Stehle, T; Diefenbach, B; Zhang, R; Dunker, R; Scott, D; Joachimiak, A; Goodman, S; and Arnaout, MA. Crystal Structure of the Extracellular Segment of Integrin $\alpha_V\beta_3$. *Science*. 2001. 294:339-345.
[3] Shimizu, H; Koyama, N; Asada, M; and Yoshimatsu, K. Aberrant expression of integrin and erbB subunits in breast cancer cell lines. *International Journal of Oncology*. 2002. 21:1073-1079.
[4] Edlund, M; Miyamoto, T; Sikes, R; Ogle, R; Laurie, GW; Farach-Carson, MC; Otey, CA; Zhau, HE; and Chung, LWK. Integrin Expression and Usage by Prostate Cancer Cell lines on Laminin Substrata. *Cell Growth & Differentiatiion*. 2001. 12:99-107.
[5] Moschos, Stergios J, Laura M Drogowski, Shelley L Reppert, and John M Kirkwood. "Integrins a nd Cancer." *Oncology (Williston Park, NY)* 21, no. 9 (2007): 13-20.
[6] Springer TA, Zhu J, Xiao T, Structural basis for distinctive recognition of fibrinogen gammaC peptide by the platelet integrin alphaIIbbeta3. J Cell Biol. 2008 Aug 25;182(4):791-800
[7] Xie C, Zhu J, Chen X, Mi L, Nishida N, Springer TA. Structure of an integrin with an alphaI domain, complement receptor type 4. EMBO J. 2010 Feb 3;29(3):666-79. Epub 2009 Dec 24.
[8] Hynes, Richard O. "Integrins: Versatility, Modulation, and Signaling in Cell Adhesion." *Cell* 69 (April 1992): 11-25.
[9] Ramirez-Carrozzi, V; Kerppola, T. Dynamics of Fos-Jun-NFAT1 complexes. 2001. *Proceedings of the National Academy of Sciences (USA)*. 98: 4893-4898.
[10] Meta, A; Nakatake, H; Imamura, T; Nozaki, C; and Sugimura, K. High-yield production and characterization of biologically active recombinant aprotinin expressed in *Saccharomyces cerevisiae*. *Protein Expression and Purification*. 2009. 66: 22-27.

Development of computer software for general area detector diffraction system (GADDS)

Hosung Kim[1], Hohyuk Kim[2]

[1]*School of Materials Science & Engineering, Chonnam National University, 300, Yongbong-dong, Puk-gu, Gwangju 138-863, Korea*
[2]*Department of Application, Korea I.T.S. Co.,Ltd., 4F. Seoil Bldg., 222, Jamsil-dong, Songpa-gu, Seoul 138-863, Korea*
E-mail: icosahedron@naver.com

We have developed the software which determines the orientation of the single crystal using General Area Detector Diffraction System(GADDS). The developed software is possible to determines the orientation for all kinds of crystal system and to analyze the single crystal when Detector's position was laid down at every directions against the beam direction. In case a uncertainty of the position of diffraction spots is below a millimeter, the orientation can be determined the right way by the least squares fitting.

The diffraction patterns can be simulated by the data of crystals and diffraction conditions. After the crystal orientation is determined, we can calculate the way of rotating the crystal for the next process. The GADDS Analysis Program is developed with C++ programming language and can be applied to the instruments of X-ray diffraction.

References

[1] Azarofff, Leonid V., "*Element of X-ray Crystallography*", Techbooks, (1992).
[2] Borchardt-Ott, Walter, "*Crystallography*", Springer, (1995).
[3] Catti, M., "*Fundamentals of Crystallography*", Oxford University, (2002).
[4] Cullity, B.D., "*Elements of X-ray Diffraction*", Addison Wesley Publishing Company, (1978).
[5] Duncan, Mckie, Christine, Mckie, "*Essentials of Crystallography*", Blackwell Science, (1986).

MS17-P05

Mineralogy and geochemistry of volcanic rocks of Poledokhtar, Myaneh (NW Iran)

Amin Kamali[*2], Mohssen Moayed[1], Hadi Pirooj[1], Mohamade Mehri[2]

1) Department of geology, faculty of natural science, Tabriz University. Tabriz-Iran.
2) Department of geology, faculty of natural science, tarbiat moalem University. Tehran-Iran
E-mail : Aminkamali63@yahoo.com

The volcanic rocks of Poledokhtar which are Located in 15 kilmetrs Myaneh. Rhyolites and dacites structured region flows, phenoceryst hornblend samples manually, contains major minerals such as plagioclase, hornblende and shows porphyry and microlitic porphyry textures. In these rocks plagioclase shows mesh texture and oscillatory zoning. The hornbelande also having opacity margin. These rocks are fall in rhyolite calc-alkaline and meta-aluminous characters and From the genetic classification point of view the studied silica domes is from I type granite and it belongs to magnetite series.These rocks are enriched in LIL, LREE, however, they are depleted in HREE and Y. In addition, they show negative anomalies of Nb, Ta, P and Ti, and positive anomaly of Pb. The negative anomalies of Nb and Ta may indicate the effect of mantle wedge metasomatism by oceanic crust. The positive anomaly of Pb may demonstrate continental crust assimilation by magma associam ated with mantle metasomatism. Based on the tectonic setting discrimination diagrams, this volcanic is belong to VAG type and therefore it has been resulted from subduction of neotethys oceanic crust beneath the central Iran continental crust.

Key words:Poledokhtar, Myaneh, Rhyolite, I Type, VAG

[2*] Corresponding author

MS17-P06

Evolution and development of CrysAlis^{Pro}

Zoltan Gal, Alexandra Griffin and Oliver Presly

Agilent Technologies XRD (formerly Oxford Diffraction)
E-mail: zoltan.gal@agilent.com

CrysAlis^{Pro} is the software used to collect and reduce data for Agilent Technologies XRD systems (formerly Oxford Diffraction). In order to achieve the best results, it is important for the software to be user-friendly and function just as well as the diffraction hardware. Encouraging feedback from users allows the provision of a continually evolving program and new features and bug fixes are frequently implemented according to the community's requirements. The presentation will highlight several examples of user-inspired software tools, alongside the addition of new utilities for protein screening, simplistic multi-temperature and wavelength experiment strategies and extended options for high pressure data collection and reduction. The updates are presented here with a discussion of how the new tools may be implemented to improve data quality.

Also highlighted will be Agilent's AutoChem module. This is a software plugin which solves and refines structures in real time, concurrent with data collection and data reduction. This is fully automated, and also enables very simple and comprehensive structure report generation, particularly useful in service crystallography.
Keywords: crysalis pro, high pressure, protein screening, autochem

MS17-P07

Structure of hibiscus latent Singapoie virus by fiber diffraction: Insights into into evolution of a distinct *Tobamovirus*

Kunchithapadam Swaminathan[1], Sunil Kumar Tewary[1], Toshiro Oda[2], Amy Kendall[3], Wen Bian[3], Gerald Stubbs[3], Sek-Man Wong[1]

[1]*Department of Biological Sciences, National University of Singapore, Singapore 117543*
[2]*Structural Physiology Research Group, RIKEN SPring-8, Center Kouto 1-1-1, Sayo, Hyogo, Japan 679-5148*
[3]*Department of Molecular Biology, Vanderbilt University, Nashville, TN 37235, U.S.A.*
E-mail: dbsks@nus.edu.sg

Hibiscus latent Singapore virus (HLSV) is a rigid rod shaped plant virus [1], a new member of the *Tobamovirus* family. Functionally, it differs from other known *Tobamoviruses*, like Tobacco mosaic virus (TMV), Cucumber green mottle mosaic virus (CGMMV), Sun-hemp mosaic virus (SHMV), Ribgrass mosaic virus (RMV) and Odontoglossum ringspot virus (ORSV, also known as TMV-O). Being unique among *Tobamovirus*, the HLSV genome contains a poly(A) tract at the 3′-UTR, which controls viral infectivity. The virion is made up of a monomeric coat protein (CP) unit of 18 kDa, arranged as a right handed helix around the virus axis. We have determined the structure of HLSV at 3.5 Å by fiber diffraction and refined to an R-factor of 0.096. While the overall structure of the HLSV CP resembles that of other *Tobamoviruses*, there are marked differences. There is a kink in the LR helix (residues 112-133) due to the close proximity of Asp116 and Glu124 with the RNA phosphates and the presence of two adjacent positively charged residues (His122 and Lys123), which destabilize the LR helix. The carboxyl-carboxylate interactions that drive viral assembly and disassembly are different and more complex in HLSV than that of other subgroup 1 and 2 *Tobamoviruses*. Furthermore, while being similar to that in Ribgrass mosaic virus (RMV) [2], the nucleotide recognition mechanism in HLSV (which is responsible for the assembly of *Tobamovirus*) deviates from that of TMV [3] and CGMMV [4]. These results, along with several defined genomic, molecular and structural differences, suggest that a new taxonomic group must be assigned for HLSV.

References

[1] Srinivasan K.G., Narendrakumar R. and Wong S.M., "Hibiscus virus S is a new subgroup II *Tobamovirus*: evidence from its unique coat protein and movement protein sequences", Arch. Virol., Vol. 147, (2002), pp 1585-1598.

[2] Wang H., Culver J.N. and Stubbs G., "Structure of *Ribgrass mosaic virus* at 2.9 Å resolution evolution and taxonomy of *Tobamoviruses*", J. Mol. Biol., Vol. 269, (1997), pp769-779.

[3] Pattanayek R. and Stubbs G., "Structure of the U2 strain of Tobacco mosaic virus refined at 3.5 Å resolution using X-ray fiber diffraction", J. Mol. Biol., Vol. 228, (1992). Pp 516-528.

[4] Wang H. and Stubbs G., "Structure determination of *Cucumber green mottle mosaic virus* by X-ray fiber diffraction. Significance for the evolution of *Tobamoviruses*", J. Mol. Biol., Vol. 239, (1994), pp 371-384

AsCA2010

The 10th Conference of the Asian Crystallographic Association

AUTHOR INDEX

A

B

C

D

H

I

K

P

T

U

X

Y

Z

AsCA2010

The 10th Conference of the Asian Crystallographic Association

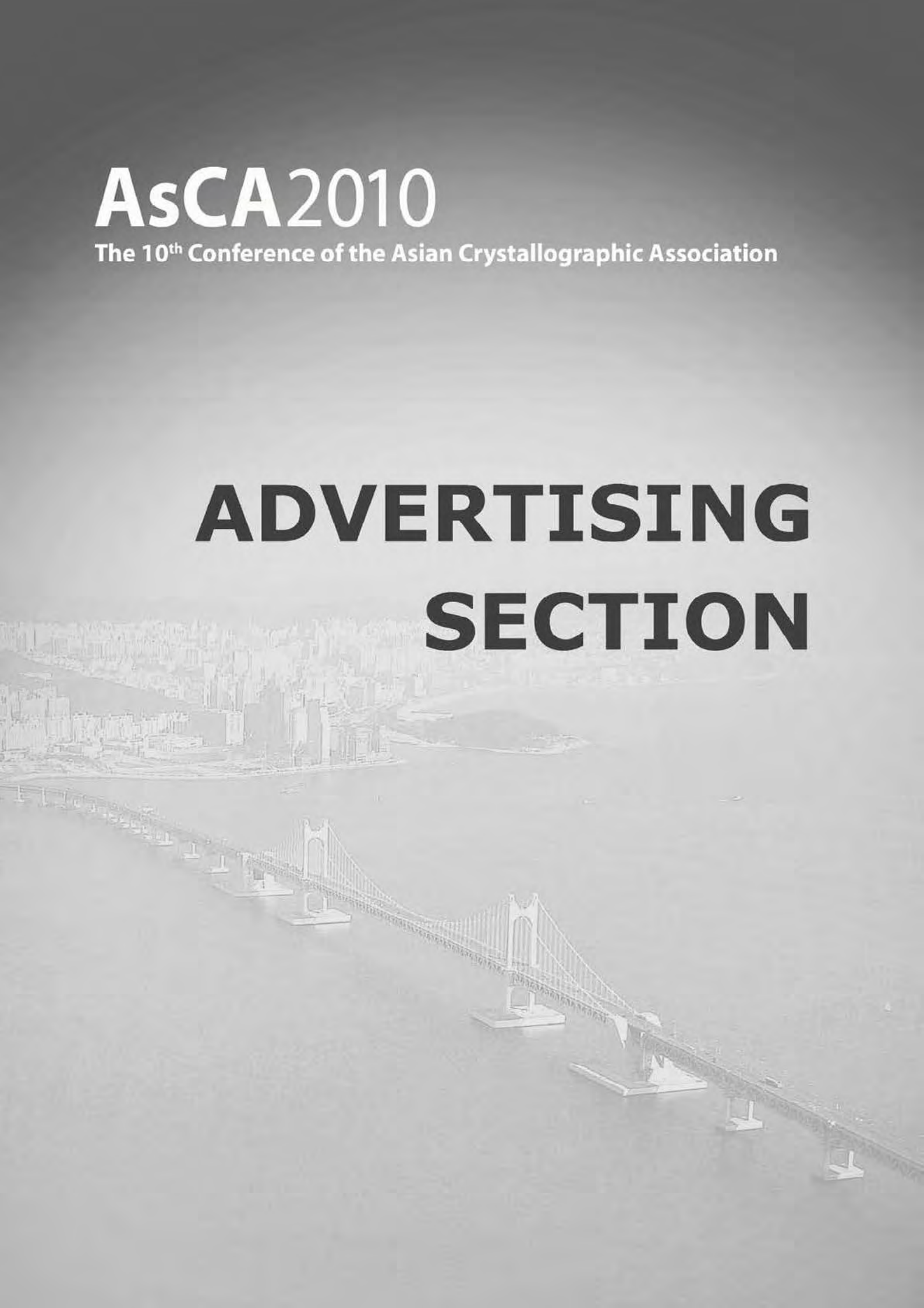

ADVERTISING SECTION

INCOATEC
innovative coating technologies gmbh

Protein Crystallography

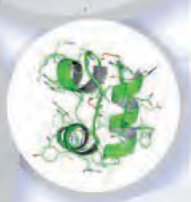

Small Molecule Crystallography

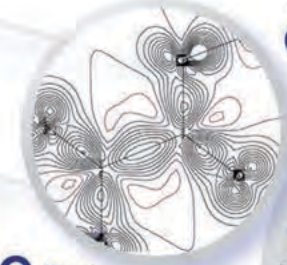

IμS Incoatec Microfocus Source

30 W

air-cooled

Quazar multilayer optics

for Cu and Mo
Ag and Cr

unprecedented
flux density

low maintenance

2D focusing or collimating

XRD

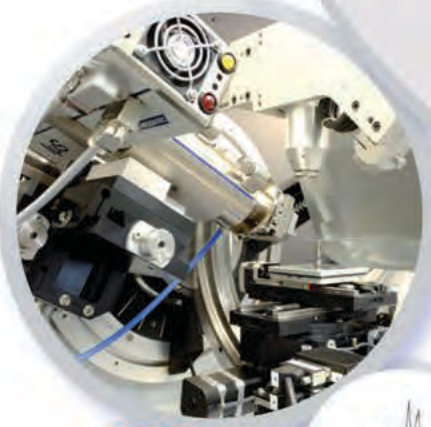

3 years warranty

High Brilliance Sealed Tube

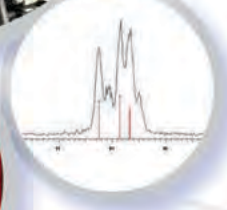

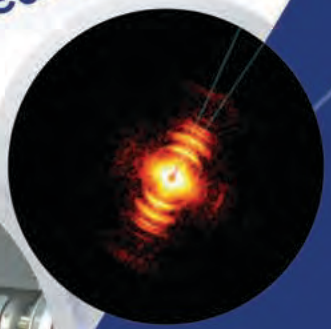

SAXS

www.incoatec.de

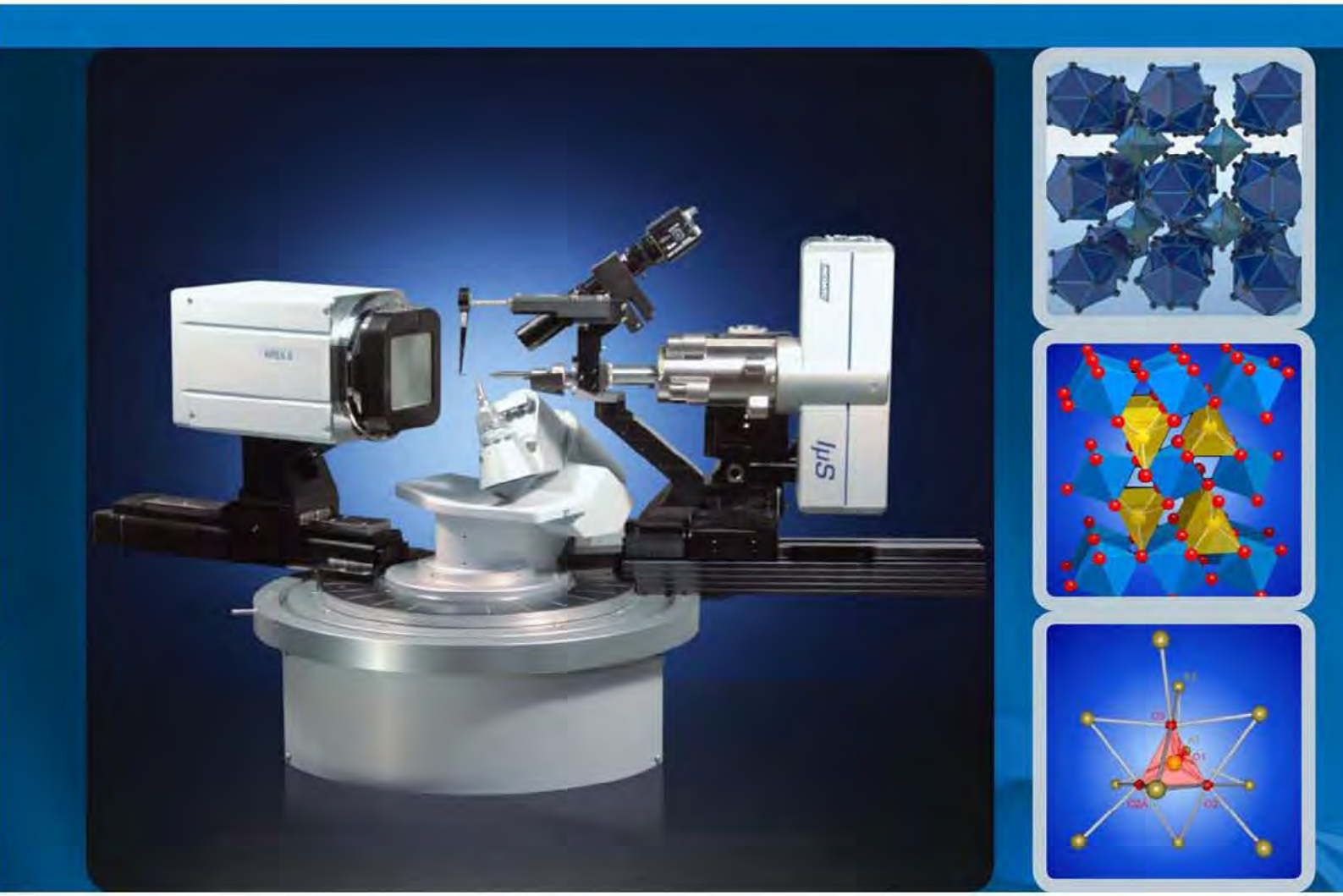

APEX II QUAZAR

World's First High-Intensity Ag Microfocus for Solid State Chemistry

- 90 µm beam size for optimal signal to noise ratio for small crystals and high pressure experiments
- Improved data quality due to lower absorption and reduced extinction
- Shorter wavelength for higher resolution charge density data
- 3 year warranty on air-cooled and maintenance free source

think forward

www.bruker-axs.de

BRUKER

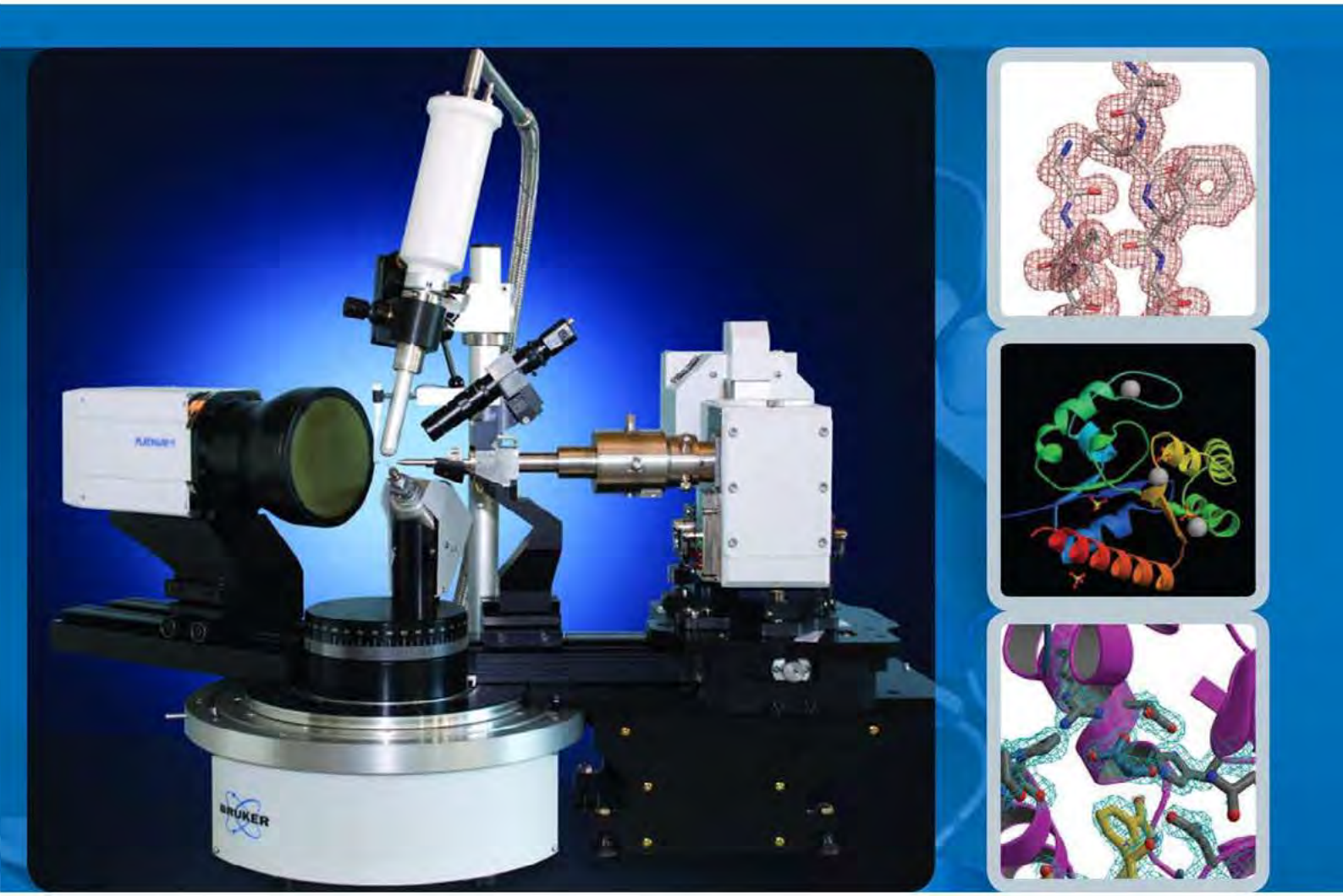

X8 PROTEUM

Your Personal Beamline

- High-throughput screening and SAD-phasing quality data in an uncompromised package
- Compact goniometer-mounted source ensures highest beam stability and most reliable alignment
- PLATINUM^{135} CCD detector with large dynamic range and high sensitivity
- Kappa goniometer for easy sample handling
- Powerful, easy-to-use PROTEUM2 software

Crystallography

PAL XFEL

The synchrotron radiation source, the light of dream to open high-tech scientific world.

Millions of times brighter than normal in X-rays, the 3rd generation light source presented new horizons of science in 20th century.

The characteristics of ultra-fast , ultra-small and coherent of X-ray Free Electron Laser will provide high lever of scientific research in the 21st century.

PAL POHANG ACCELERATOR LABORATORY

EMPYREAN

The world of X-ray diffraction is no longer flat

0D

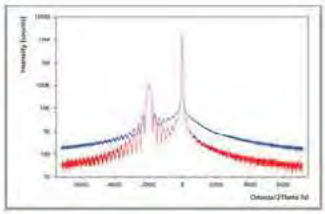

1D

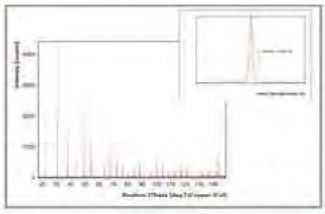

2D

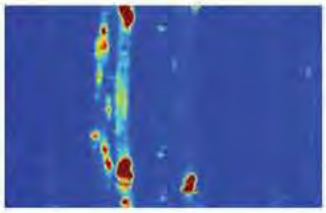

3D

The only XRD platform that does it all

- Powders
- Thin films
- Nanomaterials
- Solid objects

The new Empyrean from PANalytical is truly innovative, with cutting-edge technology in every aspect. Empyrean brings the idea of the perfect XRD platform to life:

- The widest range of samples
- The highest data quality on every sample, no compromises
- Exceptional tube performance
- The highest performance goniometer
- 2nd generation PreFIX for optics and sample platforms
- PIXcel^{3D}: the only detector for 0D, 1D, 2D and even 3D applications
- Unmatched area detector dynamic range, linearity and resolution
- See inside your samples with the world's first 3D detector

PANalytical
7F SH Energy Bldg., 16-6,
Sunae-Dong,Bundang-Gu,
Seongnam-City
Kyeonggi-Do,463-825
Korea
T 82-31-786-0940
F 82-31-786-0950
M 81-11-1731-7666
nayoon.kim@panalytical.com
www.panalytical.com

Cutting-edge technology. Ultimate commitment.

The Analytical X-ray Company

PANalytical

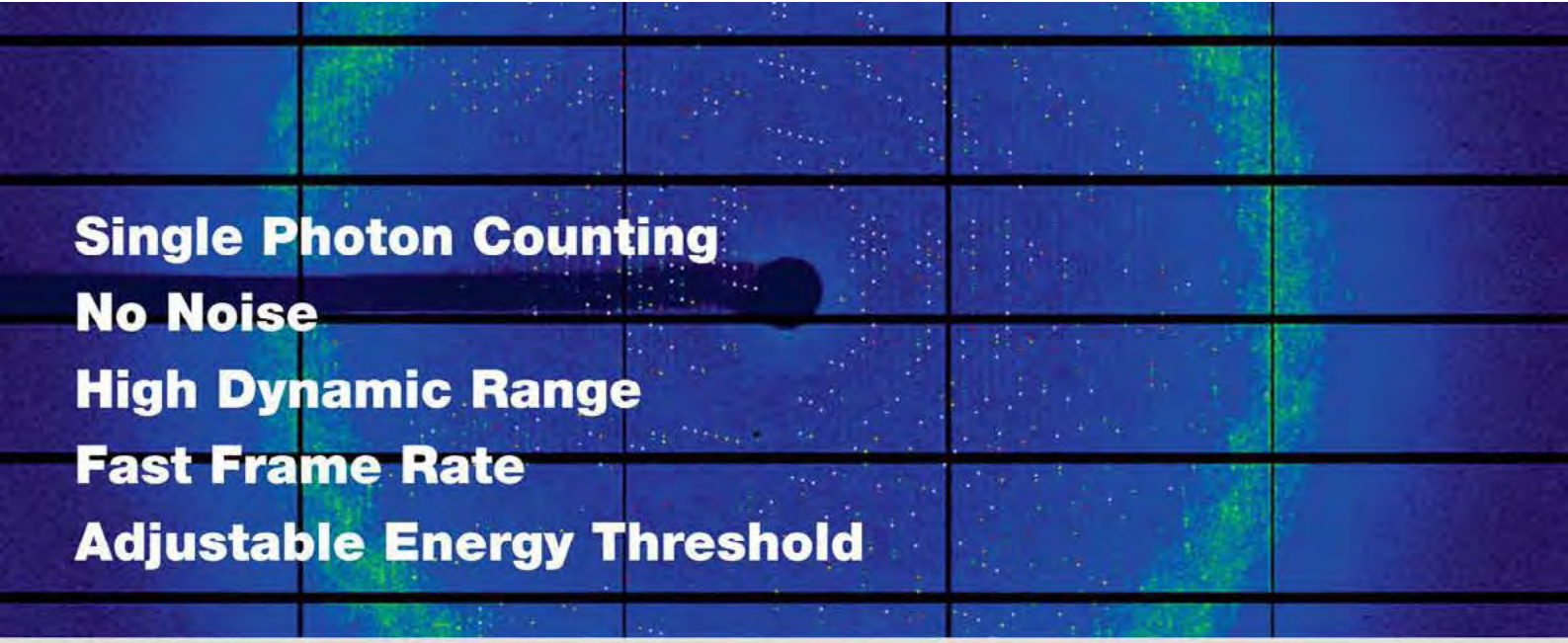

DECTRIS X-ray detector systems

DECTRIS offers a wide variety of detector systems for a broad range of applications

PILATUS 2-D detector systems

PILATUS detector systems are based on CMOS hybrid-pixel technology and deliver outstanding results in various applications. A wide range of models ensures that a suitable PILATUS detector can be chosen for every measurement.

MYTHEN 1-D detector systems

MYTHEN is a one dimensional silicon strip detector system, which can be combined to form multi-detector arrays covering large angles (MYTHEN 6K).

XBPM Beam Position Monitors

XBPM4 is a 4-quadrant x-ray beam position monitor based on CVD diamond technology, suitable for hard x-ray synchrotron beam lines.

DECTRIS
Next Generation X-Ray Detectors

DECTRIS Ltd. | Neuenhoferstrasse 107 | 5400 Baden | Switzerland | info@dectris.com | www.dectris.com

SuperNova

Dual Source
Proven Success

Now as Agilent Technologies, Oxford Diffraction continues to lead the way in dual wavelength crystallography with nearly 100 dual wavelength systems installed worldwide. The most advanced dual wavelength system, the SuperNova, features:

- Automatic wavelength switching between Mo and Cu X-ray microfocus sources
- 50W X-ray sources, which provide up to 3x more intensity than a 5kW rotating anode
- The fastest, highest performance CCD
  Large area 135mm Atlas or highest sensitivity Eos with 330 e^-/X-ray Mo gain
- A full 4-circle kappa goniometer
- AutoChem, automatic structure solution and refinement software
- An extremely compact, low maintenance design

www.agilent.com/chem xrdsales@agilent.com

The Measure of Confidence

Agilent Technologies

More Capability—you've got it!
More Analysis Power—you bet!

Designed for materials identification, the Powder Diffraction File offers comprehensive, high-quality data. Independent of whether phase identification is performed by classic d,I pair analysis or by total pattern comparisons, the accuracy of the reference in comparison to an unknown is improved with higher quality reference data. Enhance your competitive analysis with more high-quality data, more capability and more analysis power—found only in the Powder Diffraction File!

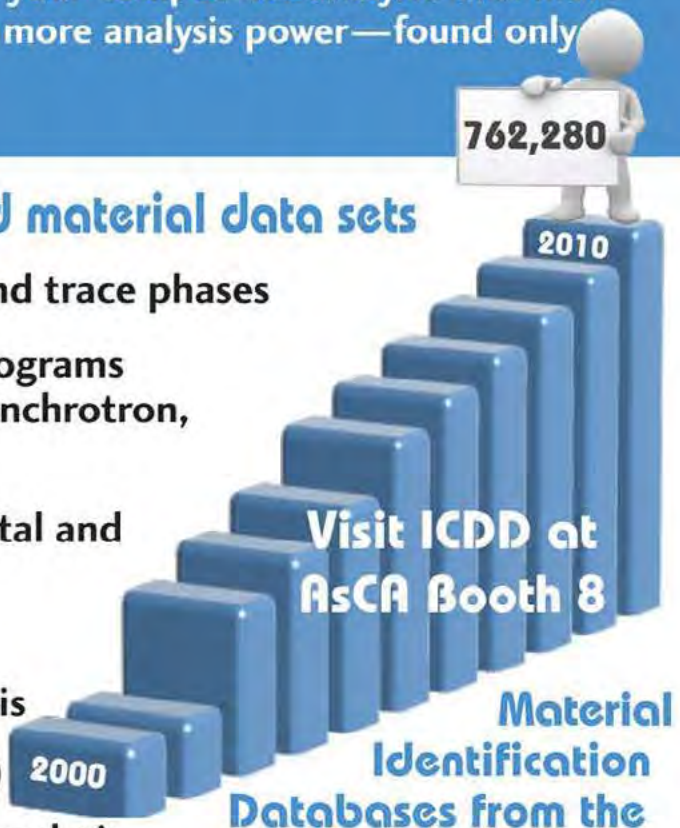

Comprehensive: 762,280 published material data sets

Improve your ability to analyze minor and trace phases

Exploit a full suite of data simulation programs enabling the use of neutron, electron, synchrotron, and X-ray data

Tailor simulations for various instrumental and specimen characteristics

Utilize quantitative analysis methods:

- Atomic parameters for Rietveld analysis
- I/I_c for Reference Intensity Ratio (RIR)
- Full digital patterns for total pattern analysis

The Powder Diffraction File

PDF-2 Release 2010	230,346 material data sets
PDF-4+ 2010	301,282 material data sets
PDF-4/Minerals 2010	36,036 material data sets
PDF-4/Organics 2011	436,901 material data sets

The International Centre for Diffraction Data

marketing@icdd.com
www.icdd.com
610.325.9814
Toll-free U.S. & Canada: 866.378.9331

ICDD®
International Centre for Diffraction Data

ISO 9001:2008 QUALITY ASSURED COMPANY CERT.NR 11409.1

Split Frame Transfer CCD

higher resolution, higher Quantum Efficiency, faster data rate exclusively from Rayonix

rayonix mx SERIES HS

- move to shutterless data collection
- permanent factory calibration, valid for all sources and all bunch structures
- no count rate limitations, no count rate corrections required
- up to 150 MegaPixel/Second
- 1 msec dead time

1880 Oak Avenue
Evanston, IL 60201 USA
info@rayonix.com

Tel: +1 (847) 869-1548
Fax: +1 (847) 869-1587
Toll Free in USA: (877) 627-XRAY

www.rayonix.com

GE Healthcare

MicroCal™

Ultrasensitive **Calorimetry** for Life Sciences

MicroCal™ is Ultrasensitive Biocalorimeter which can measure biomolecular interactions and determine the stability of biological systems.

- Investigate any biomolecular interactions (Protein, Lipid, Nucleic acid, Small Compoud etc.) with high sensitivity
- No immobilization or labeling required. No buffer restrictions. Easily handles turbid solutions
- Provides insights into mechanisms of folding and domain structure of unknown proteins
- Designed for ease-of-use,all functions are operated through software to facilitate fast and accurate analyses

GE imagination at work

지이헬스케어코리아(주)
(Tel) 0262013800, (Fax) 0262013804
www.gelifesciences.com/korea

For more information, visit :
www.gelifesciences.com/Microcal

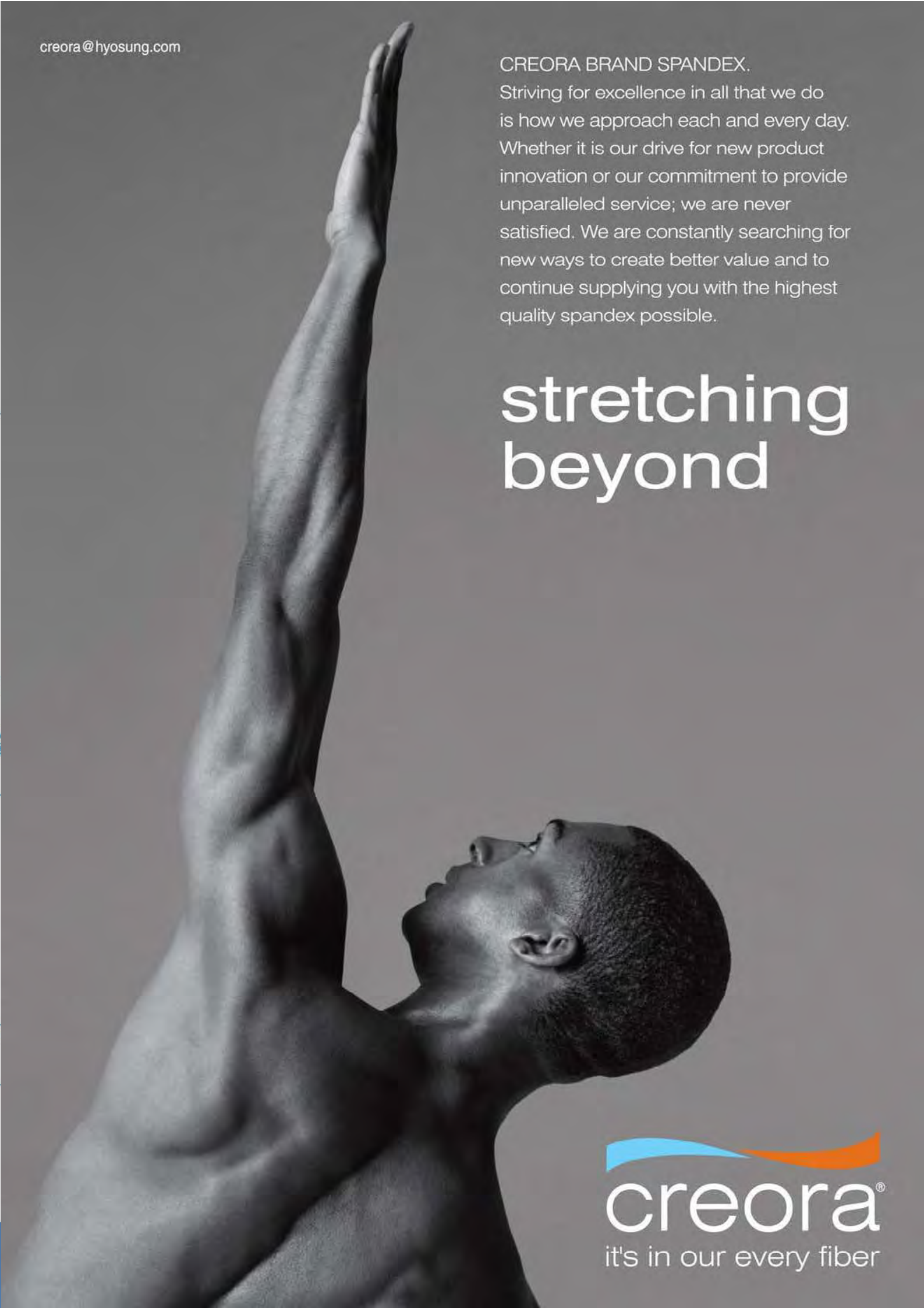
creora@hyosung.com
CREORA BRAND SPANDEX.
Striving for excellence in all that we do is how we approach each and every day. Whether it is our drive for new product innovation or our commitment to provide unparalleled service; we are never satisfied. We are constantly searching for new ways to create better value and to continue supplying you with the highest quality spandex possible.
stretching beyond
creora®
it's in our every fiber

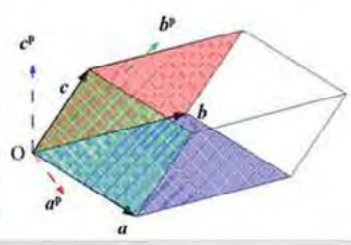

SPECIAL ISSUE ONLINE NOW

Journal of Applied Crystallography

Crystallography education and training for the 21st century

CONTENTS

AUTHORS

Frank H. Allen, Gary M. Battle, Helen M. Berman, Elena Boldyreva, Graeme L. Card, Aina E. Cohen, Nora Darowski, Zbigniew Dauter, Kay Diederichs, Tzanko I. Doukov, Pete W. Dunten, Shuchismita Dutta, Thomas Eriksson, Annette Faust, Gregory M. Ferrence, Nicholas Furlani, Ana M. Gonzalez, David S. Goodsell, Robert M. Hanson, Mariusz Jaskolski, Katherine A. Kantardjieff, Cora Lind, Joseph R. Luft, Scott E. McPhillips, Irimpan I. Mathews, Uwe Mueller, Rachel NeMoyer, Massimo Nespolo, Joseph D. Ng, Santosh Panjikar, Elliott J. Penna, Virginia B. Pett, Stephen A. Potter, Sandra Puehringer, Bernhard Rupp, Bernard Santarsiero, Clyde A. Smith, Edward H. Snell, M. Elizabeth Snell, Alexei Soares, S. Michael Soltis, Jinhu Song, Bernd Souvignier, Robert M. Sweet, Brian H. Toby, Manfred S. Weiss, Jennifer R. Wolfley, Christine Zardecki

Publication date: October 2010

Order your print copy at http://journals.iucr.org/services/specialissues.html

Sponsored by Bruker, Dectris, Huber, ICDD, Molecular Dimensions, Oxford Cryosystems, Taylor & Francis

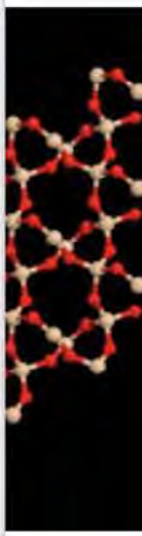

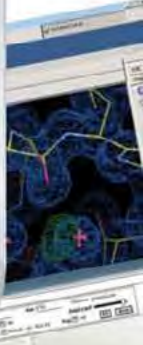

Rigaku proudly introduces...

The ScreenMachine

As synchrotron beamlines have become more prevalent for research in structural biology, many home lab X-ray systems are used mainly for screening crystals in advance of synchrotron data collection. To meet the needs of this type of work flow, Rigaku has developed the ScreenMachine, a self-contained unit that is optimized for safe crystal mounting and recovery, optimized for evaluating small crystals, designed for minimal maintenance and, best of all, collects amazingly high quality data.

Screen Protein Crystals,
Teach crystallography,
and Solve Protein Structures

Rigaku

Rigaku Americas Corporation phone: +1 (281) 362-2300 | e-mail: info@rigaku.com | www.rigaku.com
Rigaku Bejing Corporation (China) phone: +86-10-82800840 | Rigaku Corporation (Japan) phone: +81 (0)3-3479-0618

Perform more analyses, produce more results: Rigaku benchtop solutions!

MiniFlex™ II

- D/teX Ultra collects data up to 100X faster
- Graphite monochromator optimizes peak to background measurements
- 6-position sample changer for high throughput and ultimate ease of use

XtaLAB mini

- Automatic intelligent space group determination and chemical-knowledge-based structure solution
- Simple, rugged design with small footprint
- Needs only standard AC power anywhere in the world
- Exceptional data quality with built-in optic and Mercury3 detector
- Video crystal viewing and face indexing
- Option for complete handling of twins

Supermini

- Sequential measurement F-U
- 200 W high-powered benchtop design
- Meets WEEE/RoHS directives
- Vacuum or helium environments

Rigaku

Rigaku Americas Corporation phone: +1 (281) 362-2300 | e-mail: info@rigaku.com | www.rigaku.com
Rigaku Bejing Corporation (China) phone: +86-10-82800840 | Rigaku Corporation (Japan) phone: +81 (0)3-3479-0618